

**SUSTAINABLE ENERGY SYSTEMS**  
**Limitations and challenges based on exergy analysis**

**Proefschrift**

ter verkrijging van de graad van doctor  
aan de Technische Universiteit Delft,  
op gezag van de Rector Magnificus prof. ir. K.C.A.M. Luyben,  
voorzitter van het College voor Promoties  
in het openbaar te verdedigen op dinsdag 23 oktober 2012 om 10.00 uur

door

NICO WOUDSTRA, ingenieur

werktuigkundig ingenieur  
geboren te Sneek

Dit proefschrift is goedgekeurd door de promotor:

Prof.dr.ir. A.H.M. Verkooijen

Samenstelling promotiecommissie:

Rector Magnificus,	voorzitter
Prof.dr.ir. A.H.M. Verkooijen,	Technische Universiteit Delft, promotor
Prof.dr.ir. B.J. Boersma,	Technische Universiteit Delft
Prof. Dr.-Ing. G. Tsatsaronis,	Technische Universität Berlin
Prof.dr.ir. T.H. van der Meer,	Universiteit Twente
Prof.ir. P.G. Luscuere	Technische Universiteit Delft
Dr. K. Hemmes,	Technische Universiteit Delft
Dr.ir. F.P.J.M. Kerkhof	Jacobs

ISBN/EAN: 978-94-6191-441-5

Copyright © 2012 by N. Woudstra

All rights reserved. No part of the material protected by this copyright notice may be reproduced or utilized in any form or by any means, electronic or mechanical, including photocopying, recording or by any information storage and retrieval system, without the prior permission of the author.

Dedicated to:

*Diego Raphaël* and all other children that didn't get the chance to develop

## TABLE OF CONTENTS

### Summary

### Nomenclature

<b>1</b>	<b>INTRODUCTION.....</b>	<b>1</b>
<b>1.1</b>	<b>Problem description.....</b>	<b>1</b>
<b>1.2</b>	<b>Objectives.....</b>	<b>3</b>
<b>1.3</b>	<b>Outline.....</b>	<b>4</b>
<b>2</b>	<b>EXERGY ANALYSIS .....</b>	<b>9</b>
<b>2.1</b>	<b>Introduction.....</b>	<b>9</b>
2.1.1	The need for exergy analysis .....	9
2.1.2	Exergy losses.....	10
2.1.3	Exergoeconomic evaluation .....	10
<b>2.2</b>	<b>The exergy concept.....</b>	<b>11</b>
2.2.1	General definition.....	11
2.2.2	Thermo-mechanical and chemical exergy .....	12
2.2.3	The exergy balance .....	13
<b>2.3</b>	<b>The calculation of exergy of heat, cold and matter.....</b>	<b>13</b>
2.3.1	The exergy of heat.....	13
2.3.2	The exergy of cold .....	14
2.3.3	The thermo-mechanical exergy of matter .....	17
2.3.4	The chemical exergy of matter.....	18
2.3.5	The exergy loss of open steady state systems .....	24
<b>2.4</b>	<b>The exergy of solid and liquid fuels.....</b>	<b>26</b>
2.4.1	Introduction.....	26
2.4.2	The equations of Szargut and Styrylska.....	26
2.4.3	The calculation method of Baehr-I .....	27
2.4.4	The calculation method of Baehr-II .....	29
2.4.5	Comparison of the various methods for the calculation of the specific exergy .....	32
<b>2.5</b>	<b>Value diagrams and exergy flow diagrams.....</b>	<b>38</b>
2.5.1	Introduction.....	38
2.5.2	Value diagrams for heat transfer .....	39
2.5.3	Value diagrams for thermal power plants .....	41
2.5.4	Exergy flow diagrams .....	44
<b>2.6</b>	<b>Exergy efficiencies.....</b>	<b>45</b>
2.6.1	Introduction.....	45
2.6.2	Exergy efficiencies of energy conversion plants .....	46
2.6.3	Exergy efficiencies of apparatuses and sub-systems .....	47

2.6.4	The thermodynamic equivalent temperature of heat transfer .....	52
2.6.5	The internal exergy efficiency of thermal power cycles.....	53
<b>3</b>	<b>OPTIONS FOR FUTURE ENERGY SYSTEMS.....</b>	<b>55</b>
<b>3.1</b>	<b>Introduction.....</b>	<b>55</b>
<b>3.2</b>	<b>The application of renewable energy sources.....</b>	<b>56</b>
3.2.1	Introduction.....	56
3.2.2	Renewable sources.....	56
3.2.3	System configurations and conversion technologies.....	58
3.2.4	Secondary fuel, transport, distribution and storage of energy.....	59
3.2.5	The importance of high system efficiencies.....	59
<b>3.3</b>	<b>Possibilities for higher efficiencies.....</b>	<b>60</b>
<b>3.4</b>	<b>The effects of alternative options for the generation of heat.....</b>	<b>61</b>
<b>3.5</b>	<b>Conclusions.....</b>	<b>67</b>
<b>4</b>	<b>FUEL CONVERSION.....</b>	<b>69</b>
<b>4.1</b>	<b>Introduction.....</b>	<b>69</b>
<b>4.2</b>	<b>Atmospheric combustion.....</b>	<b>70</b>
4.2.1	Introduction.....	70
4.2.2	Options to decrease the exergy loss of combustion.....	71
4.2.3	System evaluation.....	73
4.2.4	General remarks about the heating value and specific exergy of fuels.....	75
4.2.5	Description of the reference case.....	76
4.2.6	Effect of the type of fuel.....	77
4.2.7	Effect of the air factor.....	78
4.2.8	Affect of air preheating.....	79
4.2.9	Conclusions.....	81
<b>4.3</b>	<b>Pressurized combustion.....</b>	<b>84</b>
<b>4.4</b>	<b>Conversion into a secondary fuel.....</b>	<b>85</b>
4.4.1	Introduction.....	85
4.4.2	Coal gasification.....	86
4.4.3	Biomass gasification.....	87
4.4.4	Reforming of natural gas.....	88
<b>4.5</b>	<b>Exergy analysis of fuel conversion in literature.....</b>	<b>90</b>
<b>4.6</b>	<b>Conclusions.....</b>	<b>94</b>
<b>5</b>	<b>THERMAL POWER CYCLES.....</b>	<b>97</b>
<b>5.1</b>	<b>Introduction.....</b>	<b>97</b>
<b>5.2</b>	<b>Steam turbine cycles.....</b>	<b>98</b>
5.2.1	Conventional steam turbine plant (reference system).....	98
5.2.2	Advanced steam conditions.....	100

5.2.3	Prospects of advanced steam conditions .....	108
<b>5.3</b>	<b>Potassium topping cycles .....</b>	<b>109</b>
5.3.1	Introduction .....	109
5.3.2	Description of the potassium topping cycle plant .....	111
5.3.3	Plant performance .....	114
<b>5.4</b>	<b>Gas turbine cycles .....</b>	<b>115</b>
5.4.1	Introduction .....	115
5.4.2	Reference system of an open cycle gas turbine .....	117
5.4.3	Performance evaluation of an open cycle gas turbine.....	118
5.4.4	Development of gas turbine performance .....	124
<b>5.5</b>	<b>Combined cycles .....</b>	<b>126</b>
5.5.1	Introduction .....	126
5.5.2	Plant designs .....	132
5.5.3	Evaluation of system results.....	134
5.5.4	Discussion of results .....	142
5.5.5	Conclusions .....	145
<b>5.6</b>	<b>Conclusions .....</b>	<b>146</b>
<b>6</b>	<b>FUEL CELL SYSTEMS .....</b>	<b>151</b>
<b>6.1</b>	<b>Introduction .....</b>	<b>151</b>
<b>6.2</b>	<b>Status of fuel cell development and applications.....</b>	<b>152</b>
<b>6.3</b>	<b>Thermodynamic losses of fuel cells.....</b>	<b>154</b>
6.3.1	Introduction .....	154
6.3.2	Polymer Electrolyte Membrane Fuel Cell (PEMFC).....	155
6.3.3	Molten Carbonate Fuel Cell (MCFC) .....	157
6.3.4	Solid Oxide Fuel Cell (SOFC) .....	158
<b>6.4</b>	<b>Fuel conversion and purification .....</b>	<b>159</b>
6.4.1	Introduction .....	159
6.4.2	Conversion and purification processes.....	161
6.4.3	Evaluation of reforming processes .....	162
<b>6.5</b>	<b>The design of Fuel Cell Systems.....</b>	<b>166</b>
6.5.1	Introduction .....	166
6.5.2	PEMFC systems .....	167
6.5.3	MCFC systems .....	171
6.5.4	SOFC systems .....	180
<b>6.6</b>	<b>Conclusions .....</b>	<b>190</b>
<b>7</b>	<b>COMBINED HEAT AND POWER SYSTEMS .....</b>	<b>193</b>
<b>7.1</b>	<b>Introduction .....</b>	<b>193</b>
<b>7.2</b>	<b>Thermodynamic aspects of CHP .....</b>	<b>195</b>
7.2.1	How CHP can be useful .....	195

7.2.2	CHP plants, a variety of applications.....	201
<b>7.3</b>	<b>Thermodynamic concepts for the evaluation of CHP.....</b>	<b>203</b>
7.3.1	The conversion of energy values into exergy values for heat and fuel.....	203
7.3.2	Lost power and generated heat in the case of thermal power cycles with heat rejection at elevated temperatures (e.g. back pressure steam cycles) .....	204
7.3.3	The power loss ratio in the case of steam cycles with steam extraction.....	205
7.3.4	The efficiency of a reference system .....	206
<b>7.4</b>	<b>Merit indicators.....</b>	<b>207</b>
7.4.1	Options to indicate the thermodynamic merits of CHP .....	207
7.4.2	Comparison of some arbitrarily chosen CHP systems.....	212
7.4.3	Evaluation of merit indicators.....	216
<b>7.5</b>	<b>Evaluation of CHP design data.....</b>	<b>217</b>
7.5.1	The industrial gas turbine with waste heat boiler (IND. GT + WHB).....	217
7.5.2	The combined cycle district heating plant (CC/DH).....	220
7.5.3	The micro-CHP unit.....	221
7.5.4	Extraction condensation plants .....	222
<b>7.6</b>	<b>Conclusions .....</b>	<b>225</b>
<b>8</b>	<b>CONCLUSIONS .....</b>	<b>229</b>
8.1	Introduction.....	229
8.2	Options for sustainable energy systems.....	230
8.3	Conventional power plant technologies.....	231
8.4	Fuel cell systems.....	232
8.5	Combined heat and power systems.....	233
8.6	Exergy analysis .....	235
<b>APPENDICES</b>		
Appendix 2.1	Tabulated data .....	237
Appendix 2.2	Exergy efficiencies for the apparatuses of Cycle-Tempo .....	239
Appendix 2.3	Properties of solid and liquid fuels.....	251
Appendix 3.1	Evaluation of renewable energy sources .....	263
Appendix 4.1	Exergy losses of a conventional power plant (a reference system).....	317
Appendix 4.2	The thermodynamic equivalent temperature of heat transfer to the gas turbine cycle.....	339
Appendix 4.3	Fuel data .....	343
Appendix 5.1	Steam cycles with advanced steam conditions. Assumptions concerning system design and design parameters.....	351

Appendix 5.2 Thermodynamic performance of closed cycle gas turbine systems ..... 357  
Appendix 5.3 Evaluation of methods to determine the internal exergy efficiency ..... 371

Appendix 6.1 Thermodynamics of fuel cells ..... 377  
Appendix 6.2 Conversion of molar ratios into mass ratios for different fuels ..... 397  
Appendix 6.3 Calculation of the SOFC target system with Cycle-Tempo ..... 401

Appendix 7.1 Off-design evaluation of CHP systems..... 411

**References ..... 419**  
**Acknowledgements**  
**Curriculum Vitae**

## SUMMARY

### SUSTAINABLE ENERGY SYSTEMS

#### Limitations and challenges based on exergy analysis

##### General

There is a general understanding that the so-called “developed countries” have to change their way of life including their energy supply into a more sustainable way. But even in the case of unanimity with regard to the direction, there are still many opinions about the way to follow. This thesis discusses problems and possibilities of more sustainable energy systems first of all for the energy supply of the Netherlands. The “trias energetica” is used to distinguish the steps that have to be taken for this purpose. It considers the following sequence of steps:

- 1) reduce final energy consumption
- 2) make use of renewable energy sources
- 3) improve overall conversion efficiencies.

The importance of the first step is obvious, but this thesis focuses on the other two steps with great emphasis on the last one. The consequences of the application of available sources of renewable energy in the Netherlands are discussed in Chapter 3. The application of wind and solar energy will result in serious higher costs of energy supply. These higher costs are not only caused by the primary conversion by wind turbines, photovoltaic cells and so on, but also by the need of energy storage and the corresponding conversions. Biomass is supposed to offer a more affordable alternative, but the biomass available today in the Netherlands for energy conversion is not sufficient to cover the present demand. The required primary energy is determined by the final energy demand as well as the efficiency of the necessary conversions from the primary source to the final demand. Today thermodynamic losses associated with the conversion of primary energy into electricity and heat are very serious. Further reduction of these losses is necessary to arrive at more sustainable energy systems.

A rough indication of the effects of higher conversion efficiencies is shown in Chapter 3. Simplified systems for the supply of electricity and heat for the Netherlands have been compared based on the use of one single primary fuel (natural gas). The total heat demand is divided into a low temperature and a high temperature heat demand. A reference system, consisting of power plants for the generation of electricity and boilers for the generation of steam and hot water, was considered first. The calculations in Chapter 3 show fuel savings up to 30% to 40% are achievable by the application of power plants with high efficiencies (80%), improved CHP for the high temperature (industrial) heat demand and improved Heat Pumps for the low temperature heat demand. It is obvious that high power generation efficiencies are in favor of Heat Pump application.

Most of this thesis focuses on possibilities to reduce the thermodynamic losses of current energy conversion systems for the generation of electricity and heat. The exergy concept is used comprehensively to quantify these losses and to provide a better understanding of their causes. Fuel conversion processes and thermal power cycles are primarily used today for the generation

of power and heat. The limitations of these processes and cycles are discussed respectively in the Chapters 4 and 5. Possibilities to improve the thermodynamic performance of power and heat generation with the use of fuel cells and CHP (Combined Heat and Power) are discussed in Chapter 6 and 7.

### Exergy

The fundamentals of the exergy concept as well as possibilities to use this concept for the analysis of energy conversion systems are presented in Chapter 2. A separate section is dedicated to the determination of the specific exergy of solid and liquid fuels. Because of the complex chemical composition of these fuels it is not possible to calculate the specific exergy only with the use of fundamental equations. Szargut and Styrylska have determined regression equations from the calculated exergy values for a large number of pure substances. These equations are frequently used in particular within the area of chemical engineering. Baehr has described a more fundamental method to calculate the exergy of solid and liquid fuels. With the method of Baehr-I only the entropy of the fuel has to be estimated. For all other parameters exact values are available. Based on this method Baehr presented also a simplified method, called Baehr-II. For this method the mass fractions of the fuel in the method of Baehr-I are eliminated by using statistical relations between mass fractions and heating values. Then equations are obtained that enable the calculation of the specific exergy of a fuel if only the heating value is known. A comparison of the three methods is made, assuming that Baehr-I gives the most accurate results. It appears that the method of Szargut and Styrylska agrees good in the case of fuels in the dry and ash free condition. Large deviations might occur in the case of fuels in the as received condition. The results from the Baehr-II method do correspond quite well with the results from Baehr-I for coal in the as received condition. For wood, wood chips and peat the correspondence is good for the fuel in the as received condition as well as in the dry and ash free condition. The chapter further describes various tools for analyzing energy conversion systems like value diagrams, exergy flow diagrams, and exergy efficiencies for apparatuses, plants and thermal power cycles. The application of these tools is evaluated in the other chapters.

### Fuel conversion

The thermal conversion of a primary fuel into heat or into a secondary fuel causes substantial thermodynamic losses. These losses (exergy losses) are usually in the order of 20%-30% or even higher and have a considerable effect on the overall performance of plants using fossil or renewable fuels. The losses are in general higher if the quality of the fuel is lower as is e.g. the case with biomass. In the case of atmospheric combustion the exergy losses are affected mainly by the temperature of the combustion air and the air factor. A comprehensive evaluation of these effects for various fuels is presented in Chapter 4. Air preheating appears to be the most effective way to reduce the exergy loss of combustion. Usually the full flue gas flow is used to preheat the combustion air. Then the maximum achievable temperature of the combustion air is limited because of the difference in thermal strength of the air flow and the flue gas flow. Higher air preheat temperatures are conceivable by splitting the flue gas flow. But even in the case of the combustion of natural gas with an air preheat temperature of 1000°C the exergy loss is still higher than 20% of the fuel exergy. Pressurized combustion is usually associated with gas turbine

units. In the case of simple gas turbine cycles the exergy loss of combustion is determined primarily by the pressure ratio and the  $TIT$  (Turbine Inlet Temperature). It is shown that even in the case of a pressure ratio of 50 and a turbine inlet temperature of 1900°C the exergy loss of combustion is higher than 20%. Alternative gas turbine cycles, like recuperated cycles and cycles with reheat and intercooling, have been proposed in the past. Such cycles can reduce the exergy loss of combustion. But even with these cycles it is unlikely that exergy losses of combustion seriously lower than 20% can be realized.

For the thermal conversion of primary fuels into secondary fuels examples of three processes are discussed: coal gasification, biomass gasification and reforming of natural gas. In general the exergy losses of the gasifier or reformer can be significant lower than the exergy loss of combustion. But the conversion of a primary fuel into an appropriate fuel for power systems will require various auxiliaries (e.g. the generation of steam) and also further processing of the gas. The total exergy loss of the fuel conversion system depends also on the quality of integration into the power plant but is usually higher than 20%. This means that the highest efficiencies achievable for power plants using solid fuels are roughly 20 to 25% lower than the efficiencies of natural gas fuelled systems using similar power cycles.

#### Thermal power cycles

Thermal power cycles are primarily used today for the generation of power. High overall plant efficiencies do require an appropriate match between combustion process and power cycle. Large conventional power plants consisting e.g. of a coal fired boiler and steam turbine cycle have total exergy losses of around 60%<sup>1</sup>. The application of advanced steam conditions is an option to reduce these losses. Net thermal efficiencies higher than 45% are supposed to be feasible today and higher efficiencies up to 50% (LHV) are expected to become feasible in the future. At present IGCC plants have not serious higher efficiencies and without CO<sub>2</sub> capture IGCC is not economic competitive with PC or CFBC plants. But the IGCC might benefit in the future from the further development of the CC (combined cycle) and more rigorous requirements with regard to CCS (carbon capture and storage). The application of alternative topping cycles like e.g. potassium topping cycles will not enable significant higher efficiencies. Natural gas fired CC (combined cycle) plants can reach net thermal efficiencies up to 60% today. Determining for these efficiencies are primarily the thermodynamic equivalent temperature of heat transfer to the combined cycle ( $\bar{T}_{H,CC}$ ) and the internal exergy efficiency of the combined cycle ( $\eta_{ex, intern, CC}$ ). Heat transfer to the combined cycle occurs only in the gas turbine, thus the thermodynamic equivalent temperature of heat transfer to the combined cycle is the same as the thermodynamic equivalent temperature of heat transfer to the gas turbine cycle. During a period of 25 years, from 1983 to 2008, the temperature  $\bar{T}_{H,CC}$  of large heavy duty gas turbines has been raised from around 650°C to around 800°C because of the application of higher turbine inlet temperatures and pressure ratios. The internal exergy efficiency has been increased during this period from around

---

<sup>1</sup> The thermal efficiency of such a plant is roughly 40% to 43%.

0.7 to 0.8. Thermal efficiencies of 0.62 to 0.71 are achievable with CC plants if  $\bar{T}_{H,CC}$  is increased to 1140°C and the internal exergy efficiencies are in between 0.8 and 0.9. Considering the developments in the past, it is expected that thermal efficiencies around 0.7 might be achievable after serious development efforts during several decades.

#### Fuel cell systems

The strive for higher power plant efficiencies is hindered primarily by the high thermodynamic losses of thermal combustion. These fuel conversion losses can be reduced seriously by replacing the thermal conversion of fuel by the electrochemical conversion as is the case in fuel cells. In particular with high temperature fuel cells (MCFC or SOFC) the exergy loss is less than 2% of the total exergy that enters the cell, or less than 4% of the chemical exergy that enters the cell. The exergy losses in low temperature fuel cells like the PEMFC are significantly higher<sup>2</sup>. Overall system efficiencies of fuel cell systems will depend highly on the system design and in particular on the overall design of the fuel conversion system. Natural gas is initially the most likely primary fuel for fuel cell systems. With low temperature fuel cells the fuel has to be converted first into almost pure hydrogen. CO removal at ppm level is required to avoid poisoning of the electrodes. Because of the higher exergy loss of the cell and the additional losses of fuel conversion and purification the efficiency of low temperature fuel cell systems will always be much lower than the efficiencies achievable with high temperature fuel cell systems. High temperature fuel cells offer the opportunity to raise conversion efficiencies of power generation based on natural gas to values around 80%. This has been confirmed by system calculations for a target system, a so-called SOFC-GT hybrid system. The assumed design data of the fuel cell stack of the target system are based on the application of existing materials and an operation temperature of 700°C. The high efficiency can be achieved at plant power levels around 30 MW<sub>e</sub> or even lower and without the need for cooling water. Further improvement of the system efficiency appears to be conceivable by using the residual heat. The application of a bottoming cycle (e.g. ORC) will raise the exergy efficiency even above 80%. It is obvious that lifetime and costs of HT fuel cell stacks have to be at the appropriate levels before these systems will be considered seriously for commercial application.

#### Combined heat and power

During the generation of heat in natural gas fired hot water boilers or industrial steam boilers, most of the fuel exergy is lost. Also the highly recommended high efficiency hot water boilers have exergy efficiencies below 15%. A substantial reduction of these losses is possible only by the application of alternative heat generation processes like heat pumps and combined heat and power plants (CHP plants). The fuel savings achievable with these technologies (roughly 30% to 40%) are discussed in Chapter 3. In Chapter 7 a more comprehensive discussion of various concepts for CHP plants is presented. In the literature on CHP plants it is often assumed that the thermodynamic advantages are obvious. If merit indicators are presented, thermal efficiencies (electrical, thermal and overall efficiencies) are frequently used. Exergy

---

<sup>2</sup> The exergy loss of a PEMFC is more than 20% of the total exergy supplied to the system.

efficiencies are only mentioned occasionally. Besides a general description of the thermodynamic aspects of CHP and the thermodynamic concepts for the evaluation of these plants Chapter 7 focuses on the definition and application of true merit indicators. It appeared that both, thermal efficiencies and exergy efficiencies, don't indicate the merits of CHP in the right way. Finally, the true merit indicators are used to discuss the characteristics of different CHP plants like industrial CHP plants, CC plants for district heating and micro-CHP units.

The evaluations in Chapter 7 are made for design conditions of the considered plants. An evaluation of off-design conditions is discussed in Appendix 7.1 but is useful only for the optimization of specific CHP plants. Fuel savings up to 20% are achievable with CHP plants in operation today (see Table 7.4.1). For the future higher savings are conceivable depending on the development of the electrical efficiencies of CHP plants and power stations. A literature evaluation shows that determining the merits of CHP is a serious problem. Useful indicators will require any kind of comparison with separate generation of heat and power. If there is no need to consider external requirements, the fuel savings factor of a CHP plant in comparison with separate generation is a true indicator of the thermodynamic quality of the CHP plant. In the case of a government or an owner of an industrial site who is looking for minimum fuel consumption of a wider system, it has to be checked first how the overall energy demand affects the maximum installed power of CHP. If the maximum installed CHP power is limited by the power demand, the fuel energy savings factor per unit electricity is the true criterion to achieve the maximum benefit from combined generation. If the heat demand is limiting the maximum installed CHP power, the fuel exergy savings factor per unit heat exergy is more appropriate. The application of different fuels will complicate the discussion about merit indicators. True values of the merit indicators can be obtained only if CHP and reference system use the same fuel. If for the generation of power always other primary fuels are used than for the generation of heat, additional (arbitrary) criteria are needed to define the merits of CHP.

With CHP plants for the generation of low temperature heat in general higher fuel savings can be achieved than with CHP plants for the generation of high temperature heat. Thus, the application of CHP plants for the generation of low temperature heat is more attractive than the application of industrial CHP. For the generation of low temperature heat, however, the Heat Pump is an alternative option to reduce the thermodynamic losses of heat generation. A general conclusion with regard to the preferred technology is impossible. Useful conclusions can be drawn only for specific cases and require more detailed evaluation of the alternatives. Micro-CHP units with high electrical efficiencies will enable high fuel savings as well as high fuel energy savings per unit electricity. The application of units with electrical efficiencies lower than 20% is not really beneficial with regard to fuel savings, but might be useful for the implementation of micro-CHP into the market. Natural gas fuelled fuel cell systems with high electrical efficiencies are very attractive. The development of reliable and cheap micro-CHP fuel cell systems with electrical efficiencies of 40% or higher seems to be attractive. Combined Cycle plants with heat extraction for district heating show high values for the relevant merit indicators, in particular the fuel energy savings per unit electricity. In the evaluations the heat losses of the district heating system due to transport and distribution are ignored. These losses can be

substantial and have a serious effect of the thermodynamic merits of the CHP plant. They have to be considered in particular if e.g. the application of small scale units has to be compared with the application of large scale plants. However, the selection of true values of these losses is in general not easy. Detailed evaluation of the losses of transport and distribution for a specific case is necessary to come to the right conclusions. Suggestions that an optimum value for the heat to power ratio of CHP units does exist are obviously false.

## SAMENVATTING

### DUURZAME ENERGIESYSTEMEN

#### Beperkingen en uitdagingen gebaseerd op exergie analyses

##### Algemeen

Het besef dat de ontwikkelde landen hun levenswijze inclusief hun energievoorziening meer duurzaam dienen te maken is algemeen aanwezig. Maar zelfs in geval van unanimiteit over de richting die moet worden gekozen, zijn er nog veel meningsverschillen over de te volgen weg. In dit proefschrift worden problemen en mogelijkheden besproken voor meer duurzame energiesystemen, primair gericht op de energievoorziening van Nederland. De “trias energetica” wordt gebruikt om aan te geven welke stappen moeten worden gemaakt. De volgende stappen worden daarbij onderscheiden:

- 1) beperk het finale energiegebruik
- 2) maak gebruik van duurzame bronnen
- 3) verbeter totale omzettingsrendementen

Het belang van de eerste stap is duidelijk, maar dit proefschrift richt zich op de andere stappen met een sterke nadruk op de laatste. De gevolgen van het gebruik van in Nederland beschikbare bronnen van hernieuwbare energie zijn besproken in hoofdstuk 3. Het gebruik van wind en zonne-energie resulteert in duidelijk hogere kosten voor de energievoorziening. Deze hogere kosten worden niet alleen veroorzaakt door de primaire omzetting met windturbines, fotovoltaïsche cellen etc., maar ook door de noodzaak van energieopslag en de daarbij behorende omzettingen. Verondersteld is dat biomassa een voordeliger alternatief biedt, maar de thans in Nederland beschikbare hoeveelheden voor energieomzetting zijn niet toereikend om te voorzien in de huidige vraag. De vereiste primaire energie wordt bepaald door zowel de finale vraag naar energie als door het rendement van de verlangde omzettingen van primaire bron tot de uiteindelijke vraag. De thermodynamische verliezen bij de huidige omzetting van primaire energie in elektriciteit en warmte zijn aanzienlijk. Een verdere reductie van deze verliezen is vereist om te komen tot meer duurzame energiesystemen.

In hoofdstuk 3 is een ruwe indicatie gegeven van het effect van hogere omzettingsrendementen. Uitgaande van aardgas als primaire brandstof zijn enkele vereenvoudigde systemen voor de energievoorziening van Nederland met elkaar vergeleken. De totale warmtevraag is verdeeld in een lage temperatuur en een hoge temperatuur warmtevraag. Eerst is een referentiesysteem gekozen bestaande uit centrales voor de productie van elektriciteit en ketels voor de opwekking van stoom en warm water. De berekeningen in hoofdstuk 3 laten zien dat brandstofbesparingen van 30% tot 40% mogelijk zijn door gebruik te maken van centrales met hoge rendementen (80%), verbeterde WK installaties voor de hoge temperatuur (industriële) warmtevraag en verbeterde warmtepompen voor de lage temperatuur warmtevraag. Het is duidelijk dat hoge rendementen bij de elektriciteitsproductie de toepassing van warmtepompen aantrekkelijker maakt.

Het grootste deel van dit proefschrift is gericht op het verminderen van de thermodynamische verliezen van de huidige energieomzettingssystemen voor de opwekking van elektriciteit en warmte. De grootheid exergie is uitvoerig gebruikt voor het kwantificeren van deze verliezen en het verkrijgen van een beter inzicht in de oorzaken. De huidige opwekking van elektriciteit en warmte maakt voornamelijk gebruik van brandstofomzettingssystemen en thermische kringprocessen. De beperkingen van deze processen zijn besproken in respectievelijk de hoofdstukken 4 en 5. Mogelijkheden om de thermodynamische rendementen bij de opwekking van elektriciteit en warmte te verbeteren met gebruikmaking van brandstofcellen en WKK (Warmte Kracht Koppeling) worden besproken in hoofdstuk 6 en 7.

### Exergie

De theoretische basis van de grootheid exergie en mogelijkheden om deze grootheid te gebruiken voor de analyse van energiesystemen zijn gepresenteerd in hoofdstuk 2. Een afzonderlijke paragraaf is gewijd aan de bepaling van de specifieke exergie van vaste en vloeibare brandstoffen. Vanwege de complexe chemische samenstelling van deze brandstoffen is het niet mogelijk om de specifieke exergie te berekenen met gebruikmaking van alleen fundamentele vergelijkingen. Szargut en Styrylska hebben regressie vergelijkingen bepaald gebaseerd op de berekende exergiewaarden voor een groot aantal zuivere stoffen. Deze vergelijkingen worden vaak gebruikt, vooral voor toepassingen in de procesindustrie. Baehr heeft een meer fundamentele methode voor de berekening van de exergie van vaste en vloeibare brandstoffen beschreven. De methode aangeduid als Baehr-I verlangt alleen een schatting van de brandstofentropie. Voor alle overige parameters zijn exacte waarden beschikbaar. Uitgaande van deze methode heeft Baehr ook een vereenvoudigde methode gepresenteerd, hier aangeduid als Baehr-II. Bij deze methode zijn de massafracties in de brandstof, zoals verlangd voor Baehr-I, geëlimineerd door gebruik te maken van statistische relaties tussen massa fracties en verbrandingswaarden. Daarmee worden vergelijkingen verkregen waarmee de specifieke exergie van een brandstof kan worden berekend door alleen gebruik te maken van de verbrandingswaarde. De drie genoemde methoden zijn onderling vergeleken er van uitgaande dat Baehr-I de meest nauwkeurige resultaten geeft. Het blijkt dat de methode van Szargut en Styrylska goede overeenstemming vertoont in geval van brandstoffen in droge en asvrije toestand. Voor brandstoffen in de werkelijke toestand (“as received”) kunnen grote afwijkingen optreden. De overeenkomst tussen Baehr-I en Baehr-II is redelijk goed in geval van steenkool in de werkelijke toestand. In geval van hout, houtsnippers en turf is de overeenkomst goed voor brandstof in zowel de werkelijke als in de droge en asvrije toestand. Het hoofdstuk beschrijft verder verschillende gereedschappen voor de analyse van energiesystemen zoals waardediagrammen, exergiestroomdiagrammen en exergierendementen voor apparaten, totale installaties en arbeidskringprocessen. De toepassing van deze gereedschappen is geëvalueerd in de overige hoofdstukken.

### Brandstofomzetting

De thermische omzetting van een primaire brandstof in warmte of in een secundaire brandstof gaat gepaard met aanzienlijke thermodynamische verliezen. Deze verliezen (exergieverliezen) zijn doorgaans in de orde van 20%-30% en zijn van grote invloed op de totale

prestaties van installaties die gebruik maken van fossiele of hernieuwbare brandstoffen. De verliezen zijn doorgaans groter als de kwaliteit van de brandstof laag is, wat bijv. het geval is bij biomassa. In geval van atmosferische verbranding worden de exergie verliezen vooral beïnvloed door de verbrandingstemperatuur en de lucht factor. Een uitgebreide evaluatie van deze effecten voor verschillende brandstoffen is gepresenteerd in hoofdstuk 4. Luchtvoorwarming blijkt het meest effectief om het exergieverlies van verbranding te verlagen. Het is gebruikelijk om hiervoor de volledige rookgasstroom te gebruiken. De maximaal haalbare temperatuur van de verbrandingslucht is dan beperkt vanwege het verschil in thermische sterkte tussen de luchtstroom en de rookgasstroom. Hogere luchtvoorwarmingstemperaturen zijn denkbaar door de rookgasstroom te splitsen. Maar zelfs in geval van verbranding van aardgas met een luchtvoorwarmingstemperatuur van 1000°C is het exergieverlies nog steeds meer dan 20% van de brandstofexergie. Verbranding onder hogere druk is doorgaans gekoppeld aan gasturbines. In geval van een eenvoudig gas turbine kringproces wordt het exergieverlies van verbranding voornamelijk bepaald door de drukverhouding en de *TIT* (Turbine Inlaat-Temperatuur). Berekeningen laten zien dat zelfs in geval van een drukverhouding van 50 en een turbine inlaattemperatuur van 1900°C het exergieverlies van verbranding groter is dan 20%. Alternatieve gasturbinekringprocessen, zoals recuperatieve processen en kringprocessen met herverhitting en tussenkoeling, zijn in het verleden voorgesteld. Zulke processen kunnen het exergieverlies bij verbranding verminderen. Maar zelfs met dergelijke kringprocessen is het onwaarschijnlijk dat exergie verliezen bij verbranding duidelijk lager dan 20% haalbaar zijn.

Voor de thermische omzetting van primaire brandstoffen in secundaire brandstoffen zijn voorbeelden van drie processen bekeken: steenkoolvergassing, biomassavergassing and aardgasreforming. In het algemeen kunnen de exergie verliezen van de vergasser of reformer duidelijk lager zijn dan het exergieverlies van verbranding. Maar de omzetting van een primaire brandstof in een geschikte brandstof voor elektriciteitopwekking verlangt diverse hulpsystemen (bijv. stoomopwekking) en processen voor de verdere behandeling van het gas. Het totale exergieverlies van het brandstofomzettingssysteem is mede afhankelijk van de kwaliteit van integratie in de elektriciteitsproductie-installatie, maar is doorgaans hoger dan 20%. Dit betekent dat de hoogst haalbare rendementen van elektriciteitsproductie-installaties op basis van vaste brandstoffen doorgaans ruwweg 20% tot 25% lager zijn dan de rendementen van aardgas gestookte installaties met soortgelijke arbeidskringprocessen.

#### Thermische kringprocessen

Voor de opwekking van arbeid wordt heden ten dage voornamelijk gebruik gemaakt van thermische kringprocessen. Een goede afstemming tussen kringproces en verbrandingsproces is verlangd om tot een hoog totaal rendement te komen. Het totale exergieverlies van grootschalige elektriciteitscentrales bestaande uit een steenkool gestookte ketel en een stoomturbine bedraagt circa 60%<sup>3</sup>. De toepassing van geavanceerde stoomcondities biedt een mogelijkheid om deze verliezen te verminderen. Netto rendementen hoger dan 45% worden verondersteld haalbaar te

---

<sup>3</sup> Het thermisch rendement van een dergelijke centrale bedraagt circa 40% tot 43%.

zijn vandaag de dag en hogere rendementen tot 50% (op basis van de stookwaarde) worden naar verwachting haalbaar in de toekomst. Kolenvergassing/STEG<sup>4</sup> (KV/STEG) installaties hebben tegenwoordig geen duidelijk hogere rendementen en zonder CO<sub>2</sub> verwijdering is de KV/STEG economisch niet aantrekkelijk in vergelijking met poederkoolverbranding of circulerend wervelbedverbranding. Doch de KV/STEG kan in de toekomst profiteren van de verdere ontwikkeling van het gecombineerde gasturbine/stoomturbine kringproces en strengere eisen met betrekking tot CO<sub>2</sub> verwijdering en opslag. Het gebruik van andere voorgeschakelde kringprocessen, zoals bijv. een kalium kringproces, maakt geen duidelijk hogere rendementen mogelijk. Vandaag de dag kunnen aardgas gestookte STEG installaties rendementen bereiken tot 60%. Bepalend voor het rendement zijn voornamelijk de thermodynamisch equivalente temperatuur van warmteoverdracht naar het kringproces ( $\bar{T}_{H,CC}$ ) en het interne exergierendement van het gecombineerde kringproces ( $\eta_{ex, intern, CC}$ ). De warmtetoevoer aan het gecombineerde kringproces geschiedt uitsluitend in de gasturbine. De thermodynamisch equivalente temperatuur van warmteoverdracht naar het gecombineerde kringproces is dus dezelfde als de thermodynamisch equivalente temperatuur van warmteoverdracht naar het gasturbine kringproces. Gedurende een periode van 25 jaar, van 1983 tot 2008, is de  $\bar{T}_{H,CC}$  van gasturbines voor industrieel gebruik verhoogd van circa 650°C tot circa 800°C door de toepassing van hogere turbine inlaattemperaturen en drukverhoudingen. Het interne exergierendement is in die periode verhoogd van circa 0.7 tot 0.8. Thermische rendementen van 0.62 tot 0.72 zijn bereikbaar met STEG installaties als de  $\bar{T}_{H,CC}$  kan worden verhoogd tot 1140°C en het interne exergierendement een waarde heeft tussen 0.8 en 0.9. Gelet op de ontwikkelingen in het verleden mag worden verwacht dat thermische rendementen van circa 0.7 kunnen worden behaald na aanzienlijke ontwikkelingsinspanningen gedurende meerdere tientallen jaren.

#### Brandstofcellen

Het streven naar hogere rendementen van elektriciteitscentrales wordt vooral belemmerd door hoge thermodynamische verliezen bij de thermische verbranding. Deze verliezen bij de brandstofomzetting kunnen aanzienlijk worden geminderd indien de thermische omzetting van de brandstof wordt vervangen door een elektrochemische omzetting zoals in brandstofcellen. In het bijzonder bij hoge temperatuur brandstofcellen (MCFC of SOFC) is het exergieverlies minder dan 2% van de totale exergie die aan de cel wordt toegevoerd, of minder dan 4% van de toegevoerde chemische exergie. De exergieverliezen in lage temperatuur brandstofcellen zoals de PEMFC zijn duidelijk hoger<sup>5</sup>. Totale rendementen van brandstofcellen zijn in hoge mate afhankelijk van het systeemontwerp, in het bijzonder het ontwerp van het brandstof omzettingssysteem. Aardgas is in eerste instantie de meest voor de hand liggende primaire brandstof voor brandstofcellen. In geval van lage temperatuur brandstofcellen moet de

<sup>4</sup> STEG (StoomTurbine En Gasturbine) is een stoomturbine met een voorgeschakelde gasturbine

<sup>5</sup> Het exergieverlies van een PEMFC is meer dan 20% van de totaal aan het systeem toegevoerde exergie.

brandstof eerst worden omgezet in vrijwel zuivere waterstof. CO verwijdering tot ppm niveau is noodzakelijk om vergiftiging van de elektroden te vermijden. Vanwege het grotere exergieverlies van de cel en de additionele verliezen van brandstofomzetting en zuivering zal het rendement van lage temperatuur brandstofcelsystemen altijd duidelijk lager zijn dan de rendementen die met hoge temperatuur brandstofcelsystemen haalbaar zijn. Hoge temperatuur brandstofcelsystemen bieden de mogelijkheid om de rendementen van elektriciteitsproductie op basis van aardgas te verhogen tot waarden rond de 80%. Dit is bevestigd door systeemberekeningen voor een beoogd systeem (target system), een zogenaamd hybride SOFC-GT<sup>6</sup> systeem. De veronderstelde ontwerpgegevens van de brandstofcelstapeling van dit beoogde systeem zijn gebaseerd op het gebruik van thans beschikbare materialen en bedrijfstemperatuur van 700°C. Het hoge rendement kan worden behaald met installaties met een vermogen van circa 30 MW<sub>e</sub> of zelfs lager zonder dat koelwater is verlangd. Verdere verbetering van het rendement is denkbaar door benutting van restwarmte. The toepassing van een nageschakeld kringproces (bijv. een ORC) kan het rendement opvoeren tot boven de 80%. Het is duidelijk dat levensduur en kosten van HT brandstofcelstapelings op een geschikt niveau moeten zijn willen deze serieus in aanmerking kunnen komen voor commerciële toepassing.

#### Warmte/kracht koppeling

Bij de opwekking van warmte in aardgas gestookte ketels of industriële stoomketels gaat het grootste deel van de exergie van de brandstof verloren. Ook de zeer aanbevolen hoge rendementsverwarmingsketels hebben exergierendementen lager dan 15%. Een aanzienlijke reductie van dit exergieverlies is alleen mogelijk door gebruik te maken van alternatieve warmte opwekkingsprocessen zoals warmtepompen en warmte/kracht (WK) installaties. De brandstofbesparing die met deze technologieën te bereiken zijn (ruwweg 30% tot 40%), zijn besproken in hoofdstuk 3. In hoofdstuk 7 zijn diverse mogelijkheden voor warmte/kracht installaties uitvoeriger gepresenteerd. In de literatuur over WK installaties wordt doorgaans verondersteld dat de thermodynamische voordelen evident zijn. Als er profijt factoren worden vermeld, worden veelal thermische rendementen (elektrische, warmte en totale rendementen) gebruikt. Slechts af en toe wordt gebruik gemaakt van exergie rendementen. Naast een algemene beschrijving van de thermodynamische aspecten van warmte/kracht en de thermodynamische begrippen voor de evaluatie van deze installaties is hoofdstuk 7 gericht op de definitie en het gebruik van correcte profijt factoren. Het blijkt dat zowel thermische rendementen als exergie rendementen de verdiensten van WK niet correct weergeven. Correcte profijt factoren zijn tenslotte gebruikt om de kenmerken van de verschillende WK installaties zoals industriële WK, STEG installaties voor stadsverwarming and micro-WK installaties, te bespreken.

De evaluaties in hoofdstuk 7 zijn gemaakt voor de installaties in ontwerptoestand. In Appendix 7.1 is een evaluatie van off-design toestanden besproken, maar die is alleen bruikbaar voor de optimalisatie van specifieke WK installaties. Met thans gebruikelijke WK installaties zijn brandstofbesparingen van 20% bereikbaar (zie tabel 7.4.1). Voor de toekomst zijn grotere

---

<sup>6</sup> SOFC-GT is combinatie van vaste oxide brandstofcellen (SOFC) met een gas turbine (GT).

besparingen denkbaar afhankelijk van de ontwikkeling van elektrische rendementen van WK installaties en elektriciteitscentrales. Een evaluatie van de literatuur laat zien dat het bepalen van het profijt van een WK installatie een serieus probleem is. Bruikbare indicatoren verlangen op enigerlei wijze een vergelijking met gescheiden opwekking van warmte en elektriciteit. Als het niet nodig is rekening te houden met externe factoren is de relatieve brandstofbesparing van een WK installatie ten opzichte van gescheiden opwekking een correct beoordelingscriterium voor de thermodynamische kwaliteit van een WK installatie. In geval van een overheid of een eigenaar van een industriecomplex, die streeft naar minimalisatie van het brandstofverbruik van een groter systeem, moet eerst worden nagegaan op welke manier de totale energievraag van invloed is op het maximaal te installeren WK vermogen. Indien dit vermogen wordt beperkt door de elektriciteitsvraag, dan is de “brandstofenergie besparingsfactor per eenheid elektriciteit” de juiste criterium om maximaal te profiteren van gecombineerde opwekking. Wordt het maximaal te installeren WK vermogen beperkt door de warmtevraag dan dient de “brandstofenergie besparingsfactor per eenheid warmte-exergie” te worden toegepast. Het gebruik van verschillende brandstoffen is een complicatie bij de discussie over profijt factoren. Juiste waarden van de profijt factoren kunnen alleen worden verkregen als WK installatie en referentiesysteem gebruik maken van dezelfde brandstof. Indien voor de elektriciteitsproductie altijd andere primaire brandstoffen worden gebruikt dan voor de opwekking van warmte, zijn additionele criteria verlangd om het profijt van WK te definiëren.

Met WK installaties voor de opwekking van lage temperatuur warmte kunnen doorgaans grotere brandstofbesparingen worden behaald dan met WK installaties voor de opwekking van hoge temperatuur warmte. De toepassing van WK installaties voor de opwekking van lage temperatuur warmte is dus doorgaans aantrekkelijker dan de toepassing van industriële WK. Voor de opwekking van lage temperatuur warmte vormt de warmtepomp echter een alternatief om de thermodynamische verliezen bij de warmteopwekking te beperken. Een algemene conclusie met betrekking tot de gewenste technologie is daarom niet mogelijk. Zinnige conclusies zijn alleen te trekken voor specifieke gevallen en verlangen een meer gedetailleerde evaluatie van de alternatieven. Grote brandstofbesparingen zowel als grote brandstofenergie besparingen per eenheid elektriciteit kunnen worden behaald met micro-WK eenheden met hoge elektrische rendementen. Het gebruik van eenheden met elektrische rendementen lager dan 20% is niet echt interessant uit het oogpunt van brandstofbesparing, maar kan zinvol zijn voor de invoering van micro-WK. Vooral aardgas gestookte brandstofcelsystemen met hoge elektrische rendementen zijn aantrekkelijk. De ontwikkeling van betrouwbare en voordelige micro-WK brandstofcelsystemen met elektrische rendementen van 40% of meer lijkt aantrekkelijk. STEG installaties met warmteonttrekking voor stadsverwarming hebben hoge waarden voor de relevante profijt factoren, in het bijzonder de brandstofenergie besparing per eenheid elektriciteit. In de beschouwingen zijn de warmteverliezen van het stadsverwarmingssysteem als gevolg van transport en distributie verwaarloosd. Deze verliezen kunnen aanzienlijk zijn en zijn wel degelijk van invloed op het thermodynamische profijt van de WK eenheid. Zij moeten in het bijzonder in beschouwing worden genomen indien bijv. het gebruik van kleinschalige eenheden wordt vergeleken met het gebruik van grootschalige installaties. De selectie van betrouwbare waarden

van deze verliezen is echter niet eenvoudig. Een gedetailleerde evaluatie van de verliezen van transport en distributie voor een specifieke situatie is noodzakelijk om tot de juiste conclusies te komen. Suggesties dat er een optimale waarde voor de warmte/kracht verhouding van WK eenheden bestaat zijn overduidelijk onjuist.



## NOMENCLATURE

$c$	velocity	[m/s]
$ex$	specific exergy	[kJ/kg]
$ex^{\text{mol}}$	molar exergy	[kJ/kmol]
$Ex$	exergy	[kJ]
$Ex_{\text{loss}}$	exergy loss	[kJ]
$Ex_Q$	exergy of heat	[kJ]
$F$	Faraday constant ( $= 96485 \times 10^3$ )	[C/kmol]
$F_{\text{fuel ratio}}$	the relative fuel consumption of the CHP plant compared to the reference case	[-]
$F_{\text{fuel savings}}$	the relative fuel savings of the CHP plant compared to the reference case	[-]
$F_{\text{FESUE}}$	fuel energy savings per unit electricity	[-]
$F_{\text{FEXSUE}}$	fuel exergy savings per unit electricity	[-]
$F_{\text{FESUQ}}$	fuel energy savings per unit heat	[-]
$F_{\text{FEXSUEXQ}}$	fuel exergy savings per unit heat exergy	[-]
$f_{ex}$	exergy fraction	[-]
$f_{ex, F}$	exergy factor of fuel	[-]
$f_{ex, Q}$	exergy factor of heat	[-]
$G$	Gibbs free energy	[kJ]
$g$	gravitational acceleration	[m/s <sup>2</sup> ]
$g$	specific Gibbs free energy	[kJ/kg]
$g^{\text{mol}}$	molar Gibbs free energy	[kJ/kmol]
$g_{298}^{0, \text{mol}}$	molar Gibbs free energy at standard pressure and temperature	[kJ/kmol]
$\Delta_f g_{298}^{0, \text{mol}}$	Gibbs free energy of formation	[kJ/kmol]
$H$	enthalpy	kJ
$H_0$	enthalpy at environmental conditions	kJ
$HHV_F$	higher heating value of the fuel	[kJ/kg]
$\Delta_R H$	reaction enthalpy	[kJ]
$h$	specific enthalpy	[kJ/kg]
$h^{\text{mol}}$	molar enthalpy	[kJ/kmol]
$h_{298}^{0, \text{mol}}$	molar enthalpy at standard pressure and temperature	[kJ/kmol]
$i$	number of components in one mole of a gas mixture	[-]

$j$	number of elements in one mole of a compound	[-]
$K_{\text{power loss}}$	power loss ratio (for systems with heat extraction)	[-]
$LHV_F$	lower heating value of the fuel	[kJ/kg]
$m$	mass (or mass flow)	[kg]
$n$	number of moles	[-]
$n$	number of electrons per molecule fuel	[-]
$P$	power	[kW]
$p$	pressure	[bar]
$p_0$	pressure of the environment	[bar]
$Q$	heat	[kJ]
$Q_C$	heat to or from a cold reservoir	[kJ]
$Q_H$	heat to or from a hot reservoir	[kJ]
$Q_0$	heat to or from the environment	[kJ]
$R$	gas constant	[kJ/kg K]
$R^{\text{mol}}$	universal gas constant	[kJ/kmol K]
$S$	entropy	[kJ/K]
$S_0$	entropy at environmental conditions	[kJ/K]
$\Delta_R S$	reaction entropy	[kJ/K]
$s$	specific entropy	[kJ/kg K]
$s^{\text{mol}}$	molar entropy	[kJ/kmol K]
$s_{298}^{0, \text{mol}}$	molar entropy at standard pressure and temperature	[kJ/kmol K]
$T$	temperature	[K]
$T_C$	temperature of heat transfer from the cycle	[K]
$T_H$	temperature of heat transfer to the cycle	[K]
$T_0$	temperature of the environment	[K]
$\bar{T}$	thermodynamic equivalent temperature of heat transfer	[K]
$\bar{T}_C$	thermodynamic equivalent temperature of heat transfer from the cycle	[K]
$\bar{T}''_C$	elevated temperature of heat transfer from power cycle	[K]
$\bar{T}_H$	thermodynamic equivalent temperature of heat transfer to the cycle	[K]
$\Delta T$	temperature difference	[K]
$V$	volume	[m <sup>3</sup> ]
$V$	voltage	[V]
$V_{\text{cell}}$	actual cell voltage	[V]
$V_{\text{rev}}$	reversible cell voltage	[V]

$W$	work	[kJ]
$W_{\text{rev}}$	work from a reversible cycle	[kJ]
$x$	mass fraction	[-]
$y$	mole fraction	[-]
$z$	height above reference level	[m]

### GREEK CHARACTERS

$\Delta$	change of conditions	[-]
$\nu$	stoichiometric number	[-]
$\eta_{\text{ex}}$	exergy efficiency	[-]
$\eta_{\text{ex, intern}}$	internal exergy efficiency of a thermal power cycle	[-]
$\eta_{\text{ex, electr}}$	electric exergy efficiency	[-]
$\eta_{\text{ex, } Q}$	heat exergy efficiency	[-]
$\eta_{\text{ex, total}}$	total exergy efficiency	[-]
$\eta_{\text{FC}}$	fuel cell efficiency	[-]
$\eta_{\text{th}}$	thermal efficiency	[-]
$\eta_{\text{th, electr}}$	electric thermal efficiency	[-]
$\eta_{\text{th, } Q}$	heat thermal efficiency	[-]
$\eta_{\text{th, total}}$	total thermal efficiency	[-]
$\eta''_{\text{ex, } Q, \text{ CHP}}$	assigned heat exergy efficiency	[-]
$\eta_{\text{th, rev}}$	thermal efficiency of a reversible power cycle	[-]

### SUBSCRIPTS AND SUPERSCRIPTS

bc	bottoming cycle
C	cold, cold reservoir
CHP	combined heat and power
ch	chemical
electr	electricity, electrical
ex	exergy
F	fuel
f	formation
H	hot, hot reservoir
in	inlet
irrev	irreversible
max	maximum
min	minimum
out	outlet

p	primary
Q	heat
R	reaction
ref	reference case
rev	reversible
s	secondary
tc	topping cycle
th	thermal
tm	thermo-mechanical
univ	universal

### **ABBREVIATIONS**

AFC	Alkaline Fuel Cell
ATR	AutoThermal Reformer or AutoThermal Reforming
CC	Combined Cycle
CCS	Carbon Capture and Storage
CFB	Circulating Fluidized Bed (boiler)
CFBC	Circulating Fluidized Bed Combustion
CHP	Combined Heat and Power
GT	Gas Turbine (cycle)
DCFC	Direct Carbon Fuel Cell
DH	District Heating
DMFC	Direct Methanol Fuel Cell
GT	Gas Turbine
HDS	Hydro-DeSulfurization
HP	High Pressure
HRSG	Heat Recovery Steam Generator
ICE	Internal Combustion Engine
IGCC	Integrated Gasification Combined Cycle
IND	Industrial
L-ICE	Large-ICE
IP	Intermediate Pressure
LP	Low Pressure
MCFC	Molten Carbonate Fuel Cell
MHD	Magneto-HydroDynamic conversion
PAFC	Phosphoric Acid Fuel Cell
PC	Pulverized Coal / Potassium Cycle
PEMFC	Proton Exchange Membrane Fuel Cell
POX	Partial OXidation reactor
PROX	PReferential OXidation reactor
PSA	Pressure Swing Absorption

SC	Super Critical (steam conditions) / Steam Cycle
SOFC	Solid Oxide Fuel Cell
SR	Steam Reformer or Steam Reforming
ST	Steam Turbine (cycle)
USC	Ultra Super Critical (steam conditions)
WHB	Waste Heat Boiler



## 1 INTRODUCTION

### 1.1 Problem description

There is a general understanding that the so-called “developed countries” live in strong disharmony with their environment with regard to the use of energy and raw materials. This has resulted in worldwide discussions on the sustainability of our way of life and more specifically on the future of our industrial production systems and energy systems. This thesis focuses primarily on options for future energy systems and discusses the problems and possibilities of a more sustainable energy supply. The evaluations are primarily considering applications for the energy system of the Netherlands but the results are also valid for many other countries.

The choice for sustainable development gets support from many scientists and politicians worldwide. However, in the discussion about the final goal and the first steps that have to be taken, opinions are highly diverging. The definitions as formulated in the political area are not very helpful for a useful specification. In the last century the discussions about sustainability were intensified by the publication of the Brundtland report [1.8]. In this report the following definition was presented:

“Humanity has the ability to make development sustainable to ensure that it meets the needs of the present without compromising the ability of future generations to meet their own needs”.

The definition is not more than a first outline of the goal of sustainable development and is not very useful to discuss the possibilities of sustainable energy systems. A more specific definition was given by Angela Merkel (from [1.1], Introduction):

“Using resources no faster than they can regenerate themselves and releasing pollutants to no greater extent than natural resources can assimilate them”.

This definition is more useful for the discussions on sustainable energy systems, but it considers only resources and environmental criteria. A full evaluation of sustainability requires the consideration of resources, environment, social and economic aspects. It appears that the development of methods and tools for the evaluation of the sustainability of energy systems (see e.g. [1.2] to [1.7]) tends to become a new scientific discipline that needs contributions from different areas. As this thesis focuses on the thermodynamics of energy system, the practical approach of the “trias energetica” is considered to be more useful here. This approach is supposed to be adequate to discuss what can be learned from the thermodynamics for energy conversion systems for the realization of a sustainable energy system. To improve the degree of sustainability of our energy system the “trias energetica” considers the following sequence of steps:

- 1) reduce final energy consumption
- 2) make use of renewable energy sources
- 3) improve overall conversion efficiencies.

The first step focuses primarily on consumer behavior and the efficiency of energy consuming equipment. In principle huge savings are possible in this area (see e.g. [1.10]).

Unfortunately, as the introduction of new lighting equipment shows, the effect of improved technologies are partly overruled by undesired changes of the consumer behavior. The actual savings are therefore lower than expected (see [1.9]). This first step, however, is not the main area of interest of this thesis and will be considered only occasionally.

The second step is often seen as crucial for sustainable energy systems. And it is obvious that the use of renewable energy sources is essential for such systems. For large scale application in the Netherlands wind, sun and biomass are supposed to be available in the future. Contributions from other renewable sources like e.g. hydro-electric power are limited in the Netherlands. But, from studies made in the past it appeared that the economical feasibility of wind and solar energy is doubtful. The consequences of wind and solar energy are outlined in this thesis to emphasize that additional measures are necessary to make the application of these renewable sources attractive. Biomass is considered to be the most attractive renewable energy source. As a solid fuel it has similar possibilities and problems as other solid fuels like coal. Of course, the conversion technologies (e.g. combustion, gasification) are not fully identical, but the options for application are in principle the same. The characteristics of biomass are comprehensively discussed during the evaluation of the energy conversion systems. In particular for wet biomass additional technologies are under development but these are not included in the evaluations presented in this thesis. Various other renewable sources, like geothermal energy, etc. are investigated today. They too are not included in the evaluations here because it is not expected that large scale application of these sources will be possible in the Netherlands.

This thesis will primarily focus on the thermodynamics of energy conversion systems which is actually the main topic of the third step of the trias energetica. The thermodynamic efficiency of most of the processes for energy conversion is poor. Usually these efficiencies are in between 10 and 60% for the conversion of fuels into electricity and heat. For the production of heat high thermal efficiencies, even around 100%, are mentioned, but these efficiencies ignore the thermodynamic value of the energy and are therefore no true thermodynamic efficiencies. Thus, there is significant potential for further improvement of the thermodynamic efficiencies of energy conversion processes. High conversion efficiencies are beneficial not only for systems based on fossil fuels but also for renewable fuels like biomass and solar thermal systems. High conversion efficiencies are actually useful for any kind of energy system because they might reduce the power of the primary sources and thus the fuel costs as well as the capital costs of the primary energy conversion step.

To achieve high efficiencies for the production of electricity and heat first the weaknesses of the present conversion technologies have to be understood. Entropy generation has been used in the past to quantify the thermodynamic losses of energy conversion processes. More recently the use of the exergy concept was given more attention for engineering purposes, since exergy losses are easier to understand in an engineering environment. However, the application of the exergy concept is not well developed today. Therefore, in this thesis various new performance indicators (specific exergy efficiencies, merit indicators) have been defined and their application has been demonstrated for specific system evaluations.

## Chapter 1 Introduction

Thus, exergy analysis is used here to identify the thermodynamic losses of energy conversion systems and to understand the causes of these losses. In conventional systems a substantial part of the exergy losses is caused by the combustion of fuel. The actual losses do depend also on the type of fuel. For solid fuels, and in particular biomass, the losses are significantly higher than for natural gas. Options to reduce these losses have been investigated and discussed. Heat from the combustion system is often transferred to a closed thermal power cycle. Thermal power cycles usually have high thermodynamic efficiencies but losses due to heat transfer from the combustion system to the thermal power cycle can be high depending on the temperatures of heat transfer to the cycle. Therefore, cycles with internal combustion can achieve higher efficiencies than systems with closed power cycles. A technology for the conversion of fuel with potentially higher efficiencies is the electro-chemical conversion with fuel cells. Reversible fuel conversion is conceivable with this technology and studies on high temperature fuel cell systems have shown that achievable efficiencies are significantly higher than with thermal power cycles.

The production of heat, in particular the production of low temperature heat, is in general involved with very high thermodynamic losses. The exergy efficiency of hot water boilers is usually below 15%. It is necessary to apply alternative technologies like heat pumps (HP) and combined heat and power (CHP) to improve the thermodynamic efficiency of heat generation. Since the heat demand depends on environmental conditions, which may vary widely for a specific application, CHP units have to operate at varying power levels. Furthermore, the achievable savings with CHP are depending also on the demands of heat and power. Therefore, it is in general not easy to predict the benefits of combined generation. In the literature on CHP different merit indicators are used like thermal efficiencies and exergy efficiencies. Both efficiencies are not appropriate under all circumstances. Therefore, some new merit indicators have been presented and evaluated together with the usual indicators.

### 1.2 Objectives

The objective of this thesis is to identify steps that are necessary to make our future energy system more sustainable. The present energy system is primarily based on fossil fuels like natural gas, oil, and coal. Just replacing these sources by renewable sources like wind, solar and biomass, without additional measures will result into a significant increase of the energy systems total yearly cost. The thesis will show that economic affordable sustainable energy systems require additional measures like higher conversion efficiencies and reduced energy demands. As the thesis focuses primarily on higher conversion efficiencies for the generation of power and heat, the following questions have to be answered:

- what are the limitations of the most important technologies used today;
- what improvements of these technologies might be expected in the future;
- what improvements are conceivable by the application of fuel cell systems;
- how will the application of CHP be useful for this purpose.

These general objectives have been translated into the following specific objectives for the various chapters of this thesis:

#### Chapter 2 Options for future energy systems

The objective of this chapter is to show the consequences of the introduction of renewable sources and the need for higher conversion efficiencies. In addition two important questions with regard to the design of future energy systems are answered roughly:

- 1) is hydrogen considered to be a suitable secondary fuel
- 2) what might be expected roughly from the application of CHP and Heat Pumps

#### Chapter 3 Exergy analysis

The exergy concept is used comprehensively to investigate the considered energy conversion systems. The objective of this chapter is to define and evaluate methods that are useful for the exergy analysis of energy conversion systems like value diagrams, exergy flow diagrams, exergy efficiencies of apparatuses, thermal power cycles, power plants and CHP plants. Furthermore, the accuracy of different methods for the determination of the specific exergy of solid and liquid fuels is checked.

#### Chapter 4 Fuel conversion

The thermodynamic performance (exergy efficiency) of energy conversion systems is affected seriously by the losses of fuel conversion processes like combustion and gasification. The objective of this chapter is to show the magnitude of the losses of these process and the effects of conceivable developments of combustion processes. A comprehensive evaluation of processes for the production of secondary fuels is not subject of this thesis.

#### Chapter 5 Thermal power cycles

The chapter shows the internal exergy efficiencies that are achievable with thermal power cycles like steam turbine cycles, open gas turbine cycles, combined cycles and potassium topping cycles. It shows further if overall plant efficiencies seriously higher than 70% achievable with thermal power cycles.

#### Chapter 6 Fuel cell systems

The objective of this chapter is to show that mature fuel cell systems can reach plant (electrical) efficiencies around 80% and even higher. The thermodynamic performance of high temperature fuel cell systems depends seriously on the system design. Guidelines for the realization of thermodynamic as well as economic attractive system designs have to be formulated. It will be shown further that high efficiencies around 80% and higher cannot be achieved with natural gas fuel systems using low temperature fuel cells.

#### Chapter 7 Combined heat and power

With the use of value diagrams it will be shown how thermal power cycles can be used in a suitable way for combined heat and power generation. An overview of existing concepts for the evaluation of CHP plants is given too. Finally, thermodynamic true merit indicators for the evaluation of CHP systems will be defined. And it will be demonstrated how these indicators can be used to identify attractive design characteristics of various CHP plants like industrial CHP, CC plants for district heating and micro-CHP.

### **1.3 Outline**

The thesis is outlined here by presenting a short description of each chapter. As the evaluation of the energy conversion systems is primarily based on the application of the

## Chapter 1 Introduction

exergy concept, the thesis starts with a chapter about exergy analysis. The next chapter about future energy systems provides the framework for the discussions on sustainable energy systems and thus the motivation for the further chapters.

### Chapter 2 Exergy analysis

The application of the exergy concept is generally seen as a useful tool for the evaluation of energy conversion systems. In publications, however, the application is usually limited to the calculation of exergy values of mass flows and exergy losses of processes. Applied definitions and calculation methods are not always exactly the same. Therefore the chapter starts with a description of definitions and calculation methods as applied in this thesis. This description is also useful for the derivation of more specific methods for the evaluation of energy systems like value diagrams, exergy flow diagrams, exergy efficiencies of apparatuses, thermal power cycles and conversion plants. The description is in agreement with the methods applied in the computer program Cycle-Tempo, a computer program for the evaluation of energy conversion systems developed by the energy systems group of the TU Delft<sup>1</sup>. The program is frequently used for the studies presented in this thesis. As the exact chemical composition of liquid and solid fuels is unknown, the specific exergy of these fuels cannot be calculated exactly. Methods from different authors (Szargut and Baehr) are available to estimate the specific exergy for different fuels. A comparison of these methods is made to check the applicability for various fuels. The definition of value diagrams, exergy flow diagrams, exergy efficiencies and further concepts are described in Chapter 2, but the application of these methods and concepts is presented and discussed in the other chapters.

### Chapter 3 Options for future energy systems

Sustainable energy systems have to use renewable energy sources. Wind and solar energy are frequently mentioned as important energy sources for the future. The straightforward use of wind turbines and photovoltaic energy conversion, however, appears to be significantly more expensive than the use of fossil fuels. This was one of the conclusions of studies made in the eighties of the last century by the energy systems group of the TU Delft. These studies have considered the total energy system of the Netherlands globally. As the studies have not been published before, a summary is presented in Appendix 3.1. Another conclusion from these studies is that the costs of systems based on alternative fuels like nuclear energy and biomass are of the same order as the costs of systems based on fossil fuels. Even, if in the case of wind and solar energy the costs of the primary conversion equipment is assumed to be minimum, the total yearly costs are still dominated by the costs of wind turbines or photovoltaic generators. The economic feasibility of this concept is hindered further by the costs of large scale energy storage and the required conversion equipment. The results from Appendix 3.1 are further discussed in Chapter 3. with respect to the preferred

---

<sup>1</sup> Cycle-Tempo is a flow sheeting program for the thermodynamic modeling and optimization of energy systems like steam turbine cycles, gas turbine cycles, combustion and gasification systems, heat transfer systems, combined heat and power systems, fuel cell systems, organic Rankine cycles, refrigeration systems and heat pumps. It can be used also for combinations of these systems. Detailed information is available from <http://www.cycle-tempo.nl/>. The program uses FluidProp (<http://www.fluidprop.com/>) for the calculation of thermodynamic values of the fluids. Facilities for the calculation of exergy values, exergy efficiencies and drawing of value diagrams are integrated in the program.

renewable sources, conversion technologies and secondary fuels. Also the importance of higher conversion efficiencies is emphasized. Biomass appears to be an attractive renewable fuel. The term biomass covers a range of fuel from algae to clean wood. In this thesis biomass is specified as clean wood. The effects of alternative options for the generation of heat are evaluated for a fossil fuel based system and show what fuel savings are achievable in principle by appropriate application of CHP and Heat Pumps. The calculations are rough but they give at least a first indication of the conceivable savings.

#### Chapter 4 Fuel conversion

The thermal conversion of primary fuel into heat or a secondary fuel occurs in general with substantial thermodynamic losses, usually 20 to 30% or even more of the fuel input. The effects of fuel type and combustion parameters on the exergy loss of atmospheric combustion systems is evaluated comprehensively. The preheating of combustion air appears to be an useful method to reduce the exergy loss of combustion. Usually the combustion air temperature is preheated to temperatures not higher than 500°C. However, higher temperatures are conceivable. Therefore, the effect of very high air preheat temperatures (up to 1000°C) is considered. In the case of pressurized combustion in gas turbines, the combustion conditions are depending on the design parameters of the gas turbine cycle. Further improvements of the gas turbine cycle and the effects on the exergy loss of combustion are discussed also. Finally, the losses of thermal conversion of a primary fuel into a secondary fuel are discussed. For that purpose calculations are presented for some examples of gasification and reforming processes.

#### Chapter 5 Thermal power cycles

For the generation of power, thermal power cycles are primarily used today. High total efficiencies of power plants require an appropriate match of combustion process and power cycle. The losses of the heat transfer from the combustion process to the power cycle are primarily determined by the properties of the working fluid and the selected fluid parameters. The chapter starts with presenting the exergy loss of a conventional power plant consisting of a steam boiler and a steam turbine cycle. The effects of the application of advanced steam conditions and a potassium topping cycle on plant efficiency and internal exergy efficiency of the cycles are discussed using studies done in the past. The perspectives of advanced steam conditions are discussed based on information from literature. Serious attention is paid to the most popular (natural gas fired) topping cycle today: the so-called Combined Cycle (gas turbine + steam turbine). This part starts with a discussion of the performance of gas turbine cycles and the effects of developments in the past. The performance of CC (Combined Cycle) plants is discussed using an evaluation of plants with different HRSG (Heat Recovery Steam Generator) designs: single pressure, double pressure and triple pressure steam generators. The future prospects of CC's are discussed based on an evaluation of the effects of the development of gas turbine cycles and combined cycles during a period of 25 years. The internal exergy efficiency of the thermal power cycle is used extensively for these evaluations.

#### Chapter 6 Fuel cell systems

Thermal combustion of fuels can be avoided by the application of fuel cells. Thus, fuel cell systems will eliminate the high thermodynamic losses of thermal combustion. Various

## Chapter 1 Introduction

studies on fuel cells systems have shown, however, that the application of fuel cells will not automatically result in high net efficiencies (see e.g. [6.2], [6.19], [6.44], [6.45], [6.72] and [6.73]). The chapter starts with a comparison of the thermodynamic losses of the PEMFC, MCFC and SOFC. Natural gas is initially the most likely primary fuel for fuel cell systems. Then, thermal conversion into hydrogen or an hydrogen rich mixture will be necessary. Different reforming processes like steam reforming (SR), partial oxidation (POX) or autothermal reforming (ATR) can be used for this purpose. A comparison of the thermodynamic performance of SR and ATR is made to get a better understanding of the losses of the fuel conversion system. Various options for the design of PEMFC, MCFC and SOFC systems are discussed to provide general guidelines for the system design. The discussion is helpful also to understand the effect of the various design parameters on the performance of these systems. High system efficiencies do require careful integration of the various subsystems (fuel conversion and processing, air preheating, fuel cell stacks, utilization of residual heat). Finally a target system (natural gas fuelled SOFC-GT system) is defined that will achieve an electrical efficiency around 80%. This system can be used as a target for the further development of high temperature fuel cell systems.

### Chapter 7 Combined heat and power

During the generation of heat in natural gas fired hot water boilers or industrial steam boilers, most of the fuel exergy is lost. Even the highly recommended high efficiency hot water boilers have exergy efficiencies below 15%. A substantial reduction of these losses is possible only by the application of alternative heat generation processes like heat pumps and combined heat and power plants (CHP plants). The fuel savings achievable with these technologies are discussed roughly in Chapter 3. In this chapter a more comprehensive discussion of various concepts for CHP plants is presented. In the literature on CHP plants it is often assumed that the thermodynamic merits are obvious. If merit indicators are presented, thermal efficiencies (electrical, thermal and overall efficiencies) are frequently used. Exergy efficiencies are only mentioned occasionally. After a general description of the thermodynamic aspects of CHP and the thermodynamic concepts for the evaluation of these plants the chapter focuses on the definition and application of true merit indicators. It appeared that both, thermal efficiencies and exergy efficiencies, are not true merit indicators. Finally, the preferred merit indicators are used to discuss the characteristics of different CHP plants like industrial CHP plants, CC plants for district heating and micro-CHP units.



## 2 EXERGY ANALYSIS

### 2.1 Introduction

#### 2.1.1 The need for exergy analysis

Energy conversion processes have in general high exergy losses. In many cases this is not obvious from the thermal efficiencies that are usually presented to indicate the performance of these processes (see e.g. Table 2.1). Hot water boilers and combined heat and power plants can have reasonable high thermal efficiencies. These efficiencies do suggest that further improvements are hardly possible. However, the thermal efficiency does not always represent the true thermodynamic performance of an energy conversion plant. This is e.g. obvious from the thermal efficiency of a heat pump. Electrical driven compression heat pumps for the generation of hot water for space heating have thermal efficiencies of 300% or higher. As true efficiencies higher than 100% do not exist it has to be concluded that the thermal efficiency is not a true efficiency. Therefore, the thermal performance of heat pumps is usually presented as a Coefficient Of Performance (COP). It appears actually that the true thermodynamic losses (irreversibilities) are not really recognized if only thermal energy values are considered. The exergy concept has been introduced to determine the true thermodynamic losses and thus the true thermodynamic performance of energy conversion systems. However, it is also useful for the analysis of chemical plants.

In this thesis exergy analysis is used primarily to discover possibilities to reduce the thermodynamic losses of energy conversion systems. Therefore exergy

plant	efficiency
electrical power plant	55 %
hot water boiler	95 %
combined heat and power (CHP) plant	80 %

values and exergy losses have to be calculated and presented. For the calculation of exergy values somewhat different concepts and assumptions can be used. A comprehensive description of calculation methods and underlying considerations is given in this chapter to clarify the basis for the evaluations in the other chapters of this thesis. The methods as described in this chapter are in fact a continuation of the work of prof. J.J.C. van Lier (e.g. [2.1] and [2.3]). In addition to his work the books of Baehr [2.2], Szargut et al [2.4] and Kotas [2.5] have been used for the further development of concepts and calculation methods. For the development of specific concepts and methods, much more literature has been used of course.

In the case of large, complex systems it is useful to present the results not only by listing the losses of apparatuses (unit operations), sub-systems or the total system. Graphical presentation in diagrams is in general useful for the quick understanding of results, and to get a better insight from the results. The application of value diagrams and exergy flow diagrams is discussed in Section 3.4. In Section 3.5 the use of exergy efficiencies is discussed. The

methods as described in these sections correspond with the methods applied in Cycle-Tempo<sup>1</sup>, a tool frequently used for this research.

### 2.1.2 Exergy losses

Some authors (e.g. Kotas [2.5]) propose to distinguish between internal irreversibilities and external irreversibilities. Internal irreversibilities occur within the space in which the process takes place as e.g. irreversibilities due to combustion and heat transfer within a boiler. External irreversibilities occur within the immediate environment outside the boiler, and are associated with degradation of thermal energy in the environment, dissipation of kinetic energy of the exhaust gasses, and irreversibility due to mixing of the exhaust gasses with atmospheric air. Kotas mentions also that such a division can involve some degree of arbitrariness. Differentiation is not always easy and is not always necessary. E.g. the combustion air of large steam boilers is usually taken from the boiler house because of the somewhat higher temperature. In that case lost heat from the boiler is used to preheat the combustion air. In this way a small part of the lost exergy is reused within the system.

Another distinction that can be made is the difference between avoidable and unavoidable irreversibilities (see e.g. [2.5], [2.12], [2.18], [2.19], [2.20]). The avoidable irreversibility, also called intrinsic irreversibility, is the minimum irreversibility within the limits imposed by physical, technological, economic, and other constraints. The difference between the actual and the intrinsic irreversibility is the avoidable irreversibility.

A further distinction that is proposed in literature is the split in an endogenous and an exogenous part of the exergy loss (see e.g. [2.11], [2.12], [2.20]). The endogenous exergy destruction is the exergy destruction of a component in the case that all other components operate in an ideal way (reversible mode). Thus, the endogenous exergy destruction is due exclusively to imperfections of the processes within the considered component. The exogenous exergy destruction is the remaining part of the total exergy destruction within the considered component. The total exergy destruction of the component is caused partly by imperfections of the considered component and for another part by imperfections of the other components of the system.

The determination of avoidable and unavoidable exergy losses as well as the endogenous and exogenous parts of the exergy, is rather complicated and requires serious efforts and sometimes arbitrary decisions. For the calculation of the endogenous exergy loss all other components within the system are supposed to operate in a reversible way. In the case of combustion and chemical conversions a true reversible alternative is not easily to define. Furthermore, if an irreversible process is replaced by a reversible one this might affect the value of conditions (e.g. temperatures) of other apparatuses. It is obvious that splitting the exergy losses as proposed will require serious efforts. As the benefits are not quite clear for the purpose of this thesis a split of irreversibilities or exergy losses is not considered.

### 2.1.3 Exergoeconomic evaluation

---

<sup>1</sup> Cycle-Tempo is a computer program for the thermodynamic evaluation and optimization of energy conversion systems, developed at the TU Delft by the Energy Systems group.

The optimization of energy conversion system requires that the thermodynamic performance is balanced against overall system costs. For that purpose the exergy analysis is combined with costs evaluations resulting in so-called thermoeconomic or exergoeconomic analyses. The application of these methods focuses primarily on the actual design of energy conversion plants (see e.g. [2.17], [2.18], [2.19]) or the diagnosis of system malfunctions and on-line monitoring of power plants (see e.g. [2.13], [2.14], [2.15], [2.22] and [2.23]).

The objective of this thesis is, however, to find the most profitable technologies and process conditions for future energy conversion systems that might improve the sustainability of the energy supply system. For that purpose also new technologies like biomass gasification and fuel cells have to be considered for future application. Accurate economic data for the evaluation of these systems are not sufficiently available at this moment and if they should be available the development of technologies, system and apparatus design, prices for resources and residues, and costs of depreciation are quite uncertain over periods of ten years or even longer. Therefore, exergoeconomic evaluations are not be considered for this thesis.

## 2.2 The exergy concept

### 2.2.1 General definition

The word “exergy” was proposed in 1953 by Z. Rant (see e.g. [2.1]) to indicate the fraction of energy that can be converted completely into other types of energy. The remainder, the part that cannot be converted into other types of energy, was called “anergy”. Thus, a quantity of energy can be split into a quantity of exergy and a quantity of anergy. Some other characteristics as described by Baehr [2.1] from the first and second law of thermodynamics are:

- In a process the sum of exergy and anergy will not change.
- In all irreversible processes exergy is converted into anergy. In a reversible process the exergy will remain unchanged.
- It is impossible to convert anergy into exergy.

Anergy is actually the useless part of energy and consequently only exergy is of interest for the designers of energy systems. Anergy is ignored in this thesis.

The initial definitions of exergy were highly based on theoretical considerations. To stimulate the application of the exergy concept more practical definitions are usual in recent literature. Exergy can be defined briefly as:

*the maximum theoretical work that can be obtained from an amount of energy or matter.*

This definition expresses the meaning of the exergy concept and shows the difference with heat (thermal energy), but is too rough for the selection of a calculation procedure. Work can be generated from an amount of energy or matter if these sources are not in equilibrium with the environment. The maximum theoretical work from each of these sources is obtained from a reversible system that brings the considered source into equilibrium with the environment. To enable this conversion, it might be necessary that the conversion system exchanges heat or matter with the environment. Since this heat or matter are in equilibrium with the environment

their exergy is zero. These considerations will result into the following somewhat more comprehensive definition:

*the exergy of an amount of energy or matter is the work generated by a system in which the amount of energy or matter is converted under ideal conditions using only the environment as a reservoir of heat and matter.*

For the calculation of the exergy of an amount of energy or matter, suitable systems have to be chosen that will bring the energy or matter into equilibrium with the environment. Different systems can be necessary depending on the characteristics of the source. Figure 2.1 shows schematically a system that will be used for the calculation of the exergy of an amount of matter. The system satisfies the requirements as mentioned before. Matter enters the system at its actual conditions  $(T, p)$  and leaves the system at environmental conditions  $(T_0, p_0)$ . Only reversible processes are used in the system for the conversion of matter. Heat is transferred to or from the environment at environmental temperature  $(T_0)$ . The work transferred from the system of Figure 2.1 is presented as reversible work because of the reversible processes in the system. This is the maximum work that can be achieved from the converted matter and thus this work also represents the exergy of this amount of matter. For simplicity it is assumed that in this case the composition of the matter is not changed. Thus, the matter is brought only into thermo-mechanical equilibrium with the environment. The calculated exergy is actually the thermo-mechanical exergy<sup>2</sup>.

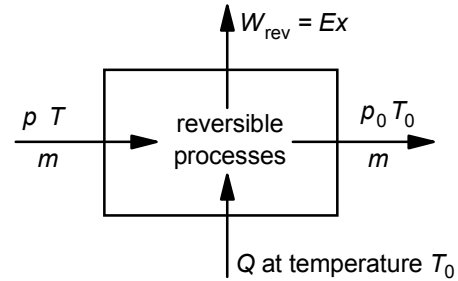


Figure 2.1

*System for the calculation of the thermo-mechanical exergy of an amount of matter*

### 2.2.2 Thermo-mechanical and chemical exergy

The total exergy of an amount of matter is usually split into the thermo-mechanical part and a chemical part. To determine the total exergy, it is necessary to bring the matter into thermo-mechanical as well as chemical equilibrium with the environment. The total exergy cannot be calculated using just a single conversion system. The chemical exergy must be calculated in addition to the thermo-mechanical exergy, using a separate conversion step as shown in Figure 2.2. The first system brings the matter in thermo-mechanical equilibrium with the environment and the second system brings the matter, at environmental temperature and

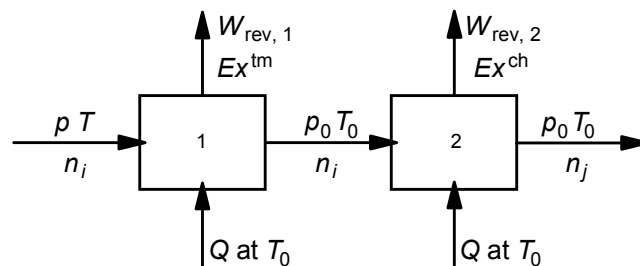


Figure 2.2

*Reversible systems for the calculation of the total exergy of an amount of matter*

<sup>2</sup> The thermo-mechanical exergy is also presented as the physical exergy.

pressure, into chemical equilibrium with the environment. Then, the total exergy of the matter equals the total reversible work from the two systems:

$$Ex_{\text{matter}} = Ex_{\text{matter}}^{\text{tm}} + Ex_{\text{matter}}^{\text{ch}} \quad (2.1)$$

Detailed calculation procedures are presented in the next section.

### 2.2.3 The exergy balance

The evaluation of energy systems in this thesis primarily focuses on open steady state systems. The schematic presentation of such a system is shown in Figure 2.3. Processes in real systems are in principle irreversible. The exergy loss of the system can be calculated if the exergy of all flows of energy and matter are determined, then:

$$Ex_{\text{loss}} = \sum Ex_{\text{in}} - \sum Ex_{\text{out}} \quad (2.2)$$

Thus, it is necessary to determine the exergy of work, heat and matter. Since exergy is the potential to do work, the work generated by the system is 100% exergy. Thus, all exergy flows of the exergy balance of open steady state systems can be calculated if equations for the calculation the exergy of heat and matter are available. The derivation of these equations is presented in Section 2.3.

The energy content of an amount of matter is not only determined by its thermo-mechanical conditions and chemical composition but also by its velocity and its distance to a reference level. The last two characteristics are determining the kinetic energy and potential energy of the matter. These energies will also contribute to the total exergy of matter that enters or leaves the system. If kinetic energy and potential energy are converted into work by a

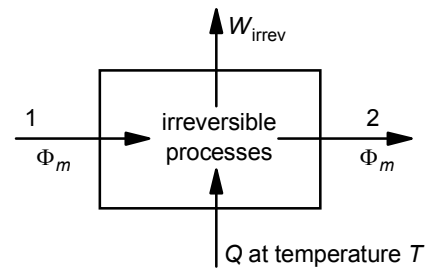


Figure 2.3  
General presentation of an open system with irreversible processes

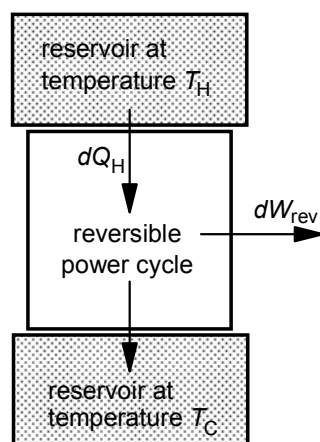


Figure 2.4  
Thermal power cycle operating between two heat reservoirs at different temperatures

reversible process, the work from the conversion system will be the same as the energy input. This means that the exergy content of kinetic energy and potential energy is the same as the energy content. Usually kinetic energy and potential energy are ignored in system evaluations because their contribution is in general negligible. If necessary they can easily be included in system calculations. Therefore, they will not be discussed separately in this chapter.

## 2.3 The calculation of exergy of heat, cold and matter

### 2.3.1 The exergy of heat

The conversion of heat into work is possible by using a thermal power cycle operating between heat reservoirs at different temperatures (see Figure 2.4). The hot reservoir transfers heat to the cycle that has to be converted into work. From the second law it is known that not all heat can be

converted into work. A certain amount of heat is transferred from the cycle to a cold reservoir. The work from a reversible power cycle is given by the following equation:

$$dW_{\text{rev}} = \left(1 - \frac{T_C}{T_H}\right) \cdot dQ_H \quad (2.3)$$

This equation can be used also to determine the exergy of an amount of heat at a specific temperature. To calculate the work of an amount of heat in a way that it equals the exergy the following conditions have to be satisfied:

- The heat transferred from the hot reservoir to the system should have the temperature of the considered heat.
- The heat transferred from the system to the cold reservoir must have the temperature of the environment.

Then, the system as shown in Figure 2.5 can be used to calculate the exergy of heat. In this case Equation 2.3 becomes:

$$dW_{\text{rev}} = dEx_Q = \left(1 - \frac{T_0}{T}\right) \cdot dQ \quad (2.4)$$

The thermal power cycle is a closed cycle. Besides the considered heat, the cycle only transfers heat to and from the environment. In this case the environment is defined only by its temperature. In practice heat is usually transferred from flows of matter at varying temperatures. The total exergy of the heat at varying temperatures becomes:

$$Ex_Q = \int_1^2 dEx_Q = \int_1^2 \left(1 - \frac{T_0}{T}\right) \cdot dQ = \left(1 - \frac{T_0}{\bar{T}}\right) \cdot Q \quad (2.5)$$

The temperature  $\bar{T}$ , the thermodynamic equivalent temperature of heat transfer, is defined by Equation (2.5). If all the heat is transferred to the system at  $\bar{T}$ , the exergy of the heat will be the same as the exergy of the heat transferred at varying temperatures. The ratio of exergy and heat is called the exergy factor of the heat. This factor is defined as:

$$f_{\text{ex}, Q} = \frac{Ex_Q}{Q} = 1 - \frac{T_0}{\bar{T}} \quad (2.5a)$$

The exergy of 1 kW heat is presented in Figure 2.6 as a function of temperature, assuming that the environmental temperature equals 298.15 K. This function equals actually also the exergy factor of heat.

### 2.3.2 The exergy of cold

In [2.7] it is concluded that the exergy of cold is considered by several authors. However, the discussions are often quite brief and the conclusions and comments are not always clear. Apparently, a more fundamental discussion of the exergy of cold is useful. Several authors discuss the exergy of cold just by using Equation 2.4 without consideration of the thermodynamic fundamentals behind this equation. In the case of cold the temperature of the considered cold ( $T$ ) is lower than the temperature of the environment ( $T_0$ ), thus:  $T < T_0$ .

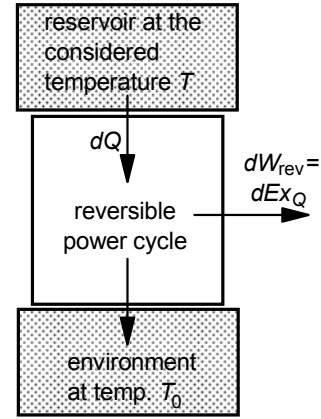


Figure 2.5  
Thermal power cycle  
used to determine the  
exergy of heat

## Chapter 2 Exergy analysis

Then, Equation 2.4 results into a negative value of the exergy of cold. Some authors use practical arguments to come to a positive value of the exergy of cold.

Exergy is defined as the maximum theoretical work that can be obtained from an amount of energy or matter. The process used to calculate the exergy should only use the environment as a source of heat and matter. In

thermodynamics heat is defined in a way that it is positive when it is transferred to the considered system. If the system in Figure 2.7 is considered, the first law of thermodynamics requires that the work done by the system equals the total heat transferred to the system, thus:

$$W = Q_H + Q_C \quad (2.6)$$

Then, if all terms are divided by  $Q_H$  :

$$\frac{W}{Q_H} = 1 + \frac{Q_C}{Q_H} \quad (2.7)$$

The heat transferred to the cold reservoir ( $Q_C$ ) must have a negative value, because it is

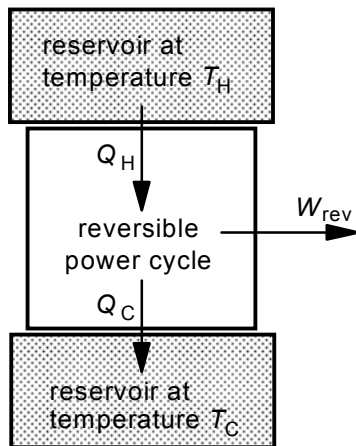


Figure 2.7 Thermal power cycle operating between two heat reservoirs at different temperatures

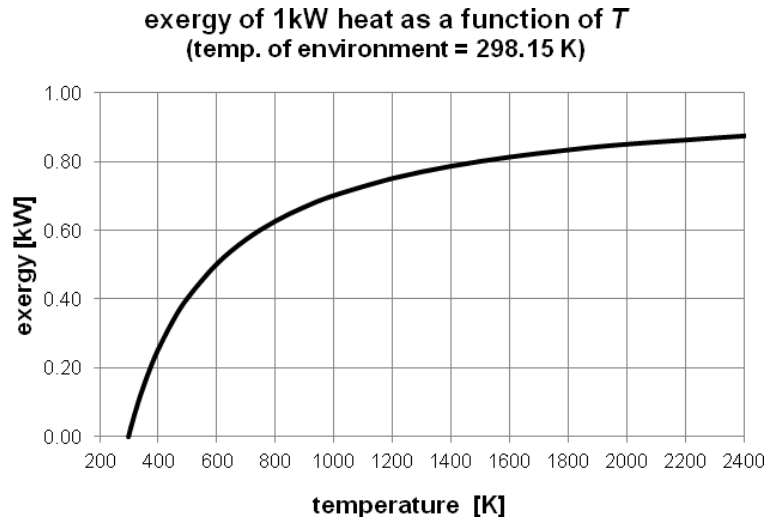


Figure 2.6 The exergy of 1kW heat as a function of  $T$  ( $T_0 = 298.15$  K.)

transferred from the system. Using the absolute value of the ratio of  $Q_H$  and  $Q_C$ , Equation 2.6 can be written as:

$$\frac{W}{Q_H} = 1 - \left| \frac{Q_C}{Q_H} \right|$$

The definition of the thermodynamic temperature results from the second law of thermodynamics. The thermodynamic temperature is defined such that in the case of a reversible system the ratio of the temperatures equals the ratio of the temperatures:

$$\left| \frac{Q_C}{Q_H} \right| = \frac{T_C}{T_H} \quad \text{and thus:} \quad \frac{W_{\text{rev}}}{Q_H} = 1 - \frac{T_C}{T_H} \quad \text{or:}$$

$$W_{\text{rev}} = \left( 1 - \frac{T_C}{T_H} \right) \cdot Q_H \quad (2.8)$$

This is actually the same equation as Equation 2.3.

The temperature of cold is always lower than the temperature of the environment, thus  $T_C < T_0$ . The system presented in Figure 2.8 can be used to determine the maximum theoretical work that can be achieved from  $Q_C$ . If in the Equations 3.6 – 3.8  $T_H$  and  $Q_H$  are replaced by  $T_0$  and  $Q_0$ , the following equation is derived:

$$W_{rev} = \left(1 - \frac{T_C}{T_0}\right) \cdot Q_0 \quad (2.9)$$

However, Equation 2.9 gives the work from the quantity of heat transferred to the system from the environment, in this case the hot reservoir. To find the reversible work achievable from the heat to the cold reservoir, the heat from the environment must be replaced by the heat to the cold reservoir. This can be done by applying the energy balance of the system:

$$W_{rev} = Q_0 + Q_C \quad (2.10)$$

With this equation  $Q_0$  can be replaced by  $W_{rev} - Q_C$  in Equation 2.10. Further rearrangement of the equation results into:

$$W_{rev} = Ex_{Q_C} = \left(1 - \frac{T_0}{T_C}\right) \cdot Q_C \quad (2.11)$$

In this equation the heat  $Q_C$  has a negative value; but also the term within the brackets, the exergy factor of cold, is negative. Thus, for the exergy of the cold  $Ex_{Q_C}$  a positive value is obtained if the definition of exergy is applied consistently.

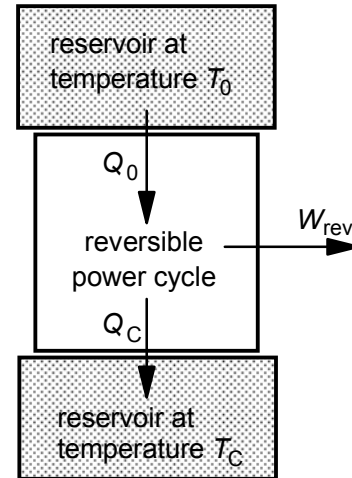


Figure 2.8 Thermal power cycle used to determine the exergy of cold

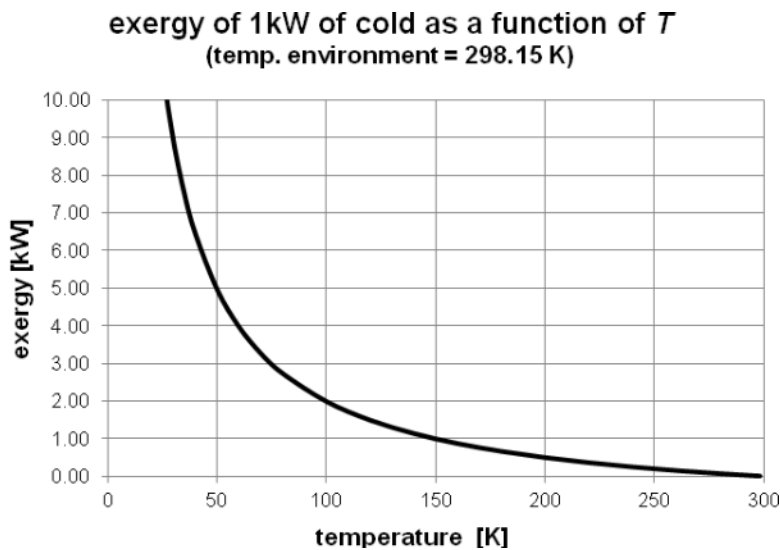


Figure 2.9 The exergy of 1kW cold as a function of T ( $T_0 = 298.15$  K)

From the equations derived for the exergy of heat and cold it must be concluded that the exergy of cold as well as the exergy of heat is positive. This means that both heat and cold have the potential to generate work. And because of the reversibility of the applied systems, the generation of heat or cold will require work.

## Chapter 2 Exergy analysis

The exergy of 1 kW cold is shown in Figure 2.9 for the case that the environmental temperature is 298.15 K. At temperatures lower than 150 K the exergy (= reversible work) from a quantity of cold will be higher than 1 kW and becomes infinite for 0 K. This is a well-known thermodynamic characteristic of cold and it explains why in practice the temperature of 0 K can technically not be reached.

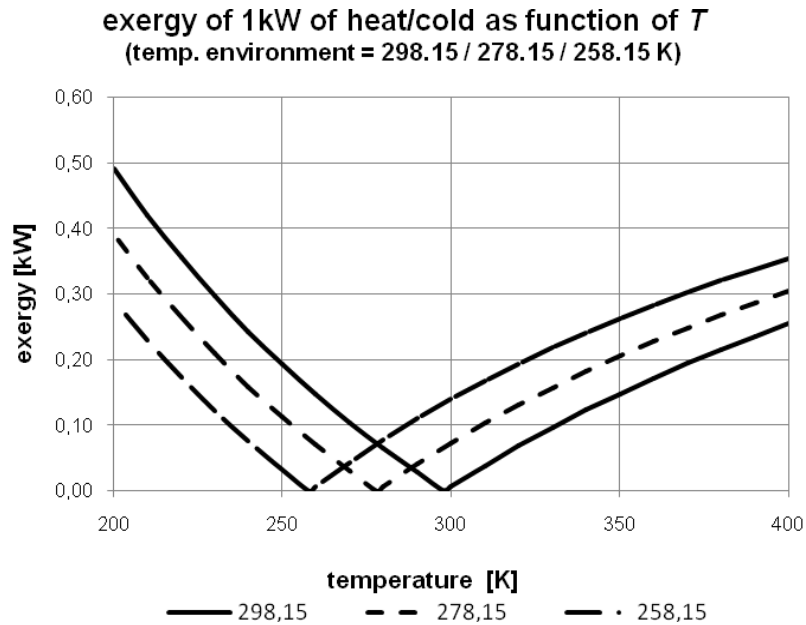


Figure 2.10 The exergy of 1kW heat/cold as a function of  $T$

The interest for the application of exergy analysis in the build area is growing recently. For the heating and cooling of buildings large quantities of low exergy heat and cold are required. At near environmental temperatures the exergy values of heat and cold are quite sensitive for the used environmental temperature as is demonstrated in Figure 2.10. This is a serious complication for the application of exergy analysis in this area.

### 2.3.3 The thermo-mechanical exergy of matter

The work that can be derived from an amount of matter can be determined in two different ways: the amount of matter can be brought into equilibrium with the environment in an open or in a closed system. The reversible work for these two cases will not be the same. In [2.6] e.g. the work from an appropriate closed system is defined as the exergy of an amount of matter and the work from an appropriate open system is called the “flow exergy”. In the original literature about exergy and the application for power systems, like [2.1] and [2.2], the exergy of matter was considered to be the work obtained by using an open system. This appeared to be suitable also for the investigations presented in this thesis. Therefore, the exergy of matter is defined here as the work from an appropriate open system as presented before in Figure 2.1. By neglecting the kinetic and potential energy of the matter entering and leaving the system, the energy balance for this system in steady state can be written as:

$$Q = (H_{\text{out}} - H_{\text{in}}) + W_{\text{rev}} \quad (2.12)$$

The exergy of the matter that enters the system can be calculated using this energy balance. The matter should leave the system in equilibrium with the environment, thus, the conditions at the outlet must equal the environmental conditions ( $T_0, p_0$ ). Since all processes in the

system are reversible and heat transfer to or from the environment should occur at temperature  $T_0$ , the transferred heat can be written as:

$$Q = \int_{\text{in}}^{\text{out}} T \cdot dS = T_0 \cdot (S_0 - S) \quad (2.13)$$

The reversible work from this system equals the exergy of the matter that enters the system. With Equations 2.6 and 2.7 this exergy becomes:

$$Ex^{\text{tm}} = W_{\text{rev}} = (H - H_0) - T_0 \cdot (S - S_0) \quad (2.14)$$

As no changes of the composition of the matter have been considered, the exergy determined with Equation 2.8 is just the thermo-mechanical exergy of matter.

### 2.3.4 The chemical exergy of matter

#### Options for the definition of an environment

The chemical exergy has to be determined in an additional step as mentioned before. This step should bring the matter in chemical equilibrium with the environment at environmental pressure and temperature. The unambiguous calculation of exergy values requires an environment with constant pressure, temperature and chemical potential of the environmental components. The environment should be such that its parameters are not affected by the use or exhaust of heat and matter by the technical process. The composition of the environment should be constant, thus, the components in the environment should not be able to react with each other. However, various compositions of the environment are conceivable that satisfy these requirements. Useful results can be achieved mainly if the environment applied for the calculations is in good agreement with the actual environment.

If the natural environment is considered, it must be concluded that the environment is not homogeneous; the environmental parameters mentioned before are dependent on location and time. In [2.9] the results of a study by J. Ahrendts are discussed. He has investigated different environments that are in equilibrium with itself. For this purpose he took the earth's atmosphere, all the water of the seas and oceans and layers of the earth's crust with varying thickness (1 to 1000 m) and assumed that all matter in this system is in chemical equilibrium at a temperature of 298.15K. With the resulting equilibrium compositions, he calculated the exergy values of a large number of chemical compounds. It appeared that, with increasing the thickness of the upper layer of the earth's crust that is included into the environment, the exergy of oxygen increases whereas the exergy of regular fuels decreases. With a crust thickness of 1000m the exergy of oxygen is even much higher than the exergy of fuel. The results of Ahrendts show that large quantities of solid oxides are formed if chemical equilibrium is achieved. In reality these oxidation processes are blocked by strong diffusion resistances. Baehr concluded that the application of an environment in complete equilibrium in itself is useless for practical purposes.

#### The environment proposed by Baehr and Schmidt

Baehr and Schmidt decided to use a subsystem of the environment for the calculation of the exergy of fuels. This subsystem consists of saturated air and water. In such a system evaporation and condensation of water is possible without the transfer of exergy. The resulting composition was presented in [2.2] (see Table 2.2) for a temperature of 25°C. In

## Chapter 2 Exergy analysis

Western Europe energy systems are often evaluated at a temperature of 15°C. The composition at this temperature was added to Table 2.2 to show the differences caused by the reduced water fraction. Baehr and Schmidt didn't try to

*Table 2.2 Reference environment by Baehr and Schmidt [2.2]*

	$T_0 = 25^{\circ}\text{C}$ $p_0 = 1.01325 \text{ bar}$	$T_0 = 15^{\circ}\text{C}$ $p_0 = 1.01325 \text{ bar}$
component	mole fraction	mole fraction
CO <sub>2</sub>	0.0003	0.0003
N <sub>2</sub>	0.7565	0.7677
O <sub>2</sub>	0.2030	0.2060
H <sub>2</sub> O	0.0312	0.0168
Ar	0.0090	0.0091

answer the question about the chemical equilibrium of the environmental components. They mention further that this model has the disadvantage that it is not able to calculate the exergy of sulfur containing fuels, because none of the environmental components does contain sulfur.

#### The environment proposed by Szargut

A comprehensive list of exergy values of elements and compounds has been determined by Szargut, Morris and Steward [2.4]. They didn't bother about the chemical equilibrium of the environment but they were looking for reference species that are supposed to be stable in our actual environment. The average concentrations at which these reference species are available in the environment is determining the exergy of the corresponding compounds and elements. Szargut has introduced the idea of the standard chemical exergy. The standard chemical exergy of a substance is defined as the exergy of the substance in the standard state at normal temperature (298.15K, 1.01325bar), assuming that it is available at the assumed average concentrations of the reference species in the environment. The earth's atmosphere, its hydrosphere and the earth's surface are used to select species for this purpose. The earth's atmosphere is an appropriate reference state but it can be used for the determination of the standard chemical exergy of only 10 elements (Ar, C, D<sub>2</sub>, H<sub>2</sub>, He, Kr, N<sub>2</sub>, Ne, O<sub>2</sub> and Xe). The exergy values were calculated assuming that the relative humidity of the air is 70%. The assumed composition is not exactly the same as the air composition of Baehr and Schmidt; this causes small differences in exergy values. Solid species from the earth's surface resulting from weathering processes, like oxides, carbonates and sulfates, are considered to be convenient reference species for other elements. The authors mention, however, that the chemical composition of the earth's surface is somewhat ill defined and an exact calculation of the thermodynamic functions of such solid reference species is difficult to make in a consistent way. Therefore, they proposed that first ions or compounds dissolved in seawater should be used as the reference species for some elements. Based on available data of mass fractions of elements contained in seawater and a calculation scheme of the standard chemical exergy for this purpose, they calculated the standard chemical exergy of quite a number of elements. On the other hand, they concluded that the thermodynamic conditions on land surfaces can be different from those in seawater. Minerals present on the land surface can interact with fresh water and oxygen, producing weathering products which are not in equilibrium with seawater. Therefore, they concluded that it is unavoidable to assume solid reference species present on the land surface for some elements. For 13 species (Al, Co, Cr, Fe, Mg, Mn, P, Sb, Si, Sn, Ti, U, and V) solid reference species from the earth's surface have been used. The calculated standard chemical exergy of elements are summarized in Table 2.3.

*Table 2.3 Standard chemical exergy of elements [2.4]*

element	$ex^{ch,mol}$ [kJ/mol]	element	$ex^{ch,mol}$ [kJ/mol]	element	$ex^{ch,mol}$ [kJ/mol]
Ag (s)	70.2	D <sub>2</sub> (g)	263.8	O <sub>2</sub> (g)	3.97
Al (s)	888.4	F <sub>2</sub> (g)	466.3	P (s, red)	863.6
Ar (g)	11.69	Fe (s, $\alpha$ )	376.4	Pb (s)	232.8
As (s)	494.6	H <sub>2</sub> (g)	236.1	Rb (s)	388.6
Au (s)	15.4	He (g)	30.37	S (s, rhombic)	609.6
B (s)	628.5	Hg (l)	115.9	Sb (s)	435.8
Ba (s)	747.7	I <sub>2</sub> (s)	174.7	Se (s, black)	346.5
Bi (s)	274.5	K (s)	366.6	Si (s)	854.6
Br <sub>2</sub> (l)	101.2	Kr (g)	34.36	Sn (s, white)	544.8
C (s, graphite)	410.26	Li (s)	393.0	Sr (s)	730.2
Ca (s)	712.4	Mg (s)	633.8	Ti (s)	906.9
Cd (s, $\alpha$ )	293.2	Mn (s)	482.3	U (s)	1190.7
Cl <sub>2</sub> (g)	123.6	Mo (s)	730.3	V (s)	721.1
Co (s, $\alpha$ )	265.0	N <sub>2</sub> (g)	0.72	W (s)	827.5
Cr (s)	544.3	Na (s)	336.6	Xe (g)	40.33
Cs (s)	404.4	Ne (g)	27.19	Zn (s)	339.2
Cu (s)	134.2	Ni (s)	232.7		

The calculated standard chemical exergy of compounds are not considered here. They can easily be derived from the standard chemical exergy of the elements.

The calculation of standard chemical exergy values appeared to be possible only by making arbitrary assumptions. The elements in solids appear usually in complicated mixtures or solid solutions. However, for the calculations relatively simple compounds have been assumed. In spite of the uncertainties with regard to the accuracy of the exergy values, the standard chemical exergy values of Szargut et al. are commonly used. At this moment no alternatives are available and apparently the application does not require further improvements.

More authors have specified somewhat different environments for the calculation of exergy values. Most of them use a simplified composition of humidified air. The specifications of Baehr and Schmidt, and Szargut et al. appeared to be the most useful. The specification of Baehr is primarily chosen for the evaluations in this thesis. The available elements in air are usually sufficient for the calculation of exergy values for the evaluation of conventional energy systems. The exergy values from Szargut are used only to check the inaccuracy in cases that specific elements that are not available from the specification of Baehr are ignored.

#### Chemical exergy of elements, compounds, and well defined mixtures

In Figure 2.2 it was shown that the chemical exergy of an amount of matter should be calculated after the matter was brought into thermo-mechanical equilibrium with the environment. For the calculation of the chemical exergy a reversible system is required that converts the considered matter isothermally into components of the reference environment. At the outlet of the system the pressure of these components should be the same as the pressure at which the reference components are available in the environment. The system might

## Chapter 2 Exergy analysis

exchange heat and matter with the environment. It appears that the calculation of the chemical exergy of matter is in general not possible by applying one single conversion system. The calculation procedure in this thesis is based on the specification of

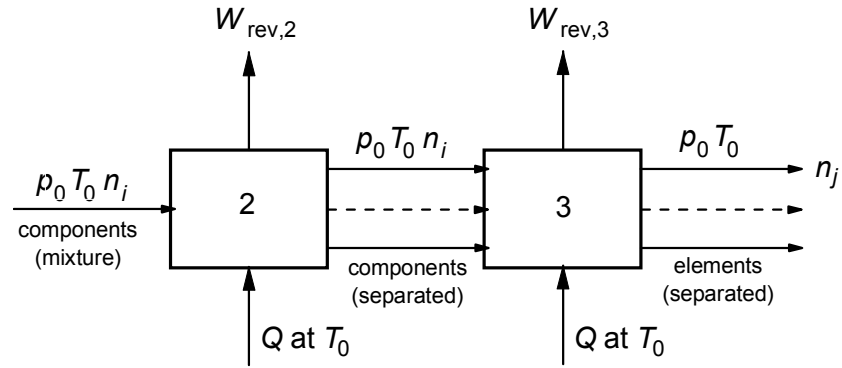


Figure 2.11 The systems used for the calculation of the chemical exergy of a mixture

the reference components of air (as specified by Baehr). However, to make a comparison possible with the exergy values calculated by Szargut, the calculation procedure is split into two steps. In the first step the exergy of matter is calculated assuming that the exergy values of the elements are known. In the second step the exergy of the elements is calculated based on the specified composition of air. The systems necessary for the calculation of the first step are presented in Figure 2.11. The considered mixture is available at environmental pressure ( $p_0$ ) and temperature ( $T_0$ ). That means that the components of the mixture are available at their partial pressures in the mixture at the inlet of system 2<sup>3</sup>. It is assumed that all components are separated by using reversible membranes. Through each of the membranes only one component can pass without friction, while all other components are blocked. Thus, the pressure after separation will be the same as the partial pressure in the mixture. After separation, the components are compressed reversibly from their partial pressure in the mixture to standard (environmental) pressure. The work necessary for reversible compression or expansion can be calculated using the following fundamental equation:

$$W_{\text{rev}} = - \int_{\text{in}}^{\text{out}} V \cdot dp - \frac{(c_{\text{out}}^2 - c_{\text{in}}^2)}{2} - g \cdot (z_{\text{out}} - z_{\text{in}}) \quad (2.15)$$

The kinetic energy and potential energy can be ignored because the exergy of matter is considered at steady state at one specific location. The compression occurs isothermal at  $T_0$ , and because of the low pressures ( $p \leq p_0$ ) gases are supposed to behave as ideal gas, then:

$$W_{\text{rev}} = - \int_{\text{in}}^{\text{out}} V \cdot dp = - \int_{\text{in}}^{\text{out}} \frac{R \cdot T}{p} \cdot dp = -R \cdot T_0 \cdot \int_{\text{in}}^{\text{out}} \frac{dp}{p} = -R \cdot T_0 \cdot \ln \frac{p_{\text{out}}}{p_{\text{in}}}$$

In the case of reversible compression or expansion of  $n$  mole of a gas, the following equation is derived to calculate the exchanged work:

$$W_{\text{rev}} = n \cdot R^{\text{mol}} \cdot T_0 \cdot \ln \frac{p_{\text{in}}}{p_{\text{out}}} \quad (2.16)$$

<sup>3</sup> System 1 is the system used for the calculation of thermo-mechanical exergy

For one mole of mixture the total work for compression is the sum of the reversible isothermal compression work for all components, thus:

$$W_{\text{rev}, 2} = \sum_i -y_i \cdot R^{\text{mol}} \cdot T_0 \cdot \ln \frac{p_0}{y_i \cdot p_0} \quad (2.17)$$

The separated and compressed components enter system 3 at standard conditions. In system 3 the compounds are isothermally converted into their elements using reversible processes and exchanging heat only with the environment. Under these circumstances the conversion of a compound into its elements represents the reverse formation reaction at standard pressure and temperature. The system should meet the conditions necessary for the derivation of Equation 2.14, thus:

$$W_{\text{rev}} = (H_{\text{in}} - H_{\text{out}}) - T_0 \cdot (S_{\text{in}} - S_{\text{out}}) \quad (2.18)$$

The change of enthalpy or entropy during the dissociation of 1 mole of compound  $i$ , as depicted in Figure 2.12, is written as:

$$(H_{\text{in}} - H_{\text{out}}) = 1 \cdot h_{i, 298}^{0, \text{mol}} - \sum_j \nu_j \cdot h_{j, 298}^{0, \text{mol}} \quad (2.19)$$

$$(S_{\text{in}} - S_{\text{out}}) = 1 \cdot s_{i, 298}^{0, \text{mol}} - \sum_j \nu_j \cdot s_{j, 298}^{0, \text{mol}} \quad (2.20)$$

Then, Equation 2.18 becomes:

$$W_{\text{rev}} = 1 \cdot \left( h_{i, 298}^{0, \text{mol}} - T_0 \cdot s_{i, 298}^{0, \text{mol}} \right) - \left( \sum_j \nu_j \cdot h_{j, 298}^{0, \text{mol}} - T_0 \cdot \sum_j \nu_j \cdot s_{j, 298}^{0, \text{mol}} \right)$$

which can be written also as:

$$W_{\text{rev}} = \left( h_{i, 298}^{0, \text{mol}} - T_0 \cdot s_{i, 298}^{0, \text{mol}} \right) - \sum_j \nu_j \cdot \left( h_{j, 298}^{0, \text{mol}} - T_0 \cdot s_{j, 298}^{0, \text{mol}} \right) = \Delta_f g_{i, 298}^{0, \text{mol}} \quad (2.21)$$

Obviously the reversible work from the reverse formation reaction at standard pressure and temperature equals the change of Gibbs free energy of formation. If the mixture consists of more than one compound the total work from system 3 becomes:

$$W_{\text{rev}, 3} = \sum_i y_i \cdot \Delta_f g_{i, 298}^{0, \text{mol}} \quad (2.22)$$

To find the chemical exergy of the mixture entering system 2 the exergy of the elements that leaving systems 3 has to be added to the work from the systems 2 and 3. Then, the exergy of the mixture becomes:

$$ex_{\text{mixture}}^{\text{ch}, \text{mol}} = W_{\text{rev}, 2} + W_{\text{rev}, 3} + \sum_j \nu_j \cdot ex_{\text{element}}^{\text{ch}, \text{mol}} \quad (2.23)$$

This results into the following equation for the calculation of the chemical exergy of a mixture of gases:

$$ex_{\text{mixture}}^{\text{ch}, \text{mol}} = \sum_i -y_i \cdot R^{\text{mol}} \cdot T_0 \cdot \ln \frac{p_0}{y_i \cdot p_0} + \sum_i y_i \cdot \Delta_f g_{i, 298}^{0, \text{mol}} + \sum_j \nu_j \cdot ex_j^{\text{ch}, \text{mol}} \quad (2.24)$$

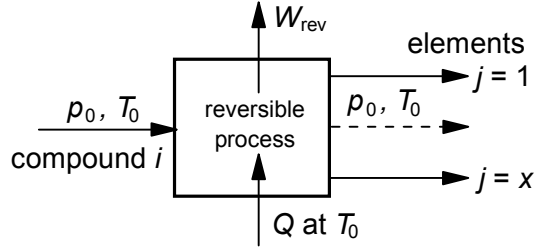


Figure 2.12 System for the reverse formation of a compound

## Chapter 2 Exergy analysis

The chemical exergy of mixtures is calculated by using tabulated data (see e.g. Appendix 1) if the composition of the mixture is known. The mole number  $\nu_i$  equals the number of moles of the respective elements that result from the conversion of 1 mole of the mixture.

The calculation of the chemical exergy of the elements is supposed to be done in another step. The system used for this purpose is shown in Figure 2.13. If

the element as such does not exist in the environment it has to be converted first into an environmental compound. Hydrogen and carbon e.g. have to be converted into water and carbon dioxide. This conversion, which is actually a formation reaction, occurs in system 4. The necessary oxygen is taken from the environmental air by assuming that the oxygen can be separated using a reversible membrane. Then, system 6 brings the oxygen at standard pressure as required for the formation reaction in system 4. Finally the environmental component has to be expanded to its partial pressure in the environmental air. After expansion the component can be transferred to the environment via a reversible membrane without exchange of work. The processes in the systems 4 to 6 are reversible and isothermal. Then, the work generated by these systems equals the exergy of the considered element.

The process of system 4 is actually an isothermal formation reaction. The work from this reaction is calculated using the same equation as for system 3. Since, in this case the reaction has the reverse direction, the sign has to be changed, and the mole number has to equal the number of moles that are produced from 1 mole of element. If the formation of 1 mole of compound requires  $\nu$  mole of the considered element, then:

$$W_{\text{rev}, 4} = -\frac{1}{\nu} \cdot \Delta_f g_{298}^{0, \text{mol}} \quad (2.25)$$

The processes of the systems 5 and 6 are isothermal expansion and compression processes. Thus, Equation 2.16 is used to calculate the reversible work. In the expansion process of system 5 the mole number equals the number of moles from system 4, thus:

$$W_{\text{rev}, 5} = \frac{1}{\nu} \cdot R^{\text{mol}} \cdot T_0 \cdot \ln \frac{p_0}{y_i \cdot p_0} \quad (2.26)$$

The parameter  $y_i$  is the mole fraction of the considered component in the air mixture. The work exchanged by system 6 is calculated as:

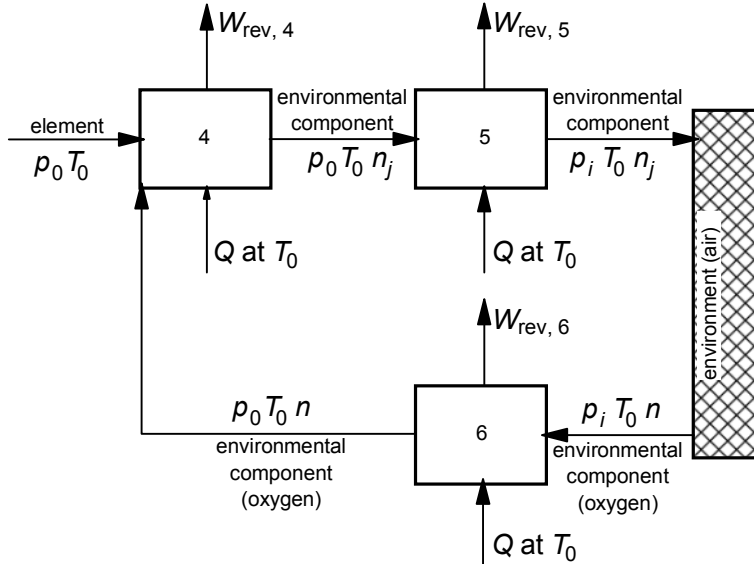


Figure 2.13 Systems used for the calculation of the chemical exergy of elements

$$W_{\text{rev},6} = \nu_0 \cdot R^{\text{mol}} \cdot T_0 \cdot \ln \frac{y_i P_0}{p_0} \quad (2.27)$$

In this equation  $y_i$  is the mole fraction of the considered component (usually oxygen) in the air mixture, and  $\nu_0$  is number of moles of the considered environmental component necessary for the conversion of 1 mole of element. By using Equations 2.25 to 2.27 the following equation for the calculation of the chemical exergy of an element is formulated:

$$ex_{\text{element}}^{\text{ch, mol}} = \frac{1}{\nu} \cdot \left( R^{\text{mol}} \cdot T_0 \cdot \ln \frac{p_0}{y_i P_0} - \Delta_f g_{298}^{0, \text{mol}} \right) + \nu_0 \cdot R^{\text{mol}} \cdot T_0 \cdot \ln \frac{y_i P_0}{p_0} \quad (2.28)$$

The parameter  $y_i$  in this equation may represent the mole fraction of different air components and, therefore, can have different values.

The method for the calculation of the chemical exergy of a gas mixture as described before calculates the exergy in two steps: first the exergy values of the elements are calculated based on the composition of the environmental air and second the exergy of the mixture is calculated using the exergy values of the elements. The calculation procedure as used in Cycle-Tempo differs somewhat from the method described before. In Cycle-Tempo the components from the mixture are converted directly into environmental components. The used systems are presented in Figure 2.14. In this figure the systems 3 and 4 are combined. The used equations are actually the same.

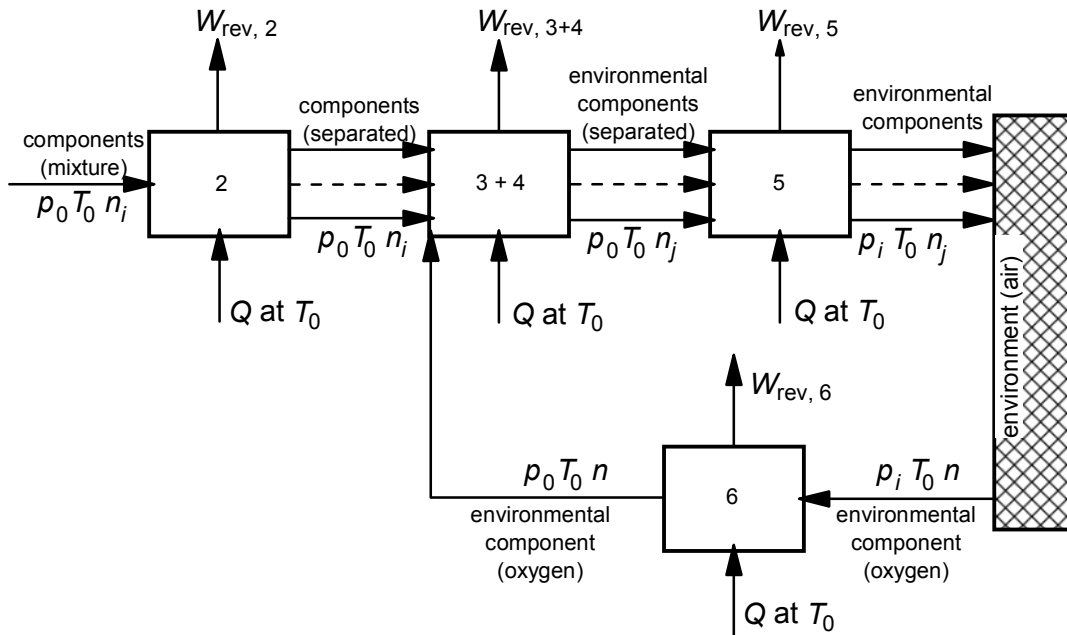


Figure 2.14 Systems used for the calculation of the chemical exergy of a gas mixture

### 2.3.5 The exergy loss of open steady state systems

In technical processes driving forces are necessary to make sure that these processes will take place within the available time and space. If a process has to take place in a short period and a small space high driving forces are necessary. Process time and space are

actually determining equipment size and consequently system costs. In an economic evaluation system costs have to be balanced against system performance or actually the driving forces. Such an evaluation is usually part of a wider evaluation that considers also emissions and sustainability aspects. During design and optimization of a plant quick determination of the exergy losses is in general useful. The magnitude of losses shows e.g. to what extent improvements are achievable.

In traditional thermodynamics the irreversible entropy increase (or entropy production) is used to indicate the degree of irreversibility of a process. A drawback of this indicator is that it is not easily to understand whether the actual entropy increase is reasonable. In exergy analysis the exergy losses can be compared with the total exergy input and show directly what percentage is lost at individual parts of a system. The relation between the irreversible entropy increase and exergy loss can be demonstrated by deriving a general equation for the exergy losses in open steady state systems as depicted before in Figure 2.3. The exergy loss due to irreversible processes in the system are determined by using the exergy balance of the system:

$$Ex_{\text{loss}} = Ex_{\text{in}} - Ex_{\text{out}} \quad (2.29)$$

The ingoing exergy equals the exergy  $Ex_1$  of mass flow 1 and the exergy of the heat to the system at temperature  $T$ . The exergy leaving the system equals the exergy  $Ex_2$  of mass flow 2 and the flow of work  $W_{\text{irrev}}$ . Equation (2.29) is then rewritten as:

$$Ex_{\text{loss}} = Ex_1 + \int_1^2 \left(1 - \frac{T_0}{T}\right) \cdot dQ - Ex_2 - W_{\text{irrev}} \quad (2.30)$$

The exergy change of the flow of matter through the system is calculated using Equation (2.14):

$$Ex_1 - Ex_2 = (H_1 - H_2) - T_0 \cdot (S_1 - S_2) \quad (2.31)$$

Assuming that changes of the potential energy and kinetic energy are neglected, the energy balance of the system of Figure 2.3 will be:

$$H_2 - H_1 + W_{\text{irrev}} - Q = 0 \quad (2.32)$$

Combining Equations 2.30, 2.31 and 2.32 results into the following equation for the exergy loss of the system:

$$Ex_{\text{loss}} = T_0 \cdot \left( (S_2 - S_1) - \int_1^2 \frac{dQ}{T} \right) \quad (2.33)$$

In the system of Figure 2.3 an amount of matter is converted from state 1 into state 2. The entropy change due to this conversion is:

$$S_2 - S_1 = \int_1^2 \frac{dQ}{T} + \Delta S_{\text{irrev}} \quad (2.34)$$

Combining Equation 2.34 with Equation 2.33 gives:

$$Ex_{\text{loss}} = T_0 \cdot \Delta S_{\text{irrev}} \quad (2.35)$$

From this equation it appears that the exergy loss in an open system with steady flow equals the product of ambient temperature and the irreversible entropy increase (entropy production) of the flow of matter through the system.

## 2.4 The exergy of solid and liquid fuels

### 2.4.1 Introduction

The exact composition of commercially available solid and liquid fuels is in general unknown. Therefore, it is not possible to calculate the exact heating value or the specific exergy of these fuels. Accurate heating values are determined in practice by measurements and associated correction calculations according to a well-defined procedure. Exergy values, however, cannot be determined by measurements but have to be estimated using the available information. Reasonable values of the specific exergy are achieved by using the ultimate analyses and heating values of solid or liquid fuels. The specific exergy of these fuels is primarily determined by the heating value. For the evaluations in this thesis mainly the lower heating value ( $LHV_F$ ) is used. The difference between the specific exergy and the heating value of commercially available solid and liquid fuels is usually not higher than 10%. Therefore, the specific exergy of fuels is often presented as the exergy factor of the fuel, which is defined as:

$$f_{ex, F} = \frac{ex_F}{LHV_F} \quad (2.36)$$

Initially Rant has proposed a constant exergy factor for solid and liquid fuels. However, the exergy factor appeared to depend significantly on the chemical composition of various organic substances. More accurate methods to calculate the exergy of solid and liquid fuels are presented by Szargut and Styrylska [2.4], and by Baehr [2.8], [2.9]. These methods are discussed in the following sections. Szargut and Styrylska proposed a statistical method using primarily the exergy of well-known chemical substances. Baehr presented in [2.8] a more fundamental method. He showed that the specific exergy of the fuel can be calculated with reasonable accuracy if the entropy of the fuel is estimated as good as possible. For coal and oil estimated entropy values are presented. This method is indicated in the following sections as Baehr-I. A second method, indicated as Baehr-II has been presented in [2.9]. This method combines the results of Baehr-I with the results of a statistical analysis of a large number of fuels by F. Brandt [2.10]. Brandt has determined simple linear equations between the mass fractions available from the ultimate analysis of the fuel and the higher and lower heating value of coal and oil. Baehr used this method to get simple equations for the exergy of solid and liquid fuels. With these equations the specific exergy can be determine with only the heating value as variable. A comparison of the three methods is presented in Section 2.4.5.

### 2.4.2 The equations of Szargut and Styrylska

Szargut and Styrylska determined regression equations from the calculated exergy values of a large number of pure organic substances. These equations express the dependence of the exergy factor ( $f_{ex, F}$ ) on the atomic ratios H/C, O/C, N/C and S/C. The ratios have to be specified as ratios of mass fractions. Separate regression equations have been obtained for different groups of organic substances. For solid and liquid fuels as used in practice the following equations are derived:

- bituminous coal, lignite, coke, peat:

$$f_{ex} = 1.0437 + 0.1896 \cdot \frac{x_{H_2}}{x_C} + 0.0617 \cdot \frac{x_{O_2}}{x_C} + 0.0428 \cdot \frac{x_{N_2}}{x_C} \quad (2.37)$$

$$\text{range of application: } \frac{x_{O_2}}{x_C} \leq 0.667 \quad \text{mean accuracy: } \pm 1\%$$

- liquid technical fuels:

$$f_{ex} = 1.0401 + 0.1728 \cdot \frac{x_{H_2}}{x_C} + 0.0432 \cdot \frac{x_{O_2}}{x_C} + 0.2169 \cdot \frac{x_S}{x_C} \left( 1 - 2.0628 \cdot \frac{x_{H_2}}{x_C} \right) \quad (2.38)$$

$$\text{mean accuracy: } \pm 0.5\%$$

- wood:

$$f_{ex} = \frac{1.0412 + 0.2160 \cdot \frac{x_{H_2}}{x_C} - 0.2499 \cdot \frac{x_{O_2}}{x_C} \cdot \left( 1 + 0.7884 \cdot \frac{x_{H_2}}{x_C} \right) + 0.0450 \cdot \frac{x_{N_2}}{x_C}}{1 - 0.3035 \cdot \frac{x_{O_2}}{x_C}} \quad (2.39)$$

$$\text{range of application: } \frac{x_{O_2}}{x_C} \leq 2.67 \quad \text{mean accuracy: } \pm 1.5\%$$

These equations are generally used for the determination of specific exergy values of solid and liquid fuels in system studies.

#### 2.4.3 The method of Baehr-I

The system as shown in Figure 2.15 is used in [2.8] to calculate the work from reversible combustion reactions of solid and liquid fuels. Reactants and products are transferred to and from the system separately at standard pressure and temperature. The reaction product consists of carbon dioxide, water, sulfur dioxide and nitrogen; excess oxygen and ash have no effect on the reversible work since composition and properties of these components are not changed. Equation 2.18 is used to determine the reversible work from this system. The enthalpy change equals the reaction enthalpy and the entropy change equals the reaction entropy, thus:

$$H_{out} - H_{in} = \Delta_R H(T_0, p_0) \quad \text{and} \quad S_{out} - S_{in} = \Delta_R S(T_0, p_0)$$

Then, Equation 2.18 will become:

$$W_{rev} = -\Delta_R H(T_0, p_0) + T_0 \cdot \Delta_R S(T_0, p_0) \quad (2.40)$$

If the system in Figure 2.15 is considered for the conversion of 1 kg of fuel the exergy balance of the system has to be written as:

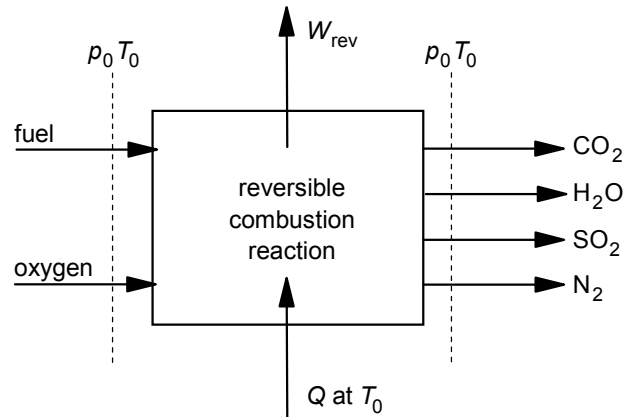


Figure 2.15 System for the reversible isothermal and isobaric combustion of fuel

$$ex_F(T_0, p_0) + m_{O_2} \cdot ex_{O_2}(T_0, p_0) = W_{rev} + \sum_{\substack{\text{reaction} \\ \text{products}}} m_i \cdot ex_i(T_0, p_0) \quad (2.41)$$

The heat transferred to or from the system has the temperature of the environment, thus, the exergy is zero. The last term of Equation 2.41 represents the exergy of the gaseous components that leave the system and can be written as:

$$\sum_{\substack{\text{reaction} \\ \text{products}}} m_i \cdot ex_i(T_0, p_0) = m_{CO_2} \cdot ex_{CO_2}(T_0, p_0) + m_{H_2O} \cdot ex_{H_2O}(T_0, p_0) \\ + m_{SO_2} \cdot ex_{SO_2}(T_0, p_0) + m_{N_2} \cdot ex_{N_2}(T_0, p_0) \quad (2.42)$$

The nitrogen in this equation is the nitrogen from the fuel.

The reversible work can be eliminated by combining Equations 2.40 and 2.41. That will give the following equation:

$$ex_F = -\Delta_R H(T_0, p_0) + T_0 \cdot \Delta_R S(T_0, p_0) + \sum_{\substack{\text{reaction} \\ \text{products}}} m_i \cdot ex_i(T_0, p_0) - m_{O_2} \cdot ex_{O_2}(T_0, p_0) \quad (2.43)$$

The specific exergy of the fuel can be calculated if it is possible to solve the various terms in this equation. The reaction enthalpy  $\Delta_R H(T_0, p_0)$  can be replaced by the higher heating value but with a negative sign:

$$HHV_F(T_0, p_0) = -\Delta_R H(T_0, p_0) \quad (2.44)$$

This is because the reaction enthalpy is defined as the heat that must be transferred to the system while the heating value is defined as the heat that must be transferred from the system. Then, Equation 2.43 is written as:

$$ex_F = HHV_F(T_0, p_0) + T_0 \cdot \Delta_R S(T_0, p_0) + \sum_{\substack{\text{reaction} \\ \text{products}}} m_i \cdot ex_i(T_0, p_0) - m_{O_2} \cdot ex_{O_2}(T_0, p_0)$$

Or with: 
$$\Delta Ex = \sum_{\substack{\text{reaction} \\ \text{products}}} m_i \cdot ex_i(T_0, p_0) - m_{O_2} \cdot ex_{O_2}(T_0, p_0)$$

this equation becomes:

$$ex_F = HHV_F(T_0, p_0) + T_0 \cdot \Delta_R S(T_0, p_0) + \Delta Ex \quad (2.45)$$

The exergy of the ash is ignored in this equation. This is acceptable since the ash exists at environmental temperature and is assumed to be chemically stable.

For the reaction entropy in Equation 2.45 can be written:

$$\Delta_R S(T_0, p_0) = m_{CO_2} \cdot s_{CO_2}(T_0, p_0) + m_{H_2O} \cdot s_{H_2O}(T_0, p_0) + m_{SO_2} \cdot s_{SO_2}(T_0, p_0) \\ + m_{N_2} \cdot s_{N_2}(T_0, p_0) - s_F(T_0, p_0) - m_{O_2} \cdot s_{O_2}(T_0, p_0) \quad (2.46)$$

If the ultimate analysis of the fuel is known, all parameters of this equation can be calculated except the entropy of the fuel. Then:

$$\Delta_R S(T_0, p_0) = 0.719 \times x_C - 16.154 \times x_{H_2} + 1.3431 \times x_S + x_{N_2} \times 6.8360 \\ - s'_F(T_0, p_0) \cdot (1 - x_{water} - x_{ash}) + 6.4074 \times x_{O_2} \quad [\text{kJ/kg K}] \quad (2.47)$$

In this equation the entropy of the fuel ( $s_F(T_0, p_0)$ ) is replaced by the entropy of the dry and ash free fuel ( $s'_F(T_0, p_0)$ ), because, it is easier to make an estimate of the entropy of the dry and ash free fuel. The entropy of the real fuel (as received) is then written as:

## Chapter 2 Exergy analysis

$$s_F(T_0, p_0) = s'_F(T_0, p_0) \cdot (1 - x_{\text{water}} - x_{\text{ash}})$$

The last term of Equation 2.45 actually is (see Equation 2.43):

$$\begin{aligned} \Delta Ex = & m_{\text{CO}_2} \cdot ex_{\text{CO}_2}(T_0, p_0) + m_{\text{H}_2\text{O}} \cdot ex_{\text{H}_2\text{O}}(T_0, p_0) + m_{\text{SO}_2} \cdot ex_{\text{SO}_2}(T_0, p_0) \\ & + m_{\text{N}_2} \cdot ex_{\text{N}_2}(T_0, p_0) - m_{\text{O}_2} \cdot ex_{\text{O}_2}(T_0, p_0) \end{aligned} \quad (2.48)$$

The mass of the various components is calculated by using the ultimate analysis of the fuel.

The exergy at standard conditions is calculated using the environment as defined by Baehr.

By doing so, the following equation is achieved:

$$\begin{aligned} \Delta Ex = & 1345.00 \times x_C - 980.49 \times x_{\text{H}_2} + 9433.84 \times x_S \\ & + 24.70 \times x_{\text{N}_2} + 123.54 \times x_{\text{O}_2} \quad [\text{kJ/kg}] \end{aligned} \quad (2.49)$$

The details of the derivation of Equations 2.47 and 2.49 are presented in Appendix 2.3.

In the case of solid and liquid fuels the actual chemical composition of the fuel is unknown and consequently the specific entropy of the fuel cannot be determined accurately. And, if the entropy of the fuel is not known, also the reaction entropy cannot be calculated. This problem can be solved only by estimating a value of the specific entropy of the fuel. In [2.8] Baehr concluded that the entropy of solid and liquid fuels at standard conditions can be estimated with reasonable accuracy from tabulated data of the entropy for a number of pure substances. He proposed the use of the following values for coal and oil:

$$\text{solid fuels (coal)} \quad s'_F(T_0, p_0) = 1.7 \pm 1.0 \quad \text{kJ/kg K}$$

$$\text{liquid fuels (oil)} \quad s'_F(T_0, p_0) = 3.5 \pm 1.0 \quad \text{kJ/kg K}$$

The choice of these values is based on the following considerations:

- the specific entropies of a large number of pure solids are in between 0.4 and 2 kJ/kg K
  - the specific entropies of liquid hydrocarbons and alcohols are in between 2 and 4 kJ/kg K
- Entropy values of pure substances are used for this evaluation. The entropy values of coal and oil estimated in this way are supposed to be the entropies of pure fuel without inert components like water and ash. Thus the values are considered to be true for water and ash free fuels.

#### 2.4.4 The calculation method of Baehr-II

In [2.9] equations for the calculation of the specific exergy of solid and liquid fuels are presented with only the heating value (higher or lower heating value) as the independent variable. These equations are based on the Baehr-I equations derived before. But the Baehr-I equations have been simplified by using linear relations between the heating value and the mass fractions from the ultimate analysis of the fuel as presented in [2.10]. These relations are based on a careful statistical analysis of a variety of fuels. The derivation of the equations for the calculation of the specific exergy of coal and oil is presented here separately.

##### 1) The specific exergy of coal

The following relations between the mass fractions of elements and the lower heating value of coal are taken from Brandt [2.10] (for heating values within the range  $10 \text{ MJ/kg} < LHV_F < 35 \text{ MJ/kg}$ ):

$$x_C = 0.054829 + 0.023736 \times LHV_F$$

$$x_{\text{H}_2} = 0.018054 + 0.0008215 \times LHV_F$$

$$x_{\text{S}} = 0.000555 + 0.000240 \times LHV_F$$

$$x_{\text{O}_2} = 0.158524 - 0.003385 \times LHV_F$$

$$x_{\text{N}_2} = 0.000909 + 0.0003935 \times LHV_F$$

$$x_{\text{water}} = 0.746737 - 0.023637 \times LHV_F$$

$$x_{\text{ash}} = 0.020392 + 0.001831 \times LHV_F$$

To enable the transformation from equations based on the lower heating value into equations based on the higher heating value, the following relation between the heating values is given:

$$HHV_F = 2.2180 + 0.9602 \times LHV_F$$

If these relations are used to calculate the entropy with Equation 2.47, the following equation is achieved:

$$\Delta_R S(T_0, p_0) = 0.77046 - 0.01488 \times LHV_F - s'_F(T_0, p_0) \cdot [0.23287 + 0.021806 \times LHV_F]$$

For solid fuels Baehr proposed:  $s'_F(T_0, p_0) = 1.7 \pm 1.0$  kJ/kg K

The use of this entropy results into the following equation for the reaction entropy:

$$\Delta_R S(T_0, p_0) = 0.37458 - 0.05159 \times LHV_F \pm (0.23287 + 0.021806 \times LHV_F) \quad (2.50)$$

This equation gives the reaction entropy in kJ/kg K. The result deviates slightly from the equation presented by Baehr:

$$\Delta_R S(T_0, p_0) = 0.374 - 0.0368 \times LHV_F \pm (0.233 - 0.0218 \times LHV_F)$$

The reversible work from the system of Figure 2.15 can be calculated using the following equation:

$$W_{\text{rev}} = HHV_F(T_0, p_0) + T_0 \cdot \Delta_R S(T_0, p_0)$$

With  $HHV_F = 2.2180 + 0.9602 \times LHV_F$  and Equation 2.50 this results into:

$$W_{\text{rev}} = 2.3297 + 0.94471 \times LHV_F \pm (0.069430 + 0.006501 \times LHV_F) \text{ [MJ/kg]} \quad (2.51)$$

This equation is quite similar to the equation presented by Baehr in [2.9]:

$$W_{\text{rev}} = 2.3295 + 0.9447 \times LHV_F \pm (0.0694 + 0.00650 \times LHV_F)$$

For the calculation of  $\Delta Ex$  with Equation 2.49 the mass fractions of the various components can be replaced using the relations of Brandt, then:

$$\Delta Ex = 0.080886 + 0.032975 \times LHV_F \text{ [MJ/kg]} \quad (2.52)$$

Baehr presented slightly different coefficients:

$$\Delta Ex = 0.0805 + 0.03281 \times LHV_F \text{ [MJ/kg]}$$

With Equation 2.51 and Equation 2.52 and by using the equation of Brandt for the relation between the higher and the lower heating value ( $HHV_F = 2.2180 + 0.9602 \times LHV_F$ ) the following equation for specific exergy of coal is achieved:

$$ex_F = 2.4106 + 0.97949 \times LHV_F \pm (0.06943 + 0.0065015 \times LHV_F) \quad (2.53)$$

This is very close to the equation presented by Baehr [2.9]:

$$ex_F = 2.410 + 0.9775 \times LHV_F \pm (0.069 + 0.00650 \times LHV_F)$$

Replacing the lower heating value by the higher heating value gives the following equation:

$$ex_F = 0.14805 + 1.02004 \times HHV_F \pm (0.05441 + 0.00677 \times HHV_F) \quad (2.54)$$

## Chapter 2 Exergy analysis

Baehr presented for the specific exergy as function of the higher heating value:

$$ex_F = 0.152 + 1.018 \times HHV_F \pm (0.054 + 0.00680 \times HHV_F)$$

The equations derived by using the basic data as presented by Baehr are not exactly the same as the equations presented in [2.9], but the differences are not significant. The derived equations are used for comparison with the other methods and the differences with the equations as published by Baehr are ignored.

2) The specific exergy of fuel oil (37 MJ/kg < 43 MJ/kg)

The following relations between the mass fractions of elements and the lower heating value of fuel oil are taken from Brandt [2.10] (for heating values within the range 37 MJ/kg <  $LHV_F$  < 43 MJ/kg):

$$x_C = 0.68309 + 0.0040776 \times LHV_F$$

$$x_{H_2} = -0.224265 + 0.0082625 \times LHV_F$$

$$x_S = 0.276035 - 0.0062774 \times LHV_F$$

$$x_{O_2} = 0.21356 - 0.0048612 \times LHV_F$$

$$x_{N_2} = 0.05158 - 0.0012015 \times LHV_F$$

The relation between the higher and the lower heating value is presented as:

$$HHV_F = -4.8954 + 1.18036 \times LHV_F$$

These relations can be used to calculate the reaction entropy with Equation 2.47. This results into the following equation:

$$\Delta_R S(T_0, p_0) = 6.2056 - 0.17833 \times LHV_F - s_F(T_0, p_0)$$

For liquid fuels Baehr proposed:  $s_F = 3.5 \pm 1.0$  kJ/kg

The liquid fuels do not contain water or ash. Then, the equation for the reaction entropy becomes:

$$\Delta_R S(T_0, p_0) = 2.7056 - 0.17833 \times LHV_F [\text{MJ/kg}] \pm 1.0 \text{ kJ/kg} \quad (2.55)$$

With the lower heating value in MJ/kg the reaction entropy is calculated in kJ/kg K. Baehr did present the following equation:

$$\Delta_R S(T_0, p_0) = 2.715 - 0.17875 \times LHV_F \pm 1.0$$

The reversible work from the system of Figure 2.15 is calculated using the following equation:

$$W_{\text{rev}} = HHV_F(T_0, p_0) + T_0 \cdot \Delta_R S(T_0, p_0)$$

With  $HHV_F = -4.8954 + 1.18036 \times LHV_F$  and Equation 2.55 this results into:

$$W_{\text{rev}} = -4.0887 + 1.12719 \times LHV_F \pm 0.29815 \text{ [MJ/kg]} \quad (2.56)$$

This equation was presented by Baehr [2.9] as:

$$W_{\text{rev}} = -4.086 + 1.1271 \times LHV_F \pm 0.298$$

The differences are actually negligible. In Equation 2.49 for the calculation of  $\Delta Ex$  the mass fractions of the various components can be replaced using the relations of Brandt, then:

$$\Delta Ex = 3.7704 - 0.062467 \times LHV_F \text{ [MJ/kg]} \quad (2.57)$$

The same equation was presented by Baehr as:

$$\Delta Ex = 3.766 - 0.06250 \times LHV_F$$

With Equations 2.56 and 2.57 and using the equation of Brandt for the relation between the higher and the lower heating value ( $HHV_F = -4.8954 + 1.18036 \times LHV_F$ ) the following equation for specific exergy of fuel oil is achieved:

$$ex_F = -0.3183 + 1.0647 \times LHV_F \pm 0.29815 \text{ [MJ/kg]} \quad (2.58)$$

This is very close to the equation presented by Baehr:

$$ex_F = -0.320 + 1.065 \times LHV_F \pm 0.298$$

Replacing the lower heating value by the higher heating value gives the following equation:

$$ex_F = 4.0975 + 0.90203 \times HHV_F \pm 0.29815 \text{ [MJ/kg]} \quad (2.59)$$

This equation based on the higher heating value was presented by Baehr as:

$$ex_F = 4.059 + 0.902 \times HHV_F \pm 0.298$$

Even if  $ex_F$  is calculated, using the equations presented by Baehr for  $W_{rev}$  and  $\Delta Ex$ , the following equation is obtained:

$$ex_F = 4.0953 + 0.90193 \times LHV_F \pm 0.298$$

Obviously, the equations as presented by Baehr in [2.9] are not entirely correct. In the case of fuel oil as well as in the case of coal the derived equations are not exactly the same as the equations presented in [2.9]. But, in all cases the differences are not really significant. For the comparison of Baehr-II with the other methods (Baehr-I and Szargut) the equations [2.53] and [2.58] as derived in this Section are used.

#### 2.4.5 Comparison of the various methods for the calculation of the specific exergy

The equations for the calculation of the specific exergy of solid and liquid fuels, as presented in the previous sections, have been used to check the credibility of the results for a variety of fuels. The considered fuels are proposed before for default purposes in Cycle-Tempo and are listed in the Tables 2.5, 2.6 and 2.7.

##### Coal

The overview of solid fuels like coal, cokes and lignite is given in Table 2.5. The ultimate composition and the heating values for the fuel in the as received state are shown first. Then the calculated exergy values are presented. The specific exergy as well as the exergy factor is calculated for each of the fuels using the three calculation methods Baehr-I, Baehr-II and Szargut. Except for lignite and cokes, the values derived with the three methods do in general agree quite well, as demonstrated in Figure 2.16. For most of the coal types the differences are lower than 1%. Very serious deviations are found for lignite and somewhat higher deviations for cokes, Ohio#6 and Illinois#6 coal. Since Baehr-I is the most accurate method the deviations of Baehr-II and Szargut from Baehr-I are discussed below. For coke the deviation of the specific exergy calculated with Baehr-II is 2.3%. In the case of Ohio#6 coal the calculated value is 1.3% lower. With Szargut the calculated value for Illinois#6 coal is 1.85% lower. However, it should be emphasized that the method of Szargut is defined for dry and ash free fuels. But the accuracy of the results for coal in the as received state appear to be quite reasonable. The highest deviations are found for lignite. The value calculated by using Szargut is 3.33% lower and the deviation when using Baehr-II is 15.9% higher. In the case of

<i>Table 2.5 Specific exergy of various solid fuels</i>										
FUEL	units	cokes	coal	coal	coal	coal	coal	coal	coal	lignite
mass fractions			Ruhr	Saar	Drayton	Ohoi #6	El Correjon	Illinois #6	Wambo	Rheinland
<b>as received</b>										
water	[-]	0.090	0.025	0.025	0.095	0.022	0.167	0.161	0.091	0.570
ash		0.090	0.060	0.060	0.122	0.064	0.074	0.101	0.102	0.120
C	[-]	0.800	0.840	0.790	0.650	0.751	0.611	0.589	0.660	0.213
H	[-]	0.002	0.033	0.050	0.042	0.050	0.040	0.039	0.043	0.016
O	[-]	0.002	0.024	0.053	0.070	0.061	0.084	0.075	0.182	0.077
N	[-]	0.008	0.012	0.013	0.012	0.014	0.015	0.012	0.017	0.003
S	[-]	0.007	0.006	0.009	0.009	0.040	0.008	0.024	0.004	0.002
Cl	[-]	0.000	0.000	0.000	0.000	0.000	0.000	0.000	0.000	0.000
F	[-]	0.000	0.000	0.000	0.000	0.000	0.000	0.000	0.000	0.000
total	[-]	1.000	1.000	1.000	1.000	1.000	1.000	1.000	1.000	1.000
$HHV_F$	[MJ/kg]	27.39	32.85	32.57	26.89	31.91	25.31	24.47	27.25	8.31
$LHV_F$	[MJ/kg]	27.12	31.98	31.32	25.67	30.67	24.26	23.23	26.05	7.68
<b>Baehr-I</b>										
$ex_F$	[MJ/kg]	28.30	33.64	33.27	27.52	32.87	25.93	25.21	27.86	8.57
$f_{ex} = ex_F/LHV$	[-]	1.044	1.052	1.062	1.072	1.072	1.069	1.085	1.069	1.117
<b>Baehr-II</b>										
$ex_F$	[MJ/kg]	28.97	33.74	33.09	27.55	32.45	26.17	25.17	27.93	9.93*)
$f_{ex} = ex_F/LHV$	[-]	1.068	1.055	1.056	1.073	1.058	1.079	1.083	1.072	1.293*)
<b>Szargut</b>										
$ex_F$	[MJ/kg]	28.33	33.70	33.22	27.30	32.57	25.85	24.74	27.75	8.29
$f_{ex} = ex_F/LHV$	[-]	1.045	1.054	1.061	1.063	1.062	1.066	1.065	1.065	1.080
<b>dry and ash free</b>										
$HHV_F$	[MJ/kg]	33.40	35.90	35.60	34.34	34.88	33.35	33.14	33.77	26.81
$LHV_F$	[MJ/kg]	33.34	35.12	34.40	33.16	33.69	32.20	32.00	32.60	25.72
<b>Baehr-I</b>										
$ex_F$	[MJ/kg]	34.51	36.77	36.36	35.15	35.93	34.17	34.14	34.53	27.65
$f_{ex} = ex_F/LHV$	[-]	1.035	1.047	1.057	1.060	1.067	1.061	1.067	1.059	1.075
<b>Baehr-II</b>										
$ex_F$	[MJ/kg]	35.06	36.81	36.10	34.89	35.41	33.95	33.76	34.34	27.60
$f_{ex} = ex_F/LHV$	[-]	1.052	1.048	1.050	1.052	1.051	1.054	1.055	1.053	1.073
<b>Szargut</b>										
$ex_F$	[MJ/kg]	34.83	36.99	36.48	35.27	35.78	34.32	34.08	34.72	27.78
$f_{ex} = ex_F/LHV$	[-]	1.045	1.053	1.061	1.063	1.062	1.066	1.065	1.065	1.080

Baehr-II the heating value of this fuel is out of the range for this equation (10 – 35 MJ/kg).

The use of Szargut and Baehr-II for the calculation of lignite in the as received state is actually not allowed.

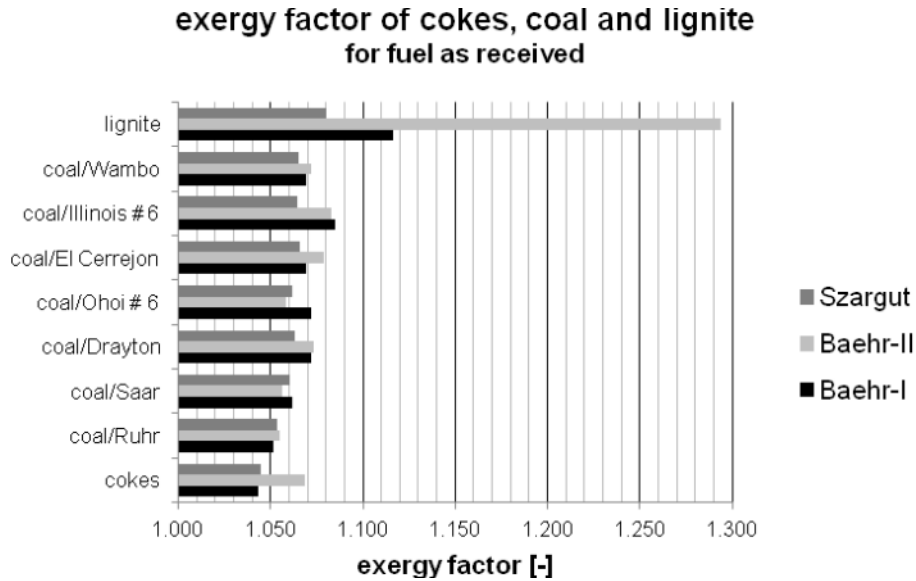


Figure 2.16 The exergy factor of coal, cokes, and lignite calculated for fuel in the as received state

FUEL		petrol	kerosine	diesel oil	fuel oil	fuel oil	fuel oil	fuel oil
					[general]	[light]	[medium]	[heavy]
mass fractions								
C	[-]	0.855	0.859	0.857	0.844	0.855	0.853	0.849
H	[-]	0.145	0.140	0.134	0.138	0.125	0.116	0.106
O	[-]	0.000	0.000	0.000	0.013	0.008	0.003	0.005
N	[-]	0.000	0.000	0.000	0.000	0.000	0.003	0.005
S	[-]	0.001	0.001	0.009	0.005	0.012	0.025	0.035
total	[-]	1.000	1.000	1.000	1.000	1.000	1.000	1.000
$HHV_F$	[MJ/kg]	46.50	46.50	45.40	42.00	44.80	43.30	42.30
$LHV_F$	[MJ/kg]	43.35	43.44	42.48	38.99	42.07	40.77	39.99
<b>Baehr-I</b>								
$ex_F$	[MJ/kg]	45.96	45.99	45.00	41.55	44.50	43.17	42.33
$f_{ex} = ex_F/LHV$	[-]	1.060	1.059	1.060	1.066	1.058	1.059	1.059
<b>Baehr-II</b>								
$ex_F$	[MJ/kg]	45.83	45.94	44.90	41.19	44.48	43.09	42.26
$f_{ex} = ex_F/LHV$	[-]	1.057	1.057	1.057	1.057	1.057	1.057	1.057
<b>Szargut</b>								
$ex_F$	[MJ/kg]	46.35	46.42	45.39	41.71	44.93	43.55	42.73
$f_{ex} = ex_F/LHV$	[-]	1.069	1.068	1.069	1.070	1.068	1.068	1.069

## Chapter 2 Exergy analysis

To enable a true comparison of Szargut and Baehr-II with Baehr-I fuels are also considered in the dry and ash free state. The corresponding heating values and the calculated exergy values are presented in the lower part of Table 2.5 as well as in Figure 2.17. The

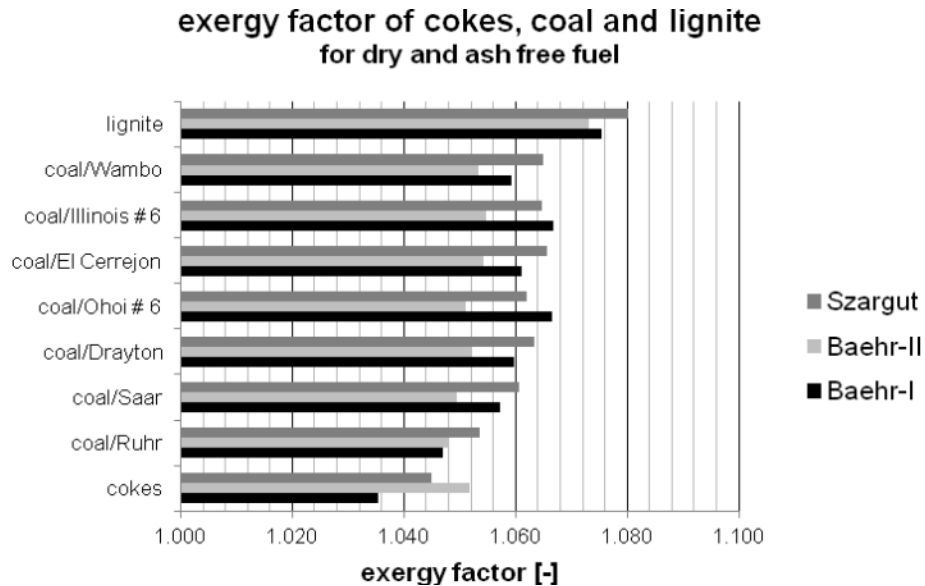


Figure 2.17 The exergy factor of coal, cokes, and lignite calculated for fuel in the dry and ash free state

method of Szargut calculates the exergy factor of the fuel ( $f_{ex, F}$ ) based on the atomic ratios of some components. Since these ratios do not depend on the state of the fuel, the same values of the exergy factor are calculated as for the as received state. In the dry and ash free state the deviations of the exergy values calculated using Szargut are all lower than 1%, thus within the mean accuracy range as specified by Szargut (see Equation 2.37). The values calculated with Baehr-II show deviations higher than 1% for cokes (+1.6%), Ohio#6 coal (-1.5%), and Illinois#6 coal (-1.1%). But the value for lignite is within the 1% range now.

Szargut specified for Equation 2.37, that can be used for bituminous coal, lignite, coke and peat, a mean accuracy of  $\pm 1\%$ . Baehr has mentioned an uncertainty with regard to the estimated value of the fuel entropy ( $\pm 1.0$  kJ/(kg K)). No additional uncertainties for the method of Brandt [2.10] have been specified. The specified uncertainties are used to calculate maximum and minimum values of the exergy factor of Ruhr coal (see Figure 2.18). It appears that the uncertainty range is almost the same for the three methods.

### Liquid fuels

The results for the liquid fuels are presented in Table 2.6. The deviations of the specific exergy values calculated with Baehr-II and Szargut are lower than

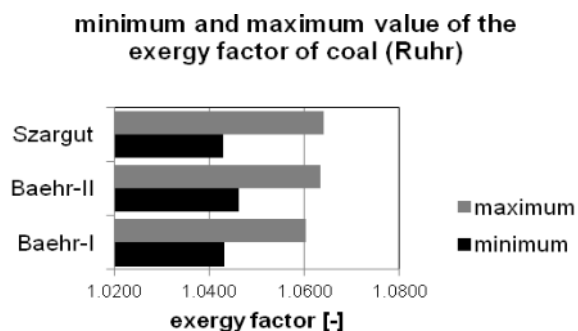


Figure 2.18 The minimum and maximum value of the exergy factor of coal (Ruhr)

Table 2.7 Specific exergy of some biomass fuels

FUEL		wood	wood chips	peat	wood	wood chips	dry peat
mass fractions		as received			dry and ash free		
water	[-]	0.494	0.303	0.482	-	-	-
ash		0.032	0.006	0.023	-	-	-
C	[-]	0.284	0.356	0.285	0.600	0.515	0.576
H	[-]	0.030	0.043	0.028	0.063	0.062	0.058
O	[-]	0.149	0.289	0.172	0.315	0.418	0.347
N	[-]	0.009	0.003	0.009	0.020	0.004	0.018
S	[-]	0.001	0.000	0.001	0.001	0.000	0.002
Cl	[-]	0.000	0.000	0.000	0.000	0.000	0.000
F	[-]	0.000	0.000	0.000	0.000	0.000	0.000
total	[-]	1.000	1.000	1.000	1.000	1.000	1.000
$HHV_F$	[MJ/kg]	11.09	13.36	10.89	23.41	19.33	22.00
$LHV_F$	[MJ/kg]	9.23	11.69	9.09	22.02	17.98	20.75
<b>Baehr-I</b>							
$ex_F$	[MJ/kg]	11.45	13.91	11.30	24.16	20.13	22.82
$f_{ex} = ex_F/LHV$	[-]	1.241	1.190	1.243	1.097	1.119	1.100
<b>Baehr-II</b>							
$ex_F$	[MJ/kg]	11.45	13.86	11.31	23.98	20.02	22.73
$f_{ex} = ex_F/LHV$	[-]	1.241	1.186	1.245	1.089	1.114	1.096
<b>Szargut</b>							
$ex_F$	[MJ/kg]	10.14	13.11	10.01	24.19	20.17	22.85
$f_{ex} = ex_F/LHV$	[-]	1.098	1.122	1.101	1.098	1.122	1.101

1%. Szargut specified a mean accuracy of  $\pm 0.5\%$  for Equation 2.38. The deviation from the values calculated with Baehr-I are for almost all fuels around 1.0%. For the method of Baehr-I and Baehr-II an inaccuracy of  $\pm 1.0$  kJ/(kg K) is specified for the fuel entropy of solid as well as liquid fuels. The inaccuracy ranges of the three methods are shown in Figure 2.19 for the specific exergy of general fuel oil. The ranges of Baehr-II and Szargut show a clear overlap with the range of Baehr-I.

#### Biomass

The results for some biomass fuels in the as received state as well as in the dry and ash free state are presented in Table 2.7. The results of Szargut are determined by using Equation 2.39 for wood and wood chips; Equation 2.37 has been used for peat. Baehr has not defined specific equations for biomass fuels; therefore, the equations as derived for coal

minimum and maximum values of the exergy factor of fuel oil (general)

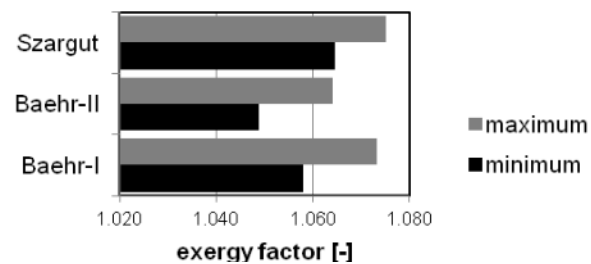


Figure 2.19 The minimum and maximum value of the exergy factor of fuel oil (general)

## Chapter 2 Exergy analysis

are applied. The results are presented too for fuels in the as received state in Figure 2.20 and in the dry and ash free state in Figure 2.21. For the fuel in the as received state, the agreement between Baehr-II and Baehr-I is quite good. But the values found by using the Szargut equations differ seriously: the values for wood and peat more than 11% lower. If the fuel is considered in the dry and ash free state the deviations of Szargut and Baehr-II from Baehr-I are low. Differences between Szargut and Baehr-I are not higher than 0.1% to 0.2%.

### Conclusions

From the three considered methods for the calculation of the specific exergy of solid and liquid fuels, the method of Baehr-I is supposed to be the most reliable because this method uses primarily fundamental thermodynamics. Only the fuel entropy cannot be determined exactly. However, the inaccuracy of the fuel entropy on the specific exergy of the fuel is very limited: roughly  $\pm 1\%$ . For the application of this method the ultimate analysis of the fuel as well as the heating value (higher or lower heating value) have to be available. The method is suitable for any kind of fuel that consists of the considered elements. If not, the model can be modified and the equations fitted to the actual circumstances.

The Baehr-II method has the advantage over the Baehr-I method that no information is needed about the composition of the fuel. The specific exergy is calculated by using only the

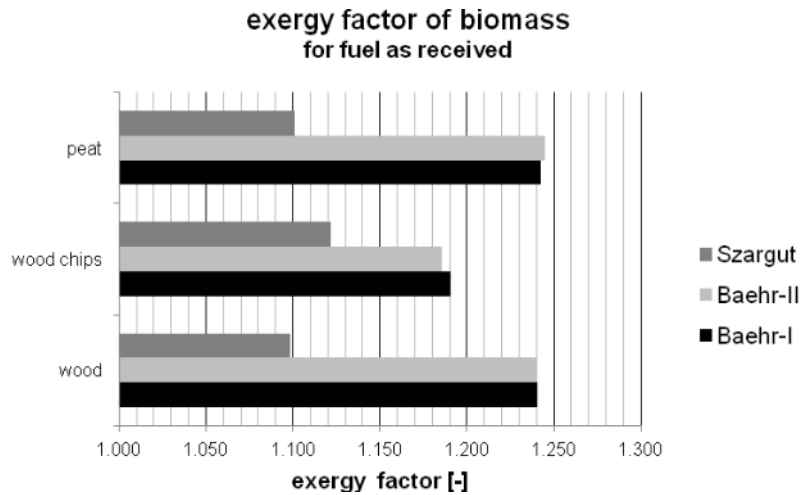


Figure 2.20 The calculated exergy factors of peat, wood chips, and wood in the as received state

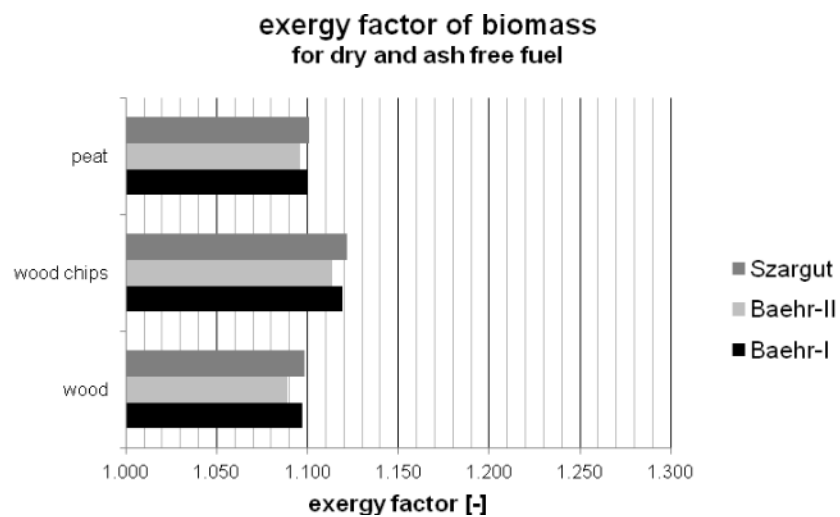


Figure 2.21 The calculated exergy factors of peat, wood chips and wood in the dry and ash free state

heating value as independent variable. The Baehr-II method actually combines the Baehr-I method with equations for the relation between the fuel composition and its heating value as determined by Brandt [2.10]. This relation is based on statistical information of a large number of fuels and causes an additional inaccuracy. Thus, the accuracy of the calculated specific exergy should be less than the values calculated by using the Baehr-I method. The results from the Baehr-II method do correspond quite well with the results from the Baehr-I method for coal in the as received condition; for cokes the agreement is poor and for lignite bad. For coal in the dry and ash free condition the agreement is not that good, but for coke and in particular lignite the agreement is much better. For the considered biomass fuels, wood, wood chips and peat, the correspondence between the methods of Baehr-II and Baehr-I is good for the fuel in the as received condition as well as in the dry and ash free condition.

The equations of Szargut for solid technical fuels are suitable only for fuel in the dry and ash free condition. The comparison of the calculation methods as presented in this section shows that application of Szargut for fuels in the as received state might cause serious deviations. The method corresponds quite good with the results of the Baehr-I method for all considered fuels in the dry and ash free condition. The exergy factors calculated with the Szargut method are the same for fuels in the as received state and in the dry and ash free state. It appeared that application of the method of Szargut for fuels in the as received state might cause serious inaccuracies.

## 2.5 Value diagrams and exergy flow diagrams

### 2.5.1 Introduction

The exergy analysis of plants for the conversion of energy or the production of chemical substances requires primarily the determination of all exergy flows that are transferred between the distinguished apparatuses or unit operations of a plant. The resulting exergy losses can provide useful information with regard to the overall plant performance as well as the performance of subsystems. In the case of large, comprehensive systems these calculations will result into a extensive list of apparatuses and their losses. The evaluation of long lists with data is time consuming and provides only limited understanding of the results. Graphical presentation of the results is in general useful for quick and correct understanding of the data as well as for discussions with regard to system optimization.

Property diagrams, like  $T,s$ -diagrams and  $h,s$ -diagrams, are commonly used to describe thermal power cycles. With appropriate understanding of the thermodynamics it is possible to read also exergy values and exergy losses from these diagrams. This will be demonstrated in the following chapters. More specific diagrams for the presentation of exergy

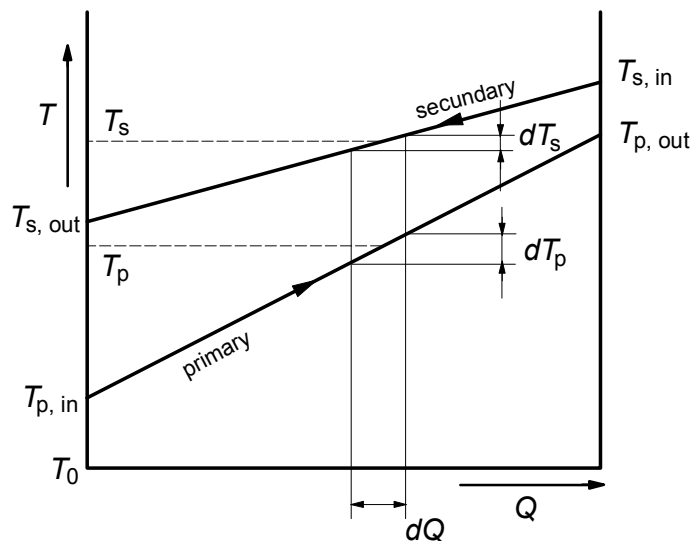


Figure 2.22  $T,Q$ -diagram of a heat exchanger

## Chapter 2 Exergy analysis

losses are the “value diagram” and the “exergy flow diagram”. Actually both diagrams are modifications of the general used  $T, Q$ -diagrams and energy flow diagrams. Value diagrams and exergy flow diagrams are frequently used in this thesis. The basics are described in the following sections.

### 2.5.2 The value diagram for heat transfer

Heat transfer processes are often depicted in  $T, Q$ -diagrams. An example of such a diagram is shown in Figure 2.22. In this diagram the temperature of the primary (= the heated) and secondary (= the cooled) flows in a heat exchanger are given as a function of the transferred heat. In Figure 2.23 the temperature curves of the same flows are shown in the value diagram. In this diagram the temperature at the vertical axis is replaced by the term  $(1 - T_0/T)$ . The vertical axis starts at  $T = T_0$  and goes up to  $T = \infty$ . Then, the values on the vertical axis will go from 0 to 1. If the transfer of an infinitesimal quantity of heat  $dQ$  is considered, the temperature of the heat from the secondary system is  $T_s$ . The exergy of this heat is:

$$dEx_s = \left(1 - \frac{T_0}{T_s}\right) \cdot dQ \quad (2.60)$$

The area 1-3-4-6-1 in Figure 2.23 equals the amount of heat  $dQ$ , while the area 1-2'-5'-6-1 equals the exergy  $dEx_s$  of this heat. The exergy fraction  $(1 - T_0/T_s)$  indicates which part of the considered heat can be converted into work. The total exergy transferred from the secondary flow can be determined by integrating Equation 2.60 from the inlet temperature  $T_{s,in}$  to the outlet temperature  $T_{s,out}$ :

$$Ex_s = \int_{T_{s,in}}^{T_{s,out}} \left(1 - \frac{T_0}{T_s}\right) \cdot dQ \quad (2.61)$$

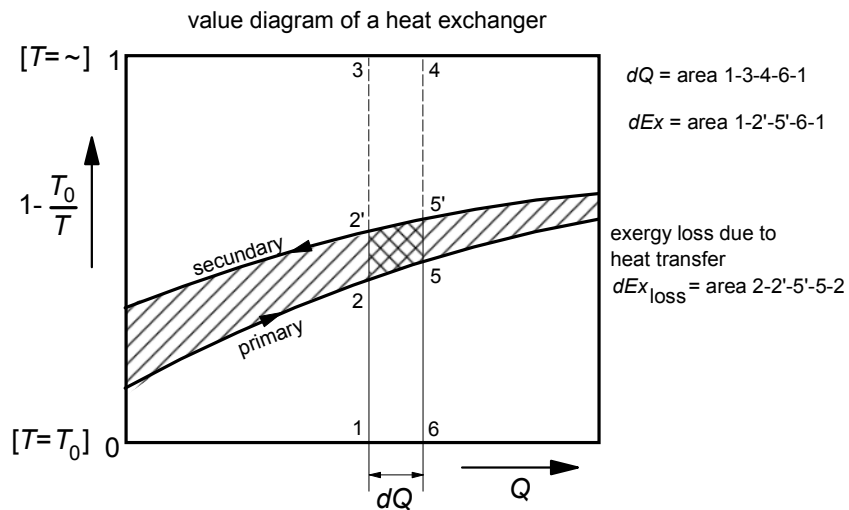


Figure 2.23 Value diagram of a heat exchanger

Thus, the exergy transferred from the secondary flow equals the whole area below its temperature curve in the value diagram. The heat  $dQ$  from the secondary flow is transferred to the primary flow. The exergy of the heat transferred to this flow is:

$$dEx_p = \left(1 - \frac{T_0}{T_p}\right) \cdot dQ \quad (2.62)$$

This exergy is represented by the area 1-2-5-6-1 in the value diagram of Figure 2.23. Obviously, the exergy transferred to the primary flow is smaller than the exergy transferred from the secondary flow. The difference, the area 2-2'-5'-5-2, is the exergy that is lost due to the temperature difference necessary to transfer the heat from the secondary to the primary flow. The total exergy transferred to the primary flow can be calculated by integrating Equation 2.62 from inlet to outlet of the heat exchanger:

$$Ex_p = \int_{T_{p,in}}^{T_{p,out}} \left(1 - \frac{T_0}{T_p}\right) \cdot dQ \quad (2.63)$$

The exergy transferred to the primary flow equals the area below its temperature curve in the value diagram. The total exergy loss due to heat transfer,  $Ex_s - Ex_p$ , is represented by the shaded area between the two temperature curves. Therefore value diagrams are convenient to present exergy losses of heat transfer processes. From this diagram it is obvious that higher temperature differences between the secondary and the primary flow will increase the exergy loss due to heat transfer. The temperature difference is in fact the driving force for the heat transfer process; increasing the driving force will accelerate the process. Higher driving forces will reduce the size of the heat exchanger, but will cause higher exergy losses too.

Value diagrams can also be used to depict the heat transfer to or from a flow when this heat transfer takes place in more than one heat exchanger. Figure 2.24 shows the value-diagram of the heat transfer in

the waste heat boiler of a simple combined cycle plant. The off-gasses from the gas turbine exhaust are cooled successively in the superheater, evaporator and economizer of the waste heat boiler. After leaving the economizer, the flue gas is used to heat water in a water boiler for a district heating cycle. After leaving the water boiler the flue gasses are emitted to the environment through the stack. The residual heat is called the stack loss. The shaded areas represent the

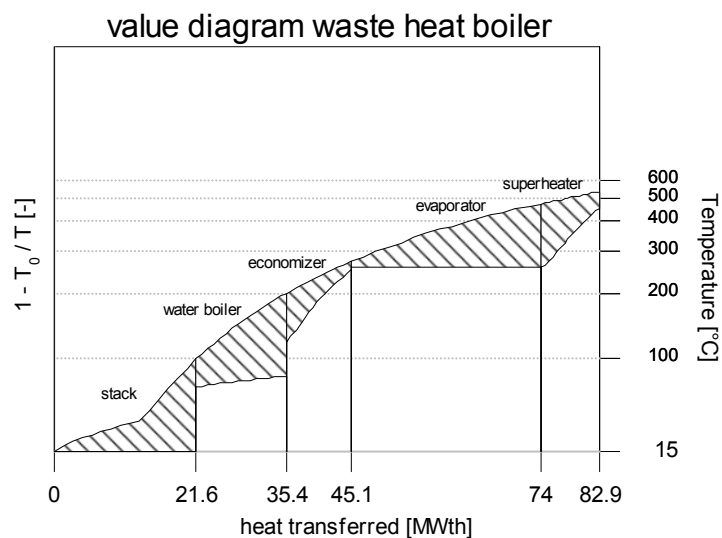


Figure 2.24 Value diagram of the heat transfer in a waste heat boiler

## Chapter 2 Exergy analysis

exergy losses due to the heat transfer and the stack loss<sup>4</sup>.

### 2.5.3 Value diagrams for thermal power plants

The value diagram is primarily developed for the evaluation of heat transfer processes. But with some ingenuity it can be used also for the evaluation of thermal power plants as well as combined heat and power plants. Starting point for the exergy analysis of power plants is the fuel exergy supplied to the plant. In general the fuel exergy has not the same value as the heating value of the fuel. However, the differences between the exergy value and the lower heating value of fossil fuels are limited. The difference between exergy and lower heating value is indicated before by the exergy factor of the fuel:

$$f_{ex,F} = \frac{ex_F}{LHV_F} \quad (2.64)$$

In Table 2.4 approximate values of the exergy factor are given. The exergy factors of coal and fuel oil are estimated values, derived from [2.8] and [2.9]. These values do correspond quite well with the exergy factors calculated in the Tables 2.5 and 2.6. The exergy factor of natural gas is the value calculated for Slochteren natural gas.

The width of a value diagram represents an amount of heat; this can also be e.g. the lower heating value of 1 kg of fuel. But, instead of the lower heating value, also the exergy of the fuel can be used to determine the width of the diagram. This is done in Figure 2.25, assuming natural gas as the fuel. In the case of coal or fuel oil the ratios between the exergy and the heating values will be somewhat different. Since the vertical axis of the diagram

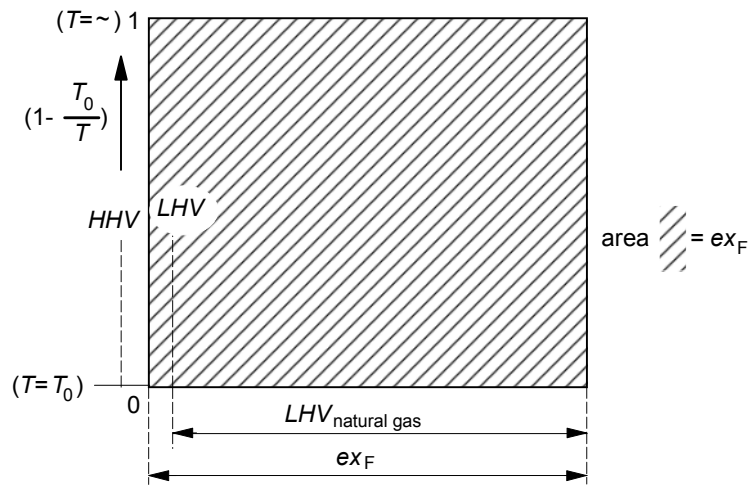


Figure 2.25 Value diagram based on the exergy of the considered fuel

starts at  $T = T_0$  and ends at  $T = \infty$  the length of the vertical axis equals 1. Thus, the total area of the diagram equals the exergy of the fuel.

For the thermodynamic evaluation of combustion processes it is necessary to assume that fuel is combusted adiabatically before heat from the generated flue gas can be used. After adiabatic combustion of a fuel, the flue gasses have usually a high temperature (up to 2000°C). As fuel and oxidizer are supposed to enter the combustion chamber at ambient temperature, the heat that is transferred from the flue gas by cooling down till ambient

<sup>4</sup> The value diagram in Figure 2.24 is depicted directly by Cycle-Tempo. The program is provided with the facilities to construct easily  $T, Q$ -diagrams as well as value diagrams for a quick analysis of the results.

temperature will equal the lower heating value if it is assumed that water vapor in the flue gas will not condense. The cooling curve of the flue gas, when cooling the gas to environmental temperature, is depicted in Figure 2.26. In the case of natural gas the exergy factor  $f_{ex,F}$  is higher than 1. The temperature  $T_{fg}$  is the adiabatic combustion temperature. Combustion processes are supposed to generate heat, thus, the heat that is transferred from the flue gas is considered as the product of the process. The exergy of this heat equals the area below the temperature curve. Then, the difference between the exergy of the fuel (the total area of the diagram) and the exergy of the heat from the flue gas (the area below the temperature curve) is the exergy loss of the combustion process. This equals the shaded area in Figure 2.26.

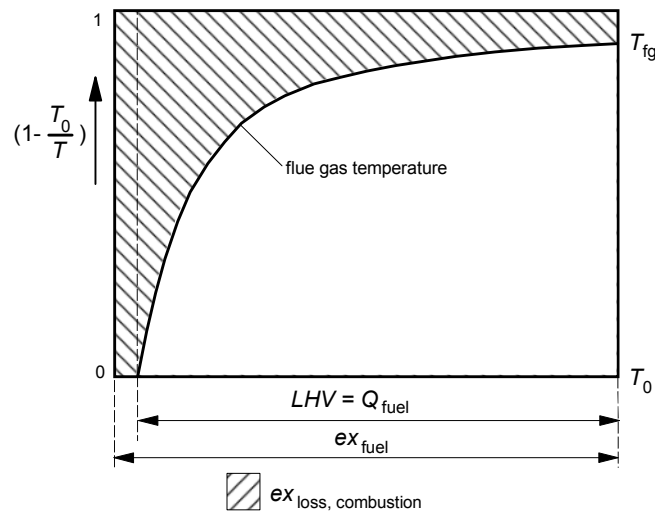


Figure 2.26 Value diagram with the flue gas cooling curve

In a steam boiler heat from the flue gas is transferred to the steam cycle. The feedwater that enters the boiler is heated in the economizer till approximately saturation temperature, evaporated and superheated respectively. In the value diagram shown in Figure 2.27 also the temperature curve of the water/steam in the boiler is depicted. The flue gasses are cooled in the boiler to the temperature  $T_{stack}$  at which they are discharged to the environment. The residual heat from the flue gas is lost. The corresponding exergy loss, the horizontally shaded area in Figure 2.27, is the stack exergy loss which is serious lower than the stack heat loss. The area below the water/steam temperature curve equals the exergy transferred to the steam cycle. Thus, the area between the temperature curves of flue gas and water/steam, the vertically shaded area, is the exergy loss due to heat transfer in the boiler. The steam generated in the boiler is expanded in a steam turbine; the main part of the exergy transferred to steam cycle is

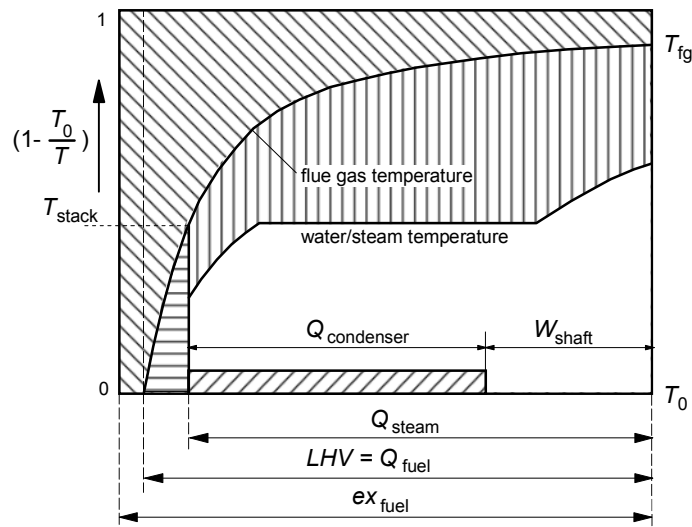


Figure 2.27 Value diagram of a conventional steam cycle power plant

converted into mechanical energy (= 100 % exergy). After expansion the steam is condensed. The condensation heat is transferred to the environment. Water or air are generally used as cooling fluids. The difference between condensation temperature and ambient temperature causes a small exergy loss as indicated in the value diagram. This loss is determined by the temperature increase of the cooling fluid in the condenser as well as the temperature difference between the primary and secondary fluid. The heat of condensation is much higher than the work transferred to the turbine shaft, but because of the low temperature of this heat the exergy is almost negligible. The blank area in the diagram of Figure 2.27 equals the work transferred to the shaft of the steam turbine. It appears that most of the exergy losses are presented quite well in the value diagram of a conventional steam cycle power plant. All losses shown in the value diagram of a conventional power station are losses occurring outside the steam cycle. Additional diagrams as e.g. a value diagram of the feedwater heaters are necessary to show also internal cycle losses. The steam turbine losses cannot easily be shown in value diagrams.

Value diagrams are used also to depict closed cycle as well as open cycle gas turbine processes. An example of an open cycle process is shown in Figure 2.28. Also in this case the internal exergy losses of the gas turbine cycle, like the losses due to friction in compressor and turbine, are ignored. In an open cycle gas turbine heat is transferred to the cycle in the combustion chamber. Air enters the combustion chamber at elevated temperature because of the temperature increase due to

compression. The temperature is raised further in the combustion chamber. The temperature increase in the combustion chamber is represented by the upper temperature curve of Figure 2.28. The area below this curve represents the exergy that is transferred to the gas turbine cycle. The shaded area above this curve, together with the strip at the right side of the diagram due to the difference between the heating value and the exergy of the fuel, equals the exergy loss of combustion. After expansion in the turbine the temperature of the flue gasses is still high (around 500 °C). The lower temperature curve of Figure 2.28 represents the temperature of the flue gas if it is cooled down to ambient temperature. The area below the flue gas cooling curve represents the exergy that is achieved from the turbine exhaust gas. If the flue gas is directly discharged to the environment, this exergy is lost. In stationary applications however the residual heat of the turbine exhaust gasses is normally used to generate steam in a waste heat boiler or heat recovery steam generator. In the case of industrial application waste heat boilers usually generate saturated steam. In the case of large scale power generation with combined cycle plants the heat recovery steam generator produces superheated steam that is expanded in a bottoming steam

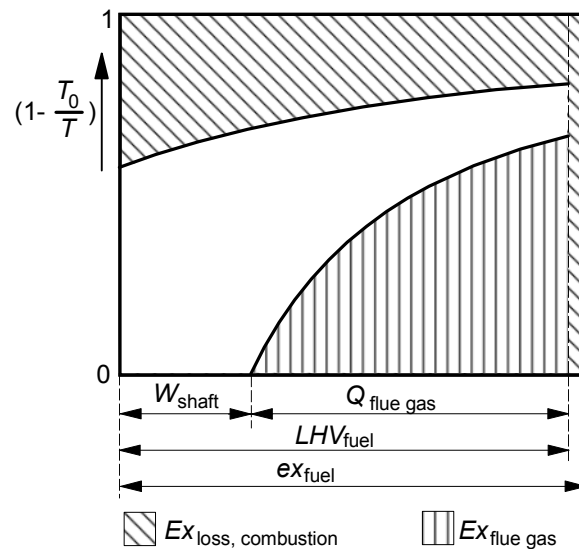


Figure 2.28 Value diagram of an open gas turbine cycle

turbine cycle. Figure 2.29 shows the value diagram of a gas turbine with steam bottoming cycle. The diagram clearly shows the part of the exergy from the off-gases that is recovered under these circumstances.

2.5.4 Exergy flow diagrams

Exergy flow diagrams provide an opportunity to get a rough overview of the exergy losses of a system. They present relative or absolute quantities of exergy flows and losses in a system without relation with process properties like in the value diagram. In principle the exergy flow diagram is similar to the energy flow diagram, but the flows are depicted as exergy flows instead of energy flows. A simple example for a large hot water boiler with a heat output of 500 kW is presented in Figure 2.30. For the purpose of this analysis, the hot water boiler is assumed to consist of a combustion chamber and a heat exchanger, as shown in the system diagram in the middle. The assumed temperatures are depicted also in this diagram. The main processes in the boiler, combustion and heat transfer, are distinguished for this purpose. These two processes are considered also in the exergy flow diagram: an adiabatic combustion process and a process of heat transfer from flue gas to hot water. The overall thermal efficiency of the hot water boiler is supposed to be 0.93. After calculating the exergy of the flue gas after combustion, the exergy increase of the hot water in the heat exchanger and the exergy of the flue gas discharged through the stack, the exergy flow diagram can be sketched. The exergy efficiency of the combustion process is 66.1% and the exergy efficiency of the heat transfer process is 22.3%. Finally, from the 559.2 kW fuel exergy only 81.1 kW is transferred to the water. This results into an overall exergy efficiency of 14.5%. The energy flow diagram is added also to Figure 2.30. This example shows

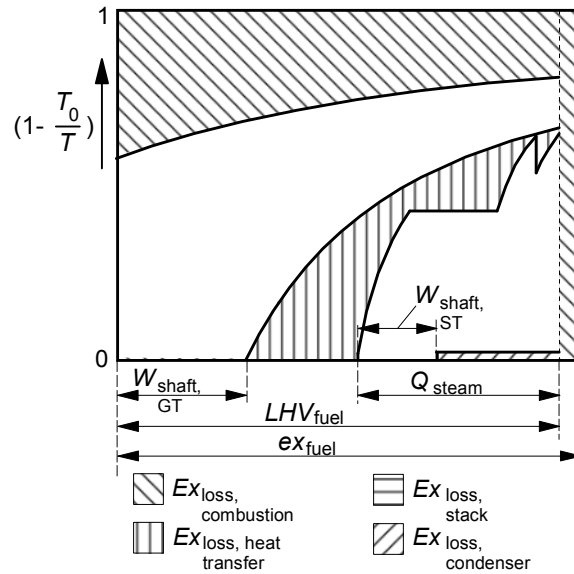


Figure 2.29 Value diagram of a combined cycle plant

the energy flow diagram is added also to Figure 2.30. This example shows

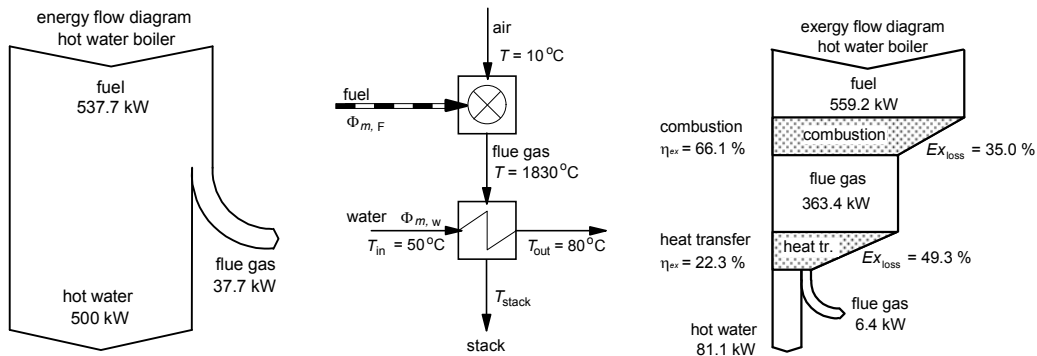


Figure 2.30 Energy flow diagram, system diagram and exergy flow diagram of a hot water boiler

obviously that the evaluation of energy conversion systems based only on thermal values (energy values) can be highly misleading.

In the case of large complex conversion plants it is actually impossible and also not very useful to present all conversion processes separately in the exergy flow diagram. In general, the plant must be split up arbitrarily in a limited number of sub-systems which are presented in the overall exergy flow diagram of the plant. Recycle flows have to be avoided as far as possible to achieve orderly results. If more detailed information is useful, exergy flow diagrams of the various sub-systems can be depicted in addition to the overall diagram. Several exergy flow diagrams of larger systems are presented in the following chapters.

## 2.6 Exergy efficiencies

### 2.6.1 Introduction

Efficiencies are generally used to indicate the performance of processes and systems. As demonstrated before, the thermal efficiency is not a reliable indicator of the thermodynamic performance of energy conversion systems. The true thermodynamic value of a quantity of energy is determined by the exergy value, and therefore, exergy efficiencies will give a true indication of the thermodynamic performance of conversion processes. Exergy efficiencies can be used for different purposes and they can be defined in different ways. The exergy efficiency should compare in principle the actual performance of a process with the ideal performance, actually the performance of the corresponding reversible process. However, it is not easy and sometimes even impossible to define a corresponding reversible process unambiguously. In [2.18] and [2.19] discussions are presented about avoidable and unavoidable exergy losses in apparatuses. But even in this literature alternative definitions for the exergy efficiency of apparatuses have been used. The way exergy efficiencies are defined is primarily determined by the application. That's why in this section three options for the application of exergy efficiencies are discussed:

- exergy efficiencies of energy conversion plants
- exergy efficiencies of apparatuses and sub-systems
- exergy efficiencies of thermal power cycles.

The exergy efficiencies of apparatuses and sub-systems are discussed comprehensively. The efficiencies of apparatuses as defined in this section are applied too in Cycle-Tempo. The definitions are fit to the available information from the various apparatus models. A comprehensive description of these efficiencies is in general necessary for the right understanding of the calculated values.

It is often difficult to judge thermodynamic losses without further reference. Usually a comparison with the thermodynamic performance of specific apparatuses or sub-systems from alternative plants is required to judge the calculated efficiencies correctly. A quick overview of the most important information of the thermodynamic performance of complex plants is achieved by combining exergy efficiencies and exergy flow diagrams. This combination appeared to be very instructive during plant evaluations.

### 2.6.2 Exergy efficiencies of energy conversion plants

The importance of exergy efficiencies for the evaluation of power plants is limited. The generated electricity is the same as the produced exergy. And the exergy of common fuels for electricity production is only slightly higher than the *LHV* (see Equation 2.64 and Table 2.4). Therefore, the difference between the thermal efficiency and the exergy efficiency of power plants is normally not higher than 2 or 3 percentage points. The information achieved by using exergy efficiencies instead of thermal efficiencies does not really provide additional information. In the case of heat generating plants or combined heat and power plants (CHP) the situation is quite different. The exergy of generated heat is normally much lower than the thermal energy and, therefore, the exergy efficiency will in general differ seriously from the thermal efficiency of these plants. If exergy efficiencies of CHP plants are considered, it has to be realized that these plants generate two different products. The economical value of these products will be different even if the exergy values are the same. Market prices of electricity and heat are not determined by their exergy value. If the exergy of electricity and heat are added up to calculate the total exergy efficiency of a CHP plant, this exergy efficiency primarily indicates the extent of the overall thermodynamic losses. In the case of economic evaluations the use of product prices is still necessary.

Efficiencies for plants compare in general the generated product with the source that is needed to generate the product. This will result into the following general equation for exergy efficiencies:

$$\eta_{ex, \text{ plant}} = \frac{Ex_{\text{product}}}{Ex_{\text{source}}} \quad (2.65)$$

In the case of a power plant the generated electricity is the product and the fuel exergy is the exergy source. If the plant generates more than one product as in the case of CHP plants the product exergy usually represents the exergy of the generated electricity and heat. By doing so this equation ignores several exergy flows that enter and leave the system normally. Not considered are for example: the exergy value of materials used to capture harmful components in the off-gasses as well as the products from the capture processes. Furthermore the exergy of exhausted flue gas and the heat rejected by the condenser are considered to be an exergy loss. The exergy efficiency calculated with Equation 2.69 takes into account internal irreversibilities as well as external irreversibilities of a system. For fundamental evaluations it is not really appropriate but it is in agreement with currently used thermal efficiencies.

The use of thermal efficiencies is complicated by the fact that the heating value of a fuel can be defined in two ways: the higher heating value (*HHV*) and the lower heating value (*LHV*). A fuel will have only one value for the specific exergy if it is assumed that the exergy of water vapor at environmental conditions is the same as the exergy of liquid water. In that case there is also one exergy efficiency of an energy conversion plant. If the exergy of water vapor and liquid water are not the same the specific exergy of the fuel depends on the amount of water in the fuel and the assumed condition of the reaction products after combustion. Another problem that complicates the discussions on plant efficiencies is the way the auxiliary power consumption is included in the calculations. In practice the gross efficiency ignores the auxiliary power consumption while the net efficiency takes all auxiliary power into account. The system evaluations in this thesis are not always considering all auxiliaries

necessary to operate an energy conversion plant. In such cases the used net efficiencies will count only the power of the auxiliary equipment included in the system diagram. This is in agreement with the procedures followed by the computer program Cycle-Tempo; if no additional auxiliary powers are specified, the program will calculate the net efficiency using the calculated power for the auxiliary equipment included in the system diagram.

The application of exergy efficiencies will not provide always new insights with regard to the performance of energy conversion plants. But at least it can be seen as a correction or modest improvement of currently used thermal efficiencies.

### 2.6.3 Exergy efficiencies of apparatuses and sub-systems

Exergy efficiencies of apparatuses and sub-systems don't have a useful thermal counterpart. In these cases thermal efficiencies indicate only the thermal losses of the considered system parts. Since the thermal losses are usually estimated based on historic data, the accuracy of thermal loss data is very low in the case of advanced energy conversion systems for which historic data are very limited available.

Exergy losses of the apparatuses and eventually specified sub-systems can easily be calculated if the system calculation is extended with a calculation of the exergy values of all flows of the system flow diagram. For an exergy evaluation of the system it is often sufficient to present these losses as a percentage of the exergy of the source. A presentation of the relative exergy losses clearly shows the contribution of the various apparatuses and sub-systems to the total exergy loss of the system.

In the case of a system optimization, it is in general useful to know to what extent further improvements of apparatuses or subsystems are feasible. To enable a comparison with components of alternative plants with sometimes different capacities, the calculation of exergy efficiencies might be useful. A more detailed evaluation of the exergy efficiency of an apparatus or sub-system can show whether the resulting exergy loss is acceptable or not. In these discussions the search for avoidable and unavoidable exergy losses will become of interest.

Exergy efficiencies of apparatuses and sub-systems can also be useful to check the correctness of process calculations. Unrealistic input data or incorrect assumptions can result into unusual efficiencies. Obviously, incorrect input data are noticed only if the deviations are sufficiently high.

#### Definition of efficiencies

Exergy efficiencies are discussed in the past by several authors like e.g. [2.16] and [2.17]. In fact they all come to the conclusion that the general definition of the exergy efficiency of a system, apparatus or sub-system should be:

$$\eta_{ex} = \frac{Ex_{\text{product}}}{Ex_{\text{source}}} \quad (2.66)$$

A further specification is necessary to use this general definition for specific apparatuses. However, the mentioned literature has presented this specification only for a limited number of apparatuses and processes. For the specification of the exergy efficiency of all apparatuses available in Cycle-Tempo careful consideration appeared to be necessary of the requirements that have to be fulfilled by these efficiencies.

Efficiencies have to be defined such that in principle all values between 0 and 1 are possible; values higher than 1 and lower than 0 should not be possible. Only then the sensitivity for changes of the irreversible processes in the apparatuses is appropriate. Only data that are achievable from the Cycle-Tempo output can be used for the calculation of the efficiencies. The program calculates the thermo-mechanical and chemical exergy of all flows of a system flow diagram. That means that only the exergy of explicitly defined flows in the system diagram can be included in the specified efficiency definitions. The need for additional calculations should be avoided.

To determine the exergy efficiency for a specific apparatus, the exergy of the product and the source must be defined. The problem is, however, that it appears not to be possible to define the product exergy for all apparatuses as available in Cycle-Tempo; e.g. what will be the product of a steam condenser that rejects heat to the environment, or what will be the product of a heat sink. Therefore, initially two different exergy efficiencies have been proposed: the “functional efficiency” which is actually the efficiency as defined before and the “universal efficiency”. In this thesis the functional efficiency will be used as the exergy efficiency and the universal efficiency is used only if the definition of a usual efficiency (“functional efficiency”) is not possible.

The *universal efficiency* is defined as the ratio between the total exergy that leaves the system and the total exergy that enters the system; it is defined as follows:

$$\eta_{Ex, univ} = \frac{\sum Ex_{out}}{\sum Ex_{in}} \tag{2.67}$$

Since:  $\sum Ex_{in} = \sum Ex_{out} + Ex_{loss}$  Equation (2.67) can be written as:

$$\eta_{ex, univ} = \frac{\sum Ex_{in} - \sum Ex_{loss}}{\sum Ex_{in}} \tag{2.68}$$

The universal efficiency can be calculated for all apparatuses, but it doesn't fulfill the requirements as mentioned before. Because very low efficiency values (near to 0) are in general not possible.

To emphasize the difference between the two exergy efficiencies, the *functional efficiency* (Equation 2.66) is written as:

$$\eta_{ex} = \frac{Ex_{source} - Ex_{loss}}{Ex_{source}} \tag{2.69}$$

As  $Ex_{source} \leq Ex_{in}$  it is obvious that

$$\eta_{ex} \leq \eta_{ex, univ}$$

The difference of the two exergy efficiencies can be demonstrated further by considering the exergy flow diagram of a heat exchanger (see Figure 2.31) in which the primary flow is heated by cooling the secondary flow. The heat transfer to the primary flow causes an exergy

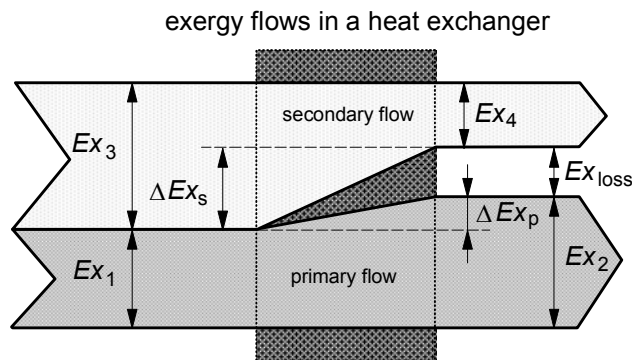


Figure 2.31 Exergy flow diagram of a heat exchanger

## Chapter 2 Exergy analysis

increase of this flow from  $Ex_1$  to  $Ex_2$ ; the exergy increase of the primary flow is considered to be the product of the heat transfer process, because this exergy increase is the desired result of the process. The heat transfer from the secondary flow causes a reduction of the exergy of this flow from  $Ex_3$  to  $Ex_4$ ; this exergy decrease is supposed to be the exergy source of the heat transfer process, because it is the exergy that is used to realize the increase of the primary flow. Then, the exergy efficiencies can be written as:

$$\eta_{ex} = \frac{\Delta Ex_s - Ex_{loss}}{\Delta Ex_s} \quad \text{and} \quad \eta_{ex,univ} = \frac{Ex_1 + Ex_3 - Ex_{loss}}{Ex_1 + Ex_3}$$

From Figure 2.31 it is obvious that  $\eta_{ex} \ll \eta_{ex,univ}$ , and that the value of  $\eta_{ex}$  can vary in principle from 0 to 1. It appears that only a limited part from the exergy that enters the heat exchanger is transferred during the process. That means that a breakdown of the incoming exergy flows into an active part (the source or the product) and a non-active part might be useful. The non-active part is not involved into the heat transfer process and is considered to be a ballast flow.

### Examples of exergy efficiencies of apparatuses

The general efficiency, as presented by Equation 2.66, has to be specified further for specific apparatuses or processes. A specification for each apparatus available in Cycle-Tempo is described in Appendix 3.2. A somewhat extended description is given here for three examples of apparatuses: the turbine, heat exchanger and combustor.

#### *Turbine (type 3)<sup>5</sup>*

The turbine model of Cycle-Tempo is a general model that can be applied for steam turbines, gas turbines, potassium turbines, turbines in organic rankine cycles etc.. Steam turbines in rankine cycles can have one or more extraction points. For the specification of the exergy efficiency of the turbine, a steam turbine with one extraction point is considered. The corresponding Cycle-Tempo system diagram is shown in Figure 2.32. The steam turbine generates shaft power that is transferred to an electrical generator. The generator does not belong to the turbine system. Steam that enters the turbine is expanded to the exhaust pressure; a part of the steam is extracted at a higher pressure. The expansion process converts the thermo-mechanical energy of the steam into mechanical energy delivered by the shaft. The kinetic energy of the turbine exhaust flow is included in the calculation of the enthalpy of the steam at turbine outlet. Therefore, it is not necessary to consider this kinetic energy separately for the exergy calculation. The objective of the expansion process is to generate shaft work, thus, the generated shaft work is supposed to be the product of the turbine process:

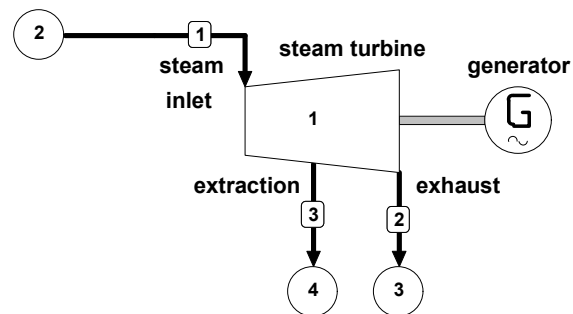


Figure 2.32 Cycle-Tempo system diagram of steam turbine

<sup>5</sup> The type number refers to the numbering of apparatuses in Cycle-Tempo

$$Ex_{\text{product}} = W_{\text{shaft}} \quad (2.70)$$

The shaft work is obtained from the expansion of steam in the turbine. During the expansion process the exergy of the steam is used only partly. At the extraction point and at the turbine exhaust the residual exergy of the steam is not negligible. In the case of a condensing turbine the exergy of the turbine exhaust is lost; useful application is not possible. However, ignoring the exergy of the exhausted steam means that the exergy loss of the condenser is included in the exergy efficiency of the turbine. For the definition of an exergy efficiency that purely represents the quality of the expansion process in the turbine, the efficiency should not be influenced by the quality of other processes. Thus, the exergy source of the turbine should include only the change of the thermo-mechanical exergy of the steam in the turbine. Since the chemical exergy of the working fluid does not change, the change in thermo-mechanical exergy equals the change in total exergy of the steam. By doing so, the exergy efficiency is also appropriate for back-pressure turbine units.

Since the turbine used for this description has more than one outlet, the exergy source must be written as:

$$Ex_{\text{source}} = Ex_{\text{in}}^{\text{tm}} - \sum Ex_{\text{out}}^{\text{tm}} = Ex_{\text{in}} - \sum Ex_{\text{out}} \quad (2.71)$$

Then, the exergy efficiency of the turbine becomes:

$$\eta_{\text{ex, turbine}} = \frac{W_{\text{shaft}}}{Ex_{\text{in}} - \sum Ex_{\text{out}}} \quad (2.72)$$

#### Heat exchanger (types 6 and 12)

In a heat exchanger, the primary fluid is heated by transferring heat from the secondary fluid. A system model of a heat exchanger as considered in Cycle-Tempo is shown in Figure 2.33. The apparatus model can be used for a variety of designs, including co-flow, counter-flow and cross-flow heat exchangers. This high flexibility for the application, however, makes that the user has to check whether the resulting temperature profiles do obey the second law of thermodynamics. The facilities of Cycle-Tempo for drawing  $T, Q$ -diagrams and value diagrams are very helpful in this respect. The purpose of the considered heat exchanger types is in general the transfer of heat to the primary fluid. The heat transfer to the primary fluid will increase the thermo-mechanical exergy of this fluid. Therefore, the increase of the thermo-mechanical exergy of the primary fluid is supposed to be the product of the heat transfer process. As the chemical composition of the fluids in the heat exchanger are not changed, the increase of the thermo-mechanical exergy is the same as the increase of the total exergy, thus:

$$Ex_{\text{product}} = Ex_{\text{p, out}} - Ex_{\text{p, in}} \quad (2.73)$$

The primary fluid is heated by transferring heat from the secondary fluid. This heat transfer will require in general a limited part of the exergy of the secondary fluid at the inlet of the heat exchanger. Therefore the decrease of thermo-mechanical exergy of the secondary fluid in the heat exchanger is supposed to be the exergy source of the heat transfer process. As the

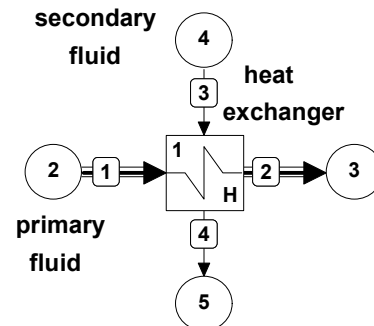


Figure 2.33 Cycle-Tempo system diagram of heat exchanger

## Chapter 2 Exergy analysis

chemical composition does not change during heat transfer, the decrease of thermo-mechanical exergy of the secondary fluid will be the same as the decrease of total exergy, thus:

$$Ex_{\text{source}} = Ex_{s, \text{in}} - Ex_{s, \text{out}} \quad (2.74)$$

Then, the exergy efficiency of the heat exchanger can be written as:

$$\eta_{ex, \text{heat exchanger}} = \frac{Ex_{p, \text{out}} - Ex_{p, \text{in}}}{Ex_{s, \text{in}} - Ex_{s, \text{out}}} \quad (2.75)$$

Heat exchangers can have under specific circumstances more than one inlet for the secondary fluid, e.g. in the case of feedwater preheaters where extraction steam as well as condensate from other preheaters is used to heat the feedwater. Then, the secondary side has more than one inlet; the secondary fluids are mixed in the heat exchanger and leave the apparatus as one single secondary flow. Then, the exergy efficiency becomes:

$$\eta_{ex, \text{heat exchanger}} = \frac{Ex_{p, \text{out}} - Ex_{p, \text{in}}}{\sum Ex_{s, \text{in}} - Ex_{s, \text{out}}} \quad (2.76)$$

In Cycle-Tempo the heat losses of a heat exchanger are included in the energy balance and are therefore included also in the calculated exergy values. Then, the heat losses are automatically included in the exergy efficiency.

### Combustor (type 13)

Figure 2.34 presents a Cycle-Tempo system model of a combustor. Fuel and oxidizer are supplied to the combustor separately. In general, the oxidizer will be air but the specification of other compositions is possible. The combustion process is supposed to be adiabatic. If heat losses have to be considered, as usual in steam boiler models, these losses can be taken into account in the heat transfer system. Ash (or slag) is removed from the combustor at specified conditions by a separate ash

outlet. The thermodynamic effects of the ash removal are included in the resulting energy and exergy balances. The purpose of the combustion process is the generation of a hot gas (flue gas), from which only the thermo-mechanical exergy will be utilized. Therefore, the thermo-mechanical exergy of the hot flue gas is supposed to be the product of the combustion chamber. Fuel and oxidizer are fed to the combustion chamber, often at elevated temperature and pressure. The thermo-mechanical exergy necessary to increase pressure and temperature of fuel and oxidant is not generated by the combustion process. Thus, the thermo-mechanical exergy of fuel and oxidizer must be subtracted from the thermo-mechanical exergy of the hot flue gas. Then, the product of the combustion chamber is written as:

$$Ex_{\text{product}} = E_{\text{flue gas}}^{\text{tm}} - Ex_{\text{fuel}}^{\text{tm}} - Ex_{\text{oxidizer}}^{\text{tm}} \quad (2.77)$$

In principle the chemical exergy of the fuel is used as the exergy source. If the composition of the oxidizer is not exactly the same as the composition of reference air used for the determination of the chemical exergy values, the exergy of the oxidizer will not be zero, and has to be included in the exergy balance of the system. The chemical exergy of the flue gas

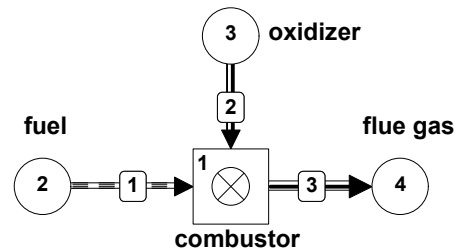


Figure 2.34 Cycle-Tempo system diagram of combustor

flow is discharged to the environment and will not become available as product. Thus, the net available exergy source is:

$$Ex_{\text{source}} = Ex_{\text{fuel}}^{\text{ch}} + Ex_{\text{oxidizer}}^{\text{ch}} - Ex_{\text{flue gas}}^{\text{ch}} \quad (2.78)$$

Then, the exergy efficiency of the combustor is defined as:

$$\eta_{\text{ex, combustor}} = \frac{Ex_{\text{flue gas}}^{\text{tm}} - Ex_{\text{fuel}}^{\text{tm}} - Ex_{\text{oxidizer}}^{\text{tm}}}{Ex_{\text{fuel}}^{\text{ch}} + Ex_{\text{oxidizer}}^{\text{ch}} - Ex_{\text{flue gas}}^{\text{ch}}} \quad (2.79)$$

This definition does not consider the presence of non-combustible components in the fuel that are separated in the combustion chamber in the form of ash or slag. The chemical exergy of these substances is not utilized for the production of heat and must, therefore, be subtracted from the chemical exergy of the fuel. In general, most of the ash and slag is discharged from the gas at high temperature in the combustion chamber. In principle the heat from ash and slag can be utilized; if not, its thermo-mechanical exergy is lost externally and is considered to be an external loss. The ash remaining in the flue gas will leave the combustor as fly ash that will be utilized together with the flue gas. Thus, the thermo-mechanical exergy of the non-combustible solid or liquid components (further indicated as ash) is considered to be a product of the combustion process. Then, if the exergy of non-combustible components cannot be ignored, the exergy efficiency of the combustor becomes:

$$\eta_{\text{ex, combustor}} = \frac{Ex_{\text{flue gas}}^{\text{tm}} + Ex_{\text{ash}}^{\text{tm}} - Ex_{\text{fuel}}^{\text{tm}} - Ex_{\text{oxidizer}}^{\text{tm}}}{Ex_{\text{fuel}}^{\text{ch}} + Ex_{\text{oxidizer}}^{\text{ch}} - Ex_{\text{ash}}^{\text{ch}} - Ex_{\text{flue gas}}^{\text{ch}}} \quad (2.80)$$

In practice, due to incomplete combustion not all fuel will be converted in the combustion chamber. In the ideal case the non-converted fuel will be heated and cooled but does not participate to the conversion process and is only considered to be a ballast flow.

#### 2.6.4 The thermodynamic equivalent temperature of heat transfer

The thermodynamic equivalent temperature of heat transfer has been defined before with Equation 2.5. This temperature is used frequently in this thesis for the evaluation of thermal power cycles. The methods used to calculate the thermodynamic equivalent temperature are derived and discussed in this section.

Heat transfer to or from a fluid flow will in general change the temperature of the fluid; only in the case of phase changes of pure fluids the temperature will remain constant. The exergy of the heat transferred to the fluid can be determined with Equation 2.5:

$$Ex_Q = \int_{\text{in}}^{\text{out}} \left(1 - \frac{T_0}{T}\right) \cdot dQ = \left(1 - \frac{T_0}{\bar{T}}\right) \cdot Q \quad (2.5)$$

The thermodynamic equivalent temperature ( $\bar{T}$ ) is defined such that, if the same amount of heat is transferred to the system at this temperature, the exergy transferred to the system will be the same as in the case of the actual system with varying temperature. This definition will be used to find methods to calculate this temperature.

A system for the transfer of heat to a fluid is shown in Figure 2.35. The exergy balance of the system can be written as:

$$\Delta Ex = Ex_{\text{out}} - Ex_{\text{in}} = Ex_Q - Ex_{\text{loss}} \quad (2.81)$$

## Chapter 2 Exergy analysis

If it is assumed that heat is transferred to the fluid at fluid temperature friction is the only conceivable cause of exergy losses. In energy conversion systems the exergy loss due to friction is usually small and often considered to be negligible. If the exergy loss is ignored, the exergy change of the fluid in the system equals the exergy of the heat that is transferred to the system. Then, combining Equation 2.5 and Equation 2.81 results into:

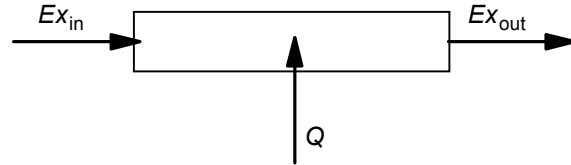


Figure 2.35 System for the transfer of heat to a fluid

$$H_{\text{out}} - H_{\text{in}} - T_0 \cdot (S_{\text{out}} - S_{\text{in}}) = \left(1 - \frac{T_0}{\bar{T}}\right) \cdot (H_{\text{out}} - H_{\text{in}}) \quad (2.82)$$

From Equation 2.82 the following expression for the thermodynamic equivalent temperature of heat transfer is achieved:

$$\bar{T} = \frac{H_{\text{out}} - H_{\text{in}}}{S_{\text{out}} - S_{\text{in}}} = \frac{m \cdot (h_{\text{out}} - h_{\text{in}})}{m \cdot (s_{\text{out}} - s_{\text{in}})} \quad (2.83)$$

If the fluid flowing through the system is supposed to be an ideal gas the changes of enthalpy and entropy can be written as:

$$h_{\text{out}} - h_{\text{in}} = \int_{\text{in}}^{\text{out}} c_p \cdot dT \quad \text{and} \quad s_{\text{out}} - s_{\text{in}} = \int_{\text{in}}^{\text{out}} \frac{c_p}{T} \cdot dT$$

If it is assumed also that the specific heat is constant, these equations can be written:

$$h_{\text{out}} - h_{\text{in}} = c_p \cdot (T_{\text{out}} - T_{\text{in}}) \quad \text{and} \quad s_{\text{out}} - s_{\text{in}} = c_p \cdot \ln \frac{T_{\text{out}}}{T_{\text{in}}}$$

Thus, in the case of ideal gas with constant specific heat Equation 2.83 becomes:

$$\bar{T} = \frac{T_{\text{out}} - T_{\text{in}}}{\ln \frac{T_{\text{out}}}{T_{\text{in}}}} \quad (2.84)$$

This equation can be used to determine  $\bar{T}$  for ideal gases if the specific heat is constant or nearly constant and can be used if only temperatures are known. Equation 2.84 is sometimes used also in the case of fluids that do not really obey the conditions used for this derivation. This can be useful for a rough estimate of  $\bar{T}$  if no high accuracy is required<sup>6</sup>.

### 2.6.5 The internal exergy efficiency of thermal power cycles

The internal exergy efficiency of a thermal power cycle is actually an exergy efficiency of a subsystem. Equation 2.65 has been used to define the exergy efficiencies discussed so far. In that case the exergy efficiency compares the exergy product with the exergy source. This method can be used also to determine the exergy efficiency of a thermal power cycle. But, in the introduction of this chapter (Section 2.6.1) it has been mentioned that the exergy efficiency should indicate preferably the performance ratio of the actual process and the ideal, reversible, process. In the case of thermal power cycles this method is conceivable by

<sup>6</sup> The accuracy in the case of heat transfer to an open gas turbine cycle is discussed in Appendix 4.2

comparing the performance of the actual power cycle with a reversible power cycle operating with the same temperatures of heat transfer to and from the cycle. A comparison of the actual cycle with the true reversible cycle is in general hindered by the fact that the temperatures of heat transfer to and from the actual cycle are often affected by the irreversibilities within the cycle. Nevertheless, the internal exergy efficiency as defined in this section is supposed to be useful in addition to the general exergy efficiency as defined by Equation 2.65. The evaluations in the Chapters 5 and 7 will demonstrate the advantages of this additional exergy efficiency.

For the description of the internal exergy efficiency a general system for the evaluation of thermal power cycles as shown in Figure 3.26 will be used. From the second law of thermodynamics it is known that in the case of a reversible power cycle the thermal efficiency only depends on the temperatures at which heat is transferred to and from the cycle. By applying the thermodynamic temperature (Kelvin temperature) the thermal efficiency of a reversible power cycle is calculated using the following equation:

$$\eta_{th, rev} = \frac{W_{rev}}{Q_H} = 1 - \frac{T_C}{T_H} \quad (2.85)$$

For real (irreversible) systems the efficiency will always be lower because of friction and other losses within the cycle. The effect of all these losses can be included in a so-called internal efficiency ( $\eta_{ex, intern}$ ). Then, the thermal cycle efficiency can be written as:

$$\eta_{th} = \frac{W}{Q_H} = \eta_{ex, intern} \cdot \left( 1 - \frac{T_C}{T_H} \right) \quad (2.86)$$

The Equations 2.85 and 2.86 show that the internal efficiency is actually defined as:

$$\eta_{ex, intern} = \frac{W}{W_{rev}} \quad (2.87)$$

This means that the internal efficiency is defined as the ratio of two amounts of work. Therefore, it can be seen as an exergy efficiency. The internal exergy efficiency is a true indicator of the thermodynamic quality of a power cycle or a combination of power cycles. Heat transfer to and from a power cycle does not occur in general at constant temperatures. In that case thermodynamic equivalent temperatures have to be used to calculate the thermal efficiency of the thermal power cycle. Then, the general equation for the efficiency of thermal power cycles becomes:

$$\eta_{th} = \eta_{ex, intern} \cdot \left( 1 - \frac{\bar{T}_C}{\bar{T}_H} \right) \quad (2.88)$$

This equation can be used for a single power cycle as well as for combined cycles. In the case of combined cycles the effect of the exergy loss due to the heat transfer from the high temperature cycle (the topping cycle) to the low temperature cycle (the bottom cycle) is included in the internal exergy efficiency.

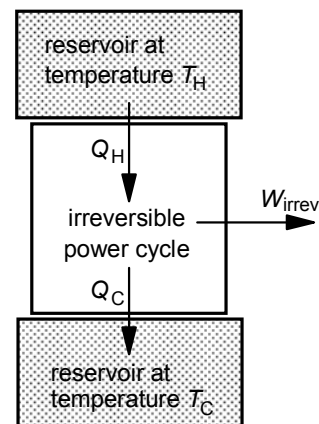


Fig. 2.36 Thermal power cycle operating between two heat reservoirs at different temperatures

### 3 OPTIONS FOR FUTURE ENERGY SYSTEMS

#### 3.1 Introduction

It has been mentioned in Chapter 1 that this thesis will primarily focus on the third step of the “trias energetica”. Comprehensive discussions with regard to possibilities to reduce the thermodynamic losses of conversion systems for the generation of power and combined heat and power are presented in the Chapters 4 to 7. In this chapter various options for future energy systems are discussed globally in order to emphasize the importance of higher conversion efficiencies. It will be demonstrated that also in the case of energy systems based on renewable sources higher conversion efficiencies are necessary to make the higher costs affordable. This chapter can be seen as an extended and updated version of a conference paper [3.1] presented before.

The application of wind and solar energy is hindered by the fact that the costs of conversion into useful energy (power or heat) are relatively high. Also the generated power does not match quite well with the energy demands. In the case of high contributions of wind and solar additional measures are required to match generation and demand. This match can be improved by controlling the energy demand as intended by the application of so-called smart grids or intelligent grids. Some first investigations in this area have started recently but it is not clear yet to what extent these technologies are able to eliminate the mismatch between generation and demand. It is very likely that the large scale use of wind and solar energy will require the application of back-up systems or energy storage. Energy storage, in particular the storage of electricity and heat, is very expensive. Only the storage of solid, liquid or gaseous fuels is affordable if large scale storage is needed. In that case of renewable sources energy must be converted first into an appropriate fuel that must be converted afterwards into the demanded energy (electricity, heat or transport fuel). But even in the case of storage systems that need no additional conversion, charging and discharging as well as losses from the store will cause energy loss. The costs of energy systems is determined highly by the costs of the plants for the primary conversion. Reduction of the specific costs as well as the required power is required to make these costs affordable. Minimization of the thermodynamic losses will contribute to the economic feasibility of energy systems based on renewable sources. Various options for such energy systems are discussed in Section 3.2. The conclusions of that section are based on studies made in the past which are summarized in Appendix 3.1. These studies show that the generation of heat, and first of all the generation of LT heat for space heating, highly determines the overall thermodynamic losses and costs of the considered systems. A rough evaluation of some alternatives for the production of heat is given in Section 3.4. This evaluation shows that the highest savings are achieved by the application of different technologies for the generation of heat. In Section 3.3 possibilities for improving the efficiency of power generation are discussed roughly.

## 3.2 The application of renewable energy sources

### 3.2.1 Introduction

The introduction of renewable energy sources in the Netherlands was studied by the Energy Systems group of the TU Delft during the years 1983-1988 on request of the ministry of economic affairs. The results are useful for this thesis but unfortunately they have never been published before. Only some results have been used for [3.1]. Therefore, a comprehensive summary is presented in Appendix 3.1. At the start the study focused on the application of wind and solar energy in combination with hydrogen as the secondary fuel at the time that oil and natural gas are no longer available for large scale use. It was supposed that this will be the case around the year 2040. From the current fuels only coal and uranium were supposed to be available in 2040. Total costs and emissions should be used primarily to indicate the attractiveness of system alternatives.

The evaluations are made for the energy supply of the Netherlands. The considered energy system was defined as the total system necessary for the conversion, transport and storage of energy within the Netherlands in between the current locations at which imported fuels are available and the consumers of energy. In Figure 3.1 the system is schematically presented with all optional primary energy sources for large scale application. The evaluation was initially based on data of the year 1980 for the energy demand and for wind and solar data. Hourly averaged data were used for the system calculations. For the last evaluations demand data have been modified with the purpose to have estimated data for the year 2040. The effect of the modified demand data on the attractiveness of the evaluated systems appeared not to be really significant.

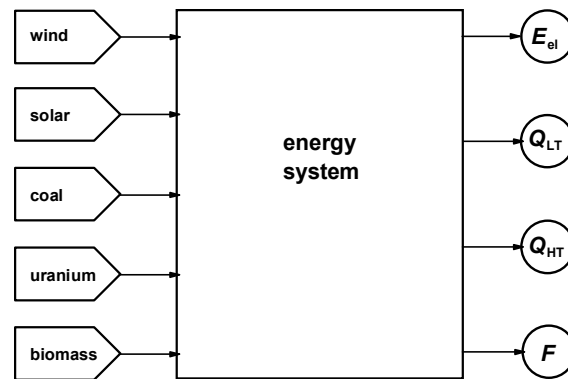


Figure 3.1 Energy system

### 3.2.2 Renewable sources

Biomass has not explicitly been considered for the system evaluations. In the eighties it was not clear whether biomass would be accepted as a renewable energy source. Today biomass is expected to be an important source of renewable energy for the future; but the available biomass from the Netherlands is far from sufficient for the Dutch energy supply. In [3.2] the available biomass for energy conversion was estimated to be 125 PJ in 2009 whereas the total energy demand (electricity, heat and transport fuel) is in the order of 2000 PJ. It should be possible to increase the amount of biomass for energy conversion, but it is likely that in the future the cultivation of all kind of plants will be necessary first of all for food and more valuable industrial products. But even then the residues from these processes might become available for energy conversion. A realistic estimate of the available amounts of

### Chapter 3 Options for future energy systems

biomass for energy conversion in the future is impossible at the moment. Just a policy focusing on maximization of the available biomass for energy conversion might be advisable.

For the conversion of biomass roughly the same technologies as for the conversion of other solid fuels are conceivable. Solid fuels like coal are primarily combusted for the generation of heat that can be converted further into power. The technologies for the conversion of coal into secondary gaseous or liquid fuels are available but economically feasible only in the case of very high prices for crude oil and natural gas. For the same reasons biomass is primarily combusted today. But the conversion into secondary fuels is supposed to be an important option for the future. In principle the same conversion processes as for the conversion of coal can be used for the conversion of biomass into secondary fuels. The term biomass is used for a large variety of materials from clean wood to purely waste. The properties of these materials will be very different and the development of more appropriate conversion processes based on e.g. gasification, pyrolysis, extraction, digestion or fermentation is going on. Today it is not clear what combination of biomass materials and conversion processes will become the most successful for the future. But it is obvious that there is a strong need for processes that are able to generate secondary fuels at affordable costs from types of biomass that can be made available abundantly.

Costs and efficiencies of biomass conversion processes are roughly of the same order as the processes for the conversion of coal<sup>1</sup>. In general the capital costs of biomass conversion systems are higher and the efficiencies lower. The differences are primarily determined by the lower heating value and the higher water content of the fuel. Further optimization of the biomass conversion processes might cause further reductions of the differences between biomass and coal. The studies summarized in Appendix 3.1 show that an energy system for the Netherlands based only on coal as the primary fuel results in significant lower total yearly costs than systems based only on wind turbines or photovoltaic generators. It is supposed that the total yearly costs of systems based on biomass will not be much higher than the costs of coal fuelled systems. Thus, from the renewable fuels considered for large scale use, biomass will be the most attractive.

The application of wind and solar energy appeared to be much more expensive than coal and it is expected that they will also be much more expensive than biomass. The higher costs of the systems are caused not only by the costs of the wind turbines and the photovoltaic generators but also by the costs of systems necessary to match the generated and demanded powers. Even very optimistic assumptions regarding the capital costs of photovoltaic generators were not able to make these generators more attractive than wind turbines. The study shows that the total yearly costs are roughly doubled if photovoltaic generators are used instead of wind turbines. In both cases renewable sources have replaced fossil fuels completely. The difference between solar and wind is primarily caused by the higher yearly load factor of the wind turbines and lower seasonal fluctuations of wind energy. The applied data resulted in a load factor of the wind turbines of 25.3% and a load factor of the photovoltaic generators of 12.6%. During winter time the energy demand of the Netherlands

---

<sup>1</sup> This statement is right only within the framework of the system evaluations presented in Appendix 3.1. Because of the limited accuracy of these evaluations only differences higher than at least 30 to 40% are considered to be significant.

is higher than during the summer period. But the power generation by the photovoltaic generators is highest in the summer period and lower during winter time. Power generation by the wind turbines does not show significant fluctuations of the seasons. Thus, in the case of photovoltaic generators the need for energy storage is much higher. If the power of the photovoltaic generators or the wind turbines is higher than the electricity demand and the surplus electricity is used to generate a secondary fuel, the differences between wind and solar energy will also have consequences for the systems that convert electricity into the secondary fuel. If hydrogen is used as the secondary fuel and electrolysis plants are used to convert electricity into hydrogen, the large difference between actual generated and demanded electricity appears to be a serious disadvantage in the case of photovoltaic generators. The combination of photovoltaic generators and electrolysis plants appears to be very expensive.

Other options for the use of solar energy is the application of thermal solar power plants of solar collectors for the generation of LT heat. Thermal solar power plants have not been considered in the studies presented in Appendix 3.1. During the eighties available information on technology, operation modes and costs was not sufficient to make useful estimates of the required input data. Today application of this technology in the Netherlands does not seem to be very likely. Application of solar collectors was considered for the generation of LT heat. Cost data of this technology as used for this study were much more realistic than the data used for photovoltaic generators. This might have been the reason that the study has shown a strong increase of the total yearly costs if hydrogen fuelled boilers were replaced by solar collectors for the generation of LT heat. Heat storage in hot water tanks was considered to balance daily as well as seasonal fluctuations. Large scale heat storage was considered to balance seasonal fluctuations. With the considered cost data large scale heat storage appeared not to be attractive. It should be mentioned that only straightforward systems have been considered. More sophisticated solutions of aquifers for the storage of heat and cold eventually in combination with heat pumps are not considered.

### 3.2.3 System configurations and conversion technologies

For the conversion of the energy from the primary sources into demanded energy quite a number of conversion and storage systems are available. In Appendix 3.1 various system configurations and conversion technologies are considered. The evaluated configurations and technologies are primarily determined by the choice of primary energy sources and secondary fuel. Alternative technologies for one specific energy conversion process are in general direct competitors and it is not expected that they will cause significant differences in holistic system evaluations. The generation of heat and in particular LT heat, however, appeared to be an exception in this respect. LT heat can be generated by applying very different technologies e.g. by the combustion of a secondary fuel in hot water boilers or the application of electrical driven compression heat pumps, CHP systems or solar collectors. Unfortunately a comprehensive evaluation of the various technologies for the generation of LT heat was not explicitly done in this study. Therefore, conclusions have to be drawn with reservation. More specific evaluations of heat pump applications and the use of combined heat and power are presented in Section 3.4 and Chapter 7. The attractiveness of hot water boilers using a secondary fuel depends primarily on the actual fuel costs. If the fuel is generated by an expensive system, as is the case with hydrogen, the actual costs of the fuel are high.

## Chapter 3 Options for future energy systems

Furthermore, the thermodynamic efficiency of hot water boilers is very poor (less than 15%). From the exploring system studies it appeared that the application of heat pumps is much more attractive than the combustion of hydrogen. But general application of heat pumps will require extension of the grid for electricity transport and distribution. However, the extra costs for the extension of the grid were not included in the exploring studies. It is not expected, however, that these additional costs will cancel out the advantages of heat pump applications. The application of solar collectors is primarily depending on the specific costs of the system including the required heat storage. With the used cost data, representing the costs at the time of evaluation, solar collectors appeared not to be very attractive.

### 3.2.4 Secondary fuel, transport, distribution and storage of energy

From the studies presented in Appendix 3.1 it appeared that type of fuel selected as the secondary fuel has a significant effect on the total yearly system costs. Systems with secondary fuels from coal have resulted in serious lower total yearly costs than hydrogen based systems. It was assumed that coal can be converted directly into gaseous or liquid hydrocarbon fuels. In comparison with hydrogen the generation of secondary fuels from coal is less expensive and more efficient. If biomass has to be used instead of coal as the primary fuel, the same system configuration can be used but the specific costs of the conversion processes will be higher and the conversion efficiencies will be lower. It is expected that the costs of gaseous and liquid fuels from biomass can be of the same order as the costs of the fuels from coal. Thus, it is expected that also systems based on hydrocarbon fuels from biomass are less expensive than hydrogen based systems.

The high costs of systems based on hydrogen are primarily caused by the thermodynamic losses as well as the high capital costs of the conversion equipment of the conversion chain for the generation of hydrogen. Therefore hydrogen will be used on large scale only if very cheap and efficient methods for the generation of hydrogen become available. At the moment the use of hydrocarbon fuels from biomass is expected to be more attractive than the application of pure hydrogen (see also [3.3]). But if the available biomass is not enough for the required fuel production hydrogen has to be considered too. The application of hydrocarbon fuels also have their disadvantages. Surplus power from wind turbines and photovoltaic generators can be converted directly into hydrogen by using electrolysis plants. In the case of hydrocarbon fuels application of surplus power is not possible, which might limit the application of wind and solar. Thus, systems using hydrogen as the secondary fuel are more flexible with regard to the installed power of wind turbines and photovoltaic generators.

The calculated total costs for transport and distribution of the considered energy carriers are in general not higher than 10 to 20% of the total yearly costs. These costs are dominated by the costs for transport and distribution of electricity. It appears that the costs for transport and distribution of energy cannot be ignored, but on the other hand they are also not really determining and will have little effect on the choice of a secondary fuel.

### 3.2.5 The importance of high system efficiencies

The system calculations presented in Appendix 3.1 have demonstrated clearly the importance of high overall system efficiencies, not only for the case of systems based on

fossil fuels or biomass, but even more for systems based on renewable sources. Assuming the given energy demands, the power needed for the primary conversion processes (power plants or power generators using renewable energy) is determined by the efficiencies of the various processes necessary for the conversion and storage of power into the demanded energy. The costs of the primary conversion processes are determining the total yearly costs usually more than 50%. Therefore, high efficiencies of conversion and storage systems are very important to limit the costs of the primary conversion processes and to achieve affordable total yearly costs. Thus the need for high efficiencies of the conversion processes is true for all kinds of systems using fossil fuels, biomass, wind or solar energy.

### 3.3 Possibilities for higher system efficiencies

After the selection of primary energy sources the overall system efficiency is primarily determined by the chosen system configuration and the performance of the individual conversion processes. It is obvious that high efficiencies of the individual conversion processes are a prerequisite to achieve high overall conversion efficiencies. In the systems as presented in Appendix 3.1 a variety of conversion processes have been considered. An overview of the considered conversion processes is presented in the Tables 2, 6 and 10 of the appendix. In general the conversion of a fuel into heat (LT or HT heat), the conversion of a primary or secondary fuel into power and the conversion of a primary fuel into a secondary fuel will cause relatively high thermodynamic losses.

The conversion factors in the tables are representing usual thermal efficiencies. The thermal efficiency of hot water boilers are high, around 90%. However, the true thermodynamic efficiencies (exergy efficiencies) are much lower as will be demonstrated in Chapter 7. In that chapter also options to reduce of the thermodynamic losses of heat generation are discussed. In the case of power generating plants the thermodynamic efficiencies are almost the same as the thermal efficiencies. The before mentioned tables show that thermal efficiencies of power plants are roughly in the range of 40 to 60%. The origin of the thermodynamic losses as well as possibilities to improve the efficiencies of power plants are discussed in the Chapters 4, 5 and 6. In Chapter 4 also a short discussion will be dedicated to the losses of the conversion of primary fuels into secondary fuels. Obviously higher efficiencies of power generation are necessary to achieve more efficient energy systems. Characteristics and limitations of thermal power cycles are discussed in Chapter 5. Finally, Chapter 6 shows how efficiencies up to 80% and even higher are conceivable by the application of high temperature fuel cells with natural gas as the primary fuel. Similar systems can be used for the conversion of solid fuels, but the preceding conversion of the solid primary fuel into secondary gaseous fuel will cause additional thermodynamic losses resulting into significant lower plants efficiencies.

The overall system efficiency depends to a large extent on the efficiency of the heat generation processes. For economic reasons hot water and steam boilers are primarily used today for the generation of heat. The thermodynamic efficiency of these boilers, and in particular hot water boilers, is very poor. As the efficiency of a boiler is primarily determined by the conditions of the heated fluid, it is impossible to achieve significant improvements without the use of alternative technologies. Even the so-called high efficiency hot water

### Chapter 3 Options for future energy systems

boilers with thermal efficiencies of more than 100% if based on the *LHV* have thermodynamic efficiencies of roughly 10 to 15%. The application of lower water temperatures to enable higher thermal efficiencies might even cause a reduction of the thermodynamic efficiency of the boiler. Various alternative technologies for the generation of heat, like CHP, heat pumps, solar collectors etc. are available today. Unfortunately, in many cases they appear not to be economically attractive. In the Netherlands large CHP plants are applied for district heating systems and industrial plants; smaller systems are in use for the heating of buildings and greenhouses. Stimulation by the government has resulted in a serious increase of the total CHP power in the Netherlands. The system calculations in Appendix 3.1 did indicate that electrical driven compression heat pumps can be attractive for the generation of LT heat if only more expensive secondary fuels are available for the combustion in hot water boilers. Finally it appears that the application of alternative options depends on the actual economic conditions.

Obviously the highest savings of primary fuel are achievable by the application of solar collectors for the generation of LT heat. The unfavorable mismatch between generation and demand of LT heat requires the storage of LT heat if no back-up facilities are involved.

This hinders the economic attractiveness. The application of CHP or heat pumps appeared to be more attractive but only limited savings of primary fuel are achievable. A rough estimate of the maximum achievable

	Yearly energy consumption	Relative values
Electricity	309 PJ/a	0.274
LT heat	429 PJ/a	0.381
HT heat	389 PJ/a	0.345
Total energy demand	1127 PJ/a	1.000

savings with CHP and heat pumps is presented in the following section. In these evaluations the system costs are not considered.

#### **3.4 The effects of alternative options for the generation of heat**

The effects of CHP and heat pumps application are indicated roughly by the evaluation of a number of systems for the generation of electricity and heat for a hypothetic country. For the purpose of this evaluation the values of the total yearly demands of electricity, low temperature heat and high temperature heat are taken from Appendix 3.1. The energy demands used for the calculations do represent estimated values for the Netherlands in the year 2040. The values are shown in Table 3.1. It has to be emphasized that the evaluation is only an attempt to discuss the effects of different technologies for the generation of heat and does not reflect the real situation in a specific country. But the data are not far away from the conditions in the Netherlands. For a fair comparison of the different technologies it is assumed that only natural gas is used for the generation of electricity and heat. It is assumed for simplicity that only one kind of plant is used for each of the conversions. An overview of the considered system cases is presented in Table 3.2. Case 1 (reference)

In the reference system (case 1A) electricity is generated by power plants, LT heat for space heating and hot water services by hot water boilers and HT heat for industrial heating

purposes by steam boilers. The respective performance data of the conversion plants are presented in Table 3.3. The standard performance values are supposed to represent the status of today (Case 1A), while the improved performance data are representing values that perhaps will be achieved in the future (Case 1B). The calculated yearly energy input and output of the conversion systems are shown in Table 3.5. The total yearly fuel consumption of Case 1A (the reference system with standard performance) is:

$$E_{F, \text{total, ref}} = 1.328 \times E_{\text{demand}}$$

The diagram of Figure 3.2 shows the relative sizes of the amounts of energy in a single bar. The grey parts at both ends of the bar represent the energy losses; at the left the losses of electricity generation at the right the total energy loss of heat generation (the losses of LT heat generation and HT heat generation).

True thermodynamic losses, however, are shown by the diagram in Figure 3.3. In this diagram the exergy fraction of the energy demands as well as the necessary fuel is plotted on the vertical axis. The exergy factor of electricity is 1.0, the exergy factor of natural gas (Slochteren quality) 1.040 and the exergy factors of LT and HT heat are supposed to be 0.108 and 0.319 respectively. The exergy values of heat are based on the assumed temperatures of

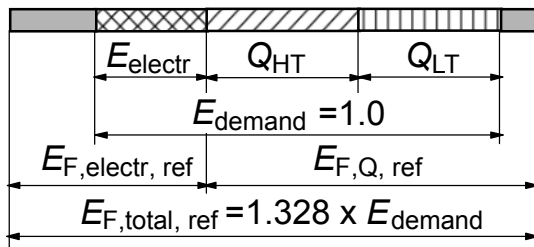


Figure 3.2 Energy demand and fuel energy of Case 1A

the generated hot water ( $\bar{T} = 323.15 \text{ K}$ ) and steam ( $\bar{T} = 423.15 \text{ K}$ ) and an environmental temperature of  $288.15 \text{ K}$ . The total area of the diagram in Figure 3.3 represents the fuel exergy, the cross shaded area the exergy of the demanded electricity, the slantly shaded area the exergy of the demanded HT heat and the vertical shaded area the exergy of the demanded low temperature heat. The grey area, the

*Table 3.2 Overview of cases*

System	Conversion systems	performance	
		Standard	Improved
Reference	Power plants for $E_{\text{electr}}$ Hot water boilers for $Q_{\text{LT}}$ Steam boilers for $Q_{\text{HT}}$	<u>Case 1A</u>	<u>Case 1B</u>
CHP for $Q_{\text{LT}}$	CHP for $E_{\text{electr}}$ and $Q_{\text{LT}}$ Hot water boilers for $Q_{\text{LT}}$ Steam boilers for $Q_{\text{HT}}$	<u>Case 2A</u>	<u>Case 2B</u>
CHP for $Q_{\text{HT}}$	CHP for $E_{\text{electr}}$ and $Q_{\text{HT}}$ Hot water boilers for $Q_{\text{LT}}$ Steam boilers for $Q_{\text{HT}}$	<u>Case 3A</u>	<u>Case 3B</u>
HP for $Q_{\text{LT}}$	Power plants for $E_{\text{electr}}$ Heat pumps for $Q_{\text{LT}}$ Steam boilers for $Q_{\text{HT}}$	<u>Case 4A</u>	<u>Case 4B</u>
HP for $Q_{\text{LT}}$ CHP for $Q_{\text{HT}}$	Power plants for $E_{\text{electr}}$ Heat pumps for $Q_{\text{LT}}$ CHP for $E_{\text{electr}}$ and $Q_{\text{HT}}$	<u>Case 5A</u>	<u>Case 5B</u>

## Chapter 3 Options for future energy systems

difference between the exergy of the fuel and the exergy of the demanded energy, represents the overall exergy loss. Obviously the high exergy loss is primarily caused by the generation of heat. The calculated exergy efficiency, the ratio of the exergy of the generated energy and the exergy of the required fuel, is only 0.308 for the Case 1A. The calculated results are shown in Table 3.4. The table also shows the results for Case 1B, the reference case with the supposed improved performance of the conversion plants. The higher efficiencies of these plants reduces the total fuel consumption with almost 17% compared to the reference case (Case 1A). The overall exergy efficiency increases to 0.369.

		standard	improved
Power plants	$\eta_{th, electr}$	0.55	0.80
Hot water boilers	$\eta_{th, Q_{LT}}$	0.90	1.0
Steam boilers	$\eta_{th, Q_{HT}}$	0.85	0.90
CHP for $Q_{LT}$	$\eta_{th, CHP, electr}$	0.55	0.80
	$\eta_{th, CHP, Q_{LT}}$	0.35	0.20
CHP for $Q_{HT}$	$\eta_{th, CHP, electr}$	0.40	0.60
	$\eta_{th, CHP, Q_{HT}}$	0.45	0.30
Heat pumps	$COP_{th, Q_{LT}}$	3.0	4.0

	A (standard performance)			B (improved performance)		
	$\frac{E_{F, total}}{E_{demand}}$	$\frac{E_{F, total}}{E_{F, total, ref}}$	$\eta_{ex, overall}$	$\frac{E_{F, total}}{E_{demand}}$	$\frac{E_{F, total}}{E_{F, total, ref}}$	$\eta_{ex, overall}$
Case 1	1.328	1.0	0.308	1.106	0.833	0.369
Case 2	1.134	0.854	0.360	1.038	0.782	0.394
Case 3	1.152	0.867	0.355	1.068	0.804	0.383
Case 4	1.136	0.855	0.360	0.845	0.636	0.484
Case 5	0.936	0.705	0.436	0.793	0.597	0.515

#### Case 2 (maximum use of CHP for LT heat)

The poor thermodynamics of Case 1 are primarily due to the low exergy efficiency of the boilers, first of all the hot water boilers. For Case 2 it is assumed that electricity will be generated by CHP (Combined Heat and Power) plants that generate LT heat. It is arbitrarily assumed that the generation of heat will not affect the generation of electricity; the electrical efficiency of the CHP plants then will be 0.55, the same as the efficiency of the power plants.

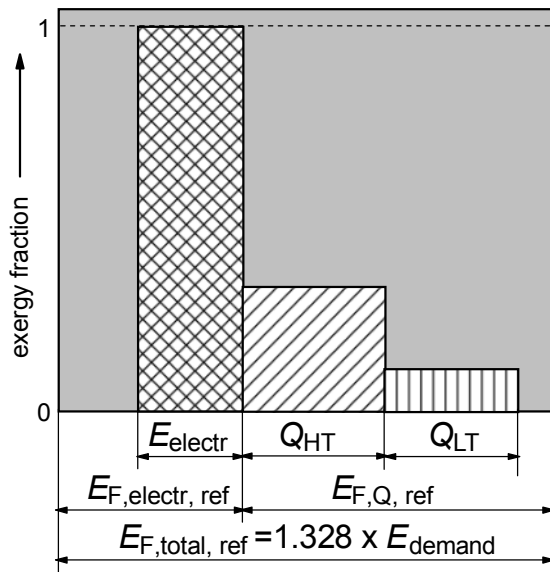


Figure 3.3 Exergy demand and fuel exergy of Case 1A (reference)

The total efficiency of the CHP plants is supposed to be 0.90, the same as the efficiency of the hot water boilers. This results into a heat efficiency ( $\eta_{th, CHP, Q_{LT}}$ ) of 0.35 for the CHP plants. With these data the CHP plants are only able to generate 46% of the demanded LT heat. The remainder is supposed to be generated by conventional hot water boilers. All HT heat is generated by steam boilers. The results are presented in Figure 3.4 and Table 3.5. The LT heat generated by the CHP plants is shown at the left of the diagram, the LT heat generated by the hot water boilers is shown at the right. The application of CHP for the generation of LT heat in this case will reduce the total fuel consumption with almost 15% (see Table 3.4)

and results in an overall exergy efficiency of 0.360. If the improved performance data of the conversion plants are used (Case 2B) the fuel consumption is reduced with almost 22% and an overall exergy efficiency of 0.394 is achieved. The improvement of the overall efficiency is mitigated by the fact that only 18% of the demanded LT heat is generated by the CHP plants. The generated LT heat is lower than in the Case 2A because of the higher electrical efficiency of the CHP plants.

#### Case 3 (maximum use of CHP for HT heat)

If all electricity is generated by CHP plants that generate HT heat, more heat can be generated in coproduction because of the lower electrical efficiency (0.40) of these CHP plants. With the assumed performance data ( $\eta_{th, CHP, electr} = 0.40$  and  $\eta_{th, CHP, Q_{HT}} = 0.45$ ) these plants generate 89% of the demanded HT heat. The remainder of the HT heat demand is supposed to be generated by conventional steam boilers (see Table 3.5). LT heat is generated by hot water boilers as in Case 1. The overall exergy efficiency is 0.355 (see Table 3.4). This is almost the same as for Case 2A. Application of the improved performance data (Case 3B) limits the heat generation by the CHP plants to 40% of the HT heat demand. Nevertheless the total fuel consumption is almost 20% lower than for the reference (Case 1A) and the exergy efficiency becomes 0.383. Apparently the

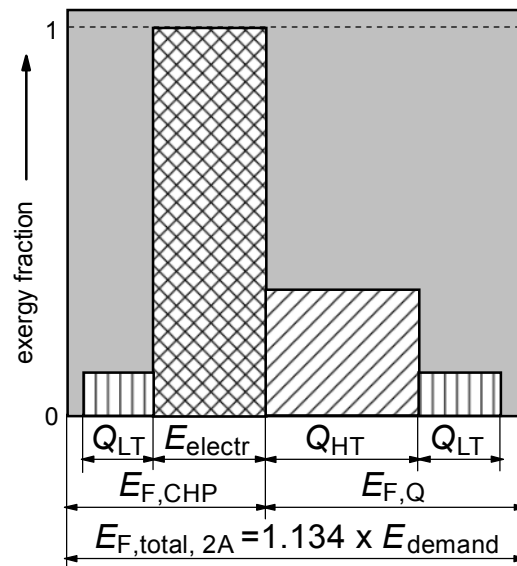


Figure 3.4 Exergy demand and fuel exergy of Case 2A

### Chapter 3 Options for future energy systems

differences between the Cases 2 and 3 are rather limited; the results demonstrate that it does not really matter whether CHP plants are used for the generation of LT heat or HT heat.

#### Case 4 (maximum use of heat pumps)

If it is assumed that all LT heat is generated by electrical driven compression heat pumps, a substantial increase of the generated electricity is required. The horizontal shaded area in Figure 3.5 represents the additional electric power generated to drive the heat pumps. The fuel consumption of the power plants increases proportionally as shown in Table 3.5. HT heat is generated by conventional steam boilers. In this case fuel is needed only for the generation of electricity and HT heat; no additional fuel is necessary for the generation of the LT heat. From the results in Table 3.4 it appears that the overall exergy efficiency of Case 4A is almost the same as of Case 2A; thus, with the assumed performance data the application of electrical driven compression heat pumps results almost into the same overall efficiency as the application of CHP for the generation of LT heat. But comparison of Case 4B and Case 2B, the same cases with the considered improved performance, shows that the overall efficiency of Case 4B is significantly higher. Case 4B benefits twice from the improved performance data, because the fuel consumption necessary for the generation of LT heat is reduced by the higher efficiency of electricity generation as well as by the higher value of the COP of the heat pumps. The improved performance data on the other hand have only a limited effect on Case 2; the higher electrical efficiency of the CHP reduces the heat generation by the CHP plants and therefore more LT heat must be generated by the hot water boilers.

#### Case 5 (maximum use of heat pumps in combination with CHP for HT heat)

The application of electrical driven heat pumps requires the generation of more electricity. The Cases 2 and 3 have shown that the electricity demand limits the power of the CHP plants and thus the advantages of CHP. Therefore the combination of heat pumps for LT heat and CHP for HT heat appears to be very attractive. If the standard performance data are considered, all HT heat can be generated by the CHP plants (see Table 3.5 and Figure 3.6). In that case the HT heat demand limits the maximum power generated by the CHP plants; only 77% of the needed electricity can be generated by the CHP plants. The remaining 23% is generated by power plants. If the improved performance data for the conversion plants are applied for these calculations, it appears that all electricity can be generated by the CHP plants but then the CHP plants are only able to generate 53% of the demanded HT heat. The remaining 47% are generated by steam boilers which mitigates the benefits of this case. The calculated results as presented in Table 3.4 show that the total fuel consumption of Case 5A is

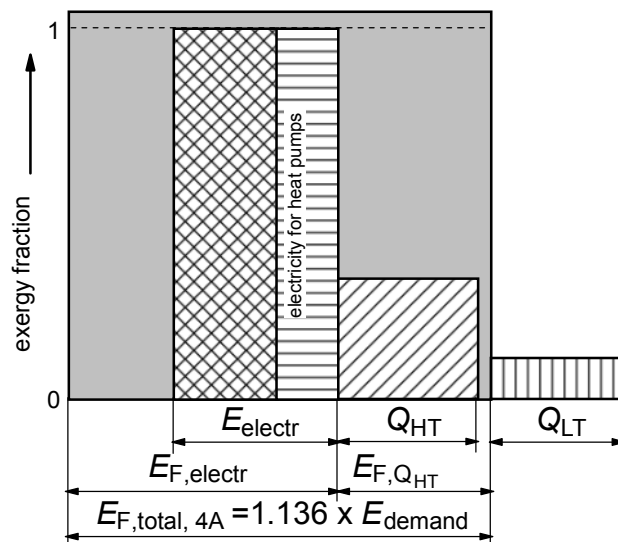


Figure 3.5 Exergy demand and fuel exergy of Case 3A

significant lower than the total fuel consumption of the other cases; the total fuel consumption is only 70.5% of the total fuel consumption of the reference case, Case 1A. Due to the application of the heat pumps, the energy of the fuel is even lower than the total energy demand. The overall exergy efficiency of Case 5A is 0.436. Application of the improved performance data of the conversion plants results in an exergy efficiency of 0.515 (Case 5B).

*Table 3.5 Yearly energy input and output of conversion plants*

Case	1A	1B	2A	2B	3A	3B	4A	4B	5A	5B
Power plants										
fuel (PJ/a)	562	386	-	-	-	-	822	520	193	-
electricity (PJ/a)	309	309	-	-	-	-	452	416	106	-
Hot water boilers										
fuel (PJ/a)	477	429	258	352	477	429	-	-	-	-
LT heat (PJ/a)	429	429	232	352	429	429	-	-	-	-
Steam boilers										
fuel (PJ/a)	458	432	458	432	48	260	458	432	-	201
HT heat (PJ/a)	389	389	389	389	41	234	389	389	-	181
CHP plants (LT heat)										
fuel (PJ/a)	-	-	562	386	-	-	-	-	-	-
electricity (PJ/a)	-	-	309	309	-	-	-	-	-	-
LT heat (PJ/a)	-	-	197	77	-	-	-	-	-	-
CHP plants (HT heat)										
fuel (PJ/a)	-	-	-	-	773	515	-	-	864	693
electricity (PJ/a)	-	-	-	-	309	309	-	-	346	416
HT heat (PJ/a)	-	-	-	-	348	155	-	-	389	208
Heat pumps										
electricity (PJ/a)	-	-	-	-	-	-	143	107	143	107
LT heat (PJ/a)	-	-	-	-	-	-	429	429	429	429

#### Conclusions of this evaluation

The rough evaluation of different technologies for the generation of heat shows how the considered technologies will affect the total fuel consumption needed to generate the demanded electricity and heat. More accurate system evaluations are complicated by the fact that it is impossible to predict the layout and boundary conditions of future energy systems. The rough evaluation is helpful to understand and discuss the need for new and improved technologies and to get better insight in the interactions.

The possibilities to reduce the total fuel consumption appear to be more or less the same for CHP and heat pumps if performance data as usual today are considered. The total installed power of the CHP plants is limited by the total electricity demand. CHP plants can be used for the generation of LT heat or HT heat; the reduction of the total fuel consumption is not really different for the two CHP options. The reduction of the total fuel consumption is not quite high, and is primarily determined by the actual plant performance. The combined application of heat pumps for the generation of LT heat and CHP for the generation of HT heat appears to

### Chapter 3 Options for future energy systems

be most attractive. The achievable reduction of the total fuel consumption is roughly two times the reduction that is achievable with CHP or heat pumps alone. Further improvement of the efficiencies of the conversion plants will enable significant reductions of the total fuel consumption. Systems based on the application heat pumps are in particular sensitive for higher conversion efficiencies. They will benefit twice if the efficiency of power generation as well as the COP of heat pumps are improved.

### 3.5 Conclusions

#### Renewable energy sources

The studies summarized in Appendix 3.1 have shown that conceivable energy systems for the Netherlands based on wind turbines or photovoltaic generators will result into significantly higher total yearly costs than systems based on a solid fuel like coal. It is expected that the total yearly costs of systems based on biomass will be relatively close to the costs of the coal fuelled systems. Thus, biomass is supposed to be the more attractive renewable source for large scale use. Unfortunately the available biomass in the Netherlands appears to be far from sufficient to cover the total energy demand of the Netherlands at this moment. It is almost impossible today to make a realistic estimate of available quantities of biomass for energy conversion in the future. But it seems to be advisable to maximize the available biomass for energy conversion in the future.

#### Secondary fuel

The application of a secondary fuel seems to be indispensable regarding the need for transport, distribution and storage of energy. Hydrogen and some hydrocarbon fuels are most frequently suggested for this purpose. In general hydrogen will require serious adjustment of the fuel infrastructure while the hydrocarbon fuels can be chosen such that optimum use of the existing infrastructure can be achieved. In Appendix 3.1 it was concluded that hydrogen offers maximum flexibility with regard to the introduction of renewable sources in the national energy system. Electrical energy from these sources can easily be converted into hydrogen by electrolysis plants. A disadvantage of hydrogen, however, is that the use of hydrogen results in high overall system costs. The production of hydrogen requires in general additional conversion steps resulting in high thermodynamic losses and high capital costs. In [3.3] a comprehensive evaluation of various chains for the conversion of biomass into power and heat has been made. Also from this evaluation it was concluded that overall chain efficiencies in the case of hydrocarbon fuels like syngas or SNG (synthetic natural gas) are significantly higher than in the case of hydrogen.

The application of hydrocarbon fuels in a system based on renewable energy depends on the availability of suitable sources of renewable energy. If only biomass is available for the

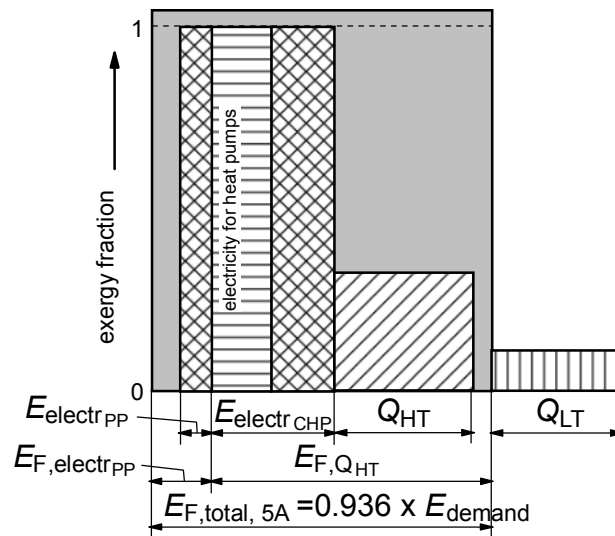


Figure 3.6 Exergy demand and fuel exergy of Case 5A

generation of hydrocarbon fuels it is unlikely that total amounts of biomass are sufficient to cover the total demand on secondary fuels. In that case hydrogen can be used in addition to the hydrocarbon fuels. Further evaluations and comparison with other secondary fuels, like e.g. ammonia, are necessary to get a better understanding of the consequences.

#### System configuration and conversion technologies

The selected primary sources and secondary fuel of the national energy system are primarily determining the system configuration and the conversion technologies that can be applied. Usually the primary conversion processes are determining more than 50% of the total yearly costs. To limit the costs of the primary conversion processes and to achieve affordable total yearly costs, high efficiencies of the storage and conversion processes are required. Thus, the need for high efficiencies of the conversion processes is true for all kind of systems irrespective the used primary sources, fossil fuels, biomass, wind or solar energy.

The thermodynamic efficiency of LT heat generation in fired hot water boilers is very poor (less than 15%). More efficient generation of LT heat is necessary to achieved significant higher overall system efficiencies. From the studies reported in Appendix 3.1 it was concluded that the application of heat pumps is attractive for this purpose. The evaluations in Section 3.4 do confirm this conclusion. The application of electrical driven heat pumps for LT heat generation in combination with CHP plants for the generation of HT heat will reduce the total amount of fuel necessary for the generation of the demanded electricity and heat to roughly 70% of the energy consumption of a system that uses only boilers for heat generation.

High overall conversion efficiencies are of major importance. Further improvement of the conversion efficiencies of power plants, CHP plants and heat pumps is necessary under all circumstances. The rough evaluation of systems for the generation of electricity and heat as shown in Section 2.4 indicated that the overall exergy efficiency of the system can be raised from around 30% to 50% by improving the performance of conversion plants. This will reduce the total fuel consumption with 40%..

## 4 FUEL CONVERSION

### 4.1 Introduction

Primary fuels have to be converted into heat or a secondary fuel to get the energy available in a useful way. Further conversions are necessary in the case of power generation or for the production of high quality fuels. Thermal conversion of a primary fuel into heat or a secondary fuel causes substantial thermodynamic losses. These losses (exergy losses) are usually in the order of 20-30% or even higher. A comprehensive overview of exergy losses in a conventional coal fired power plant are presented in Appendix 4.1. The calculated exergy loss due to combustion is 26% of the fuel exergy, and the total exergy loss of the boiler is 51% resulting in an overall net exergy efficiency of the power plant of 39.91%. Obviously the exergy loss due to combustion has a considerable effect on the overall plant performance. High overall plant efficiencies will require first of all minimization of the boiler exergy losses.

Atmospheric combustion is used for the conversion of various types of fuel, gaseous, liquid and solid fuels, into heat. The exergy loss due to combustion will vary considerable depending on the type of fuel, the air factor and the preheating temperature of the combustion air. The effects of air preheat and air factor on the combustion losses are quantified in this chapter for three different fuels: natural gas, coal and biomass. Also possibilities for loss reduction are discussed. The results have been presented before in [4.1].

Pressurized combustion is done primarily in gas turbines fuelled with oil or natural gas. The pressurized combustion of solid fuels can be done e.g. in pressurized fluidized beds, but the application of PFBC is limited so far. In this chapter the exergy loss of combustion in a non reheat gas turbine without recuperation is briefly discussed. The effects of the applied pressure ratio and the turbine inlet temperature are evaluated quantitatively.

Conversion of a primary fuel into a secondary fuel is used for several reasons in power and heat generating systems.

Power generating system like gas turbines and fuel cells are not able to convert solid fuels directly. Gasification of solid fuels like coal and biomass is required before they can be used in gas turbine or fuel cell systems. Fuel cells are highly demanding with regard to the applied fuel. Low temperature fuel cells can operate only on almost pure hydrogen. Conversion of natural gas or the secondary gas from

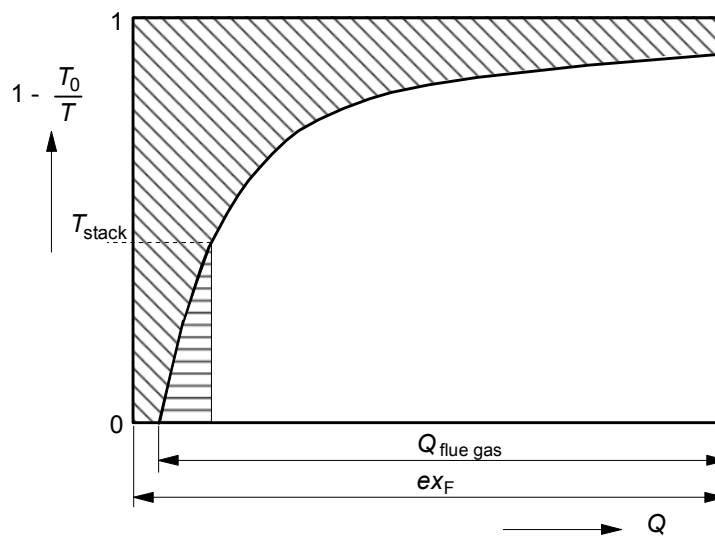


Figure 4.1 Value diagram of adiabatic fuel combustion

gasification processes is necessary to get the required fuel quality. To get an indication of the exergy losses of the conversion of primary fuels into secondary fuels three examples of conversion processes are considered: a coal gasification process, a biomass gasification process and the reforming of natural gas.

## 4.2 Atmospheric combustion

### 4.2.1 Introduction

The production of power and heat in industrialized countries is almost entirely based on the combustion of commercial available fuels. Usually atmospheric combustion takes place in boilers or furnaces; well designed boilers have thermal efficiencies of more than 90 %. Even very high efficiencies, close to 100 %, can be achieved depending on the applied fuel and boiler type. These high thermal efficiencies do suggest perhaps that combustion processes are highly optimized and do not need further improvement with regard to their thermodynamic performance. Second law (entropy or exergy) evaluations however show that the thermodynamic losses of boilers and furnaces are much higher than the thermal efficiency suggests. With thermal losses of around 5% the thermodynamic losses still can be in the order of 30%. These high thermodynamic losses (exergy losses) are primarily caused by the combustion process as can be demonstrated by the value diagram of Figure 4.1; the shaded areas represent the thermodynamic losses (see also Section 2.5.3).

Because of availability and costs, air is normally used for fuel combustion. In the case of the usual fossil fuels (coal, oil or natural gas) adiabatic combustion temperatures are around 2000 °C. Heat will become available by cooling down the flue gas from the adiabatic temperature to the ambient temperature. The temperature curve is shown in Figure 4.1; the area below the curve equals the exergy of the heat transferred from the flue gas. The condensation of water vapor from the flue gas is ignored in this diagram. As the total area of the diagram equals the exergy of the fuel, the slantly shaded area represents the exergy loss of combustion. In a boiler however flue gas is not cooled down to ambient temperature, but leaves the boiler at “stack temperature” (see Figure 4.1). The residual heat from the flue gas is lost also. In Figure 4.1 the horizontal shaded area equals the corresponding exergy loss. From the value diagram it is obvious that the rather low combustion temperature and the need for cooling the flue gas in order to extract the required heat, are the main causes of the large exergy loss. The thermodynamic equivalent temperature of heat transfer from the flue gas is around 1000 °C. The application of pure oxygen instead of air to oxidize the fuel will enable significant higher adiabatic combustion temperatures which will result in a higher thermodynamic equivalent temperature of heat transfer from the flue gas. This option is worthwhile only if the high temperature heat can be used appropriately in a process that will need or convert this heat at high temperature. In general this is not possible up to now. Thus, the parameters that determine primarily the exergy loss are the fuel type (fuel composition and moisture content) the air temperature and the air factor at combustor inlet.

Reduction of the thermodynamic losses of combustion in atmospheric combustion systems does not automatically result into higher overall plant efficiencies. In the case of power plant, the generated heat has to be transferred to a power cycle. If the thermodynamic equivalent temperature at which heat is transferred to the power cycle is unaffected, the overall plant efficiency will be the same and only the flue gas temperature is raised. The

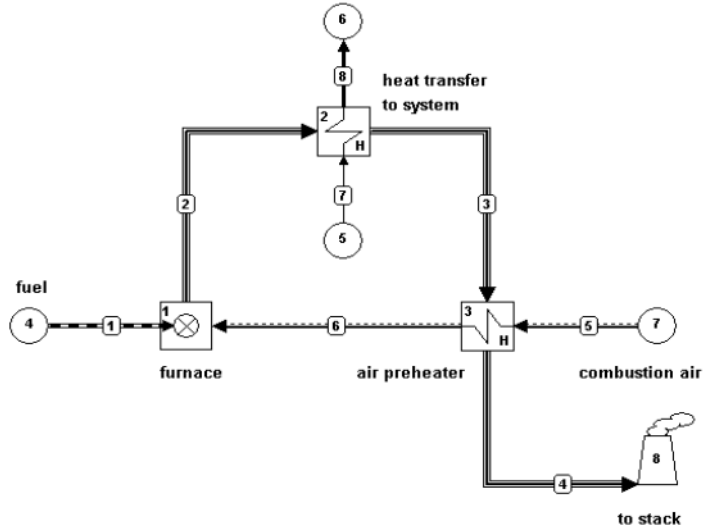


Figure 4.2 Combustion system with air preheat

higher flue gas temperature reduces the thermodynamic losses of combustion but at the same time it increases the thermodynamic losses due to heat transfer in the boiler. Thus, measures taken to decrease the thermodynamic losses of combustion are useful only if they are accompanied by improved power cycles that absorb heat at higher temperatures.

4.2.2 Options to decrease the exergy loss of combustion

In actual combustion plants it has to be assured that fuel is converted completely. Complete combustion of fuel will be possible only if the air quantity is higher than the stoichiometric air quantity. Therefore, some excess air is necessary to realize complete fuel

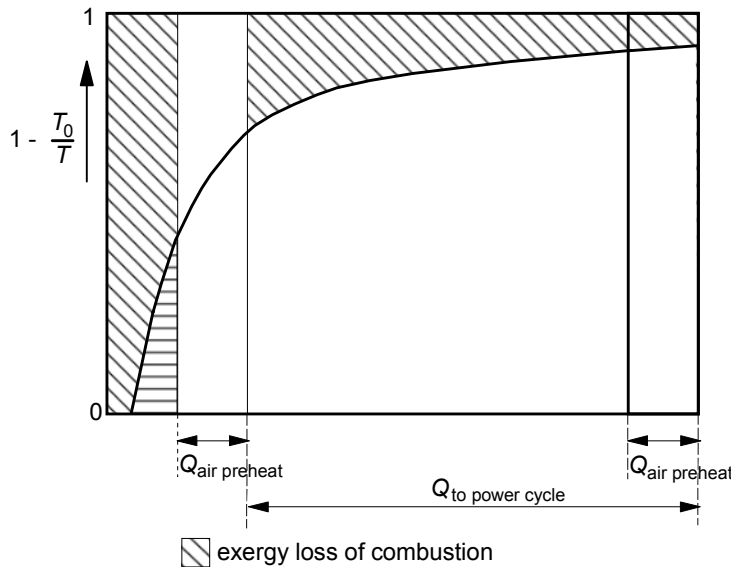


Figure 4.3 Value diagram of a combustion system with air preheat

conversion within the limited time and space available in a boiler furnace. However, the air factor, defined as the ratio between the actual air quantity divided by the stoichiometric quantity, should be as low as possible, since the excess air reduces the adiabatic combustion temperature and consequently the thermodynamic equivalent temperature of heat transfer. The actual air factor depends on the type of fuel and the boiler design. Solid fuels will require higher air factors than

gaseous fuels. The required air factor might depend further on the desired combustion temperature, the residence time of the reactants in the combustion chamber or furnace, and the way of mixing, the turbulence of fuel and air. An air factor of 1.05 and 1.10 is normally sufficient for gaseous fuels, while solid fuels require higher air factors like 1.10 to 1.20 to ensure almost complete combustion.

Air preheating enables higher combustion temperatures and consequently higher thermodynamic equivalent temperatures of heat transfer from the flue gas. Assuming a theoretical combustion system as shown in Figure 4.2, air is preheated before it is supplied to the furnace. After adiabatic combustion in the furnace hot flue gas is passed to the heat transfer system that supplies heat to a power cycle or any other process. Then, flue gas is cooled further in the air preheater and finally discharged to the stack. The resulting cooling curve of the flue gas is shown in the value diagram of Figure 4.3. In this diagram it is supposed that heat transfer in the preheater will take place without temperature difference between air and flue gas. This is not a realistic assumption of course, but it simplifies the explanation of the effect of air preheat. The higher air temperature in the case of air preheat results in a higher adiabatic combustion temperature. Since the flue gas composition is not really affected by the higher combustion temperature, the total heat that can be transferred from the flue gas when it is cooled to environmental temperature will increase. The total available heat from the flue gas equals the sum of the heating value of the fuel and the heat transferred to the preheated air.

Therefore, the value diagram of Figure 4.3 is achieved by extending the horizontal axis of the value diagram of Figure 4.1 with the heat from the preheated air. The flue gas temperature curve is extrapolated to the point of the elevated combustion temperature. The slantly shaded area in Figure 4.3 represents the exergy loss of combustion in the case of a boiler with air reheat. The air preheater causes internal heat exchange in the combustion system. If the value diagram considers only the external heat transfer to the system the diagram as shown in

Figure 4.4 is achieved. Comparing this diagram with the diagram of Figure 4.1, it is obvious that the air preheater reduces the exergy loss of combustion. The difference in exergy loss between the two diagrams is shown in Figure 4.5 together with the exergy loss of the air preheater. The exergy loss of the air preheater was ignored so far but for a real case the reduced exergy loss of combustion is partly compensated by the exergy loss of the air preheater. The difference between the two areas is the net exergy gain due to air preheat.

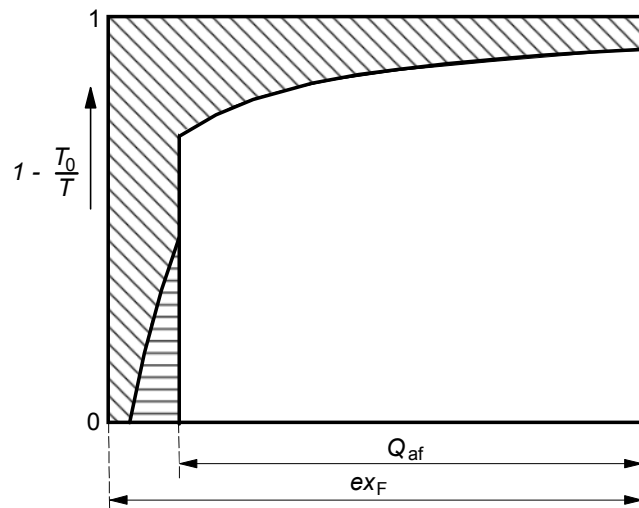


Figure 4.4 Value diagram of a combustion system with air preheat (if only external heat transfer is considered)

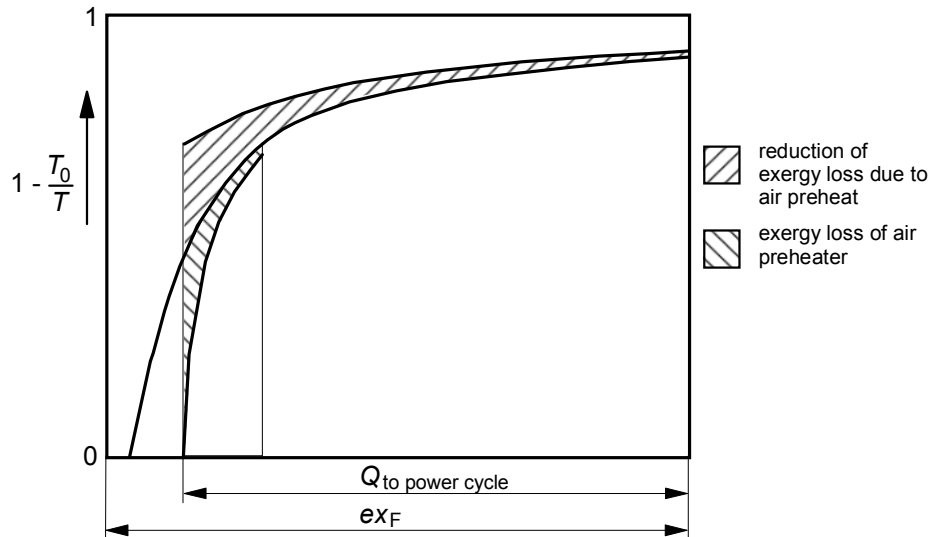


Figure 4.5 Value diagram with exergy loss reduction due to air preheat and additional exergy loss of the preheater

#### 4.2.3 System evaluation

To quantify the effects of the various design options for combustion systems three system designs are specified for calculation with the computer program Cycle-Tempo. The three system designs are presented in this section. The objective of this evaluation is to understand the effects of the various design parameters on the performance of combustion systems. Therefore, technical limitations are sometimes ignored.

The first system model represents a simple combustion system without air preheat as shown in Figure 4.6. An air blower (nr.2) brings the air to the combustion chamber (nr.3). The combustion chamber is assumed to operate adiabatic. Then, the flue gas leaves the combustion chamber at high temperature. Hot flue gas is cooled from the adiabatic combustion temperature to 100°C in a heat exchanger (nr.5) and then discharged to the atmosphere by the forced draft fan (nr.6) through the stack (nr.7). Thus, the flue gas temperature at the inlet of the forced draft fan is 100°C. This temperature is applied for all system alternatives disregarding the type of fuel. This is done to get a useful comparison of the performance of the various system alternatives. As the utilization of the heat transferred in the heat exchanger (nr.5) is beyond the scope of this evaluation, only the heat transferred from the flue gas is included in the system models.

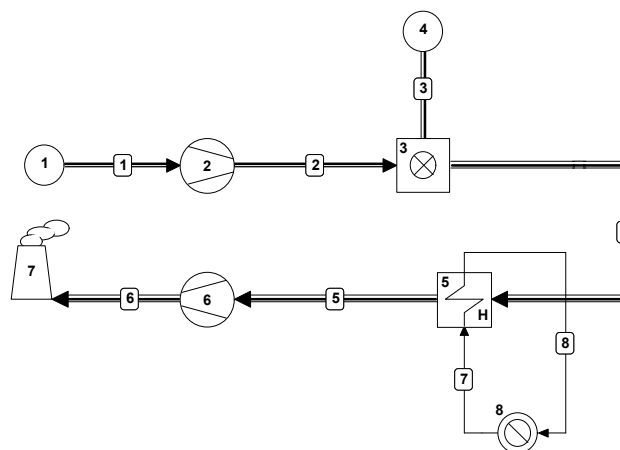


Figure 4.6 Combustion system without air preheat

A second system model represents a combustion system with air preheat and is shown in Figure 4.7. The only difference with the first model (without air preheat) is the air preheater (nr.2). Heat is transferred in the air preheater from the flue gas flow to the air flow. The temperature difference between flue gas and air will become smaller with increasing air temperature, since the flue gas flow is stronger than the air flow with regard to the heat capacities. The minimum allowable temperature difference is supposed to be 40 K. If this temperature difference is reached at the hot side of the air preheater the maximum air preheat temperature is achieved. The highest air temperature that can be achieved depends as well on the type of fuel as on the chosen air factor.

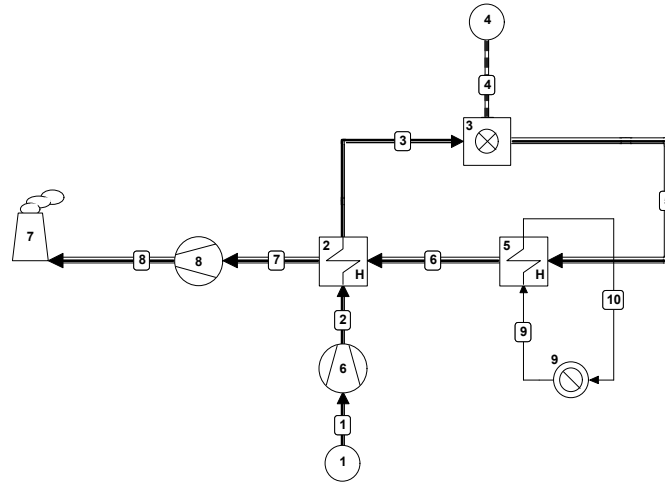


Figure 4.7 Combustion system with air preheat

Higher air temperatures are achievable only if the flue gas flow is split. In that case the flue gas flow that goes through the air preheater is just large enough to deliver the heat necessary to preheat the combustion air. The remainder of the flue gas flow is cooled in a heat exchanger placed in parallel (nr. 11 in Figure 4.8), where heat is transferred to a thermal power cycle or another heat absorbing process. With this flue gas system any desired air temperature can be achieved in principle. For this evaluation it is assumed that air temperatures up to 1000°C achievable.

Limitations with respect to the technical feasibility of these systems are ignored. In all cases with split flue gas flow the temperature difference between air and flue gas at the hot side of the air preheater is assumed to be 40 K.

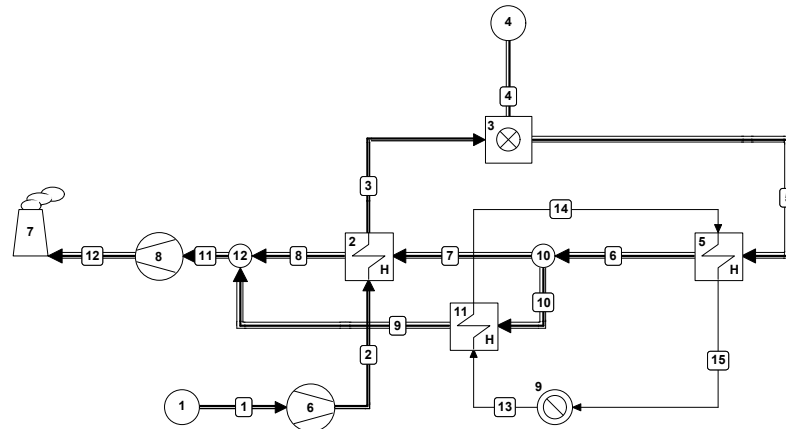


Figure 4.8 Combustion system with split flue gas flow for air preheat

Three kinds of fuels are considered to evaluate the effect of the fuel on the exergy loss of the combustion system: natural gas, hard coal and biomass (wood). For natural gas the composition of Slochteren gas has been chosen. The composition of the fuels (ultimate analysis for the solid fuels) as fed to the combustor is shown in Table 4.1. The lower heating value ( $LHV_F$ ) and the exergy ( $ex_F$ ) of the fuel are

## Chapter 4 Fuel conversion

presented too. The exergy values of the solid fuels are calculated by Cycle-Tempo; the program uses the calculation method of Baehr-II (see Section 2.4.4). The definition of the

environment necessary to determine the exergy values is based on [2.9]. Complete combustion is assumed for all considered system cases. The stack temperature is determined by the assumption that the flue gas is cooled to 100°C. Then, the actual stack temperature is supposed to be almost the same for all alternatives.

natural gas		solid fuels		
components	mole fraction	elements/ components	mass fractions	
			coal	wood
CH <sub>4</sub>	0.8129	C	0.5990	0.4496
C <sub>2</sub> H <sub>6</sub>	0.0287	H <sub>2</sub>	0.0534	0.0475
C <sub>3</sub> H <sub>8</sub>	0.0038	N <sub>2</sub>	0.0115	0.0148
C <sub>4</sub> H <sub>10</sub>	0.0015	O <sub>2</sub>	0.1694	0.2361
C <sub>5</sub> H <sub>12</sub>	0.0004	S	0.0135	0.0011
C <sub>6</sub> H <sub>14</sub>	0.0005	Cl <sub>2</sub>	0.0030	-
N <sub>2</sub>	0.1432	F <sub>2</sub>	0.0002	-
O <sub>2</sub>	0.0001	H <sub>2</sub> O	-	0.2000
CO <sub>2</sub>	0.0089	ash	0.1500	0.0509
total	1.000	total	1.000	1.000
$LHV_F$ (MJ/kg)	38.00		24.61	16.01
$ex_F$ (MJ/kg)	39.39		26.47	18.06
$f_{ex, F}$	1.037		1.076	1.128

#### 4.2.4 General remarks about the heating value and specific exergy of fuels

Useful energy from primary fuels is obtained by converting fuel components into chemical components as available in the environment. Common fuels consist of hydrocarbon components that are converted, actually oxidized, into CO<sub>2</sub> and H<sub>2</sub>O. In general oxygen from air is used as the oxidizer. The energetic value of a fuel is normally expressed by the (lower or higher) heating value of a fuel which is defined as the amount of heat that must be transferred from the combustion process after the fuel is converted completely into environmental components. The higher and lower heating value have to be distinguished if the flue gas, the product of the combustion process, contains water vapor. Most of the water vapor will condense if the flue gas is cooled down to the temperature of the environment. The amount of water vapor that is still available in the flue gas after achieving equilibrium at environmental temperature depends on the actual ambient temperature. The higher and lower heating values are theoretical values that are not related to the actual system conditions. The lower heating value of the fuel is the heat that must be transferred from the combustion process if it is assumed that water vapor does not condense at all. Thus, after cooling the reaction products to environmental temperature it is assumed that all water in the flue gas is still available as water vapor. In the case of the higher heating value it is assumed that the water vapor in the flue gas is completely condensed. Thus the flue gas at the final conditions does contain liquid water only. The difference between the two heating values depends on the water fraction in the flue gas which is determined by the amount of hydrogen in the fuel, assuming that dry air is used for the combustion process. Obviously, the heat that can be transferred from the flue gas in actual processes will have a value anywhere in between the higher and the lower heating

value depending on the actual environmental temperature. The available water vapor in the combustion air will affect the exact value, but in general this effect will be very small.

The exergy of the fuel represents the total work that can be obtained from the fuel by converting the fuel (with reversible processes) into environmental components and expanding or compressing these components to their partial pressure in the environment as discussed in Chapter 3. After defining the composition of the environment as well as its temperature (and pressure) the exergy (maximum theoretical work) of the fuel is fixed. In principle the calculated exergy value is only correct if the actual composition of the environment is exactly the same as the composition used for the exergy calculation. It is obvious that this is not always guaranteed. The exergy of common fuels is primarily determined by the composition of air. The air composition is supposed to be quite homogeneous worldwide. Appropriate exergy values are obtained for fuel conversion systems if standard air is used as the basis for the calculation.

#### 4.2.5 Description of the reference case

A reference system is chosen to have a basis for the judgment of the results of the various systems. The reference system is a natural gas fueled system with air preheat; the full flue gas flow is used to heat the combustion air to a temperature of 279°C. The system diagram used for the calculations by Cycle-Tempo is shown in Figure 4.7. The system is used in this section also

	units	natural gas
air factor	-	1.05
temp. combustion air	°C	279
adiabatic comb. temp.	°C	2106
system exergy efficiency	%	72.80
exergy losses		
combustor	%	23.14
air preheater	%	1.01
stack	%	3.34

to explain the parameters that are used to evaluate the performance of the various systems. The relevant results for the reference case are presented in Table 4.2. The value diagram as derived from Cycle-Tempo is presented in Figure 4.9. The length of the horizontal axis of the diagrams from Cycle-Tempo equals the heat transferred from the flue gas if it is cooled from the adiabatic combustion temperature to ambient temperature<sup>1</sup> (for the combustion of 1 kg of fuel). This amount of heat is not the same as the fuel exergy. Thus, the total area of the diagram depicted by Cycle-Tempo is not exactly the same as the fuel exergy. But the differences are small.

Natural gas is combusted assuming an air factor of 1.05. The temperature difference between air and flue gas at the hot side of the air preheater is 40 K; the maximum air temperature that can be achieved under these circumstances is 279°C. The calculated adiabatic combustion temperature is 2106°C. The main performance parameter used in this evaluation is the system exergy efficiency. This parameter is defined as the exergy of the heat transferred from the flue gas in heat exchanger 5 (see Figure 4.7) divided by the exergy of the combusted fuel. Exergy losses are presented for the combustor, air preheater and stack. They are presented as a percentage of the fuel exergy. In addition to the exergy of the fuel, the electric motor driven air blower and forced draft fan also supply exergy to the system. For the

<sup>1</sup> The ambient temperature is assumed to be 15°C.

## Chapter 4 Fuel conversion

reference case the electrical input of the motors is 0.35% of the fuel exergy. Therefore the total exergy loss of combustor, air preheater and stack (27.49%) is somewhat higher than the total loss if calculated from the system exergy efficiency (27.20%).

The value diagram in Figure 4.9 shows the cooling curve of the flue gas as well as the heating curve of the combustion air in the air preheater. At low temperatures the slope of the cooling curve changes because of the condensation of water vapor. This occurs in the environment after the flue gas has left the stack. At environmental temperature most, but not all, of the water vapor is condensed. This means

that the length of the horizontal axis is almost, but not exactly, the same as the  $HHV_F$ . The shaded area below the cooling curve in heat exchanger (nr. 5) represents the exergy that is transferred from the flue gas. The shaded areas of the air preheater (nr. 2) and the stack represent the corresponding exergy losses. It is obvious from the value diagram that the effect of condensation of water vapor from the flue gas on the exergy loss of the stack (nr. 7) is not negligible.

It appears that in the reference case more than one quarter of the fuel exergy is lost in the combustion system. The bulk of this loss (27.49%) is caused by the combustion process (23.14%). The contributions of the air preheater (1.01%) and the stack (3.34%) are quite limited.

### 4.2.6 Effect of the type of fuel

The effect of the combustion of different fuels (natural gas, coal and wood) on the system exergy efficiency are shown in Table 4.3. An air factor of 1.10 and combustion without air preheat is assumed. Thus, air is supplied to the combustor at almost ambient temperature. Under these circumstances, the exergy efficiency of the combustion system with natural gas are much lower than for the reference case. Without air preheat the adiabatic combustion temperature is 1874°C (2106°C for the reference case) and the system exergy efficiency 67.74 (72.80 for the reference case).

In the case of coal combustion the system exergy efficiency appears not to be much lower than in the case of natural gas combustion. Wood combustion, however, has a significant lower system exergy efficiency (60.52% vs 66.03 for coal and 67.74 for natural gas). Since the combustion of coal requires less air per kilogram fuel than the combustion of

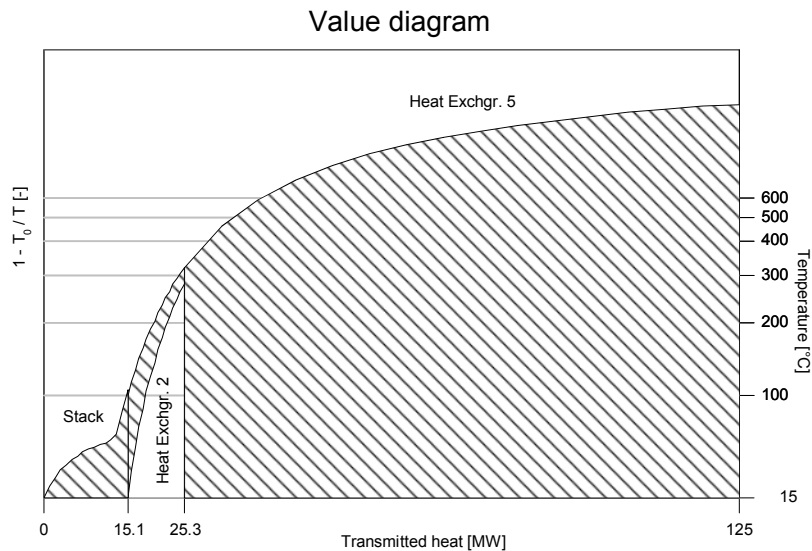


Figure 4.9 Value diagram of the reference case

natural gas, a somewhat higher adiabatic combustion temperature is achieved (1902 instead of 1874°C). Nevertheless, the exergy loss of the combustor in the case of coal combustion is higher. This is caused by the higher exergy factor (the ratio

	units	nat. gas	coal	wood
air factor	-	1.10	1.10	1.10
temp. combustion air	°C	15	15	15
adiab. comb. temp.	°C	1874	1902	1682
system exergy eff.	%	67.74	66.03	60.52
exergy losses:				
combustor	%	29.40	30.66	35.46
stack	%	3.26	3.51	4.25

between the exergy value and the lower heating value) of the coal. Also the stack losses are somewhat higher in the case of coal combustion which results from the higher specific exergy (caused by the gas composition) of the flue gas at stack conditions. The significant lower system exergy efficiency in the case of wood combustion is caused by the lower adiabatic combustion temperature, the higher exergy factor of wood and higher stack losses. It has to be noticed that the stack loss is not only determined by the temperature and quantity of the flue gas but also by the chemical exergy. In the case of coal and wood the chemical exergy of the flue gas is higher than in the case of natural gas.

It appears that the fuel type might have a considerable effect on the system exergy efficiency depending on the characteristics of the fuel. In the case of wood the system exergy efficiency is around 10% lower than in the case of natural gas (60.52 vs. 67.74%). It is expected that in general the exergy efficiency of usual conversion plants will be seriously lower if biomass fuels are used.

#### 4.2.7 Effect of the air factor

The highest adiabatic combustion temperature is obtained when fuel and air are supplied to the combustor at their stoichiometric ratio. In actual combustion systems excess air is always necessary to achieve near to 100 % combustion of the fuel. For gaseous fuels air factors below 1.10 are usual while solid fuels in general require higher air factors. Increasing the air factor will dilute the stoichiometric flue gas

mixture with non-reacting gases that reduce the adiabatic combustion temperature. The effect of the air factor on the overall system exergy efficiency is shown in Figure 4.10 for combustion systems without air preheat and air factors in the range of 1.05 to 1.20. Raising the air factor from 1.05 to 1.20 causes a decrease in system exergy efficiency of 1.80 % in

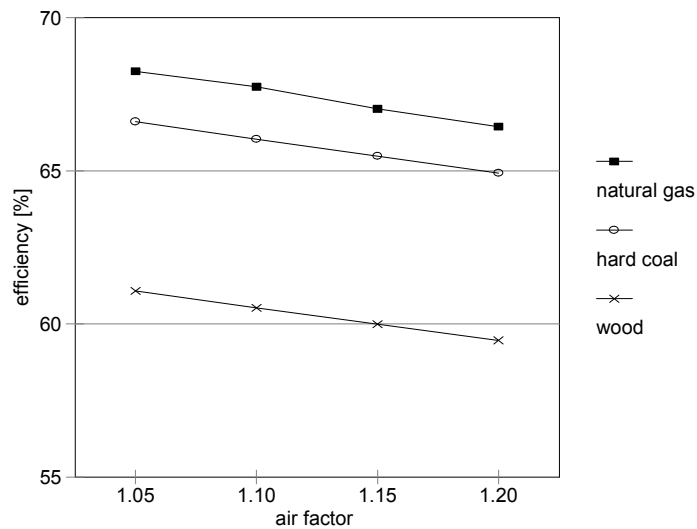


Figure 4.10 System exergy efficiencies versus air factor; without air preheat

## Chapter 4 Fuel conversion

case of natural gas, 1.67 % in case of hard coal and 1.61 % in case of wood combustion. Thus, increasing the air factor results in all considered cases only into a slight decrease of the system exergy efficiency.

4.2.8 Effect of air preheatingAir preheat with full flue gas flow

The advantages of air preheat have been outlined before in Section 4.2.2. In this section the advantages are quantified and discussed in more detail. The effect of air preheat in the case of natural gas combustion is shown

in Table 4.4. The system calculations are based on the following assumptions: the total flue gas flow is cooled in the air preheater, the

	units	natural gas			
air factor	-	1.05	1.10	1.15	1.20
temp. combustion air	°C	279	288	298	307
adiab. comb. temp.	°C	2106	2050	1998	1950
system exergy eff.	%	72.80	72.48	72.21	71.92
exergy losses:					
combustor	%	23.14	23.46	23.74	24.00
preheater	%	1.01	1.09	1.16	1.26
stack	%	3.34	3.28	3.23	3.18

minimum temperature difference between flue gas and air in the air preheater is 40 K, the flue gas leaves the air preheater at a temperature of 100°C and air is preheated to the maximum achievable temperature. The thermal strength of the air flow and the flue gas flow are different because of the fuel that is added in the combustion chamber. The difference in thermal strength will be smaller if the air factor increases. Thus, higher air factors will enable higher preheat temperatures of the combustion air as is shown also in Table 4.4. On the other hand a higher air factor will decrease the adiabatic combustion temperature. The results in Table 4.4, however, show that the positive effect of the higher air preheat temperature is overruled by the negative effect of the lower adiabatic combustion temperature, because the system exergy efficiency decreases with increasing air factor. The increase of the total exergy loss with increasing air factor is not only caused by the higher exergy loss of the combustor. Also the exergy loss of the preheater increases. But, the stack loss decreases if the air factor increases.

A comparison of system exergy efficiencies for combustion systems with and without air preheat is made for a better understanding of the various effects. For the two options the air

	units	natural gas			
air factor	-	1.05	1.10	1.15	1.20
system exergy eff.					
with air preheat	%	72.80	72.48	72.21	71.92
without preheat	%	68.24	67.74	67.02	66.44
difference	%	4.56	4.74	5.19	5.49

factor is used as the independent variable. The cases with air preheat are the same as shown in Table 4.4. The differences with a system without air preheat are presented in Table 4.5. For both options the system exergy efficiency decreases with increasing air factor. For the systems without air preheat the decrease of the system exergy efficiency is somewhat higher

because they miss the mitigating effect of the air preheat. Thus, the advantage of air preheat increases at higher air factors. The effect of air preheat on the system exergy efficiency is shown in Figure 4.11 for the three considered fuels. It is assumed for all cases that air is preheated with the full flue gas flow. The efficiency decrease is almost the same for all fuels. In the case of wood combustion the efficiencies are much lower but the efficiency drop is almost the same.

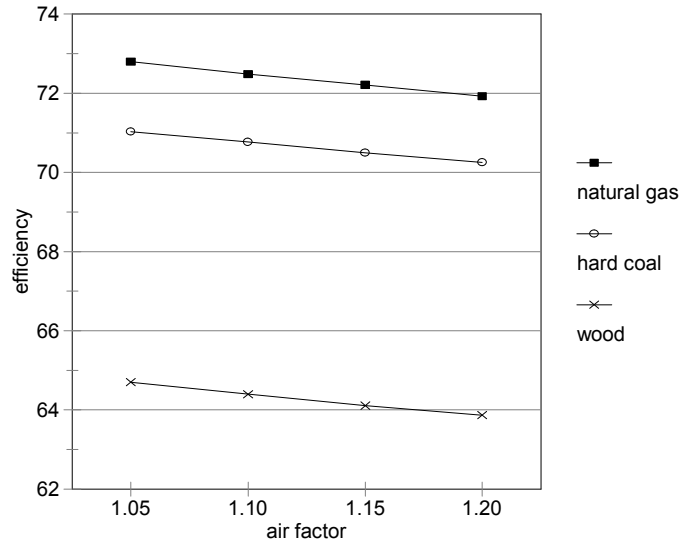


Figure 4.11 System exergy efficiencies for different fuels; air preheat with full flue gas flow

#### Air preheat with split flue gas flow

In the case of air preheat with the full flue gas flow the maximum air preheat temperature is limited because of the difference in thermal strength of the heated and cooled flows. Higher air preheat temperatures are conceivable by adjusting the thermal strength of the two flows. This is possible e.g. by increasing the air flow through the air preheater or decreasing the flue gas flow. In the following it is assumed that the flue gas through the air preheater is reduced by splitting the flow after cooling in heat exchanger (nr. 6) into a flow to the air preheater (nr. 2) and a flow to another heat exchanger (nr. 11) as shown in Figure 4.8. The heat exchangers 6 and 11 transfer heat to a power cycle or other heat absorbing process. The exergy transferred from the flue gas in these heat exchangers is considered as the product of the combustion system. It has to be emphasized that this is just a theoretical evaluation. The technical feasibility of such a system is questionable. In a real combustion system it is necessary to divide a very large flue gas flow in a controlled way over two channels. Operational problems and costs have hindered the application of this kind of solutions so far. Furthermore, the costs of air preheaters will increase serious if air preheat temperatures higher than 600°C are required. Nevertheless, it might be good to be aware of the thermodynamic merits of this solution.

	units	natural gas				
air factor	-	1.05	1.05	1.05	1.05	1.05
temp. combustion air	°C	15	300	500	750	1000
adiab. comb. temp.	°C	1983	2120	2153	2425	2604
system exergy eff.	%	68.24	73.06	75.10	76.92	78.25
exergy losses:						
combustor	%	28.66	22.83	20.46	18.37	16.84
preheater	%	-	1.06	1.39	1.66	1.86
stack	%	3.33	3.34	3.34	3.34	3.34

With the system model of Figure 4.8 any air preheat temperature can be achieved in theory. The results of an number of system cases for the combustion of natural gas are presented in Table 4.6. The air factor is assumed to be 1.05 and the combustion air temperature ranges from 15°C to 1000°C. It is obvious that air preheating has a considerable effect on the exergy loss of combustion. The combustor loss reduces from 28.66% for the case without air preheat to 16.84% for the case with an air preheat temperature of 1000°C. The effect on the system exergy efficiency is

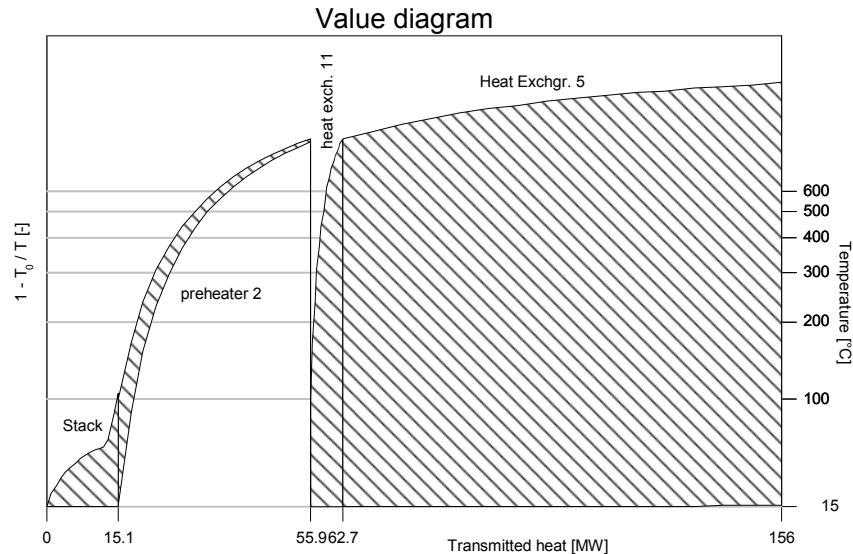


Figure 4.12 Value diagram, combustion of natural gas with an air preheat temperature of 1000 °C

is somewhat mitigated by the exergy loss of the air preheater, but the increase of the system exergy efficiency from 68.24% to 78.25% is still considerable. Since the overall exergy loss of the combustion system is about 30%, a loss reduction of 10% points means that the overall loss is reduced by one third.

The value diagram of the natural gas fired system with split flue gas flow and an air preheat temperature of 1000°C is shown in Figure 4.12. From the heat supplied to the system by the fuel, almost 40% is transferred in the air preheater. About 7% is transferred in the bypass heater (heat exch. 11). The shaded area under the temperature curves of the heat exchangers 5 and 11 represents the exergy that is transferred from the flue gas. This exergy can be used in principle for the generation of power in a thermal power cycle. Coal and wood fired systems with the same air preheat temperatures are considered too for this evaluation. The system exergy efficiencies are presented in Figure 4.13. The effects of varying the air preheat temperature are more or less the same. An efficiency increase of 10% (points) is roughly achievable for all considered fuels.

#### 4.2.9 Conclusions

Thermal combustion of fuel is associated with large exergy losses. The type of fuel can seriously affect the system exergy efficiency, depending on the characteristics of the fuel. In the case of combustion without air preheat a somewhat lower system exergy efficiency (66.03 %) was calculated for the considered coal than for the case with natural gas (67.74 %). The combustion of wood resulted in a significantly lower system exergy efficiency (60.52 %).

The air factor has a limited effect on the system exergy efficiency. An increase of the air factor from 1.05 to 1.20 in the case of natural gas decreases the system exergy efficiency from

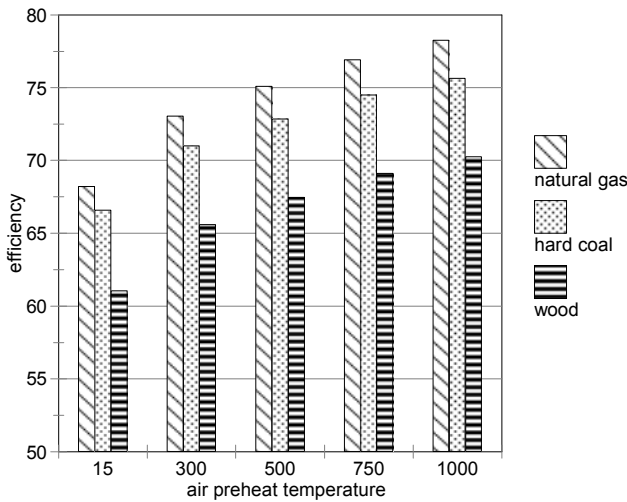


Figure 4.13 Comparison of different fuels; air preheat with split flue gas flow

68.24% to 66.44%, a difference of 1.80% (points). The application of air preheating mitigates this effect. If air is preheated to the highest achievable temperature the increase of the air factor from 1.05 to 1.20 results in a decrease of the system exergy efficiency from 72.80% to 71.92%, a difference of only 0.88% (points).

An effective method to reduce the exergy loss of combustion is the preheating of combustion air. Preheating of air with the full flue gas flow as usual in large steam boilers is limited by the difference in the thermal

strength of the air and flue gas flows. Higher air factors will enable higher air preheat temperatures. In the case of natural gas combustion with an air factor of 1.05 the maximum air preheat temperature is 279°C under the assumed conditions. An increase of the air factor to 1.20 enables a maximum air preheat temperature of 307°C. Thus, the efficiency improvement due to air preheating depends also on the applied air factor. In the case of natural gas combustion the maximum achievable increase of the system exergy efficiency due to air preheating is 4.56 % (points) in the case of an air factor of 1.05 and 5.48 % if an air factor of 1.20 is used.

Higher air preheat temperatures are achievable if only a part of the flue gas flow is used for air preheating. The remainder of the flue gas flow can be used for heat transfer to a power cycle or another heat absorbing process. With the split flue gas flow an air preheat temperature of 1000°C can be achieved in principle. This high air preheat temperature will increase the exergy efficiency of the combustion system with 10% (points) compared to a system without air preheat. It is obvious that it is only useful to increase the air preheat temperature if heat transfer from the flue gas to the thermal power cycle occurs also at

**Gas turbine model**

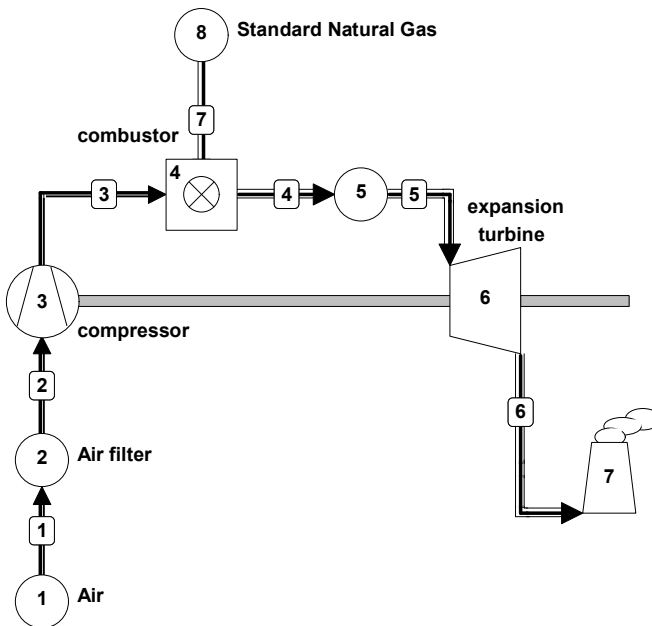


Figure 4.14 Simple gas turbine model

## Chapter 4 Fuel conversion

higher temperatures. Otherwise a reduction of the exergy loss of combustion increases only the exergy loss of the heat transfer to the power cycle. The technical and economic feasibility of air preheat temperatures higher than about 500°C is uncertain. High temperature air preheating is applied for industrial processes for many decades, but the application for energy conversion plants appeared not to be attractive so far.

Even with very high air preheat temperatures the exergy loss of atmospheric combustion systems is still higher than 20 % of the fuel exergy. This relative high exergy loss is a serious obstacle for the realization of high overall plant efficiencies.

*Table 4.7 Input data of the simplified gas turbine model*

Nr.		units	
1	Air inlet	temperature	15
		pressure	1.01325
3	Compressor	pressure ratio	40
		isentropic efficiency	0.87
4	Combustor	pressure loss	0.1
8	Fuel (standard natural gas)	temperature	15
		pressure	42
6	Expansion turbine	inlet temperature (ISO)	1300
		isentropic efficiency	0.86
7	Stack	pressure	1.01325
	Generator	efficiency	0.98

### compressor outlet temp. vs pressure ratio

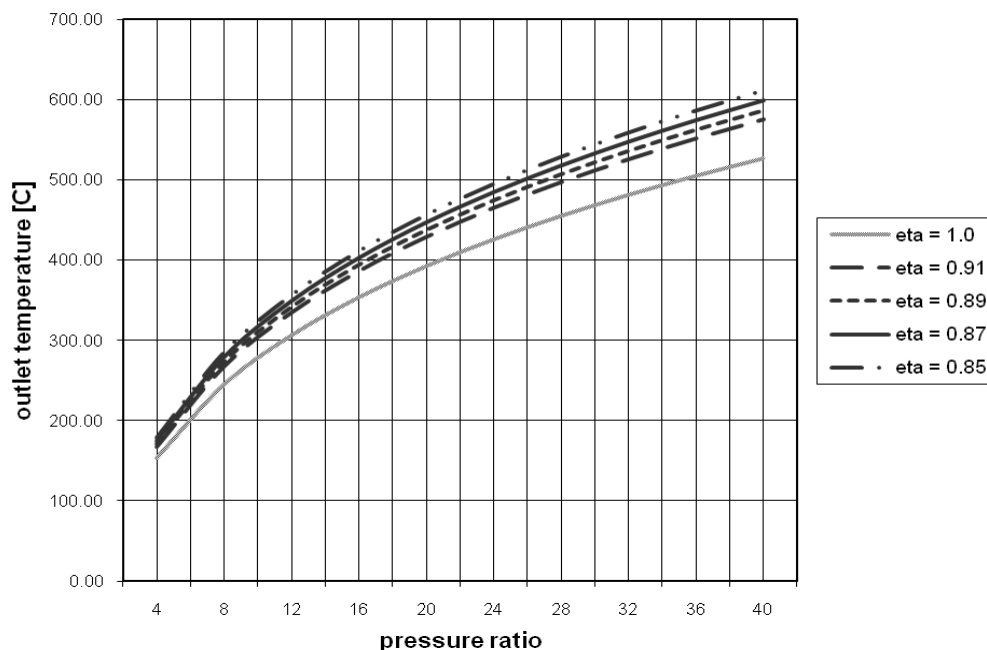


*Figure 4.15 compressor outlet temperature as function of pressure ratio and isentropic compressor efficiency*

### 4.3 Pressurized combustion

In the conventional power plant as presented in Appendix 4.1 heat from the flue gas is transferred to a steam cycle for conversion into power. The exergy flow diagram shows that

*Table 4.7 Input data of the simplified gas turbine model*

Nr.		units	
1	Air inlet	temperature	°C
		pressure	bar
3	Compressor	pressure ratio	40
		isentropic efficiency	0.87
4	Combustor	pressure loss	bar
8	Fuel (standard natural gas)	temperature	°C
		pressure	bar
6	Expansion turbine	inlet temperature (ISO)	°C
		isentropic efficiency	-
7	Stack	pressure	bar
	Generator	efficiency	-

the losses due to heat transfer are higher than 20% of the fuel exergy. If the hot flue gas can be used directly for the generation of power as is usual in gas turbines, the high loss due to heat transfer can be avoided. This explains why high efficiencies are achievable with power generating systems based on gas turbines. Possibilities to reduce the exergy loss of combustion in the case of pressurized combustion are not the same for atmospheric combustion because of the different process conditions. The simple gas turbine model as shown in Figure 4.14 is used to discuss these possibilities. The assumed input data for a reference case are presented in Table 4.7. The

conditions of the combustion air at the inlet of the combustor are primarily determined by the pressure ratio of the air compressor; the isentropic efficiency is of minor importance (see Figure 4.15). The adiabatic combustion temperature is determined by the inlet conditions of the expansion turbine. Large

gas turbines for power generation have today pressure ratios of 20 and higher and turbine inlet temperatures are around 1300°C. With the assumed conditions for the reference case the calculated overall exergy efficiency of the gas turbine cycle is 35.9% which corresponds with a thermal efficiency of 37.7%. The temperature of the compressed air is 447°C and the exergy loss of combustion is 27.6% of the fuel exergy. Thus, the

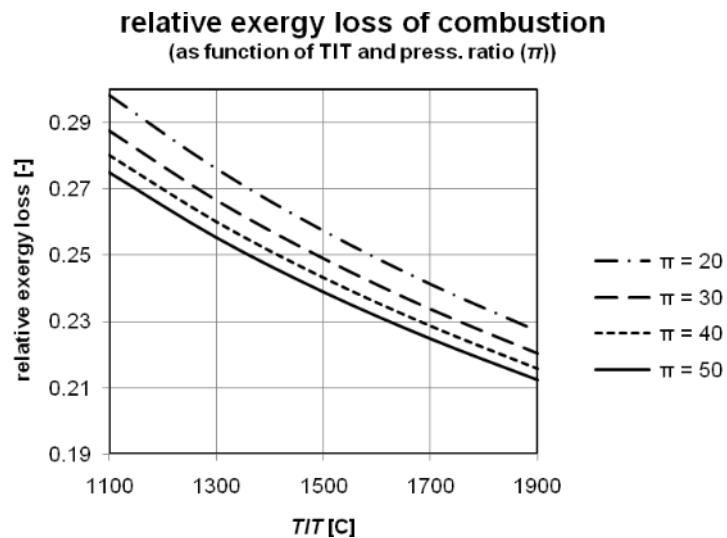


Figure 4.16 Relative exergy loss of combustion as function of the TIT and the pressure ratio

## Chapter 4 Fuel conversion

exergy loss of combustion is also higher than one quarter of the fuel exergy. Further improvement of the gas turbine performance in the futures might be expected. Figure 4.16 shows what happens with the exergy loss of combustion if the turbine inlet temperature and the pressure ratio is increased. Other parameters like the isentropic efficiencies of compressor and expansion turbine are supposed to be the same for all cases. It appears that even in the case of a  $TIT$  of  $1900^{\circ}\text{C}$  the exergy loss of combustion is still higher than 20%.

In this evaluation only the simple gas turbine process is considered. Alternative gas turbine cycles which will enable higher system efficiencies are technically more complicated. Very high efficiencies have been claimed in the past for recuperated gas turbine cycles with low pressure ratios and high  $TIT$ 's. But these systems appear to be very sensitive for the pressure loss of the recuperator. These losses are not easy to predict accurately. The recuperated gas turbine as well as the reheat gas turbine are thermodynamically attractive, but the application of these systems is limited so far because of technical difficulties. The thermodynamic characteristics of these processes are discussed more comprehensively in Chapter 5. However, it is unlikely that these processes will reduce the exergy loss of combustion seriously below 20%.

### 4.4 Conversion into a secondary fuel

#### 4.4.1 Introduction

In this section three examples of fuel conversion processes are discussed. These examples are used to give an impression of the performance that is achieved with state of the art technology and to discuss the prospects of these processes. It is not the intention to present an exhaustive evaluation of fuel conversion processes. Therefore, conclusions have to be formulated with appropriate reservation.

The considered fuel conversion processes are a process for the gasification of coal, a biomass gasification process, and a process for the reforming of natural gas. The conversion of solid fuels like coal and biomass into a gaseous fuel is attractive in combination with power systems based on gas turbines or fuel cells. It is an option to achieve higher efficiencies for solid fuel based power plants. Since gas turbines and fuel cells are quite sensitive for impurities in the fuel, the need for intensive gas cleaning will result automatically in attractive emission levels. Industrial scale steam reforming processes are in use for the generation of hydrogen from natural gas. Small scale reforming processes are developed for the conversion of natural gas into hydrogen or a hydrogen rich fuel in fuel cell systems. This is still supposed to be an option for the future. The fuel conversion processes are described briefly in this section together with the calculated exergy losses. The auxiliary

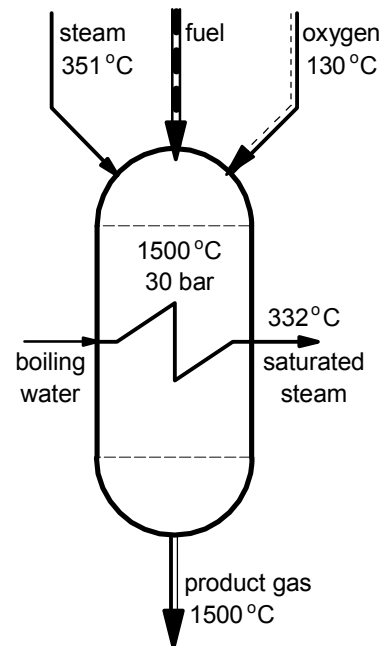


Figure 4.17 Coal gasification in an entrained coal gasifier

systems needed for the operation of these processes are not included in the presented exergy calculations. In general the auxiliary systems will increase the exergy loss in the case of actual power plants.

ultimate composition coal		composition product gas			
mass fractions		mole fractions			
C	0.7260	H <sub>2</sub>	0.282	mass ratios	
H <sub>2</sub>	0.0477	CO	0.576	oxygen to coal	0.89
N <sub>2</sub>	0.0184	CO <sub>2</sub>	0.026	steam to coal	0.14
O <sub>2</sub>	0.0902	H <sub>2</sub> O	0.045	<i>LHV</i>	
S	0.0047	N <sub>2</sub>	0.036	coal	28.94 MJ/kg
ash	0.1124	Ar	0.010	product gas	10.96 MJ/kg
		H <sub>2</sub> S	0.001		
		C	0.004		
		ash	0.019		

#### 4.4.2 Coal gasification

An entrained flow gasification process is chosen for this evaluation. The gasification process is schematically depicted in Figure 4.17. Pulverized coal enters the gasifier at the top where it is mixed with steam and oxygen. The steam enters the reactor at a temperature of 351°C and air at a temperature of 130°C. In Table 4.8 the ultimate composition of the fuel as well as the mass ratios of oxygen to coal and of steam to coal are presented. It is assumed that the gasification reaction takes place at a temperature of 1500°C. The raw product gas leaves the reactor without further cooling. The composition of the product gas is presented too in Table 4.8. In the table also the lower heating value of the coal and the product gas are presented. The reactor walls are cooled with water. The water enters and leaves the cooling system at saturated conditions.

The calculated energy and exergy flows are shown in Table 4.9. The exergy of the product gas is 1545 MW from which 237 MW (15%) is thermo-mechanical exergy and 1308 MW (85%) is chemical exergy. The exergy loss is calculated from the exergy balance and is 239 MW, which is 13.4% of the fuel exergy. Thus the exergy efficiency of the gasification process is almost 86.6%. But it has to be realized

	energy [MW]	exergy [MW]
fuel	1741	1780
steam	25	10
oxygen	5	20
boiling water	397	138
saturated steam	448	164
product gas	1722	1545 ( $Ex^{tm} = 237$ ) ( $Ex^{ch} = 1308$ )
exergy loss		239 (= 13.4%)

that this efficiency does not include all processes necessary for a coal gasification system. Exergy necessary for the generation of steam and oxygen has to be added to find the total exergy loss of the gasification plant. Furthermore exergy losses will occur due to cooling and processing of the gas before it can be used for power generation or other applications. These

## Chapter 4 Fuel conversion

losses have been calculated in a system study on large scale integrated gasification combined cycle (IGCC) plants and are published in [4.19]. The results for a case with low temperature gas cleaning (SBAS) are summarized in Figure 4.18. The exergy loss of the total fuel conversion system, including coal treatment, air separation, gas cooling, gas cleaning and gas conditioning, appears to be 25.5%. The exergy loss calculated for the gasifier is 14.2% in this case. Thus, the total exergy loss of the gasification system is substantial higher than the exergy loss of the gasifier alone.

The exergy of the product gas as presented in Table 4.9 is 1545 MW. Roughly 85% of the exergy is available as chemical exergy (or cold gas exergy), the remainder (15%) is available as thermo-mechanical exergy, primarily because of the high temperature of the product gas. Efficient use of the thermo-mechanical exergy requires in general careful integration of the power generation plant. If the gasification process has to be used just for the generation of fuel, combination with appropriate heat consumers is recommended.

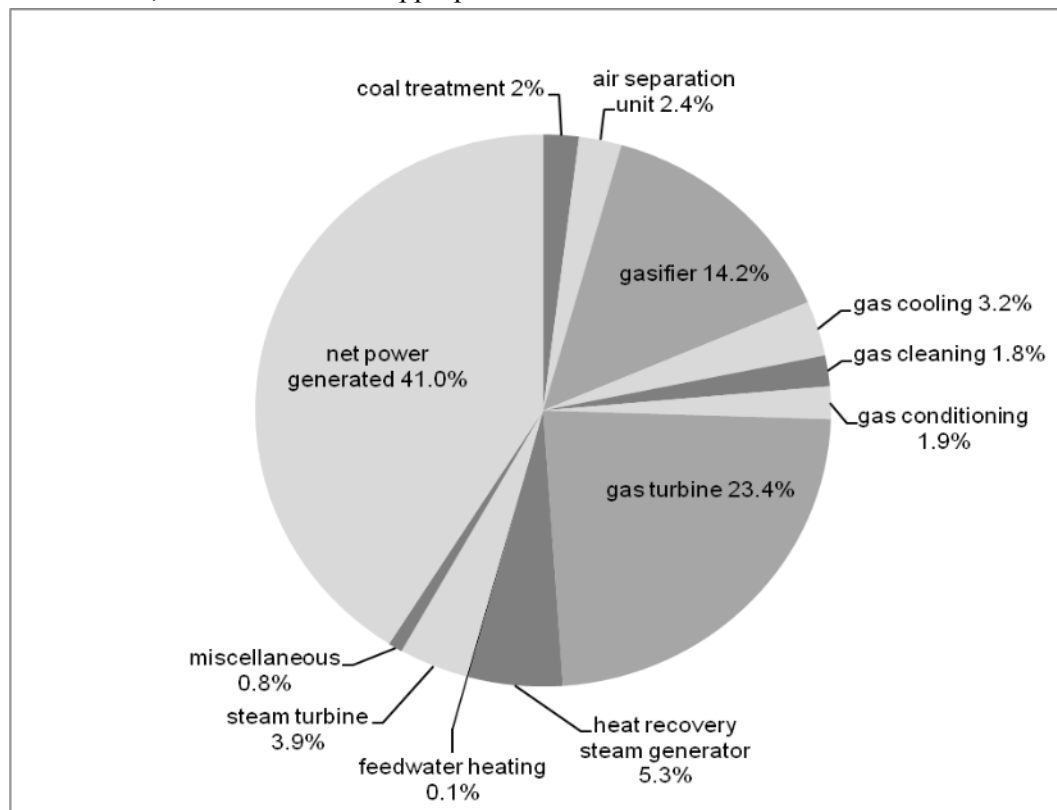


Figure 4.18 Exergy losses of an IGCC system

### 4.4.3 Biomass gasification

An air blown pressurized fluidized bed gasifier is considered for this evaluation operating at a temperature of 950°C and a pressure of 18 bar. The biomass gasifier is schematically outlined in Figure 4.19. Clean wood is supposed to be the fuel. Air enters the reactor at the bottom of the reactor vessel at a temperature of 433°C. The mass ratio air to biomass is supposed to be 1.5. The ultimate composition of the wood and the resulting composition of the product gas are shown in Table 4.10. The gasification process generates a

low calorific gas that leaves the reactor at 950°C. The lower heating value of the product gas is 4.88 MJ/kg.

The calculated energy and exergy flows are presented in Table 4.11. The exergy of the product gas is 9.62 MW from which 1.67 MW (17%) is thermo-mechanical exergy and 7.95 MW (87%) is chemical exergy. The gasifier exergy loss is 2.11 MW which is 18.6%. Then, the exergy efficiency of the gasifier is 81.4%. Also in the case of biomass gasification it has to be noticed that the exergy loss of a total system for the gasification of wood must be higher because of the exergy loss of auxiliary equipment and the gas treatment system. In [4.20] an evaluation of various gasification processes is presented. Only one air blown gasifier (the Värnamo gasifier) was considered. The other processes are using steam or oxygen for the gasification process because finally the processes have to generate hydrogen. In that evaluation the Värnamo gasifier has an exergy loss of more than 20%. The exergy loss was calculated for the gasification system without gas cleaning and gas processing.

Also in the case of biomass gasification a substantial part of the exergy of the product gas becomes available as thermo-mechanical exergy (approx. 17%). Efficient use of the heat from the product gas is required to minimize the exergy loss of the total system.

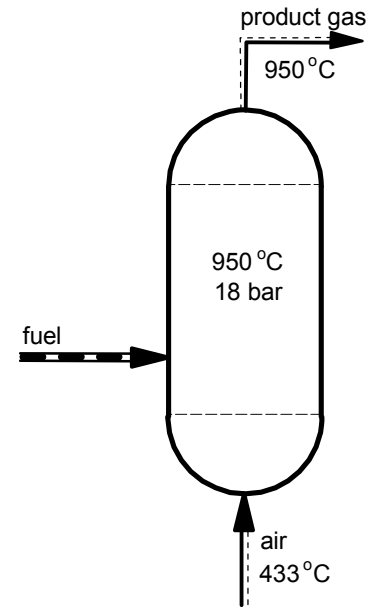


Figure 4.19 Biomass gasification in a fluidized bed gasifier

ultimate composition wood		composition product gas				
mass fractions		mole fractions				
C	0.4248	H <sub>2</sub>	0.108	mass ratio air to biomass	1.50	
H <sub>2</sub>	0.0520	CO	0.156			
H <sub>2</sub> O	0.1500	CO <sub>2</sub>	0.138	<i>LHV</i> biomass (wood) 15.47 MJ/kg product gas 4.88 MJ/kg		
N <sub>2</sub>	0.0047	H <sub>2</sub> O	0.111			
O <sub>2</sub>	0.3612	N <sub>2</sub>	0.413			
S	0.0005	Ar	0.005			
ash	0.0068	CH <sub>4</sub>	0.068			
		ash	0.019			

#### 4.4.4 Reforming of natural gas

The steam reforming process is in industry used for the conversion of natural gas into hydrogen. The reforming process is an endothermic process:



Heat is usually generated by the combustion of primary fuel in a furnace and transferred to reactor tubes placed in that furnace. More recently the process is considered too for application in fuel cell systems. Natural gas is an attractive primary fuel for fuel cells, but in the case of low temperature fuel cells it has to be converted first into almost pure hydrogen. Steam reforming is often used to convert natural gas in a mixture of hydrogen and carbon

## Chapter 4 Fuel conversion

monoxide. Further processing to convert and remove carbon monoxide is not considered here, but discussed in Chapter 6. Heat required for the reforming process can be obtained from the combustion of primary fuel or residual fuel from the fuel cell system.

A two stage natural gas reformer for application in a fuel cell system is schematically outlined in Figure 4.20. A hot flue gas flow is supposed to be available to deliver heat for the reforming process. It is assumed that the hot flue gas flow that enters the reformer at 1200°C and is cooled in the reformer to 600°C.

Steam and natural gas enter the reformer at 200°C. The steam gas mixture is heated and partly converted in the first catalyst bed by the flue gas and the hot product gas from the second stage. The mixture leaves the first stage at a temperature of 675°C and is heated by the hot product gas from the second stage. The heated product gas from the first stage is used to exchange heat with the second catalyst bed before it enters the second stage reactor. It is assumed that the mixture achieves chemical equilibrium at the highest temperature in the catalyst bed (830°C). The hot product gas is used to heat the first stage reactor. The product gas leaves the reformer system at a temperature of 600°C.

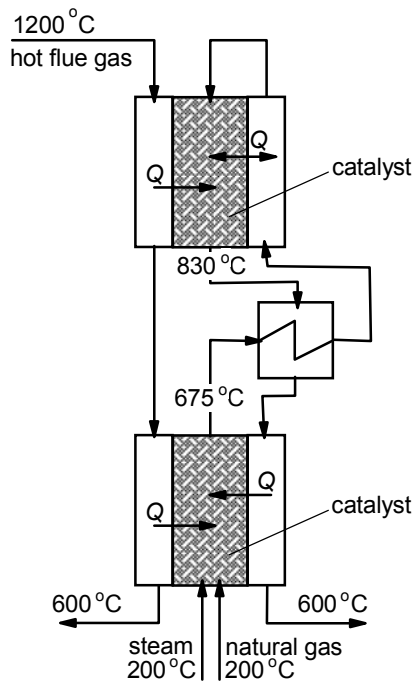


Figure 4.20 Two stage natural gas reformer

*Table 4.11 Energy and exergy to and from the gasifier and the exergy loss of the biomass gasification process*

	energy [MW]	exergy [MW]
fuel	10.97	11.34
air	0.44	0.39
product gas	11.41	9.62 ( $Ex^{\text{tm}} = 1.67$ ) ( $Ex^{\text{ch}} = 7.95$ )
exergy loss		2.11 (= 18.6%)

The calculated energy and exergy transferred to and from the reformer are presented in

Table 4.12. The exergy loss (23 kW) is only 5.8% of the exergy of the primary fuel that enters the process. This loss as such does not seem to be very harmful. The total exergy as well as the chemical exergy of the product gas are higher than the total exergy and chemical exergy of the natural gas. This is due to the endothermic character of the process. It has to be noticed, however, that the considered process does not comprise all processes necessary for the generation of hydrogen suitable for conversion in low temperature fuel cells. The generation of steam as well as the gas processing (shift reactors) and CO removal are not considered. Furthermore, the conversion of natural gas in a steam reformer is only a partial conversion of the primary fuel. That complicates the assessment of the exergy loss of such a process. An alternative and perhaps in this case a more appropriate method to assess the performance of the reforming process is the exergy efficiencies as discussed in Appendix 2.2. The exergy efficiency of a reformer was specified by Equation 31 in that appendix:

<i>Table 4.12 Energy and exergy to and from the reformer and the exergy loss of the reforming process</i>				
	energy	exergy		
		total	thermo- mechanical	chemical
	[kW]	[kW]	[kW]	[kW]
natural gas	425	395	1	394
steam	70	16	16	0
hot flue gas in	296	166	157	9
reformed gas	628	488	28	460
hot flue gas out	163	66	57	9
exergy loss		23		

$$\eta_{ex, \text{reformer}} = \frac{Ex_{\text{productgas}}^{\text{ch}} - (Ex_{\text{fuel}}^{\text{ch}} + Ex_{\text{steam}}^{\text{ch}})}{(Ex_{\text{flue gas, in}} - Ex_{\text{flue gas, out}}) - (Ex_{\text{productgas}}^{\text{tm}} - (Ex_{\text{fuel}}^{\text{tm}} + Ex_{\text{steam}}^{\text{tm}}))}$$

Using the data from Table 4.12 gives:

$$\eta_{ex, \text{reformer}} = \frac{460 - (394 + 0)}{(166 - 66) - (28 - (1 + 16))} = 0.742$$

This efficiency shows that 25.8% of the exergy that is made available for conversion is lost during the reforming process. In Chapter 6 the meaning of these losses for complete fuel cell systems are discussed further.

#### 4.5 Exergy analysis of fuel conversion in literature

The exergy analysis of fuel conversion processes as discussed in this chapter considers only the global exergy losses of these processes. That means that a detailed understanding of the origin and causes of the exergy losses (or entropy production) will not be achieved. This knowledge might be useful for the further development and optimization of fuel conversion processes. Considering the number of papers on the thermodynamic losses of fuel conversion processes, this topic has apparently fascinated many researchers. Some of these papers are discussed in this section to see in how far they offer additional insights.

In [4.2] Dunbar and Lior compare the global entropy production of combustion with the entropy production of the separate sub-processes of combustion as assumed for that evaluation like constituent mixing, oxidation and internal heat exchange. They consider four conceivable representative paths of the global combustion process for the quantification of sub-processes. Hydrogen and methane are considered as the fuels for the evaluations. When increasing the excess air from 0% to 100% the exergy efficiency of hydrogen combustion ranges from 66% to 77% and decreases with increasing the amount of excess air. Air and fuel are supposed to enter the combustion process at ambient conditions (25°C). In the case of methane combustion and considering the same conditions, the exergy efficiency ranges from 60% to 72%. Again the efficiency decreases with increasing the amount of excess air. The results of the four hypothetical process paths have revealed that the internal heat exchange is responsible for more than 2/3 of the global exergy loss. The exergy loss due to internal heat exchange increases seriously with the percentage of excess air. The differences in exergy loss

## Chapter 4 Fuel conversion

due to internal heat exchange between the considered paths are small. The exergy loss due to the mixing sub-process is rather limited and no perceptible differences between the modes of mixing are found. To reduce the entropy production during combustion it is necessary “to seek means for reducing the amount of conversion of the reactants chemical energy to the form of thermal energy”. In this respect they refer to a theoretical concept of reversible combustion as discussed by Keenan (1941). The concept was expanded further by Obert (1948, 1973) and Beretta et al. (1992). They all had to acknowledge the practical difficulties associated with this conceptual procedure. Another way, employing fuel cells, is being explored by the authors. Fuel oxidation in fuel cells produces work during the process, thus generating less internal thermal energy and entropy. This results in a significantly more efficient process.

Another paper [4.5] presents the state of the art of exergy analysis in combustion. Studies with regard to gaseous, liquid and solid fuels are evaluated with serious attention for the various combustion characteristics. The major observations relating to the reduction of thermodynamic irreversibility's in combustion processes are:

- The internal thermal energy exchange is in general the major source of irreversibility
- The rate of exergy loss by chemical reaction is reduced if the flame temperature is kept high; this can be done by oxygen enrichment of air through an exergy efficient method
- Combustion should be controlled to occur with less temperature gradient in the combustor; this can be attained by air preheating, fuel-air staging, and controlling the jet velocities.

These conclusions are in good agreement with the conclusions in Section 4.2.8.

A detailed analysis of fuel conversion processes (combustion and gasification) is presented in [4.6]. For all the considered processes a detailed analysis as well as a global analysis is made. The conversion process is divided into sub-processes like heat transfer from reaction products to reactants, instantaneous chemical reaction and product mixing. Hypothetical sequences of sub-processes are assumed in the same way as done in [4.2]. Then the entropy production can be calculated for each sub-process. Two hypothetical sequences are considered: an isothermal case and an adiabatic case. Three conversion processes are analyzed: the oxidation of solid carbon with air, the gasification of solid carbon with oxygen and the gasification of solid carbon with steam/oxygen mixtures. For the stoichiometric combustion of carbon with air it was found that the exergy loss due to internal heat transfer (14-16% of the expended exergy) is higher than the loss due to the chemical reaction (9-11% of expended exergy). For the gasification of solid carbon with air at an equivalence ratio of 0.5 an exergy efficiency of 82.7% has been calculated and for the gasification with oxygen at the same equivalence ratio an efficiency of 87.6%. If the losses of oxygen separation and the generation of the required electrical power are taken into account, the exergy efficiency of gasification with oxygen is only 77.4%. Of course this value will depend on the assumed processes for oxygen separation and required power generation. In the case of gasification with air or oxygen, the exergy loss due to chemical reaction is higher than the loss due to heat transfer. The actual rate of these losses depends somewhat on the applied sequence of sub-processes. The main consequence of the introduction of steam is that the losses for oxygen generation are largely reduced. The overall exergy efficiency does not differ much from the

oxygen blown plant. The application of solid carbon in this study instead of commercially available coal hampers the use of the conclusions for actual conversion plants. However the overall efficiency of the gasification process is close to the calculated value for the gasification of coal in Section 4.4.2.

The gasification of biomass is evaluated in [4.7] for the production of biofuels. The presented results for wood gasification are taken from [4.12]. In this paper exergy efficiencies have been calculated for the gasification of dry wood. Gasification with air and gasification with steam are considered. The exergy efficiency appears to be maximum at the carbon boundary point, the point at which all carbon is consumed. In the case of gasification with air the exergy efficiency at the carbon boundary point is 80.5% and with steam 87.6%. The gasification temperature at this point is rather low and the gasification reactions will become slow. For practical processes much higher gasification temperatures are necessary which requires higher air to fuel or steam to fuel ratios; the process conditions have to be adjusted also to the required product gas. In practice the water content of biomass is quite high. That means that process conditions and the resulting exergy efficiencies will deviate from the before mentioned values. In [4.8] it is concluded that the gasification efficiencies for other biomass fuels like straw, treated wood and grass/plants are almost similar. Only in the case of fuels like sludge and manure the gasification efficiencies are significantly lower. The most promising route to biofuels appears to be a two-stage process involving the production of syngas from biomass gasification, followed by the synthesis of transportation fuels. All reported biomass-to-biofuels routes have lower exergy efficiency compared to fossil fuels. The conversion efficiency of all investigated biomass-to-biofuel routes can be increased by improving the operation of biomass gasifiers. Of all the processes of the biomass-to biofuel route the gasifiers show the highest exergy loss.

In most of the papers on fuel conversion no special attention is given to the exergy efficiency. Usually a simple expression is used that compares the total exergy of the flows leaving the conversion system with the total exergy of the flows that enter the system. However, in [4.10] it is demonstrated that a second law efficiency defined in this way is in particular not appropriate for chemical processes. In agreement with the definitions of the exergy efficiencies presented in Section 3.6 the authors try to cancel the contribution of what they call the transiting exergy, which is the exergy of components that transit the process without participating into the reaction<sup>2</sup>. The new proposed true efficiency is called the intrinsic efficiency. Unfortunately a further specification of the intrinsic efficiency by using a break-down of exergy values into a chemical and a thermo-mechanical part as shown in Appendix 3.2 is missing in [4.10]. But the example of a chemical process for which the second law efficiency<sup>3</sup> is compared with the intrinsic exergy efficiency<sup>4</sup> as a function of the chemical conversion rate is very instructive.

In [4.11] a new coefficient was introduced: the utilizable exergy coefficient. This coefficient was proposed for the simultaneous assessment of internal and external exergy

---

<sup>2</sup> The exergy of components that do not participate into the reaction was also called: ballast exergy. The few authors in this area all use their own parameters, coefficients, specifications and nomenclature.

<sup>3</sup> The second law efficiency is the same as the universal exergy efficiency (Equation 2.67) as presented in Section 2.6.

<sup>4</sup> The intrinsic exergy efficiency is defined in the same way as the (functional) exergy efficiency (Equation 2.66) as presented in Section 3.6.

losses and the characterization of the conversion performance of chemical reactors. The application of the coefficient was demonstrated for a steam methane reforming process. The coefficient is primarily an alternative for cases in which exergy efficiencies are used in an incorrect way to draw conclusions from process evaluations. The coefficient is applied also in [4.13]. The paper describes the development of a new procedure for process synthesis of large chemical plants: the so-called exergy load distribution analysis. The application is not expected to be useful for energy conversion plants.

Most exergy evaluations of combustion processes are considering continuous flow systems. In [4.16] the exergy loss of combustion in adiabatic constant volume systems is examined. The paper focuses on the application to internal combustion engines. Therefore, special attention is given to combustion at high pressures. For the conditions of this study the calculated exergy losses range between 5 and 25%. The lower losses are derived for very high, unusual, combustion temperatures. It was found further that the dependence of the exergy loss of combustion on the reactant pressure is weak.

An exergy analysis of a bio-ethanol production process from lingo-cellulosic feedstock is presented in [4.17]. The thermodynamic efficiency of the process for biofuel production was found to be 34.7%. The major inefficiencies are caused by two processes. The combustion of lignin for process heat and power production accounts for 67% of the losses, the simultaneous scarification and co-fermentation process for 27%. Another example of the analysis of a fuel conversion process is presented in [4.18]. The paper presents an exergo-environmental analysis of a steam methane reforming process for the production of hydrogen. From the viewpoint of overall environmental impact, the study combines an exergy analysis and a life cycle assessment. The exergy efficiency of the total system appears to be 67%. By far the highest exergy losses are calculated for the combustion chamber. Also the reformer and the hydrogen separation unit show high exergy losses. The study shows that the environmental impact of the exergy losses in the components of the steam methane reforming plant are significantly higher than the component (equipment) related environmental impact. Therefore it was concluded that the overall environmental impact can be reduced by reducing the exergy losses within the components, even if this would require efficient modern equipment that requires the use of expensive materials.

This literature review offers useful information in addition to the evaluations presented first in this chapter. For the evaluation of fuel conversion systems focusing on system improvement or optimization, the calculation of global exergy losses of the apparatuses or processes is appropriate. More detailed evaluations as presented e.g. in [4.2] and [4.6] that consider various (arbitrarily chosen) sub-processes are primarily helpful to improve and optimize specific process steps. A systematic evaluation of complete combustion systems including air preheating as presented in this chapter is rather unusual but nevertheless helpful for the design and development of combustion systems. In Section 4.4 it was found that the exergy losses of systems for the conversion of primary fuels into secondary fuels are considerable. These high exergy losses are confirmed by various papers. The variety of definitions for exergy efficiencies of processes with chemical conversions complicate however the comparison of the results. Uniform definitions of exergy efficiencies are helpful for clear discussions on system performances in the future.

## 4.6 Conclusions

The thermal conversion (combustion) of fuels is associated with serious exergy losses. In general these losses are in the order of 20 to 30% of the exergy of the fuel. Exergy losses around 20% are achievable only if design parameters are used that are either economically or technically not feasible today. This conclusion is true for atmospheric as well as pressurized combustion systems. For the evaluation of pressurized systems a simple gas turbine cycle was considered. The thermodynamic equivalent temperature of heat transfer to the cycle ( $\bar{T}_0$ ) can be raised by using more complicated cycles like recuperated cycles or cycles with staged combustion. The various options are discussed more comprehensively in Chapter 5. They will enable a reduction of the exergy loss of combustion, but because of technical complications and costs such applications are rare so far.

The exergy loss of combustion is primarily determined by the thermodynamic equivalent temperature of heat transfer from the flue gas. This temperature is easily estimated by applying Equation 2.84. For quick and dirty evaluations this equation can be very useful, but it has to be noticed that under specific circumstances deviations from the true value can be significant.

Some processes for the conversion of primary fuels into secondary fuels are considered: coal gasification, biomass gasification, and steam reforming of natural gas. The exergy loss of the gasification process alone (roughly 13 to 19%) is lower than the exergy loss of combustion. But the conversion of a solid fuel into an appropriate fuel for power systems will require various auxiliaries and also further processing of the raw fuel gas. This will increase the total exergy loss of fuel conversion. The exergy loss of total fuel conversion systems is of the same order as the exergy loss of combustion systems. The exergy of the product gas can be split in chemical exergy and thermo-mechanical exergy. The relatively high thermo-mechanical exergy of the product gas (approx. 15 to 17%) is primarily caused by the high temperature of the gas as it leaves the gasifier. Efficient use of the heat from the product gas is required to minimize the exergy loss of the total system. The exergy loss of steam reforming is considered first by calculating the exergy loss of a steam reformer. The exergy loss is less than 6% of the exergy of the primary fuel. For a complete steam reforming system the exergy loss of additional process e.g. steam generation and the necessary processing of the reformed gas have to be included. In Chapter 6 a more comprehensive evaluation of steam reforming processes is given.

The conversion of natural gas in a steam reformer is only a partial conversion of the primary fuel. That complicates the assessment of the exergy loss of such a process. If the exergy loss is related to the total exergy that is involved in the process, which is actually done by the exergy efficiency, the loss appears to be 25.8%.

The exergy losses of combustion are depending also on the quality of the fuel. In the case of solid fuels like coal and in particular biomass the exergy loss of combustion appears to be higher than in the case of natural gas. The total loss of the combustion system (including the stack losses) can be more than 7% (points) higher in the case of wood combustion than in the case of natural gas.

## Chapter 4 Fuel conversion

Similar power systems as used for power generation from natural gas can be used in the case of solid fuels, if these fuels are converted first into a gaseous secondary fuel. However, the exergy loss this fuel conversion is significant. Exergy losses of gasification processes are usually in the range of 13 to 19%; additional losses for processing the gas are around 7%. This means that the highest efficiencies achievable for power plants using solid fuels are roughly 20 to 25% lower than the efficiencies of natural gas fuelled systems using similar power cycles. In the general it is concluded that the exergy losses of processes for the conversion of a primary fuel into a secondary fuel are significant. This exergy loss hinders the realization of very high ( $> 60\%$ ) overall conversion efficiencies of power plants using solid fuels.



## 5 THERMAL POWER CYCLES

### 5.1 Introduction

A large variety of thermal power cycles has been developed up to now for the generation of power, e.g. internal combustion engines, steam turbine cycles, gas turbine cycles, organic rankine cycles. This chapter will primarily focus on power cycles for large scale power generation based on steam turbine and gas turbine cycles. But, the fundamental thermodynamic approach might be useful also for other types of thermal power cycles. Insights and conclusions derived from these evaluations can be used in general for the development of thermal power cycles.

The objective of this chapter is primarily to demonstrate the application of the exergy concept for the thermodynamic design and development of thermal power cycles and to discuss the limitations as well as the options for further improvement of the thermodynamic performance. The thermodynamic equivalent temperature and the internal exergy efficiency of a thermal power cycle as presented in the Sections 2.6.4 and 2.6.5 are extensively used for this purpose.

In Section 5.2.1 the various options for improving the efficiency of thermal power plants are discussed. The exergy calculation of the conventional power plant as presented in Appendix 4.1 shows that the exergy loss due to heat transfer from the flue gas to the power cycle is quite high (21.1%). This chapter will focus on the possibilities to reduce or to avoid these losses. For that purpose different methods are conceivable. The most obvious way is to apply steam conditions that enable heat transfer to the power cycle at higher temperatures. Steam turbine cycles with so-called “advanced steam conditions” make use of supercritical steam pressures ( $p > 221.20 \text{ bar}$ ) and higher steam temperatures ( $600 < T < 700 \text{ }^\circ\text{C}$ ) at the inlet of the HP turbine (see e.g. [5.3], [5.4] and [5.5]). The resulting efficiency improvements are discussed in Section 5.2.2. The combination of high pressures and high temperatures is a real challenge with regard to materials that have to be used for the last superheater of the boiler, the life steam pipe and the HP turbine. The application of topping cycles makes it possible to mitigate the material loads or to limit the material quantities. For that purpose a variety of topping cycles has been evaluated in the past, in particular after the oil crises of the seventies. In Section 5.3 the potassium topping cycle is discussed as an example. At the time this topping cycle was considered (around 1980) it was expected that coal should be the suitable fuel for large scale power generation. However, the only topping cycle that has been applied successfully up to now is the gas turbine topping cycle. Gas turbine topping cycles have been applied primarily for natural gas fired systems. In the case of coal fired systems the IGCC has to compete with conventional combustion plants with supercritical steam cycles and it is still uncertain which of these technologies will be the most attractive for future applications.

The exergy efficiency of a process or system pretends to indicate the difference between the actual performance of the system and the performance of a reversible system operating under identical thermodynamic conditions. The true value of the ratio between the actual and

the reversible system is important to see what savings are achievable by further improvement of the system. In various discussions the question was raised whether the exergy efficiency represents the true ratio between the actual and the

*Table 5.1 Exergy losses of the conventional steam cycle (reference system)*

	MW	rel. ex. loss (%)
exergy losses		
boiler	753.23	51.05
steam cycle	97.36	6.60
cooling water system	19.22	1.30

reversible system. The primary reason to doubt about the true ratio is that the exergy flows that leave the system unused are affected by the quality of the system itself. If the quality of the system increases, the exergy flows that leave the system will decrease. The decrease of this exergy flow will cause an additional increase of the performance of the reversible system. This is in general also the case if Equation 2.65 is used to define the exergy efficiency of thermal power cycles. Therefore, the internal exergy efficiency of a thermal power cycle has been defined in Section 2.6.5. It is expected that the internal exergy efficiency as defined by Equation 2.87 and Equation 2.88 gives a better approximation of the true ratio between the actual cycle and the ideal cycle than the usual exergy efficiency. A comparison of the two exergy efficiencies is made in the Sections 5.2 and 5.5.

## 5.2 Steam turbine cycles

### 5.2.1 Conventional steam turbine plant (reference system)

A conventional power plant that has been used within the Energy Systems group as a reference system for the evaluation of advanced power plants is described in Appendix 4.1. The steam turbine cycle of this conventional power plant is used as the starting point for the discussions in this section. Heat from external sources is transferred to the steam cycle in the evaporator, the superheaters, the reheaters, and the economizer. Equation 2.83 in Section 2.6.4 has been derived to calculate the thermodynamic equivalent temperature of heat transfer to a fluid. However, in the case of this reference system heat is transferred to two fluid flows with different flow rates: the fluid through the economizer, evaporator and superheaters and the fluid through the reheaters. Then Equation 2.83 has to be written as:

$$\bar{T} = \frac{\sum m \cdot (h_{\text{out}} - h_{\text{in}})}{\sum m \cdot (s_{\text{out}} - s_{\text{in}})} \quad (5.1)$$

Then, the thermodynamic equivalent temperature of heat transfer to the cycle is:

$$\bar{T}_H = 645.76 \text{ K } (= 372.61^\circ\text{C})$$

Heat is transferred from the cycle at the temperature of condensation of the steam in the condenser, thus:  $\bar{T}_C = 295.51 \text{ K } (= 22.36^\circ\text{C})$

Because of the thermal losses of the boiler only 94.14% of the heat from the fuel is transferred to the power cycle. Then, the heat transferred to the cycle is:

$$Q_{\text{to}} = 1310090 \text{ kW}$$

The gross electrical power delivered by the cycle is 600 MW. If the losses of the electrical generator are included in the thermal efficiency of the cycle, the thermal efficiency is:

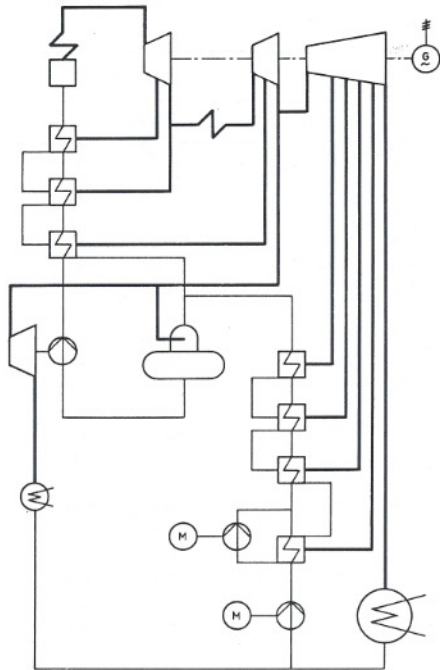


Figure 5.1 Steam cycle with single reheat

values for in principle the same quality factor. Theoretically the internal exergy efficiency gives the true value if it is assumed that the temperatures of heat transfer to and from the cycle are not affected by the losses within the cycle. This seems to be a reasonable assumption in the case of steam cycles.

The value of the internal exergy efficiency is determined by the quality of the various system components: the steam turbine, the feedwater heaters, the boiler feedwater pump and feedwater pump turbine. From Appendix 4.1 it appears that the exergy losses of the steam turbine are responsible for 70% of the total exergy loss of the steam cycle. A further reduction of

$$\eta_{th} = 0.4580$$

Then, the internal exergy efficiency of the cycle can be calculated using Equation 2.88:

$$\eta_{ex, \text{intern}} = 0.8444$$

This means that the actual generated electrical power is 84.44% of the theoretical maximum achievable electrical power generated by the cycle<sup>1</sup>.

The exergy efficiency of the power cycle can be defined as the ratio of the generated shaft power and the available exergy. The available exergy is actually the difference between the exergy transferred to the cycle and the exergy transferred from the cycle. Thus:

$$\eta_{ex, \text{ST cycle}} = \frac{P_{\text{shaft}}}{Ex_{\text{to}} - Ex_{\text{from}}} = 0.8631$$

It appears that the two efficiencies give different

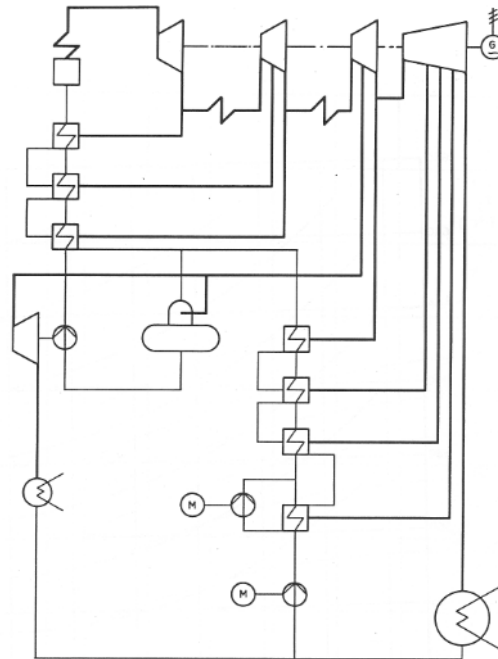


Figure 5.2 Steam cycle with double reheat

<sup>1</sup> In this evaluation it is assumed that heat is transferred from the cycle at condenser temperature. Thus, the exergy loss of the condenser is not included in the internal exergy efficiency of the cycle ( $\eta_{ex, \text{intern}}$ ). If it is preferred to include the condenser losses in the internal efficiency the temperature of the environment has to be used to determine the ideal cycle efficiency (Carnot efficiency). In that case the internal exergy efficiency of the cycle is 82.70% instead of 84.44%.

the losses of the steam cycle is conceivable but the actual value is normally the result of balancing costs against performance. It is expected that only limited improvements are achievable in the future.

From Appendix 4.1 it appeared that the gross exergy efficiency of the conventional power plant is only 40.70%. The exergy losses of the plant are summarized in Table 5.1 and in the exergy flow diagram presented in Figure 8 of this appendix. The diagram shows that the highest exergy losses occur in the boiler primarily due to combustion and heat transfer. A further reduction of the losses due to combustion is conceivable as shown in Chapter 4, but the achievable reduction is rather limited. The most effective option for improving the efficiency of thermal power plants is the reduction or the elimination of the exergy losses due to heat transfer. A reduction of the losses due to heat transfer is possible by raising  $\bar{T}_H$ , the temperature of heat transfer to the cycle. This can be achieved by applying advanced steam conditions or rankine topping cycles. The elimination of heat transfer and its corresponding losses can be realized by integration of the combustion process in the power cycle as usual in e.g. gas turbines and MHD (magneto-hydrodynamic) systems. Some of these options are discussed in the following sections.

### 5.2.2 Advanced steam conditions

The term “advanced steam conditions” is used for the application of steam cycles with higher steam temperatures ( $> 540^\circ\text{C}$ ) and supercritical pressures at the inlet of the steam turbine. The effect of the application of advanced steam conditions was investigated by the Energy Systems group of the TU Delft in 1985 [5.1]. The original report was presented in Dutch. Therefore a summary of the assumptions and results is presented in Appendix 5.1. A further evaluation of the results is presented in this section.

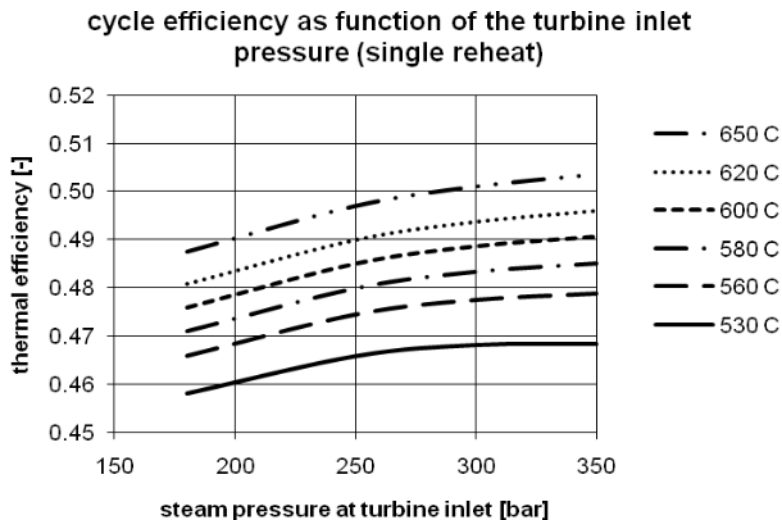


*Figure 5.3 Cycle efficiency as function of the turbine inlet pressure, with the turbine inlet temperature as parameter (single reheat)*

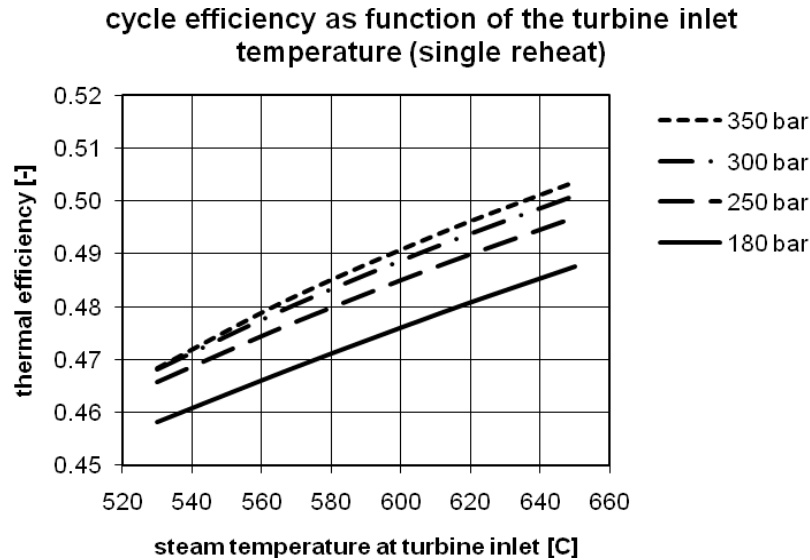


Figure 5.4 Cycle efficiency as function of the turbine inlet temperature, with turbine inlet pressure as parameter (single reheat)

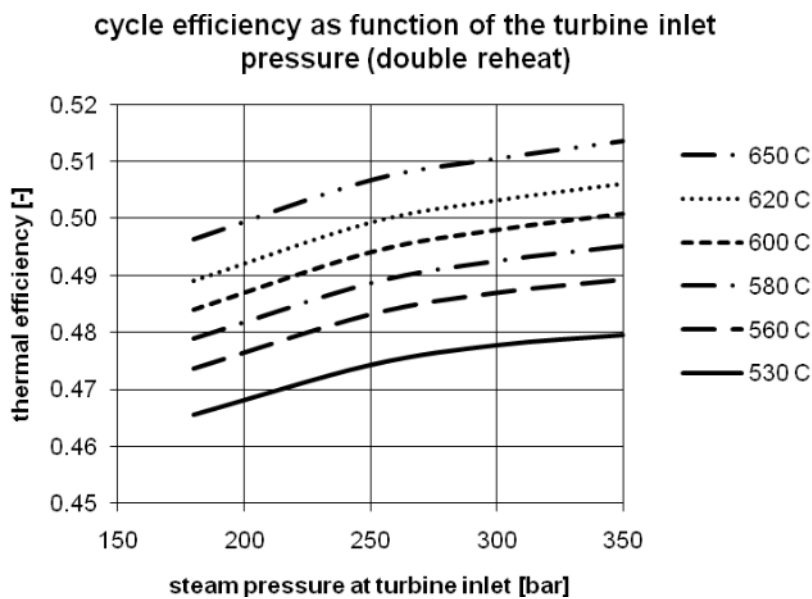
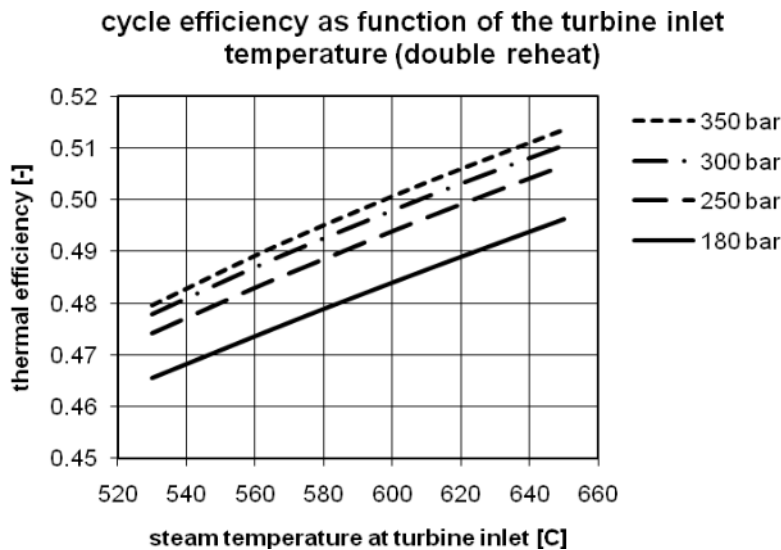


Figure 5.5 Cycle efficiency as function of the turbine inlet pressure,

System calculations are made for two configurations, one with a single reheat steam cycle (see Figure 5.1) and one with a double reheat steam cycle (see Figure 5.2). The steam cycle of the reference system presented in Appendix 4.1 has the same configuration as the cycle with single reheat but the efficiencies are not exactly the same because of some minor differences of the design data. For the evaluation of advanced steam cycles a system with turbine inlet conditions of 180 bar and 530°C, the same as for the reference system, is chosen as the starting point. Further system calculations are made for steam pressures of 250, 300 and

350 bar and steam temperatures of 560, 580, 600, 620 and 650°C, in total 24 system calculations for each configuration. The assumptions with regard to system design and design parameters necessary for the system calculations are presented in Appendix 5.1 together with the results. The calculated thermal efficiencies of the various cycles are presented in the Figures 5.3 and 5.4 for the single reheat steam cycles and in Figures 5.5 and 5.6 for the double reheat steam cycles. It should be noticed that in a detailed evaluation of steam cycles the results are always susceptible to the chosen design parameters, in particular the assumptions with regard to the steam turbine. In this case the dimensions of the last stage of the LP turbine are relatively small. This increases the effect of the LP turbine exhaust loss.



*Figure 5.6 Cycle efficiency as function of the turbine inlet temperature, with turbine inlet pressure as parameter (double reheat)*

Figure 5.3 shows that for all considered turbine inlet temperatures an increase of the steam pressure up to 250 bar is useful. A further increase of the pressure is effective only in combination with higher inlet temperatures. Figure 5.4. shows that the thermal efficiency increases almost linear with the turbine inlet temperature. The calculated increase of the thermal efficiency is roughly 2.5% to 2.9% (percentage points) per 100 K. The lower value is calculated for the cycle with a steam pressure of 180 bar, the higher value for the cycle with a steam pressure of 350 bar. Thus, the efficiency increase appears to be higher at higher steam pressures.

The results for the steam cycles with double reheat show more or less the same tendencies. Figure 5.5 shows, however, that the double reheat cycle will benefit slightly more from a higher turbine inlet pressure. The efficiency increases with increasing pressure even in the case of lower steam temperatures. Also in this case the thermal efficiency of the cycle increases almost linear with the steam temperature at turbine inlet (see Figure 5.6). The calculated increase is roughly 2.6% to 2.8% (percentage points) per 100 K. The lower value is for the cycle with a steam pressure of 180 bar, the higher value for the cycle with a steam

## Chapter 5 Thermal power cycles

pressure of 350 bar. The application of double reheat results in somewhat higher thermal efficiencies in comparison with single reheat. The increase in efficiency is about 0.8% (point) for the 180 bar cycles up to about 1.0% for the 350 bar cycles.

For a better understanding of the results of the cycle calculations the internal exergy efficiency was calculated for all considered cases. Unfortunately, some data necessary for the calculation of these efficiencies are estimated since the original system calculations are no longer available. Only the data presented in Appendix 5.1 are available for this purpose. For the calculation of the internal exergy efficiency of the cycle Equation 2.88 is used. This equation writes the thermal efficiency of a steam cycle as:

$$\eta_{\text{th, cycle}} = \eta_{\text{ex, intern}} \cdot \left(1 - \frac{\bar{T}_C}{\bar{T}_H}\right)$$

All systems use the same condenser temperature, thus,  $\bar{T}_C$  is constant. Then, the thermal efficiency is determined only by the value for  $\bar{T}_H$ , the thermodynamic equivalent temperature

*Table 5.2 Results of cycle calculations (single reheat steam cycle)*

$p_{\text{steam}}$	$T_{\text{steam}}$	$\bar{T}_H$	$\bar{T}_C$	$\eta_{\text{rev}}$	$\eta_{\text{th, cycle}}$	$\eta_{\text{ex, intern}}$
180	530	643.86	295.55	0.5410	0.4581	0.8468
	560	651.44	295.55	0.5463	0.4660	0.8530
	580	656.66	295.55	0.5499	0.4711	0.8567
	600	662.00	295.55	0.5536	0.4760	0.8599
	620	667.40	295.55	0.5572	0.4808	0.8629
	650	675.77	295.55	0.5626	0.4876	0.8666
250	530	663.33	295.55	0.5544	0.4658	0.8401
	560	671.77	295.55	0.5600	0.4745	0.8473
	580	677.41	295.55	0.5637	0.4799	0.8513
	600	683.01	295.55	0.5673	0.4851	0.8551
	620	689.00	295.55	0.5710	0.4900	0.8581
	650	697.87	295.55	0.5765	0.4970	0.8621
300	530	672.87	295.55	0.5608	0.4681	0.8348
	560	682.04	295.55	0.5667	0.4775	0.8426
	580	688.05	295.55	0.5705	0.4833	0.8472
	600	694.06	295.55	0.5742	0.4887	0.8511
	620	700.55	295.55	0.5781	0.4938	0.8542
	650	710.14	295.55	0.5838	0.5010	0.8581
350	530	678.53	295.55	0.5644	0.4683	0.8297
	560	690.15	295.55	0.5718	0.4788	0.8374
	580	696.74	295.55	0.5758	0.4850	0.8423
	600	703.38	295.55	0.5798	0.4907	0.8463
	620	709.74	295.55	0.5836	0.4961	0.8501
	650	719.72	295.55	0.5894	0.5035	0.8543

of heat transfer to the cycle, and  $\eta_{\text{ex, intern}}$ . The temperature  $\bar{T}_H$  is calculated with Equation 5.1. Then, the enthalpies and entropies at the inlet and outlet of the boiler and the reheaters have to

be known as well as the ratio of the mass flows to boiler and reheaters. However, the actual data for the mass flows and the inlet temperatures of the reheaters are missing. It appears that the value of the ratio of the mass flows to the boiler and the reheater has very little effect on the value of  $\bar{T}_H$ . Therefore, it was decided to use the mass flow ratio of the reference system (Appendix 4.1) for the cycles with single reheat; for the cycles with double reheat the mass flow rate of the first reheater is assumed to be 90% of the mass flow rate of the boiler and the mass flow rate of the second reheater is assumed to be 75%. The inlet temperature of the reheater is supposed to be near to its optimum value. The optimum value is obtained more or less inlet temperature of the reheater equals the thermodynamic equivalent temperature of heat transfer to the boiler. Moreover, the optimum is very flat. It was decided to take the thermodynamic equivalent temperature of the boiler as the inlet temperature of the first reheater. The thermodynamic equivalent temperature of boiler and first reheater together is used as the inlet temperature of the second reheater. The resulting values of  $\bar{T}_H$  are presented

*Table 5.3 Results of cycle calculations (double reheat steam cycle)*

$p_{\text{steam}}$	$T_{\text{steam}}$	$\bar{T}_H$	$\bar{T}_C$	$\eta_{\text{rev}}$	$\eta_{\text{th, cycle}}$	$\eta_{\text{ex, intern}}$
180	530	646.26	295.55	0.5427	0.4655	0.8578
	560	655.48	295.55	0.5491	0.4736	0.8625
	580	662.03	295.55	0.5536	0.4789	0.8651
	600	668.33	295.55	0.5578	0.4840	0.8677
	620	674.82	295.55	0.5620	0.4890	0.8701
	650	684.95	295.55	0.5685	0.4963	0.8730
250	530	664.08	295.55	0.5555	0.4743	0.8539
	560	674.16	295.55	0.5611	0.4831	0.8610
	580	680.83	295.55	0.5648	0.4886	0.8651
	600	687.73	295.55	0.5685	0.4940	0.8690
	620	694.68	295.55	0.5722	0.4992	0.8723
	650	705.30	295.55	0.5777	0.5067	0.8771
300	530	672.69	295.55	0.5618	0.4778	0.8505
	560	683.69	295.55	0.5678	0.4869	0.8575
	580	690.84	295.55	0.5716	0.4925	0.8616
	600	698.02	295.55	0.5754	0.4979	0.8653
	620	705.65	295.55	0.5794	0.5031	0.8683
	650	716.66	295.55	0.5851	0.5105	0.8725
350	530	678.34	295.55	0.5657	0.4796	0.8478
	560	691.28	295.55	0.5730	0.4892	0.8538
	580	698.86	295.55	0.5770	0.4951	0.8580
	600	706.44	295.55	0.5810	0.5007	0.8618
	620	714.03	295.55	0.5848	0.5060	0.8653
	650	725.41	295.55	0.5906	0.5136	0.8696

## Chapter 5 Thermal power cycles

in Table 5.2 for the single reheat cycles and in Table 5.3 for the double reheat cycles. With these values the thermal efficiencies of the reversible cycles are calculated with the following equation:

$$\eta_{\text{rev}} = 1 - \frac{\bar{T}_C}{\bar{T}_H}$$

The values of  $\eta_{\text{th, cycle}}$  are available from the calculations with the Cycle-Tempo models. Finally, the values for  $\eta_{\text{ex, intern}}$  as shown in Table 5.2 and Table 5.3 are calculated.

It is obvious that higher steam temperatures and steam pressures will result in higher thermal efficiencies of the reversible cycle because of the higher thermodynamic equivalent temperature of heat transfer to the cycle. But, it appears that also the internal thermodynamic losses of the cycle are affected by the changing the steam conditions. Therefore, the effects on the thermal efficiency of the reversible cycle (the Carnot efficiency) and on the internal exergy efficiency are considered separately. The thermal efficiencies of the reversible cycles are depicted in Figure 5.7 for the single reheat cycle and in Figure 5.8 for the double reheat cycle. The results of the single reheat cycle show that the thermal efficiencies of the reversible cycle increase almost linearly with the steam temperature at turbine inlet. And the increase per K appears to be practically independent of the steam pressure. The only exception is the step from 530°C to 560°C for the 350 bar case. This deviation is apparently

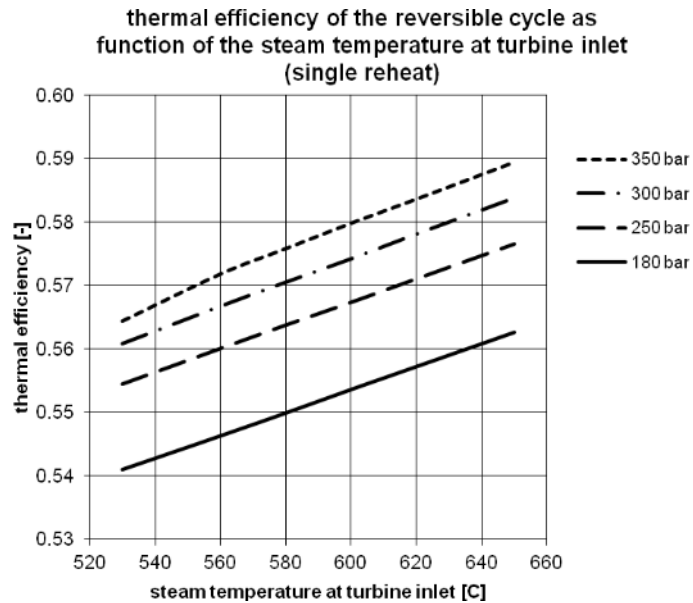


Figure 5.7 The thermal efficiency of the reversible cycle as function of the turbine inlet temperature, with the turbine inlet pressure as parameter (single reheat)

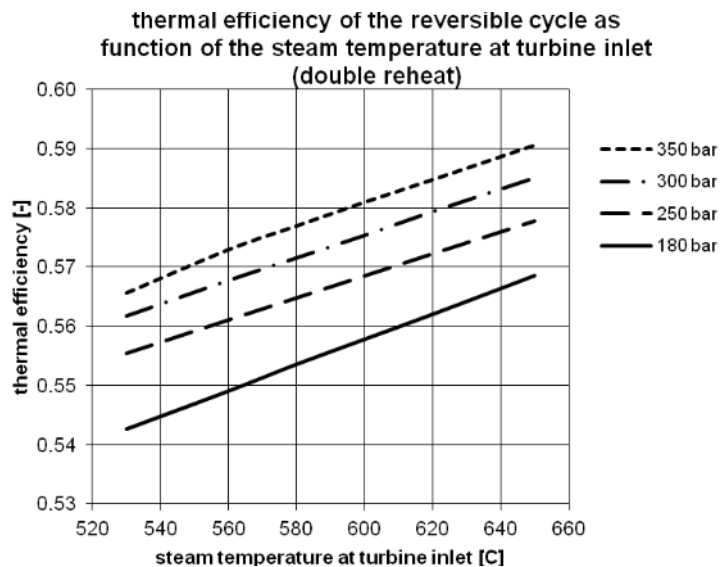


Figure 5.8 The thermal efficiency of the ideal cycle (carnot efficiency) as function of the turbine inlet temperature, with the turbine inlet pressure as parameter (double reheat)

caused by the relatively low boiler inlet temperature (see Table 2 of Appendix 5.1). As there is no reasonable explanation for this assumption, the chosen boiler inlet temperature is

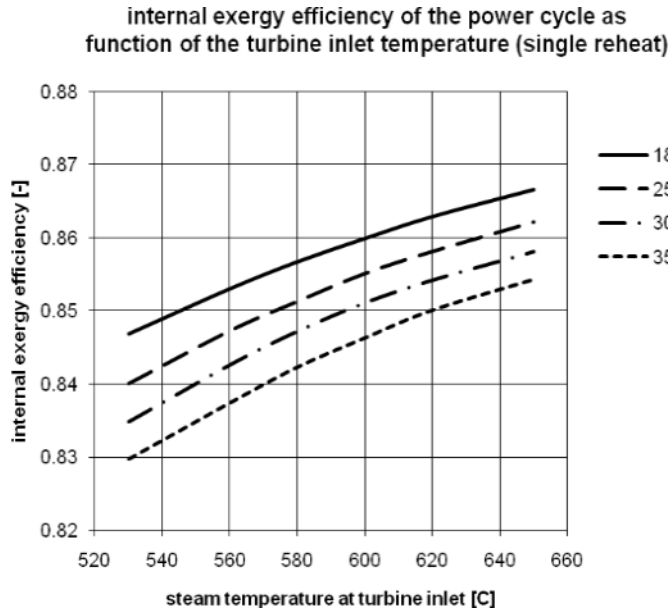


Figure 5.9 The internal exergy efficiency of the power cycle as function of the turbine inlet temperature, with the turbine inlet pressure as parameter (single reheat)

5.9 for the single reheat systems and in Figure 5.10 for the double reheat systems. The internal exergy efficiencies are primarily determined by the isentropic efficiencies of the steam turbines. In general these isentropic efficiencies are higher as the steam volume flow rate is higher. The internal efficiencies of the single reheat systems are in full agreement with this rule. The internal exergy efficiencies of the power cycles are higher if the steam temperature is higher, and are lower if the steam pressure is

supposed to be incorrect for a systematic evaluation. The same effect is observed in Figure 5.8 for the double reheat cycles. Another difference is the slope of the curve for the systems with a turbine inlet pressure of 180 bar. This curve appears to be somewhat steeper than the others. Obviously, the systems with a turbine inlet pressure of 180 bar benefit somewhat more from a temperature increase than the systems with higher turbine inlet pressures.

The internal exergy efficiencies of the power cycles are depicted in Figure

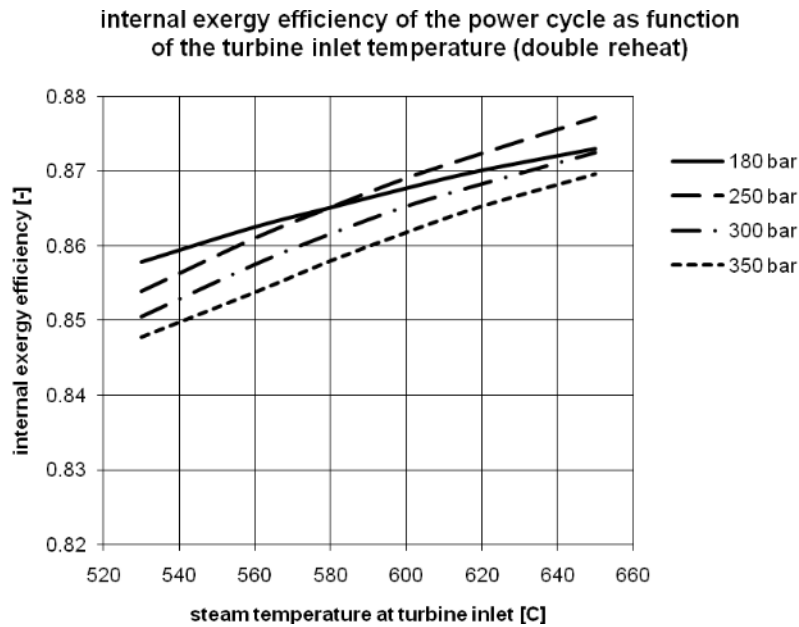
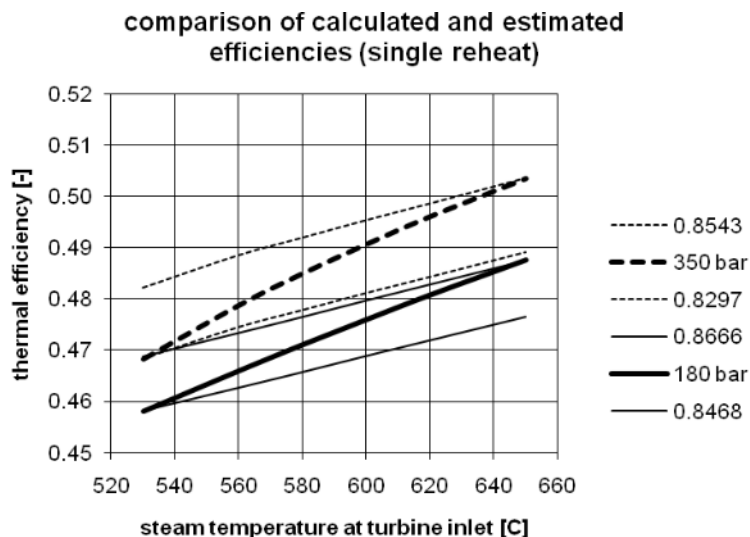


Figure 5.10 The internal exergy efficiency of the power cycle as function of the turbine inlet temperature, with the turbine inlet pressure as parameter (double reheat)

## Chapter 5 Thermal power cycles

higher. The efficiency values of the double reheat cycle show the same tendencies if the turbine inlet pressure is higher than 250 bar. Since the double reheat increases the average steam volume, the internal exergy efficiencies of the double reheat cycle are significantly higher than of the single reheat cycles. Obviously, the results of the cycle with a steam turbine inlet pressure of 180 bar are not in line with the other results. The increase of the internal exergy efficiency with the turbine inlet temperature is lower than for the series with higher steam pressures. In Table 4 of Appendix 5.1 also the isentropic turbine efficiencies are presented for the double reheat case. Evaluation of the efficiencies of the HP turbine of the 250 bar series learns that the increase of the isentropic efficiency when increasing the turbine inlet temperature is much higher than for the other series. Probably this is caused by the large changes of the inlet pressure of the IP turbine (see Table 4 of Appendix 5.1). These pressures are chosen by using data from literature. It is questionable if the chosen values are really appropriate for this cycle evaluation. However, no serious effects have been noticed if only the thermal cycle efficiencies are considered. The effect on the overall results is very limited.



*Figure 5.11 Comparison of the actual efficiencies of the power cycles (for 180 and 350 bar) with estimated thermal efficiencies based on constant internal exergy efficiencies (max. and min value of considered series)*

The evaluation of the results of the cycle calculations shows that the application of the internal exergy efficiency of the power cycle can be helpful for analyzing the results. The internal exergy efficiency can also be applied for “quick and dirty” cycle evaluations. E.g. if the effect of a variable on the thermodynamic equivalent temperatures of heat transfer to and from the cycle is known, a rough estimate of the cycle performance can be made using an estimated value for the internal exergy efficiency. Depending on the actual conditions such an evaluation can be rough. In Figure 5.11 the thick lines represent the actual calculated thermal efficiencies for the series with a turbine inlet pressure of 180 bar and 350 bar. The thin lines do represent estimated values of the thermal cycle efficiencies when using the ideal cycle efficiency in combination with a constant (estimated) internal exergy efficiency. For the estimated values the minimum and maximum values of each of the considered series are applied. It appears that the application of a constant internal exergy efficiency underestimates the effect of the steam temperature on the thermal efficiency of the cycle. Nevertheless, the application of the internal exergy efficiency can be useful if no more appropriate information is available. But it has to be noticed that the inaccuracy might be considerable.

### 5.2.3 Prospects of advanced steam conditions

The application of advanced steam cycles is primarily considered for coal fired systems. If natural gas or oil are available for power generation, the application of CC plants is in general more attractive. Worldwide, however, coal is often preferred for power generation because of availability and lower fuel price. In [5.3] it was mentioned that thermal power plants using conventional fossil fuels cover more than 70% of the total world's electricity production, with more than 40% coal contribution. In the case of coal fired systems, the IGCC (Integrated Gasification Combined Cycle) is a serious alternative for the direct combustion of coal. But usually the application of direct combustion of coal in combination with a steam cycle is preferred for economical reasons. In general steam cycles with advanced conditions are combined with pulverized coal combustion systems. But, as concluded in [5.2], also CFB boilers can operate with advanced USC steam conditions (365 bar, 700°C) in a conventional configuration provided materials with sufficient strength, fire side corrosion resistance, and steam side oxidation resistance, are developed for these conditions.

Up to the nineties conventional steam parameters (approximately: temperature 535°C and pressure 180 bar) were limited because of the properties of available materials for the critical parts of the cycle: primarily the superheater and reheater of the boiler, the piping and flow control from boiler to steam turbine, and the HP and IP sections of the steam turbine. The progress with regard to the development of high strength ferritic steels stimulated the interest for higher steam conditions. In a study by MAN and GEC ALSTHOM [5.7], published in 1993, it was concluded that steam conditions up to 300 bar and 580 to 600°C might be feasible for 800 MW steam turbine cycles. Fuel savings of around 6% are calculated if steam conditions are increased from 160 bar and 535°C to 300 bar and 580°C/600°C. In the case of advanced steam conditions the temperature of reheated steam to the IP turbine is supposed to be 20K higher than the temperature at the inlet of the HP turbine. The same advanced conditions are mentioned in [5.8], a study performed by SK Power Company in Denmark and published in 1994. Supercritical steam plants like Hemweg 8, coming into operation at that time, had steam conditions like 250 bar/535°C and 48 bar/563°C [5.9]. An overview of the state of the art in Denmark in 1999 is presented in [5.10]. The application of the 9% chromium steel P91 has enabled steam conditions like 290 bar/582°C/580°C/580°C for the plant Nordjylland 3 that came into operation in 1998. It was expected at that time that after 2001 life steam temperatures up to 640°C will become possible with the application of P92. It was mentioned too that in 1998 a project of large power industries and power companies was started focusing on a demonstration project called "Advanced (700°C) coal fired power plant". The goal of the project was the introduction of new nickel based super alloys for application at temperatures up to 700°C. Depending on fuel type and location the efficiency of such a power plant is expected to be 52-55%. The project will take a period of 17 years.

Several German companies cooperated into a study to come to a sustainable reference design for a coal fired power plant as published in 2004 [5.11]. Assuming a commissioning date of 2008, steam conditions selected for the reference power plant are 285 bar/600°C/620°C, and the net efficiency is supposed to be 45.9% (with cooling tower). Location of the plant at a costal site on the North Sea coast of Germany might increase the net

## Chapter 5 Thermal power cycles

efficiency with 1 percentage point. In a publication by Siemens in 2009 [5.4] these performance data were confirmed for a carbon capture ready (CCR) design. Net efficiencies of 45.5–46.0%, depending on site and fuel conditions, are mentioned for a plant with steam parameters 280 bar/600°C/610°C. Net efficiencies above 50% are expected to be achievable at coastal sites if nickel-based alloys prove their economic readiness for use. The first Siemens reference plant in the USA was applied in the Longview Power Project [5.6]. It was expected that the plant will start commercial operation in 2011. Steam conditions are 265 bar/569°C/557°C, and the net efficiency is 40.8% (LHV).

In [5.5] various options for high efficiency power generation are discussed and compared. Natural gas fired as well as coal fired systems are considered. It was mentioned that with mature technology and commercial US boiler plant practice efficiencies of 41.5% (LHV) can be achieved with SC steam parameters of 250 bar/540°C. It is expected that 50% (LHV) efficiency will be achievable with 700°C USC plants. Some interesting concluding remarks from [5.5] are:

- Efficiency improvement is far the most predictable and lowest cost method to reduce all emissions including CO<sub>2</sub>.
- In the near term, the choice of coal-based generating technology without CCS is PC or CFBC in supercritical, or for PC also USC cycle. While IGCC has a smaller cost differential between no-capture and capture plant, IGCC without CO<sub>2</sub> capture it is not presently competitive on cost and on availability with PC or CFBC plants.
- IGCC with CCS technology is likely to emerge as the eventual sustainable coal fuelled option; it has the advantage of providing the base for the future hybrid fuel cell/GT/steam coal plant with 60% cycle efficiency and near zero emission.

### 5.3 Potassium topping cycles

#### 5.3.1 Introduction

After the first oil crisis in 1973 the interest for energy conversion technologies with higher conversion efficiencies was growing. At that time various advanced energy conversion technologies were investigated or under development by the NASA for space applications. Therefore the NASA was requested by the US Department of Energy to evaluate various technologies for terrestrial application. This has resulted in the so-called Energy Conversion Alternatives Study (ECAS). Also in Europe the search for higher conversion efficiencies for the power industry was going on. In 1979 the Dutch government approved the evaluation of the Potassium Rankine Cycle as a contribution to an IEA study, together with German and Austrian partners, and a national comparison of topping cycles (MHD + steam cycle, potassium cycle + steam cycle, coal gasification CC). In all cases coal

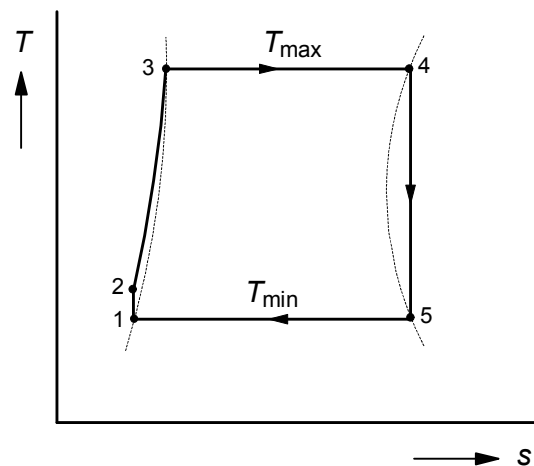


Figure 5.12  $T,s$ -diagram of a hypothetical cycle fluid

was considered as the primary fuel. In this section some results of the study on potassium topping cycles are discussed.

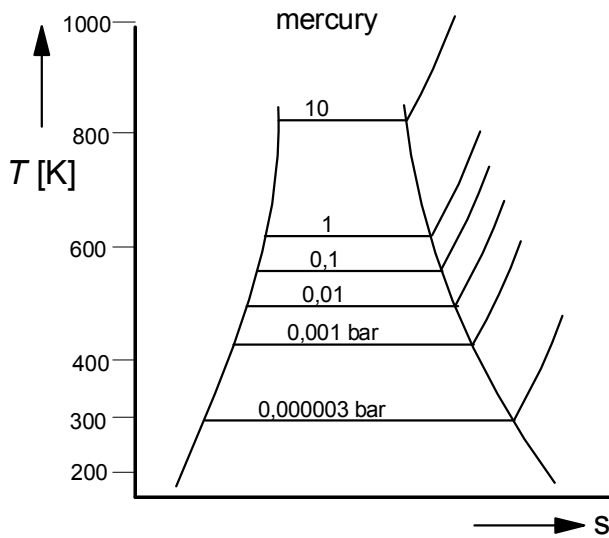


Figure 5.13  $T,s$ -diagram of mercury

The  $T,s$ -diagram of a hypothetical cycle fluid, as shown in Figure 5.12, can be used to explain the attractiveness of liquid metals as the working fluid of a rankine cycle. The dotted lines are the left and right border of the two phase area and the cycle is represented by the solid lines between the points 1 to 5. In the case of a cycle fluid with ideal properties, the compression work and thus the enthalpy difference  $h_2 - h_1$  should be small. The curve from point 2 to 3 must be steep, then the heat transferred to the cycle at temperatures lower than  $T_{\max}$  will be small. If the fluid has a high critical temperature heat

transfer during evaporation  $Q_{3-4}$  can occur at high temperature and if the saturation pressure is not too high material stresses in the high temperature parts of the system are limited. The right border of the two phase area must preferably be such that that the expansion end point (point 5) lies just within the two phase area. Then, the fluid in the last stages of the turbine will contain almost no liquid drops and heat transfer from the cycle occurs only at  $T_{\min}$  the lowest temperature of the cycle. The pressure during condensation must be not very low to avoid very large dimensions of the last turbine stages. Furthermore, the fluid should not be toxic, corrosive or very expensive.

The application of liquid metal rankine cycles has attracted interest already before the second world war in order to transfer heat to the power cycle at higher temperatures. At that time mercury was considered as cycle fluid. The very high temperature at the critical point of mercury (around 1764 K) allowed for vaporization at high temperature in combination with reasonable pressure. The  $T,s$ -diagram of mercury, as sketched roughly in Figure 5.13, shows that the fluid properties are in many respects close to the ideal fluid properties. However, condensation at low temperatures causes huge vapor volumes. To limit the dimensions of the low pressure turbine, condensation of the fluid occurred at higher temperatures. For that reason combination with a steam bottoming cycle was necessary to achieve high overall efficiencies. Furthermore, mercury is very poisonous. In the period from 1928 to 1950 some plants have been build and operated. But the results of actual plant operation were not sufficient to continue application of this technology. During the sixties the application of mercury power cycles has been considered by NASA for electricity generation in space. But this has not resulted into actual application.

The development of sodium cooled fast breeder nuclear reactors during the seventies of the last century has provided a serious boost of liquid metal technology. After the termination of the fast breeder program, the development of a potassium topping cycle could provide a

## Chapter 5 Thermal power cycles

new opportunity for the application of the knowledge of liquid metal technology. Various alkali metals like sodium, potassium and cesium were considered for rankine cycle application. Potassium appeared to be the most promising. A serious disadvantage of alkali metals is that they are in the solid state under environmental conditions. Experiences from the fast breeder program have shown, however, that this problem can be solved without large difficulties.

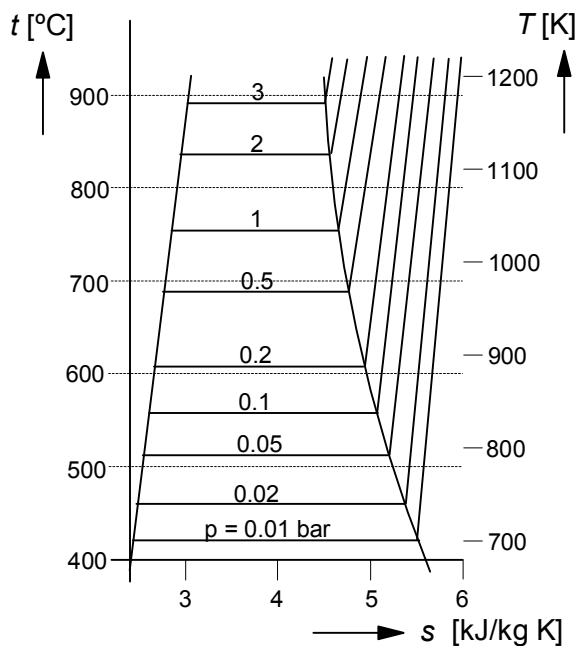


Figure 5.14  $T,s$ -diagram of potassium

The  $T,s$ -diagram of potassium is sketched roughly in Figure 5.14. The critical temperature of potassium is around 1950°C. The diagram shows that saturation pressures below 3 bar are achievable in the case of power cycles with evaporation temperatures around 850°C. Condensation temperatures should not be seriously lower than 500°C to avoid very high volume flow rates at the turbine exhaust. At a pressure of 0.05 bar the saturation temperature is 510°C (783 K) and the specific volume is 33.3 m<sup>3</sup>/kg which corresponds with water vapor of around 30°C. A potassium condensation temperature of around 500°C is suitable for heat transfer to a bottoming steam cycle.

### 5.3.2 Description of the potassium topping cycle plant

In [5.17] various system designs for power plants with potassium topping cycles are investigated. Three plants with pulverized coal combustion are considered as well as two plants with fluidized bed combustion. Differences are primarily determined by the combustion system. Therefore, the reference system, a system with pulverized coal combustion, is used for this thesis. The system flow diagram is presented in Figure 5.15. The combustion system is actually a conventional system with an air preheat temperature of 420°C and a flue gas exhaust temperature of 144°C. Facilities for gas cleaning are not considered in this diagram. Potassium evaporation occurs in the tubes of the furnace walls as well as in radiation screens in the upper part of the furnace and tube bundles in the horizontal

During the seventies various studies of power plants using alkali metals as the cycle fluid are presented (e.g. [5.12] - [5.16]). For the Dutch evaluation it was decided to reject the treble rankine cycle as considered for the IEA study. For the treble rankine cycle unusual high air preheat temperatures higher than 900°C are proposed and an organic rankine cycle was placed in between the potassium cycle and the steam cycle. It appeared that the use of the high air preheat temperature and the additional organic power cycle is not necessary to achieve plant thermal efficiencies around 60%. Furthermore, it was expected that they might seriously complicate the introduction of the potassium topping cycle.

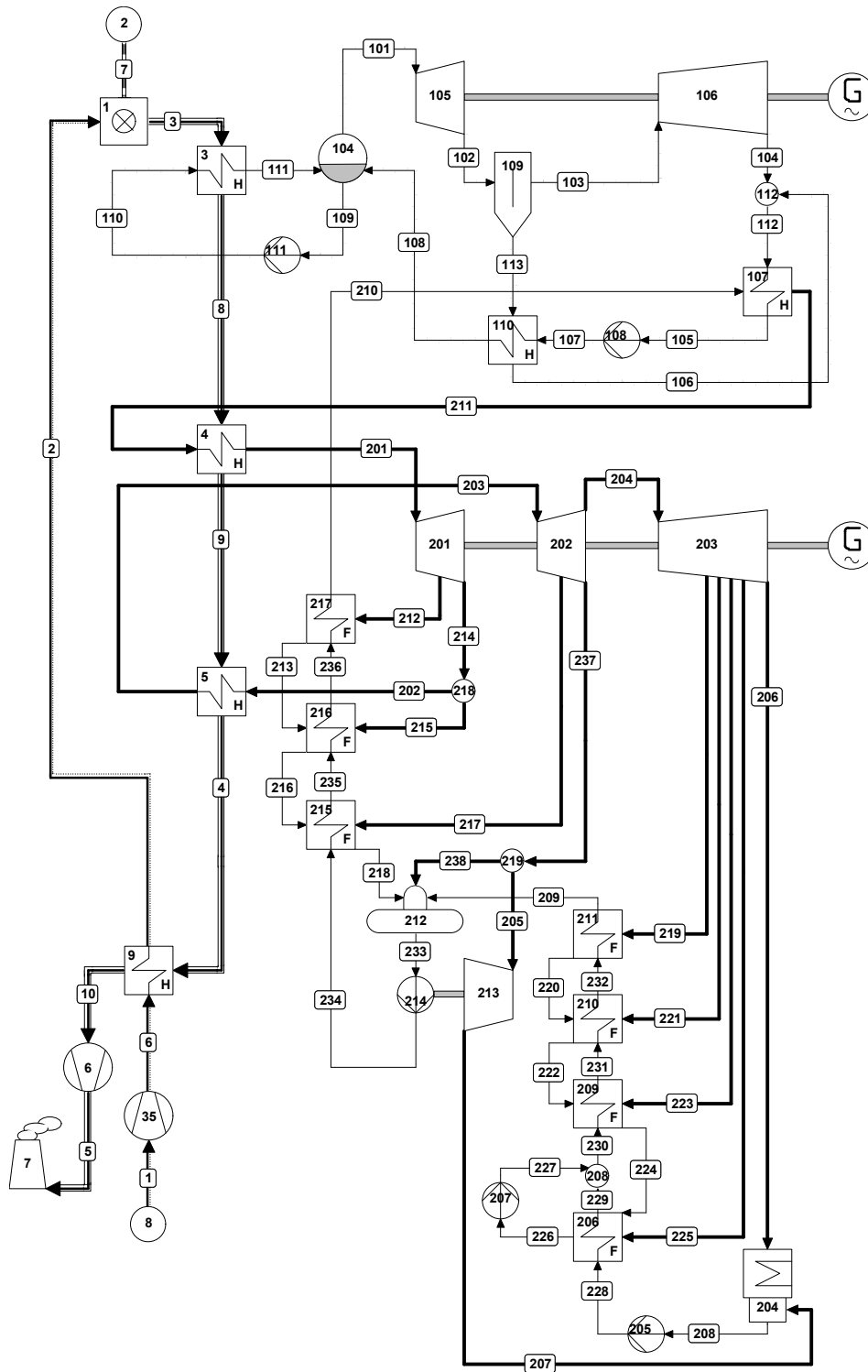


Figure 5.15 Flow diagram potassium topping cycle plant

## Chapter 5 Thermal power cycles

flue gas duct. The flue gases leave the potassium evaporator (3)<sup>2</sup> at a temperature of 1025°C. Further cooling of the flue gases takes place in respectively the steam superheater (4) and reheater (5). Finally the flue gases are cooled in the air heater (5) from 484°C to 144°C and passed to the stack via an electrostatic filter, a draft fan and a desulfurization plant.

The potassium evaporator generates saturated vapor at a temperature of 850°C. The saturation pressure at this temperature is 2.24 bar. The saturated vapor is passed to the first potassium turbine (105) via a number of pipes in parallel. In this turbine potassium vapor is expanded to a pressure of 0.36 bar. The moisture content of the vapor after this expansion is about 10%. The potassium vapor must be dried before it is passed to the second potassium turbine (106). The moisture is partly removed in a vapor dryer (109) in a way that the moisture content of the vapor to the second turbine is around 2%. The removed liquid is passed to a boiler feed preheater (110) together with a small amount of vapor. The dried vapor is expanded in the second potassium turbine to a pressure of 0.028 bar corresponding with a saturation temperature of 477°C. The moisture content of the vapor at the turbine exhaust is slightly lower than 13%. Because of the large vapor volume at the turbine exhaust the low pressure turbine must consist of three double flow units in parallel. The potassium condensers (107) are positioned immediately below the LP turbines. The condenser tubes are cooled by the feedwater of the steam bottoming cycle. Feedwater is evaporated and slightly superheated in the potassium condenser. The potassium condenser actually operates as a once-through steam boiler. A feedpump (108) passes the potassium condensate from the condenser to respectively the feed preheater (110) and the boiler drum (104). In the potassium condenser also serious amounts of argon must be removed. Argon is used as seal gas in the rotating equipment of the potassium cycle. Some gas will be mixed up with the potassium flows and is separated finally in the potassium condenser. There it is discharged by a vacuum-pump.

For the steam turbine cycle supercritical conditions are chosen at the steam turbine inlet. The temperature of the steam generated in the potassium condenser is rather low, approximately 460°C, because of the low condensation temperature of the potassium. Further superheating to a temperature of 565°C occurs in the boiler flue gasses (4). The steam pressure at the inlet of the HP turbine (201) is 240 bar. After expansion in the HP steam turbine, steam is reheated by the flue gasses (5) and passed to the IP turbine (202). Steam from the exhaust of the IP turbine is used to feed the feedpump turbine (213) and the deaerator (212). The main flow is passed to the LP turbine and expanded to condenser pressure (0.027 bar). The condensate is preheated first by four low pressure feedwater heaters, using extraction steam

fuel (coal) consumption	[kg/s]	48.76
<i>LHV</i>	[MJ/kg]	24.61
fuel power	[MW <sub>th</sub> ]	1200
potassium turbine power	[MW <sub>e</sub> ]	210.4
steam turbine power	[MW <sub>e</sub> ]	436.2
gross electrical power	[MW <sub>e</sub> ]	646.6
auxiliary power consumption	[MW <sub>e</sub> ]	22.7
net electrical power	[MW <sub>e</sub> ]	623.9
gross electrical efficiency	[-]	0.539
net electrical efficiency	[-]	0.520

<sup>2</sup> The numbers refer to the apparatus numbers in the system flow diagram of Figure 5.15.

from the LP turbine. Further preheating occurs in the deaerator and three high pressure feedwater heaters with extraction steam from the HP and IP turbines. A relatively high final feedwater temperature (312°C) is chosen in order to avoid large temperature differences between the primary and secondary fluids in the potassium condenser/steam generator.

### 5.3.3 Plant performance

The plant performance was investigated by using Cycle-Tempo. Some of the final results are presented in Table 5.4 and Table 5.5. The potassium topping cycle plant should generate approximately 600 MW<sub>e</sub>. Since the plant will have a thermal efficiency close to 50%, a fuel power of 1200MW<sub>th</sub> was chosen as the starting point for the system calculations. Only design conditions are considered. Coal is combusted with environmental air that enters the system at a temperature of 15°C and a relative humidity of 60%. The coal type is a modified Illinois nr. 6 and has a lower heating value of 24.61 MJ/kg. Roughly 70% of the heat transferred in the boiler is transmitted to the potassium cycle (777.5 MW<sub>th</sub>). The remainder (338.0 MW<sub>th</sub>) is transferred directly to the steam cycle. The electrical power generated by the potassium turbine is 210.4 MW<sub>e</sub>; this is about one third of the total generated electricity. The heat transferred to the steam cycle in the potassium condenser is 563.0 MW<sub>th</sub>. Thus, through potassium condenser, steam superheater and steam reheater in total 901.0 MW<sub>th</sub> is transferred to the steam cycle.

The electrical power delivered by the steam turbo-generator is 436.2 MW<sub>e</sub>. Then, the gross generated electrical power by the potassium turbine and steam turbine together is 646.6 MW<sub>e</sub>. A detailed estimate is made of the

*Table 5.5 Process data potassium topping cycle plant*

pipe nr	temperature [°C]	pressure [bar]	mass flow [kg/s]	enthalpy [kJ/kg]	entropy [kJ/kg K]
101	850	2.24	380	2769	4.5247
104	477	0.028	321	2349	4.8705
105	477	0.50	380	596	2.5359
106	487	0.34	59	604	2.5460
108	647	6.0	380	726	2.6916
201	565	240	365	3398	6.2681
202	308	41	275	2981	6.3876
203	565	36	275	3596	7.3285
210	312	265	365	1393	3.2956
211	451	260	365	2936	5.6368

auxiliary power. For the boiler system including flue gas desulfurization the required auxiliary power was calculated to be 14.2 MW<sub>e</sub>. The power of the air fans and flue gas fans are taken from the system calculation by Cycle-Tempo. The power of the coal mills and the desulfurization plant (in total 10.3 MW<sub>e</sub>) are based on literature data. The auxiliary power for the potassium cycle and the steam cycle is calculated to be respectively 2.8 and 1.7 MW<sub>e</sub>. The auxiliary power of the potassium cycle includes a power of 1.5 MW<sub>e</sub> necessary for the cooling system of the potassium turbine. With 4.0 MW<sub>e</sub> supposed to be necessary for transport, air conditioning, ventilation, lighting etc. the total auxiliary power is 22.7 MW<sub>e</sub>. The gross electrical efficiency of the potassium topping cycle plant appears to be 0.539 and the net electrical efficiency is 0.520.

## Chapter 5 Thermal power cycles

In Table 5.6 the calculated values of  $\eta_{ex, intern}$  are presented for the potassium cycle, the steam cycle and the combined potassium/steam cycle. The thermodynamic equivalent temperatures of heat transfer to and from the cycles are calculated by using the process data shown in Table 5.5. The temperature of heat transfer to the potassium cycle is 841°C, very

<i>Table 5.6 Calculated data potassium topping cycle plant</i>		
Potassium cycle		
$\bar{T}_{H, PC}$	[°C]	841
$\bar{T}_{C, PC}$	[°C]	478
$\eta_{th, PC}$	[-]	0.2706
$\eta_{ex, intern, PC}$	[-]	0.8303
Steam cycle		
$\bar{T}_{H, SC}$	[°C]	398
$\bar{T}_{C, SC}$	[°C]	22
$\eta_{th, SC}$	[-]	0.4841
$\eta_{ex, intern, SC}$	[-]	0.8639
Combined cycle		
$\bar{T}_{H, CC}$	[°C]	669
$\bar{T}_{C, CC}$	[°C]	22
$\eta_{th, CC}$	[-]	0.5792
$\eta_{ex, intern, CC}$	[-]	0.8433

close to the evaporation temperature of potassium in the boiler. The temperature of heat transfer from the potassium cycle equals almost the condensation temperature. The internal exergy efficiency of the potassium cycle ( $\eta_{ex, intern, PC} = 0.8303$ ) is somewhat lower than usual for steam cycles. This relatively low value might result from the limited expansion rate but might also be caused by a rather pessimistic estimate of the component performance data assumed for this study. The internal exergy efficiency of the steam cycle ( $\eta_{ex, intern, SC} = 0.8639$ ) is slightly higher than the values in Table 5.2. This might be the result of somewhat different performance data assumed for the various system components. It is supposed that the deviation is within usual boundaries. The temperature of heat transfer to the combined cycle ( $\bar{T}_{H, CC}$ ) appears to be significant lower than the temperature of heat transfer to the potassium cycle. This is due to the heat transfer from the flue gas to the steam cycle in the boiler.  $\bar{T}_{H, CC}$  can be increased by increasing the percentage of the heat from the boiler that is transferred directly to the potassium cycle. This can be realized e.g. by raising the air preheat

temperature. The internal exergy efficiency of the combined cycle ( $\eta_{ex, intern, CC} = 0.8433$ ) has a value in between the values of the two consisting cycles.

## 5.4 Gas turbine cycles

### 5.4.1 Introduction

In this section the thermodynamic performance of the so-called simple cycle open gas turbine process is discussed. This kind of gas turbine processes is by far the most frequently applied for airplane propulsion, mechanical drive in industry as well as for power plants. The evaluation of open cycle processes is complicated by the fact that the composition of the working fluid in the cycle changes because of the addition of fuel in the combustion chamber. Thus, fluid properties and mass rates will differ before and after combustion which is inconvenient for more fundamental thermodynamic evaluations. That's why the closed cycle air turbine is used in Appendix 5.2 to discuss a variety of options to improve the thermodynamic performance of gas turbine cycles. The conclusions and insights from the evaluation of closed cycle systems are in general also applicable for open cycle systems in the case of high air to fuel ratios. Thus, open cycle systems will differ more from closed cycle

systems if low calorific fuels, high turbine inlet temperatures and low compression ratios are applied.

The evaluation of the performance of actual gas turbine systems is in general hindered by the lack of information on the performance of the various processes within the system. Gas turbine manufacturers usually specify the overall performance as presented e.g. in the Gas Turbine World performance specs. These specs show the generated power, thermal efficiency, pressure ratio, air mass flow and turbine exhaust temperature for all commercially available gas turbines for power generation, mechanical drive and marine propulsion. But important data like isentropic efficiencies of compressor and turbine, heat losses as well as the turbine inlet temperatures are missing. The available data are specified for ISO base load output conditions. That means that operation on natural gas<sup>3</sup> is assumed at sea level with air at a temperature of 15°C and 60% relative humidity. To reproduce the data of a specific gas turbine with a thermodynamic model various assumptions and adjustments are necessary to achieve reasonable agreement between modeling results and specified data.

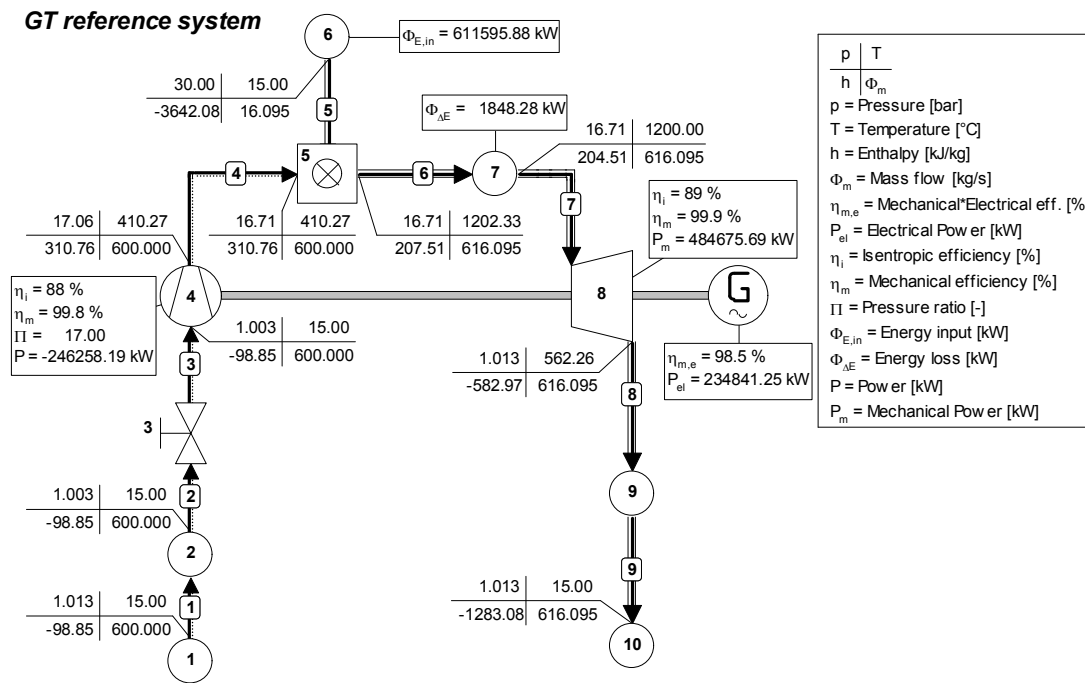


Figure 5.16 Flow diagram with calculated results of an open cycle gas turbine (ref. cycle)

The description of the open gas turbine cycle in this section focuses on the comparison of the reversible cycle efficiency (Carnot efficiency) and the internal exergy efficiency ( $\eta_{ex, intern}$ ) of thermal power cycles. This efficiency cannot be determined by using only manufacturers data. Therefore system models are established to determine the efficiency. A reference system is defined first to have a starting point for the systematic evaluation of the effects of some design parameters. In addition the effect of deviations from the assumed

<sup>3</sup> Natural gas is specified as pure methane for this purpose.

## Chapter 5 Thermal power cycles

values of some parameters have been checked. Finally the results of the systematic evaluation are used to discuss the performance improvements of three large scale gas turbines during a period of 25 years (1983-2008).

app			units	
1	air inlet	pressure	[bar]	1.01325
		temperature	[°C]	15
		mass flow	[kg/s]	600
2	inlet filter	pressure loss	[bar]	0.01
4	compressor	pressure ratio	[-]	17
		mechanical efficiency	[-]	0.998
		isentropic efficiency	[-]	0.88
5	combustor	relative pressure loss	[%]	2
6	fuel inlet (CH <sub>4</sub> )	pressure	[bar]	30
		temperature	[°C]	15
7	sink	heat loss	[kJ/kg]	3
8	turbine	<i>TIT</i>	[°C]	1200
		mechanical efficiency	[-]	0.999
		isentropic efficiency	[-]	0.89
	electrical generator	mech. + electr. efficiency	[-]	0.985
9	exhaust duct	pressure loss	[bar]	0.0
10	flue gas outlet	pressure	[bar]	1.01325

#### 5.4.2 Reference system of an open cycle gas turbine

The system flow diagram used for the reference system is shown in Figure 5.16. The corresponding input data of the system model established with Cycle-Tempo are presented in Table 5.7. The input data are arbitrarily chosen but are supposed to represent usual gas turbine data for large scale power generation. Air at a temperature of 15°C, a pressure of 1 atm and with a relative humidity of 60% enters the system in apparatus 1 (source). The air inlet filter is represented by a sink (apparatus 2) which is used to specify the pressure loss caused by the filter. The apparatus 3 has no meaning for this calculation and is ignored. The compressor (apparatus 4) has a pressure ratio of 17; the

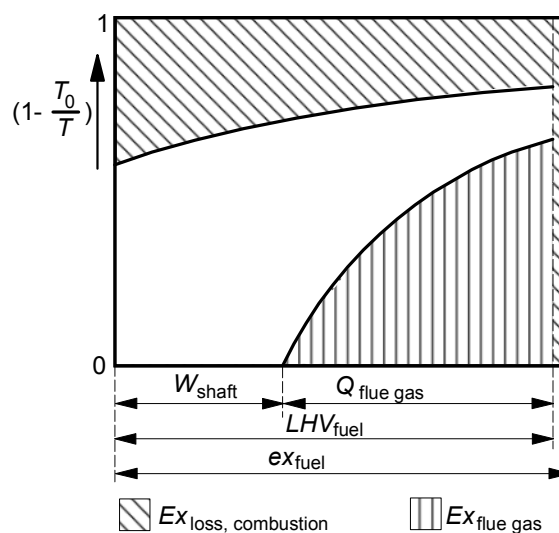


Figure 5.17 Value diagram of open cycle gas turbine (ref. cycle)

isentropic efficiency is 88% and the mechanical efficiency 99.8%. For the combustor (apparatus 5) a relative pressure loss of 2% is specified. It is assumed that fuel is transferred to the system at a pressure of 30 bar and at environmental temperature (apparatus 6). Pure methane is considered to be the composition of the natural gas. To specify a general heat loss a sink (apparatus 7) is included in the system model in between the

combustor and the turbine. The heat loss is specified as a decrease of the specific enthalpy of the flue gas from the combustor. The flue gas enters the turbine at a temperature of 1200°C. The turbine (apparatus 8) has an isentropic efficiency of 0.89 and a mechanical efficiency of 0.999. For the mechanical and electrical losses of the generator an efficiency of 0.985 is assumed. However, this efficiency does not play a role in these evaluations as the shaft power to the generator is considered to be the generated power by the cycle. The pressure at the turbine exhaust is 1 atm. Pressure losses of the exhaust duct are ignored. The results of the calculation with Cycle-Tempo are shown in Figure 5.16. The value diagram of the reference cycle is presented in Figure 5.17 and the overall results in Table 5.8. In the value diagram the

*Table 5.8 Overall results reference GT system*

	unit	energy	exergy
fuel to system	[kW]	611596	640926
shaft power	[kW]	238417	238417
efficiency	[-]	0.3898	0.3720
electrical power	[kW]	234841	234841
efficiency	[-]	0.3840	0.3664

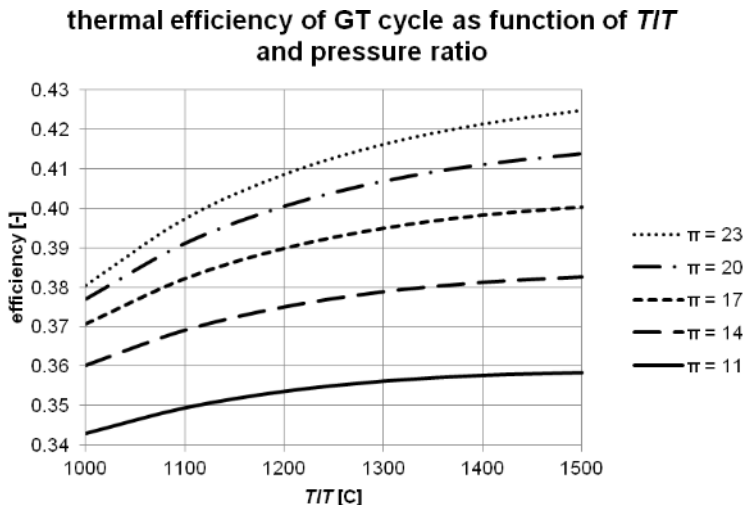


*Figure 5.18 Thermal efficiencies of open gas turbine cycle as function of the turbine inlet temperature (TIT) and the pressure ratio ( $\pi$ )*

effects of the entropy increase in compressor and turbine are ignored. The thermal efficiency of the cycle based on the shaft power is 0.3898 and the corresponding exergy efficiency is 0.3720. A break-down of the calculated exergy losses is presented in Table 5.9. In this table the exergy losses are split into internal and external losses<sup>4</sup>. This done with regard to the evaluation of the methods for the calculation of the internal

exergy efficiency of the cycle, as presented in Appendix 5.3.

### 5.4.3 Performance evaluation of an open cycle gas turbine

The effects of the pressure ratio and the gas turbine inlet temperature on the

<sup>4</sup> The negative exergy loss by the air source (= an exergy transfer to the system) results from the 60% relative humidity of the combustion air. The reference air for the exergy calculation is saturated with water vapor.

## Chapter 5 Thermal power cycles

performance of the gas turbine cycle is investigated with the reference cycle as starting point. The pressure ratio is varied from  $\pi = 11$  to  $\pi = 23$  and the turbine inlet temperature from  $TIT = 1000$  °C to  $TIT = 1500$  °C. The calculated thermal efficiencies are presented in Figure 5.18. The results clearly show

that high pressure ratios are not very useful at low turbine inlet temperatures and high temperatures are not useful in the case low pressure ratios. The results are derived by assuming that the isentropic efficiencies of the compressor and turbine are constant. In real systems the isentropic efficiencies of the compressor will decrease with increasing pressure ratio and the isentropic efficiency of the turbine will decrease with increasing turbine inlet temperature. This means

that the effect of increasing the pressure ratio and the turbine inlet temperature on the thermal efficiency is somewhat overestimated in this evaluation. Within the considered ranges of pressure ratio and turbine inlet temperature the values of the isentropic efficiencies can differ more than 2% (points). The sensitivity of the thermal efficiency of the cycle for the isentropic efficiencies of compressor and turbine are shown in Figure 5.19. The isentropic efficiency of

				units	
internal exergy losses					
turbine	app 8	[kW]			22281
compressor	app 4	[kW]			13364
heat losses	app 7	[kW]			1487
comb. press. loss	pipe 4	[kW]			1006
air inlet filter	app 2	[kW]			494
total				[kW]	38632
external exergy losses					
combustion	app 5	[kW]			186733
fuel throttling	pipe 5	[kW]			1210
exhaust loss	pipe 8	[kW]			176010
air source	app 1	[kW]			-77
total				[kW]	363879
total exergy loss				[kW]	402508

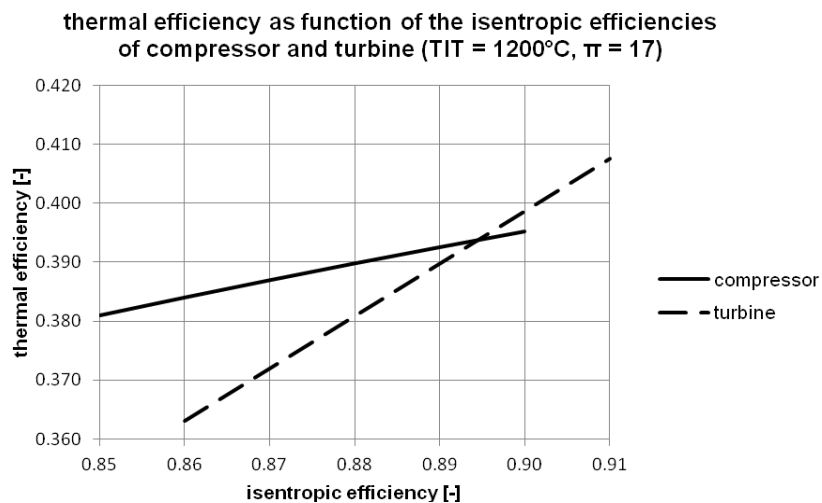


Figure 5.19 Thermal efficiency of open gas turbine cycle as function of the isentropic efficiencies of turbine and compressor ( $\pi = 17$ ;  $TIT = 1200^\circ\text{C}$ )

the compressor is varied from 0.85 to 0.90 and the isentropic efficiency of the turbine from 0.86 to 0.91. The sensitivity for the isentropic efficiency of the turbine is more than two times

the sensitivity for the isentropic efficiency of the compressor. If e.g. the isentropic efficiencies in the case of a gas turbine cycle with  $TIT = 1500 \text{ }^\circ\text{C}$  and  $\pi = 23$  should be 2% (points) lower, 0.86 for the compressor and 0.87 for the turbine, the thermal efficiency of the cycle should be almost 3% (points) lower, 0.3968 instead of the initially calculated value 0.4247. Thus, the actual thermal efficiencies of open cycle gas turbine processes might deviate significantly from the data used for this evaluation.

For a better understanding of the results the thermal efficiency of the reversible cycle and the internal exergy efficiency of the cycle are considered separately. The relation between these two efficiencies is defined by Equation 2.88 derived in Chapter 2:

$$\eta_{th} = \eta_{ex, \text{intern}} \cdot \left(1 - \frac{\bar{T}_C}{\bar{T}_H}\right) \quad (2.88)$$

The application of this equation is complicated by the fact that in the case of gas turbine cycles the exact calculation of  $\bar{T}_C$  and  $\bar{T}_H$  of the reversible cycle is not possible if only data of the actual cycle are available. Various options to estimate of these temperatures are evaluated in Appendix 5.3. In this appendix it was concluded that the options 1 and 6 are the most appropriate for the evaluation of gas turbine cycles. Only these two methods are applied in this section.

#### Method 1 (= option 6)

This method is based on the original definition of the internal exergy efficiency as presented in Equation 2.87:

$$\eta_{ex, \text{intern}} = \frac{W}{W_{rev}} \quad (2.87)$$

and can be used if the results of a calculation with Cycle-Tempo are available. From this calculation the actual power generated by the gas turbine cycle is known. The power from the corresponding reversible cycle is supposed to be the difference between the exergy transferred to the cycle and the exergy transferred from the cycle. Then:

$$\eta_{ex, \text{intern}} = \frac{P_{\text{shaft}}}{Ex_H - Ex_C} \quad (5.2)$$

With:  $Ex_H = Ex_F - Ex_{\text{loss, app } 5} - Ex_{\text{loss, pipe } 5}$  and  $Ex_C = Ex_{\text{pipe } 8} - Ex_{\text{pipe } 1}$

Apparatus numbers and pipe numbers refer to the system diagram presented in Figure 5.16. This method enables also the calculation of the thermal efficiency of the reversible cycle, since:

$$\eta_{ex, \text{intern}} = \frac{\eta_{th}}{\eta_{th, rev}} \quad (5.3)$$

However, this method does not provide values of thermodynamic equivalent temperatures of heat transfer to and from the cycle. Method 1 can be used only if results from a cycle calculation are available. This will not always be the case. Furthermore, Equation 5.3 just gives the usual exergy efficiency of the gas turbine cycle. Therefore, method 2 is considered as an alternative in this investigation.

#### Method 2 (= option 1)

This method is based on the application of Equation 2.88. The thermodynamic equivalent temperature of heat transfer to the cycle is calculated as follows:

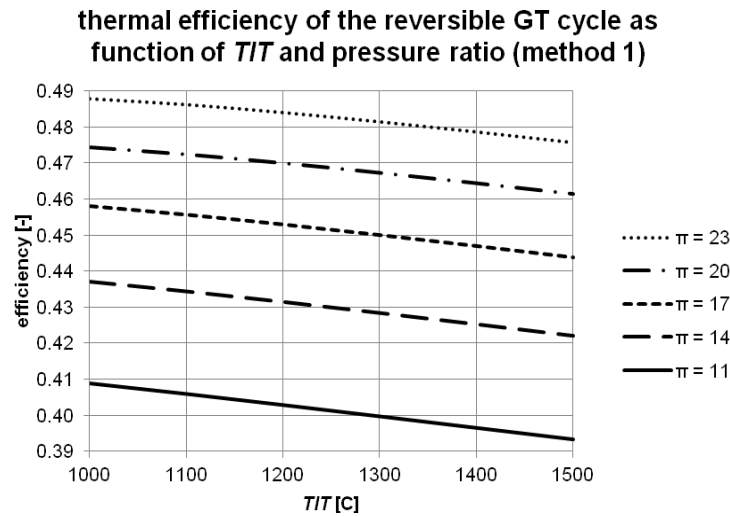


*Figure 5.20 Thermal efficiency of the reversible gas turbine cycle as function of the turbine inlet temperature ( $TIT$ ) and the pressure ratio ( $\pi$ ) (method 1)*

$$\bar{T}_H = \frac{T_7 - T_4}{\ln \frac{T_7}{T_4}} \quad (5.4)$$

and the thermodynamic equivalent temperature of heat transfer from the cycle:

$$\bar{T}_C = \frac{T_8 - T_0}{\ln \frac{T_8}{T_0}} \quad (5.5)$$

In this case the thermal efficiency of the reversible cycle is:

$$\eta_{th, rev} = 1 - \frac{\bar{T}_C}{\bar{T}_H}$$

The application of these equations is actually allowed only if the cycle fluid is an ideal gas with constant  $c_p$ . But, as demonstrated in Appendix 5.3, application can be useful in addition to method 1 which is actually just the usual exergy efficiency of the gas turbine cycle. However, the accuracy of the efficiency values is limited and will be discussed later in this section.

The thermal efficiencies of the reversible gas turbine cycle calculated by using method 1 and method 2 are presented in respectively Figure 5.20 and Figure 5.21 for the considered ranges of pressure ratio and turbine inlet temperature. It appears that the reversible cycle efficiencies calculated with method 2 are significantly higher than the reversible cycle efficiencies calculated with method 1. But the trends are highly similar. The diagrams show that the efficiency of the reversible cycle decreases if the turbine inlet temperature increases at constant pressure ratio<sup>5</sup>. At low pressure ratios the decrease per K is almost the same for the

<sup>5</sup> In Appendix 5.2, Section 2.2 it has been shown that in the case of a closed cycle gas turbine the increase of the turbine inlet temperature has no effect on the efficiency of a reversible cycle if the cycle fluid is an ideal gas with constant specific heat.

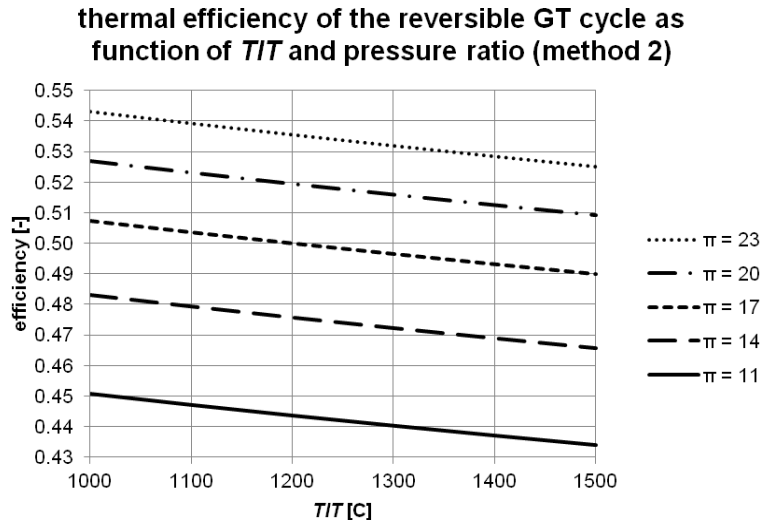


Figure 5.21 Thermal efficiency of the reversible gas turbine cycle as function of the turbine inlet temperature ( $TIT$ ) and the pressure ratio ( $\pi$ ) (method 2)

two methods, but at higher pressure ratios method 2 slightly overestimates the effect on the efficiency. For rough evaluations the trends do agree quite well. The internal exergy efficiencies are calculated with Equation 5.3. The efficiencies calculated with the two methods are presented in Figure 5.22 and Figure 5.23. As the internal exergy efficiency is calculated by dividing the thermal efficiency of the actual cycle which is taken from the Cycle-Tempo calculation and the thermal efficiency of the reversible cycle which is calculated in two different ways (method 1 and method 2), the differences between the internal exergy efficiencies from these two methods are opposite proportional with the differences between the thermal efficiencies of the reversible cycles. It has been mentioned before that the effect of higher turbine inlet temperatures and higher pressure ratios on the thermal efficiency of the cycle is somewhat overestimated as the effect of these variables on the isentropic efficiency of compressor and turbine is ignored. That means that the effect of changes of the isentropic efficiencies of compressor and expansion turbine due

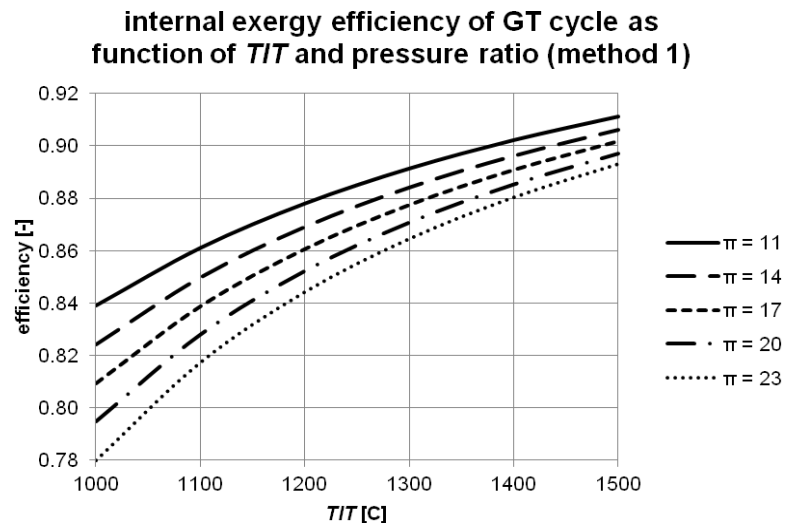
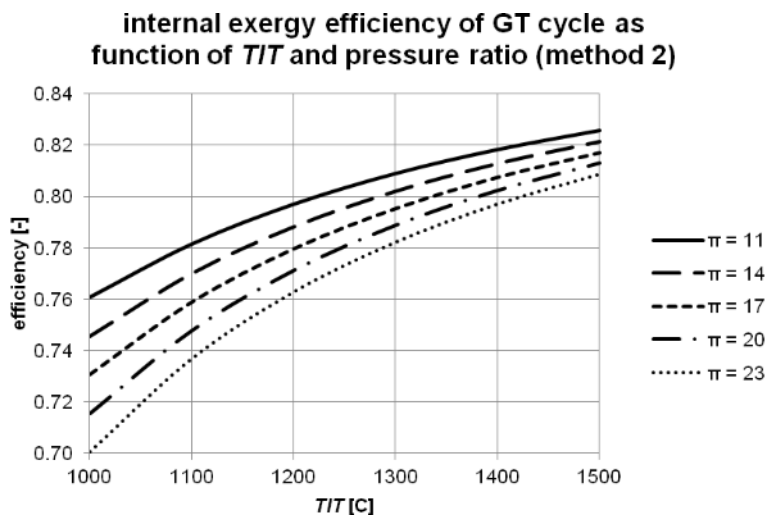


Figure 5.22 The internal exergy efficiency of the gas turbine cycle as function of the turbine inlet temperature ( $TIT$ ) and the pressure ratio ( $\pi$ ) (method 1)

## Chapter 5 Thermal power cycles

to variation of the pressure ratio or  $TIT$  are also not included in the values of the internal exergy efficiency. Thus, the actual increase of these values in the case of higher pressure ratios and higher turbine inlet temperatures will be lower than presented in these figures. But from the diagrams it is obvious that the increase of the thermal efficiency of the cycle due to higher turbine inlet temperatures at constant pressure ratio is caused by the higher internal exergy efficiency. At higher turbine inlet temperatures the exergy loss of the turbine will increase because of the higher entropy increase, but despite this effect the relative loss of the cycle is reduced.

It appears that the differences between the two calculation methods are quite serious. For a better understanding of the origin of these differences calculations are made for gas



*Figure 5.23 The internal exergy efficiency of the gas turbine cycle as function of the turbine inlet temperature ( $TIT$ ) and the pressure ratio ( $\pi$ ) (method 2)*

turbine cycles with thermodynamic losses only in the compressor and the expansion turbine. Flow resistances and heat losses are ignored. The isentropic efficiency of the compressor and the turbine are varied but have the same value. The calculated internal exergy efficiencies by the two methods are shown in Figure 5.24. In this case the thermal efficiency of true reversible gas turbine cycle is available. With this thermal efficiency it is possible to calculate also the true internal exergy efficiency. This true efficiency is presented too in Figure 5.24. From this figure it appears that method 2 approximates the true internal exergy efficiency of the cycle quite well. Higher losses in compressor and turbine cause a serious increase of the thermodynamic equivalent temperatures of heat transfer to and from the cycle, but the effect on the thermal efficiency of the reversible process is limited. The deviation of method 1 from the true efficiency value is significant higher. Method 1 is actually the usual exergy efficiency of a thermal power cycle as specified by Equation 2.66. This shows that the usual exergy efficiency is in general not an accurate approximation of the ratio between the actual and the reversible process.

The application of method 2 for the evaluation of open cycle gas turbine processes offers the possibility to determine the internal exergy efficiency without complete cycle calculations and without the additional calculation of the corresponding reversible cycle. The inaccuracy is limited and the method is useful for the evaluation of trends and the credibility of results.

reversible gas turbine cycle is available. With this thermal efficiency it is possible to calculate also the true internal exergy efficiency. This true efficiency is presented too in Figure 5.24. From this figure it appears that method 2 approximates the true internal exergy efficiency of the cycle quite well. Higher losses in compressor and turbine cause a serious increase of the thermodynamic equivalent temperatures of heat transfer to and from the cycle, but the effect on the thermal efficiency of the reversible process is limited. The deviation of method 1 from the true efficiency value is significant higher. Method 1 is actually the usual exergy efficiency of a thermal power cycle as specified by Equation 2.66. This shows that the usual exergy efficiency is in general not an accurate approximation of the ratio between the actual and the reversible process.

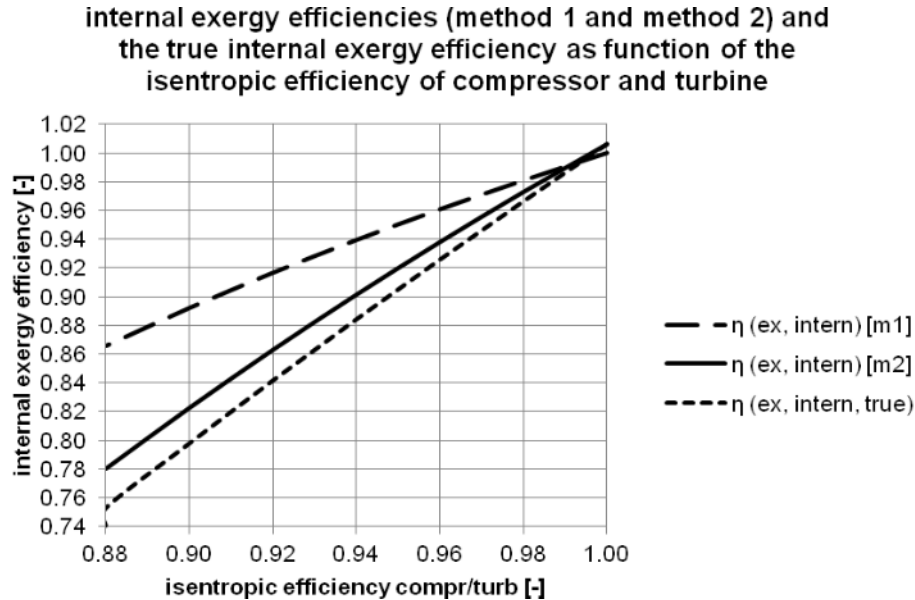


Figure 5.24 The internal exergy efficiencies (method 1 and 2, and the true efficiency) of the gas turbine cycle as function of the isentropic efficiency of compressor and turbine (flow resistances and heat losses are ignored)

#### 5.4.4 Development of gas turbine performance

An impression of the performance improvements of gas turbines for electricity production is given by comparing the data of 3 large heavy gas turbines. For the purpose of this evaluation the largest gas turbines for the 50 Hz market delivered by Siemens, General Electric and Alstom are considered. The data are summarized in Table 5.10. The largest gas turbine delivered by Alstom is actually the GT26. A comparison with this engine (ISO base rating of 288 MW in the 2008 specs) is complicated because of the reheat and the very high pressure ratio (33.9). Therefore the GT13E was chosen for this evaluation instead of the GT26.

The comparison is based on data from the Gas Turbine World 2008 Performance Specs (the upper part of Table 5.10) and the Gas Turbine World Handbook 1982-83 (the lower part of Table 5.10). The data give an impression of the developments over a period of 25 years. In the first rows manufacturer data are shown. For each of the gas turbines a Cycle-Tempo model was build to calculate the internal exergy efficiency using the two methods discussed before. The models use the manufacturer data with the exception of the specified flow. In the performance specs it was mentioned that the flow represents the air mass flow through the turbine. However, adjustment of the air mass flow appeared to be necessary to achieve an accurate fit. The models are fitted in a way that the heat loss is approximately 1% of the ISO base rating. The corresponding data of the reference cycle are added in the last column for comparison with the data presented in the previous sections. It shows that the thermal efficiency of the reference cycle is within the range of the real engines. Also the internal exergy efficiency calculated with method 1 is within the range. The calculated efficiency with method 2 is a bit higher than the value of the Siemens turbine. Also  $\bar{T}_H$  and  $\bar{T}_C$  are in reasonable agreement with the data calculated for the real gas turbines. It should be

<b>GTW 2008</b>					
manufacturer data	units	Siemens SGT5-4000F	GE PG9371 (FB)	Alstom GT13E2	Ref Cycle
ISO base rating	[MW]	286.60	279.20	179.90	234.84
efficiency	[-]	0.395	0.379	0.369	0.384
pressure ratio	[-]	17.9	18.3	16.5	17.0
flow	[kg/s]	689	655	564	-
exhaust temperature	[°C]	577	629	510	562
calculated data					
$TIT$	[°C]	1248	1305	1108	1200
air flow	[kg/s]	681	644	554	600
heat loss	[kW]	2930	2849	1826	1848
$\eta_{ex, intern}$ (method 1)	[-]	0.8797	0.8688	0.8451	0.8606
$\eta_{ex, intern}$ (method 2)	[-]	0.7771	0.7540	0.7377	0.7797
$\bar{T}_H$ (method 2)	[°C]	783	809	717	755
$\bar{T}_C$ (method 2)	[°C]	246	265	222	241
<b>GTW 1983</b>					
manufacturer data		KWU V94	PG9151 E	BBC type 13	
ISO base rating	[MW]	130.6	106.7	88.9	
efficiency	[-]	0.304	0.298	0.301	
pressure ratio	[-]	10.4	11.6	11.8	
flow	[kg/s]	487	398	374	
exhaust temperature	[°C]	590	540	526	
calculated data					
$TIT$	[°C]	1076	1034	1009	
air flow	[kg/s]	460	428	362	
heat loss	[kW]	1337	1104	911	
$\eta_{ex, intern}$ (method 1)	[-]	0.8294	0.7968	0.7957	
$\eta_{ex, intern}$ (method 2)	[-]	0.7040	0.6679	0.6690	
$\bar{T}_H$ (method 2)	[°C]	649	641	638	
$\bar{T}_C$ (method 2)	[°C]	251	233	228	
improvements					
$\Delta TIT$	[K]	172	271	99	
$\Delta \bar{T}_H$	[K]	134	168	79	
$\Delta \eta_{ex, intern}$ (method 1)	[-]	0.0503	0.0720	0.0494	
$\Delta \eta_{ex, intern}$ (method 2)	[-]	0.0731	0.0861	0.0687	

emphasized that the calculated data in Table 5.10 are the result of model calculations that necessarily imply some uncertainties. Thus, the accuracy of these data is not very high but it is assumed that the accuracy is good enough for a discussion about trends for future developments.

Large heavy duty gas turbines are primarily applied today in combined cycle plants. The temperature of the exhaust gas should be high enough to allow for suitable steam conditions of the steam bottoming plant. Therefore, the pressure ratios are relatively low in comparison with e.g. the aeroderivative gas turbines. Further increase of  $\bar{T}_H$  is of main importance for the efficiency of combined cycle plants. During the considered period this is primarily done by raising the turbine inlet temperature as well as the pressure ratio. Siemens raised the *TIT* apparently from 1076°C in 1983 to 1248°C<sup>6</sup> in 2008 an increase of 172 K; GE achieved in this period an increase from 1034°C to 1305°C an increase of 271 K. The achieved improvements are presented in the last rows of Table 5.10. The increase of the turbine inlet temperature of the Alstom turbine is only 99 K, but it has to be noticed that the GT13E2 is perhaps not really representative for the development at Alstom since this engine is actually replaced by the GT26. The increase of the turbine inlet temperatures affects of course the value of the  $\bar{T}_H$ . The increase of this temperature is 134 K for the Siemens gas turbine and 168 K for the GE engine. With Figure 5.22 and Figure 5.23 the increase of the internal exergy efficiency can be estimated for the case that the isentropic efficiencies of compressor and turbine are supposed to be fixed. Using these diagrams to determine the effects of increased *TIT* and pressure ratio results into the following increases of  $\eta_{ex, intern}$ : around 0.03 for GE, 0.02 for Siemens and 0.00 for Alstom<sup>7</sup>. The calculated increases of  $\eta_{ex, intern}$  when using the methods 1 and 2 discussed before are shown in Table 5.10. These increases are significantly higher: for Siemens, GE and Alstom respectively 0.0503, 0.0720 and 0.0494 with method 1 and 0.0731, 0.0861 and 0.0687 with method 2. This shows that also the internal thermodynamic losses, primarily determined by the isentropic efficiencies, are reduced during the considered period of 25 years.

## 5.5 Combined cycles

### 5.5.1 Introduction

For power generation the highest efficiencies are achieved today by the combination of a gas turbine with a steam turbine cycle. This combination became popular in particular in countries where natural gas is abundantly available for the generation of electricity. With the gas turbine technology of today Combined Cycle plants can achieve thermal efficiencies even higher than 60% based on the lower heating value of the fuel. The thermodynamic equivalent temperature of heat transfer to the combined cycle is determined by the gas turbine

<sup>6</sup> The *TIT* is not the actual temperature, but specified as the ISO inlet temperature. This is calculated inlet temperature if it is assumed that the total air flow (actual air flow through combustor + cooling air) is used for the combustion process

<sup>7</sup> These numbers are almost the same for the two methods.

## Chapter 5 Thermal power cycles

technology since normally the steam cycle uses just the heat from the gas turbine exhaust. The temperature of heat rejection is actually the same as for a steam turbine cycle and is very close to the ambient temperature. As discussed before the thermal efficiency of the plant is determined not only by  $\bar{T}_H$  and  $\bar{T}_C$  but also by the internal exergy efficiency. The purpose of this section is to determine the internal exergy efficiency and its dependence on the plant design, in particular the design of the heat recovery steam generator (HRSG), the interface between the two cycles.

The attractiveness of the Combined Cycle plant is demonstrated too by the attention paid in literature on the further optimization of these plants. A variety of system improvements is investigated in references [5.20] to [5.31]. In almost all papers any kind of exergy evaluation, based on flow sheet calculations, is used to elucidate the effects of system modifications. Only in [5.21] no explicit results of exergy calculations are shown. The added value of the exergy evaluations is not always obvious. Results from exergy calculations are usually presented as exergy losses (often called exergy destruction) in system components (like combustors, heaters, compressors and expanders) or subsystems and relative exergy losses (exergy destruction rates). Relative exergy losses are usually defined as the exergy loss divided by the total exergy supplied to the system by the fuel. Several references present primarily (relative) exergy losses of subsystems [5.23], [5.24], [5.26], [5.27] and [5.29]. Data are summarized in tables or bar graphs. More detailed results of exergy calculations are presented in [5.20], [5.22] and [5.31]. In references [5.22] and [5.28] the exergy concept has been used in combination with an economic assessment of system alternatives. It is obvious that a final optimization of energy conversion systems has to be based on economic considerations. But, a separate thermodynamic evaluation is useful to understand the thermodynamic qualities and weaknesses of the considered system configurations. Furthermore, the selection of arbitrary data for avoidable thermodynamic inefficiencies and cost numbers, needed for an exergoeconomic analysis, might hamper the credibility of the results. Nevertheless, an exergoeconomic evaluation is considered to be useful but primarily as an additional step in the final phase of plant optimization.

A graphical presentation of the results from exergy calculations appears not to be very common. In [5.23] the results are summarized in combined energy and exergy diagrams. In [5.30] the size of the exergy flows are shown in a simplified system flow diagram. References [5.24], [5.25] and [5.29] show trends in (summarized) exergy values and exergy destruction ratios as a function of the considered variable. In [5.26]  $T,h$ -diagrams are used to illustrate the results of HRSG optimization. However, these diagrams do not explicitly show exergy values or exergy losses. Exergy efficiencies, also called second law efficiencies, are not used abundantly in the referred papers. References [5.22] and [5.24] show well specified exergy efficiencies of plant components. Many of the other references mainly present exergy efficiencies of power cycles and/or the considered power plants. For thermal cycles and power plants, the overall exergy efficiencies do not give really more information than the overall thermal efficiencies. For a comparison of the performance of plants and plant components well specified, suitable exergy efficiencies are useful. Exergy efficiencies, like all other efficiencies, cause primarily confusion if they are not clearly specified.

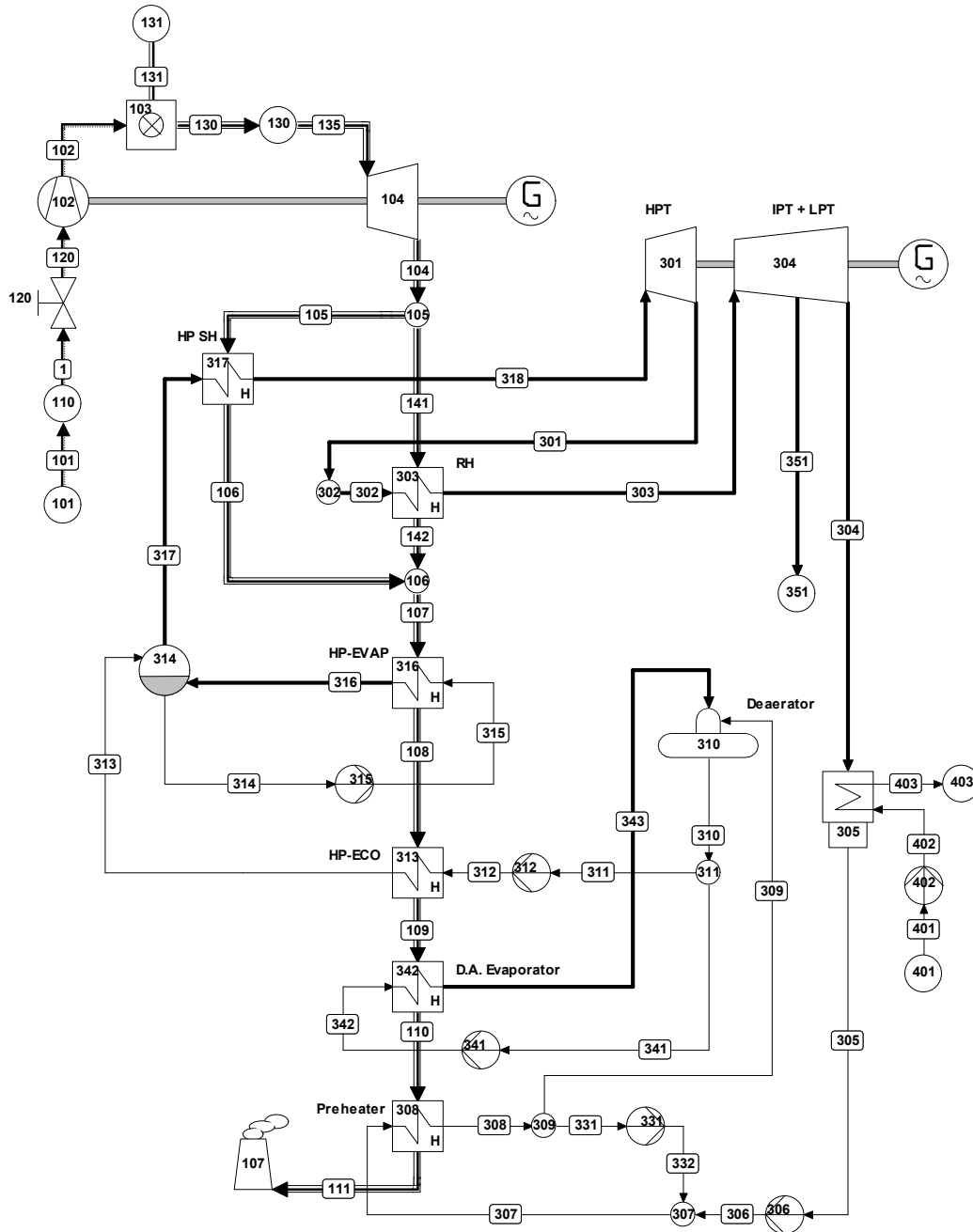


Figure 5.25 CC plant with single reheat (Cycle-Tempo flow diagram)

In this chapter three system designs of CC plants are systematically evaluated. Models of these plants are established by using Cycle-Tempo. The system designs are based on the same gas turbine, but are different with regard to the steam turbine cycle. Steam cycles are derived for respectively single pressure, double pressure and triple pressure HRSG's. The steam pressures are optimized using a multi-parameter optimization routine as available in Cycle-Tempo. The program also calculates exergy values of all fluid flows of the system by using the composition of environmental air as the reference state. This air is supposed to be

## Chapter 5 Thermal power cycles

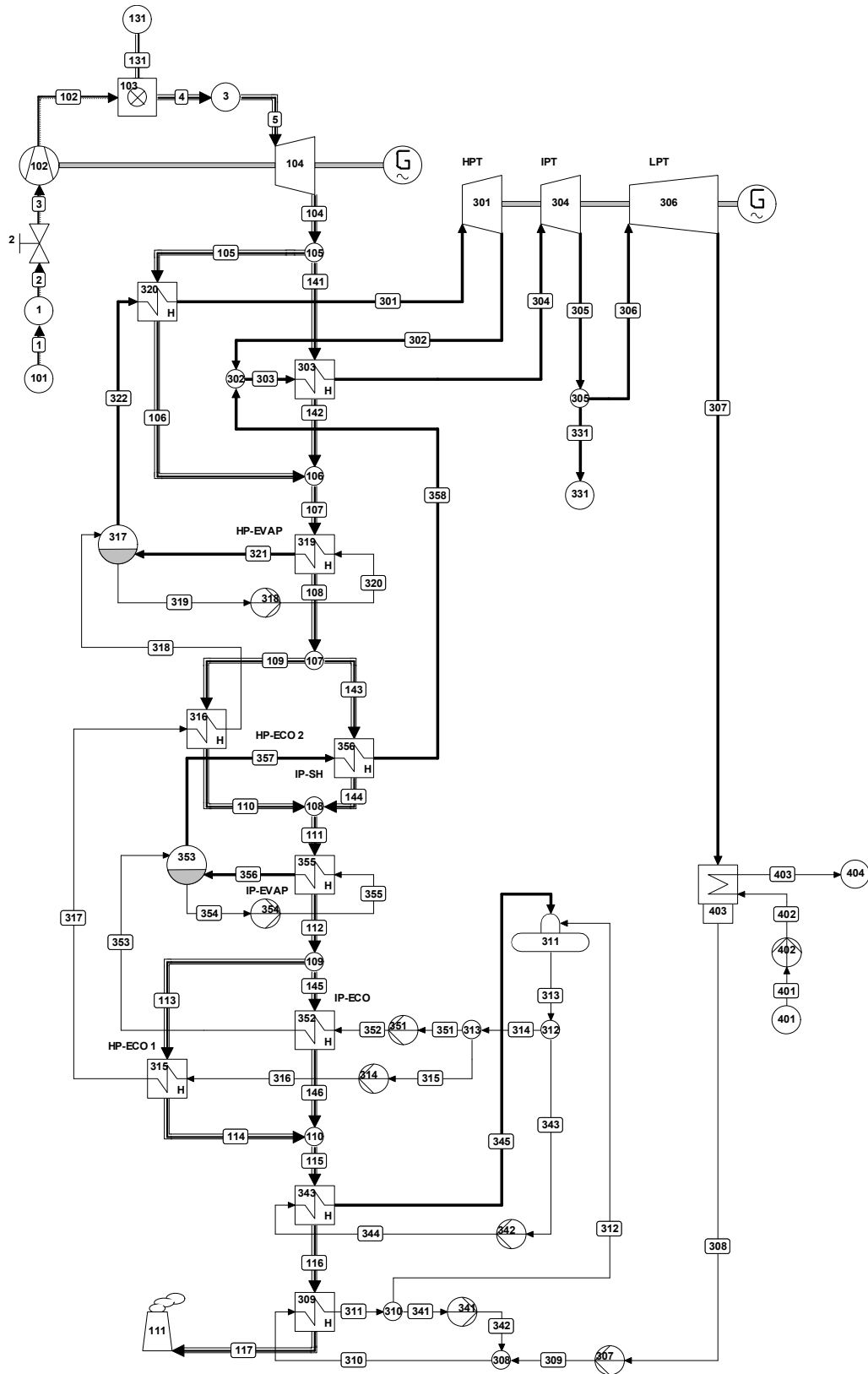


Figure 5.26 CC plant with double reheat (Cycle-Tempo flow diagram)



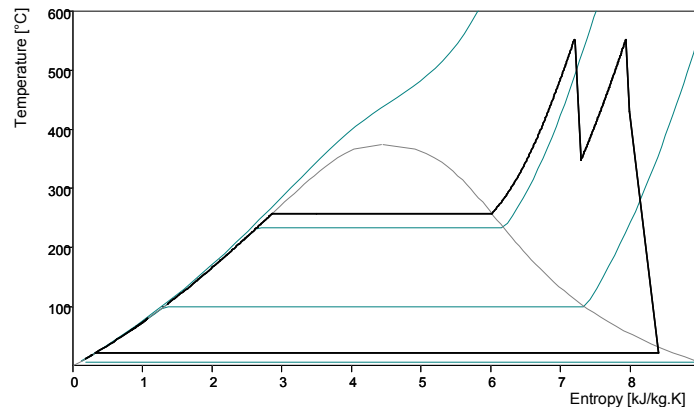


Figure 5.28 *T,s*-diagram of the single pressure steam cycle

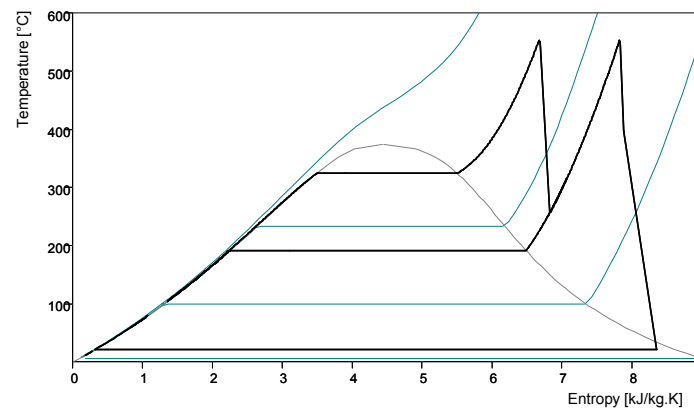


Figure 5.29 *T,s*-diagram of the double pressure steam cycle

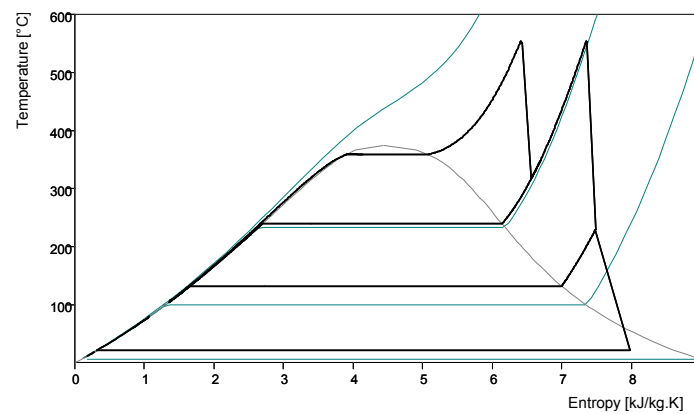


Figure 5.30 *T,s*-diagram of the triple pressure steam cycle

saturated with water vapor, at a temperature of 15°C. Furthermore, the program calculates exergy losses and efficiencies of all apparatuses as specified for the system, and is able to draw value diagrams. Also exergy flow diagrams are presented for the considered plants. The study has been presented before as a journal paper [5.19].

### 5.5.2 Plant designs

System configurations are established for three different combined cycle plants. The plants are characterized by the number of pressure levels for steam generation in the HRSG (see Figures 5.25 to 5.27). The same gas turbine data, based on published data of the Siemens V94.3A [5.34], are used for all plants. The gas turbine is fuelled with natural gas (Slochteren quality). Overall results and some characteristic data of the plants are presented in Table 5.11. The results confirm that significant higher overall thermal efficiencies (1.60 and 2.25% (points)) are achieved if the number of pressure levels at which steam is generated in the HRSG is increased.

	units	1 press.	2 press.	3 press.
<b>Overall results</b>				
net electrical power	MWe	364.26	374.84	379.13
thermal efficiency	-	0.5514	0.5674	0.5739
increase in efficiency	-	-	0.0160	0.0225
<b>gas turbine cycle</b>				
fuel flow	MW	660.62	660.62	660.62
pressure ratio	-	17.12	17.12	17.12
turbine inlet temp. (ISO)	°C	1227.81	1227.81	1227.81
GT outlet temp.	°C	581.60	582.43	583.92
stack temperature	°C	160.78	119.03	81.88
<b>steam turbine cycle</b>				
HP inlet temp.	°C	550.00	549.75	550.40
HP inlet press.	bar	41.54	112.9	175.0
IP inlet temp.	°C	550.22	550.96	552.31
IP inlet press.	bar	9.261	11.62	31.45
LP inlet temp.	°C			226.68
LP inlet press.	bar			2.711
condenser press.	bar	0.02643	0.02643	0.02643

The gas turbine has a compressor pressure ratio of 17.12 and a turbine inlet temperature (ISO temperature) of 1227.81°C. It is arbitrarily assumed that the increased complexity of the HRSG will result in higher pressure losses. This results into slightly higher GT outlet temperatures for the 2 and 3 pressure alternatives. Steam turbine data are chosen without considering constructional limitations. The steam turbine cycles are single reheat cycles with

## Chapter 5 Thermal power cycles

steam turbine inlet temperatures of 550°C. The slight deviations from this temperature are caused by the calculation process. Steam pressures are the result of a multi-parameter optimization that minimizes the overall exergy losses. In the case of the single pressure steam cycle (see Figure 5.25), steam is generated only at a pressure level corresponding to the HP turbine inlet pressure. After expansion in the HP turbine, steam is reheated in the HRSG and further expanded in the IP and LP turbine. In the HRSG of the double pressure system (see Figure 5.26) steam is generated at pressure levels corresponding with the inlet pressures of the HP and IP turbines. Expanded steam from the HP steam turbine is mixed with steam from the IP steam generator before it is reheated to the IP turbine inlet temperature. In the case of the triple pressure system (see Figure 5.27) steam is generated in the HRSG at three pressure levels corresponding with the inlet pressure of the HP, IP and LP steam turbines. Steam from the LP steam generator is mixed with the IP outlet flow. The temperature of the LP steam (approx. 227°C) almost equals the outlet temperature of the IP steam turbine. The condenser pressure is based on the availability of cooling water of 12 °C at condenser inlet and a temperature increase of 7 K. The three steam turbine cycles are depicted in  $T,s$ -diagrams shown in the Figures 5.28 to 5.30. The detailed system models are used for design point calculations. Steam turbine efficiencies are calculated by Cycle-Tempo; the applied calculation method is based on [5.36] and results in somewhat conservative values for the steam turbine efficiencies.

*Table 5.12 Results of the gas turbine cycles*

GAS TURBINE CYCLE	units	1 press.	2 press.	3 press.
<b>overall cycle data</b>				
heat flow to cycle ( $LHV$ )	MW	660.62	660.62	660.62
net electrical power from cycle	MW	251.36	250.75	249.65
$\eta_{th, GT}$	-	0.3805	0.3796	0.3779
$\bar{T}_H$	K	1040.0	1040.0	1040.0
$\bar{T}_{C, GT}$	K	521.1	521.4	521.9
$\eta_{th, rev, GT}$	-	0.4989	0.4987	0.4982
$\eta_{ex, intern, GT}$	-	0.7626	0.7612	0.7586
<b>exergy balance</b>				
<b>combustor</b>				
fuel exergy	MW	691.48	691.48	691.48
exergy loss combustor	MW	204.61	204.61	204.61
exergy transferred to GT cycle	MW	486.87	486.87	486.87
<b>GT cycle</b>				
internal exergy loss	MW	41.27	41.20	41.10
net electrical power	MW	251.36	250.75	249.5
exergy of exhaust gas	MW	194.24	194.92	196.12
$\eta_{ex, GT cycle}$	-	0.8590	0.8589	0.8586

### 5.5.3 Evaluation of system results

#### Gas turbine cycle

The fuel flow rate to the gas turbine (17.387 kg/s) is the same for the three systems. The corresponding heat flow (660.62 MW) is based on the lower heating value of the fuel. The exergy flow of the fuel, as shown in Table 5.12, is 691.48 MW. The exergy loss due to combustion is 204.61 MW; this means that 29.59% of the exergy transferred to the plant is lost during combustion. The exergy efficiency of the combustion process is then 70.41%. Table 5.12 shows that the generated net electrical power by the gas turbine cycle is not the same for the three systems. The differences in net electrical power result from differences in GT outlet pressure. It was arbitrarily assumed that a higher number of pressure levels should result in higher gas side pressure losses of the HRSG. The assumed overall pressure losses are 24, 29 and 38 mbar for respectively the 1, 2, and 3 pressure HRSG. Then, also the thermal cycle efficiency ( $\eta_{th,GT}$ ) slightly decreases if the number of pressure levels increases. The thermal efficiency of the cycle ( $\eta_{th,GT}$ ) represents the fraction of the heat flow to the cycle that is converted into electrical power. For the calculation of the thermodynamic equivalent temperature of heat transfer to the GT cycle, which is also the thermodynamic equivalent temperature of heat transfer to the combined cycle, the following equation is applied:

$$\bar{T}_H = \frac{T_{out} - T_{in}}{\ln \frac{T_{out}}{T_{in}}} \quad (5.6)$$

with the compressor outlet temperature as  $T_{in}$  and the turbine inlet temperature as  $T_{out}$ . In Section 5.4.3 it was concluded that this method is fairly accurate. The accuracy is at least sufficient for the evaluation of trends. For that reason this method is assumed to be appropriate in this case. The thermodynamic equivalent temperature of heat transfer from the gas turbine cycle ( $\bar{T}_{C,GT}$ ) is also calculated by applying Equation 5.6 with the turbine outlet temperature as  $T_{in}$  and the temperature of the environment (288.15 K) as  $T_{out}$ . The thermal efficiencies of the reversible gas turbine cycle ( $\eta_{th,rev,GT}$ ) are calculated with the following equation:

$$\eta_{th,rev,GT} = 1 - \frac{\bar{T}_{C,GT}}{\bar{T}_H} \quad (5.7)$$

The determination of these values is based on temperatures of the irreversible process. As no attempt is made to define a corresponding reversible cycle only the temperatures from the system calculation are available. The calculation of the internal exergy efficiency of the gas turbine cycle ( $\eta_{ex,intern,GT}$ ) is based on Equation 2.88. Differences between the values of the three plants are caused by differences in gas turbine outlet temperature caused by the different pressure losses of the HRSG's. The internal exergy efficiency of the gas turbine cycles is approximately 76% when using the calculated values for  $\eta_{th,rev,GT}$  and  $\eta_{th,GT}$ <sup>8</sup>. In Table 5.12 also the exergy balance of the combustor and the gas turbine cycle are shown. The fuel

<sup>8</sup> In Section 5.3.3 it is shown that the internal exergy efficiencies calculated in this way are not exact but in reasonable agreement with the true internal exergy efficiencies.

## Chapter 5 Thermal power cycles

exergy, the exergy loss of combustion and the exergy transferred to the gas turbine cycle are all the same for the considered cases. The exergy loss of the gas turbine cycle, the net electrical power and the exergy of the exhaust gas show slight differences due to the differences in the gas turbine exhaust temperature. The exergy efficiency of the cycle is calculated using the following equation:

$$\eta_{ex, GT\ cycle} = \frac{Ex_{product}}{Ex_{source}} = \frac{P_{electr, net}}{Ex_{to\ GT\ cycle} - Ex_{exhaust\ gas}} \quad (5.8)$$

The calculated values of the exergy efficiencies of the gas turbine cycle are almost 86%. These efficiencies are significant higher than the calculated internal exergy efficiencies. Equation 5.8 is almost the same as Equation 5.2, only in Equation 5.8 also the losses of the generator are included.

STEAM TURBINE CYCLE	units	1 press.	2 press.	3 press.
<b>overall cycle data</b>				
heat flow from GT exhaust gas	MW	400.28	400.90	402.02
heat flow to ST cycle	MW	300.73	329.72	355.91
net electrical power from cycle	MW	112.90	124.09	129.48
$\eta_{th, ST}$	-	0.3754	0.3763	0.3638
$\bar{T}_{H, ST}$	K	522.7	529.7	526.6
$\bar{T}_C$	K	295.2	295.2	295.2
$\eta_{th, rev, ST}$	-	0.4352	0.4427	0.4394
$\eta_{ex, intern, ST}$	-	0.8626	0.8501	0.8279
<b>exergy balance</b>				
exergy from HRSG to ST cycle	MW	133.51	149.27	160.32
net electrical power	MW	112.90	124.09	129.48
exergy from ST cycle to condenser	MW	4.38	4.79	5.27
internal exergy loss	MW	16.23	20.39	25.57
$\eta_{ex, ST\ cycle}$	-	0.8743	0.8589	0.8351

### Steam turbine cycle

The results of the calculations of the steam turbine cycles are presented in Table 5.13. The heat flow obtained from the GT exhaust gas by cooling this gas to ambient temperature is based on the assumption that water vapor in the flue gas will not condense but remains completely in the vapor phase. Then, approximately 400 MW of heat can be extracted from this gas flow. In the case of the single pressure system only 300.73 MW from the 400.28 MW is transferred to the steam turbine cycle. The net electrical power from the steam turbine cycle

is 112.90 MW which results in a thermal efficiency of the (irreversible) steam cycle ( $\eta_{th, irrev, ST}$ ) of 0.3754. This efficiency is determined by dividing the net electrical power from the ST cycle by the heat transferred to de ST cycle. It appears that the heat transferred to the ST cycle is markedly affected by the number of pressure levels at which steam is generated in the HRSG. In the case of the triple pressure system the heat flow to the ST cycle is about 18% higher then in the case of the single pressure system. Increasing the extraction of heat in the HRSG results into lower outlet temperatures of the flue gas (= stack temperature, see Table 5.11) and into a serious reduction of the heat lost through the stack. However, the generated net electrical power is not proportional with the heat transferred to the cycle. It appears that

the thermal efficiency of the cycle ( $\eta_{th, ST}$ ) is affected also by the number of pressure levels. Table 5.13 shows that  $\eta_{th, ST}$  is higher in the case of the double pressure system and lower in the case of the triple pressure system. The thermodynamic equivalent temperature of heat transfer to the cycle ( $\bar{T}_{H, ST}$ ) is calculated by applying Equation 5.1:

$$\bar{T} = \frac{\sum m \cdot (h_{out} - h_{in})}{\sum m \cdot (s_{out} - s_{in})} \quad (5.1)$$

In this equation the enthalpy and entropy transfer by all heat exchangers (within the HRSG) is included. It appears that the double pressure system enables a somewhat higher temperature of heat transfer to the cycle (529.7 K) than the other two; the temperature of the triple pressure system however appears to be slightly lower than the temperature of the double pressure system (526.6 K). The low stack temperature results in additional heat transfer at low temperatures. Heat transfer from the ST cycle occurs in the condenser at constant temperature. The condenser temperature is used as the temperature of heat transfer from the ST cycle ( $\bar{T}_C$ ). This temperature is the same for the three cases. The thermal efficiency of the reversible cycle ( $\eta_{th, rev, ST}$ ) is calculated by using the thermodynamic equivalent temperatures of heat transfer to and from the cycle. As the temperature of heat transfer from the cycle is constant, the thermal efficiency of the reversible cycle is only a function of the thermodynamic equivalent temperature of heat transfer to the cycle ( $\bar{T}_{H, ST}$ ). Thus the highest value is achieved for the two pressure case. The internal exergy efficiency of the steam cycle ( $\eta_{ex, intern, ST}$ ) is calculated also here as the ratio between the irreversible and the reversible thermal efficiency. It appears that the internal cycle efficiency of the steam turbine cycle decreases if the number of pressure levels increases. The accuracy of the internal efficiencies is limited since the exergy losses that are determining these efficiencies are depending on the assumed performance data. But it seems to be plausible that the higher complexity of the 3 pressure steam cycle and the addition of steam at lower pressure and temperature than the live steam will result in higher internal losses of the cycle. Since:

$$P_{net\ electr} = \eta_{ex, intern, ST} \cdot \eta_{th, rev, ST} \cdot \dot{Q}_{H\ to\ ST} \quad (5.9)$$

the net generated electrical power is obviously dominated by the increase of heat transfer to the cycle. However, the effect of the higher heat flow to the ST cycle is mitigated by higher

## Chapter 5 Thermal power cycles

internal losses. The exergy transferred in the HRSG to the steam cycle is calculated by summarizing the exergy transfer to the steam cycle in all heat exchangers of the HRSG:

$$Ex_{\text{to ST in HRSG}} = \sum_i \Phi_{m,w} (ex_{\text{out,w}} - ex_{\text{in,w}}) \quad (5.10)$$

The values in Table 5.13 show that the increase of the number of pressure levels has a significant effect on the exergy flow to the steam turbine cycle (+12% in the case of double pressure and +20% in the case of triple pressure). But also the exergy transfer from the steam cycle to the condenser as well as the internal exergy loss of the steam cycle increases. Therefore, the net generated electricity is not proportional to the exergy flow to the cycle. The exergy efficiency of the steam turbine cycle is calculated in the same way as for the gas turbine cycle. The following equation is used for this purpose:

$$\eta_{\text{ex, ST cycle}} = \frac{Ex_{\text{product}}}{Ex_{\text{source}}} = \frac{P_{\text{electr, net}}}{Ex_{\text{to ST cycle}} - Ex_{\text{to condenser}}} \quad (5.11)$$

The differences between the internal cycle efficiency ( $\eta_{\text{ex, intern, ST}}$ ) and the exergy efficiency of the cycle ( $\eta_{\text{ex, ST cycle}}$ ) are seriously lower than in the case of the gas turbine cycle.

<i>Table 5.14 Results of the Combined Cycle plants</i>				
COMBINED CYCLE PLANT	units	1 press.	2 press.	3 press.
<b>overall cycle data</b>				
heat into cycle	MW	660.62	660.62	660.62
net electrical power	MW	364.26	374.84	379.13
$\eta_{\text{th, CC}}$	-	0.5514	0.5674	0.5739
$\bar{T}_H$	K	1040.0	1040.0	1040.0
$\bar{T}_C$	K	295.2	295.2	295.2
$\eta_{\text{th, rev, CC}}$	-	0.7162	0.7162	0.7162
$\eta_{\text{ex, intern, CC}}$	-	0.7699	0.7923	0.8014
$\eta_{\text{ex, CC}}$	-	0.8070	0.8157	0.8195
<b>exergy balance</b>				
fuel exergy	MW	691.48	691.48	691.48
net electrical power	MW	364.26	374.84	379.13
overall exergy loss	MW	327.22	316.64	312.35
exergy efficiency CC plant	-	0.5268	0.5421	0.5483

### Combined cycle plant

The CC plants are evaluated assuming that the gas turbine cycle and the steam turbine cycle together are considered as one single thermal power cycle. The overall results of the CC plants are shown in Table 5.14. The net electrical power generated by the combined cycles equals the sum of the net electrical powers from the gas turbine cycle and the steam cycle. It appears that the thermal efficiency of the combined cycle increases from 0.5514 for the single pressure plant to 0.5739 for the triple pressure plant. Heat transfer to the combined cycle

occurs only in the combustor of the GT; therefore the thermodynamic equivalent temperature of heat transfer to the cycle is the same as for the gas turbine cycle (1040 K). Heat transfer from the combined cycle to the environment occurs in the steam condenser (at 295.2 K). Thus the heat transferred to the cycle as well as the thermal efficiency of the reversible cycle ( $\eta_{th, rev, CC}$ ) are the same for all the considered cases. It is obvious from Equation 5.9 that the differences between the thermal efficiencies of the irreversible cycles are only due to differences between the internal efficiency of the cycles. Increasing the number of pressure levels for steam generation in the HRSG increases the internal efficiency ( $\eta_{ex, intern, CC}$ ) from 0.7699 for the single pressure case to 0.8014 for the triple pressure case. The exergy efficiency of the combined cycle is calculated in the same way as of the GT and the ST cycles. But in the CC case also the exergy discharged to the environment through the stack has to be subtracted in the denominator. Thus, the following equation is used:

$$\eta_{ex, CC} = \frac{Ex_{product}}{Ex_{source}} = \frac{P_{electr, net}}{Ex_{to GT cycle} - Ex_{to stack} - Ex_{to condenser}} \quad (5.12)$$

The differences between the internal exergy efficiency of the cycle ( $\eta_{ex, intern, CC}$ ) and the exergy efficiency of the cycle ( $\eta_{ex, CC}$ ) are again much lower than in the case of the gas turbine cycle.

The exergy balance of the combined cycle in Table 5.14 shows the overall exergy losses and the exergy efficiencies of the considered plants. The overall exergy loss is the difference

HRSG	units	1 press.	2 press.	3 press.
<b>exergy balance</b>				
exergy transferred from GT cycle	MW	194.24	194.92	196.12
exergy transferred to ST cycle	MW	133.51	149.27	160.32
exergy loss HRSG	MW	29.64	23.12	18.99
exergy flue gas to stack	MW	31.09	22.53	16.81

between the fuel exergy and the net electrical power; the exergy efficiency is calculated as the ratio of the net electrical power and the fuel exergy and increases from 0.5268 for the single pressure case to 0.5483 for the triple pressure case. The efficiency increase results primarily from differences of the heat transfer in the HRSG. Therefore, the exergy loss of the HRSG is considered in more detail. The exergy balance of the HRSG's is shown in Table 5.15. From the exergy transferred from the GT cycle, 194.24 MW in the single pressure case, 29.64 MW is lost due to heat transfer in the HRSG, 133.51 MW is transferred to the steam cycle and the remainder, 31.09 MW, is passed to the stack. It appears that when increasing the number of pressure levels the reduction of the exergy loss to the stack is even higher than the reduction of the exergy loss due to heat transfer in the HRSG. The reduction of the two exergy losses results in a 20% higher exergy transfer to the steam cycle for the triple pressure case compared to the single pressure case. However, the effect on the overall plant efficiency is somewhat mitigated because of the higher internal exergy loss of the ST cycle (see Table 5.13).

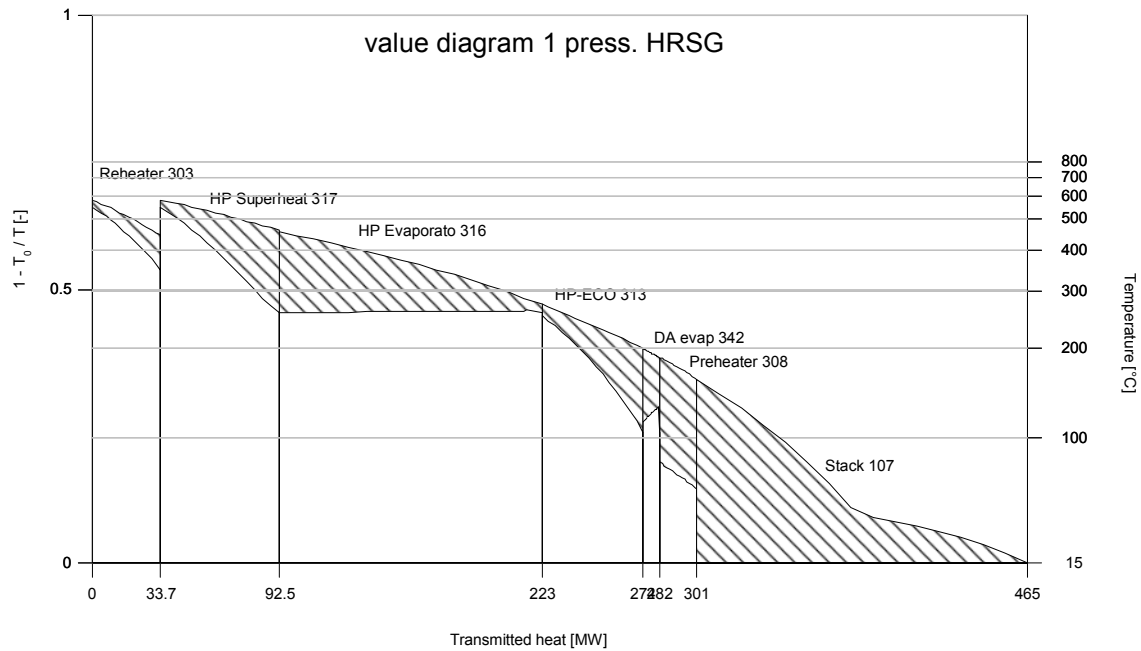


Figure 5.31 Value diagram of the HRSG, steam generated at 1 pressure level

The effect of increasing the number of pressure levels is demonstrated by the value diagrams of the HRSG's as shown in Figure 5.31, 5.32 and 5.33 for respectively the single, the double and the triple pressure case. The shaded areas do represent the exergy loss due to heat transfer. The temperature curve of the flue gas, if cooled to environmental temperature after leaving the stack, shows clearly the effect of the condensation of water vapor available

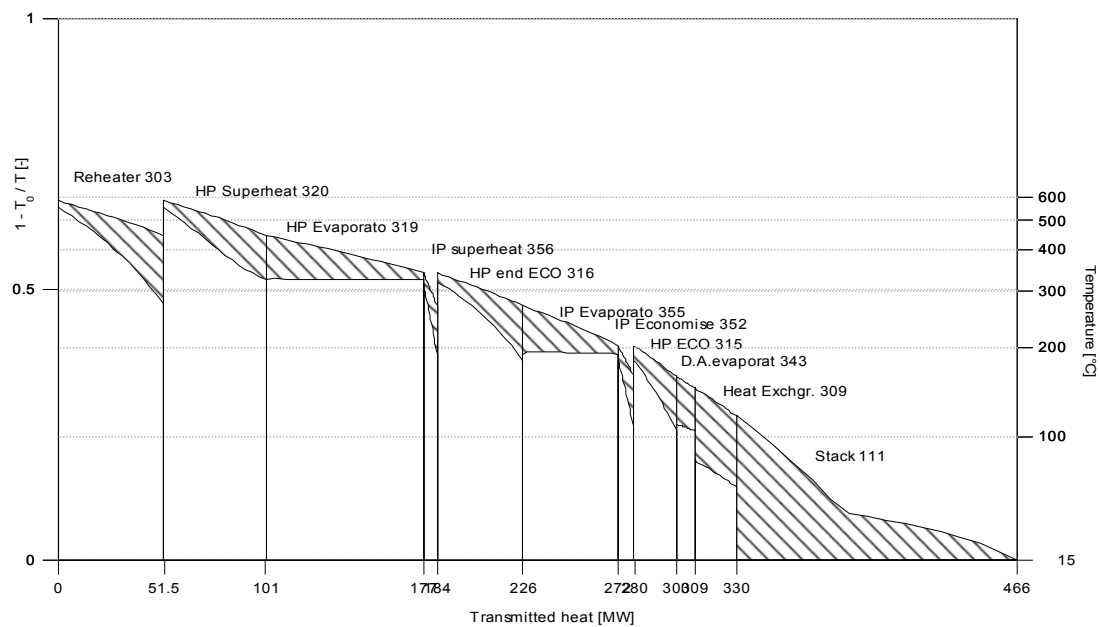


Figure 5.32 Value diagram of the HRSG, steam generated at 2 pressure levels

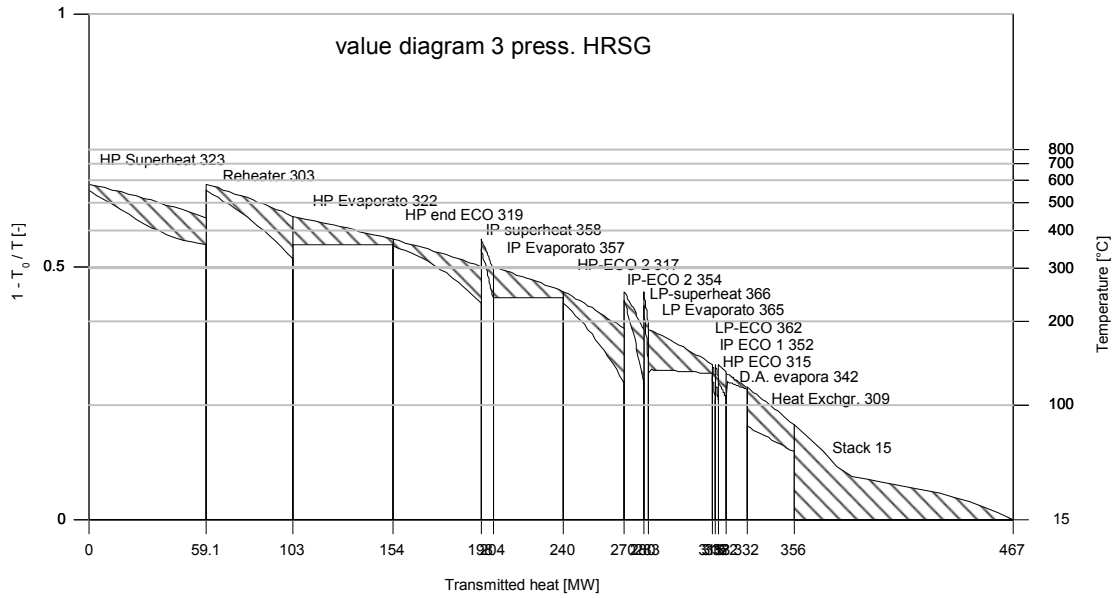


Figure 5.33 Value diagram of the HRSG, steam generated at 3 pressure levels

in the flue gas. An overview of all exergy losses and exergy flows of the Combined Cycle plants is given by the exergy flow diagrams in Figure 5.34, 5.35 and 5.36. The diagrams clearly show the exergy loss reduction of the HRSG and the stack for the double pressure and triple pressure case. They also show that the large exergy losses due combustion and friction

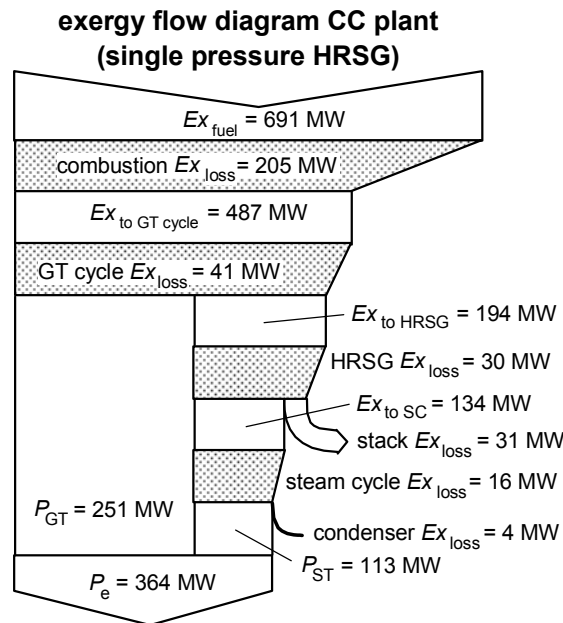


Figure 5.34 Exergy flow diagram of the CC plant, single pressure HRSG

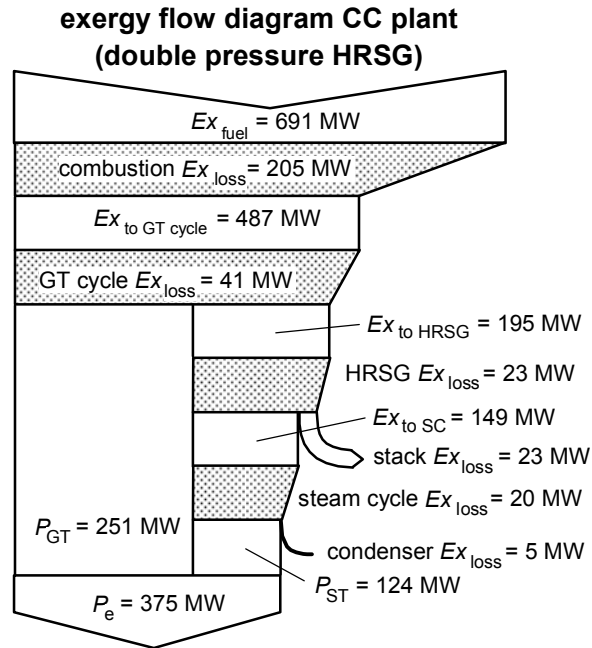


Figure 5.35 Exergy flow diagram of the CC plant, double pressure HRSG

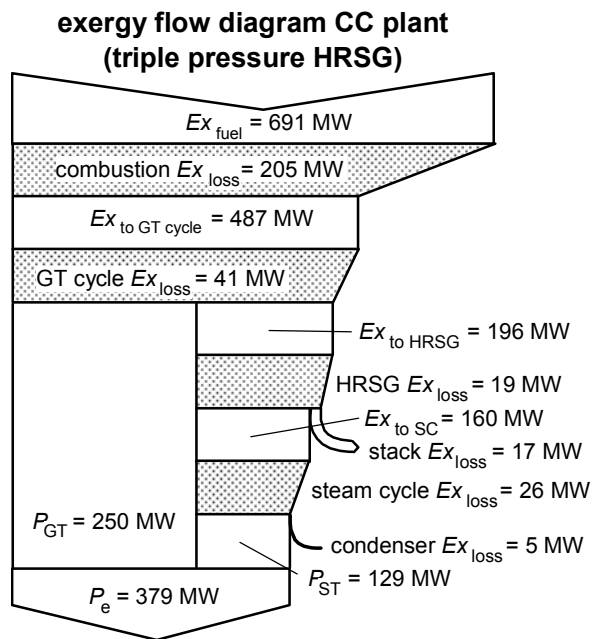


Figure 5.36 Exergy flow diagram of the CC plant, triple pressure HRSG

in the gas turbine cycle remain unaffected. Serious higher efficiencies are achievable only if these losses can be reduced or eliminated.

#### 5.5.4 Discussion of results

##### Exergy flow diagram and value diagram

The exergy flow diagrams of the CC plants and the value diagrams of the HRSG's present a clear and useful overview of all exergy losses. The exergy flow diagrams (Figure 5.34, 5.35 and 5.36) show that more than 35% (205 + 41 MW) of the fuel exergy entering the CC plant is lost due to combustion and friction within the gas turbine cycle. The exergy losses of HRSG, stack and steam cycle together are in the case of the single pressure system only 11.1% (30 + 31 + 16 MW) and are reduced to 9.6% and 9.0% for respectively the double pressure and the triple pressure case. The increase of the number of pressure levels at which steam is generated in the HRSG obviously influences just the exergy losses of system parts that have only a limited effect on the overall plant exergy loss.

More detailed insight into the effect of an increased number of pressure levels is obtained from the value diagrams of the HRSG's. The value diagram of the single pressure case (Figure 5.31) shows that substantial exergy losses occur in most of the heat exchangers and in particular in the stack. The value diagram of the double pressure case, as presented in Figure 5.32, shows that the exergy loss due to heat transfer as well as the exergy of the flue gas discharged to the stack is significantly reduced. Figure 5.33, the value diagram of the triple pressure HRSG, clearly shows that the use of an extra pressure level enables further reduction of these exergy losses. It is also obvious from this diagram that the effect of further attempts to reduce these losses will be very limited.

##### Exergy efficiencies and internal exergy efficiencies of the cycles

In the previous sections different parameters are applied to indicate the performance of systems and subsystems. The internal exergy efficiency of the cycle as well as the exergy efficiency are used for the power cycles. The difference between these two exergy efficiencies is discussed in Section 2.6.5. The exergy efficiency of the power cycle is the usual exergy efficiency as defined by Equation 2.66. This exergy efficiency compares the product exergy with the balance of all other exergy flows to and from the system. The balance of all other exergy flows is actually the exergy that is available for conversion into the product, thus, the exergy efficiency compares the actual product with the maximum that could have been generated under these circumstances. But this maximum differs from the product exergy in the case of a reversible system, because of the fact that in general the exergy of the flows that leave the actual system (the discharged exergy) is increased due to the irreversibilities of the system. Thus, in the case of an irreversible system the exergy available for conversion into the product exergy is less than in the case of a reversible system. This means that the exergy efficiency depends on the irreversibilities of the system itself, and does not represent the ratio between the actual system and its corresponding reversible system.

The internal exergy efficiency of a thermal cycle is actually defined as the performance ratio of the actual cycle and the corresponding reversible cycle. In the case of thermal power cycles it is possible to approximate this ratio quite well without the exact specification of the reversible cycle (see Section 5.4.3). Since the available exergy for conversion into the product is always higher in the case of a reversible system, the internal exergy efficiency will always be lower than the usual exergy efficiency of a power cycle. This is confirmed by the calculations shown in the previous sections.

## Chapter 5 Thermal power cycles

Another observation from the results of the combined cycle evaluation is that in the case of a gas turbine cycle the difference between the exergy efficiency and the internal exergy efficiency much higher is than in the case of a steam turbine cycle or a combined cycle. This can be explained by considering the effects of the internal irreversibilities on the exergy flows to and from the cycle. The internal irreversibilities are dominated by the losses due to compression and expansion. Also in the case of the gas turbine cycle the losses due expansion are serious higher<sup>9</sup> than the losses due to compression because of the higher change of enthalpy. And also the entropy increase in the expansion turbine will be higher. The exergy transferred from the irreversible cycle is raised because the entropy increase in the turbine increases the amount as well as the temperature of the discharged heat. The exergy transferred to the cycle is effected by the entropy increase of the compressor. That causes an increase of the temperature of heat transfer to the cycle, but it decreases the amount of heat. The net effect will be serious lower. In the case of an irreversible steam turbine cycle the entropy increase in the turbine will only increase the amount of heat discharged by the cycle. The temperature is not affected if the end point of expansion is within the two phase region. The exergy of the discharged heat is low anyhow. Since the exergy discharge is much more susceptible to internal irreversibilities in the case of gas turbine cycles than in the case of steam turbine cycles or combined cycles, the difference between the exergy efficiency and the internal exergy of the cycle will also be higher in the case of gas turbine cycles.

#### Further developments

The exergy efficiencies of the CC plants differ from 0.5268 for the single pressure case to 0.5483 for the triple pressure case; the corresponding thermal efficiencies are respectively 0.5514 and 0.5739. These values are somewhat lower than the highest achievable values (around 0.60) today. Thus, also combined cycles with the highest thermodynamic performance today are wasting more than 40% of the available exergy from the fuel. Equation 2.88 shows what kind of improvements are actually necessary to reduce the overall exergy loss. The options are in principle: a further increase of the temperature of heat transfer to the cycle and a reduction of the internal exergy losses of the cycles including the losses of heat transfer between the cycles. The effect of increasing  $\bar{T}_H$  and the overall value of  $\eta_{ex, intern}$  on the overall thermal efficiency is shown in Figure 5.37. The temperature at the horizontal axis is the thermodynamic equivalent temperature of heat transfer to the cycle ( $\bar{T}_H$ ) and curves are depicted for different values of the internal exergy efficiency. The solid line represents the ideal case, the Carnot efficiency. The efficiency curves are depicted assuming that the temperature of heat transfer from the system is 22°C<sup>10</sup>. In the diagram also the state of the art of the gas turbine development is indicated. In 1983 the temperature  $\bar{T}_H$  was roughly 650°C (see Table 5.10,  $\pi = 11$  and  $TIT = 1050^\circ\text{C}$ ). The data of the gas turbines from 2008 show that this temperature was increased to around 800°C ( $\pi = 17$  and  $TIT = 1300^\circ\text{C}$ ). And a value of

<sup>9</sup> In the case of gas turbine used for the evaluation of combined cycle plants the exergy loss of the expansion turbine is almost 60% higher than the exergy loss of the compressor.

<sup>10</sup> This temperature equals the condensation temperature of a steam turbine cycle if cooling water of 12°C is heated 7 K and the minimum temperature difference is 3 K.

910°C is supposed to be the value of an advanced gas turbine ( $\pi = 23$  and  $TIT = 1500^\circ\text{C}$ ). The exergy losses within the cycles are the result of a trade-off between driving forces (for primarily heat transfer and mass flow rate) and capital costs. Technology development and increasing fuel prices are supposed to result in a gradual reduction of these losses. The internal exergy efficiencies of the combined cycles today are somewhere in the region of 82%, thus the remaining space for further improvements is limited. An increase of the internal exergy efficiency to 85 or 90% will raise the plant thermal efficiency with roughly 2 to 6% points; the necessary efforts will certainly take a long period of continued development.

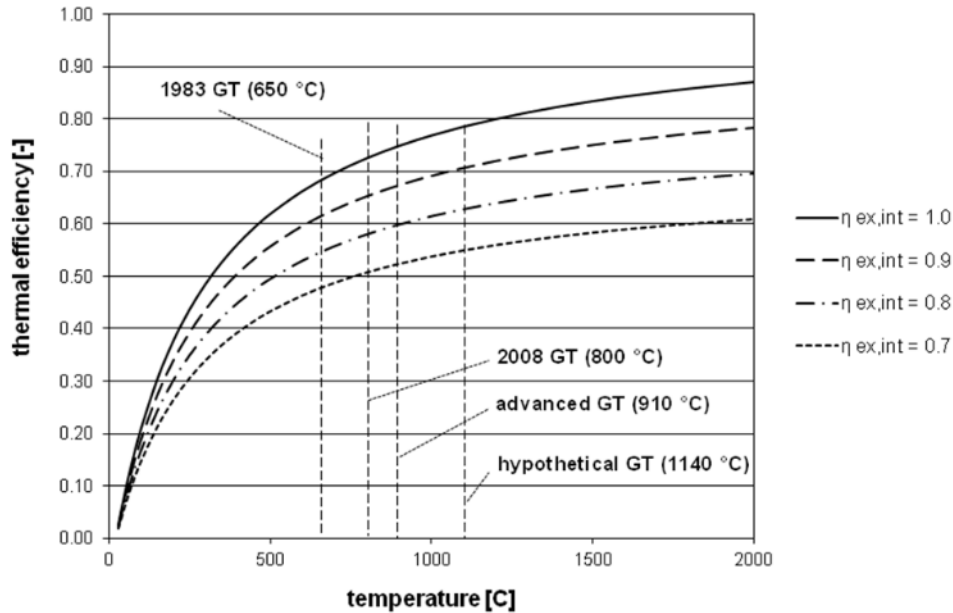


Figure 5.37 Thermal efficiency as function of  $\bar{T}_H$  and  $\eta_{ex, \text{intern}}$  ( $\bar{T}_C = 22^\circ\text{C}$ )

The other way to increase the thermal efficiency is increasing the thermodynamic equivalent temperature of heat transfer to the cycle. This can be achieved by increasing the gas turbine inlet temperature ( $TIT$ ) as well as by increasing the pressure ratio or the application of one or more reheats. The efficiency increase caused by the step from the 2008 GT to the advanced GT is roughly 2.0 to 2.5% (points) depending on the internal exergy efficiency. For this step the turbine inlet temperature was increased from  $1300^\circ\text{C}$  to  $1500^\circ\text{C}$ . In Figure 5.37 also an hypothetical GT with a  $\bar{T}_H$  of  $1140^\circ\text{C}$  is indicated. This value is achieved if  $\pi = 30$  and  $TIT = 2000^\circ\text{C}$ . The thermal efficiency of the hypothetical GT is roughly 5% (points) higher than the thermal efficiency of the 2008 GT and 3% higher than the thermal efficiency of the advanced GT if it is assumed that the internal exergy efficiency is constant. Thus, CC plant efficiencies significant higher than the 60% level of today will require very serious improvements of the gas turbine.

Today the gas turbine with the highest  $TIT$  is the GE H-series (S109H, S107H) [5.35] with steam cooled blades. Because of the steam required for the blade cooling these turbines are available only for combined cycle operation. Further increase of the turbine inlet temperatures will require substantial efforts from gas turbine manufactures. Because of the limited benefits it is uncertain that they will opt for this development. The application of

## Chapter 5 Thermal power cycles

reheat is another option to increase the thermodynamic temperature of heat transfer to the cycle. The introduction of a reheat gas turbine by Alstom (GT26) [5.35] is the only attempt into this direction so far; further developments are not announced. Therefore, the prospects of combined cycle efficiencies significantly higher than the present 60% are not obvious.

### 5.5.5 Conclusions

The application of combined cycles has resulted in a significant increase of power plant efficiencies during the last decades. Overall plant (thermal) efficiencies around 60% are achievable today if heat from the gas turbine exhaust gases is efficiently used. The evaluation of exergy losses in combined cycle plants shows that these losses are primarily dominated by the exergy losses of thermal combustion. Possibilities to reduce these losses are limited. The exergy flow diagrams (Figures 5.34, 5.35 and 5.36) show that the highest losses are caused by (thermal) combustion of the fuel. The further enhancement of plant efficiencies to 70% or higher by only the further development of the open cycle GT does not seem to be very likely.

The comparison of CC plants with increasing number of pressure levels of steam generation in the HRSG shows that the efficiency gain of a triple pressure system in comparison with a single pressure system is caused by the reduction of the exergy loss of heat transfer in the HRSG as well as the lower exergy of the flue gasses discharged to the stack. The last effect is even more important than the reduction of exergy losses due to heat transfer as can be learned from the value diagrams of the HRSG's (Figures 5.31, 5.32 and 5.33). In the case of the triple pressure steam generation the remaining exergy losses of heat transfer and flue gas discharge together are about 5% of the fuel exergy. A further increase of the number of steam pressure levels in the HRSG does not seem to be really beneficial; it enables only a small reduction of the overall exergy loss of the plant.

Different parameters can be used to assess the thermodynamic performance of power plants or the different cycles. The traditionally used thermal efficiency does not indicate the thermodynamic losses correctly as it ignores the temperature of heat transfer to and from the cycles. Therefore, the application of exergy efficiencies is recommended. Overall exergy efficiencies of power plants do indicate clearly the difference with the ideal case. In the case of thermal power cycles the exergy efficiency as defined in Chapter 2 does not really compare the actual process with the ideal process. The considered exergy source depends in general on the internal irreversibilities of the power cycle<sup>11</sup>. The internal exergy efficiency of thermal power cycles is introduced to get a better comparison of the actual process with the ideal process. In the case of gas turbine cycles the exergy flow that leaves the cycle is significant more sensitive for the internal irreversibilities of the cycle than in the case of steam turbine cycles. Therefore, the difference between the exergy efficiency and the internal exergy efficiency is serious higher for gas turbine cycle than for steam turbine cycles. It has been demonstrated in Section 5.4.3 that even in the case of gas turbine cycles the internal exergy efficiency is a good approximation of the demanded comparison.

---

<sup>11</sup> This is not only true for thermal power cycles. Also in the case of exergy efficiencies as defined for a variety of processes in Chapter 2 the exergy source depends on the irreversibilities of the considered process. In general the used exergy source is a poor approximation of the product in the case of a reversible process. But, a better approximation will require in general serious additional efforts. In the case of thermal power cycles a better approximation is achievable with limited additional effort.

The internal exergy efficiency of power cycles is a useful performance indicator in particular in the case of complicated power cycles. It is shown also in Section 5.5 that the internal exergy efficiency is useful for single cycles as well as combined cycles.

## 5.6 Conclusions

In this chapter the thermodynamic characteristics of thermal power cycles are discussed. The thermodynamic losses of general used cycles for power generation, like steam cycles and combined cycle, are outlined and options for further improvements are discussed by using the internal exergy efficiency. The conclusions with regard to these three topics are presented below.

### Steam cycles

For the thermal efficiency of a conventional steam cycle (530°C, 180 bar) a value of 0.4580 was calculated resulting in a net electrical plant efficiency of 0.4228. The thermal efficiency of the steam cycle can be increased by applying advanced steam conditions. If the steam temperature is increased to 650°C and the steam pressure to 350 bar the thermal efficiency of the cycle raises to 0.5035 for the single reheat case and to 0.5136 for the double reheat case. Considering the same ratio between the net plant efficiency and the cycle efficiency, the net plant efficiency will become 0.4648 for a single reheat plant and 0.4741 for a double reheat plant. The further development of steam turbine plants with advanced steam conditions depends primarily on the progress of materials research for the high temperature components of the steam cycle: the boiler superheater, the high pressure and the intermediate pressure turbine, the high temperature piping and control valves. For the long term thermal efficiencies of steam turbine plants up to 50% are achievable. Also the reduction of internal cycle losses will be helpful to achieve this goal. It is not very likely that efficiencies serious higher than 50% are achievable in the future.

*Table 5.16 Rough data of CC plants for various stages of GT development*

	units	1983 GT	2008 GT	advanced GT	hypothetical GT
$\bar{T}_{H,CC}$	[°C]	650	800	910	1140
$TIT$	[°C]	1050	1250	1500	2000
$\pi$	[-]	11	18	23	23
$\eta_{ex, intern, CC}$	[-]	0.7	0.8	0.8 – 0.9	0.8 – 0.9
$\eta_{th, CC}$	[-]	0.47	0.58	0.60 – 0.67	0.62 – 0.71

### Combined cycles

Combining steam cycles with topping cycles (gas turbine, potassium turbine etc.) will enable significant higher overall plant efficiencies. The preferred technology of the topping cycle depends primarily on the available fuel. In the case of natural gas the application of a gas turbine is very attractive with regard to overall plant efficiency as well as system costs. Overall plant (thermal) efficiencies of around 60% are achievable today for CC plants. In the future higher plant efficiencies will result from further increases of  $\bar{T}_H$  and increases of the

## Chapter 5 Thermal power cycles

internal exergy efficiency ( $\eta_{ex, intern}$ ). The effects of these two parameters on the thermal efficiency of a thermal power plant are shown in Figure 5.37. It is assumed for this figure that heat transfer to the environment takes place at 22°C. The curve for  $\eta_{ex, intern} = 1.0$  represents the Carnot efficiency. The internal exergy efficiency of modern CC plants is around 0.8. The vertical dotted lines in the diagram represent various levels of development of the gas turbine. The data assumed for these levels of development are presented in Table 5.16. In the year 1983 the thermodynamic equivalent temperature of heat transfer to the gas turbine cycle of the best performing heavy duty gas turbines was around 650°C. The thermal efficiency of a CC plant at that time was around 0.47 which corresponds with an internal exergy efficiency of around 0.7. In 2008 the temperature  $\bar{T}_{H,CC}$  was raised to around 800°C because of the application of higher turbine inlet temperatures and pressure ratios. The thermal efficiencies of these CC plants are around 0.58. Apparently not only the temperature of heat transfer to the cycle has been increased by 150 K but also the internal exergy efficiency has been increased from 0.7 to 0.8. A further increase of the turbine inlet temperature to 1500°C together with a pressure ratio of 23 (indicated as the advanced GT) will raise the  $\bar{T}_{H,CC}$  to 910°C. If the internal exergy efficiency is still 0.8 the thermal efficiency of the CC plant will be 0.60. Further improvement of the internal exergy efficiency to e.g. 0.9 will increase the thermal efficiency of the plant to 0.67. If it is assumed that the  $TIT$  can be raised further to 2000°C the  $\bar{T}_{H,CC}$  will increase to 1140°C and thermal efficiencies of 0.62 to 0.71 are achievable with internal exergy efficiencies ranging from 0.8 to 0.9. The actual improvements in the future are not easy to predict. But the development of CC plants with efficiencies around 70% will require serious efforts. Looking at the developments in the past, it is expected that these efforts will take several decades.

In the case of solid fuels the preference for gas turbine topping cycles is less obvious. The gasification plant necessary to convert the solid fuel into a gaseous fuel suitable for combustion in current gas turbines is quite expensive and reduces the plant overall efficiency significantly. Even with modern gas turbines efficiencies higher than 50% are not easily achievable with Integrated Gasification Combined Cycle (IGCC) plants. Nevertheless, the interest for IGCC plants is growing because of the possibilities to remove CO<sub>2</sub>. Atmospheric pulverized coal combustion in combination with post combustion CO<sub>2</sub> removal reduces the overall plant efficiency dramatically and the equipment necessary to process the large flue gas volume flow rates will be expensive. The gasification process enables pre-combustion carbon removal. In that case the gas flow rate that has to be processed is much smaller than after combustion. The attractiveness of alternative topping cycles as e.g. the potassium topping cycle is very uncertain at the moment. Significant higher efficiencies than 50% are not expected. Under these circumstances the development of a new topping cycles for large scale power plants is not very likely.

### Internal exergy efficiency

The exergy efficiency as well as the internal exergy efficiency have been applied in this chapter for the evaluation of various thermal power cycles. The general definition of the exergy efficiency is formulated as:

$$\eta_{ex} = \frac{Ex_{\text{product}}}{Ex_{\text{source}}} \quad (2.66)$$

For a thermal power cycle this equation was specified as:

$$\eta_{ex} = \frac{P_{\text{shaft}}}{Ex_{\text{H}} - Ex_{\text{C}}} \quad (5.2)$$

The internal exergy efficiency is defined as:

$$\eta_{ex, \text{intern}} = \frac{W}{W_{\text{rev}}} \quad (2.87)$$

Which can be converted into:

$$\eta_{ex, \text{intern}} = \frac{\eta_{\text{th}} \cdot Q_{\text{H}}}{\left(1 - \frac{\bar{T}_{\text{C}}}{\bar{T}_{\text{H}}}\right) \cdot Q_{\text{H}}} = \frac{\eta_{\text{th}}}{\eta_{\text{rev}}} \quad (2.88)$$

The Equations 5.2 and 2.88 are used in Section 5.2.1 to determine the efficiencies of the reference cycle. The calculated values are:  $\eta_{ex} = 0.8631$  and  $\eta_{ex, \text{intern}} = 0.8444$ .

In the introduction of this chapter (Section 5.1) it was stated that the exergy efficiency intends to present the ratio between the actual performance of a system and the performance of a reversible system operating under identical thermodynamic conditions. Obviously Equation 5.2 will not result into a true value for this ratio. This can be explained by assuming that  $Ex_{\text{H}}$  is fixed. Then, in the case of an irreversible system  $P_{\text{shaft}}$  will be lower than in the case of a reversible system. But the term  $Ex_{\text{H}} - Ex_{\text{C}}$  is also affected by the internal irreversibilities of the cycle, since  $Ex_{\text{C}}$ , the exergy transfer from the system, increases. Thus, by applying the exergy values of the actual cycle in Equation 5.3 the generated power ( $P_{\text{shaft}}$ ) is not divided by the maximum work achievable from the reversible cycle but by the maximum work achievable from an irreversible cycle. And, since  $Ex_{\text{C}}$  is higher in the case of an irreversible cycle, the calculated efficiency value will be higher than the true power ratio between the actual cycle and the reversible cycle.

In the case of a steam cycle without reheat the value of  $\eta_{\text{rev}}$  is practically independent of the performance of the irreversible cycle. Then, the internal exergy efficiency presents the true ratio between the powers generated by the actual cycle and the reversible cycle. In the case of a steam cycle with reheat, the conditions of the steam at the inlet and outlet of the reheater are affected by the performance of the HP turbine. This might affect the value of  $\bar{T}_{\text{H}}$  and thus also the value of  $\eta_{\text{rev}}$ . Then the value of  $\eta_{ex, \text{intern}}$  represents the power ratio of the actual cycle and the reversible cycle not exactly. But, the deviation is in general very small. The exergy transfer from the cycle,  $Ex_{\text{C}}$ , is in general small in the case of condensing steam cycles. The irreversible entropy increase during expansion in the steam turbine will increase of course the exergy transferred from the cycle, but also this increase is small. Then, the difference between the exergy efficiency and the internal exergy efficiency of a steam cycle is also small. This is also true in the case of combined cycles that use a steam bottoming cycle with condensing steam turbine.

## Chapter 5 Thermal power cycles

In the case of gas turbine cycles the difference between  $\eta_{ex}$  and  $\eta_{ex, intern}$  is usually significant. The internal irreversibility's of the cycle will affect the heat transfer to the system as well as the heat transfer from the system. The irreversibilities will change  $Ex_H$  as well as  $Ex_C$ , but the effect on  $Ex_C$  is serious higher. The exergy transferred to the cycle increases because of the higher temperature of heat transfer to the cycle due to the higher compressor outlet temperature, but the amount of heat decreases. The net effect on  $Ex_H$  is mitigated because of these conflicting effects. The internal irreversibilities will increase the temperature as well as the amount of heat transferred from the cycle. Thus, the exergy transferred from the cycle is certainly increased. The evaluation of the gas turbine cycle in Section 5.4 has shown that the difference between  $\eta_{ex}$  and  $\eta_{ex, intern}$  is significant. It is shown further that  $\eta_{ex, intern}$  approximates the true ratio between the powers of the actual cycle and the corresponding reversible cycle quite well.



## 6 FUEL CELL SYSTEMS

### 6.1 Introduction

In the Chapters 4 and 5 it is shown that for the conversion of primary fuels into electricity or work overall efficiencies higher than 60 to 70% are difficult to achieve, even in the case of clean primary fuels like natural gas. During the thermal conversion of fuel into heat in general more than 20% of the fuel exergy is lost and the subsequent conversion of heat into power causes an additional loss of 10 to 20%. In the case of solid fuels the total exergy loss is in general serious higher. The combustion of solid fuels is usually combined with the application of steam turbine cycles. The overall system thermal efficiencies are below 50% today. Conversion of a solid fuel into a clean secondary gaseous fuel enables the application of more efficient thermal power cycles, but the exergy loss of this additional conversion step neutralizes roughly the higher efficiency of the thermal power cycle. Today, thermal efficiencies of modern large scale power plants are in the range of 45 to 60% depending on the primary fuel. A further increase of power plant efficiencies to e.g. 80% for natural gas fuelled systems is a serious challenge for the future. It seems to be unlikely that these high efficiencies can be achieved by using only thermal power cycles. Electrochemical conversion of the fuel might be necessary to avoid the large exergy losses associated with thermal combustion. Hence, the development of fuel cells is considered to be an indispensable step to achieve more sustainable power generating systems. In this chapter various options for fuel cell applications in future power systems are discussed. As large scale commercial application of fuel cell systems has not been realized today the evaluations are based on the expected performance of fuel cell stacks and the balance of plant equipment.

Natural gas is primarily considered as the primary fuel for the evaluations in this chapter. It is obvious that sustainable energy systems will require fuel from renewable sources. Various options for the conversion of biomass into suitable fuels for fuel cells have been modeled and are discussed in [6.19], primarily with regard to their thermodynamic performance. The study has shown that also with the use of fuel cells decentralized power generation will cause high exergy losses for the total conversion chain. The exergy efficiency of the best case with centralized gasification and decentralized conversion in micro-CHP units is roughly 30% while the exergy efficiency of a reference plant with integrated biomass gasification and SOFC/GT plant is almost 49%. Thus, centralized power generation is in general preferred. This chapter, however, focuses primarily on the design of fuel cell systems in order to show what efficiencies are achievable by the application of various types of fuel cells. It is implicitly supposed that the most attractive system on natural gas will also be the most attractive in combination with biomass gasification.

Fuel cells enable the electrochemical conversion of fuel directly into electricity, thus, avoiding the exergy loss of thermal fuel conversion and in the case of closed thermal power cycles the exergy loss due to heat transfer from the flue gas to the power cycle. The electrochemical conversion in fuel cells is not free of exergy loss as explained e.g. in [6.1] and [6.3] and also in Appendix 6.1. The actual losses depend on the operation temperature

and the type of fuel cell as is discussed in Section 6.3. In general fuel cell systems for power generation have to be fuelled with available primary fuels. Even in the case of natural gas the fuel has to be converted first into hydrogen or in a hydrogen rich gas mixture, since most of the fuel cells under development today are hydrogen fuel cells. The fuel supplied to the fuel cell should be free of contaminants. Therefore, fuel cell systems have to include suitable processes for conversion and purification of the primary fuel. Apart from fuel cells operating on pure hydrogen, complete utilization of the fuel cannot be realized. The unconverted fuel is usually combusted in an after-burner. Efficient use of the heat generated by the fuel cell as well as the after-burner requires careful heat integration of the system. Various options are discussed in Section 6.4 based on the results from system studies made by the Energy Systems group of the department P&E of the TU Delft. Most of these results have been presented before in [6.2] but are discussed here more comprehensively.

Fuel cell systems are proposed so far for a variety of applications. Each of these applications has to fulfill its own requirements because of the available primary fuel, the required products, the power level and possibilities for system integration. Actual system designs usually depend on the state of development. Plants build to demonstrate the feasibility of a technology do in general not include all facilities necessary for optimum commercial performance. In the case of high performance fuel cell systems facilities might be necessary that are not presently available for commercial application. Therefore, an overview of fuel cell applications and their state of development is presented first in Section 6.2.

## 6.2 Status of fuel cell development and applications

A short overview of the most important fuel cell types and some characteristics is shown in Table 6.1. More specific types like the direct methanol fuel cell (DMFC) and the direct carbon fuel cell (DCFC) are not included in this overview, because they are in principle based on one of more of the considered technologies. The DMFC seems to be attractive primarily to replace batteries in portable systems for military applications and consumer electronics. Also PEMFC is considered for these devices. The application of very small power generators is not subject of discussion in this study. The thermodynamic performance is often not of primary importance for these applications.

fuel cell type	operating temperature	electrolyte	charge carrier
AFC	50-200°C	potassium hydroxide	OH <sup>-</sup>
PEMFC	50-80°C	ion exchange membrane	H <sup>+</sup>
PAFC	205-220°C	phosphoric acid	H <sup>+</sup>
MCFC	650°C	molten carbonate	CO <sub>3</sub> <sup>2-</sup>
SOFC	500-1000°C	ceramic	O <sup>2-</sup>

In the beginning of the fuel cell development the focus was primarily on low temperature cells with liquid electrolytes. The alkaline fuel cell (AFC) and the phosphoric acid fuel cell (PAFC) have been developed first for space applications. The development for terrestrial application appeared not to be very successful. The AFC has the disadvantage that air and fuel have to be completely free of CO<sub>2</sub>. This requires rigorous purification of the gas

## Chapter 6 Fuel cell systems

flows to the fuel cell. For the PAFC the  $\text{CO}_2$  in the fuel is not a problem, it appeared to be only a diluent. But the overall system for both types is rather complex. The use of a liquid electrolyte is also an extra complication. Electrolyte losses have to be compensated and concentrations have to be controlled and maintained. As the PAFC appeared to be less sensitive for impurities in the fuel and air, this type was initially preferred for stationary power generation. Efficiencies of 42%, based on the *LHV*, are achieved on natural gas. This was considered to be insufficient to compensate the high capital costs of the PAFC system. Serious performance improvements, however, are limited by the slow oxygen reaction rate at the cathode.

High temperature fuel cells like MCFC and SOFC have the possibility to allow for internal reforming of hydrocarbon fuels and they appeared to be less sensitive for impurities in the fuel. That's why these fuel cells are supposed to be more appropriate for stationary power generation. However, materials selection is essential for high temperature fuel cells. Degradation, sealing and thermal expansion of construction materials require serious consideration. Since the 1980s the research in the Netherlands has focused first on the MCFC. The initial enthusiasm was tempered by various problems resulting from the application of the liquid and very corrosive electrolyte. During the 1990s the interest for the SOFC was growing worldwide. The solid electrolyte was considered to be a serious advantage over the MCFC but the very high temperatures (up to  $1000^\circ\text{C}$ ) required the application of unconventional and expensive materials, also for components outside the SOFC stack. Operation at lower temperatures, down to  $500^\circ\text{C}$ , is an important target of the SOFC research today. Attempts to prove that high system efficiencies can be maintained during many years of operation as required for stationary power generation are still going on.

Before 1990 the main focus was on small to large scale power generation systems assuming that coal and natural gas have to be seen as the available primary fuels. Primarily MCFC and later on also SOFC were supposed to be most attractive technologies for these applications. The progress made with the development of the PEMFC resulted in increased interest for transport applications, in particular light duty vehicles, during the 1990s. The low operating temperature, high power density and fast response times makes the PEMFC in particular attractive for this kind of applications. Most of the big car manufacturers (like e.g. Daimler, Ford, General Motors, Honda, Hyundai, Nissan, Renault, Toyota, Volkswagen) are involved in the development, usually in co-operation with fuel cell manufacturers and large energy companies. Several PEMFC demonstration cars have been presented and tested. The SOFC is considered too, but up to now proposed only for auxiliary power generation by BMW. The demonstration vehicles are fuelled with hydrogen or methanol. Hydrogen enables the simplest system design but the storage of amounts of fuel sufficient to enable driving ranges similar to conventional cars requires the development of new storage systems. On-board storage of hydrogen is done at high pressure (up to 700 bar) or with liquefied hydrogen. Metal hydride storage is under investigation. The on-board storage of methanol seems to be less complicated, but reforming and purification of the fuel before conversion in the fuel cell stack complicates the overall system design and requires additional space. Up to now early announcements for market introduction of fuel cell cars are overruled again and again. Nevertheless, the development of fuel cell cars is making serious progress. The PEMFC is

also used for propulsion as well as power generation in a number of special projects, usually with hydrogen as fuel. Application of the PEMFC appears to be attractive in particular at industrial plants where hydrogen is available as a by-product.

Since 2000, the interest for small to medium-scale power generation is increasing again. PEMFC and SOFC are primarily considered for this purpose but also MCFC is proposed as a candidate. The micro-CHP for the energy supply of single dwellings with electrical powers from 1 kW and higher is often seen as a serious option for the future. Units using conventional technologies like internal combustion engines and Stirling engines are commercially available already for several years. But their market share is very limited so far. Micro-CHP units based on fuel cells, primarily PEMFC but also SOFC, will enable significant higher electrical efficiencies. It is obvious that successful market penetration will require high electrical efficiencies, maintenance free operation during long periods, and low costs. These characteristics cannot be guaranteed today. SOFC and MCFC are supposed to be suitable too for small and large-scale CHP units. MCFC pilot plants have been build with powers up to 2 MW. A further decrease of costs is necessary, however, to make commercial application attractive.

In principle high efficiencies are achievable by applying high temperature fuel cells. The residual heat from these fuel cells can be released at high temperature and has consequently a high exergy value. The conversion of heat into power can be done in a more efficient way at higher power levels, depending on the conversion technology. Since the thermodynamic performance of fuel cells increases at higher operation pressures, the combination of fuel cells and gas turbines seems to be attractive. In particular the SOFC is potentially suitable for very efficient large scale power generation. The highest efficiencies are achievable already at power levels ( $< 30 \text{ MW}_e$ ) that are serious lower than usual with conventional power plants (see e.g. Section 6.5.4). The combination of high efficiency and relative small scale power plants makes the fuel cell a very attractive option for future power generation. It has to be noticed, however, that large scale power generation requires total operation times of more than 40,000 hours which is quite a challenge with the present state of the art.

A more comprehensive and detailed overview of the state of technology development and fuel cell applications can be achieved from literature (see e.g. [6.4], [6.5], [6.6] and [6.7]). In [6.4] primarily the technology status of the PEMFC and SOFC are presented but also applications of other types of fuel cells are discussed. A short overview of fuel applications is presented in [6.7]. The paper presents first of all the fundamentals of fuel cells but discusses also the system design. A general discussion of applications is given in [6.5] while vehicle applications are discussed in more detail in [6.6].

### **6.3 Thermodynamic losses of fuel cells**

#### **6.3.1 Introduction**

Hydrogen fuel cells will generate power as well as heat even in the case of a reversible process. The heat generated by a reversible fuel cell is often called reversible heat.

## Chapter 6 Fuel cell systems

Irreversibilities will reduce the generated power and in general increase the generated heat<sup>1</sup>. Heat is transferred from the fuel cell by the process flows or by a separate cooling system. Separate cooling systems are often used in low temperature fuel cells. In high temperature fuel cells the cells are usually cooled by the process flows. In general the desired in- and outlet temperatures are maintained by controlling the flow rate of the oxidizer. The way of heat transfer can have a serious effect on the overall performance of a fuel cell system.

In the next sections exergy losses of three fuel cell types are discussed based on the data of some arbitrarily chosen system studies. The considered design and the assumed performance data will of course affect the rate of the various exergy flows. It is obvious that these will differ from case to case. The examples are used here primarily to demonstrate the differences between the fuel cell types, without comprehensive discussion of all details.

A comprehensive description of the technology of the various fuel cells is presented in [6.1] and [6.3]. A general description of the thermodynamics of fuel cells is given in Appendix 6.1.

### 6.3.2 Polymer Electrolyte Membrane Fuel Cell (PEMFC)

Operating temperatures of the Polymer Electrolyte Membrane Fuel Cells are typically in the range of 60-80°C. The fuel entering the anode of the fuel cell consists of hydrogen diluted with various inert components depending on the fuel conversion process. Humidified air is normally used as oxidizer. The operating pressure is usually not higher than 2 to 5 atmosphere. PEMFC stacks have normally a separate cooling system with water or air as the cooling fluid. The reactants as well as the coolant flow enter the stack at a temperature somewhat higher than the temperature of the environment. An overview of the exergy flows to and from a PEMFC stack is shown in Figure 6.1 for a PEMFC, operating at atmospheric pressure and a temperature of 70°C, and fueled with gas from an auto-thermal reformer. The exergy flows are presented as percentages of the total exergy input. The exergy input of the stack does not consist of only the chemical exergy of the fuel but also the thermo-mechanical exergy of the ingoing fluids. Because of the low temperature this thermo-mechanical exergy is only 4.27%. In this case the fuel is a mixture of hydrogen and various inert gas components. Thus, not all hydrogen can be converted. The chemical exergy of the fuel that leaves the stack (20.76%) depends on the composition of the fuel and the fuel utilization of the stack. With a fuel utilization of 80% a relative high percentage of the fuel remains unconverted. The chemical exergy of the flows that leave the stack is 20.76%. The fuel is converted in the stack into electricity and heat. In this example it is assumed that the fluids at the inlet and the outlet of the stack have the same temperatures.

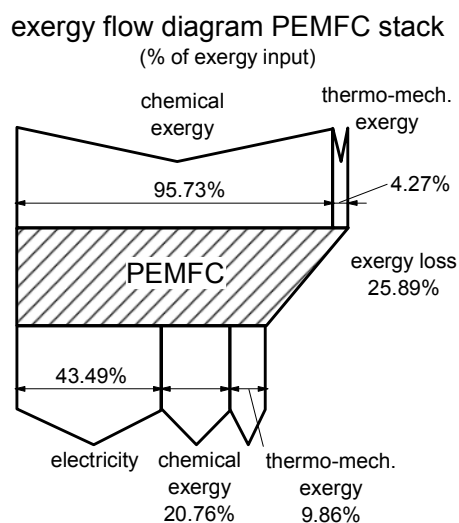


Figure 6.1 Exergy flow diagram of a PEMFC stack (fuel is gas from auto-thermal reforming)

<sup>1</sup> The irreversibility's of fuel cells are described in Appendix 6.1.

The generated heat is transferred to the cooling fluid. Because of the low operating temperature of the PEMFC, the thermo-mechanical exergy that leaves the stack is limited (9.86%)<sup>2</sup>. This is the main reason for the relatively high exergy loss (25.89%) of the PEMFC stack. If the temperature of the heat from the stack outlet flows is not high enough to use this heat for internal or external heating purposes, the thermo-mechanical heat from the stack has to be considered as an exergy loss too. The anode exhaust flow still contains combustible components that might be used within the fuel cell system. Usually the anode exhaust flow is used to deliver heat for the fuel reforming process.

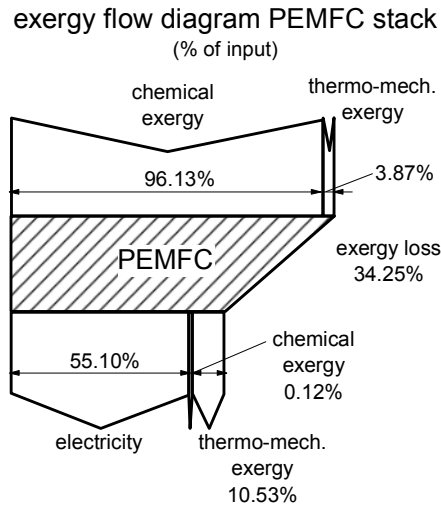


Figure 6.2 Exergy flow diagram of a PEMFC stack (fuel is hydrogen)

The generated power of a PEMFC will be higher if fuel of high quality used. In the case of pure hydrogen 100% utilization can be achieved in principle. The exergy flow diagram of a PEMFC stack using pure hydrogen and with 100% fuel utilization is shown in Figure 6.2. The generated electricity, 55.10% of the total exergy to the stack, is significantly higher than in the case of the fuel from auto-thermal reforming. But also the exergy loss (34.25%) is significantly higher. The thermo-mechanical exergy that leaves the system (10.53%) is only slightly higher. Because of the 100% fuel utilization the chemical exergy that leaves the system is almost zero. The reduced oxygen content of the cathode air causes the deviation from zero (0.12%).

In Appendix 6.1 it is demonstrated that the efficiency of a fuel cell primarily depends on the cell voltage. And the cell voltage appeared to be a function of the current density of the cell. High cell voltages are hindered by the relatively high activation losses in the case of low temperature fuel cells. In general high power densities and consequently high current densities are required to reduce the capital costs of fuel cell plants. The need for high current densities will limit the cell voltage in the case of real fuel cell systems. In the considered cases cell voltages of 0.73 V are arbitrarily assumed. If in the case of pure hydrogen the cell voltage can be increased to 0.80 V, 60.13% of the exergy that enters the stack is converted into electrical power. And the exergy loss of the PEMFC is 29.81%. It appears that even under these favorable conditions the exergy loss of a PEMFC is still considerable. This relatively high exergy loss is primarily caused by the low temperature of the generated heat and is unavoidable in the case of low temperature fuel cells. This also explains the interest for high temperature PEMFC systems.

The practical application of the PEMFC requires additional facilities for fuel preparation, heat discharge etc. These facilities will cause additional exergy losses depending on the fuel supplied to the system and the type of application. The additional exergy losses and possibilities for system optimization are discussed in Section 6.4.

<sup>2</sup> From the cooling system only the exergy increase of the cooling fluid is considered as an exergy flow that leaves the system.

## Chapter 6 Fuel cell systems

## 6.3.3 Molten Carbonate Fuel Cell (MCFC)

The exergy flow diagram as shown in Figure 6.3 is based on an MCFC system with external reforming. The hydrogen concentration of the fuel gas mixture is 52.85%. The cell operates around 650°C with a temperature of 600°C at the inlet and 700°C at the outlet. Because of the high temperature of the gases that enter the stack, the thermo-mechanical exergy at the system inlet is 44.83% of the total exergy input. The remainder (55.17%) is the chemical exergy of fuel and oxidizer. In the case of the MCFC the oxidizer must contain carbon dioxide that can be obtained from the anode exhaust. Therefore, the anode exhaust is combusted first and after heat transfer to the reforming process the combustion gas is mixed with preheated fresh air before it enters the cathode. Then, the oxygen concentration at the cathode inlet is relatively low. A further reduction of the oxygen concentration is caused by the application of cathode recycling necessary for the heat transfer from the stack. Finally the oxygen concentration at the cathode inlet is only 6.67%. The CO<sub>2</sub> concentration is 11.59%. Because of the difference with standard air, the chemical exergy of the gas flow to the cathode inlet is almost 10% of the total chemical exergy that enters the stack.

In spite of the rather high cell voltage (0.8503 V) the generated electricity is only 22.90% of the total exergy input of the cell. But this is more than 45% of the chemical exergy of the fuel that enters the stack. The limited power is also determined by the relatively low fuel utilization of 70%. The low fuel utilization on the other hand is also responsible for the high value of the chemical exergy (21.35%) that leaves the stack. The chemical exergy of the cathode exhaust flow is somewhat less than 15% of the total chemical exergy flow leaving the stack. Because of the high outlet temperature the thermo-mechanical exergy of the exhaust flows is 53.80%. The fuel cell is primarily cooled by the cathode flow. The mass of this flow is seriously higher than the anode mass flow. Therefore, the anode flow contains little more than 17% of the total thermo-mechanical exergy that leaves the stack.

The relative exergy loss of the fuel cell itself appears to be only 1.94%. This very low value is seriously flattered because of the high thermo-mechanical exergy that passes the stack without actually contributing to the process. The exergy efficiency of the fuel cell, calculated using the efficiency definition as presented in Section 2.15 of Appendix 3.2, is only 92.19%. But also this value shows that the exergy loss of the MCFC itself is very low, much lower than the exergy loss of the PEMFC. However, in comparison with the PEMFC, the MCFC will need additional facilities for preheating and cooling the gas flows to and from the stack. The various options for improved performance and alternatives for system designs are discussed in Section 6.4.

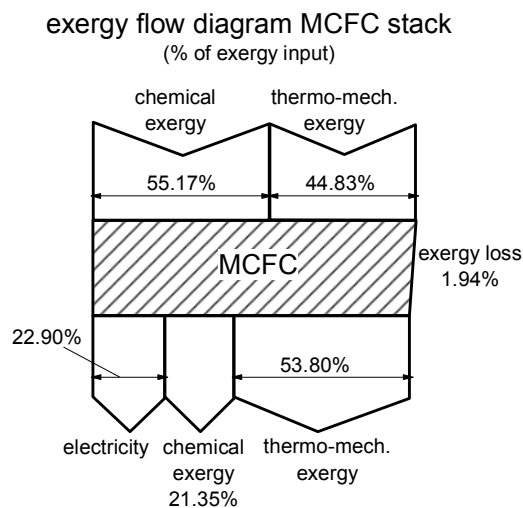


Figure 6.3 Exergy flow diagram of a MCFC stack

### 6.3.4 Solid Oxide Fuel Cell (SOFC)

It is assumed for the exergy flow diagram of a SOFC stack as presented in Figure 6.4 that the stack operates at a temperature around 850°C, with a temperature of 800°C at the stack inlet and 900°C at the outlet. The flow diagram is depicted for a stack operating at almost atmospheric pressure and external reforming. The hydrogen content of the fuel that enters the anode is around 50%. In comparison with the MCFC the higher operating temperature of the SOFC increases the thermo-mechanical exergy of the fluid flows to and from the stack. The preheated air entering the cathode has the composition of ambient air, thus, the chemical exergy of the cathode air is almost zero. The mass flow to the cathode is

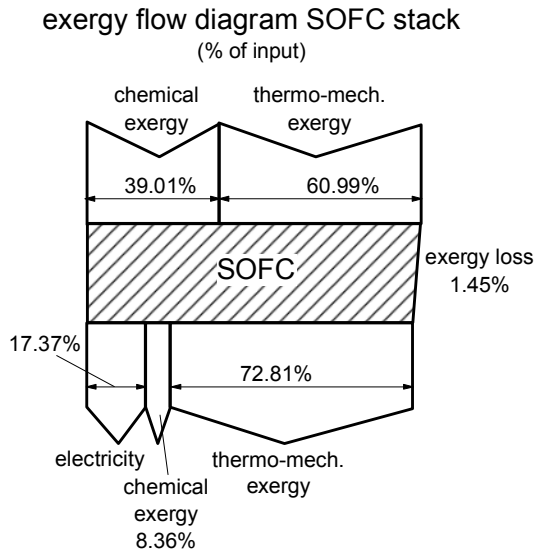


Figure 6.4 Exergy flow diagram of a SOFC stack

roughly 30 times the mass flow to the anode. The high mass flow rate is determined by the heat generated in the stack, since the stack is primarily cooled by the cathode flow. Thus, the thermo-mechanical exergy of the anode flows at the inlet as well as at the outlet is very small compared to the thermo-mechanical exergy of the cathode flow.

The cell voltage determines the electricity generated by the stack and is fixed at 0.70 V for the purpose of this evaluation. Then, the generated electricity is only 17.37% of the total exergy input of the stack. But this is still almost 45% of the chemical exergy of the fuel to the anode. The chemical exergy of the fluid flows leaving the stack is 8.36%. This number is determined by the fuel utilization that is

assumed to be 80%. The thermo-mechanical exergy leaving the stack is 72.81%. The thermo-mechanical exergy of the anode exhaust is lower than 10% of the total thermo-mechanical exergy that leaves the stack.

The exergy loss of the fuel cell stack is only 1.45%. But also this value is flattered by the high thermo-mechanical exergy that passes the stack without actually contributing to the process. The exergy efficiency of the fuel cell calculated by Cycle-Tempo according to the efficiency definition of Section 2.15 of Appendix 2.2 is 92.29%. This value is almost the same as the exergy efficiency of the MCFC stack. It appears that there are serious difference between the MCFC and SOFC with regard to their thermodynamic performance. But in how far the performance of a complete fuel cell system might benefit from the small losses of the fuel cell stack depends on the possibilities to limit the exergy losses during preheating of the fluid flows to the stack and to convert the exergy of the fluid flows from the stack into additional power.

## 6.4 Fuel conversion and purification

### 6.4.1 Introduction

Reforming processes are used to convert natural gas into hydrogen or a hydrogen rich gas. Large scale steam reforming systems are in use at petro-chemical sites for the generation of hydrogen for many years. For application in fuel cell systems highly different boundary conditions and power levels have to be considered. In particular in the case of small scale power applications like micro-CHP and passenger cars quite different designs for reformer, steam generation and the subsequent gas purification system are required because of the relatively high fuel prices, space limitations, and different possibilities for energy exchange with surrounding processes.

The development of fuel conversion and purification units is discussed in many papers during the last decades. Only a limited number is mentioned for the purpose of this study (see e.g. [6.8] to [6.18]). In [6.8] the results of a study are presented in which the feasibility of hydrogen production using alternative feedstocks, such as coke oven gas, refinery gas and biogas was evaluated. Natural gas based processes were used as a reference. The analysis of a large reformer plant at a refinery is presented in [6.9]. Energy and exergy efficiencies are calculated for the various subsections (steam reformer, shift reactor, steam generator, pressure-swing absorption (PSA), and waste heat boiler (WHB)) of the reformer plant. The calculated exergy efficiency of the steam reformer subsection is 78.23%. The description of the design and the determining process parameters, however, is far from complete. The exergy efficiency is defined as the ratio  $Ex_{out} / Ex_{in}$ , which is not really appropriate to indicate the quality of a process. But, at least it confirms that the exergy loss of the steam reformer is substantial. In [6.10] a comparison is made of three different reforming technologies: steam reforming (SR), partial oxidation (POX) and autothermal reforming (ATR). Natural gas, gasoline and diesel are considered as the hydrocarbon fuels. Natural gas appeared to be the best fuel for hydrogen production and SR and ATR are the most competitive fuel processing options. The highest fuel processing efficiency is achieved with steam reforming of natural gas. High PEMFC system efficiency levels can be achieved only with appropriate heat integration within the PEMFC system. The same reforming technologies (SR, POX and ATR) for the supply of hydrogen rich gas for PEMFCs are evaluated in [6.15]. The three processes are studied by varying relevant process parameters like reaction temperature and pressure, S/C ratio and O/C ratio. All simulations are done with a Gibbs reactor model using natural gas as the primary fuel. For a wide range of process conditions methane conversion, hydrogen yields, carbon monoxide yields and carbon yields are calculated. The methane steam reforming process appears to be the most favorable process with respect to high hydrogen yields and concentrations, high methane conversion and the relatively low CO concentration of the product gas.

Experimental results of autothermal reforming are reported in [6.11]. The considered ATR should provide the fuel for a 3 kW<sub>e</sub> fuel cell stack. Experiments with commercial diesel showed promising results but insufficient long-term stability. The so-called FLOX<sup>3</sup> steam

---

<sup>3</sup> FLOX stands for FLameless OXidation

reformer concept is roughly described in [6.12]. The concept is developed for PEMFC units with powers from 1 kW to 50 kW. It was concluded that the lead back of anode off-gas in the SR concept seems to be easier than heat recovery in ATR concepts. And efficient fuel processing appears to be important for the realization of acceptable PEMFC system efficiencies. Experimental results of a PEMFC with fuel processor are presented in [6.13]. The fuel processor comprises a pre-reformer step, a steam reformer, HT and LT shift reactors, a steam generator and a preferential oxidation step for CO removal. The thermal power of the generated hydrogen is between 0.5 kW and 2.5 kW. The fuel processor tests show a high product gas quality with less than 50 ppm CO in steady state operation. It was concluded that the PROX reactor limits the dynamic behavior of the complete system. A variety of improvements is under development. Results of lab scale experiments with a methanol steam reformer for application in passenger cars are reported in [6.16]. The experiments have shown that the reaction temperature sharply drops at the beginning of the catalyst bed. About 45% of the methanol is converted within the first 10 cm of the catalyst bed. Long-term measurements of more than 700 hours show severe ageing of catalytic activity. Higher amounts of catalyst might be able to maintain appropriate conversion rates during the required operation time. Cycled start-up and shut-down processes under nitrogen and hydrogen atmospheres do not harm the catalytic activity. The performance of a compact natural gas fuel processor for 1 kW residential PEMFCs is discussed in [6.17]. The fuel processor consists of a natural gas reformer, a water gas shift reactor, a heat exchanger and a burner, and produces hydrogen with a carbon monoxide concentration in the process gas below 7000 ppmv (dry gas base). The total volume of the integrated fuel processor is only 0.014 m<sup>3</sup>. Another small fuel processor is discussed in [6.18]. It is a fuel processor for 2 kW class residential PEMFCs. The packaged hardware system contains a steam reformer, HT and LT shift, steam generator and internal heat exchangers. A two stage PROX reactor reduces CO concentrations to less than 10 ppm. A first prototype of the fuel processor was connected to a PEMFC single cell to test the performance and reliability. During 3 days of operation no failure of fuel cell voltage has been shown.

Sulfur compounds occur naturally in hydrocarbon fuels and they are added also as odorants e.g. in natural gas. However, sulfur deactivates the catalyst materials of fuel processor and fuel cells. Removal of sulfur is necessary, preferably to concentrations below 200 ppbv. Catalytic-adsorption is attractive because of the lower maintenance costs and size. Usually hydro-desulfurization (HDS) is proposed for sulfur removal from the fuel. Hydrogen added to the fuel reacts with the sulfur compounds to form H<sub>2</sub>S using a HDS catalyst followed by H<sub>2</sub>S adsorption on zinc oxide at a temperature of 300-400°C. In [6.14] a new developed catalytic-adsorption fuel desulfurization technology is presented that is effective and environmental friendly. It selectively oxidizes sulfur compounds; the SO<sub>x</sub> species are adsorbed by an inexpensive high capacity particulate absorbent. In the case of natural gas the sulfur slip is below 10 ppbv.

It appears that primarily steam reforming (SR) and autothermal reforming (ATR) are seen as serious candidates for application in small scale fuel cell systems. For residential application steam reforming is in general preferred. Developers of fuel processors usually claim high efficiencies. However, the presented efficiency values are useless for comparison because different efficiency definitions are used based on concentrations or enthalpy changes.

## Chapter 6 Fuel cell systems

Furthermore, in- and outlet conditions are often not mentioned. Therefore, various aspects with regard to the thermodynamic design of external reformers are evaluated in the following sections. The main purpose of these evaluations is to determine appropriate process conditions for the fuel cell system calculations as presented in Section 6.5. For these evaluations natural gas is supposed to be the primary fuel.

#### 6.4.2 Conversion and purification processes

Several conversion and purification processes are necessary for the generation of hydrogen from natural gas. In the case of low temperature fuel cells almost pure hydrogen is required to avoid poisoning of the catalyst material. The higher the cell temperature the lower the sensitivity for impurities. The processes necessary in the case of PEMFC systems are mentioned in Table 6.2 together with a range of operation temperatures mentioned in literature.

	process	operation temperature [°C]
sulfur removal	hydro-desulfurization	300-400
fuel conversion	reforming (SR/ATR)	700-850/700-900
CO conversion	HT shift	300-430
	LT shift	200-250
CO removal	preferential oxidation	80-160

The removal of sulfur compounds is necessary in the case of LT fuel cells as well as HT fuel cells. Since sulfur compounds will also affect the reformer catalyst, sulfur has to be removed first before the fuel enters the reformer. Usually hydro-desulfurization (HDS) is proposed for this purpose. By adding some hydrogen to the fuel sulfur from the sulfur compounds is converted by the HDS catalyst into H<sub>2</sub>S which can be adsorbed in a zinc oxide bed at a temperature of 300-400°C according to:



A slip stream of the reformer outlet can be used to provide the hydrogen required for this process.

The desulfurization process is followed by reforming of the fuel. In the case of steam reforming, methane and higher hydro-carbon compounds are converted by adding steam. The methane reacts according:



The reaction is endothermic, thus, heat supply from an external source is required. Per mole of methane at least 1 mole of water is required for this conversion. In real systems more water is added to avoid the formation of solid carbon. Carbon formation might result from one of the following reactions:



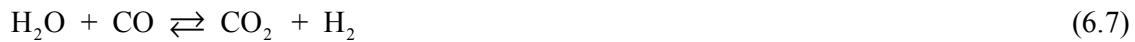
All these reaction are exothermic. At the reaction temperatures mentioned in Table 6.2 close approximation of the chemical equilibrium can be achieved by applying appropriate catalysts.

In the autothermal reformer fuel is converted by using basically the reforming reaction (6.2) and the partial oxidation reaction:



The partial oxidation reaction is exothermic and must supply the heat for the reforming process. The ATR does not require external heat supply but at the temperatures mentioned in Table 6.2 the reaction requires an appropriate catalyst. A disadvantage of the ATR process is that it generates only 2 moles of hydrogen per mole of methane. A mixture of hydrogen and carbon monoxide leaves the reformer. The mixture can be supplied to a high temperature fuel cell without further processing. In the case of a PEMFC further processing of the product gas is necessary to reduce the CO content to ppm level.

A two stage shift reactor, a HT shift followed by a LT shift is generally proposed to convert most of the CO. For this conversion the exothermic water-gas-shift reaction is used:



The two shift reactors make use of different catalyst materials. The gas that enters the shift reactor should contain sufficient water vapor to convert all CO. That means that overall, for reforming and CO conversion, a S/C ratio of 2 is required. Most of the CO is converted in the HT shift, resulting in a substantial increase of the gas temperature. After the LT shift the CO concentration will be 0.5-1.0%.

Several processes are mentioned in literature for the further reduction of the CO content like selective or preferential oxidation (PROX), methanation, selective membranes and pressure swing absorption (PSA). Preferential oxidation is most frequently proposed and should be able to bring down the CO concentration to about 5 ppm. Preferential oxidation requires the addition of some oxygen or air to convert CO into CO<sub>2</sub> using an appropriate catalyst. After the PROX the product gas is suitable for conversion in a LT PEMFC.

#### 6.4.3 Evaluation of reforming processes

An evaluation of the main process parameters for SR and ATR processes is the purpose of this section. First two reference cases are presented and starting from these reference cases the effect of some process parameters is demonstrated with special attention for the thermodynamic losses. The parameters selected for the reference cases are given in Table 6.3. The selected values are based on the literature discussed before. In general the reaction pressure will depend on the fuel cell pressure to avoid throttling or compression of the fuel gas between reformer and fuel cell stack. Actual pressures can differ seriously from atmospheric pressure.

Since the program Cycle-Tempo does not have a special model for an ATR, the gasifier model is applied for the process calculations. This model has separate inlets for fuel, air and steam and calculates the

	units	SR	ATR
inlet temperature	[°C]	300	300
reaction temperature	[°C]	830	850
outlet temperature	[°C]	450	850
reaction pressure	[bar]	1.01325	1.01325
S/C ratio	[-]	3.0	1.8

equilibrium composition at a defined reaction temperature. In this case the outlet temperature and reaction temperature are supposed to be equal. The steam to fuel mass ratio is fixed at

## Chapter 6 Fuel cell systems

1.5687 corresponding with a S/C ratio of 1.8 in the case of Slochteren natural gas (see Appendix 6.2). The inlet air flow is calculated by the program based on the specified outlet temperature. The temperature and pressure of all inlet flows are supposed to be equal. The results of the ATR process calculation are summarized in the exergy flow diagram of Figure 6.5. The diagram shows the exergy flows to and from the reformer and distinguishes between chemical exergy and thermo-mechanical exergy. It appears that 95.79% of the total exergy that enters the ATR is chemical exergy. This is just the chemical exergy of the fuel. The thermo-mechanical exergy at the ATR inlet is only 4.22%. This value is low, not only because of the inlet temperature of 300°C but primarily because of relatively small mass flows of the reactants. The exergy loss of the reformer is 13.28%. This relatively high exergy loss is caused by the partial combustion of the fuel. The product gas leaves the ATR at a temperature of 850°C. This temperature causes the relatively high value of the thermo-mechanical exergy (14.14%). Overall the ATR process results in a reduction of the chemical exergy and an increase of the thermo-mechanical exergy.

exergy flow diagram autothermal reformer  
(% of input)

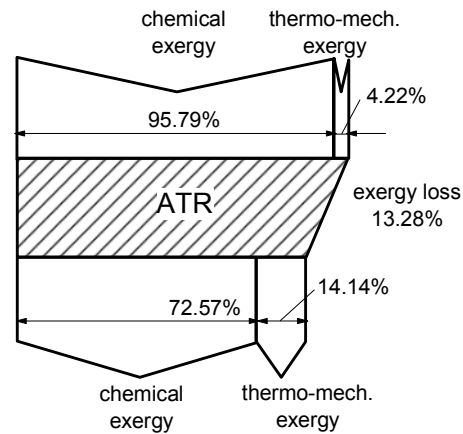


Figure 6.5 Exergy flow diagram autothermal reformer

The steam reformer model of Cycle-Tempo is applied for the process calculations of the SR. This model assures that the required heat for the reforming process is extracted from a flue gas flow. But the model does not include a check of the distance between the temperature curves of the two mass flows. In case of doubt an additional check is necessary to assure appropriate heat exchange. Fuel and steam at the inlet of the reformer have the same

exergy flow diagram steam reformer  
(% of input)

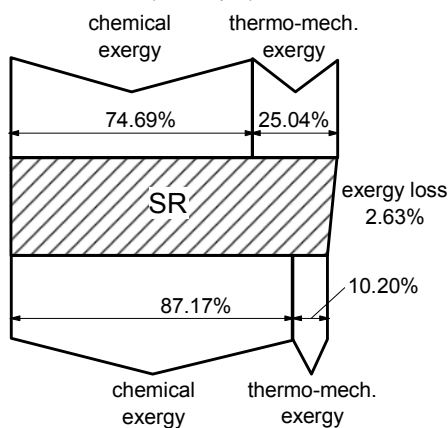


Figure 6.6 Exergy flow diagram steam reformer

temperature (300°C). The inlet temperature of the flue gas is 1000°C and the flue gas leaves the reformer at the same temperature as the product gas (450°C). The results of the SR process calculation are summarized in Figure 6.6. The thermo-mechanical exergy at reformer inlet is significant higher (25.04%) than in the case of the ATR because of the high temperature and high mass rate of the flue gas flow. The exergy loss is only 2.63% which is serious lower than in the ATR case. The chemical exergy leaving the SR appears to be 87.17% of the total exergy that enters the reformer. The thermo-mechanical exergy leaving the system is only 10.20%. Thus, in the case of steam reforming the chemical exergy increases and the thermo-mechanical exergy is reduced. Of course the

exergy loss of the SR depends on the inlet and outlet temperatures of the process fluids and the flue gas as well as the steam to carbon ratio. A decrease of the temperature of the reactants will increase the exergy loss with almost 15%.

Additional calculations are made to check the selected process parameters for the steam reformer presented in Table 6.3. In Figure 6.7 the equilibrium concentrations are shown as a function of the reaction temperature for the specified fuel, S/C ratio, and operation pressure. The diagram shows that almost full conversion of hydrocarbons is achieved at temperatures somewhat higher than 700°C. At higher temperatures the hydrogen and carbon dioxide concentrations slightly decrease while

concentrations of carbon monoxide and water vapor increase. With the available reformer catalysts chemical equilibrium is almost achievable. Thus, the selected equilibrium temperature (830°C) is quite high for atmospheric operation. However, in the case of higher pressures higher reaction temperatures are necessary to achieve complete conversion of hydrocarbons as is obvious from Figure 6.8. An equilibrium temperature of 830°C seems to be a good choice if the reaction pressure is around 6 bar. The temperature curve of the process gas is depicted in Figure 6.9. If the process heat is taken from flue gas that is cooled down from 1000°C to 430°C the temperature difference is supposed to be sufficient for proper heat transfer. The accompanying value diagram is shown in Figure 6.10. The diagram clearly shows that the exergy loss due to heat transfer is small. In integrated steam reformers (see e.g. Section 4.4.4) heat is recovered from the process gas. Then, the process gas that leaves the reforming reactor is internally cooled down to a temperature that almost equals the flue gas temperature. This

	units	SR	ATR
inlet temperature	[°C]	300	300
reaction temperature	[°C]	830	850
outlet temperature	[°C]	450	850
reaction pressure	[bar]	1.01325	1.01325
S/C ratio	[-]	3.0	1.8

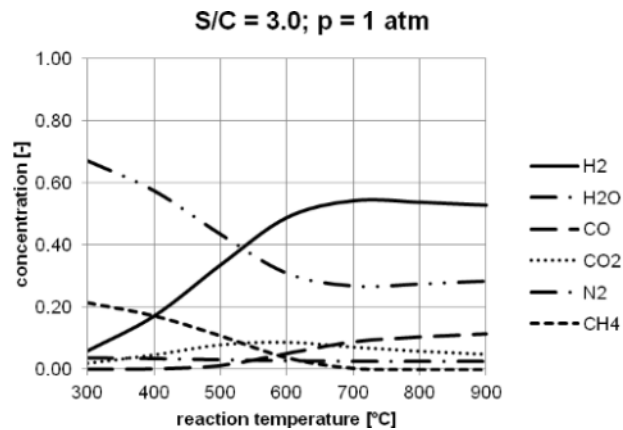


Figure 6.7 Equilibrium composition of SR as a function of the reaction temperature  
S/C = 3.0; p = 1 atm

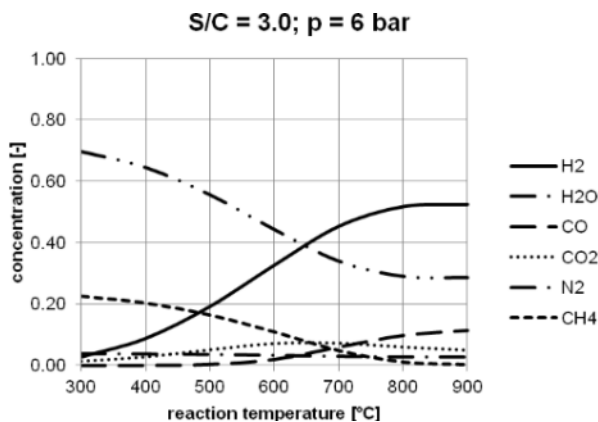


Figure 6.8 Equilibrium composition of SR as a function of the reaction temperature  
S/C = 3.0; p = 6 bar

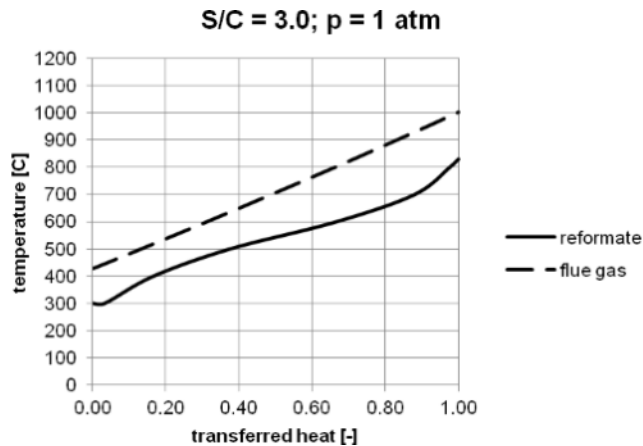


Figure 6.9  $T,Q$ -diagram of the steam reformer (without heat recovery)

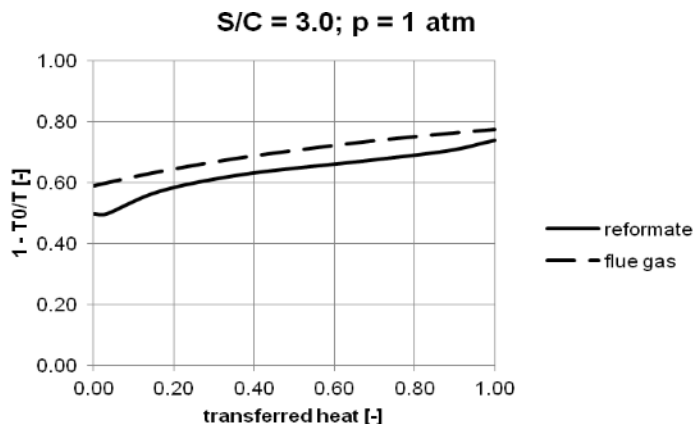


Figure 6.10 Value diagram of the steam reformer

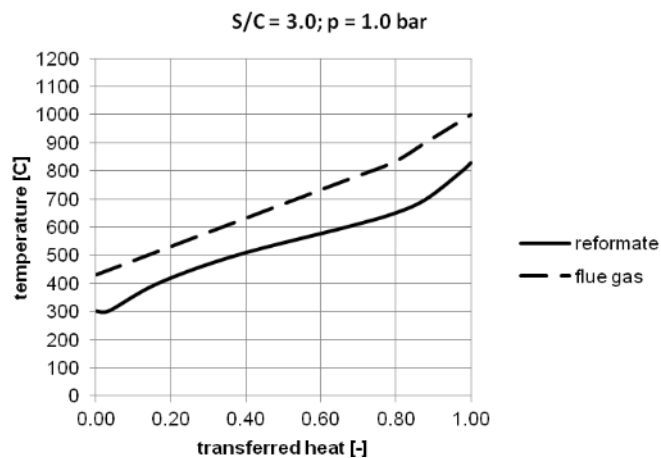


Figure 6.11  $T,Q$ -diagram of the steam reformer (with heat recovery)

reduces the heat demand of the reformer with about 20 to 30%, depending on the process conditions. The heat recovery affects the flue gas curve. The modified flue gas curve, assuming the same inlet and outlet temperatures of the flue gas, is shown in Figure 6.11. It demonstrates that the chosen flue gas temperatures are able to assure suitable heat transfer in the case of a reformer with heat recovery.

A comparison of some parameters of the two reformer cases is presented in Table 6.4. The exergy losses are shown not only as a percentage of the total exergy input but also as a percentage of the fuel exergy. The percentages are obviously different in the case of SR, but for the comparison between the two cases this appears not to be important. The product gas compositions obviously show high differences. The hydrogen concentration of the SR product gas is almost two times the concentration for the ATR case. Also the CO concentration is higher. Consequently the heating values of the SR product gas are significant higher than the heating values of the ATR product gas. This evaluation is not really a true comparison of the thermodynamic performance of the two reforming technologies. In

general the SR will require a combustor to generate the hot flue gas required to supply heat. This might raise the exergy loss seriously. High temperature gases leave the ATR. If a suitable heat demand is not available, most of the thermo-mechanical exergy of this gas will be lost. Thus, a true comparison of the technologies might be possible only in the case of complete system designs. In literature the performance of SR is often seen as superior over ATR (see e.g. [6.10], [6.12] and [6.15]). Nevertheless, because of costs and system complexity autothermal reforming might be preferred in particular for mobile applications.

	units	SR	ATR
exergy loss (% of exergy input)	[-]	2.63	13.28
exergy loss (% of fuel exergy)	[-]	3.58	13.87
product gas composition			
CH <sub>4</sub>	[-]	0.0002	0.0000
N <sub>2</sub>	[-]	0.0261	0.3616
CO <sub>2</sub>	[-]	0.0554	0.0602
H <sub>2</sub> O	[-]	0.2766	0.2364
H <sub>2</sub>	[-]	0.5330	0.2646
CO	[-]	0.1087	0.0731
$M_{\text{product gas}}$	kg/kmol	12.27	19.78
<i>LHV</i> product gas	MJ/kg	13.02	4.28
<i>HHV</i> product gas	MJ/kg	14.93	4.87

## 6.5 The design of Fuel Cell Systems

### 6.5.1 Introduction

Fuel cell systems are proposed for a variety of applications and for operation on different fuels. Today commercial application of fuel cell systems is very limited and discussions on suitable applications of the different fuel cell types are going on. As shown before, the exergy loss of a fuel cell stack, in particular of high temperature fuel cell stacks, is low and might enable high overall system efficiencies. However, experience with a variety of system designs has shown that system efficiencies are highly depending on the system design. High efficiencies are achieved only with proper overall system designs. In this section various system designs are discussed to show how efficiencies are affected by the system design and how power plants with thermal efficiencies around 80% are achievable. Primarily more general applications of PEMFC, MCFC and SOFC are considered.

The PEMFC is usually seen as the preferred fuel cell type for mobile applications and micro-CHP. In principle hydrogen is the most convenient fuel for mobile applications. But the lack of existing hydrogen distribution systems and on board fuel storage for current usual drive ranges causes serious problems. On board storage of the required quantities within an acceptable volume is conceivable with hydrogen under high pressure (up to 700 bar), liquid hydrogen or hydrogen stored in chemical or metal hydrides. But the volumetric power density is still lower than in the case of gasoline and diesel oil. Because of the problems associated with the use of hydrogen other developers of fuel cell cars prefer the use of more conventional fuels like gasoline, sulfur free diesel or methanol which requires on board fuel conversion. The kind of fuel might significantly affect the overall system design. In the case of micro-

## Chapter 6 Fuel cell systems

CHP natural gas is generally seen as the available fuel. The fuel conversion is supposed to be integrated in the overall system design. In this section primarily literature results are discussed.

MCFC systems are primarily proposed for CHP systems with power levels from roughly 100 kW and higher. Because of the high temperature at which heat is generated by the fuel cells, heat can be delivered as steam for industrial use as well as hot water for district heating. Natural gas is usually available as the fuel for these systems. A variety of system studies made by the Energy Systems group at the TU Delft are summarized and discussed in this section. The purpose of these studies was first of all to answer a number of basic design questions like: what are attractive stack operation pressures and temperatures, what are the effects of the temperature rise of the process flows through the stack, what is the significance of internal reforming, is recycling of anode and cathode gas useful.

The SOFC appears to be a candidate for a variety of applications. Applications for small scale power generation and CHP like auxiliary power units for passenger cars as well as for micro-CHP are under development. But the SOFCs are supposed to be suitable also for small to large scale CHP as well as pure power generation. Because of the good internal reforming capability of the SOFC, the SOFC can be used too for cogeneration of electricity and hydrogen (see e.g. [6.52]). Only a limited part of the generated hydrogen should be converted into electricity in that case. In [6.50] this application is proposed in combination with PEMFC systems. With respect to applications, available fuel and questions with regard to overall system design, SOFC systems appear to be highly similar to MCFC systems. System studies made by the Energy Systems group are summarized and discussed. Finally a target system is specified to show the characteristics of a system that is able to achieve a thermal efficiency of 80%.

### 6.5.2 PEMFC systems

#### Mobile application (hydrogen fuelled)

For mobile applications hydrogen as well as hydrocarbon fuelled systems have been developed for application in passenger cars (e.g. [6.4], [6.6] and [6.20]). The majority of these fuel cell cars run on hydrogen. But Daimler also developed a methanol fuelled vehicle. It seems that car manufacturers primarily focus on hydrogen fuelled vehicles for the future (see e.g. [6.23]). Apparently they have solved the problems with regard to the water management of PEMFCs. Initially, humidification of air and fuel was necessary to keep the water content of the membrane at the required level. Such facilities, however, are hindering operation at temperatures below 0°C. Today, fuel cell systems for cars are equipped with a balance-of-plant without humidification devices. Then operation at pressures slightly higher than atmospheric pressure (1.5-2.7 bar) is required [6.21]. In that case the system efficiency is determined almost entirely by the performance of the fuel cell stack. The auxiliary power necessary for the air blower, however, is significant and might require more than 10% of the generated electrical power of the stack depending on the stack operating conditions and the efficiencies of blower and electric motor.

Mobile applications require fuel cell stacks with high power densities and consequently high current densities. This hinders the realization of high efficiencies since the cell voltage

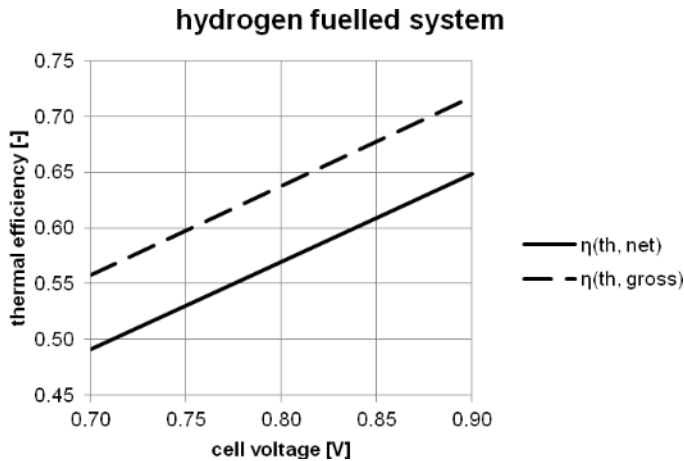


Figure 6.12 Thermal efficiencies of  $H_2$  fuelled system as function of cell voltage

decreases with increasing current density. The efficiency at design power is, however, of limited importance because power systems of passenger cars will operate most of the time at part load. Fuel cell systems have the advantage that at part load the cell voltage increases which is beneficial for the efficiency. A true comparison with conventional systems requires complex well-to-wheel evaluations that include also the losses of the hydrogen production. In [6.22]

it is mentioned that fuel savings of 35-45% are achievable because of the superior efficiency fuel cells.

Fuel cells are actually at the start of their development and further improvements are expected for the future. At present actual cell voltages at design load are roughly around 0.7 V. To give an idea of possible improvements in the future the results of system calculations for a simple system are presented in Figure 6.12. The system consists of a hydrogen fuelled PEMFC stack with air blower. The stack is supposed to operate at a pressure of 2 bar and an oxygen utilization of 50%. Net and gross thermal efficiencies are depicted as a function of the cell voltage. At a cell voltage of 0.7 V the net efficiency is almost 50%, but seriously higher efficiencies are achievable if higher cell voltages can be realized.

#### Micro-CHP (natural gas fuelled)

The interest for various types of micro-CHP units is increasing because of their potential to reduce  $CO_2$  emissions. Units with internal combustion engines and Stirling engines are commercially available today. However, the application hampers because of the limited electrical efficiencies and the high capital costs. Fuel cells have the potential to build micro-CHP units with serious higher electrical efficiencies. The effects of higher electrical efficiency on fuel savings and consequently  $CO_2$  emissions are more comprehensively discussed in Chapter 7. For the development of micro-CHP units the PEMFC was considered to be attractive because of the low operation temperature and the high power densities. Most of the companies that have developed a micro-CHP fuel cell unit have chosen for the PEMFC. To discuss the strengths and weaknesses of PEMFC micro-CHP units fuelled with natural gas, a system model with Cycle-Tempo developed for an external partner is presented first.

The system flow diagram of the micro-CHP unit with a PEMFC stack and autothermal reformer is depicted in Figure 6.13. Usually steam reforming is used for micro-CHP units but

the various aspects of the system design can be demonstrated quite well with this system.

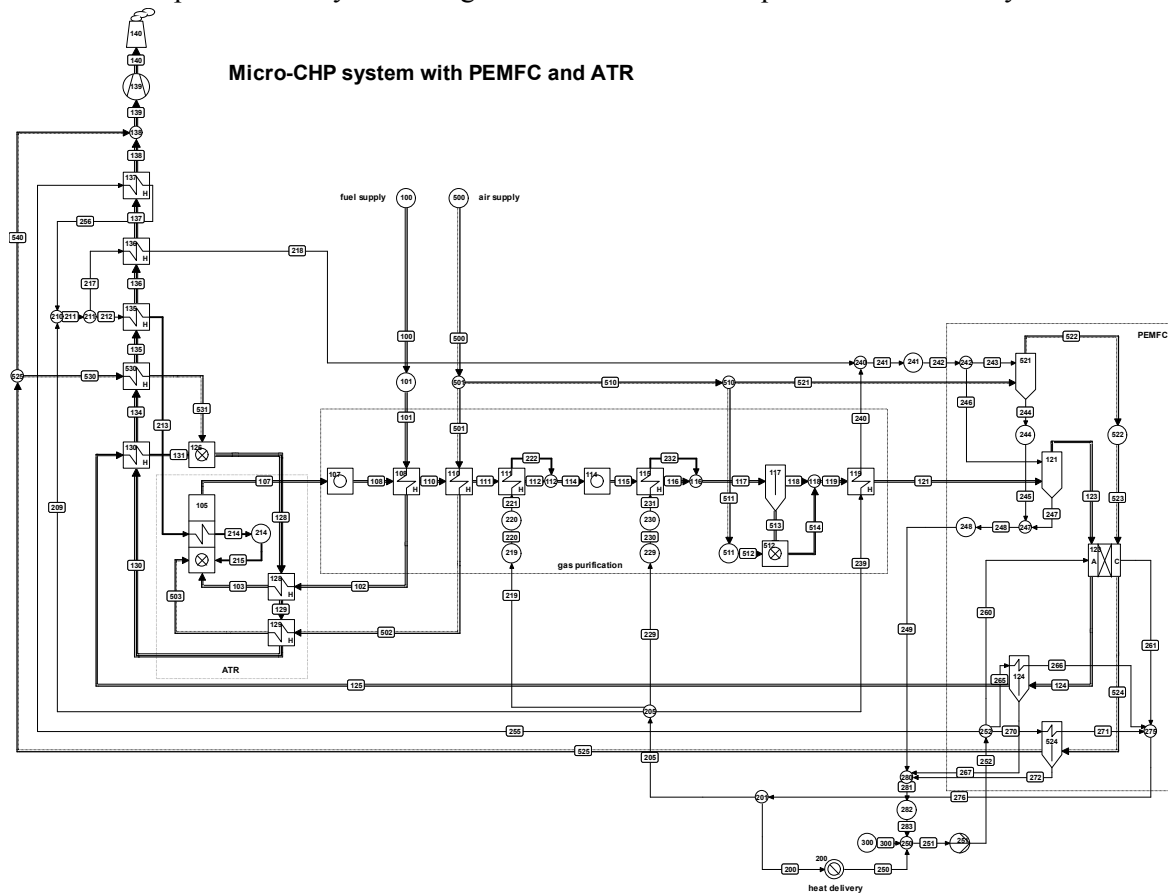


Figure 6.13 Micro-CHP plant with PEMFC and ATR

Natural gas is preheated and supplied to the ATR<sup>4</sup> together with steam and air. Desulphurization was omitted; the effect on the thermodynamic performance, however, is very limited. In the ATR the gas mixture reacts and leaves the reactor at an equilibrium temperature of 900°C. The product gas is cooled down at 400°C by process steam before it enters the HT shift. The product gas is cooled further and supplied to the LT shift at 200°C. The available heat is used to preheat natural gas and air; the remainder is used to evaporate water that is supplied to the product gas before it enters the LT shift. A preferential oxidation reactor is supposed for the final reduction of the CO concentration. Fuel gas and air are humidified before entering the water cooled PEMFC stack. The stack operates at 70°C and almost atmospheric pressure. A fuel utilization of 0.8 is assumed and the air utilization is supposed to be 0.5. The cell voltage is assumed to be 0.7326V. Fuel and air flows leaving the stack are dehydrated before they are supplied to an afterburner. The hot flue gas from this burner is used first to preheat fuel and air and to generate steam for autothermal reforming. The remaining heat is used for the generation of hot water. Heat delivery occurs at low

<sup>4</sup> Cycle-Tempo is not provided with an ATR model. But the gasifier model is used for this purpose. It is able to calculate the equilibrium composition based on specified reaction conditions and a specified ratio of the reactants and it assures the energy balance.

temperatures (65°C to 40°C). The results of the system calculation are summarized in the exergy flow diagram presented in Figure 6.14. The system is divided in four subsystems: the ATR, gas purification, PEMFC and waste heat utilization. The apparatuses that belong to the ATR, gas purification and PEMFC are indicated by rectangles with dotted lines in the system flow diagram (Figure 6.13) all other apparatuses are supposed to belong to the waste heat utilization subsystem. The net electrical efficiency is 37.31% and the heat efficiency is 5.81% based on exergy values. This corresponds with thermal efficiencies of 38.67% for electricity and 52.45% for heat. The electrical efficiency is quite high because of the relatively high cell voltage assumed for this case. In the literature mentioned below the presented values for steam reforming cases are significant lower. The low exergy value of the heat is caused by the low temperature. Higher temperatures of heat delivery will reduce the total recoverable heat power and will increase also the flue gas stack loss. The exergy loss of ATR and gas purification together is 16.95% of the exergy input and the exergy loss of the PEMFC including humidification and dehydration of the air and fuel flows is 24.97%. Perhaps, some of the assumptions made for this system calculation can be questioned. But the results give a clear insight in the thermodynamic losses of such a system. After all, it shows that operation of a PEMFC on natural gas requires a complex system design. This also hinders the economy of PEMFC-CHP systems.

The performance of micro-CHP PEMFC systems is discussed in various publications describing the results of modeling activities (e.g. [6.25], [6.26], [6.31]), laboratory experiments (e.g. [6.27], [6.30]) and field tests (e.g. [6.32], [6.33], [6.34]). A comprehensive description of a system developed by Viessmann (Germany) is presented in [6.35]. With exception of [6.30] all systems are fuelled with natural gas. For the conversion into hydrogen usually a steam reformer is applied. Presented electrical efficiencies are in between 0.28 and 0.38 (thermal). The cell voltages are usually around 0.6 V. The measured electrical performances (gross electrical efficiencies < 0.30) during a French field test with 5 units installed at different places (see [6.31] to [6.34]) are seen as disappointing. But analysis of the experimental data and additional numerical simulations do suggest various improvements.

Micro-CHP PEMFC units have been developed so far by several European manufacturers (Vaillant, Baxi Innotech, Viessmann) as well as Japanese manufacturers (Panasonic, Toyota, Toshiba, Eneos, Ebara Ballard). An overview of these units is given by [6.36]. The models of the Japanese manufacturers are commercially launched under the joint brand name “ENE FARM” and have an electrical output of 1 kW<sub>e</sub>. Only the Eneos unit has an electrical output of 0.75 kW<sub>e</sub>. From 2002 to 2008 more than three thousand units were built and installed in Japanese homes. Because of the high unit costs the Japanese products have

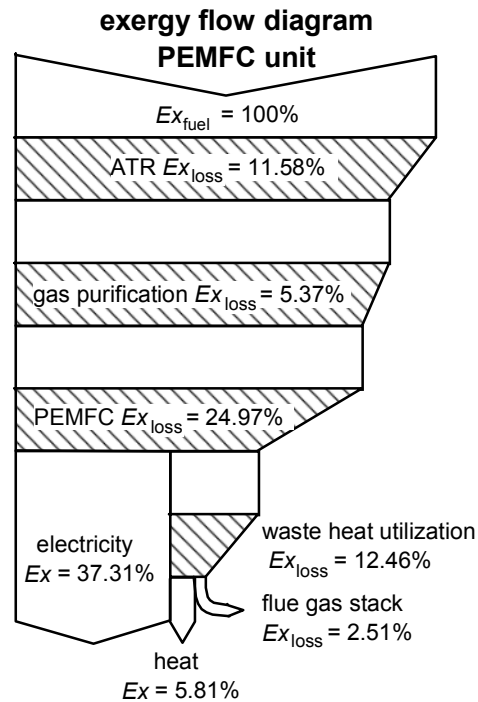


*Figure 6.14 Exergy flow diagram  
Micro-CHP plant with PEMFC  
and ATR*

been seriously subsidized by the Japanese government (see [6.28]). The average unsubsidized price of a 0.7 to 1.0 kW system is € 23,000.- (early 2009). Based on empirical experience curves it is predicted that economical viability might be met by 2025. In [6.28] it is mentioned too that manufacturing cost is distributed among all major system components. A technology breakthrough is actually required that can greatly simplify the overall system design. The European systems have just been installed as technology trials. No serious attempts are undertaken to bring these units to the market. The design of Viessmann as described in [6.35] included already several simplifications of the system. In the last prototype a low temperature reforming process with reduced CO concentration was used in combination with a single shift reactor and selective methanization for the final removal of CO. The humidifier of cathode air was omitted.

The study in [6.28] concludes that the PEMFC micro-CHP units cannot be considered as commercially available. New developments like the development of high temperature PEMFC membranes and more tolerant low- or non-platinum catalysts might cause a step-wise cost reduction and accelerate the introduction of micro-CHP fuel cell systems. Investigations on HT PEMFC are described e.g. in [6.25], [6.26], [6.27], [6.29] and [6.37] to [6.39]. Operation at temperatures higher than 120°C requires replacement of the usual Nafion membranes. In [6.37] various options for new proton conducting hybrid membranes are characterized and discussed. Also in [6.29] various solutions are mentioned and the results of tests with PBI (polybenzimidazole doped with phosphoric acid) are presented which is seen as the most successful membrane system so far. A broad review of the field of HT-PEMFCs from the perspective of materials requirements and characterization is presented in [6.39]. It was concluded in general that the area of HT-PEMFC is relatively immature and requires significant research and discovery. The higher operation temperature (considered values: 160°C - 200°C) will enhance the electrochemical kinetics of both electrodes, increase the CO tolerance and improve possibilities for heat utilization. In [6.25] and [6.26] a CO level of 0.1%-0.2% is supposed to be acceptable. With regard to the thermodynamic performance the two papers are not really consistent. For the same system design [6.25] gives thermal efficiency values of 0.8308 and 0.2762 for combined heat and power and respectively electricity. And [6.26] gives for the same parameters 0.952 and 0.388. In [6.38] savings of 9.6% are expected in the case of a system with methane reforming. But anyhow, it is uncertain whether the HT-PEMFC might solve the problems around the introduction of PEMFC micro-CHP units as mentioned before.

PEMFC systems for micro-CHP applications as well as mobile applications show enhanced thermodynamic performance in comparison with their conventional competitors. But the fuel savings resulting from higher efficiencies will not easily compensate the higher system cost. Higher capital cost make that the economic viability is still uncertain. High power densities and simplified overall system design are necessary to facilitate market introduction. Also the long term behavior of fuel cells is a point of care.

### 6.5.3 MCFC systems

The development of the Molten Carbonate Fuel Cell (MCFC) focuses primarily on small and intermediate scale CHP systems [6.40], [6.41], with electrical power levels from

roughly 100 kW to 10 MW. Also higher powers are considered. A more recent review of the status of MCFC systems development and application is presented in [6.49]. A short overview of Korean MCFC plants is shown in [6.48]. The high temperature of the residual heat from a MCFC stack enables the generation of steam and thus application for industrial CHP plants. The market of industrial CHP plants is diverse and it is expected to be a durable market. For the long term a further integration of the production of electricity and industrial products might provide new challenges for HT fuel cell systems.

#### Exploring system studies

In the 1980s system studies have been carried out to investigate the effect of various system designs on system performance. Some of the results of a system study by TU Delft, TNO and KEMA are summarized here to show the effect on system performance of internal reforming, increased cell pressure and anode gas recirculation. A more comprehensive presentation of the results was presented in [6.42]. Five alternative systems were examined: 3 at atmospheric pressure and 2 at a pressure of 10 bar. A power level of 5 MW<sub>e</sub> was considered for the atmospheric systems and a power level of 25 MW<sub>e</sub> for the pressurized systems. External reforming as well as internal reforming has been considered for the two pressure levels (see Table 6.5). System 5 is a modified version of system 1. In the case of system 5

system no.	characteristics	aux. power	$\eta_{th, electr}$	$\eta_{th, total}$
		[% of gross power]	[-]	[-]
1	IR, a	8.23	0.555	0.786
2	ER, a	17.10	0.381	0.716
3	IR, p	3.15	0.667	0.929
4	ER, p	8.72	0.541	0.957
5	IR, a, agr	7.54	0.559	0.912

ER = external reforming  
 IR = internal reforming  
 a = atmospheric pressure  
 p = elevated pressure (10 bar)  
 agr = anode gas recirculation

water vapor needed for the reforming process is supplied by recycling a part of the anode exhaust flow. The system flow diagram of system 5 is shown in Figure 6.15 as an example. All systems are supposed to operate on design power and to deliver heat to a district heating (DH) system. The supply temperature of the DH system is supposed to be 95°C and the return temperature 50°C. The fuel for all system alternatives is natural gas (Slochteren quality). The fuel utilization of the fuel cell stack is 80% in the case of external reforming and 90% for the internal reforming cases. The internal reforming systems are supposed to make use of direct internal reforming. Air and fuel gas enters the stack at a temperature of 600°C and are heated up to 650°C. The systems generate electricity to the grid. This implies a DC/AC conversion for all systems. Fuel cell performance data were derived from literature information. A cell voltage of 0.73 V at a current density of 160 mA/cm<sup>2</sup> was supposed to be a realistic value for system 1. Cell voltages for all other cases are based on this value but corrected for differences in fuel and oxidant concentrations and utilization. Preheated air is used to supply the cathode

with oxygen. For the supply of CO<sub>2</sub> cathode air is mixed with the anode outlet flow after catalytic combustion of the residual fuel from the anode outlet. Cathode recirculation is applied to assure the heat discharge from the fuel cell stack. The thermodynamic system

**atmospheric MCFC-CHP with IR and anode recirculation**

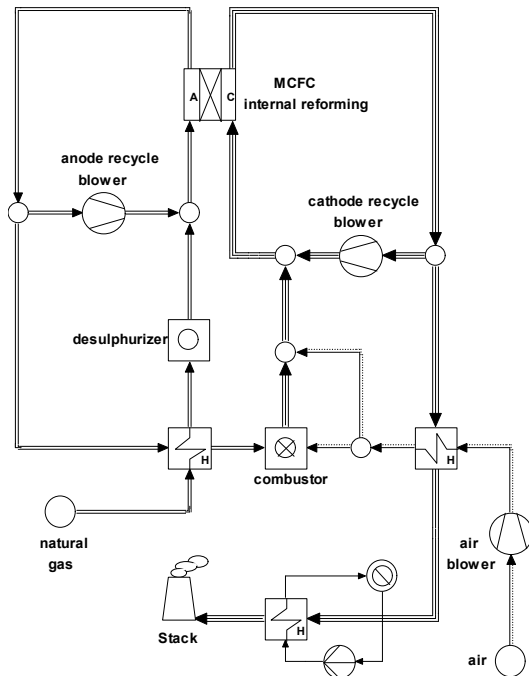


*Figure 6.15 System flow diagram of atmospheric MCFC-CHP plant with internal reforming and anode recirculation (system 5)*

calculations were carried out with Cycle-Tempo. At that time the present fuel cell model in the program was not available; the actual fuel cell calculations were made by hand. The calculated auxiliary power (as a percentage of the gross power) and thermal efficiencies are shown in Table 6.5. The efficiencies are based on the lower heating value of the fuel. The systems were checked with regard to carbon deposition. For the pressurized system with external reforming carbon deposition cannot be excluded under normal operation. System 2 operates on atmospheric pressure with external reforming and has the lowest electrical and total efficiency (0.381). All blowers and pumps are driven by electric motors. The power consumption of this equipment is relatively high (17.10% of the gross generated power). The relatively low electrical efficiency is partly due to some less favorable design conditions. Parameter optimization might raise the efficiency with some points. The

application of an ORC bottoming cycle can be considered because of the relatively high quality of the waste heat. The ORC cycle might raise the net electrical efficiency to 0.445. However, the bottoming cycle reduces the total efficiency from 0.716 to 0.541. The performance of the fuel cell stack can be improved by raising the operation pressure. In that case (system 4) an air compressor and gas expander have to be added to the system. The gas expander drives the compressor and an electrical generator. For system 4 a net electrical efficiency of 0.541 is calculated. The application of a mechanical driven compressor reduces the auxiliary power consumption to 8.72% of the gross electric power. As the heat of condensation from water vapor of the fuel cell exhaust gas can be utilized in this case, also the total efficiency will be significantly higher (0.957). The results for system 1 and system 3 show that internal reforming has a considerable effect on the electrical efficiency. In the case of atmospheric pressure (system 1) the electrical efficiency is 0.555 and in the case of elevated pressure (system 3) 0.667. Internal reforming uses a significant part of the heated generated by the fuel cell stack, thus reducing the need for cooling. As cooling of the stack is controlled by the cathode air flow, this flow can be seriously smaller in the case of internal reforming. The circulation of smaller air flows reduces the required auxiliary power. Steam needed for the internal reforming process in the systems 1 and 3 is generated in a steam

generator. However, water vapor is generated at the anode. This water vapor can be used for the reforming process by recirculating the anode off-gas as is done in system 5 (see Figure 6.15). The effect of the anode gas recirculation on the net electrical efficiency is limited but the effect on the total efficiency is significant.

#### MCFC-CHP system

Another MCFC-CHP system will be used to discuss various aspects of the system design with regard to the system performance. In Figure 6.16 the system flow diagram is depicted of a MCFC-CHP system with external reforming. The results of the system calculation are presented in Tables 6.6 and 6.7. The system design has been used before in [6.44] and [6.44] for the evaluation of various design parameters. The system design is used here primarily to demonstrate the considerations that play a role during the design process. The economic feasibility of such a system is very unlikely. The system is fuelled with natural gas of Slochteren quality. The MCFC stack operates at a pressure of 4 bar and uses a gas

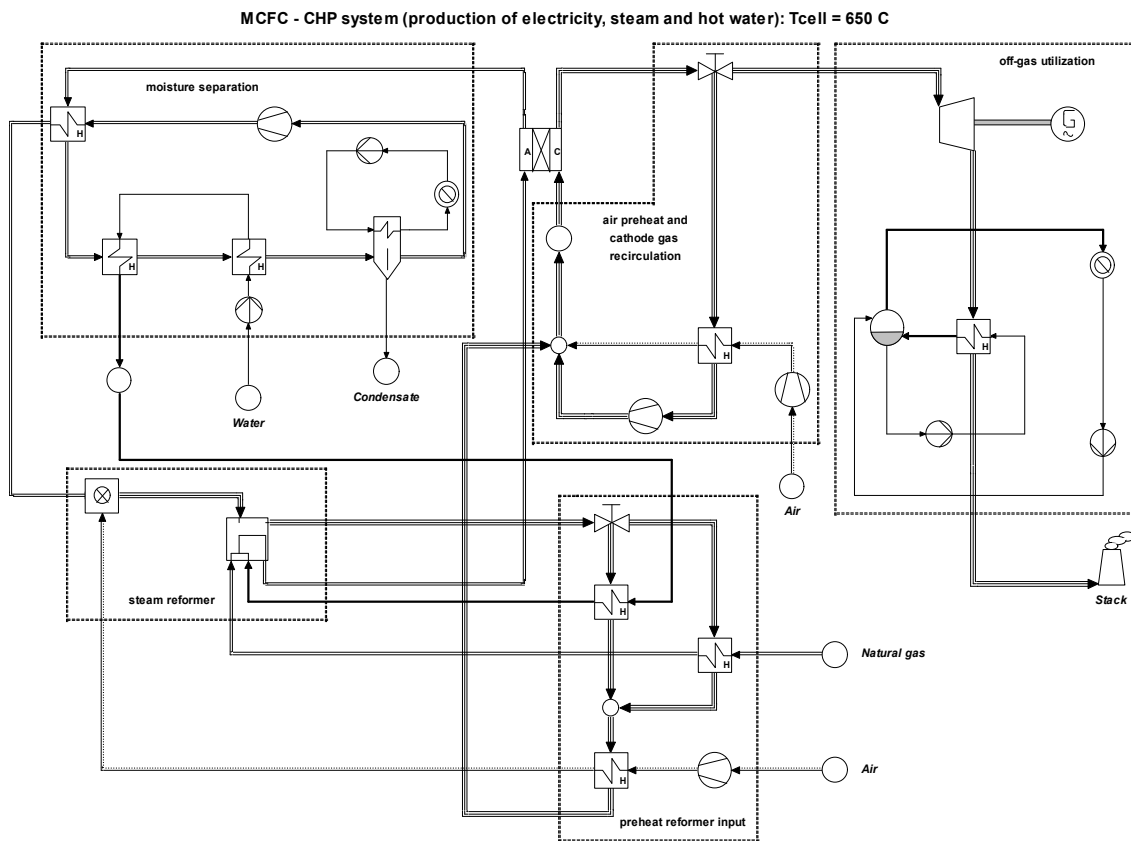


Figure 6.16 System flow diagram of a pressurized MCFC-CHP plant with external reforming

turbine that is supposed to be adjusted for this application. The surplus of the expander power is used to drive an electrical generator. Thus, electricity is generated by the fuel cell stack and the gas turbine. The stack operates at temperatures around 650°C. Fuel and air enter the stack at 600°C and leave the stack at 700°C. The heat discharge from the stack is controlled by the cathode flow. A large cathode flow is necessary because of the limited temperature rise from

*Table 6.6 Overall results pressurized MCFC-CHP with external reforming*

		energy [kW]	exergy [kW]
fuel input		557.64	580.82
generated power	fuel cell	306.11	306.11
	GT generator	60.07	60.07
gross power		366.19	366.19
auxiliary power		77.59	77.29
net power		288.59	288.59
generated heat	saturated steam	91.64	33.35
	hot water	109.49	17.54
total generated		489.72	339.48
		[-]	[-]
efficiencies	gross electrical	0.6568	0.6305
	net electrical	0.5175	0.4969
	heat	0.3607	0.0876
	total	0.8782	0.5845

*Table 6.7 Fluid composition and mass flow at inlet and outlet of the fuel cell stack (MCFC-CHP)*

component	units	anode		cathode	
		inlet	outlet	inlet	outlet
N <sub>2</sub>	[-]	0.0265	0.0182	0.6943	0.7441
O <sub>2</sub>	[-]	-	-	0.0667	0.0476
H <sub>2</sub> O	[-]	0.2783	0.4686	0.1149	0.1232
Ar	[-]	-	-	0.0081	0.0092
CO <sub>2</sub>	[-]	0.0589	0.3896	0.1159	0.0765
CH <sub>4</sub>	[-]	0.0052	0.0036	-	-
CO	[-]	0.1026	0.0346	-	-
H <sub>2</sub>	[-]	0.5285	0.0855	-	-
mass flow	[kg/s]	0.053	0.169	1.268	1.151

inlet to outlet. To avoid complete heating and cooling of the cathode air from environmental temperature to the stack temperature, a cathode gas recycle is applied. The recycle blower is positioned in the cold leg of the cathode recycle in order to reduce the required power. The stack performance is calculated assuming a quasi ohmic cell resistance of  $6.089 \times 10^{-5} \Omega \cdot \text{m}^2$ , a current density of  $1500 \text{ A/m}^2$  and a fuel utilization of 0.70. The generated DC electricity is converted into AC assuming a conversion efficiency of 0.96. The anode off-gas is combusted in an afterburner. Before combustion the moisture content of the anode off-gas is reduced from 47% to 13% in a moisture separation loop. This increases the heating value of the anode off-gas from 1.22 MJ/kg to 1.64 MJ/kg. Almost 25% of the anode off-gas mass flow is removed. Because of the difference in mass flows, the heat that is transferred by cooling the anode off-gas to condensation temperature cannot be recovered completely. The remainder is used for the generation of steam for the reformer. Condensation of water vapor starts at about  $116^\circ\text{C}$  and the gas leaves the moisture separator at  $80^\circ\text{C}$ . These temperatures enable the

utilization of the latent heat for district heating. The hot flue gasses from the combustor are used to heat the reformer. The higher combustion temperature due to moisture removal will improve the heat transfer in the reformer. Combustion air for the after-burner is preheated to 440°C resulting in a flue gas temperature of 1272°C. The S/C ratio of the reformer is 3 and a reaction temperature of 800°C is assumed. The flue gas leaves the reformer at a temperature of 670°C and is cooled to 426°C to deliver heat for fuel and air preheating and for superheating reformer steam. The cooled flue gas is mixed with the cathode air to provide the cathode flow with CO<sub>2</sub>. A CO<sub>2</sub> concentration of 11.59% at cathode inlet is achieved in this way (see Table 6.7). The oxygen utilization at the cathode is 33% and the CO<sub>2</sub> utilization 38%. Most of the cathode exhaust (77%) is recycled. A cathode recycle blower operating at a temperature of about 630°C is considered for this purpose. Replacement of the recycle blower by an ejector seems to be attractive with regard to power consumption and costs. The development of an ejector for this purpose is reported in [6.47]. The remainder of the cathode exhaust flow is discharged to the stack. However, first the gas is expanded and cooled before it is passed to the flue gas stack at a relatively high temperature of 200°C. The expander off-gas is used to generate saturated steam at 10 bar. This causes a high stack temperature. Lower stack temperatures are achievable by reducing the steam pressure or by additional hot water generation. Anyhow, the possibilities of heat generation depend on the availability of appropriate heat demands.

The calculated electric and thermal powers that can be generated by this system are shown in Table 6.6. The net electrical efficiency based on the thermal input is 0.5175 which is high for a 250 kW CHP plant. A total efficiency of 0.8782 is also attractive. This value is achieved primarily because of the generation of hot water by the moisture separation loop. The thermal power of the hot water is even higher than the thermal power of the saturated steam. But the exergy value is much lower. It appears that the auxiliary power (77.59 kW) is more than 20% of the gross electrical power, which is quite high. Another indicator for the system capital cost is the total heat power transferred within the system. This value is considered as a rough indication of the total cost of heat exchangers. From various cost studies it is known that usually the capital costs of heat exchangers dominate the total capital cost. A total heat transfer power of 487 kW is calculated for this system. It is expected that the high auxiliary power and heat transfer power will hinder the economic feasibility of this

*Table 6.8 Exergy losses subsystems pressurized MCFC-CHP with external reforming*

subsystem	exergy loss	
	[kW]	[-]
fuel cell	25.87	0.0445
air preheat and cathode air recirculation	42.62	0.0734
moisture separation	39.57	0.0681
steam reforming	67.84	0.1168
preheat reformer input	14.94	0.0257
off-gas utilization	24.78	0.0427
flue gas stack	25.72	0.0443
<b>total</b>	<b>241.34</b>	<b>0.4155</b>

system design. If heat delivery is not possible the residual heat from the flue gas can be used for additional power generation. In case of small-scale systems the application of Organic Rankine Cycles (ORC's) can be beneficial. For maximum power generation the ORC working fluid has to be adapted to the actual flue gas temperature

[6.43]. Table 6.8 gives an overview of exergy losses of the distinguished subsystems. Absolute values as well as fractions of the fuel exergy are shown. The total exergy loss of the system is 241.34 kW which is 0.4155 of the exergy input by the fuel. The exergy loss of the fuel cell stack is 4.45% of the fuel exergy, slightly more than 10% of the total exergy loss. The steam reformer (including the after-burner) causes an exergy loss of 67.84 kW, more than 28% of the total exergy loss. Also the exergy loss of the moisture separation loop is relatively is high.

The overview clearly shows that most of the exergy loss results from the balance of plant. Thus, careful design of the total system is required to realize the high efficiencies achievable in principle by molten carbonate fuel cells. The design of the fuel cell stack will affect also the system design. Higher cell voltages reduce the heat generated by the stack and, therefore, reduce the need for heat transfer and auxiliary power for blowers and compressors. A serious complication in the case of molten carbonate fuel cells is the need for carbon dioxide at the cathode. The  $\text{CO}_2$  generated at the anode can be used for that purpose, of course, but removal of water vapor from this flow requires additional equipment. The effect of vapor removal is not investigated thoroughly. Perhaps vapor removal is not really advantages. But without removal the water vapor will decrease the combustion temperature of the reformer and reduce the  $\text{O}_2$  and  $\text{CO}_2$  concentrations at the cathode.

#### Alternative stack configurations

Options for reducing the amount of heat generated in fuel cell stacks have been investigated. It was suggested in the past that the cell geometry (flat plate, circular or tubular) could affect the current density distribution and consequently the losses in the cell. In [6.44] however, it was demonstrated that in the case of fuel cells with external reforming the

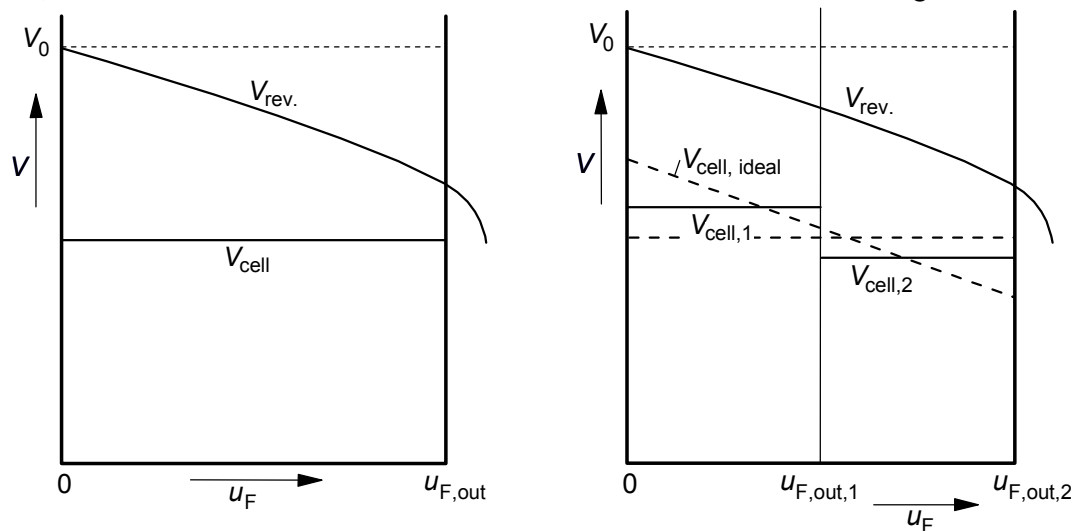


Figure 6.17 Cell voltages in the case of single stage (left) and two stage (right) operation

geometry has no or only negligible effect on the current density. In this investigation cells with internal heat transfer were not included; therefore no conclusions are drawn with respect to cells with internal reforming. An investigation of the effect of co-flow versus counter-flow of anode and cathode flows [6.44] has demonstrated that co-flow is slightly advantageous

over counter-flow. Assuming equal average current densities, co-flow offers a relatively homogeneous current distribution and a somewhat higher cell voltage at high current densities.

The concentration of hydrogen and carbon monoxide at the anode of an MCFC will change as a function of fuel utilization because of the conversion of  $H_2$  and  $CO$ , and the generation of reaction products ( $H_2O$  and  $CO_2$ ). Therefore, the reversible cell voltage will decrease as a function of fuel utilization. The resulting non-homogeneous current distribution causes higher exergy losses. A more homogeneous current distribution can be achieved by placing fuel cells in series each with its own cell voltage. Figure 6.17 shows in principle the effect of two-stage oxidation versus single stage oxidation.

In the case of two-stage oxidation the difference between the reversible voltage and the actual cell voltage at cell inlet ( $u_f = 0$ ) is lower and at cell outlet ( $u_{f, out} = 0$ ) the difference is higher. This results in a more uniform current density. If the same average current density is assumed, system calculations have demonstrated a 1% (point) higher electrical efficiency in the case of two-stage oxidation [6.44]. The difference in current density can be further reduced by increasing the number of stages. However, the additional effect of 3 or more stages is limited; in case of an infinite number of stages, in Figure 6.17 indicated as  $V_{cell, ideal}$ , the efficiency increase over the single stage case will be about 1.33 %. The calculations in [6.44] are based on the assumption that the cell resistance is constant also when the operation

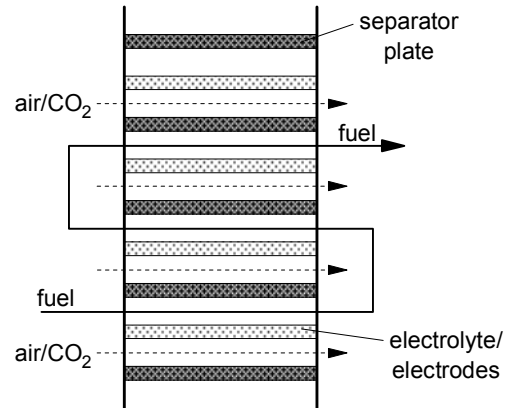


Figure 6.18 Multistage oxidation in a single stack

temperature of the cell changes. For the evaluations in [6.45] accurate relations between cell temperature and cell resistance were available and additional system calculations are made to check the influence of changes in cell resistance. From these calculations it appeared that the increase in efficiency is somewhat lower than calculated before. But, further improvements can be achieved by optimizing fuel cell temperatures and other design parameters. Multistage oxidation does not necessarily require the application of more than one stack. It can be realized also within one stack as shown in Figure 6.18. If the cells are electrically connected in series, each

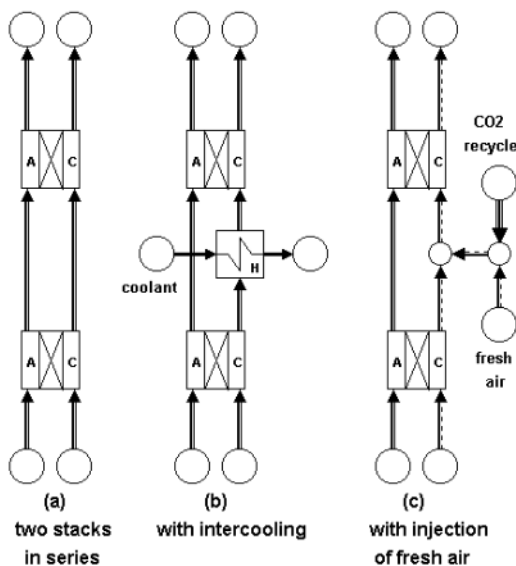


Figure 6.19 Three options for a series connection of stacks

cell will have the same current density. The voltage of the cells will, however, differ depending on the reversible voltage resulting from differences in the fuel composition.

The series connection of stacks can be used also to improve the thermal management of the fuel cell system. Because of the cathode gas recycle in the system of Figure 6.16, the supply of fresh air to the cathode is only 15% of the total cathode flow. Thus, less heat is needed for air preheating which reduces the exergy loss of heat transfer within the system significantly. However, the auxiliary power needed to drive the blower for cathode gas recycling is considerable. The application of a series of stacks makes it possible the reuse of cathode gas without the need for gas recycling. In Figure 6.19 option (a) depicts a series connection of two stacks; the inlet conditions of the second stack are determined by the outlet conditions of the first one. The total temperature rise of the cathode flow is divided over the two stacks. In that case the cathode gas flow must be almost the same as in the case of a single stack. Option (b) shows a two-stage stack arrangement with intermediate cooling of the cathode flow. In that case the maximum temperature rise of the cathode gas can be achieved in each stack. The cathode gas flow can be about half the flow of the single stack case. This might result into a significant reduction of the power needed for the recycle blower. In the case of MCFC stacks heat has to be extracted at temperatures of 600 to 700 °C; the exergy of this heat is high and can be applied for power generation in a bottoming cycle (steam or ORC) or as high temperature process heat. If for instance the power scale does not allow for the application of a bottoming cycle, the injection of fresh air in the cathode flow between both stacks (option (c)) can be considered. To balance the oxygen and the carbon dioxide concentrations the anode recycle for the supply of CO<sub>2</sub> must be divided too over the two stacks. The series connection of stacks can improve the electrical efficiency with more than 5 % (points) in the case of systems with cathode gas recycle. An increase from 46 to 55 % has been calculated for a system with four stacks in series and injection of fresh air and anode recycle gas in the cathode flow between the stacks [6.44].

The operation temperature of MCFC's is generally supposed to be optimum at 650 °C. In [6.45] the effect of the cell temperature on system performance was investigated since empirical equations for the equivalent (or quasi-Ohmic) cell resistance became available. These equations were obtained from CRIEPI. The application of these equations showed that the cell resistance decreases continuously if the cell temperature is increased from 600 to 700 °C. The cell power shows an optimum around 660 °C. The effect on overall system performance was evaluated for the system design depicted in Figure 6.16. System calculations have been made for cell temperatures from 600 to 700 °C with temperature steps of 25 °C. The highest net electrical efficiency was achieved for a system with a cell temperature of 675 °C. Also the overall exergy efficiency appeared to be maximum for this case. Only the overall thermal efficiency is still increasing with temperature. The efficiency curve is rather flat around its optimum. It is concluded that the cell temperatures for maximum system efficiency and maximum cell efficiency are not the same. But differences are practically negligible.

In MCFC systems the need for rather high concentrations of carbon dioxide at the cathode complicates the system design. Besides, the mixing of air and CO<sub>2</sub> is in conflict with future needs for CO<sub>2</sub> sequestration as discussed today. The concept of an improved MCFC (i-MCFC) might provide a solution for this problem. In the i-MCFC anode recycle gas is not

mixed with the cathode airflow but supplied through separate gas channels in the electrolyte matrix [6.46]. The concept is evaluated and discussed more comprehensively in [6.45]. A system calculation has demonstrated that replacing the MCFC by the i-MCFC does hardly affect system performance. Systems studies that fully exploit the features of the i-MCFC however have not been made. The technical feasibility seems to be unlikely.

#### MCFC-GT hybrid systems

It is expected that MCFC-GT hybrid systems will be very attractive for future applications because of the high efficiencies that are achievable. In [6.48] the MCFC-GT hybrid system is analyzed and discussed. It is mentioned too that many papers have examined such system configurations. Electrical efficiencies up to 60% and higher are reported in various papers. The combination of fuel cells and gas turbines is in general attractive in the case of high temperature fuel cells, MCFC as well as SOFC. Design options for SOFC-GT systems are discussed in the following section.

### 6.5.4 SOFC systems

#### Introduction

The development of SOFC systems is primarily focusing on small scale power generation ([6.61], [6.64], [6.65], [6.68]) and CHP systems ([6.55], [6.56], [6.57]). This focus is partly due to the present state of development; various studies have shown too the suitability for higher powers ([6.57] to [6.59], [6.62] and [6.63]). In particular the SOFC/GT hybrid system is considered frequently ([6.58] to [6.60], [6.63] to [6.74], and [6.80]). The efficiencies of SOFC/GT hybrid systems appear to be very promising also in the case of smaller powers. In [6.80] it was mentioned that gross efficiencies of 70%-80% are indicated. Most of the studies consider stationary power generation, but there is also interest for mobile applications ([6.53], [6.54] and [6.70]). In the Sections 6.4 and 6.5.2 it was demonstrated that the conversion of the primary fuel into hydrogen causes serious exergy losses. The application of the SOFC for the co-production of electricity and hydrogen as discussed in [6.51] and [6.52] offers a possibility to reduce the exergy loss of the reforming process. Also the combined application of SOFC and PEMFC is considered for this reason (see [6.50]). Natural gas appears to be a convenient fuel for HT fuel cells. But, if fossil fuels have to be replaced by renewable energy sources the combination of biomass gasification and HT fuel cell systems might become an interesting option. Comprehensive evaluations of the technological requirements as well as the various system alternatives are presented in [6.73] and [6.74] respectively. The SOFC was initially developed for operation at temperatures up to 1000°C. These high temperatures do not only exist in the fuel cell stack but also in equipment immediately connected with the stack. High fluid temperatures complicate the design and do require expensive construction materials. Also the Siemens-Westinghouse SOFC generator ([6.62]), where all high temperature components are integrated in a single vessel has not become commercially successful. The application of intermediate (600-800°C) or low temperature (500°C) SOFCs is supposed to enable the necessary cost reduction. During the last decade a lot of research has been spent on suitable materials for high performance SOFCs operating at lower temperatures (see e.g. [6.72], [6.73], [6.74], [6.77], [6.78]).

The objective of this section is primarily to discuss the effects of various options for the SOFC system design on system performance. With natural gas fuelled SOFC systems

thermal efficiencies up 80% (on LHV basis) are supposed to be achievable. Such high efficiencies require careful system design and it is useful to know what conditions have to be fulfilled to enable these high efficiencies. For that purpose the results of some system studies performed within the Energy Systems group (partly reported before in [6.57] and [6.71]) are summarized and discussed in this section.

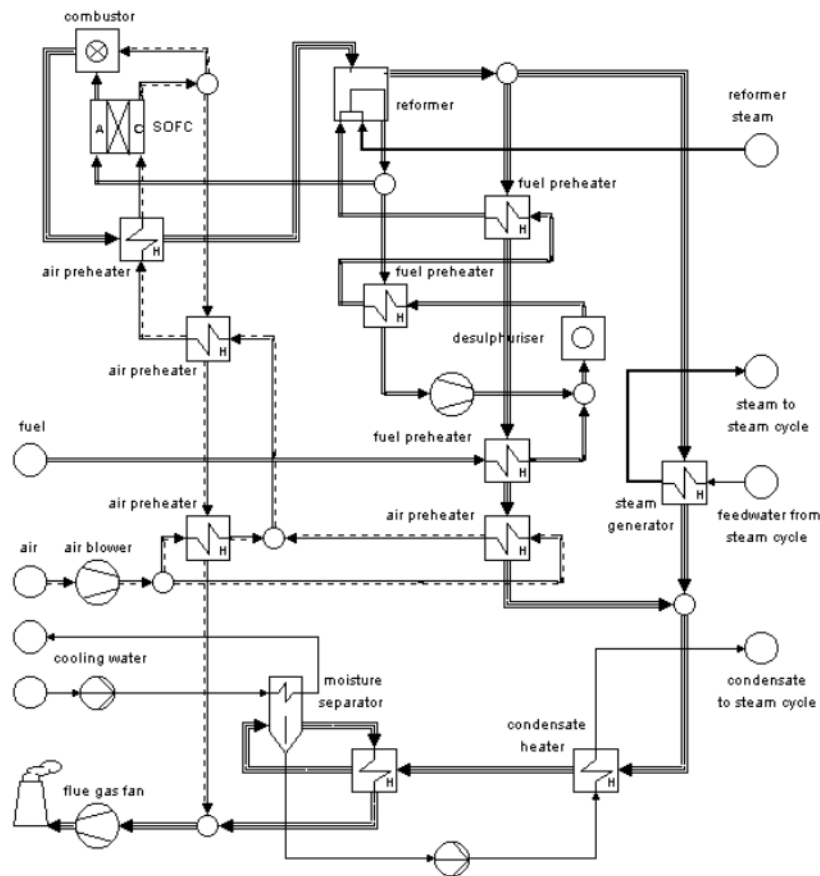


Figure 6.20 SOFC system (system 1: integrated external reforming) without steam cycle

### Exploring system studies

The results of an exploring system study has been reported in [6.57]. For this study small scale CHP systems with powers around 200 kW<sub>e</sub> as well as large scale power systems with powers around 100 MW<sub>e</sub> are considered. Only the results of the large scale power systems (5 different system configurations) are discussed here. All SOFC systems operate at atmospheric pressure. Residual heat is used for the generation of high pressure steam for additional power production with a simple steam turbine cycle. The power generated by the SOFC stacks is fixed at 100 MW<sub>e</sub>.

The configuration of the first system, a system with external reforming without recycle of the anode and cathode flows, is depicted in Figure 6.20. The steam cycle is not included in this diagram; only condensate heating and steam generation are mentioned. The actual steam cycle is a bit more complicated. Some input parameters and the main results are presented in Table 6.9. Fuel enters the system at environmental temperature (15°C) and is preheated in two

*Table 6.9 Input parameters and results of exploring SOFC system studies*

system nr.		1	2	3	4	5
<b>INPUT PARAMETERS</b>		<b>units</b>				
fuel cell						
current density	[A/m <sup>2</sup> ]	2500	2500	2500	2500	2500
quasi ohmic resistance	[Ω m <sup>2</sup> ]	1×10 <sup>-4</sup>				
fuel utilization	[-]	0.85	0.85	0.85	0.85	0.85
stack outlet temperature	[°C]	1000	1000	1000	1000	1000
ΔT anode	[K]	150	150	200	200	200
ΔT cathode	[K]	200	200	200	200	200
reformer		extern.	extern.	intern.	intern.	intern.
fraction cathode air to combustor	[-]	0.333	0.333	0.333	0.500	0.455
recycled fraction anode gas	[-]	-	0.750	-	-	0.600
recycled fraction cathode gas	[-]	-	-	-	0.500	0.545
<b>RESULTS</b>						
fuel input (based on LHV)	[MJ/s]	206.09	221.43	206.70	209.12	213.57
cell voltage	[V]	0.613	0.592	0.611	0.604	0.591
generated AC power (gross)						
SOFC stacks	[MW <sub>e</sub> ]	100.00	100.00	100.00	100.00	100.00
steam turbine	[MW <sub>e</sub> ]	16.79	27.61	26.34	30.80	40.85
auxiliary power consumption	[MW <sub>e</sub> ]	11.71	12.43	5.73	7.31	7.93
net power production	[MW <sub>e</sub> ]	105.08	115.18	120.61	123.49	132.92
net thermal efficiency	[-]	0.510	0.520	0.584	0.591	0.622
internal heat transfer	[MW <sub>th</sub> ]	616.21	658.20	384.26	342.74	397.87
estimated capital cost (relative)	[-]	1.000	0.8727	0.7734	0.7680	0.7734

stages using heat from the reformer flue gas. After the first preheating stage organic sulfur in the fuel is converted into hydrogen sulfite that will be absorbed in a zinc oxide bed. The desulphurization is supposed to occur at 400°C. To provide the fuel with hydrogen a small part of the reformer outlet flow is recycled to the inlet of the desulphurizer. At the inlet of the reformer fuel and steam are mixed at a temperature of 500°C. Extraction steam from the outlet of the HP turbine is used to generate steam for the reforming process in a steam/steam generator. In the reformer the mixture is heated to 850°C which is supposed to be the equilibrium temperature. The product gas from the reformer is passed to the anode inlet of the SOFC stack without further cooling. It is assumed that 85% of the fuel is utilized at the anode. The residual fuel is combusted in an after-burner. One third of the cathode exhaust is used as combustion air for the after-burner. The temperature of the flue gas leaving the afterburner is over 1150°C which is high enough for the last stage of air preheat. Cathode air enters the system also at environmental temperature. Air preheating occurs primarily by using heat from the cathode exhaust. Because of the oxygen consumption at the cathode and the combustion air needed for the after-burner, the heat from the cathode exhaust is not sufficient to preheat the fresh air flow. Hence, air is partly preheated by the reformer flue gas exhaust. Residual heat from the reformer flue gas exhaust is used for the generation of steam and the preheating of condensate for the steam cycle. The steam cycle is just a simple steam cycle without reheat (live steam conditions: 60 bar, 530°C). It is assumed that most water vapor from the flue gas is condensed in a moisture separator before the flue gas is mixed with the cooled cathode air

## Chapter 6 Fuel cell systems

and discharged via the flue gas stack to the environment. For the total system a net thermal efficiency of 0.510 was calculated. In Table 6.9 also the total internal heat transfer is mentioned. This is the sum of the powers of all considered heat exchangers. Together with the auxiliary power the total internal heat transfer is supposed to be a rough indicator for the system capital costs. For this study an estimate of capital cost was made by an engineering firm. Only relative cost numbers for comparison of the system alternatives are presented in Table 6.9. System 1 is used here as a reference.

System 2 is also a configuration with external reforming. Steam for the reforming process is not taken from the steam cycle, but obtained from the anode outlet by recycling 75% of the anode exhaust to the inlet of the desulphurizer. Then, more steam is available for expansion in the steam turbine resulting in a higher power output. The cell voltage is lower in this case because the anode recycle results into lower concentrations of hydrogen and carbon monoxide at the anode. Consequently more fuel is necessary to generate the same electrical power by the fuel cell stacks. The anode recycle increases the net thermal efficiency with 1% (point), but it increases also the total internal heat transfer. Nevertheless, the estimated capital costs are lower since heat transfer at lower temperatures is increased and heat transfer at higher temperatures is decreased.

In the case of system 3 it is assumed that the reforming will take place in the fuel cell stack. Steam for the reforming process is generated in a steam/steam generator heated by steam extracted from the exhaust of the HP steam turbine. The assumptions regarding the calculations of the cell voltage has resulted into a slightly lower cell voltage than for system 1 and consequently a slightly higher fuel consumption. Since the sulfur content of the anode feed is less than 10 ppm it is assumed that desulphurization of the fuel is not necessary. Due to the internal reforming the cathode air flow is reduced by almost 50%. This reduces also the necessary auxiliary power for air circulation as well as the heat transfer for air preheat. Nevertheless, more heat is available for the generation of steam and thus the power generated by the steam turbine is higher than in the previous cases. Because of the higher power generation and the reduced auxiliary power consumption the net thermal efficiency of system 3 is 0.584. The internal reforming reduces also the internal heat transfer of the system with almost 38%. The estimated capital costs are about 23% lower. The combination of higher efficiency and lower capital costs makes internal reforming very attractive.

System 4 is almost similar to system 3. The only difference is that in the case of system 4 cathode air is recirculated. This increases the overall oxygen utilization and therefore reduces the flow of fresh air that has to be supplied to the system. It is assumed that 50% of the cathode exhaust flow is recycled; the other 50% is transferred to the after-burner. The cathode recycle results into a lower mean oxygen concentration which reduces the cell voltage and increases the fuel consumption. The cell voltage calculated for this system is 0.604 V and thus the fuel input is somewhat higher than for system 3. The supply of fresh air is around 44% lower than for system 3. This means that less heat is required for LT air preheating and thus more heat is available for steam generation. Thus, the steam turbine power is increased. The auxiliary power consumption of the air supply fan will be lower, but this reduction is overcompensated by the auxiliary power of the air recirculation fan, since this fan operates at higher air temperatures. The net thermal efficiency of system 4 is 0.591 which is slightly

higher than for system 3. The internal heat transfer as well as the estimated capital costs are somewhat lower.

The results of the previous systems have shown that internal reforming, anode recycle and cathode recycle are beneficial with regard to the net thermal efficiency as well as to the system capital cost. Therefore system 5 was configured with all these facilities as depicted in

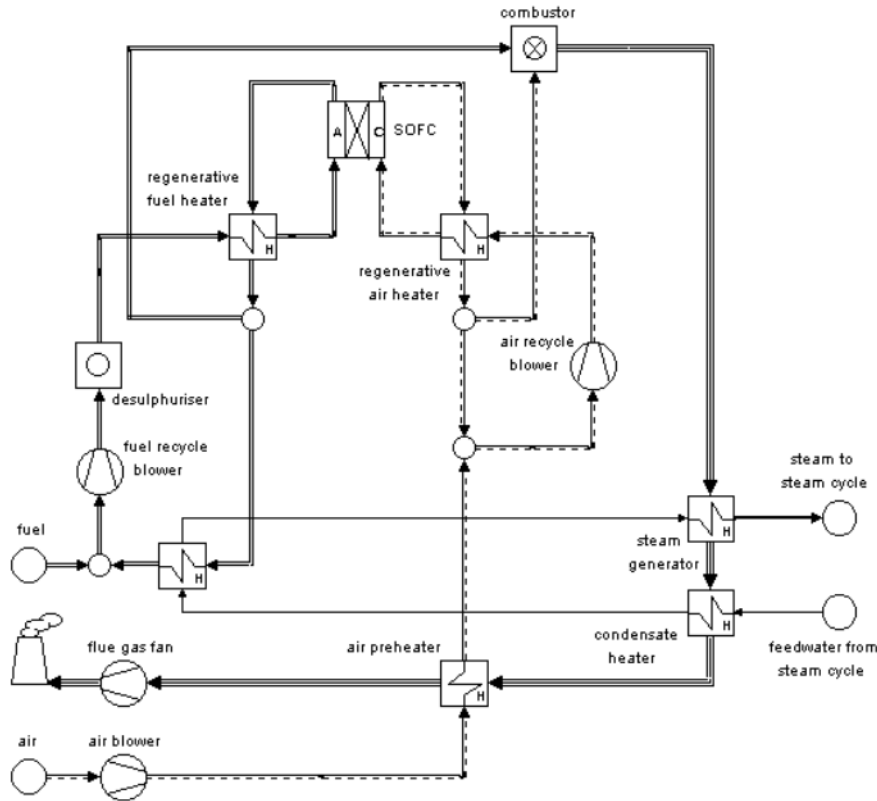


*Figure 6.21 SOFC system (system 5: internal reforming with anode and cathode gas recycle) without steam cycle*

Figure 6.21. The recycle fans are placed in the cold legs of the circuit to enable operation at lower temperatures. About 55% of the cathode air is recirculated to control the removal of residual heat from the fuel cell stacks. The remainder is passed to the after-burner for the combustion of non-converted fuel from the anode exhaust. From the anode exhaust 60% is recycled and 40% is passed to the after-burner. The hot flue gas from the afterburner is used for the generation of steam for the steam turbine and for LT preheating of cathode air. The recycle of anode gas and cathode air dilutes the gases at the electrodes of the fuel cell. This results in a lower cell voltage (0.591 V) and a higher fuel input. The power generated by the steam turbine is serious higher than for the other systems and consequently also the net thermal efficiency (62.2%). The internal heat transfer of the system is somewhat higher than for the systems 3 and 4 and the estimated capital costs are the same as for system 3.

The study has shown that the system design has significant effects on the efficiency and capital cost of SOFC power plants. The application of internal reforming as well as anode and cathode recirculation simplifies the overall system design and increases the thermal efficiency from roughly 51% for system 1 to 62% for system 5. Several input parameters for the system

## Chapter 6 Fuel cell systems

calculations are arbitrarily chosen and no attempts were made to optimize these parameters. The quasi-ohmic cell resistance was assumed to be  $10 \times 10^{-5} \Omega \text{ m}^2$ . It was expected that this value could be improved to  $5 \times 10^{-5} \Omega \text{ m}^2$  within a few years. The consequences of such an improvement are shown in Figure 6.22. In this figure the effect on the cell voltage as well as on the net thermal efficiency of the system is demonstrated. It shows that if the quasi-ohmic cell resistance is reduced from  $1.0 \times 10^{-4} \Omega \text{ m}^2$  to  $0.5 \times 10^{-4} \Omega \text{ m}^2$  the cell voltage increases from 0.59 to 0.71 V and the net thermal efficiency of the system increases from 62% to 69%.

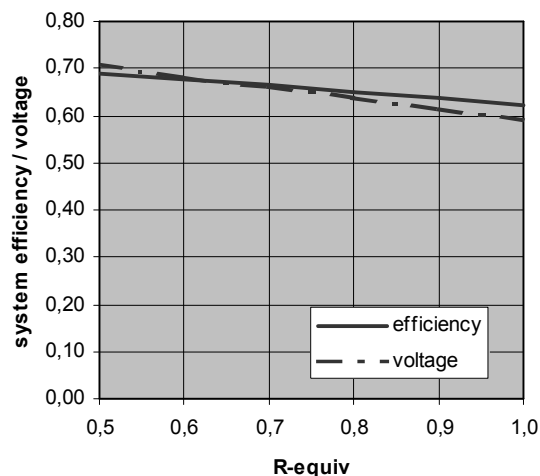


Figure 6.22 Cell voltage and net thermal efficiency as function of the quasi-ohmic cell resistance in  $\Omega \text{ cm}^2$  (system 5)

#### Intermediate scale power generation (SOFC-GT hybrid systems)

Combining SOFC's with gas turbines for intermediate to large scale power plants (roughly  $1 \text{ MW} < P_{\text{electr}} < 50 \text{ MW}$ ) seems to be very attractive. Several system studies are dedicated to this subject. Unfortunately, not many papers on this topic do present all relevant details of the considered system designs. With regard to the calculated or expected thermal efficiencies the conclusions are diverse. In [6.58], a paper published in 1993, a thermal efficiency of 77.7% was calculated for a system with external reforming and an optimized cycle configuration. The considered power was not specified but a value of 100 MW for the fuel cell stacks was mentioned. In [6.59] also powers higher than the range mentioned before are considered. The tubular SOFC module from Siemens-Westinghouse was considered for this study assuming internal reforming with anode recirculation and a pre-reformer. It was concluded that such systems can achieve electrical efficiencies close to 75% (LHV) with conventional gas turbine technology. An overview of SOFC development at Rolls-Royce was presented in [6.80]. In this paper it was mentioned that multi-megawatt hybrid systems have the potential to reach gross efficiencies of 70-80%. A general overview of SOFC systems and performance based on the Siemens-Westinghouse SOFC generator is presented in [6.62]. It was mentioned that 20 MW power plants combining an SOFC generator with integrated and more sophisticated gas turbine have the potential to reach 70% electrical efficiency. In [6.60] a system study is presented that compares an SOFC-GT system lay-out with a single stack, a system with two stacks with both reactant streams in series and a system with two stacks with the fuel streams in series and parallel air streams. The calculated thermal efficiencies range from 59.0% to 65.2%. However, the generated total powers are around 300 kW, well below the considered range for intermediate scale power generation. Further system studies are presented in [6.63] to [6.69]. A variety of results calculated for different system

configurations and design parameters is presented. A systematic evaluation of all these results is beyond the scope of this thesis. To investigate the possibilities of hybrid SOFC-GT systems for high efficiency power generation, a brief study [6.71] has been made with the aim to define a system configuration that can be used as a target for further development. The results are summarized in a conference paper [6.72] and are used also for the following discussion on the design of SOFC-GT systems.

	units	system A	system B	system C
<b>CHARACTERISTICS</b>				
external steam generation reforming		yes	yes	no
Fuel Cell stack				
power density	[kW/m <sup>2</sup> ]	2.10	2.10	2.10
operating temperature	[°C]	950	950	950
operating pressure	[bar]	7.8	8.0	8.0
cathode recycle		no	yes	yes
anode recycle		no	no	yes
quasi-ohmic resistance	[Ω m <sup>2</sup> ]	7.0×10 <sup>-5</sup>	7.0×10 <sup>-5</sup>	7.0×10 <sup>-5</sup>
Gas Turbine				
<i>TIT</i>	[°C]	1100	1100	1100
pressure ratio	[-]	8.0	8.0	8.0
fuel input (natural gas)	[kg/s]	1.0	1.0	1.0
<b>RESULTS</b>				
fuel power				
thermal	[MJ/s]	38.00	38.00	38.00
exergy	[MJ/s]	39.65	39.66	39.65
generated electrical power				
SOFC stack	[MW <sub>e</sub> ]	20.21	23.59	23.96
gas turbine	[MW <sub>e</sub> ]	8.64	7.39	6.63
aux. power consumption	[MW <sub>e</sub> ]	0.05	1.22	0.76
net power	[MW <sub>e</sub> ]	28.81	29.76	29.82
net efficiency				
thermal	[-]	0.7581	0.7833	0.7848
exergy	[-]	0.7265	0.7505	0.7520
<b>ADDITIONAL RESULTS</b>				
SOFC total cell area	[m <sup>2</sup> ]	9930	11600	11780
internal heat transfer	[MW <sub>th</sub> ]	26.10	14.43	7.62
flue gas exhaust temperature	[°C]	140	158	324

The study of [6.71] started with the comparison of six systems. The last three systems have gas turbines with two expansion stages and intermediate reheat. However, the application of a second SOFC stack to reheat the exhaust gas from the first expansion stage appeared not to be very useful. It is a serious complication of the system design and the efficiency improvement is limited. Therefore, this option is not considered here. Only for the first three systems, the systems A, B and C, some characteristics and results are considered in Table 6.10. For the evaluation of the systems it was assumed that the SOFC stack operates at a temperature of 950°C and a pressure around 8.0 bar. The quasi-ohmic resistance of the cells

## Chapter 6 Fuel cell systems

is supposed to be  $7.0 \times 10^{-5} \Omega \text{ m}^2$ , which can be seen as a rather conservative value today. The other cell parameters like cell area and fuel utilization are chosen such that the power density of the stack is the same for all systems ( $2.10 \text{ kW/m}^2$ ). Also the main conditions of the gas turbine (*TIT* and pressure ratio) are the same for the three systems. The fuel reforming is supposed to take place directly in the anode channels of the fuel cells. The fuel input is supposed to be  $1 \text{ kg/s}$  of natural gas (Slochteren quality). System A is a system configuration with external steam generation and in principle without recirculation of anode and cathode flows. Only a small part of the anode exhaust is recirculated to influence the composition at the anode inlet. The steam to fuel ratio is adjusted to assure a steam to carbon ratio of 2.5. The fuel cell stack generates  $20.21 \text{ MW}_e$  and the generator driven by the gas turbine delivers  $8.64 \text{ MW}_e$ . Only  $0.05 \text{ MW}_e$  is needed to drive the pumps and the anode blower. The system has a thermal efficiency of 0.7581 and an exergy efficiency of 0.7265. Various heat exchangers are required for steam generation and preheating of fuel and cathode air. In design condition in total  $26.10 \text{ MW}_{th}$  has to be transferred by the various heat exchangers.

In the case of system B the last stage of air preheating is done by recycling part of the cathode exhaust flow. After compression, cathode air is preheated in a recuperative heater to a temperature around  $570^\circ\text{C}$  using heat from the gas turbine off-gas. Further preheating to fuel cell inlet temperature is achieved by mixing the air flow with recycled cathode exhaust gas. This reduces the flow of fresh air with more than 20%. The reduced air flow in combination with the assumptions of similar power density of the fuel cell stack and similar turbine inlet temperature has several consequences:

- The heat required for air preheating is reduced.
- The heating value of the residual fuel that is burned in the combustor of the gas turbine can be reduced
- The fuel utilization is increased resulting in lower concentrations of  $\text{H}_2$  and  $\text{CO}$  at the anode exhaust
- The oxygen concentrations at cathode inlet and outlet are reduced.
- The cell voltage is decreased.
- The current density is increased.
- The total cell area is increased.

From the calculation with Cycle-Tempo it appears that for system B the power from the SOFC stack increases to  $23.59 \text{ MW}_e$  and the power from the gas turbine decreases to  $7.39 \text{ MW}_e$ . Also the auxiliary power consumption increases because of the power required for the cathode recycle blower. Compared to system A the net thermal efficiency of system B is 2.5% (points) higher. The net exergy efficiency is around 75%. An additional effect of cathode gas recirculation is that the total internal heat transfer within the system decreases significantly.

In the case of system C also anode recirculation is applied. The anode recirculation assures the availability of water vapor at the anode inlet that is necessary for internal reforming. Then, the separate steam generator can be cancelled. Anode recirculation dilutes the fuel flow at the stack inlet resulting into a lower cell voltage. Since the power density of the cell is assumed to be the same, the current density must be higher and also the total cell area. It appears that the thermal efficiency as well as the exergy efficiency is only slightly higher than in the case of system B. However, the temperature of the flue gas to the flue gas

stack appears to be 324°C. This means that proper utilization of the available heat might result into a further increase of the thermodynamic performance of the system. Another observation is that anode recirculation reduces also the need for steam generation within the system and consequently it reduces the internal heat transfer. It appears that the highest efficiency is achieved with the simplest system configuration but with a somewhat larger fuel cell stack.

#### SOFC-GT target system

An SOFC-GT target system is defined in order to show that electrical efficiencies around 80% are achievable with SOFC-GT systems. The configuration of the target system is the same as system C. The system flow diagram is shown in Figure 6.23. However, in the case of the target system it is assumed that the SOFC stack operates at a temperature around

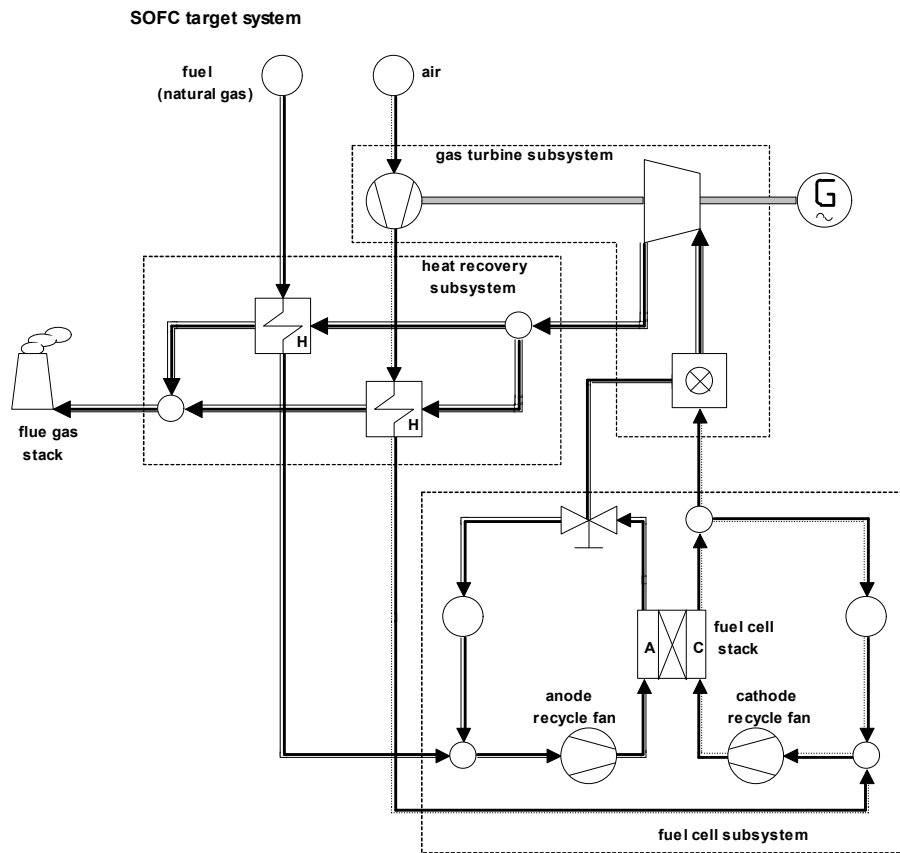


Figure 6.23 System flow diagram of the SOFC target system

700°C. And the quasi-ohmic cell resistance is supposed to be  $5.0 \times 10^{-5} \Omega \text{ m}^2$ . The research reported in [6.75] has shown that such design values are reasonable for future systems. A comparison of various design data of the target system and system C is presented in Table 6.11. The fuel flow rate to the systems is the same. Also the operating pressure of the SOFC stack and the temperature rise of the process flows in the stack is the same. The outlet temperature of the gas turbine has to be high enough to enable preheating of fuel and air to the required temperatures. Therefore, in the case of target system the fuel utilization is assumed to be 0.80. The anode recycle flow rate is fixed to assure that the steam to carbon ratio is not

	units	system C	target system
Fuel power (1kg/s, natural gas)			
thermal	[MJ/s]	38.00	38.00
exergy	[MJ/s]	39.65	39.65
Fuel Cell stack			
operating pressure	[bar]	8.0	8.0
operating temperature	[°C]	950	700
quasi-ohmic resistance	[ $\Omega \text{ m}^2$ ]	$7.0 \times 10^{-5}$	$5.0 \times 10^{-5}$
fuel utilization (per pass)	[-]	0.868	0.80
inlet temperature stack	[°C]	900	650
outlet temperature stack	[°C]	1000	750
total cell area	[m <sup>2</sup> ]	11780	10000
cell voltage	[V]	0.716	0.839
current density	[A/m <sup>2</sup> ]	2927	3335
power density	[kW/m <sup>2</sup> ]	2.10	2.80
oxygen utilization (per pass)	[-]	0.282	0.567
Gas Turbine			
TIT	[°C]	1100	945
pressure ratio	[-]	8.0	8.0
isentropic efficiency compressor	[-]	0.842	0.842
isentropic efficiency turbine	[-]	0.913	0.913
$\lambda$ combustion	[-]	10.05	2.90
Heat recovery			
internal heat transfer	[MW <sub>th</sub> ]	7.62	3.83
flue gas exhaust temperature	[°C]	324	333
Generated electrical power			
SOFC stack	[MW <sub>e</sub> ]	23.96	27.14
gas turbine	[MW <sub>e</sub> ]	6.63	4.26
aux. power consumption	[MW <sub>e</sub> ]	0.76	0.33
net power	[MW <sub>e</sub> ]	29.82	31.06
net efficiency			
thermal	[-]	0.7848	0.8175
exergy	[-]	0.7520	0.7834

lower than 2.5. The flow rate of the cathode recycle is adjusted in a way that the temperature difference in the air preheater is high enough and the oxygen utilization at the cathode is not too high. The assumed recycle flow rates are determining also the gas turbine inlet temperature. The relatively low turbine inlet temperature (945°C) for the target system reduces the power generated by the gas turbine. The calculated net thermal efficiency of the target system is 0.8175 and the corresponding exergy efficiency is 0.7834. The exergy flow diagram of the target system is depicted in Figure 6.24. Exergy flows and losses are presented as percentages of the fuel exergy. The internal exergy losses are less than 15%. The relatively high exergy loss of the flue gas stack (7.51%) is caused by high flue gas exhaust temperature (333°C). No attempts have been made to reduce this high temperature to usual levels. If the residual heat of the flue gas is utilized in a bottoming cycle (e.g. ORC) assuming that one third of the flue gas exergy can be converted into power, the net exergy efficiency of the system can be raised

to more than 80%. A complete overview of input data and results of the Cycle-Tempo calculation of the target system is presented in Appendix 6.3.

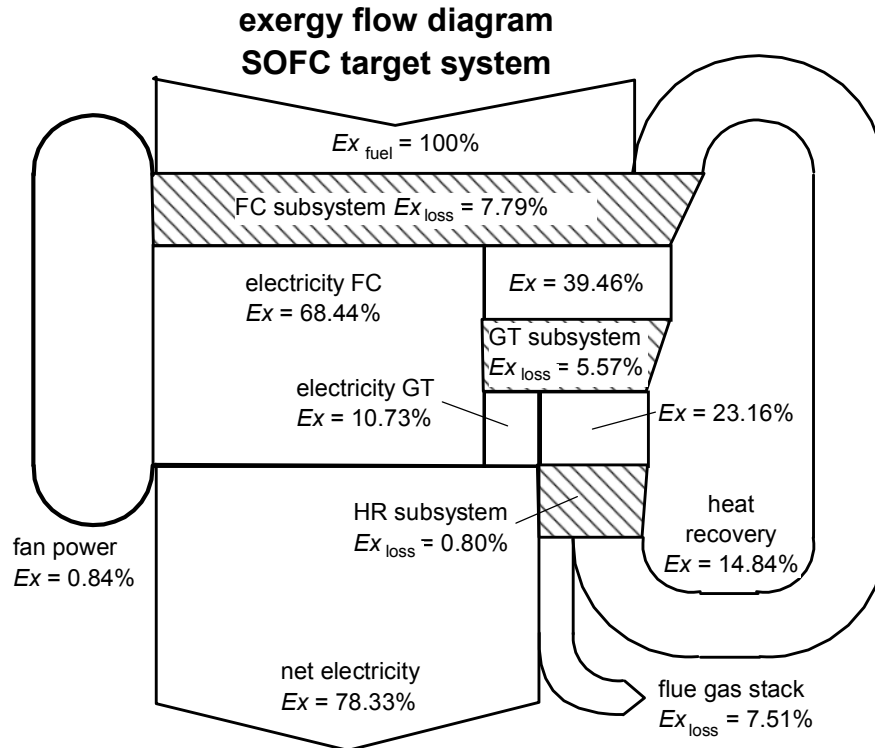


Figure 6.24 Exergy flow diagram of the SOFC target system (in percentages of fuel exergy)

The results for the target system show that efficiencies around 80% are achievable for SOFC-GT systems. The design data as used for this calculation are supposed to be achievable with the knowledge of today. An interesting point of SOFC-GT systems is that high efficiencies are achievable with plants in a power range of roughly 1 to 30 MW. It reduces e.g. the risks during the introduction of this technology and offers accurate adaptation to the development of the national power demand. Additional research is needed, however, to investigate the long term behavior and the economic feasibility of such systems.

## 6.6 Conclusions

High temperature fuel cells have the potential to raise conversion efficiencies of power generation based on natural gas to values around 80%. As demonstrated by system calculations for a target system, these high efficiencies are achievable with fuel cells stacks operating at intermediate temperature (operating temperature 700°C) in combination with gas turbines. Plant power levels in the range of roughly 1 to 30 MW<sub>e</sub> are supposed to be high enough for this purpose. Conventional gas turbine technology appears to be appropriate for the SOFC-GT power plants. The evaluation of the SOFC-GT target system shows that exergy efficiencies even higher than 80% are conceivable if residual heat is used in a bottoming cycle for additional power generation. It is obvious that lifetime and costs of HT fuel cell stacks

have to be at the appropriate levels before application of these systems can be considered seriously.

It is unlikely that similar efficiencies can be achieved with low temperature fuel cells. It has been shown that the exergy loss of PEMFCs is considerably higher than the exergy loss of high temperature fuel cells like MCFCs and SOFCs. In principle the exergy loss of the PEMFCs can be reduced by raising the operation temperature and improving the cell performance. But, even in the case of almost ideal cell performance the exergy loss of fuel conversion and purification will hinder the realization of very high efficiencies. Fuel conversion and purification can be omitted if e.g. hydrogen from renewable energy sources becomes available. The availability of hydrogen for power generation will improve the attractiveness of low temperature fuel cells.

The thermodynamic performance of high temperature fuel cell systems depends seriously on the system design. It appears that system efficiencies are determined to a great extent by the exergy losses of heat transfer processes in the system. Furthermore, heat exchangers contribute seriously to the total system costs. During the evaluation of MCFC and SOFC systems as well during the search for the SOFC target system it fortunately appeared that internal heat transfer is minimal in the case of the more efficient systems. For the design of high temperatures fuel cell systems in general the following guidelines have to be considered:

1. reduce the generation of heat in the fuel cell e.g. by minimizing the internal resistance or the application of multistage oxidation,
2. use the heat generated in the fuel cell directly for internal reforming or in an integrated gas turbine,
3. reduce the need for heat transfer in heat exchangers by applying cathode and anode recycle,
4. enable heat exchange with sufficiently small temperature differences by optimizing heat integration.



## 7 COMBINED HEAT AND POWER SYSTEMS

### 7.1 Introduction

The generation of heat, usually generated as hot water or saturated steam, in fired boilers is a process with high thermodynamic losses. In spite of the very high thermal efficiencies of steam and hot water boilers the thermodynamic efficiencies (exergy efficiencies) are rather low (roughly 10 to 30%), depending on the properties of the generated hot fluid. This means that the generation of heat in fired boilers inherently occurs with high thermodynamic losses. These losses can be reduced only by applying alternative technologies, like heat pumps or CHP. CHP is frequently presented as an option that is able to enhance the thermal efficiencies of power plants; it actually suggests that CHP offers a possibility to improve the performance of power plants. In the case of a specific power unit that is modified to make use of the waste heat without affecting the generated power, this concept might be true. The additional use of heat will increase the thermal efficiency as well as the exergy efficiency. But if different plants have to be considered or a thermodynamic optimum has to be selected, the use of thermal efficiencies to judge the performance of CHP plants is not appropriate. Actually, the real reasons for the application of CHP is not the imperfection of power plants but the need to reduce the thermodynamic losses of heat generation. This chapter discusses the causes of the high thermodynamic losses of hot water and steam boilers as well as the possibilities to reduce these losses by combining heat generation and power production. First the thermodynamic aspects of CHP will be discussed. In Section 7.2 the exergy concept is used to explain and determine the thermodynamic losses. Value diagrams, as used in this section, are very useful for qualitative evaluations and to discuss further improvements. But, additionally merit indicators are required for the quantification of the thermodynamic merits resulting from the application of CHP. The thermodynamic concepts used for the evaluation of CHP are presented in Section 7.3. Various options for merit indicators are discussed in Section 7.4. Equations for the calculation of the values of the merit indicator are derived too in this section. Calculated values for some arbitrarily chosen CHP plants are discussed to identify the true merit indicators. These true merit indicators are used in Section 7.5 to determine the effect of some important design parameters for different types of CHP plants.

The exergy concept is useful to achieve a better insight into the thermodynamic characteristics of power plants and consequently CHP (see [7.1]). Many discussions on, and pleas in favor of, CHP are based mainly on the first law of thermodynamics (see e.g. papers [7.2]-[7.14]). The number of papers using the exergy concept (like papers [7.15]-[7.20]) for the evaluation of merit indicators or design options is rather limited. The arguments in favor of CHP, based on the first law only, are not always convincing. On the other hand the need of indicators based on exergy values is also questionable. Therefore, the use of exergy values, exergy analysis and exergy based merit indicators is discussed comprehensively in this chapter.

As mentioned before thermal efficiencies (power or electric, heat and total efficiencies) are primarily used to indicate the merits of CHP. High total thermal efficiencies are supposed to show that the application of CHP will result in significant fuel savings. However, if exergy

efficiencies are determined too, it usually appears that the total exergy efficiency is within the same range as the exergy efficiencies of regular power plants. This indicates that the fuel savings are limited or even negative. The thermal efficiency is actually not an appropriate indicator for CHP plants; the true determination of the thermodynamic merits of CHP will require a more careful evaluation. The quality of merit indicators is not frequently discussed in literature. In [7.2] the EU proposal for the “quality norm” is criticized. The “quality norm” as called in that paper represents the relative fuel savings of the CHP compared to the generation of the same quantities of power and heat by a reference system, in separate generation. But, the author of [7.2] is not expecting that this quality norm will stimulate the right developments under all circumstances. The relative fuel savings are also mentioned in [7.16], but here the relative avoided irreversibility is presented as a more appropriate indicator. However, a reduction of the irreversibility’s must result in a proportional reduction of the fuel consumption. Thus, it is not expected that these indicators should give different results. Unfortunately, a quantitative comparison of the two indicators is missing in [7.16]. A variety of indicators used for legislative purposes is evaluated in [7.17]. The conclusion from this evaluation was: “that none of the investigated indicators are capable of providing a full thermodynamic evaluation of CHP systems”. This emphasizes that a more fundamental thermodynamic evaluation of merit indicators is useful.

For the evaluation in this paper it is assumed that a comparison of alternative technologies is helpful to identify the merits of CHP. However, the comparison of different technologies should not be confused by the application of different primary fuels. If a CHP plant is considered for operation on a specific primary fuel, the alternatives have to use the same fuel. Different fuels might require different combustion processes with quite different exergy losses (see Chapter 4). This might cause different fuel savings per unit generated heat. A correct comparison of the quality of plants requires the application of the same fuel. If CHP units on biomass are considered, their performance must be compared with reference plants for separate generation of electricity and heat using the same type of biomass. Only then, a true comparison of conversion technologies can be made. In the Netherlands the majority of CHP plants operate on natural gas. Therefore, only technologies based on natural gas are considered in this chapter.

The experiences with CHP in the Netherlands before 2000 have shown that the desired developments have not been achieved with inadequate regulations. Existing regulations in a number of countries are questionable with regard to their ability to achieve the highest contribution to fuel savings and reduction of CO<sub>2</sub> emissions as demonstrated in [7.17]. A comprehensive evaluation of the thermodynamic merits of CHP is necessary for further improvement of the related legislation. This paper focuses on the thermodynamic merits of CHP and results into the corresponding merit indicators. No attention is paid to additional aspects of legislative regulations.

The evaluations are made for one specific fuel (natural gas). Then, a reduction of fuel consumption will result in proportional savings of CO<sub>2</sub> emissions. And an indicator for relative fuel savings is also an indicator for the reduction of CO<sub>2</sub> emissions. The same is true if exergy efficiencies are considered. The exergy efficiency of a system is inversely proportional with the fuel consumption; the exergy efficiency can be considered also as an

## Chapter 7 Combined heat and power systems

indicator for the CO<sub>2</sub> emissions. Therefore, an additional evaluation of CO<sub>2</sub> emissions is only necessary if different fuels are considered.

All evaluations in this chapter are based on design conditions. The design conditions are primarily determining the thermodynamic performance during operation. The off-design behavior, the changes of electrical and heat efficiencies of CHP units, will not exactly be the same for different plant types. If it is expected that these differences can affect the comparison significantly, a more detailed evaluation considering the corresponding load duration curves might be necessary. However, a realistic evaluation of the actual plant performance requires a lot of work and is possible only if all relevant information is available (see Appendix 7.1).

Fuel cells are supposed to be attractive to reduce the thermodynamic losses of power generation in the future (e.g. [7.22] and [7.23]). For the near future fuel cells are considered frequently for CHP units (e.g. the papers [7.14], [7.4], [7.24], [7.25], [7.26], [7.11], [7.27], [7.12], [7.28], [7.13]). CHP units based on fuel cells (PEMFC, MCFC or SOFC) are expected to enable significant higher electrical efficiencies. The derivation of suitable merit indicators will be useful to check if these expectations are true.

If the performance of CHP has to be compared with alternative options for the generation of power and heat, also Heat Pumps have to be taken into account. The evaluation of Heat Pumps, however, would cause a serious extension of this paper. Therefore, only a few remarks are made were appropriate. It was stated in Chapter 2 and [7.29] that Heat Pumps primarily can be considered as an alternative in the case of low temperature heat generation. A rough evaluation of the long term national fuel consumption shows that the use of CHP for the generation of industrial heat and the use of Heat Pumps for the generation of low temperature heat will result into the highest fuel savings.

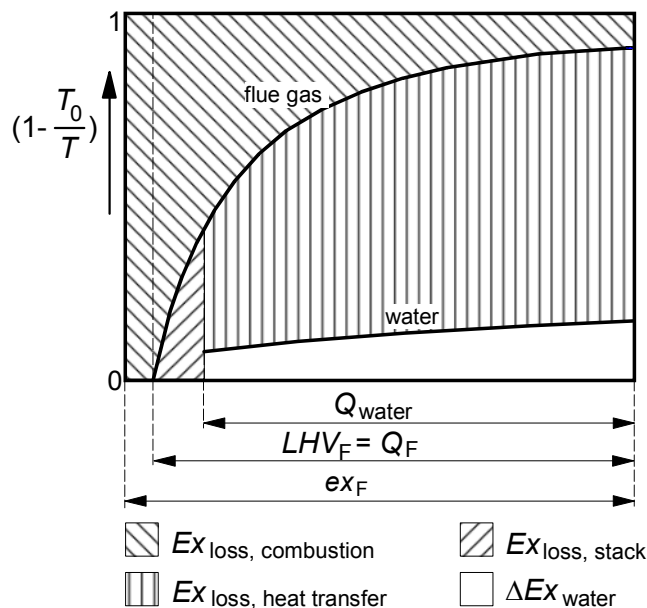


Figure 7.1 Value diagram of a hot water boiler

## 7.2 Thermodynamic aspects of CHP

### 7.2.1. How CHP can be useful

#### Exergy losses in boilers

The application of CHP makes it possible to reduce the total fuel consumption for the generation of power and heat. However, the extent of the fuel savings depends on the applied technologies and the design of the CHP plant. Heat is generated usually as hot water or steam in a fired boiler, depending on the required temperature level for final use. The poor thermodynamic performance of such boilers can be explained by the use of value diagrams as shown in Figure 7.1 and Figure 7.2. The condensation of water vapor is ignored in these

diagrams because of the use of the lower heating value. The area below the flue gas curve equals the exergy that can be obtained from the flue gas during cooling to the environmental temperature. The slantly shaded area above this curve represents the exergy lost during combustion. The slightly bent line at the bottom of the diagram in Figure 7.1 is the temperature curve of the heated water. The white area below this curve equals the exergy transferred to the water. The vertical shaded area represents the exergy loss due to heat transfer from the flue gas to the water. The flue gas is exhausted to the environment after cooling in the boiler at elevated temperature. The slantly shaded area below the flue gas curve represents the corresponding exergy loss, indicated as the stack loss. The exergy loss of the stack is usually smaller than the thermal loss of the stack. The diagram clearly shows that the exergy transferred to the water is only a small part (in general lower than 15%) of the fuel exergy. In the diagram only the thermodynamic losses (exergy losses) of the boiler are shown. If the final use of the heat is considered (i.e. space heating), additional losses caused by the heat transfer from water to air have to be taken into account. In that case the overall exergy efficiency is only a few percentage points, depending on the assumed room temperature and the temperature of the environment. Figure 7.2 shows that in the case of a steam boiler the higher exergy efficiencies are achieved because of the higher temperature of the steam. Industrial steam boilers usually generate saturated steam. Then, the exergy efficiency is primarily depending on the required steam pressure. Industrial steam boilers usually have exergy efficiencies around 30%. The generated steam is often used to transport heat to various final heat consumers. Figure 7.3 shows a specific value diagram in which also the final heat consumers are included. It will be clear that the overall exergy efficiency of the heat generating process strongly depends on the characteristics of the heat consumers and is in principle affected only by the thermal efficiency of the boiler.

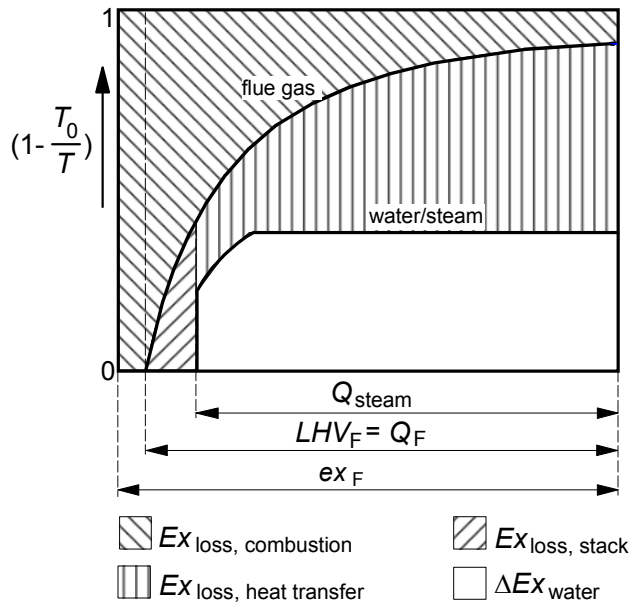


Figure 7.2 Value diagram of a steam boiler

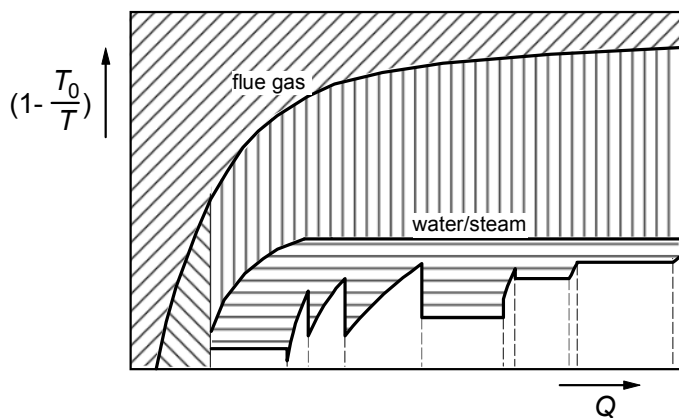


Figure 7.3 Value diagram of a steam boiler with heat consumers

Industrial steam boilers usually have exergy efficiencies around 30%. The generated steam is often used to transport heat to various final heat consumers. Figure 7.3 shows a specific value diagram in which also the final heat consumers are included. It will be clear that the overall exergy efficiency of the heat generating process strongly depends on the characteristics of the heat consumers and is in principle affected only by the thermal efficiency of the boiler.

## Chapter 7 Combined heat and power systems

The value diagrams obviously show the discrepancy between the thermal efficiencies (around 90%) and the exergy efficiencies (lower than 30%) of the boilers. Unfortunately, the exergy efficiencies represents the true thermodynamic efficiency.

<i>Table 7.1 Distinguished types of CHP (with regard to thermodynamic principles)</i>
<p><b>Systems using waste heat from power generation</b></p> <ul style="list-style-type: none"> <li>• internal combustion engines</li> <li>• gas turbines</li> <li>• Stirling engines</li> <li>• fuel cells</li> </ul>
<p><b>Systems that extract heat from power generation</b></p> <ul style="list-style-type: none"> <li>• steam turbine plants (extraction-condensation)</li> <li>• combined cycle plants (extraction-condensation)</li> </ul>

Options for combined generation of power and heat

From the preceding discussion it is obvious that heat generation with fired boilers has inherently low thermodynamic efficiencies. Higher efficiencies can be achieved only by applying alternative conversion technologies like Heat Pumps or the combined generation of heat and other products like power or chemicals. In this thesis only the combined generation of heat and other products like power or chemicals. In this thesis only the combined generation of power and heat is discussed. Two methods for the combined generation of power and heat can be distinguished, as shown in Table 7.1. Several power generating processes have to release heat to the environment at elevated temperatures. In the case of simple processes this heat is wasted. If the temperature of this is high enough the released heat can be used without affecting the power generating process. This is the case if residual heat from e.g. internal combustion engines, gas turbines, Stirling engines or fuel cells is used for the generation of

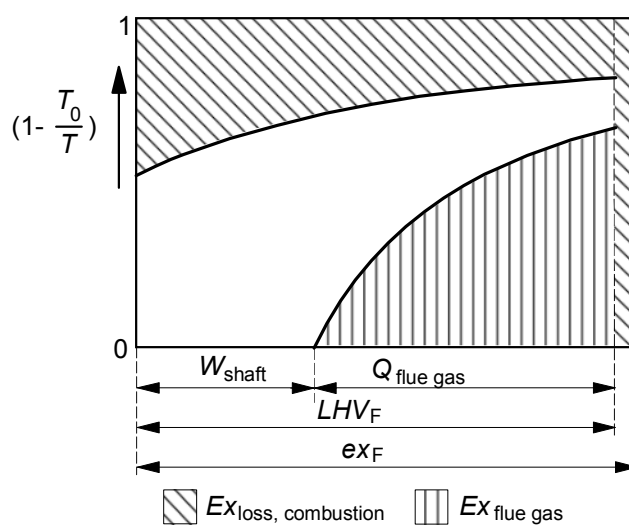


Figure 7.4 Value diagram of a gas turbine process

steam or hot water. However, the power to heat ratio of such CHP plants is almost fixed. If the generated heat does not match with the heat demand, additional heat is usually generated by auxiliary burners or boilers.

Otherwise, heat must be wasted.

Another category of CHP plants are able to replace a part of the generated power by heat generation. This is e.g. the case with steam turbine cycles.

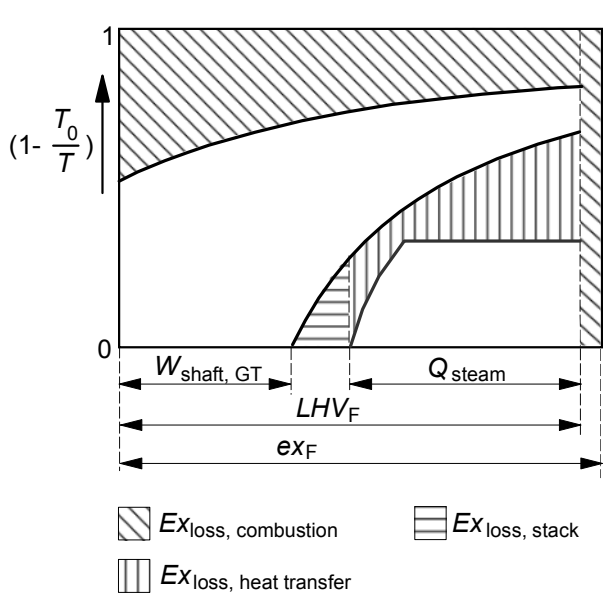
These cycles reject heat to the environment at temperatures close to environmental temperature. Because of the very low exergy, further use of this heat is not possible.

Heat rejection at higher temperatures

is possible by increasing the condensation pressure or by the condensation of extraction steam. In both cases useful heat can be generated, but as a consequence the generated power is reduced. The resulting power loss will be discussed later in this chapter. Extraction condensation turbines offer the possibility of a flexible power to heat ratio just by controlling the extracted steam flow.

Gas turbine processes and CHP

The value diagram of a gas turbine process is shown in Figure 7.4. For simplicity, the irreversibility's of compressor and expander are ignored in this diagram. The flue gas that



leaves the gas turbine contains roughly 25% of the exergy supplied by the fuel. Because of the high temperature of the turbine exhaust gas, gas turbines are often used in industry for the generation of saturated steam, as shown in the value diagram in Figure 7.5. Of course, the residual heat from the gas turbine process can be used also for the generation of hot water, but this will result in higher exergy losses. The steam pressure of industrial heating systems is usually not higher than 10 bar. Due to this pressure the exergy losses of heat transfer in the waste heat boiler are still significant. If the gas turbine process is used to generate the heat for the industrial heat demand as shown in Figure 7.3, the shaded areas shown in

Figure 7.5 Value diagram of a gas turbine with waste heat boiler

Figure 7.6 will represent the resulting exergy losses. The total exergy loss from flue gas to demanded heat is rather high. The generated power by the system considered in Figure 7.6 is relatively high. If the power generated by the gas turbine is higher than the demanded power, delivery of electricity to the grid can be considered. The economic feasibility of this option

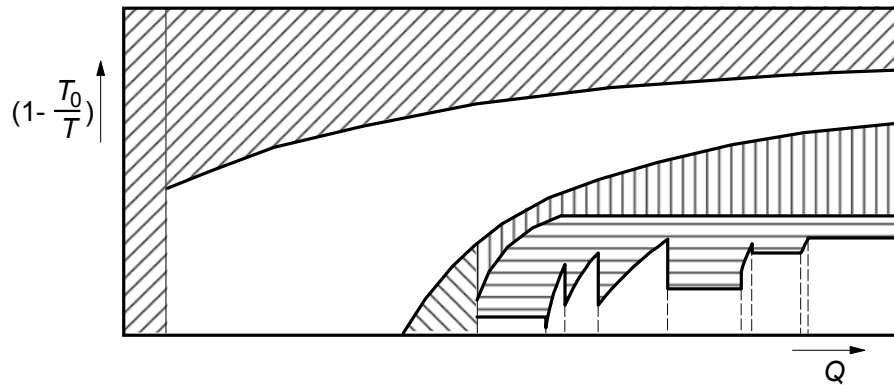


Figure 7.6 Value diagram of a GT cogeneration plant with heat consumers

## Chapter 7 Combined heat and power systems

depends on the prices of exported and imported electricity. In many cases a more appropriate solution is necessary. Further reduction of the exergy losses due to heat transfer in the waste heat boiler can be achieved by generating high pressure superheated steam for a steam turbine bottoming cycle. In large combined cycle plants, roughly 70-80% of the exergy from the exhaust gas can be transferred to the steam cycle [Chapter 5 or 7.1]. An example of the value diagram of a combined cycle plant with hot water generation for district heating is presented in Figure 7.7. This diagram shows obviously that the additional exergy losses of heat generation are very small. The generation of additional power decreases also the achievable heat to power ratio.

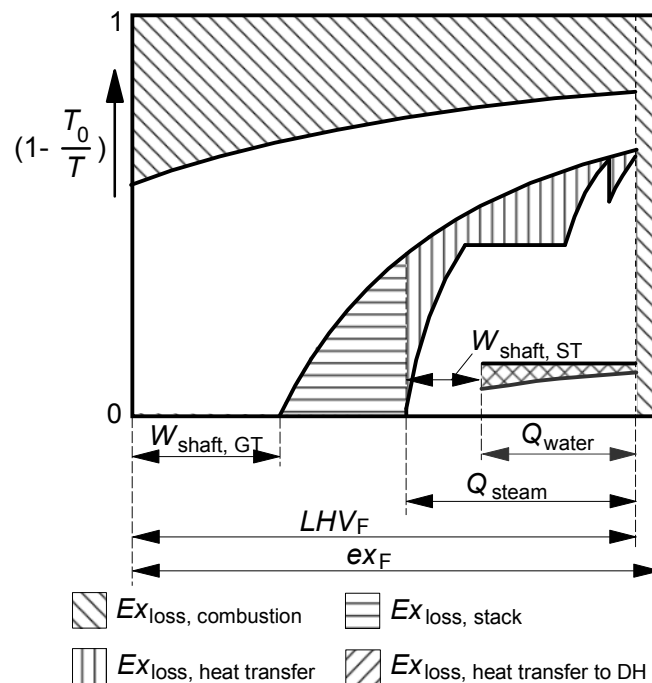


Figure 7.7 Value diagram of a combined cycle plant for district heating (DH)

#### Internal combustion engines and CHP

Large internal combustion engines (ICE) have usually thermal efficiencies of 40 to 50%. The remainder is rejected via the flue gas, cooling water, lubrication oil cooler and in the case of supercharged engines also the air cooler(s). ICEs have in general higher thermal efficiencies and somewhat lower exhaust gas temperatures than gas turbines. The temperature curves of the various fluids that transfer heat to the environment in the case of a large supercharged engine are shown in the value diagram of Figure 7.8. The diagram shows that a significant part of the residual heat is rejected by the oil cooler, supercharged air coolers (LT air and HT air) and the cooling water system. Therefore, the exergy content of the exhaust gas

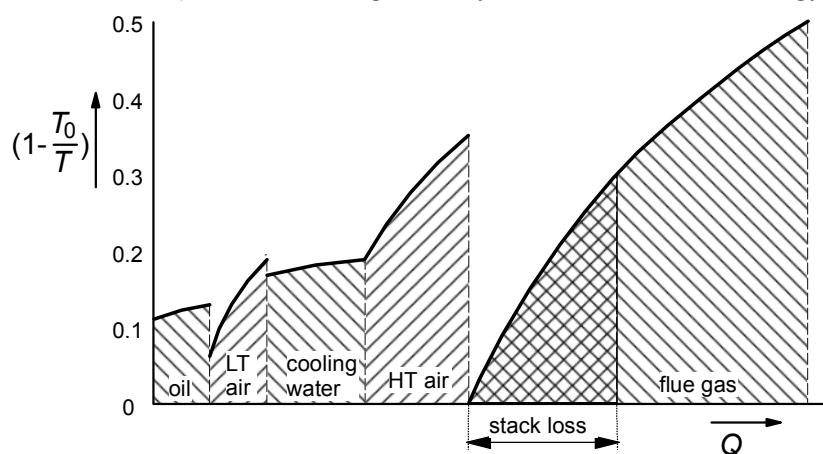


Figure 7.8 Value diagram of the residual heat from a large ICE (including stack loss)

relative low compared to the gas turbine. If the engine has to be used optimally for cogeneration, the heat from the available sources must be used in an appropriate way. It is obvious that not all heat from the flue gas can be used. It is assumed that the heat indicated as “stack loss” cannot be used.

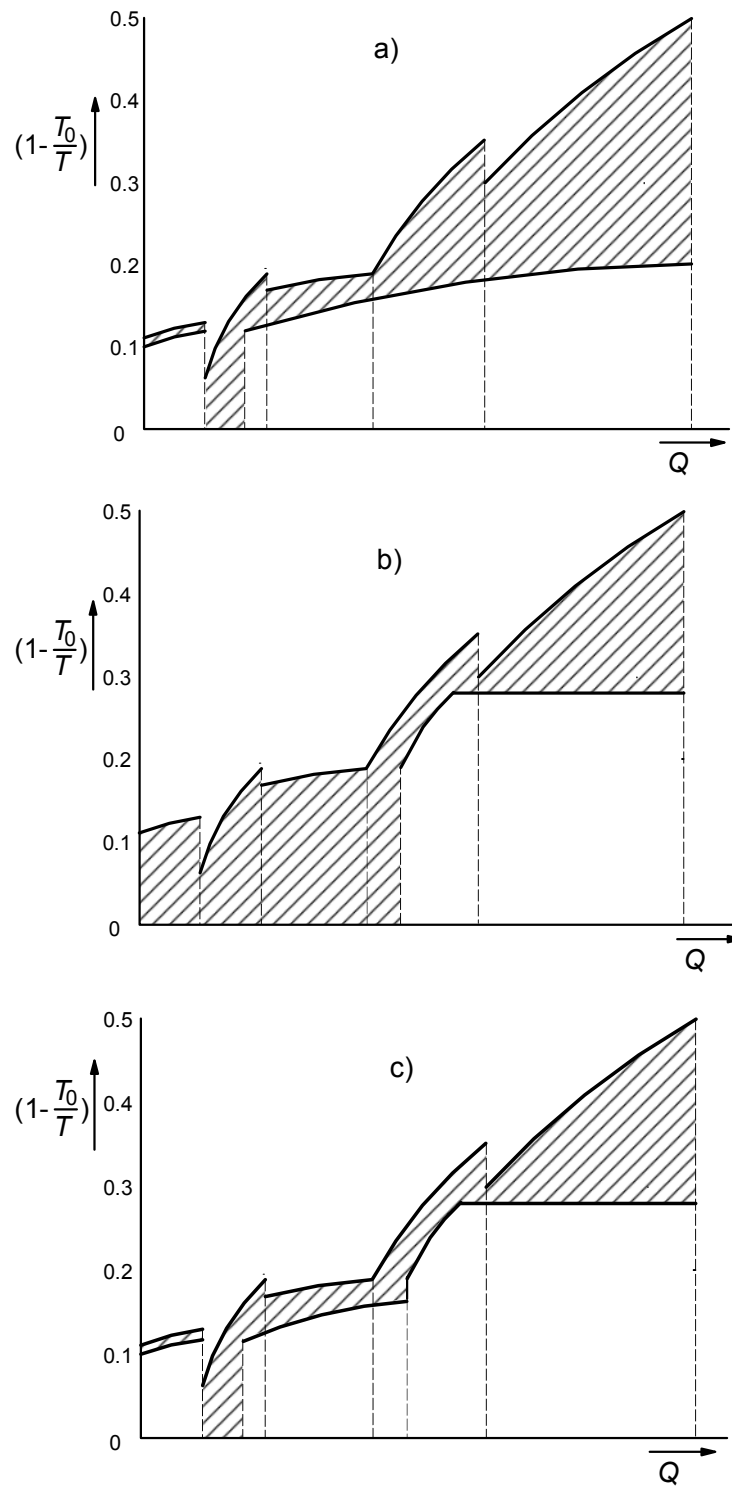


Figure 7.9 Value diagram of the residual heat from a large ICE

- a) Heat used for the generation of hot water
- b) Heat used for the generation of saturated steam
- c) Heat used for the generation of hot water and steam

## Chapter 7 Combined heat and power systems

The Figures 7.9a) and b) show how the available exergy can be used for the generation of hot water and saturated steam respectively. Apparently, both cases enable only limited use of the available exergy. The combined generation of hot water and saturated steam (see Figure 7.9c)) enables the use of most of the available exergy of the rejected heat. Of course, this solution is only useful if the generated heat matches the heat demand. As the system has to match three independent energy demands (electricity, HT heat and LT heat) the system management might cause specific problems.

*Table 7.2 Different types of CHP (with regard to application)*

### **Micro CHP (dwellings)**

- Internal combustion engine
- Stirling engine
- Fuel Cell plants

### **Small scale CHP (green houses, residential buildings)**

- Internal combustion engine

### **Industrial CHP**

- steam turbine (back pressure and extraction condensation)
- gas turbine with waste heat boiler
- combined cycle (back pressure and extraction condensation steam turbines)

### **District heating**

- steam turbine (extraction steam from large power stations)
- gas turbine with waste heat boiler
- combined cycle (extraction condensation)

### 7.2.2 CHP plants, a variety of applications

The combined production of heat and power is practiced in quite different plants from small scale to large scale, producing heat for different purposes. Plants are using different technologies for the conversion of fuel into power and heat. Table 7.2 shows a brief overview of possible applications. Micro CHP plants are proposed for the provision of residential energy demands. The plant size should enable the energy supply of single or multi-family dwellings. Electrical powers are in the range of 1 - 10 kW<sub>e</sub> [7.4], [7.30]. Micro CHP plants are supposed to replace the existing home heating systems for space heating and hot tap water. They will reduce the fuel consumption as well as the emission of greenhouse gases in the residential sector. Plants using small internal combustion engines are available commercially. However, application is hindered by the fact that it is not easy to match the generation of heat and electricity with the demands of a single dwelling. Economic feasibility is achieved in general only if various conditions regarding investment costs, customer behavior, load management, tariffs etc. are fulfilled. Recent developments have resulted in the demonstration and promotion of micro CHP plants based on Stirling engines and Fuel Cells (PEMFC and SOFC) (see e.g. [7.4], [7.11], [7.25] to [7.28]). Also the application of micro

turbines is considered. To simplify the match between power and heat demand micro-CHP plants can be combined with electrical driven Heat Pumps [7.20], [7.31]. A combined CHP/HP plant will be useful in particular if the electrical efficiency of the CHP plant is not too low. However, the economic feasibility of such plants might appear to be an obstacle, because they combine two types of systems that both are not easily accepted by the market at this moment. An important advantage of this type of systems is that they enable the application of electrical Heat Pumps without increasing the load of the electrical grid.

Small scale CHP is frequently used for the energy supply of greenhouses, hospitals, office buildings etc.. Internal combustion gas engines are dominating this application; these plants have relatively high electrical efficiencies and good overall efficiencies. Also gas turbines are used for small scale CHP, but are not very popular for this application. Heat is usually generated as hot water for space heating and hot tap water. Electrical powers can range from some 100 kW<sub>e</sub> up to 50 MW<sub>e</sub>.

Industrial use of CHP is very divers. The preferred technology depends on the history of the industrial site, the available heat sources and heat consumers. Large industries mainly use steam turbines, gas turbines and combined cycle plants. At large industrial plants, i.e. in the petrochemical industry, condensing steam turbines can be used for pure power production; but back pressure steam turbines are often used in parallel to expand high pressure steam efficiently to different pressure levels for a variety of heating purposes. The generation of power and heat can be highly integrated into the process plant. The application of gas turbines and combined cycles is mainly useful if little or no integration into the process plant is necessary. The temperature of the demanded industrial heat is in general higher than in the residential area. In many cases heat is generated as saturated steam at temperatures around 200°C. At large sites the condensate that remains after heat transfer to the heat consumers is not always returned to the boiler because of the large transport lines that are necessary.

District heating requires the availability of an expensive heat (hot water) distribution network. Therefore district heating is primarily feasible in densely populated areas and by using extended networks. Hot water can be supplied to the grid by several large power stations and auxiliary boilers. Usually steam from steam turbines or combined cycle plants is extracted for the generation of hot water. In some cases gas turbines with waste heat boilers are used. Extraction/condensation turbines are very flexible with regard to the generated heat and have a limited effect on the generated electrical power; the thermodynamic performance is good in particular if large modern combined cycle plants are applied. Water supply temperatures of district heating systems will range roughly from 80 to 120°C; return temperatures from 50 to 80°C. The actual operating temperatures are depending on the demanded heat capacity and the environmental temperature. During cold periods and high heat demands the temperature lift of the water is usually increased to raise the heat transport capacity of the grid.

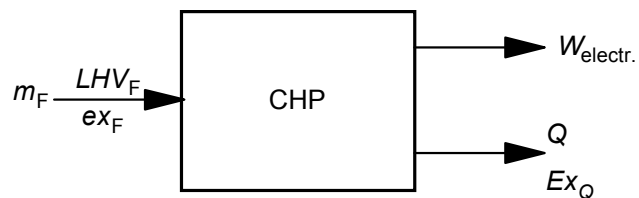


Figure 7.10 CHP system with input and outputs

### 7.3 Thermodynamic concepts for the evaluation of CHP

#### 7.3.1 The conversion of energy values of fuel and heat into exergy values

A CHP system generates two different products, heat and electricity. Heat can be generated in various ways, but in this paper only the generation of saturated steam and hot water are considered. The conditions of these fluids can vary depending on the demand. Figure 7.10 shows schematically the layout of a CHP system as used for the purpose of this evaluation. The fuel input of the CHP system can be characterized by an amount of fuel  $m_{F, \text{CHP}}$  and a heating value  $LHV_F$  or specific exergy value  $ex_F$  of the fuel. The lower heating value is actually not really appropriate for this purpose but it is generally used in Western Europe. The specific exergy of the fuel is necessary in the case of exergy calculations. The difference with the lower heating value is limited and is expressed as the exergy factor of the fuel  $f_{ex, F}$ , thus:

$$ex_F = f_{ex, F} \cdot LHV_F \quad (f_{ex, F} \text{ has roughly a value of 1.04 in case of natural gas}) \quad (7.1)$$

Electricity can be converted in principle completely into work, which means that the exergy of electricity is the same as the energy. However, the exergy of heat differs in general strongly from the energy value. If heat is transferred from a system by cooling a fluid flow, the relation between heat and exergy is defined by the following equations:

$$Ex_Q = \left(1 - \frac{T_0}{\bar{T}}\right) \cdot Q = f_{ex, Q} \cdot Q \quad \text{with} \quad f_{ex, Q} = 1 - \frac{T_0}{\bar{T}} \quad (7.2)$$

The temperature  $\bar{T}$  = the thermodynamic equivalent temperature of heat transfer from the system, and can be calculated if the fluid properties before and after heat transfer are known:

$$\bar{T} = \frac{h_2 - h_1}{s_2 - s_1} \quad (7.3)$$

Temperature  $T_0$  is the temperature of the environment. The choice of an appropriate value for this temperature is not always easy in the case of low temperature heating systems. The same equations can be used for the heat transfer to a system. Table 7.3 shows the efficiencies that

thermal efficiencies		exergy efficiencies
$\eta_{\text{th, electr}} = \frac{W_{\text{electr}}}{m_F \cdot LHV_F}$	electrical efficiency	$\eta_{\text{ex, electr}} = \frac{Ex_{\text{electr}}}{m_F \cdot ex_F}$
$\eta_{\text{th, Q}} = \frac{Q}{m_F \cdot LHV_F}$	heat efficiency	$\eta_{\text{ex, Q}} = \frac{Ex_Q}{m_F \cdot ex_F}$
$\eta_{\text{th, total}} = \frac{W_{\text{electr}} + Q}{m_F \cdot LHV_F}$	total efficiency	$\eta_{\text{ex, total}} = \frac{Ex_{\text{electr}} + Ex_Q}{m_F \cdot ex_F}$

are normally used to characterize CHP systems. Both, thermal efficiencies and exergy efficiencies are presented in order to emphasize the differences between these two kinds of efficiencies. From Equations 7.2 and 7.3 it is obvious that the difference between the exergy efficiency and thermal efficiency of heat will be higher than the difference between the

electrical efficiencies. And, because of the high difference between the heat efficiencies, also the total efficiencies will differ seriously.

### 7.3.2 Lost power and generated heat in the case of thermal power cycles with elevated temperatures of heat rejection (e.g. back pressure steam cycles)

Thermal power cycles with heat rejection temperatures close to the environmental temperature, like steam cycles, are often used for CHP plants. Then, an increase of the heat rejection temperature is required to enable heat delivery at an appropriate temperature level. This is applied e.g. in back pressure steam cycles. In Figure 7.11 two different thermal power cycles are presented schematically;

- case a) shows a power cycle for maximum power generation; the temperature of the rejected heat is too low for useful application
- case b) shows a power cycle with elevated heat rejection temperature  $\bar{T}''_C$ ; the heat from this cycle  $Q''_C$  can be used for heating purposes.

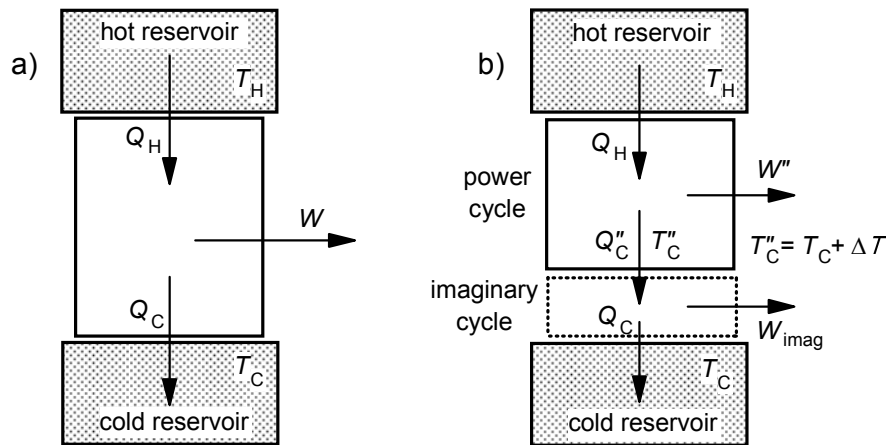


Figure 7.11 Thermal power cycles  
a) for maximum power generation,  
b) with elevated  $T_C$  for CHP

The elevated heat rejection temperature will cause a reduction of the generated power. Assuming that the temperatures of the hot and cold reservoirs and the amounts of heat ( $Q_H$ ) to the power cycles are the same for both cases, the power loss in comparison with the original cycle can be estimated as follows. The work generated by a real (irreversible) thermal power cycle can be calculated using the following equation:

$$W_{\text{irrev}} = \eta_{\text{ex, intern}} \cdot \left(1 - \frac{\bar{T}_C}{\bar{T}_H}\right) \cdot Q_H \quad (7.4)$$

In this equation the temperatures of heat transfer to and from the cycle are written as thermodynamic equivalent temperatures. The internal exergy efficiency of the thermal power cycle is defined as the ratio of the work from the actual (irreversible) power cycle and the work from a reversible power cycle using the same heat reservoirs:

$$\eta_{ex, intern} = \frac{W_{irrev}}{W_{rev}} \quad (7.5)$$

This efficiency is used to indicate the level of irreversibility of the power cycle. To estimate the effect of the elevated heat rejection temperature on the work generated by the power cycle, it is assumed that the internal exergy efficiency is the same for the cases a) and b). If  $\Delta T = \bar{T}''_C - \bar{T}_C$ , the work generated by the cycle with elevated rejection temperature is:

$$W'' = \eta_{ex, intern} \cdot Q_H \cdot \left(1 - \frac{\bar{T}_C + \Delta T}{\bar{T}_H}\right) \quad (7.6)$$

Then, the difference (= lost power due to heat generation) is (Equation 7.4 minus Equation 7.5):

$$\Delta W = W_{irrev} - W'' = \eta_{ex, intern} \cdot Q_H \cdot \frac{\Delta T}{\bar{T}_H} \quad (7.7)$$

The useful heat generated by the power cycle can be calculated from the energy balance of the power cycle:

$$Q''_C = Q_C + \eta_{ex, intern} \cdot Q_H \cdot \frac{\Delta T}{\bar{T}_H} \quad \text{with: } Q_C = Q_H \cdot \left\{1 - \eta_{ex, intern} \cdot \left(1 - \frac{\bar{T}_C}{\bar{T}_H}\right)\right\} \quad (7.8)$$

The lost power and generated heat are linear relations of the heat transferred to the cycle. With Equations 7.4 and 7.7, the lost power and the generated heat can easily be written as fractions of  $Q_H$ . It must be emphasized that these equations should be used only for first approximations. The assumption that  $\eta_{ex, intern}$  is the same for the two cases is not really true, in particular not if the temperature difference between the original temperature of heat rejection and the elevated temperature is high.

### 7.3.3 The power loss ratio in the case of steam cycles with steam extraction

The use of extraction steam from a condensing steam turbine will result in a CHP system with controllable heat generation. Steam turbines can be build such that all steam that

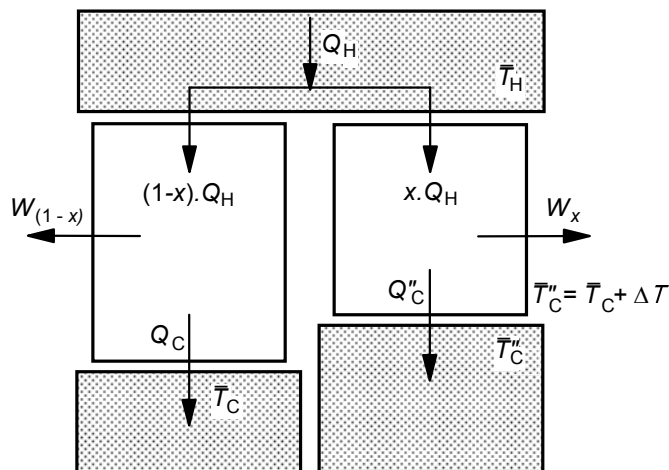


Figure 7.12 Thermal power cycle with heat extraction

enters the turbine can be extracted for heat generation. If no heat is demanded, the full steam flow will expand till condenser pressure and is used for the generation of power. Therefore, extraction condensation units are highly flexible with regard to the generated heat and are attractive for district heating systems with fluctuating heat demands. High efficiencies can be achieved by applying large combined cycle plants. The extraction of steam for heat generation will result in a decrease

of the work generated by the power cycle. The power loss ratio  $K_{\text{power loss}}$  is used to indicate the loss of work per unit generated (useful) heat. Thus:

$$K_{\text{power loss}} = \frac{\Delta W}{Q} \quad (7.9)$$

For the purpose of not very accurate exploring calculations the power generating system can be split in two cycles with the same temperature of heat transfer to the cycle but with different temperatures of heat transfer from the cycle, as shown in Figure 7.12. It is assumed again that the internal exergy efficiency will be the same if the temperature of heat transfer from the cycle is elevated. Then, the total work generated by the two cycles is written as:

$$W_{\text{total}} = W_{1-x} + W_x = \eta_{\text{ex, intern}} \cdot \left[ (1-x) \cdot Q_{\text{H}} \cdot \left( 1 - \frac{\bar{T}_{\text{C}}}{\bar{T}_{\text{H}}} \right) + x \cdot Q_{\text{H}} \cdot \left( 1 - \frac{\bar{T}''_{\text{C}}}{\bar{T}_{\text{H}}} \right) \right] \quad (7.10)$$

The maximum work from the system, with  $x = 0$  is:

$$W_{\text{max}} = \eta_{\text{ex, intern}} \cdot Q_{\text{H}} \cdot \left( 1 - \frac{\bar{T}_{\text{C}}}{\bar{T}_{\text{H}}} \right) \quad (7.11)$$

The work lost by the generation of heat is the difference between the maximum work and the actual work from the system:

$$\Delta W = W_{\text{max}} - W_{\text{total}} = \eta_{\text{ex, intern}} \cdot x \cdot Q_{\text{H}} \cdot \left( \frac{\Delta T}{\bar{T}_{\text{H}}} \right) \quad (7.12)$$

For the generated heat  $Q''_{\text{C}}$  the following equation can be derived:

$$Q''_{\text{C}} = x \cdot Q_{\text{H}} - W_x = x \cdot Q_{\text{H}} \cdot \left[ 1 - \eta_{\text{ex, intern}} \cdot \left( 1 - \frac{\bar{T}_{\text{C}} + \Delta T}{\bar{T}_{\text{H}}} \right) \right] \quad (7.13)$$

Then, the power loss ratio can be determined using Equations (7.12) and (7.13):

$$K_{\text{power loss}} = \frac{\Delta W}{Q''_{\text{C}}} = \frac{\eta_{\text{ex, intern}} \cdot \Delta T}{\bar{T}_{\text{H}} (1 - \eta_{\text{ex, intern}}) + \eta_{\text{ex, intern}} \cdot (\bar{T}_{\text{C}} + \Delta T)} \quad (7.14)$$

From this equation it is obvious that the power loss ratio decreases if the temperature of heat transfer to the cycle increases or if the temperature difference  $\Delta T$  decreases. The power loss ratio can be used e.g. to compare the performance of CHP plants with electrical driven heat pumps. The coefficient of performance ( $COP$ ) of electrical driven heat pumps is defined as:

$$COP = \frac{Q}{W} \quad (7.15)$$

This is actually the inverse of the power loss ratio. The inverse of the power loss ratio gives the quantity of heat that will be obtained per unit lost power. This value can directly be compared with the  $COP$  of heat pumps.

#### 7.3.4 The efficiency of a reference system

The fuel savings of a CHP plant compared to separate generation can be determined by comparing the efficiencies of the two options as shown schematically in Figure 7.13. The efficiency of separate generation must be determined for a system, consisting of a reference power station and a reference boiler, that generates the same quantities of power and heat as the CHP plant. The total exergy efficiency of separate generation can be written as:

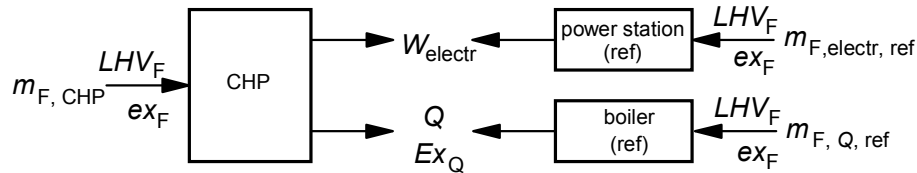


Figure 7.13 CHP system with systems for separate generation

$$\eta_{ex, ref} = \frac{W_{electr} + Ex_Q}{(m_{F, electr, ref} + m_{F, Q, ref}) \cdot ex_F} \quad (7.16)$$

Since:  $W_{electr} = \eta_{ex, electr, CHP} \cdot m_{F, CHP} \cdot ex_F = \eta_{ex, electr, ref} \cdot m_{F, electr, ref} \cdot ex_F$

it appears that:  $\frac{m_{F, electr, ref}}{m_{F, CHP}} = \frac{\eta_{ex, electr, CHP}}{\eta_{ex, electr, ref}}$

And since:  $Ex_Q = \eta_{ex, Q, CHP} \cdot m_{F, CHP} \cdot ex_F = \eta_{ex, Q, ref} \cdot m_{F, Q, ref} \cdot ex_F$

it appears that:  $\frac{m_{F, Q, ref}}{m_{F, CHP}} = \frac{\eta_{ex, Q, CHP}}{\eta_{ex, Q, ref}}$

Combining these results with Equation 7.16 gives the following equation for exergy efficiency of the reference system:

$$\eta_{ex, ref} = \frac{\frac{\eta_{ex, electr, CHP}}{\eta_{ex, electr, ref}} + \frac{\eta_{ex, Q, CHP}}{\eta_{ex, Q, ref}}}{\frac{\eta_{ex, electr, CHP}}{\eta_{ex, electr, ref}} + \frac{\eta_{ex, Q, CHP}}{\eta_{ex, Q, ref}}} \quad (7.17)$$

The total exergy efficiency of the reference system (separate generation) can be easily calculated with this equation if the exergy efficiencies of the CHP plant and the reference plants for separate generation are known. The overall thermal efficiencies of separate generation for comparison with the respective CHP plants can be derived in the same way, and results into the following equation:

$$\eta_{th, ref} = \frac{\frac{\eta_{th, electr, CHP}}{\eta_{th, electr, ref}} + \frac{\eta_{th, Q, CHP}}{\eta_{th, Q, ref}}}{\frac{\eta_{th, electr, CHP}}{\eta_{th, electr, ref}} + \frac{\eta_{th, Q, CHP}}{\eta_{th, Q, ref}}} \quad (7.18)$$

## 7.4 Merit indicators

### 7.4.1 Options to indicate the thermodynamic merits of CHP

Various concepts can be used to indicate the thermodynamic quality of energy conversion processes. A general used concept is the comparison of the actual process with the ideal case, considering conversion without losses. This concept results in the definition of the generally used efficiencies. A perfect system with regard to its thermodynamic performance is a system with no irreversibility's. It has been emphasized before that the thermal efficiency is not a true thermodynamic efficiency; a system with high thermal efficiency still can have considerable irreversibility's as explained in Section 7.2. The exergy efficiency of a plant represents the true thermodynamic quality of the energy conversion.

Another option to indicate the thermodynamic quality of energy conversion processes is the comparison with a reference system. An obvious choice in the case of CHP is the comparison with the separate generation of the same quantities of heat and electricity in respectively a reference boiler and a reference power plant. The comparison of the fuel consumption of the CHP with the quantity of fuel needed for the generation by the reference plants indicates clearly the improvement that can be achieved by the application of CHP. Since:

$$W_{\text{electr}} + Ex_Q = \eta_{\text{ex, ref}} \cdot m_{\text{F, ref}} \cdot ex_{\text{F}} = \eta_{\text{ex, CHP}} \cdot m_{\text{F, CHP}} \cdot ex_{\text{F}} \quad (7.19)$$

it appears that the ratio of the fuel consumption of the CHP and the reference system is the same as the inverse ratio of the total exergy efficiencies. However, a similar equation can be written for the energy balances of the CHP and the reference system:

$$W_{\text{electr}} + Q = \eta_{\text{th, ref}} \cdot m_{\text{F, ref}} \cdot LHV_{\text{F}} = \eta_{\text{th, CHP}} \cdot m_{\text{F, CHP}} \cdot LHV_{\text{F}} \quad (7.20)$$

Thus, it appears that:

$$F_{\text{fuel ratio}} = \frac{m_{\text{F, CHP}}}{m_{\text{F, ref}}} = \frac{\eta_{\text{ex, ref}}}{\eta_{\text{ex, CHP}}} = \frac{\eta_{\text{th, ref}}}{\eta_{\text{th, CHP}}} \quad (7.21)$$

The fuel ratio of the CHP system and the reference system represents the relative reduction of the fuel needed for the generation of the considered quantities of heat and electricity. The relative fuel savings are calculated with the following equation:

$$F_{\text{fuel savings}} = 1 - F_{\text{fuel ratio}} = 1 - \frac{m_{\text{F, CHP}}}{m_{\text{F, ref}}} = 1 - \frac{\eta_{\text{ex, ref}}}{\eta_{\text{ex, CHP}}} = 1 - \frac{\eta_{\text{th, ref}}}{\eta_{\text{th, CHP}}} \quad (7.22)$$

The fuel savings factor,  $F_{\text{fuel savings}}$ , is an important merit indicator, because it shows the percentage of the fuel that will be saved by applying CHP and at the same time it presents the percentage reduction of CO<sub>2</sub> emissions. The selection of an appropriate reference system is of main importance to determine realistic values.

The fuel savings factor, however, does not consider the wider system in which the CHP plant has to operate. In general a CHP plant will be part of a larger system (e.g. an industrial plant or a national power supply system) and the design of the CHP plant should be such that it provides the highest benefit for the total system. In the Netherlands, like in most Western European countries, the total yearly heat demand of industry and residential sector is much higher than the total yearly electricity demand. In 1990 the total heat demand was roughly 5 times the total electricity demand. Since then, the electricity consumption is steadily increasing, but today the total heat demand is still 3 to 4 times higher than the total electricity demand. Thus, the heat to power ratio of the demand is much higher than the heat to power demand of usual CHP plants. This means that, even if all electricity is generated by CHP plants, these plants will generate only a limited part of the total heat demand. Consequently, the total installed CHP power is limited by the total electricity demand. In this situation not just the “fuel savings” but the “fuel savings per unit electricity” must be considered to achieve the maximum benefit from CHP for the national power supply system. Therefore, it is useful to know what kind of CHP plants will give the highest “fuel savings per unit electricity”. The growing contribution of wind turbines and photovoltaic generators will limit further the available potential for application of CHP. This emphasizes the need to focus also in the future on the “fuel savings per unit electricity” if CHP is applied to reduce the national fuel

## Chapter 7 Combined heat and power systems

consumption as well as CO<sub>2</sub> emissions. A dimension free quantity for such a factor can be obtained if the “fuel energy savings per unit electricity” or the “fuel exergy savings per unit electricity” are determined. The values for these two factors will be slightly different, but they will result into the same ranking of CHP units. The difference between the two factors equals just the exergy factor of the fuel. The two factors are defined as follows:

The “fuel energy savings per unit electricity”:

$$F_{\text{FESUE}} = \frac{\Delta m_{\text{F}} \cdot LHV_{\text{F}}}{W_{\text{electr, CHP}}} = \frac{(m_{\text{F, ref}} - m_{\text{F, CHP}}) \cdot LHV_{\text{F}}}{\eta_{\text{th, electr, CHP}} \cdot LHV_{\text{F}} \cdot m_{\text{F, CHP}}} \quad (7.23)$$

The “fuel exergy savings per unit electricity”:

$$F_{\text{FExSUE}} = \frac{\Delta m_{\text{F}} \cdot ex_{\text{F}}}{W_{\text{electr, CHP}}} = \frac{(m_{\text{F, ref}} - m_{\text{F, CHP}}) \cdot ex_{\text{F}}}{\eta_{\text{ex, electr, CHP}} \cdot ex_{\text{F}} \cdot m_{\text{F, CHP}}} \quad (7.24)$$

With the use of Equation 7.21 the Equations 7.23 and 7.24 can be converted into:

$$F_{\text{FESUE}} = \frac{\eta_{\text{th, CHP}} - \eta_{\text{th, ref}}}{\eta_{\text{th, ref}} \cdot \eta_{\text{th, electr, CHP}}} \quad (7.25)$$

$$F_{\text{FExSUE}} = \frac{\eta_{\text{ex, CHP}} - \eta_{\text{ex, ref}}}{\eta_{\text{ex, ref}} \cdot \eta_{\text{ex, electr, CHP}}} \quad (7.26)$$

The CHP system with the highest value of the fuel energy savings (or fuel exergy savings) per unit electricity will enable the highest fuel savings of the total system if the maximum possible CHP power is installed. This indicator shows a somewhat different preference than the relative fuel savings, as will be demonstrated in the next section. The fuel savings factor ( $F_{\text{fuel savings}}$ ) and the “fuel energy savings per unit electricity” factor ( $F_{\text{FESUE}}$ ) are considered to be the most useful merit indicators if CHP plants are applied to reduce fuel consumption and CO<sub>2</sub> emissions. Only these two indicators are used in the next section for the evaluation of the effects of various plant parameters.

In addition to the indicators discussed so far, other indicators are conceivable or have been used. The fuel savings per unit electricity are supposed to be the appropriate indicator if the application of CHP is limited by the electricity demand of the wider system to which the CHP plant belongs. In the case that the application of CHP is limited by the total heat demand of the wider system, the fuel savings per unit generated heat will be the appropriate indicator. This somewhat unusual situation can occur e.g. in an industrial plant with a relatively low heat demand. A dimension free indicator can be achieved by determining the “fuel energy savings per unit heat” or the “fuel exergy savings per unit heat exergy”.

The “fuel energy savings per unit heat” ( $F_{\text{FESUQ}}$ ) is defined as:

$$F_{\text{FESUQ}} = \frac{\Delta m_{\text{F}} \cdot LHV_{\text{F}}}{Q_{\text{CHP}}} = \frac{(m_{\text{F, ref}} - m_{\text{F, CHP}}) \cdot LHV_{\text{F}}}{\eta_{\text{th, Q, CHP}} \cdot LHV_{\text{F}} \cdot m_{\text{F, CHP}}} \quad (7.27)$$

And the “fuel exergy savings per unit heat exergy” ( $F_{\text{FExSUEXQ}}$ ) as:

$$F_{\text{FExSUEXQ}} = \frac{\Delta m_{\text{F}} \cdot ex_{\text{F}}}{Ex_{\text{Q, CHP}}} = \frac{(m_{\text{F, ref}} - m_{\text{F, CHP}}) \cdot ex_{\text{F}}}{\eta_{\text{ex, Q, CHP}} \cdot ex_{\text{F}} \cdot m_{\text{F, CHP}}} \quad (7.28)$$

With the use of Equation 7.21 the Equations 7.27 and 7.28 can be converted into:

$$F_{\text{FESUQ}} = \frac{\eta_{\text{th, CHP}} - \eta_{\text{th, ref}}}{\eta_{\text{th, ref}} \cdot \eta_{\text{th, Q, CHP}}} \quad (7.29)$$

$$F_{\text{FExSUExQ}} = \frac{\eta_{\text{ex, CHP}} - \eta_{\text{ex, ref}}}{\eta_{\text{ex, ref}} \cdot \eta_{\text{ex, Q, CHP}}} \quad (7.30)$$

Further options for merit indicators are the “assigned heat efficiency” and the “assigned electric efficiency”. It has been mentioned before that the application CHP is useful in general because of the very low thermodynamic efficiency of heat generation in conventional boilers. That suggests that heat can be generated more efficient using a CHP plant. To determine the efficiency of heat generation by a CHP plant, it is necessary to assign the fuel quantities necessary for the generation of power and heat respectively. Assuming that the electricity generated by the CHP plant could have been generated by the reference power plant, the fuel assigned to the generated electricity is supposed to be the same as the fuel necessary for the generation of this electricity by a reference power plant. The remainder of the fuel is the fuel assigned to the generation of heat. The “assigned heat exergy efficiency” ( $\eta''_{\text{ex, Q, CHP}}$ ) is defined as:

$$\eta''_{\text{ex, Q, CHP}} = \frac{Ex_Q}{m''_{\text{F, CHP, Q}} \cdot ex_{\text{F}}} \quad (7.31)$$

with:  $m''_{\text{F, CHP, Q}} = m_{\text{F, CHP}} - m_{\text{F, electr, ref}}$

Equation 7.31 can be converted into Equation 7.32 by replacing the masses by efficiencies as shown before:

$$\eta''_{\text{ex, Q, CHP}} = \frac{\eta_{\text{ex, electr, ref}} \cdot \eta_{\text{ex, Q, CHP}}}{\eta_{\text{ex, electr, ref}} - \eta_{\text{ex, electr, CHP}}} \quad (7.32)$$

The relative efficiency improvement will be found if this efficiency is divided by  $\eta_{\text{ex, Q, ref}}$ , the exergy efficiency of heat generation by the reference boiler. A similar equation will be found if thermal efficiencies are used instead of exergy efficiencies. The resulting “assigned heat thermal efficiency”, however, is basically not an efficiency because values much higher than 1.0 are achievable. Because of the similarity with absorption heat pumps, it can be called the “assigned *COP*”. As the relative improvement of the “assigned *COP*” is the same as the relative improvement of the “assigned heat exergy efficiency”, the “assigned *COP*” is not considered in the evaluation further.

The “assigned electric efficiency” can be determined by assuming that the heat from the CHP plant is generated with the same efficiency as the heat in the reference boiler. The difference in fuel consumption of the CHP plant and the reference boiler is assumed to be the fuel consumption for the generated electricity. Then, the “assigned electric exergy efficiency” ( $\eta''_{\text{ex, electr, CHP}}$ ) is defined as:

$$\eta''_{\text{ex, electr, CHP}} = \frac{W_{\text{electr}}}{m''_{\text{F, CHP, electr}} \cdot ex_{\text{F}}} \quad (7.33)$$

with:  $m''_{\text{F, electr, CHP}} = m_{\text{F, CHP}} - m_{\text{F, Q, ref}}$

This will finally result into:

## Chapter 7 Combined heat and power systems

$$\eta''_{ex, electr, CHP} = \frac{\eta_{ex, Q, ref} \cdot \eta_{ex, electr, CHP}}{\eta_{ex, Q, ref} - \eta_{ex, Q, CHP}} \quad (7.34)$$

For the further evaluation of merit indicators only the assigned exergy efficiencies will be used.

<i>Table 7.4 Properties and results of various CHP systems</i>						
CHP	IND. GT + WHB	IND. CC	ICE + WHB	L-ICE + WHB	CC/DH	micro-CHP
<b>thermal efficiencies</b>						
$\eta_{th, electr, CHP}$	0.327	0.450	0.308	0.427	0.452	0.260
$\eta_{th, Q, CHP}$	0.468	0.240	0.564	0.434	0.395	0.630
$\eta_{th, total, CHP}$	0.795	0.690	0.872	0.861	0.847	0.890
heat/power ratio	1.43	0.53	1.83	1.02	0.87	2.42
<b>exergy efficiencies</b>						
$\eta_{ex, electr, CHP}$	0.313	0.431	0.295	0.409	0.433	0.249
$\eta_{ex, Q, CHP}$	0.155	0.088	0.078	0.061	0.074	0.093
$\eta_{ex, total, CHP}$	0.468	0.519	0.373	0.470	0.507	0.342
heat exergy factor ( $f_{ex, Q}$ )	0.331	0.367	0.138	0.141	0.187	0.148
<b>SEPARATE PRODUCTION (reference case)</b>						
<b>thermal efficiencies</b>						
$\eta_{th, electr, ref}$	0.550	0.550	0.550	0.550	0.550	0.550
$\eta_{th, Q, ref}$	0.900	0.900	0.950	0.950	0.950	0.950
$\eta_{th, total, ref}$	0.713	0.636	0.756	0.698	0.684	0.784
<b>exergy efficiencies</b>						
$\eta_{ex, electr, ref}$	0.527	0.527	0.527	0.527	0.527	0.527
$\eta_{ex, Q, ref}$	0.298	0.330	0.131	0.134	0.178	0.140
$\eta_{ex, total, ref}$	0.420	0.478	0.323	0.381	0.410	0.301
<b>MERIT INDICATORS CHP</b>						
$F_{fuel\ savings} = 1 - F_{fuel\ ratio}$	0.103	0.078	0.133	0.189	0.192	0.120
$F_{FESUE}$	0.350	0.189	0.499	0.546	0.526	0.523
IND. GT + WHB	= industrial gas turbine with waste heat boiler					
IND. CC	= industrial combined cycle					
ICE +WHB	= internal combustion engine with waste heat boiler					
L-ICE +WHB	= large internal combustion engine with waste heat boiler					
CC/DH	= combined cycle plant with steam extraction for district heating					
Micro-CHP	= very small internal combustion engine with waste heat boiler					

*Table 7.5 Comparison of the various merit indicators*

CHP	IND. GT + WHB	IND. CC	ICE + WHB	L-ICE + WHB	CC/DH	micro-CHP
<b>Total efficiencies</b>						
$\eta_{th, total, CHP}$	0.795	0.690	0.872	0.861	0.847	0.890
$\eta_{ex, total, CHP}$	0.468	0.519	0.373	0.470	0.507	0.342
<b>Fuel ratio and fuel savings</b>						
$F_{fuel\ ratio} = \frac{\Phi_{m, F, CHP}}{\Phi_{m, F, ref}}$	0.897	0.922	0.867	0.811	0.808	0.880
$F_{fuel\ savings} = 1 - F_{fuel\ ratio}$	0.103	0.078	0.133	0.189	0.192	0.120
<b>Savings per unit electricity</b>						
$F_{FESUE}$	0.350	0.189	0.499	0.546	0.526	0.523
$F_{FEXSUE}$	0.366	0.197	0.521	0.570	0.549	0.546
<b>Savings per unit heat or heat exergy</b>						
$F_{FESUQ}$	0.245	0.354	0.272	0.537	0.602	0.216
$F_{FEXSUEXQ}$	0.739	0.964	1.970	3.823	3.211	1.461
<b>Assigned exergy efficiencies</b>						
$\eta''_{ex, Q, CHP}$	0.382	0.484	0.177	0.273	0.415	0.176
$\eta''_{ex, Q, CHP} / \eta''_{ex, Q, ref}$	1.283	1.467	1.349	2.043	2.334	1.258
$\eta''_{ex, electr, CHP}$	0.653	0.588	0.726	0.753	0.741	0.739
$\eta''_{ex, electr, CHP} / \eta''_{ex, electr, ref}$	1.239	1.116	1.378	1.429	1.407	1.403

#### 7.4.2 Comparison of some arbitrarily chosen CHP systems

The thermodynamic merit indicators derived before can be demonstrated by comparing some CHP plants as presented in Table 7.4. The plants are defined by their electricity and heat efficiencies. Thermal efficiencies as well as the corresponding exergy efficiencies are shown. In Table 7.4 data are presented for six arbitrarily chosen plants. The first two are plants generating saturated steam for industrial heating purposes. The other four are generating hot water for the delivery of residential heat. The data are taken from different sources describing real systems and are chosen to show the usefulness of the considered merit indicators. They do not indicate the present status of the considered technologies. To define the fuel savings achieved by the application of CHP, the performance of the CHP plants is compared with a reference system consisting of conventional (separate) generation. It is supposed that the reference system generates the same quantities of electricity and heat as the CHP plant and that it uses the same primary fuel (natural gas). Different efficiency values can be chosen for the reference system depending on the objectives of the evaluation. For the purpose of this demonstration it is assumed that electricity is generated by Combined Cycle plants with an electric thermal efficiency of 0.550. The exergy efficiency of this plant (0.527) is somewhat lower because of the difference between the *LHV* and the specific exergy value of natural gas.

## Chapter 7 Combined heat and power systems

Saturated steam will be generated in natural gas fired boilers with a heat thermal efficiency of 0.900. The corresponding exergy efficiency is determined, using the equation:

$$\eta_{ex, Q} = \frac{f_{ex, Q}}{f_{ex, F}} \cdot \eta_{th, Q} \quad (7.35)$$

The exergy factors are defined by the Equations 7.1 and 7.2. The considered heat exergy factor for the CHP plants is presented also in Table 7.4. The total exergy and thermal efficiencies for separate generation are calculated using respectively Equation 7.17 and Equation 7.18. The CHP plants generating heat for residential area's have to be compared with a reference system consisting of a power station and hot water boilers. It is assumed that hot water is generated by the reference system in conventional domestic central-heating boilers with a thermal efficiency of 0.950. The corresponding exergy efficiency is derived from the thermal efficiency by using Equation 7.35. It is supposed that the quality of the generated heat (and thus the heat exergy factor) is the same.

Industrial Gas Turbine with Waste Heat Boiler (IND. GT + WHB (see Tables 7.4 and 7.5))

The industrial gas turbine with waste heat boiler (IND. GT + WHB) is a plant with a natural gas fired gas turbine. Electrical power is generated with a thermal efficiency of 0.327; the exergy efficiency is 0.313. The electrical efficiency is primarily determined by the quality of the gas turbine. The waste heat boiler generates saturated steam. The thermal efficiency of the generated heat is 0.468 resulting in a total plant thermal efficiency of 0.795. The corresponding values of the exergy efficiencies are 0.155 and 0.468. The calculated exergy factor of the generated heat is 0.331; the value is determined by the conditions of the generated steam and the boiler feedwater. The total thermal efficiency shows that 20.5% of the supplied fuel energy is lost, but the total exergy efficiency (0.468) shows that more than 50% of the thermodynamic potential of the fuel is wasted. The exergy efficiency indicates the true potential for further improvements of the performance. The heat to power ratio of the plant is 1.43. This is high compared to most of the other plants. If the performance of the CHP plant is compared with the reference system (separate generation) it appears that the use of CHP increases the total thermal efficiency from 0.713 to 0.795; a relative increase of 11.5%. The relative increase of the total exergy efficiency appears to be the same. Application of the CHP results in fuel savings (and reductions of CO<sub>2</sub> emissions) of 10.3%. The fuel savings factor is a useful indicator if this kind of CHP plants can be applied without further limitations. However, if the CHP plant should operate in a wider system in which the total power demand is limiting the installed CHP the factor  $F_{FESUE}$  (factor for fuel energy savings per unit electricity) is supposed to be more appropriate. For the IND. GT + WHB a value of 0.350 has been calculated; this means that per kW generated electricity 0.35 kW of fuel will be saved. This factor is primarily useful for comparison with the other CHP plants.

An overview of values of the considered merit indicators is presented in Table 7.5. The table starts with the total efficiencies ( $\eta_{th, total, CHP}$  and  $\eta_{ex, total, CHP}$ ) as shown before in Table 7.4. Below the second heading the fuel ratio ( $F_{fuel\ ratio}$ ) and the fuel savings factor ( $F_{fuel\ savings}$ ) are given. They show that the fuel savings of the IND. GT + WHB compared to separate generation are 10.3%. The fuel energy savings per unit electricity are 0.350; considering the

fuel exergy, the savings are somewhat higher: 0.366. If the fuel savings are related to the generated heat, quite different values are calculated: the fuel energy savings per unit heat ( $F_{\text{FESUQ}}$ ) are 0.245 and the fuel exergy savings per unit heat exergy ( $F_{\text{FESUEXQ}}$ ) are 0.739. Finally, the values of the assigned efficiencies are shown. If the fuel savings of the CHP unit are assigned completely to the heat generation, the exergy efficiency of heat generation by the CHP plant ( $\eta''_{\text{ex, Q, CHP}}$ ) is 0.382. This is 1.283 times the exergy efficiency of separate heat generation. If the fuel savings are assigned completely to the electricity generation, the exergy efficiency of the electricity generation by the CHP plant ( $\eta''_{\text{ex, electr, CHP}}$ ) is 0.653, which is 1.239 times the electrical efficiency of separate electricity generation.

Industrial Combined Cycle with steam extraction (IND. CC (see Tables 7.4 and 7.5))

The industrial combined cycle CHP plant generates heat by extracting steam from the bottoming steam cycle for the generation of saturated steam. The performance data are presented for the case of maximum heat production. The plant is characterized by a high electrical efficiency but limited heat production. The total thermal efficiency is 0.690, which is low in comparison with other CHP plants. The very low heat to power ratio emphasizes the limited heat production. But, this plant has a high total exergy efficiency (0.519). This high total exergy efficiency is actually misleading. The fuel savings compared to the reference system are not high. The calculated fuel savings factor is only 0.078, which means that the achievable fuel savings are only 7.8%. Because of the low heat to power ratio of the IND. CC plant, also the exergy efficiency of separate generation is relatively high. The fuel savings as well as the fuel savings per unit electricity show poor performance of this type of CHP. The factor for the fuel energy savings per unit electricity is 0.189, which is low in comparison with the IND. GT + WHB. Only in a system in which the heat demand limits the total installed CHP power, the IND. CC appears to be attractive. Thus, in spite of the high exergy efficiency the industrial combined cycle plant is only attractive under specific circumstances. This also demonstrates that the total exergy efficiency of a CHP plant is in general not a true indicator.

Internal Combustion Engine with Waste Heat Boiler (ICE + WHB (see Tables 7.4 and 7.5))

The internal combustion engine with waste heat boiler is supposed to generate heat for residential heating. It is a small engine that generates heat for apartment buildings or utility buildings. Because of the limited power, the electrical efficiency is rather low. The total thermal efficiency is 87.2%. Due to the low exergy factor of the generated heat, the total exergy efficiency is only 37.3%. The calculated fuel savings compared to separate generation are 13.3%. The factor for the fuel energy savings per unit electricity, however, is rather high (49.9%). These merit indicators show that the application of this kind of CHP plants will be attractive for the CHP operator as well as for the larger system to which the unit belongs. For the reference case it is assumed that heat is generated in central heating boilers with a thermal efficiency of 0.950. The efficiency is based on the lower heating value of the fuel. Higher design efficiencies are achievable today, but average operation values are usually significant lower than design values. The effect of this heat efficiency on the merit indicators will be discussed later in this paper. The fuel exergy savings per unit heat exergy are 1.970. This

## Chapter 7 Combined heat and power systems

value is high compared to the values of the industrial CHP plants. This is primarily due to the low exergy factor of the generated heat. For the same reason the value of assigned exergy efficiency of the generated heat is relatively low (0.177). The assigned exergy efficiencies of heat and power generation are 1.349 respectively 1.378 times the exergy efficiencies of separate generation.

### Large Internal Combustion Engine with Waste Heat Boiler (L-ICE + WHB (see Table 7.4 and 7.5))

The large internal combustion engine with waste heat boiler also generates heat for residential heating. It has a high electric thermal efficiency (0.427) and a high total thermal efficiency (0.861). Because of the high electric efficiency, the heat to power ratio is significant lower than for the smaller ICE + WHB unit. The size of the plant requires connection to a district heating network. Heat losses of district heating networks can be considerable, depending on the total heat demand, the size and maturity of the network. Heat losses higher than 20% are mentioned for district heating networks. For this demonstration these losses are ignored. The effect of the transport losses etc. are discussed in Section 5.2. By ignoring the transport and distribution losses, the total thermal efficiency is 86.1%. Due to the low exergy factor of the generated heat, the total exergy efficiency is only 47.0%. However, the fuel savings (18.9%) and the fuel energy savings per unit electricity (54.6%) are relatively high. These merit indicators show that the application of this kind of CHP plants is very attractive. Also the fuel energy savings per unit heat (0.537) and the fuel exergy savings per unit heat exergy (3.823) are high. The low exergy factor of the heat (0.141) increases the factor  $F_{\text{FEXSUEXQ}}$  too. The assigned exergy efficiency of the generated heat by this CHP plant (0.273) is not very high, but, nevertheless around two times (2.043) the exergy efficiency in the case of a hot water boiler. The assigned exergy efficiency of electricity generation is the highest of the considered alternatives.

### Combined Cycle plant for District Heating (CC/DH (see Table 7.4 and 7.5))

The combined cycle plant for district heating generates hot water that is heated by steam extracted from the steam turbine. The plant has a high electric thermal efficiency (0.452) and is capable to generate a reasonable amount of heat, resulting in a heat to power ratio of 0.87. The performance data presented in the Tables 7.4 and 7.5 do reflect the case of maximum heat production, and ignore the effect of heat transport losses. It appears that such a plant offers high fuel savings (19.2%). The fuel energy savings per unit electricity ( $F_{\text{FESUQ}}$ ) are also high (0.526). It should be emphasized that the total exergy efficiency of the CC/DH plant is lower than the exergy efficiency of the reference power plant. If the same technology is used for these plants these efficiencies must be almost the same. Also the values of the other merit indicators appear to be attractive. The value of the fuel exergy savings per unit heat exergy ( $F_{\text{FEXSUEXQ}}$ ) is negatively affected by the relatively high exergy factor of the generated heat (0.187). On the other hand, this factor increases the assigned exergy efficiency of heat generation by the CHP plant. The assigned exergy efficiency of electricity generation (0.741) is high as for all hot water generating CHP plants.

### Micro-CHP (see Table 7.4 and 7.5)

The performance data of the considered micro-CHP unit are specified for a small gas engine with waste heat boiler. The electric thermal efficiency is 26% and the heat thermal

efficiency 63%, resulting in a total thermal efficiency of 89.0% and a high heat to power ratio of 2.42. The total exergy efficiency is rather low (34.2%). If the presented data are compared with the data for the corresponding reference system the fuel savings appear to be 12%, which is not very high. But, the fuel energy savings per unit electricity are 0.523, almost the same as for the CC/DH plant. Because of the low fuel savings and the high heat to power ratio, the fuel energy savings per unit heat ( $F_{\text{FESUQ}}$ ) are quite low (0.216) for a LT heat generating CHP plant. Also the fuel exergy savings per unit heat exergy ( $F_{\text{FEXSUEXQ}}$ ) are relatively low. The assigned exergy efficiency of heat generation (0.176) is not high, but almost the same as for the ICE + WHB plant. And the assigned exergy efficiency of electricity generation (0.739) is at the same level as the other LT heat generating CHP plants.

### 7.4.3 Evaluation of merit indicators

An overview of the calculated merit indicators for the considered plants is shown in Table 7.5. The results for the various CHP plants are discussed in the previous section. In this section it will be discussed what indicator is most appropriate under specific circumstances and which type of CHP plant is the most attractive.

The main reasons for the application of CHP are the possibility to save fuel and costs compared to separate generation. In general the cost savings will result primarily from the fuel savings. Thus, the relative fuel savings compared to separate generation is in principle determining the merits of a CHP plant. Then the fuel savings factor ( $F_{\text{fuel savings}}$ ) is considered to be a true merit indicator. A ranking of CHP plants based on this indicator will be quite different from rankings based on the total thermal efficiency or the total exergy efficiency. Therefore, these efficiencies are not appropriate to indicate the merits of CHP.

If CHP is used to save the fuel consumption of a wider system, e.g. a large industrial plant or a nation, not the fuel savings of the individual CHP plant but the savings of the total system should be the goal. The fuel savings of the total system are determined by the fuel savings of the CHP plant as well as by the total installed power of CHP plants. If the total installed power is limited by the total electricity demand, the highest savings are achieved by applying CHP plants with maximum fuel savings per generated unit electricity ( $F_{\text{FESUE}}$ ). From Table 7.5 it appears that this results into another ranking of the CHP plants. Replacing  $F_{\text{FESUQ}}$  by  $F_{\text{FEXSUE}}$  is not really useful. It affects the numbers but not the ranking of plants. If the total installed power is limited by the total heat demand, the highest savings are achieved by applying CHP plants with maximum fuel savings per generated unit heat ( $F_{\text{FESUQ}}$ ). This will also result into a different ranking of the CHP plants mentioned in Table 7.5. The use of  $F_{\text{FEXSUEXQ}}$  instead of  $F_{\text{FESUQ}}$  will result into another ranking of the CHP plants, because it takes also the quality (exergy) of the generated heat into account. This quality is represented by heat exergy factor ( $f_{\text{ex},Q}$ ). Since it is not clear how this might improve the selection process, the use of exergy values for this purpose is not useful.

The assigned exergy efficiencies for the generation of heat or electricity can answer the question to what extent CHP can be beneficial for the generation of heat or eventually power. This might be helpful for a comparison of alternative options for the generation of a specific

## Chapter 7 Combined heat and power systems

heat demand or power demand. The assigned exergy efficiencies of heat generation are apparently not really useful for the ranking of quite different CHP plants. The ratio  $\eta''_{ex, Q, CHP} / \eta_{ex, Q, ref}$  results into the same ranking of the considered plants as  $F_{FESUQ}$ , but this might be a coincidence. The assigned exergy efficiency of heat generation as well as the ratio  $\eta''_{ex, electr, CHP} / \eta_{ex, electr, ref}$  show the same ranking as  $F_{FESUE}$ , but also here it is uncertain if this will be the case for all alternatives. Therefore, it is concluded that only  $F_{fuel\ savings}$ ,  $F_{FESUE}$  and  $F_{FESUQ}$  are useful merit indicators for a general comparison of CHP plants. For the Netherlands the electricity demand is determining the total CHP power that can be installed. If CHP has to be used to reduce the national CO<sub>2</sub> emissions, the application of plants with maximum  $F_{FESUE}$  should be favored.

From the results in Table 7.5 it is concluded that maximum fuel savings can be achieved by the application of large scale CHP plants (L-ICE + WHB and CC/DH) for the generation of LT heat. The fuel savings of the smaller plants (ICE + WHB and micro-CHP) are somewhat lower. If the fuel energy savings per unit electricity are considered, the differences between these plants are very limited. This means that all CHP plants for the generation of LT heat are suitable for the reduction of the fuel consumption and CO<sub>2</sub> emissions on a national scale. The performance of the large scale plants is apparently slightly better than of the small scale plants. However, the performance of the large scale plants can be affected negatively by losses of the required heat transport and distribution systems. This might change the ranking as obtained from Table 7.5. Unfortunately, accurate values of these losses are not easily available. The sensitivity for these losses is discussed in Section 7.5.

The fuel savings of the two industrial CHP plants (IND. GT + WHB and IND. CC) are significantly lower. This poor performance is partly caused by the low total efficiencies of these plants. If the fuel energy savings per unit electricity ( $F_{FESUE}$ ) is considered to be the determining merit indicator, application of the IND. CC should be rejected.

The comparison of industrial plants, based on the fuel savings per unit of heat, shows obviously a preference for the industrial combined cycle (IND. CC) over the industrial gas turbine with waste heat boiler (IND. GT + WHB). A comparison of the alternatives for low temperature heat generation shows a preference for the combined cycle district heating plant (CC/DH) if  $F_{FESUQ}$  is used as the determining merit indicator. In that case the micro-CHP shows a poor performance.

## 7.5 Evaluation of CHP design data

### 7.5.1 The Industrial Gas Turbine with Waste Heat Boiler (IND. GT + WHB)

From the considered industrial CHP plants in Table 7.4, the industrial gas turbine with waste heat boiler is the most attractive with regard to its potential to save fuel. Therefore this plant is used for a more detailed evaluation of the calculated merit indicators. The equations of the merit indicators, as derived in Section 7.4, show that the calculated values are determined by the efficiencies of the CHP plants and the reference plants. To calculate the data shown in Table 7.4 it was supposed that the thermal efficiency of the reference power plant is 55%. This seems to be a reasonable value if the performance of the CHP plant has to

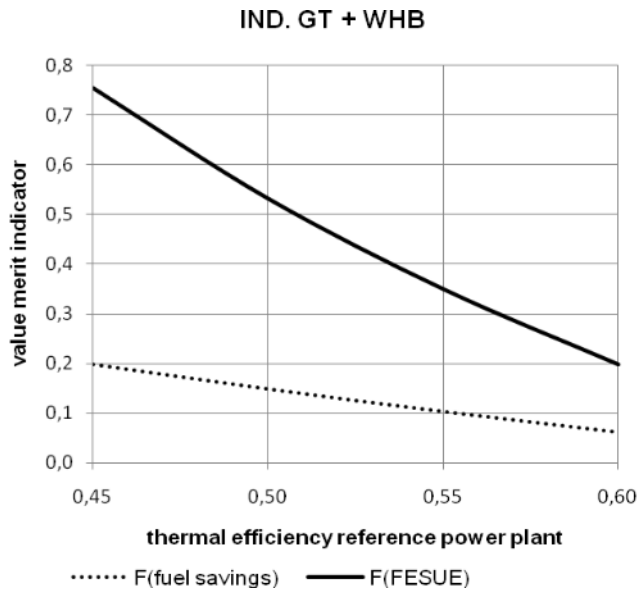


*Figure 7.14 The influence of the thermal efficiency of the reference power plant on the merit indicators of the industrial gas turbine with waste heat boiler*

reference power plant; all other efficiencies are the same as shown in Table 7.4. It is obvious that the fuel savings resulting from the application of CHP will be lower if the efficiency of the reference power plant is higher. Consequently the fuel energy savings per unit electricity decreases from about 0.75 for a power plant efficiency of 0.45 to less than 0.20 for a power plant efficiency of 0.60. This means that the efficiency of the reference power plant seriously affects the calculated fuel savings; the right choice of the reference power plant is important to get a true presentation of the merits of CHP.

The thermal efficiency of the reference steam boiler was supposed to be 0.90. However, lower efficiencies are frequently reported for industrial steam boilers. On the other hand, the available technology enables also higher efficiencies. The effects of the boiler efficiency within the range of 0.80 to 0.95 are shown in Figure 7.15. When considering the same CHP plant, the fuel savings

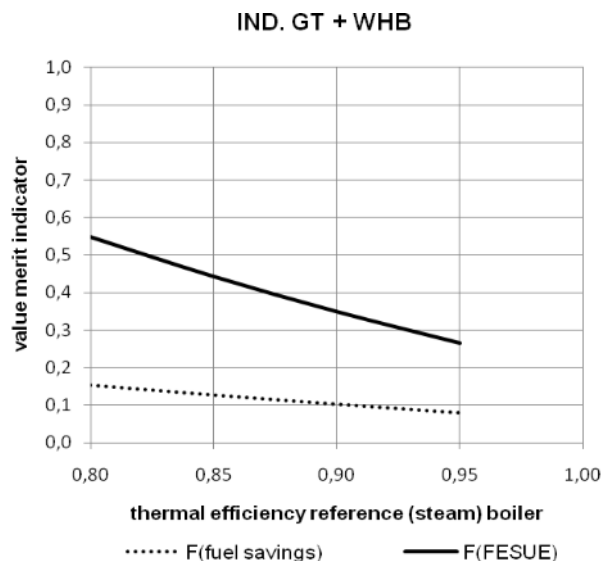


*Figure 7.15 The influence of thermal efficiency of the reference steam boiler on the merit indicators of the industrial gas turbine with waste heat boiler*

be compared with large existing power plants. But if the existing power generating capacity consists of smaller or older plants, lower values for the efficiency of the reference power plant have to be used (down to 50% or even lower). On the other hand, if a comparison is made for future application, the CHP plant should be compared with a new to build power plant with thermal efficiencies up to 60%. The effect of the efficiency of the reference power plant on the two selected merit indicators is demonstrated in Figure 7.14. The figure is obtained by varying the efficiency of the

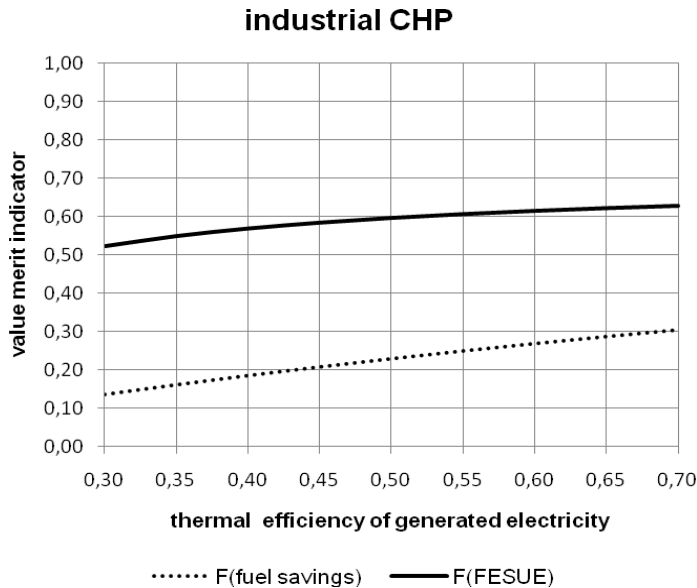


*Figure 7.16 The influence of the electric thermal efficiency on the merit indicators of an industrial CHP plant (the total thermal efficiency is supposed to be constant at 0.85)*

electrical thermal efficiencies and different total thermal efficiencies. A systematic evaluation is obtained by varying the electrical thermal efficiency of the CHP plant without changing the total thermal efficiency or by varying the total thermal efficiency without changing the electric efficiency. The effect of varying the electric thermal efficiency is shown in Figure 7.16. The values of the two merit indicators are presented if the electrical thermal efficiency is increased from 0.30 to 0.70; total thermal efficiency is supposed to be 0.85. Electrical efficiencies higher than 0.50 are not very realistic for the time being, but are included to show the importance of further developments. It appears that the electrical efficiency of the industrial CHP plant has a moderate, but still significant, effect on the fuel savings as well as on the fuel energy savings per unit electricity. The increase of the fuel savings is almost linear with the electricity thermal efficiency; the increase of the fuel energy

are reduced with almost 50% if the reference boiler efficiency increases from 0.80 to 0.95. Since the generated power is not affected by changing the reference boiler efficiency, the fuel energy savings per unit electricity ( $F_{\text{FESUE}}$ ) show the same tendency. It is obvious that also the reference boiler efficiency should to be chosen carefully.

Another question that has to be answered is what the effect will be of improved performance of the CHP plant. In Table 7.4 two different CHP plants have been compared with different

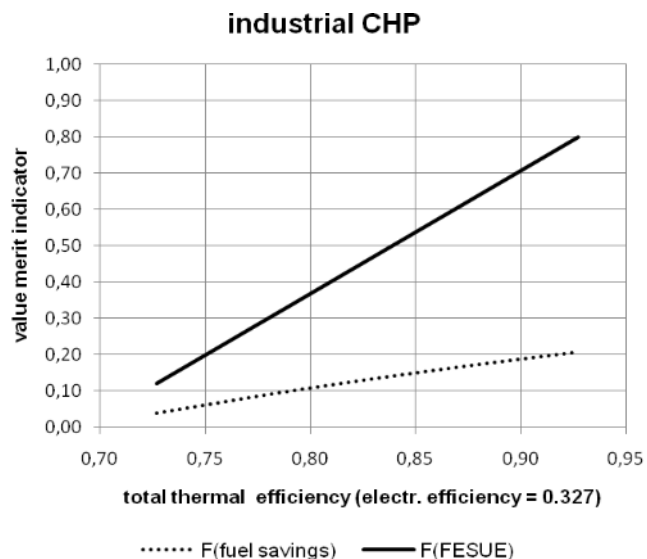


*Figure 7.17 The influence of the total thermal efficiency of the CHP plant (the electric thermal efficiency is supposed to be 0.327)*

savings per unit electricity is moderate at higher efficiencies because of the increasing electrical power. In Figure 7.17 the total thermal efficiency is varied assuming a constant electrical thermal efficiency of 0.327. It appears that the total thermal efficiency has a considerable effect on both, the fuel savings and the fuel energy savings per unit electricity. This explains also the low values of the merit indicators for the industrial combined cycle plant ( $\eta_{th, total, CHP} = 0.690$ ) in Table 7.4.

### 7.5.2 The Combined Cycle District Heating plant (CC/DH)

The combined cycle district heating plant as well as the large internal combustion engine with waste heat boiler show high fuel savings and high fuel energy savings per unit electricity. The combined cycle district heating plant, however, is more attractive because of its highly flexible heat to power ratio. Therefore, this plant is used here for a more detailed evaluation. A CHP plant for district heating should be compared with separate generation of electricity in large power plants and heat generation in individual hot water boilers. As discussed before, different values of the efficiency of the reference power plant might be appropriate for different evaluations. The effect of power plant efficiencies varying between 0.45 and 0.60 is shown in Figure 7.18. The effect is more or less similar as in the case of the industrial gas turbine with waste heat boiler, but the relative decrease of the fuel savings and the fuel energy savings per unit electricity is not that high.

The effect of the thermal efficiency of the reference boiler on the merit indicators of the CC/DH plant is shown in Figure 7.19. Modern condensing boilers have thermal efficiencies higher than 100% as the efficiencies are based on the lower heating value of the fuel. Many boilers, however, operate at lower efficiencies. And yearly averaged efficiencies are in general significant lower than the design values. Thermal efficiencies for a reference boiler can be within the range of 0.85 to 1.05. Figure 7.19 shows that within this range the variation of the merit indicators is not really high.

A true comparison of heat delivery by district heating and individual hot water boilers requires that heat losses due transport and distribution are taken into account. However, because of the many factors that are determining these heat losses, the actual heat losses can be quite different from case to case. For this evaluation it is assumed that heat losses can vary within a range of 0% to 20%. The effect of these losses on the merit indicators is shown in

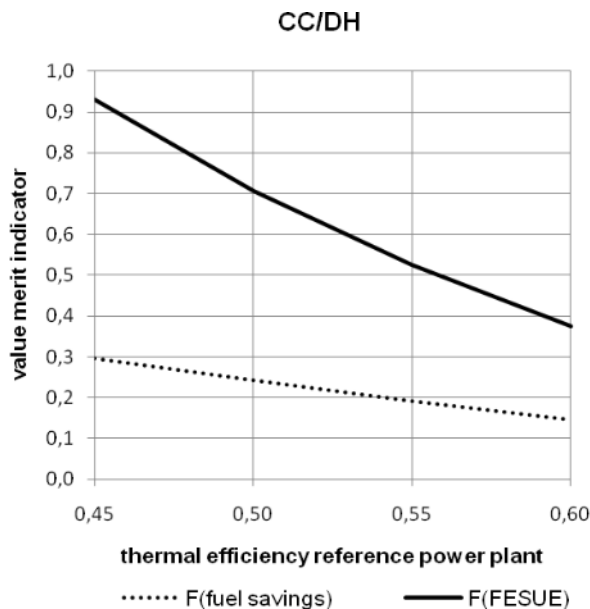


Figure 7.18 The influence of thermal efficiency of the reference power plant on the merit indicators of the combined cycle district heating plant

## Chapter 7 Combined heat and power systems

Figure 7.20. It appears that a heat loss of 20% will reduce the fuel savings from 19% (no heat loss) to 13%; the fuel energy savings per unit electricity are reduced from 53% to 34%. This shows that for a comparison of district heating with local generation, the losses of heat transport and distribution should not be ignored.

### 7.5.3 The micro-CHP unit

The efficiency values of the micro-CHP unit in Table 7.4 are based on the application of a small gas engine with waste heat boiler. The small gas engine is commercially available already for many years. The application of micro-CHP is considered to be an interesting option for fuel savings and the reduction of CO<sub>2</sub> emissions in the future. A variety of technologies is under development today based on i.e. Stirling engines, fuel cells (PEMFC and SOFC) and micro-gas turbines (see e.g. [7.4], [7.11], [7.13], [7.26]). In particular the development of fuel cell systems focuses on high electrical efficiencies. Very high efficiencies, up to 60%, are announced for SOFC units, however, without further proof. To check the importance of high electrical efficiencies of micro-CHP systems Figure 7.21 shows the influence of the thermal efficiency of electricity generation ranging from 15% to 70%. The calculations are made assuming a constant total thermal efficiency of 90%. It appears that the fuel savings are almost proportional with the electrical efficiency. The fuel energy savings per unit electricity, however, shows a steep increase in the area of moderate electrical efficiencies but this increase diminishes at higher efficiencies. Nevertheless, a further increase of the electrical efficiency is always beneficial.

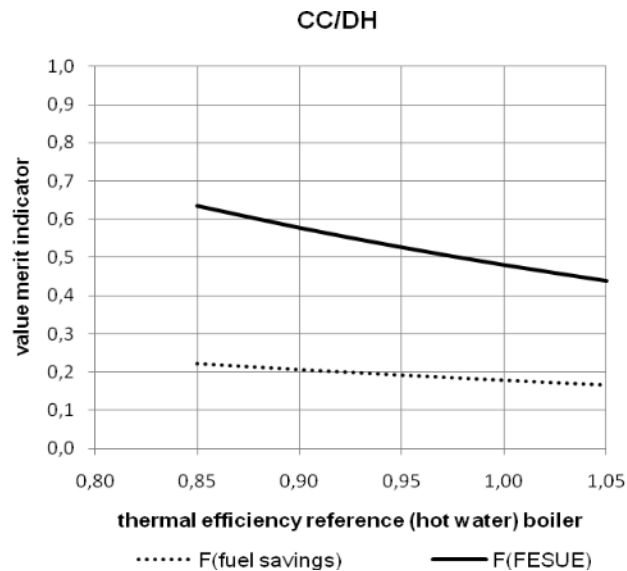


Figure 7.19 The influence of thermal efficiency of the reference hot water boiler on the merit indicators of the combined cycle district heating plant

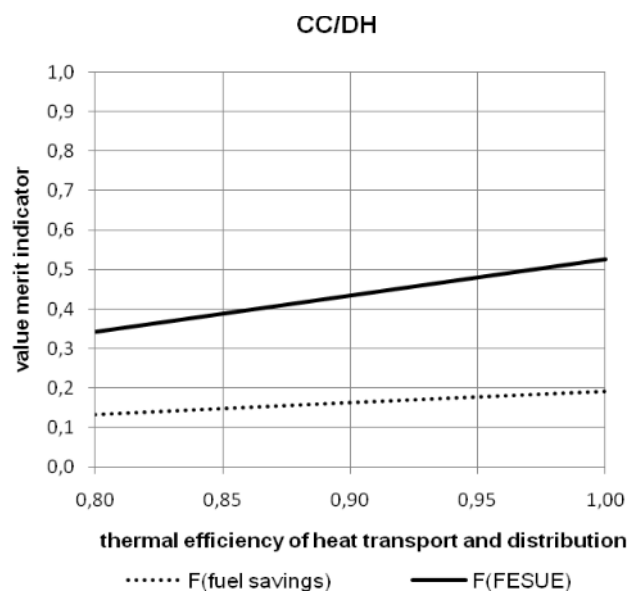


Figure 7.20 The influence of thermal efficiency of heat transport and distribution on the merit indicators of the combined cycle district heating plant

Micro-CHP systems can achieve very high total efficiencies if the heating system allows for low temperatures of the circulated water. Then, the exhaust flow(s) can be cooled till very low temperatures. The importance of high total thermal efficiencies is demonstrated in Figure 7.22. The fuel savings as well as the fuel energy savings per unit electricity will increase almost linear with the total thermal efficiency. Both indicators are almost doubled if the total efficiency increases from 85% to 95%. Thus, high total efficiencies are important to achieve maximum performance.

#### 7.5.4 Extraction condensation plants

District heating systems using large extraction condensation plants for the generation of heat are used in many European countries. These systems enable efficient generation of heat as shown before. The high initial costs of the heat transport and distribution system often hinders the realization of new projects. In new to build areas uncertainties with regard to the

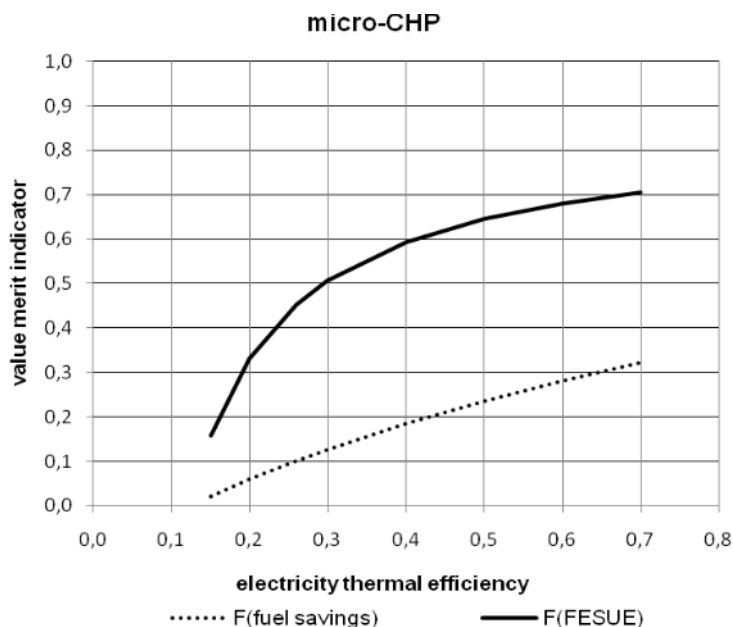


Figure 7.21 The influence of the electrical thermal efficiency on the merit indicators of the micro-CHP unit (with constant total thermal efficiency of 90%)

growth of the area is a further hindrance for the application. Because of the high costs of heat transport and distribution, the application of district heating systems is primarily attractive in densely populated areas with quite a number of large heat consumers.

The merit indicators discussed in the previous section show that district heating systems based on combined cycle plants, with properties as assumed, are attractive with respect to the fuel savings as well as fuel energy savings per unit electricity. Besides these two indicators, the power loss ratio is often used to emphasize the advantages of extraction condensation plants. In these plants heat generation reduces the generated power. Thus, the power loss ratio is defined as the reduction of the generated power divided by the generated heat:

$$K_{\text{power loss}} = \frac{\Delta W}{Q''_c}$$

Actually, the inverse of the power loss ratio  $1/K_{\text{power loss}}$ , representing the heat that will be generated per unit lost power, is often considered to be a more sensible indicator. Therefore,

## Chapter 7 Combined heat and power systems

values of the inverse of the power loss ratio are used in the following evaluations. E.g. Equation 7.14 can be used for the evaluation of the effect of various design parameters on the

*Table 7.6 The inverse value of the power loss ratio for three different power plants*

	unit	Steam cycle	Reference CC	modern CC
$\bar{T}_H$	[K]	500	950	1050
$\bar{T}''_C$	[K]	363	363	363
$\bar{T}_C$	[K]	300	300	300
$\eta_{ex, intern}$	[-]	0.75	0.75	0.80
$1/K_{power\ loss}$	[-]	8.4	10.8	9.9

power loss ratio. The equation shows that the value of the power loss ratio depends on the internal exergy efficiency of the power cycle ( $\eta_{ex, intern}$ ), the temperature of heat transfer from the cycle in the hot condenser ( $\bar{T}''_C$ ), the temperature of heat transfer from the cycle in the main condenser ( $\bar{T}_C$ ) and the temperature of heat

transfer to the cycle ( $\bar{T}_H$ ). All temperatures are considered as thermodynamic equivalent temperatures. The effect of the various design parameters can be approximated easily by assuming that the value of the internal exergy efficiency of the power cycle is constant irrespective the mode of operation<sup>1</sup>.

For the evaluation of the effects of the respective parameters 3 systems are considered: a steam cycle plant and 2 combined cycle plants (CC-1 and CC-2). The relevant parameters as well as the calculated value of the inverse of the power loss ratio are shown Table 7.6. CC-1 is a combined cycle system with a relatively low temperature (950K) of heat transfer to the

(gas turbine) cycle ( $\bar{T}_H$ ), a condensing temperature of 300K (27°C) and an internal exergy efficiency of 0.75. This internal exergy efficiency is also a low value for large combined cycle plants (see Chapter 5). If extraction steam for the generation of heat is condensed at a (thermodynamic equivalent) temperature of

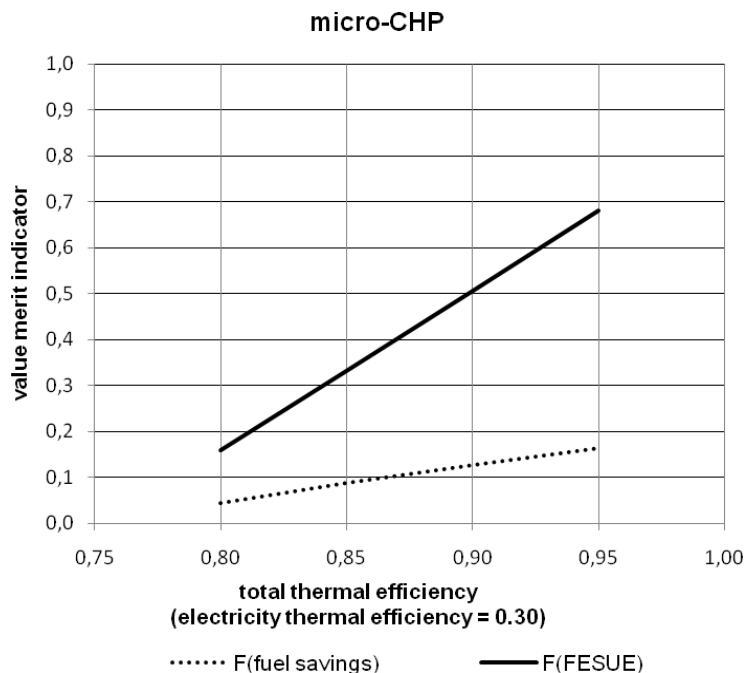


Figure 7.22 The influence of the total thermal efficiency on the merit indicators of the micro-CHP unit

<sup>1</sup> A comprehensive discussion on the thermodynamic equivalent temperatures of heat transfer to and from the cycle and the value of the internal exergy efficiency is given in Chapter 5.

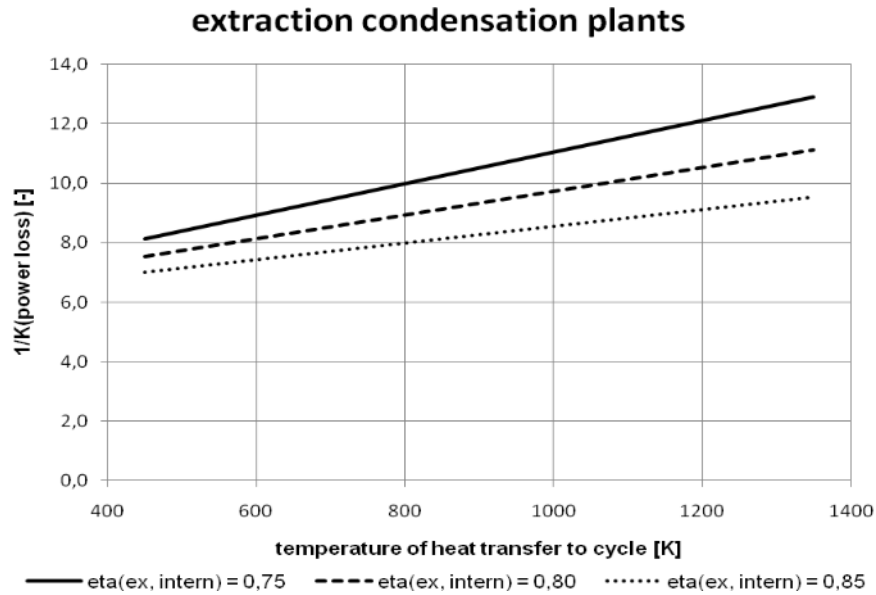
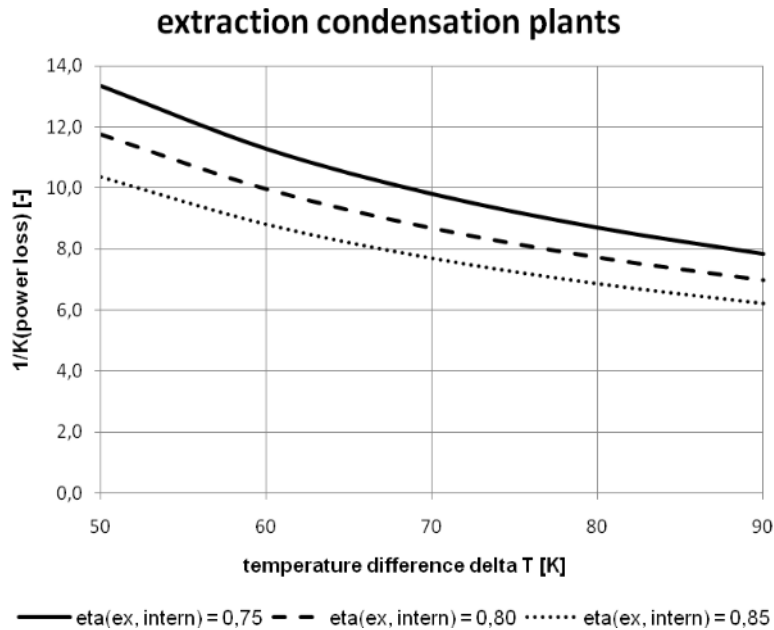


Figure 7.23 The influence of the temperature of heat transfer to the cycle and the internal exergy efficiency of the cycle on  $1/K$  (the inverse value of the power loss ratio)

363K, the inverse of the power loss ratio is 10.8. This means that the generation of 10.8 kW of heat will reduce the power production of the plant with 1 kW. This value can be compared e.g. with the  $COP$  of electrical driven Heat Pumps<sup>2</sup>. Well optimized Heat Pump systems are able to achieve a yearly averaged coefficient of performance of around 4. Thus, a combined cycle extraction condensation plant is able to generate more than two times the amount of heat for the same quantity of electricity. If CC-1 is replaced by a steam cycle with conditions as given in Table 7.6, the temperature of heat transfer to the cycle will be significant lower (500K). If the internal exergy efficiency of the steam cycle is supposed to be the same as for the combined cycle CC-1, the inverse of the power loss ratio is 8.4. In the case of a modern combined cycle plant (CC-2) with a temperature of heat transfer to the system of 1050K and a somewhat higher internal exergy efficiency of 0.80, the inverse value of the power loss ratio is 9.9. The higher temperature of heat transfer to the cycle will increase the value of  $1/K_{\text{power loss}}$ , but the higher internal exergy efficiency reduces this value. These effects are explained by Figure 7.23. The figure shows that heat generation by extraction condensation plants is attractive, irrespective of the temperature of heat transfer to the cycle. Higher temperatures of heat transfer to the cycle are beneficial, but higher internal exergy efficiencies will mitigate the effect of the higher temperatures. Thus, combined cycles with high values of  $\bar{T}_H$  as well as steam cycles with much lower values of  $\bar{T}_H$  are attractive for the efficient generation of low temperature heat.

<sup>2</sup> It should be emphasized that the temperature of the heat from the two systems is not the same. Heat Pumps with high  $COP$ 's generate low temperature heat (30 to 40°C). Heat from an extraction condensation plants has in general significant higher temperatures.



*Figure 7.24 The influence of the temperature difference  $\Delta T = \bar{T}''_c - \bar{T}_c$  and the internal exergy efficiency of the cycle on  $1/K$  (the inverse value of the power loss ratio)*

So far, the difference between the condensing temperatures in the so called hot condenser and the main condenser is supposed to be 63K, resulting in a condensing temperature of 363K (90°C) in the hot condenser. The condensation temperature in the hot condenser is primarily determined by the water supply temperature of the district heating system. During periods of high heat demands the capacity of the transport and distribution system is usually increased by raising the water supply temperature. Then, also the temperature of the hot condenser must be raised. The effect of different values of the condensation temperature in the hot condenser is shown by Figure 7.24. It is assumed that the temperature of condensation in the cold condenser is constant. It appears that the value of  $1/K_{\text{power loss}}$  is quite sensitive for the temperature difference between the hot and the cold condenser. Thus, careful optimization of the design of the district heating is required to achieve optimum economical results.

## 7.6 Conclusions

The combined generation of heat and power enables substantial fuel savings compared to the separate generation of the same quantities of heat and power. In a true comparison all considered systems are using the same fuel; in that case the reduction of CO<sub>2</sub> emissions is proportional with the fuel savings. Fuel savings up to 20% can be achieved by applying now available technologies. Higher savings are conceivable for the future, but the actual savings will depend on the further development of the electrical efficiencies of CHP plants as well as large power stations.

The application of the exergy concept and the resulting value diagrams are useful to get more insight into the performance of thermal power and CHP plants. Value diagrams obviously show the large thermodynamic losses of steam and hot water generation in fired boilers and give an idea of the reduction of thermodynamic losses in the case of combined heat and power generation. Value diagrams can be helpful also to find the optimum use of waste heat as is demonstrated for the large internal combustion engine in Section 7.2. Thorough understanding of the thermodynamics for heat and power generation is necessary to reach the maximum benefit from CHP plants. Simple equations for a preliminary evaluation of CHP plants can be derived easily. In many cases the results achieved with these equations are sufficiently accurate. The application of  $\eta_{ex, intern}$ , the internal exergy efficiency of a thermal power cycle, is helpful for the evaluation of extraction condensation steam cycles and can be used to determine the power loss ratio with reasonable accuracy.

Because of the large variety of CHP plants, appropriate merit indicators are required to determine what kind of plant will be the most beneficial for a specific situation. It is demonstrated that the optimum plant is not determined only by the properties of the CHP plant, but depends also on the characteristics of the plants for the separate generation of heat and power, and on the demand of power and heat of the wider system to which the CHP unit belongs. Useful indicators do require a comparison with separate generation of heat and power. The use of total plant efficiencies, thermal efficiencies or exergy efficiencies, is unsuitable. If the characteristics of the wider system are irrelevant, the fuel savings compared to separated generation,  $F_{fuel\ savings}$ , is a true indicator of the thermodynamic quality of a CHP plant. This indicator will be preferred if a plant operator is just looking for minimum fuel costs. A government or the owner of an industrial site, should first look how the overall energy demand will affect the total installed power of CHP. If the power demand is limiting the total installed CHP power, the fuel energy savings per unit electricity,  $F_{FESUE}$ , is the right indicator to benefit maximum from combined generation. If the heat demand is limiting the total installed CHP power, the fuel energy savings per unit heat,  $F_{FESUQ}$ , is more appropriate. In Western European countries the total electricity demand is actually limiting the total installed CHP power. In these countries the government should focus on the fuel energy savings per unit electricity.

Assigned exergy efficiencies for the generation of power or heat by a CHP plant might be interesting for specific reasons. They show exergy efficiency of the generation of one of the products assuming that the other product is generated with the same efficiency as in the case of separate generation. Assigned exergy efficiencies, however, are not appropriate to indicate the capability of CHP plants to save fuel or to reduce CO<sub>2</sub> emissions.

The highest fuel savings are achievable with CHP plants for the generation of LT heat. The fuel savings of CHP plants for the generation of HT heat are in general lower. Thus, the application of CHP plants for the generation of LT heat is in general more attractive than the application of industrial CHP. For the generation of LT heat, however, the Heat Pump is a serious alternative. A rough evaluation of future energy conversion options for the Netherlands as presented in Chapter 3 has shown that the highest fuel savings can be achieved by using industrial CHP for the generation of HT heat and Heat Pumps for the generation of

## Chapter 7 Combined heat and power systems

LT heat. Final conclusions, however, will require more detailed evaluation of the various options. The combined application of CHP systems and heat pumps, as proposed in [7.29], was not included in these evaluations, but might be attractive from a thermodynamic point of view.

It is necessary to define a reference system in order to determine the thermodynamic merits of CHP. As demonstrated, the calculated merits are rather sensitive for the efficiencies of the reference system. The choice of suitable efficiencies for the reference system should consider the purpose of the evaluation as well as the considered fuel. If CHP has to replace existing power and heat generation other efficiencies have to be used for the reference system than if it has to be seen as an extension of the future supply system. A true comparison of CHP with separate generation is possible only if all plants use the same fuel. For CHP plants using different fuels (natural gas and biomass), different reference systems are required.

Heat losses of district heating systems due to transport and distribution can be substantial and have a serious effect of the thermodynamic merits of CHP plants. The selection of true values of these losses is in general not easy. Comparison of large scale CHP plants with e.g. micro-CHP requires careful evaluation of transport and distribution losses to come to reliable conclusions.

The merit indicators are very sensitive for the total thermal efficiency of the CHP plant (see e.g. Figure 7.22). High total thermal efficiencies are required to achieve high fuel savings. Also higher electric efficiencies have a positive effect on the fuel savings as well as on the fuel energy savings per unit electricity of CHP plants. Both indicators increase if the electric thermal efficiency increases. Suggestions that an optimum value for the electric efficiency of CHP units does exist are obviously false.

High fuel savings as well as high fuel energy savings per unit electricity can be achieved with the application of Micro-CHP units with high electrical efficiencies (see Figures 7.21 and 7.22). The application of units with electrical efficiencies lower than 20% is not really beneficial with regard to fuel savings. It can be helpful, however, for the implementation of micro-CHP. Natural gas fuelled micro-CHP systems with electrical efficiencies of 40% or higher and total efficiencies like hot water boilers are attractive. The development of reliable and cheap micro-CHP fuel cell systems that can reach this performance is recommended.



## 8 CONCLUSIONS

### 8.1 Introduction

Sustainable energy systems require the use of renewable sources of primary energy. In Appendix 2.1 it has been shown that just replacing the conventional fossil sources of primary energy by renewable sources like wind and solar will result into significant higher total yearly costs of our energy supply system. The use of biomass seems to be a more attractive option. In comparison with conventional solid fuels the conversion efficiencies of biomass are lower and equipment costs are higher but it is expected that total yearly costs will differ not that much. Unfortunately, the quantities available today in the Netherlands are not sufficient to generate the total demanded powers. Thus, the application of a mix of renewable sources of primary energy is supposed to be inevitable. From Appendix 2.1 it is concluded that the transition to sustainable energy systems will require more than only the use of renewable sources. To make the costs of sustainable energy systems affordable it will be necessary:

- to reduce the energy demand (electricity, heat, fuel for transport);
- to improve the match between energy generation and demand;
- to increase conversion efficiencies (from primary energy into electricity, heat and fuel for transport).

After discussing various options for sustainable energy systems, the focus of this thesis is primarily on possibilities for higher conversion efficiencies in particular for the generation of electricity and heat. Exergy analysis is used comprehensively for that purpose.

The highest efficiencies for power plants are achieved with natural gas fired Combined Cycle plants. Net thermal efficiencies around 60% are achievable with such plants today. The thermal efficiencies are first of all determined by the large exergy loss of the combustion process. It seems not to be very likely that with this technology thermal efficiencies serious higher than 70% can be achieved within the next decades. The application of fuel cells (electrochemical fuel conversion) offers a way to avoid the large exergy loss of combustion processes. Thermal efficiencies of 80% and even higher are conceivable with high temperature fuel cells (SOFCs and perhaps also MCFCs). Such high efficiencies are calculated for so-called hybrid SOFC-GT plants (with low to intermediate temperature SOFCs) with relatively low powers (around 30 MW<sub>e</sub>) and simple system designs. The power level of these plants is primarily determined by the performance of the gas turbine. The generation of heat in hot water and steam boilers is common practice today. However, the thermodynamic efficiency (exergy efficiency) of these processes is very poor: < 15% for hot water boilers and < 30% for steam boilers. Application of other technologies like CHP and Heat Pumps is necessary to enable a serious reduction of the exergy loss of heat generation. For the evaluations in this thesis the heat demand was roughly split into a demand for low temperature heat (hot water, space heating) and a demand for high temperature heat (steam, industrial processes). For the generation of high temperature heat CHP is the preferred technology while CHP and Heat Pumps have to compete in the case of low temperature heat. The heat market is quite complex and highly depending on governmental rules, actual energy demands, technical parameters of conversion technologies, environmental parameters and so

on. In Chapter 7 it was shown that thermal efficiencies as well as exergy efficiencies are in general no true indicators for the merits of CHP. True merit indicators have to compare the performance of CHP with separate generation of power and heat. Thus, the merits of a specific CHP plant are depending on the characteristics of the total system (country, industrial plant) to which the plant belongs. The maximum power of CHP plants that can be installed, within a country or an industrial plant, is limited whether by the power demand or the heat demand. It appears that true merit indicators are appropriate only for one of these situations. Without comprehensive evaluations of the application of CHP, only rough estimates can be made of the achievable fuel savings. The calculations in Chapter 3 show fuel savings up to 30 to 40% are achievable by the application of power plants with high efficiencies (80%), improved CHP for the high temperature (industrial) heat demand and improved Heat Pumps for the low temperature heat demand. It is obvious that high power generation efficiencies are in favor of Heat Pump application.

Of course, more detailed conclusions are derived from the various evaluations. These are presented in the following sections.

## 8.2 Options for sustainable energy systems

Wind, solar energy and biomass are supposed to be the major sources of primary energy in the case of sustainable energy systems for the Netherlands in the future. As shown in Appendix 3.1, the application of wind and solar energy will cause substantial higher total yearly costs of the system. In particular the large scale application of wind and solar energy will cause substantial higher total yearly costs. The application of biomass is supposed to be somewhat more expensive than coal. In that case, biomass is a more attractive source of renewable energy for the generation of electricity and heat. Unfortunately, the available biomass in the Netherlands is not sufficient to cover the total energy demand (see [3.2]).

It is expected that the application of secondary fuels will be necessary for transport, storage and distribution of energy. Hydrogen and various hydrocarbons are most frequently suggested for this purpose. Hydrogen offers maximum flexibility for the introduction of renewable energy sources, but it requires serious adaptations of the infrastructure and will result into lower overall efficiencies and higher total yearly costs. Hydrocarbon fuels like syngas or SNG from biomass will enable higher overall efficiencies of the conversion chain (see also [3.3]).

The primary conversion processes of the considered energy systems are usually determining more than 50% of the total yearly costs. Higher efficiencies of the secondary conversions and a reduced need for energy storage will reduce the required power and costs of the primary conversion processes. Also the application of so-called “smart energy systems” that enable a better match of energy demand and generation will reduce the need for energy storage. High fuel savings are in principle achievable for the generation of heat, in particular low temperature heat. Significant reductions of the low temperature heat demand (of e.g. dwellings, buildings and greenhouses) can be realized by the application of better isolation, the use of seasonal temperature differences and improved building designs. Higher thermodynamic efficiencies of conversion equipment will provide an additional effect. Higher conversion efficiencies are realized by the application of Heat Pumps and CHP. Higher

efficiencies of electricity generation are stimulating the application of heat pumps and will improve the performance of CHP plants too.

### 8.3 Conventional power plant technologies

The highest efficiencies (thermal, *LHV* basis) for power generation today are around 60%. These efficiencies can be achieved by natural gas fired Combined Cycle plants. In the case of favorable environmental conditions net efficiencies somewhat higher than 60% are offered by plant manufacturers. During a period of 25 years an increase of about 12% (points) has been achieved for this technology. The improvements result from higher combustion temperatures in the gas turbine and lower internal losses of the gas turbine as well as the steam turbine cycle. It is expected that further increases can be realized in the future, but it seems to be unlikely that efficiencies seriously higher than 70% are achievable (see Table 5.16 and Figure 5.37). A further increase of the combustion temperature requires new solutions for existing material limitations. E.g. the application of ceramics appeared not to be feasible so far for rotating parts of the gas turbine.

Coal fired power plants are usually based on combustion processes followed by a thermal power cycle. The combustion process generates the heat that is converted into power by the thermal power cycle. The thermodynamic (exergy) efficiencies of atmospheric as well as pressurized combustion processes are within the range 70 to 80%. Values near to 80%, however, are achievable only by the application of design parameters that are either economically or technically unfeasible today. The thermodynamic efficiencies of large power cycles are usually between 80 and 90% of the theoretical value (the Carnot efficiency). In the case of closed power cycles the heat transfer from the flue gas to the power cycle causes additional thermodynamic losses. In the case of conventional steam turbine plants these losses are around 20% of the fuel exergy but they can be reduced by the application of advanced steam conditions or topping cycles. It is not expected yet that coal fired power plants using closed power cycles will be able to achieve efficiencies much higher than 50%.

The losses of heat transfer from combustion process to power cycle are avoided if the combustion process can be integrated into the power cycle. This is actually the case with internal combustion engines and gas turbines. In general the thermodynamic efficiencies of combustion engines and gas turbines are limited because of the high temperatures of heat rejection. Combination with a bottoming cycle (e.g. a steam turbine cycle or ORC), however, can almost eliminate this disadvantage. Another problem of integrated combustion processes is that the combustion parameters like pressure and maximum temperature, and thus the exergy loss of combustion, are determined by the design of the power cycle. In the case of modern gas turbines the exergy loss of combustion is usually around 25% or even higher.

The exergy loss of combustion is depending also on the quality of the fuel. In the case of solid fuels like coal and in particular biomass the exergy loss of combustion appears to be higher than in the case of natural gas. The total exergy loss of the combustion system (including stack losses) can be more than 7% higher in the case of wood combustion than in the case of natural gas.

If solid fuel are converted first into a gaseous secondary fuel, similar processes can be used for the conversion into power as for the conversion of natural gas. The exergy losses of

the conversion of a solid fuel into gaseous fuel, however, are significant. The exergy loss of gasification processes are usually in the range of 13 to 19%; additional losses for processing the gas can be around 7%. This means that the highest efficiencies achievable for power plants using solid fuels are roughly 20 to 25% lower than the efficiencies of natural gas fuelled systems if similar power cycles are used.

#### 8.4 Fuel cell systems

High temperature fuel cells have the potential to raise conversion efficiencies of power generation based on natural gas to values around 80%. This has been confirmed by system calculations for a target system (for detailed results see Appendix 6.3). The target system is a so-called SOFC-GT hybrid system with fuel cell stacks operating at intermediate temperature (operating temperature 700°C) in combination with gas turbines. The assumed design data of the fuel cell stack are based on the application of existing materials. The target system does not require unconventional gas turbine technology. The high efficiency can be achieved at plant power levels around 30 MW<sub>e</sub> or even lower and without the need for cooling water. This are attractive characteristics for the planning of new power generation capacity. Further improvement of the system efficiency appears to be conceivable by using the residual heat. The application of a bottoming cycle (e.g. ORC) will raise the exergy efficiency above 80%. It is obvious that lifetime and costs of HT fuel cell stacks have to be at the appropriate levels before these systems will be considered seriously for commercial application.

Conversion efficiencies around 80% are not achievable with natural gas fired power plants based on low temperature fuel cells. In Section 6.3 it is shown that the exergy loss of PEMFCs is considerable higher than the exergy loss of MCFCs and SOFCs. These differences are primarily caused by the operating temperatures and are therefore true also for other types. In principle the exergy loss of PEMFCs can be reduced by improving the cell performance and raising the operation temperature. But, even in the case of almost ideal cell performance, the realization of high efficiencies will be hindered by the exergy loss of fuel conversion and purification. Fuel conversion and purification are not necessary if e.g. hydrogen from renewable energy sources is available. The application of low temperature fuel cells will be more attractive if hydrogen is available for power generation.

The thermodynamic performance of high temperature fuel cell systems depends seriously on the system design. It appears that system efficiencies are determined to a large extent by the exergy losses of heat transfer processes. Furthermore, the contribution of heat exchanger costs to the total system costs is in general high. During the evaluation of MCFC and SOFC systems as well during the search for the SOFC target system it fortunately appeared that internal heat transfer is minimal in the case of the more efficient systems. For the design of high temperatures fuel cell systems in general the following guidelines have to be considered:

1. Heat generation in the fuel cell should be reduced e.g. by minimizing the internal resistance or the application of multistage oxidation.
2. Heat generated in the fuel cell has to be used directly (without heat exchange) for internal reforming and for an integrated gas turbine cycle.

## Chapter 8 Conclusions

3. The need for heat transfer in heat exchangers should be reduced by applying cathode and anode recycle.
4. Heat exchange with small temperature differences should be realized by optimizing heat integration.

### 8.5 Combined heat and power

#### General

The combined generation of heat and power enables substantial fuel savings compared to a reference system based on separate generation of the same quantities of heat and power. In a true comparison all considered systems are using the same fuel. Then, the reduction of CO<sub>2</sub> emissions will be proportional with the fuel savings. All evaluations in Chapter 7 are made for design conditions of the considered plants. The evaluation of off-design conditions is discussed in Appendix 7.1 but is useful only for the optimization of specific CHP plants. Fuel savings up to 20% are achievable with CHP plants in operation today (see Table 7.4). For the future higher savings are conceivable depending on the development of the electrical efficiencies of CHP plants and large power stations.

#### Value diagrams

The application of the exergy concept and the resulting value diagrams are very useful to improve the insight into the performance of thermal power and CHP plants. It is actually strange that these diagrams are never used appropriately in literature. The value diagrams obviously show the large thermodynamic losses of steam and hot water generation in fired boilers and indicate the reduction of thermodynamic losses in the case of combined heat and power generation. Value diagrams are also helpful to optimize the use of residual heat. This has been demonstrated for the large internal combustion engine in Section 7.2. Thorough understanding of the thermodynamics for heat and power generation is necessary to achieve the highest benefits of CHP plants.

#### Existing concepts for evaluation

Thermal efficiencies are often used to indicate the merits of CHP plants. It is obvious that, because of the different thermodynamic value of electricity and heat, exergy efficiencies are more appropriate merit indicators. Comparison with a reference system (with separate generation of electricity and heat) is necessary, however, to determine the improvement that is achieved by the application of CHP. Equations are derived for the calculation of thermal and exergy efficiency of the reference system. In Section 7.4 it is demonstrated that the also use of exergy efficiencies or assigned exergy efficiencies is not appropriate to indicate the thermodynamic quality of CHP plants. The power loss ratio is a useful merit indicator, but can be used only for specific systems (e.g. systems with steam extraction)

#### Definition of new merit indicators

The determination of the merits of CHP is apparently a serious problem. Because of the large variety of CHP plants, the use of appropriate merit indicators is necessary to determine what kind of plants are the most beneficial for a specific situation. In [7.17] a variety of

indicators<sup>1</sup> used for legislative purposes is evaluated and it was concluded that “none of the indicators are capable of providing a full thermodynamic evaluation of CHP systems”. In Section 7.4 it is demonstrated too that the optimum plant is not determined only by the properties of the CHP plant, but depends also on the characteristics of the total system to which the CHP unit belongs (see e.g. Table 7.5). Useful indicators will require any kind of comparison with separate generation of heat and power. The fuel savings factor of a CHP plant in comparison with separate generation,  $F_{\text{fuel savings}}$ , is a true indicator of the thermodynamic quality of the CHP plant if there is no need to consider external requirements. A plant operator who is looking for minimum fuel consumption of his plant will prefer the use of this indicator. A government or owner of an industrial site who is looking for minimum fuel consumption of the total system, has to check first how the overall energy demand affects the maximum installed power of CHP. If the maximum installed CHP power is limited by the power demand, the fuel energy savings factor per unit electricity,  $F_{\text{FESUE}}$ <sup>2</sup>, is the true indicator to achieve the maximum benefit from combined generation. If the heat demand is limiting the maximum installed CHP power, the fuel exergy savings factor per unit heat exergy,  $F_{\text{FEXSUEXQ}}$ , is more appropriate. In Western European countries the total electricity demand is limiting the maximum installed CHP power; thus, Western European governments should focus on the fuel energy or fuel exergy savings per unit electricity.

The application of different fuels will complicate the discussion about merit indicators. True values of the merit indicators can be obtained only if CHP and reference system use of the same fuel. If for the generation of power always other primary fuels are used than for the generation of heat, additional (arbitrary) criteria are needed to define the merits of CHP.

#### Use of merit indicators

It appears that in general higher fuel savings can be achieved with CHP plants for the generation of low temperature heat than with CHP plants for the generation of high temperature heat (see Table 7.5). Thus, the application of CHP plants for the generation of low temperature heat is more attractive than the application of industrial CHP. For the generation of low temperature heat, however, the Heat Pump is an alternative option to reduce the thermodynamic losses of conventional heat generation. A general conclusion with regard to the preferred technology is impossible. Useful conclusions can be drawn only for specific cases and require more detailed evaluation of the alternatives. A rough evaluation of future energy conversion options for the Netherlands (see Section 3.4) indicated that the highest fuel savings are achieved by the use of industrial CHP for the generation of high temperature heat and heat pumps for the generation of low temperature heat.

High fuel savings as well as high fuel energy savings per unit electricity can be achieved with the application of Micro-CHP units with high electrical efficiencies (see Figures 7.21 and 7.22). The application of units with electrical efficiencies lower than 20% is

<sup>1</sup> All indicators used for legislative purposes are based on energy values. But exergy efficiencies are considered too in the paper.

<sup>2</sup> The fuel exergy savings per unit electricity,  $F_{\text{FEXSUE}}$ , gives the same ranking but the values differ somewhat from the value of the fuel energy savings per unit electricity because of the exergy factor of the fuel.

## Chapter 8 Conclusions

not really beneficial with regard to fuel savings. It can be helpful, however, for the implementation of micro-CHP. Natural gas fuelled micro-CHP systems with electrical efficiencies of 40% or higher and total efficiencies like hot water boilers are attractive. The development of reliable and cheap micro-CHP fuel cell systems that can reach this performance is recommended.

The merit indicators are very sensitive for the total thermal efficiency of the CHP plant (see e.g. Figure 7.22). High total thermal efficiencies are required to achieve high fuel savings. Also higher electric efficiencies have a positive effect on the fuel savings as well as on the fuel energy savings per unit electricity of CHP plants. Both indicators increase if the electric thermal efficiency increases. Suggestions that an optimum value for the electric efficiency of CHP units does exist are obviously false.

Combined Cycle plants with heat extraction for district heating show high values for the appropriate merit indicators, in particular the fuel savings per unit electricity. For the evaluations in this thesis the heat losses due to transport and distribution are ignored. These losses can be substantial and have a serious effect of the thermodynamic merits of the CHP plant. The selection of true values of these losses is in general not easy. Comparison of large scale CHP with e.g. micro-CHP requires careful evaluation of transport and distribution losses to come to reliable conclusions.

### 8.6 Exergy analysis

Exergy analysis is useful to determine thermodynamic losses of energy systems. Detailed knowledge of the various losses in a system is also necessary to understand the causes of losses and to identify options for loss reduction. With the data generally needed for system calculations, exergy values of flows of matter can easily be split in values for thermo-mechanical exergy and chemical exergy. In the case of system calculations with common computer programs as Cycle-Tempo, it is not always easy to discriminate between the various causes of exergy loss like friction, heat transfer, chemical reactions, and mixing of matter. For complicated processes like e.g. high temperature fuel cells with internal reforming, the various contributions have to be determined additionally with specific, more detailed, models.

Three methods to determine the specific exergy of solid and liquid fuels are compared in Chapter 2, Szargut, Baehr-I and Baehr-II. Baehr-I, the most fundamental method, gives the most accurate results. The results from the method of Szargut do correspond quite well with Baehr-I if the fuels are specified for the dry and ash free condition. For as received conditions serious deviations might occur. The ultimate analysis and the heating value of the fuel are necessary for both methods. The method of Baehr-II can be used if only the heating value of the fuel is available. The deviations can be higher, depending on the type of fuel.

To understand the thermodynamic quality of energy systems and to discuss the calculated results, specific diagrams (exergy flow diagrams, value diagrams) and additional parameters (thermodynamic equivalent temperature, exergy efficiencies of apparatuses and power cycles) are defined and demonstrated in this thesis. They all are helpful under specific circumstances. Exergy flow diagrams can be derived from system calculations at different levels of detail. This level of detail is actually determined by the specification of a number of subsystems. In general the number of subsystems should be as low as possible. Useful

examples are shown in Chapter 5 for a steam cycle plant and three CC plants and in Chapter 6 for the SOFC-GT target system. Value diagrams are primarily useful to visualize exergy losses of heat transfer processes and are in particular helpful in the case of more complicated arrangements of heat exchangers as e.g. in HRSG's (see Chapter 5). They are also useful to discuss and optimize the design of CHP plants (see Chapter 7).

Exergy efficiencies are helpful for the comparison of alternative processes. In many papers exergy efficiencies are defined as the ratio between the exergy that leaves the system and the exergy that enters the system. Such exergy efficiencies can be very misleading because the calculated values are seriously affected by exergy flowing through the system without participating to the conversion process. Therefore, more appropriate exergy efficiencies of apparatuses of Cycle-Tempo are specified in Appendix 3.2. Such efficiencies are primarily useful for the comparison of alternative apparatuses in a system. In the case of system studies the use of the relative exergy loss of apparatuses or subsystems appears to be more appropriate.

The internal exergy efficiency of thermal power cycles is defined in Chapter 2 and used comprehensively in Chapter 5. It has shown to be a good indicator for the performance of these cycles but has to be applied with care. It turned out (see e.g. Sections 5.2 and 5.3) that the value of this efficiency depends not only on the specified losses of the apparatuses belonging to the cycle but also on the cycle parameters (temperatures and pressures).

In general exergy efficiencies do not exactly represent the ratio between the actual process and the thermodynamically ideal process. This has been comprehensively demonstrated for the exergy efficiency of thermal power cycles. For that reason the internal exergy efficiency of a thermal power cycle has been defined alternatively, as a more accurate approximation of the ratio between the performances of the actual and the ideal cycle. This example also shows that it is very difficult to define the true process data for the ideal cycle. Thus, it appears that in general the true ratio between the actual and the ideal process cannot be determined. The exergy efficiencies as defined in Chapter 2 have to be considered as a reasonable approximation of the deviation from the ideal process.

## Appendix 2.1

**APPENDIX 2.1**  
**TABULATED DATA**

In this appendix useful data are tabulated for the calculation of the chemical exergy of usual mixtures in energy systems.

**Enthalpy and entropy values at standard pressure and temperature**

COMPOUNDS		phase	$\Delta_f h_{298}^{0,\text{mol}}$	$S_{298}^{0,\text{mol}}$	$M$
			[kJ/kmol]	[kJ/kmol.K]	[kg/kmol]
methane	CH <sub>4</sub>	g	- 74 850	186.16	16.0430
ethane	C <sub>2</sub> H <sub>6</sub>	g	- 84 680	229.49	30.0701
methanol	CH <sub>4</sub> O	g	- 200 890	239.7	32.0424
	CH <sub>4</sub> O	l	-238 810	126.8	
ammonia	NH <sub>3</sub>	g	- 46 190	192.33	17.0306
carbon dioxide	CO <sub>2</sub>	g	- 393 520	213.67	44.010
carbon monoxide	CO	g	- 110 525	197.56	28.0106
nitrogen oxide	NO	g	90 370	210.7	30.0061
	NO <sub>2</sub>	g	33 850	240.5	46.0055
	N <sub>2</sub> O	g	82 050	219.7	44.0128
	N <sub>2</sub> O <sub>4</sub>	g	9 660	304.4	92.011
water	H <sub>2</sub> O	g	- 241 818	188.72	18.0153
	H <sub>2</sub> O	l	- 285 830	69.95	
sulfur dioxide	SO <sub>2</sub>	g	- 296 830	248.1	64.0628
<b>ELEMENTS</b>					
hydrogen	H <sub>2</sub>	g	0	130.57	2.0159
oxygen	O <sub>2</sub>	g	0	205.03	31.9988
nitrogen	N <sub>2</sub>	g	0	191.5	28.0134
carbon	C	s	0	5.740	12.0112
sulfur	S	s	0	31.8	32.064

**Useful constants**

universal gas constant  $R^{\text{mol}} = 8.3143 \text{ J/mol K}$

standard conditions:  $T_0 = 25 \text{ °C}$  and  $p_0 = 1 \text{ atm} (= 101\,325 \text{ Pa})$

Avogadro's number:  $N_A = 6.022137 \times 10^{26} \text{ kmol}^{-1}$

Faraday constant:  $F = 96\,485 \text{ C/mol}$  (1 C = 1 A.s)

**Composition of saturated air**

Compositions of saturated air is often used as standard composition of the environment for the calculation of the chemical exergy of matter. The composition at 25°C has been specified by Baehr. Since a standard temperature of 15 °C is often used for the evaluation of energy systems, a composition adjusted for this temperature is presented too.

	$T_0 = 25\text{ °C}$ $p_0 = 1\text{ atm}$	$T_0 = 15\text{ °C}$ $p_0 = 1\text{ atm}$
component	mole fraction	mole fraction
CO <sub>2</sub>	0.0003	0.0003
N <sub>2</sub>	0.7565	0.7677
O <sub>2</sub>	0.2030	0.2060
H <sub>2</sub> O	0.0312	0.0168
Ar	0.0090	0.0091

**APPENDIX 2.2****EXERGY EFFICIENCIES FOR THE APPARATUSES OF CYCLE-TEMPO****1 Introduction**

The exergy efficiency is defined as:

$$\eta_{ex} = \frac{Ex_{\text{product}}}{Ex_{\text{source}}}$$

To apply this efficiency to specific systems, a further specification of the product and the source is necessary. The part of the exergy of the process flow that must be attributed to the product or the source has to be determined for all ingoing and outgoing process flows. If only part of the exergy of a flow can be attributed to a source or product, a breakdown is has to be made into an active part and a passive part.

In practice the kinetic and potential energy of process flows are usually neglected. Only if fluid velocities will be very high, as in the case of the exhaust of a low pressure steam turbine, the kinetic energy has to be considered. Therefore, in the specification of the exergy efficiencies of the considered apparatuses the kinetic and potential energy are usually ignored. The calculation of the exergy values in Cycle-Tempo distinguishes between the thermo-mechanical exergy and chemical exergy. The thermo-mechanical exergy is the power generated if the flow is brought in thermo-mechanical equilibrium with the environment using reversible processes in the prescribed way. The chemical composition remains unchanged during this process. The chemical exergy is the power generated if the flow is brought in chemical equilibrium with the environment using well-defined reversible processes. Then, the exergy of an amount of matter can be written as:

$$Ex_{\text{matter}} = Ex_{\text{matter}}^{\text{tm}} + Ex_{\text{matter}}^{\text{ch}}$$

The break down of the exergy into a thermo-mechanical and a chemical part is very useful to distinguish between the active part (source, product) and the non-active part (ballast) of exergy flows.

In the following sections exergy efficiencies are specified for the apparatuses available in Cycle-Tempo. A brief description of the processes in each of the apparatuses is presented and it is explained how the product and source are selected. Sometimes arbitrary choices have been made to define a specification; furthermore, it appeared that for some apparatuses an exergy efficiency could not be defined. For that reason Cycle-Tempo calculates also the so-called “universal exergy efficiency” to enable a comparison with other cases.

In the determined equations absolute exergy quantities are used. If these quantities are chosen such that they equal the quantity per unit of time, exergy flows can be used to calculate the efficiency values. The type numbers refer to the apparatus type numbers of Cycle-Tempo.

**2 Specification of exergy efficiencies****2.1 Turbine (type 3)**

In a turbine, a working fluid is expanded in order to deliver mechanical energy by a shaft. In a steam turbine not all steam is always completely expanded to the exhaust pressure;

large steam turbines have several extraction points from which steam can be extracted for feedwater preheating or for co-generation purposes. Then, the steam turbine must have more than one outlet. The calculation of the kinetic energy of the turbine exhaust flow is included in the apparatus model. Therefore, it is not necessary to consider this kinetic energy in the exergy calculations.

The generated shaft work is supposed to be the product of the turbine process, thus:

$$Ex_{\text{product}} = W_{\text{shaft}} \quad (1)$$

The shaft work is obtained by the expansion of the working fluid in the turbine. The corresponding change of the thermo-mechanical exergy of the working fluid is considered to be the exergy source. Since the chemical exergy of the working fluid does not change, the change in thermo-mechanical exergy is identical to the change in total exergy of the working fluid. If it is assumed that the turbine has more than one outlet, the exergy source can be written as:

$$Ex_{\text{source}} = Ex_{\text{in}}^{\text{tm}} - \sum Ex_{\text{out}}^{\text{tm}} = Ex_{\text{in}} - \sum Ex_{\text{out}} \quad (2)$$

Then, the exergy efficiency of the turbine becomes:

$$\eta_{\text{ex, turbine}} = \frac{W_{\text{shaft}}}{Ex_{\text{in}} - \sum Ex_{\text{out}}} \quad (3)$$

## 2.2 Heat exchanger (types 6 and 12)

In a heat exchanger, the primary fluid is heated by transferring heat from the secondary fluid. The purpose of a heat exchanger is in general the transfer of heat to the primary fluid. The increase of the thermo-mechanical exergy of the primary fluid is then considered to be the product of the heat transfer process. It is assumed that the chemical composition of the fluids in a heat exchanger will not change; then, the increase of the thermo-mechanical exergy is the same as the increase of the total exergy, thus:

$$Ex_{\text{product}} = Ex_{\text{p, out}} - Ex_{\text{p, in}} \quad (4)$$

The necessary heat is taken from the secondary fluid. The exergy transferred from the secondary fluid is considered to be the exergy source of the heat transfer process. The exergy transferred from the secondary fluid equals the exergy decrease of the secondary fluid in the heat exchanger, thus:

$$Ex_{\text{source}} = Ex_{\text{s, in}} - Ex_{\text{s, out}} \quad (5)$$

Then, the exergy efficiency of the heat exchanger can be written as:

$$\eta_{\text{ex, heat exchanger}} = \frac{Ex_{\text{p, out}} - Ex_{\text{p, in}}}{Ex_{\text{s, in}} - Ex_{\text{s, out}}} \quad (6)$$

Sometimes heat exchangers have more than one inlet for the secondary fluid, e.g. in the case of feedwater preheater. Then, the secondary side has more than one inlet. In that case the secondary fluids are mixed in the heat exchanger and leave the apparatus as one secondary flow; then, the exergy efficiency becomes:

$$\eta_{\text{ex, heat exchanger}} = \frac{Ex_{\text{p, out}} - Ex_{\text{p, in}}}{\sum Ex_{\text{s, in}} - Ex_{\text{s, out}}} \quad (7)$$

## Appendix 2.2

*Note:*

*In Cycle-Tempo the heat losses of a heat exchanger are included in the energy balance and therefore also in the calculated exergy values. That means that these losses are automatically included in the exergy efficiency*

### 2.3 Pump (type 8)

In a pump, an incompressible fluid is increased in pressure using shaft work. The exergy increase of the fluid is considered to be the product of this compression process. The shaft work is supplied to the process as the exergy source. The exergy efficiency of the pump then becomes:

$$\eta_{ex, \text{ pump}} = \frac{Ex_{\text{out}} - Ex_{\text{in}}}{W_{\text{shaft}}} \quad (8)$$

Pumps are often driven by electric motors. Cycle-Tempo has the option to include the losses of motor and transmission into the pump losses. In that case, the exergy efficiency must be:

$$\eta_{ex, \text{ pump}} = \frac{Ex_{\text{out}} - Ex_{\text{in}}}{W_{\text{electric}}} \quad (9)$$

### 2.4 Condenser (type 4)

Condensers can be used for different purposes which can affect the definition of the exergy efficiency. The condenser of a steam turbine cycle will be used in general to transfer useless heat to the environment. This heat is just wasted and therefore it cannot be seen as a product. That means that it is not possible to define an exergy efficiency for such a condenser. However, if steam or another cycle fluid is condensed at higher temperatures utilization of the heat transferred to the primary fluid is possible. For example, the condenser of a topping cycle that transfers useful heat to a bottoming cycle and a hot condenser, that condenses extraction steam for the generation of hot water for district heating. Then the exergy increase of the primary fluid is considered as the product of the heat transfer process and the same definition of the exergy efficiency can be used as in the case of heat exchangers (see 2.2). Also condensers can have more than one inlet at the secondary side; then, the exergy efficiency can be defined in general:

$$\eta_{ex, \text{ condenser}} = \frac{Ex_{p, \text{ out}} - Ex_{p, \text{ in}}}{\sum Ex_{s, \text{ in}} - Ex_{s, \text{ out}}} \quad (10)$$

*Note*

*In condensers, non-condensable gases are discharged, together with some vapor. Usually the effect of this flow is ignored in system calculations. However, if this discharge is considered explicitly in the process calculation, the exergy of the discharged fluid must be added to Equation 10 as part of the condenser's exergy loss.*

### 2.5 Feedwater preheater

The exergy efficiency of a feedwater preheater can be defined in the same way as the exergy efficiency of a heater. As feedwater preheaters usually have more than one secondary inlet, Equation 7 can be used to specify the exergy efficiency of a feedwater preheater.

### 2.6 Deaerator (type 7)

In a steam turbine cycle a deaerator has various tasks: the removal of non-condensable gases from the feedwater, feedwater heating and the storage of feedwater. For the exergy analysis only the feedwater heating must be considered. Then, the deaerator acts as a direct contact heater in which feedwater is mixed with slightly superheated steam, usually extraction steam, and condensate from the high pressure feedwater preheaters. The resulting water mixture leaves the feedwater heater at boiling condition. The feedwater that enters the deaerator is considered to be the primary fluid; this fluid is heated by the steam and the hot condensate. The hot fluids, steam and hot condensate, are supposed to be the secondary fluid. In the same way as for the heat exchanger, the exergy of the product can be defined as:

$$Ex_{\text{product}} = m_p \cdot (ex_{\text{out}} - ex_{p, \text{in}}) = m_p \cdot ex_{\text{out}} - Ex_{p, \text{in}} \quad (11)$$

in which  $m_p$  is the mass of the condensate, the primary fluid, heated in the deaerator.

And the exergy of the source can be written as:

$$Ex_{\text{source}} = \sum (m_s \cdot ex_{s, \text{in}}) - ex_{\text{out}} \cdot \sum m_s = \sum Ex_{s, \text{in}} - ex_{\text{out}} \cdot \sum m_s \quad (12)$$

Then, the exergy efficiency of the deaerator becomes:

$$\eta_{\text{ex, deaerator}} = \frac{m_p \cdot ex_{\text{out}} - Ex_{p, \text{in}}}{\sum Ex_{s, \text{in}} - ex_{\text{out}} \cdot \sum m_s} \quad (13)$$

*Note:*

*In the deaerator the non-condensable gases are extracted, together with a small amount of steam. If the discharge of this quantity of steam is explicitly included in the process calculation, the exergy of this flow is part of the exergy loss of the deaerator has to be subtracted from the product.*

### 2.7 Compressor, fan (type 29)

In a compressor or fan, a compressible fluid is increased in pressure by means of shaft power. The exergy efficiency for compressors is specified in the same way as for pumps (see Section 2.3):

$$\eta_{\text{ex, compressor}} = \frac{Ex_{\text{out}} - Ex_{\text{in}}}{W_{\text{shaft}}} \quad (14)$$

### 2.8 Mixer, splitter, valve (type 9, 10, 11, 14)

Mixers, splitters and valves are tools that are frequently used in energy conversion systems but are not used for the conversion or transfer of energy. They may cause exergy losses, but it is not possible to define a product. Therefore, it is also not possible to specify an exergy efficiency.

*Note:*

*In system calculations splitters are often used to separate fluid components from a mixture. In that case, actually the splitter acts as a separator. However, it is also not possible to specify a meaningful functional exergy efficiency for a separator. In a calculation the separation of fluid components can easily be done and can result into an increase of exergy. Obviously, this will not be a true result. In practice the*

## Appendix 2.2

*separation of fluid components will usually require several processes with changing temperature or pressure of the fluids in between. The true exergy losses of the separation process can be determined only if the process (including all necessary apparatuses) is correctly modeled.*

### 2.9 Drum (type 15)

The drum is used to model circulating evaporators as often used in steam boilers. The evaporator circuit in general consists of a heat exchanger, circulation pump and a drum. Heating and partial evaporation of the circulating fluid occurs in the heat exchanger, the actual evaporator. In the drum, liquid and vapor are separated and the recirculated liquid is mixed with the liquid feed. If drum and heat exchanger are distinguished as individual apparatuses, the drum can be considered as an apparatus in which a liquid, the feed, is evaporated using heat transferred from the fluid from and to the evaporator circuit. Because it is assumed that the system operates in steady state, which means that the mass of the feed is the same as the mass of the steam that leaves the drum. The exergy transferred to the feed, during heating and evaporation, is considered as the exergy product. The exergy transferred from the fluid circulating through the evaporator circuit is seen as the exergy source. Then, the exergy efficiency of the drum becomes:

$$\eta_{ex, \text{ drum}} = \frac{Ex_{\text{steam, out}} - Ex_{\text{feedwater, in}}}{Ex_{\text{evaporator, out}} - Ex_{\text{evaporator, in}}} \quad (15)$$

With this equation the exergy increase of the fluid in the boiler circulation pump is ignored. If this is supposed to be unacceptable the exergy at evaporator inlet can be replaced by the exergy of the fluid at the inlet of the pump.

### 2.10 Combustor (type 13)

In a combustion chamber, fuel is combusted using air (or another oxidizer). The combustion products, the flue gases, are discharged. It is assumed that the combustion process will be adiabatic. If heat losses have to be considered, as will in general be the case in steam boiler models, these losses can be taken into account in the heat transfer system. The purpose of combustion is to generate a hot gas (flue gas), from which only the thermo-mechanical exergy is utilized. Therefore, the thermo-mechanical exergy of the hot flue gas is supposed to be the product of the combustion chamber.

Fuel and oxidizer are fed to the combustion chamber, often at elevated temperature and pressure. The exergy of the necessary heat and power for increasing the pressure and temperature of fuel and oxidant will reduce the net generated exergy. Thus the thermo-mechanical exergy of fuel and oxidizer must be subtracted from the thermo-mechanical exergy of the hot flue gas. Thus, the product of the combustion chamber can be written as:

$$Ex_{\text{product}} = E_{\text{flue gas}}^{\text{tm}} - Ex_{\text{fuel}}^{\text{tm}} - Ex_{\text{oxidizer}}^{\text{tm}} \quad (16)$$

In principle the chemical exergy of the fuel is used as the exergy source. If the composition of the oxidizer is not exactly the same as the composition of reference air used for the determination of the chemical exergy values, the exergy of the oxidizer will not be zero, and must be taken into account in the exergy balance of the system. The chemical exergy of the

flue gas flow is discharged to the environment and will not become available as product.

Thus, the net available exergy source is:

$$Ex_{\text{source}} = Ex_{\text{fuel}}^{\text{ch}} + Ex_{\text{oxidizer}}^{\text{ch}} - Ex_{\text{flue gas}}^{\text{ch}} \quad (17)$$

Then, the exergy efficiency of the combustion chamber will be defined as follows:

$$\eta_{\text{ex, combustion chamber}} = \frac{Ex_{\text{flue gas}}^{\text{tm}} - Ex_{\text{fuel}}^{\text{tm}} - Ex_{\text{oxidizer}}^{\text{tm}}}{Ex_{\text{fuel}}^{\text{ch}} + Ex_{\text{oxidizer}}^{\text{ch}} - Ex_{\text{flue gas}}^{\text{ch}}} \quad (18)$$

This definition does not consider the presence of non-combustible components in the fuel that are separated in the combustion chamber in the form of ash or slag. The chemical exergy of these substances is not utilized for the production of heat and must, therefore, be subtracted from the chemical exergy of the fuel.

In general, most of the ash and slag is discharged from the gas at high temperature in the combustion chamber. In principle the heat from the ash and slag can be utilized; if not, its thermo-mechanical exergy is lost externally and must be considered as an external loss. The ash remaining in the flue gas will leave the combustor as fly ash that will be utilized together with the flue gas. Thus, the thermo-mechanical exergy of the non-combustible solid or liquid components (further indicated as ash) is considered to be a product of the combustion process. Then, if the exergy of non-combustible components cannot be ignored, the exergy efficiency of the combustion chamber becomes:

$$\eta_{\text{ex, combustion chamber}} = \frac{Ex_{\text{flue gas}}^{\text{tm}} + Ex_{\text{ash}}^{\text{tm}} - Ex_{\text{fuel}}^{\text{tm}} - Ex_{\text{oxidizer}}^{\text{tm}}}{Ex_{\text{fuel}}^{\text{ch}} + Ex_{\text{oxidizer}}^{\text{ch}} - Ex_{\text{ash}}^{\text{ch}} - Ex_{\text{flue gas}}^{\text{ch}}} \quad (19)$$

*Note:*

*In practice, due to incomplete combustion not all fuel will be converted in the combustion chamber. In the ideal case the non-converted fuel will be heated and cooled but does not participate to the conversion process and is only considered to be a ballast flow.*

### 2.11 Boiler and reheater (type 1, 2)

Usually, a boiler is a complex installation, consisting of various apparatuses like a combustion chamber, several heat exchangers, pumps and fans. In the case of a detailed analysis of the boiler, a suitable boiler subsystem can be build up by using the available apparatus models. Then, the exergy efficiency of all apparatuses will be calculated separately. The exergy efficiency of the subsystem boiler must be defined additionally, using the calculated exergy values.

However, a detailed evaluation of the subsystem boiler is not always necessary. In many cases only a rough consideration of the boiler is appropriate; e.g. if the evaluation focuses on the cycle design. Then, the boiler can be considered as an apparatus in which a process flow is heated and evaporated. To enable the determination of an overall plant efficiency in such cases, the fuel consumption can be calculated by using a predefined thermal efficiency of the boiler. In such an evaluation, the flue gas flow to the stack is not considered explicitly and the heat discharged with the flue gases is included in the thermal efficiency of the boiler. Also the exergy of the flue gas leaving the boiler stack is unknown.

## Appendix 2.2

In the case of a steam cycle with steam reheat, a reheater must be added in a Cycle-Tempo model. For the reheater a thermal efficiency can be specified separately. In practice, the boiler and reheater are integrated and only one single thermal efficiency will exist for the boiler including the reheater. In the Cycle-Tempo model this can be realized by specifying the same thermal efficiency for the boiler and the reheater.

The purpose of the boiler and the reheater is to supply thermo-mechanical exergy to the cycle fluid. Therefore, the increase of the thermo-mechanical exergy of the cycle fluid in the apparatus, is supposed to be the exergy product of the boiler and the reheater. The chemical composition of the cycle fluid does not change during the heat transfer. Then, the increase of the thermo-mechanical exergy is the same as the increase of the total exergy. Thus, for the boiler:

$$Ex_{\text{product}} = Ex_{\text{steam}} - Ex_{\text{feedwater}} \quad (20)$$

And for the reheater:

$$Ex_{\text{product}} = Ex_{\text{steam out}} - Ex_{\text{steam in}} \quad (21)$$

Fuel is used to generate the heat for the boiler process. Then, the chemical exergy of the fuel and the oxidizer is supposed to be the exergy source, the same as in the case of the combustion chamber. But in the case of a global boiler model, the oxidizer is supposed to be air that enters the boiler subsystem at environmental temperature. Thus, the exergy of this air will be zero or very close to zero. Another reason to assume that the exergy of the combustion air may be ignored is that the air flow is not explicitly available in the boiler and reheater models and additional specification would require a modification of the existing models.

Therefore it is assumed that:

$$Ex_{\text{source}} = Ex_{\text{fuel}}^{\text{ch}} \quad (22)$$

Then exergy efficiency of the boiler and reheater can be written as:

$$\eta_{\text{ex, boiler}} = \frac{Ex_{\text{steam}} - Ex_{\text{feedwater}}}{Ex_{\text{fuel}}^{\text{ch}}} \quad (23)$$

$$\eta_{\text{ex, reheater}} = \frac{Ex_{\text{steam, out}} - Ex_{\text{steam, in}}}{Ex_{\text{fuel}}^{\text{ch}}} \quad (24)$$

The chemical exergy of the fuel corresponds of course with the part of the fuel that is necessary to heat the boiler or the reheater respectively.

*Note:*

*By using the chemical exergy of the fuel as the fuel exergy, it is implicitly assumed that fuel is supplied at ambient temperature and pressure.*

### 2.12 Moisture separator, flue gas condenser (type 22)

In a moisture separator or flue gas condenser, flue gas containing a certain amount of water vapor is cooled to a temperature below its dew point. This will cause partial condensation of the water vapor; the condensate is separated from the gas and discharged separately. The heat from condensation and gas cooling is used to heat another fluid. Therefore, the moisture separator is considered to operate like a heat exchanger; the only difference with an ordinary heat exchanger is that the condensate is discharged separately.

That means that the secondary side of this heat exchanger has two outlets. Both secondary flows can be used elsewhere in a plant; therefore, it is not assumed that the exergy of one of these flows is lost.

Thus, the exergy increase of the primary fluid is supposed to be the exergy product of the moisture separator or flue gas condenser. The exergy decrease of the secondary fluid is the exergy source. Then, the exergy efficiency of a moisture separator or flue gas condenser becomes:

$$\eta_{ex, \text{moisture separator}} = \frac{Ex_{p, \text{out}} - Ex_{p, \text{in}}}{Ex_{s, \text{in}} - \sum Ex_{s, \text{out}}} \quad (25)$$

### 2.13 Gasifier (type 23)

In a gasifier, a solid fuel (that enters the apparatus usually at elevated temperature and pressure) is converted into a gaseous fuel. Gasification takes place by using an oxidizer. The oxidizer usually consists of air, oxygen or steam, or a mixture of these fluids. Very high temperatures are required for the gasification process. Depending on the reactor design jacket cooling might be necessary to protect the reactor walls. Therefore, the gasifier model is provided with a cooling system that can be used to heat any cooling fluid. If no cooling fluid is specified the gasifier will operate adiabatic. Ash and slag are partially removed in the reactor and are discharged at elevated temperature; the thermo-mechanical exergy of this flow can be used elsewhere in the plant and is not supposed to be wasted beforehand. The remaining non-reacting components leave the reactor together with the product gas.

For the efficiency of a gasification process two kinds of efficiencies are used: the cold gas efficiency and the hot gas efficiency. Both efficiencies are specified here, but only the hot gas efficiency is presented in the Cycle-Tempo output.

#### Cold gas efficiency

If the gasifier is considered as a device that generates a fuel that should be transported and distributed to the users at environmental temperature, the thermal energy is considered not to be useful and will be ignored. Only the chemical exergy of the product gas is supposed to be of interest and is therefore seen as the exergy product of the apparatus. The chemical exergy of the fuel that must be gasified and the oxidizers are in principle transferred to the process as the exergy source. The chemical exergy of the ash (or slag) does not contribute to the chemical reaction of the process and must be distracted from the exergy source if its chemical exergy is supposed to be included in the chemical exergy of the fuel. Then, the cold gas exergy efficiency of the gasifier becomes:

$$\eta_{ex, \text{gasifier (cold gas)}} = \frac{Ex_{\text{productgas}}^{\text{ch}}}{Ex_{\text{fuel}}^{\text{ch}} + Ex_{\text{steam}}^{\text{ch}} + Ex_{\text{oxygen}}^{\text{ch}} + Ex_{\text{air}}^{\text{ch}} - Ex_{\text{ash}}^{\text{ch}}} \quad (26)$$

The cold gas efficiency ignores the thermal energy and thermo-mechanical exergy involved into the gasification process. It is the result of an incomplete evaluation and should be used only for very specific applications.

#### Hot gas efficiency

The hot gas efficiency has to consider all relevant exergy flows of the gasification process and is supposed to be the true exergy efficiency of the gasifier. It assumes that the exergy of the product gas as well as the exergy of the generated heat are the products of the

## Appendix 2.2

gasification process. The exergy product of the gasification process, thus, also includes the generated thermo-mechanical exergy, which is the difference between the thermo-mechanical exergy of the fluids that leave the system and of the fluids that enter the system. Thus, the exergy product will be:

$$Ex_{\text{product}} = Ex_{\text{productgas}} + Ex_{\text{ash}}^{\text{tm}} + (Ex_{\text{out}} - Ex_{\text{in}})_{\text{cooling}} - (Ex_{\text{fuel}}^{\text{tm}} + Ex_{\text{steam}}^{\text{tm}} + Ex_{\text{oxygen}}^{\text{tm}} + Ex_{\text{air}}^{\text{tm}}) \quad (27)$$

The exergy of the product gas includes the chemical exergy as well as the thermo-mechanical exergy. The composition of the cooling fluid doesn't change; the exergy increase is only the increase of the thermo-mechanical exergy.

The exergy source is the same as in the case of the cold gas efficiency, in fact the change of the chemical exergy of the fuel and the oxidizer during the gasification process. Thus, the hot gas exergy efficiency, the actual exergy efficiency of the gasifier, becomes:

$$\eta_{\text{ex, gasifier}} = \frac{Ex_{\text{productgas}} + Ex_{\text{ash}}^{\text{tm}} + (Ex_{\text{out}} - Ex_{\text{in}})_{\text{cooling}} - (Ex_{\text{fuel}}^{\text{tm}} + Ex_{\text{steam}}^{\text{tm}} + Ex_{\text{oxygen}}^{\text{tm}} + Ex_{\text{air}}^{\text{tm}})}{Ex_{\text{fuel}}^{\text{ch}} + Ex_{\text{steam}}^{\text{ch}} + Ex_{\text{oxygen}}^{\text{ch}} + Ex_{\text{air}}^{\text{ch}} - Ex_{\text{ash}}^{\text{ch}}} \quad (28)$$

### 2.14 Reformer (type 20)

The reformer is supposed to be a device that changes the chemical composition of a fluid flow; the product is a combustible gas. Steam is added to the fuel feed to enable the conversion into the product gas. The reforming reaction has to take place at high temperature; because of the equilibrium of the reforming reaction, reaction temperatures  $>800^{\circ}\text{C}$  are usual. The use of a suitable catalyst will limit the reaction temperature. Heat transfer to the reactor is necessary because of the endothermic reforming reaction. The heat is normally obtained from a furnace in which fuel is combusted. Heat from the combustion process is transferred to the reactor tubes by convection and radiation. Integrated reformers are often used to enable the use of residual heat from the reactor off-gases to preheat the reactor feed.

The reformer model of Cycle-Tempo is a relative simple model and does not include the combustion in the reformer furnace. It is assumed that a hot gas, from a combustor or any other hot gas generator, enters the reformer where it is cooled during heat transfer to the reactor and to the reactor feed. The present model does not inherently avoid conflicts with the second law of thermodynamics. However a more detailed reformer model can be created by building a reformer subsystem in which heat transfer and reforming reactions take place in separate apparatuses. In the present model, the chemical conversion of a fuel gas will be achieved by adding heat from a flue gas. Therefore, the change of the chemical exergy of the reactants is supposed to be the product of the reformer process:

$$Ex_{\text{product}} = Ex_{\text{productgas}}^{\text{ch}} - (Ex_{\text{fuel}}^{\text{ch}} + Ex_{\text{steam}}^{\text{ch}}) \quad (29)$$

In principle the thermo-mechanical exergy of the flue gas is available for the conversion of the fuel; thus, the change of the thermo-mechanical exergy of the flue gas can be considered to be the exergy source. But not only the chemical exergy of the product gas changes, also the thermo-mechanical exergy will change. Also this thermo-mechanical exergy can be utilized. Therefore, the net exergy source is the change of thermo-mechanical exergy of the flue gas minus the change of thermo-mechanical exergy of the reactants:

$$Ex_{\text{source}} = Ex_{\text{flue gas, in}}^{\text{tm}} - Ex_{\text{flue gas, out}}^{\text{tm}} - (Ex_{\text{productgas}}^{\text{tm}} - (Ex_{\text{fuel}}^{\text{tm}} + Ex_{\text{steam}}^{\text{tm}})) \quad (30)$$

The chemical composition of the flue gas does not change during cooling in the reformer. Thus, the change in thermo-mechanical exergy of the flue gas is the same as the change in total exergy. Then the exergy efficiency of the reformer becomes:

$$\eta_{ex, \text{ reformer}} = \frac{Ex_{\text{productgas}}^{\text{ch}} - (Ex_{\text{fuel}}^{\text{ch}} + Ex_{\text{steam}}^{\text{ch}})}{(Ex_{\text{flue gas, in}} - Ex_{\text{flue gas, out}}) - (Ex_{\text{productgas}}^{\text{tm}} - (Ex_{\text{fuel}}^{\text{tm}} + Ex_{\text{steam}}^{\text{tm}}))} \quad (31)$$

### 2.15 Fuel cell (type 21)

In a fuel cell, electricity is generated by the electrochemical reaction of a fuel and an oxidizer. Usually the air will be used as the oxidizer, but also oxygen can be used or, as in the case of Molten Carbonate Fuel Cells, a mixture of air and carbon dioxide. Fuel and oxidizer are fed separately to the anode and the cathode of the fuel cell, respectively. Not all fuel and oxidizer will be utilized in the fuel cell, because the voltage at the outlet of the cell must be sufficiently high. Furthermore, fuel and oxidizer will contain also inert components that will not take part into the electrochemical reaction; these components will be discharged together with the reaction products. The anode fluid and cathode fluid are fully separated by the anode-electrolyte-cathode layer, and leave the cell separately.

The fuel cell generates electricity as a direct current. The direct current electricity is supposed to be the product of the fuel cell. For connection with the electricity grid, a DC/AC converter will be necessary. In the Cycle-Tempo model the losses of this conversion are included in the losses of fuel cell stack if the DC/AC conversion efficiency is specified. The electrochemical reaction is actually the exergy source; thus, the change in chemical exergy of fuel and oxidizer will be the exergy source. However, also the thermo-mechanical exergy of fuel and oxidizer will change in the fuel cell because of the heat generated in the cell. The thermo-mechanical exergy transferred to the fluids can be utilized elsewhere in the system; thus, this exergy increase should be subtracted from the change in chemical exergy of the fluids. Then the exergy source becomes:

$$Ex_{\text{source}} = (Ex_{\text{in}} - Ex_{\text{out}})_{\text{fuel}}^{\text{ch}} + (Ex_{\text{in}} - Ex_{\text{out}})_{\text{oxidizer}}^{\text{ch}} - (Ex_{\text{out}} - Ex_{\text{in}})_{\text{fuel}}^{\text{tm}} - (Ex_{\text{out}} - Ex_{\text{in}})_{\text{oxidizer}}^{\text{tm}} \quad (32)$$

From this equation it appears that the exergy source equals actually the change in total exergy of fuel and oxidizer fluids. Then, the exergy efficiency of the fuel cell becomes:

$$\eta_{ex, \text{ fuel cell}} = \frac{P_{\text{electric}}}{(Ex_{\text{fuel, in}} - Ex_{\text{fuel, out}}) + (Ex_{\text{oxidizer, in}} - Ex_{\text{oxidizer, out}})} \quad (33)$$

*Note:*

*A part of the chemical exergy of the fuel is converted into electricity and another part into thermo-mechanical exergy (heat). In Equation 33 the part of the chemical exergy of the fuel that is converted into thermo-mechanical exergy is not supposed to be a product of the fuel cell process. If the fuel cell generates more heat, the generated electrical power will be less.*

*The objective of the fuel cell is to convert as the chemical exergy as far as possible into electricity. Equation 33 does not indicate really to which extent the fuel cell is able to achieve this objective.*

## Appendix 2.2

### 2.16 Scrubber, separator and saturator (type 25, 26, 28)

The objective of a scrubber, separator or saturator is to remove or to add specific components or particles to a fluid. The processes have usually a limited effect on the thermodynamic properties of the fluid. It is actually not possible to define an exergy product of these processes. Then, an exergy efficiency cannot be defined. Only the “universal exergy efficiency” can be used to indicate the height of the exergy loss of these apparatuses.

### 2.17 Chemical reactor (type 27)

Exergy efficiencies have been defined before for some specific reactors like a combustor, reformer and gasifier. The exergy efficiencies as defined are different, not only because of differences in the layout of the apparatuses, but also because of the different objectives for these reactors.

The chemical reactor of Cycle-Tempo was added to enable the calculation of a new equilibrium composition of a flow using one equilibrium reaction like e.g. the water gas shift reaction and the methane reforming reaction. Afterwards, the use of other reactions became possible by enabling the specification of reactions by a user subroutine. The reactor can have 1 to 5 inlets and should have only 1 outlet. The specification of an exergy efficiency for the chemical reactor is only possible if the objectives are known, which is not the case for a general model like this chemical reactor. Therefore, no exergy efficiency is defined for this apparatus. Only the “universal exergy efficiency” can be used to indicated the height of the exergy losses of the reactor.

### 2.18 Generator (type G) and electric motor (type M)

The models of the generator and the electric motor were initially not considered to be an apparatus model in Cycle-Tempo. The apparatuses are used only to transfer work to or from the system and to convert work into electricity or vice versa. With the introduction of the exergy calculation it appeared to include also these apparatuses in the evaluation. The exergy efficiencies for these apparatuses are straightforward, because these apparatuses have only one inlet and one outlet for exergy. The difference between the in- and outgoing exergy is the exergy loss. Then, the exergy efficiency of the generator becomes:

$$\eta_{ex, generator} = \frac{Ex_{\text{electricity}}}{Ex_{\text{shaft work}}} = \frac{W_{\text{electrical}}}{W_{\text{shaft}}} \quad (34)$$

And the exergy efficiency of the electric motor:

$$\eta_{ex, electric motor} = \frac{Ex_{\text{shaft work}}}{Ex_{\text{electricity}}} = \frac{W_{\text{shaft}}}{W_{\text{electrical}}} \quad (35)$$



## APPENDIX 2.3 PROPERTIES OF SOLID AND LIQUID FUELS

### TABLE OF CONTENTS

<b>1</b>	<b>Conversion of specified data of coal and biomass</b>
1.1	Introduction
1.2	Conversion from one state into the other
<b>2</b>	<b>The calculation of the exergy of solid and liquid fuels</b>
2.1	The method of Baehr-I
2.2	The method of Baehr-II

### 1 Conversion of specified data of coal and biomass

#### 1.1 Introduction

The composition and the heating value of solid fuels, like coal and biomass, can be specified for practical application in different ways:

- the real state of the fuel (as received) (nomenclature:  $x_i$ ,  $LHV_F$ ,  $HHV_F$ ,  $ex_F$ )
- the dry (water free) fuel ( $x_{i, \text{dry}}$ ,  $LHV_{F, \text{dry}}$ ,  $HHV_{F, \text{dry}}$ ,  $ex_{F, \text{dry}}$ )
- the dry and ash free fuel ( $x_{i, \text{daf}}$ ,  $LHV_{F, \text{daf}}$ ,  $HHV_{F, \text{daf}}$ ,  $ex_{F, \text{daf}}$ )

In general data of coal are presented for one of these states. The procedure for the calculation of fuel conversion processes is normally based on one kind of fuel specification. To enable the use of fuel data specified for any condition, it must be possible to convert the available data into the kind of data necessary for the calculation procedure. Thus, it might be necessary to convert the available data first into the data needed.

Published fuel data do not always present the lower heating value as well as the higher heating value of the fuel. If only one heating value is specified, it might be necessary that the other has to be calculated using the available data.

It is assumed that a specification of the ultimate analysis for one of the states of the fuel is available.

#### 1.2 Conversion from one state into the other

##### Conversion of data from the dry and ash free state into the as received state

The calculation is based on the following assumptions:

Known:  $x_{i, \text{daf}}$ ,  $LHV_{F, \text{daf}}$  or  $HHV_{F, \text{daf}}$ ,  $ex_{F, \text{daf}}$  and  $x_{\text{ash}}$  and  $x_{\text{water}}$

Find:  $x_i$ ,  $LHV_F$ ,  $HHV_F$  and  $ex_F$

The fractions  $x_{\text{ash}}$  and  $x_{\text{water}}$  are mass fractions of 1 kg of fuel in the real state. The mass fraction of water represents the quantity of free water in the fuel that can be removed by drying the fuel. For the dry and ash free fuel the mass fractions are specified in a way that:

$$\sum x_{i, \text{daf}} = 1$$

If it is assumed that 1 kg of fuel in the real state contains  $f_{\text{daf}}$  kg dry and ash free fuel, the total mass of the fuel in the real state can be written as:

$$\sum x_i = f_{\text{daf}} \cdot \sum x_{i, \text{daf}} + x_{\text{ash}} + x_{\text{water}} = 1$$

Thus:  $f_{\text{daf}} = 1 - x_{\text{ash}} - x_{\text{water}}$

Then, the mass fractions for the as received state can be calculated as:

$$x_i = (1 - x_{\text{ash}} - x_{\text{water}}) \cdot x_{i, \text{daf}} \quad (1)$$

Water and ash are supposed to be inert components that do not react with other components during the combustion reaction. The heat from the isothermal combustion reaction is completely determined by the reactions of the other components. The removal of the water and the ash from the fuel will increase the heat per kilogram of the fuel. If the isothermal combustion of  $m_{\text{F, daf}}$  kg of dry and ash free fuel is compared with the isothermal combustion of a quantity of  $m_{\text{F}}$  fuel as received that delivers the same amount of heat, then:

$$m_{\text{F, daf}} \cdot HHV_{\text{F, daf}} = m_{\text{F}} \cdot HHV_{\text{F}} = Q$$

Since  $m_{\text{F, daf}} = f_{\text{daf}} \cdot m_{\text{F}}$  the mass ratios of the fuels are:

$$\frac{m_{\text{F, daf}}}{m_{\text{F}}} = f_{\text{daf}} = (1 - x_{\text{ash}} - x_{\text{water}})$$

Then, the higher heating value of the fuel in the real state can be calculated using the following equation:

$$HHV_{\text{F}} = \frac{m_{\text{F, daf}}}{m_{\text{F}}} \cdot HHV_{\text{F, daf}}$$

Then, the heating value of the fuel in the real state becomes:

$$HHV_{\text{F}} = (1 - x_{\text{ash}} - x_{\text{water}}) \cdot HHV_{\text{F, daf}} \quad (2)$$

The higher heating value of the fuel is determined assuming that after the isothermal combustion process all water exists as liquid water. The water that leaves the combustion process consists of the free water in the fuel and the water generated by the oxidation of the hydrogen in the fuel.

The lower heating value of the fuel is determined assuming that after isothermal combustion all water exists as water vapor. Then, the difference between the lower and the higher heating value is heat of evaporation of the water available in the off-gasses of the combustion process:

$$LHV_{\text{F}} = HHV_{\text{F}} - m_{\text{water}} \cdot r$$

The parameter  $r$  is the heat of evaporation of water at 25°C, thus:  $r = 2442.5$  kJ/kg

The oxidation of 1 kmol of hydrogen results into the generation of 1 kmol of water, thus:

$$\text{as: } n_{\text{H}_2} = n_{\text{H}_2\text{O}} \quad \text{then: } \frac{m_{\text{H}_2}}{M_{\text{H}_2}} = \frac{m_{\text{H}_2\text{O}}}{M_{\text{H}_2\text{O}}} \quad \text{and} \quad m_{\text{H}_2\text{O}} = m_{\text{H}_2} \cdot \frac{M_{\text{H}_2\text{O}}}{M_{\text{H}_2}}$$

The dry and ash free fuel does not contain free water. Then the relation between the lower and the higher heating value of the dry and ash free fuel becomes:

$$LHV_{\text{F, daf}} = HHV_{\text{F, daf}} - x_{\text{H}_2, \text{daf}} \frac{M_{\text{H}_2\text{O}}}{M_{\text{H}_2}} \cdot r$$

## Appendix 2.3

$$LHV_{F, \text{daf}} = HHV_{F, \text{daf}} - x_{\text{H}_2, \text{daf}} \times \frac{18.0153}{2.0159} \cdot 2442.5 \text{ [kJ/kg]}$$

$$LHV_{F, \text{daf}} = HHV_{F, \text{daf}} - x_{\text{H}_2, \text{daf}} \times 21828 \text{ [kJ/kg]} \quad (3)$$

For the real fuel the equation becomes:

$$LHV_F = HHV_F - (x_{\text{water}} + x_{\text{H}_2} \frac{M_{\text{H}_2\text{O}}}{M_{\text{H}_2}}) \cdot r$$

$$LHV_F = HHV_F - (x_{\text{water}} + x_{\text{H}_2} \times \frac{18.0153}{2.0159}) \times 2442.5 \text{ [kJ/kg]}$$

$$LHV_F = HHV_F - (x_{\text{water}} + x_{\text{H}_2} \times 8.9366) \times 2442.5 \text{ [kJ/kg]} \quad (4)$$

The exergy of the fuel in the as received state differs from the exergy of the fuel in the dry and ash free state because of the difference of the mass for the same quantity of the reactants. Thus, the ratio of the exergies is the same as the ratio of the higher heating values:

$$ex_F = (1 - x_{\text{ash}} - x_{\text{water}}) \cdot ex_{F, \text{daf}} \quad (5)$$

With the Equation 1 to Equation 5 all required conversions can be made.

Conversion of data from the dry state into the as received state

The calculation is based on the following assumptions:

Available data:  $x_{i, \text{dry}}$ ,  $LHV_{F, \text{dry}}$  or  $HHV_{F, \text{dry}}$ ,  $ex_{F, \text{dry}}$  and  $x_{\text{water}}$

Demanded:  $x_i$ ,  $LHV_F$  and  $HHV_F$  and  $ex_F$

The fractions  $x_{\text{ash}}$  and  $x_{\text{water}}$  are mass fractions of 1 kg of fuel in the real state. For the dry state of the fuel the mass fractions are specified in a way that:

$$\sum x_{i, \text{dry}} = 1$$

If it is assumed that 1 kg of fuel in the real state contains  $f_{\text{dry}}$  kg dry fuel, for the total mass of the fuel in the real state can be written:

$$\sum x_i = f_{\text{dry}} \cdot \sum x_{i, \text{dry}} + x_{\text{water}} = 1$$

Thus:  $f_{\text{dry}} = 1 - x_{\text{water}}$

Then, the mass fractions for the as received state can be calculated as:

$$x_i = (1 - x_{\text{water}}) \cdot x_{i, \text{dry}} \quad (6)$$

If the isothermal combustion of  $m_{F, \text{dry}}$  kg of dry fuel is compared with the isothermal combustion of a quantity of  $m_F$  fuel as received that delivers the same amount of heat, then:

$$m_{F, \text{dry}} \cdot HHV_{F, \text{dry}} = m_F \cdot HHV_F = Q$$

Since  $m_{F, \text{dry}} = f_{\text{dry}} \cdot m_F$  the mass ratios of the fuels are:

$$\frac{m_{F, \text{dry}}}{m_F} = f_{\text{dry}} = (1 - x_{\text{water}})$$

Then, the higher heating value of the fuel in the real state can be calculated using the following equation:

$$HHV_F = \frac{m_{F, \text{dry}}}{m_F} \cdot HHV_{F, \text{dry}}$$

Then, the heating value of the fuel in the real state becomes:

$$HHV_F = (1 - x_{\text{water}}) \cdot HHV_{F, \text{dry}} \quad (7)$$

The difference between the lower and the higher heating value is heat of evaporation of the water available in the off-gasses of the combustion process, thus:

$$LHV_F = HHV_F - m_{\text{water}} \cdot r$$

The dry fuel does not contain free water. Then, the relation between the lower and the higher heating value of the dry fuel is:

$$LHV_{F, \text{dry}} = HHV_{F, \text{dry}} - x_{\text{H}_2, \text{dry}} \frac{M_{\text{H}_2\text{O}}}{M_{\text{H}_2}} \cdot r$$

$$LHV_{F, \text{dry}} = HHV_{F, \text{dry}} - x_{\text{H}_2, \text{dry}} \times \frac{18.0153}{2.0159} \times 2442.5 \text{ [kJ/kg]}$$

$$LHV_{F, \text{dry}} = HHV_{F, \text{dry}} - x_{\text{H}_2, \text{dry}} \times 21828 \text{ [kJ/kg]} \quad (8)$$

For the real fuel the Eq. A3.3-4 can be used

Thus, the ratio of the exergies is the same as the ratio of the higher heating values:

$$ex_F = (1 - x_{\text{water}}) \cdot ex_{F, \text{dry}} \quad (9)$$

With Equation 4 and Equation 6 to Equation 9 all demanded conversions from the dry fuel into the real fuel and vice versa can be made.

#### Conversion of data from the dry and ash free state into the dry state

The calculation is based on the following assumptions:

Available data:  $x_{i, \text{daf}}, LHV_{F, \text{daf}}$  or  $HHV_{F, \text{daf}}, ex_{F, \text{daf}}$  and  $x_{\text{ash}, \text{dry}}$

Demanded:  $x_{i, \text{dry}}, LHV_{F, \text{dry}}, HHV_{F, \text{dry}}, ex_{F, \text{dry}}$

The fraction  $x_{\text{ash}, \text{dry}}$  is the mass fraction ash of 1 kg of fuel in the dry state. For the dry state and ash free state of the fuel the mass fractions are specified in a way that:

$$\sum x_{i, \text{daf}} = 1$$

If it is assumed that 1 kg of fuel in the dry state contains  $f_{\text{daf/dry}}$  kg dry and ash free fuel, the total mass of the fuel in the dry state can be written as:

$$\sum x_{i, \text{dry}} = f_{\text{daf/dry}} \cdot \sum x_{i, \text{daf}} + x_{\text{ash}} = 1$$

Thus:  $f_{\text{daf/dry}} = 1 - x_{\text{ash}, \text{dry}}$

Then, the mass fractions for the dry state can be calculated as:

$$x_{i, \text{dry}} = (1 - x_{\text{ash}, \text{dry}}) \cdot x_{i, \text{daf}} \quad (10)$$

If the isothermal combustion of  $m_{F, \text{daf}}$  kg of dry and ash free fuel is compared with the isothermal combustion of a quantity of  $m_{F, \text{dry}}$  dry fuel that delivers the same amount of heat, then:

$$m_{F, \text{daf}} \cdot HHV_{F, \text{daf}} = m_{F, \text{dry}} \cdot HHV_{F, \text{dry}} = Q$$

Since  $m_{F, \text{daf}} = f_{\text{daf/dry}} \cdot m_{F, \text{dry}}$  the mass ratios of the fuels are:

$$\frac{m_{F, \text{daf}}}{m_{F, \text{dry}}} = f_{\text{daf/dry}} = (1 - x_{\text{ash}, \text{dry}})$$

## Appendix 2.3

Then, the higher heating value of the fuel in the dry state can be calculated using the following equation:

$$HHV_{F, \text{dry}} = \frac{m_{F, \text{daf}}}{m_{F, \text{dry}}} \cdot HHV_{F, \text{daf}}$$

Then, the heating value of the fuel in the real state becomes:

$$HHV_{F, \text{dry}} = (1 - x_{\text{ash, dry}}) \cdot HHV_{F, \text{daf}} \quad (11)$$

The relation between the lower and the higher heating value of the dry and ash free fuel and of the dry fuel is presented before with Equation 3 and Equation 7.

The ratio of the exergies is the same as the ratio of the higher heating values:

$$ex_{F, \text{dry}} = (1 - x_{\text{ash, dry}}) \cdot ex_{F, \text{daf}} \quad (12)$$

With Equation 3, Equation 7 and Equation 10 to Equation 12 all demanded conversions from the dry and ash free fuel into the dry fuel and vice versa can be made.

## 2 The calculation of the exergy of solid and liquid fuels

### 2.2 The method of Baehr-I

In Chapter 2 the system as shown in Figure 2.15 is used to derive an equation for the calculation of the specific exergy of solid and liquid fuels. That has resulted into the following equation:

$$ex_F = HHV_F(T_0, p_0) + T_0 \cdot \Delta_R S(T_0, p_0) + \Delta Ex \quad (13)$$

With:

$$\begin{aligned} \Delta_R S(T_0, p_0) = & m_{\text{CO}_2} \cdot s_{\text{CO}_2}(T_0, p_0) + m_{\text{H}_2\text{O}} \cdot s_{\text{H}_2\text{O}}(T_0, p_0) + m_{\text{SO}_2} \cdot s_{\text{SO}_2}(T_0, p_0) \\ & + m_{\text{N}_2} \cdot s_{\text{N}_2}(T_0, p_0) - s_F(T_0, p_0) - m_{\text{O}_2} \cdot s_{\text{O}_2}(T_0, p_0) \end{aligned} \quad (14)$$

And:

$$\begin{aligned} \Delta Ex = & m_{\text{CO}_2} \cdot ex_{\text{CO}_2}(T_0, p_0) + m_{\text{H}_2\text{O}} \cdot ex_{\text{H}_2\text{O}}(T_0, p_0) + m_{\text{SO}_2} \cdot ex_{\text{SO}_2}(T_0, p_0) \\ & + m_{\text{N}_2} \cdot ex_{\text{N}_2}(T_0, p_0) - m_{\text{O}_2} \cdot ex_{\text{O}_2}(T_0, p_0) \end{aligned} \quad (15)$$

Then, the specific exergy of the fuel can be calculated if the various terms of the right-hand side of these equations can be solved. The mass of the combustion products can be calculated using the mass fractions of the combustible elements in the fuel:

The combustion of 1 mole of carbon will result in 1 mole of carbon dioxide. Then, as

$x_C$  kg of carbon equals  $\frac{x_C}{M_C}$  mole, the mass of  $\frac{x_C}{M_C}$  mole of carbon dioxide will be

(using the data from Appendix 3.1):

$$m_{\text{CO}_2} = \frac{M_{\text{CO}_2}}{M_C} \cdot x_C = \frac{44.010}{12.0112} \times x_C = 3.6641 \times x_C$$

The combustion of 1 mole of hydrogen will give 1 mole of water. Thus, the mass of water produced by the combustion of 1 kg of fuel will be:

$$m_{\text{H}_2\text{O}} = \frac{M_{\text{H}_2\text{O}}}{M_{\text{H}_2}} \cdot x_{\text{H}_2} = \frac{18.0153}{2.0159} \times x_{\text{H}_2} = 8.9366 \times x_{\text{H}_2}$$

The combustion of 1 mole of sulfur will give 1 mole of sulfur dioxide. Thus, the mass of sulfur dioxide produced by the combustion of 1 kg of fuel will be:

$$m_{\text{SO}_2} = \frac{M_{\text{SO}_2}}{M_{\text{S}}} \cdot x_{\text{S}} = \frac{64.0628}{32.064} \times x_{\text{S}} = 1.9980 \times x_{\text{S}}$$

The oxygen mass for stoichiometric combustion of the fuel must be determined also to solve the before mentioned equations. The number of moles of oxygen can be calculated from the ultimate analysis of the fuel, because:

$$n_{\text{O}_2, \text{ stoich}} = 1 \times n_{\text{C}} + 0.5 \times n_{\text{H}_2} + 1 \times n_{\text{S}} - n_{\text{O}_2}$$

With:  $n_i = \frac{x_i}{M_i}$  and:  $m_{\text{O}_2} = M_{\text{O}_2} \cdot n_{\text{O}_2}$  the oxygen mass for stoichiometric

combustion becomes:

$$m_{\text{O}_2, \text{ stoich}} = 1 \times \frac{M_{\text{O}_2}}{M_{\text{C}}} \cdot x_{\text{C}} + 0.5 \times \frac{M_{\text{O}_2}}{M_{\text{H}_2}} \cdot x_{\text{H}_2} + 1 \times \frac{M_{\text{O}_2}}{M_{\text{S}}} \cdot x_{\text{S}} - x_{\text{O}_2}$$

$$\text{Then: } m_{\text{O}_2, \text{ stoich}} = 1 \times \frac{31.9988}{12.0112} \cdot x_{\text{C}} + 0.5 \times \frac{31.9988}{2.0159} \cdot x_{\text{H}_2} + 1 \times \frac{31.9988}{32.064} \cdot x_{\text{S}} - x_{\text{O}_2}$$

This results into the following equation for the oxygen mass:

$$m_{\text{O}_2, \text{ stoich}} = 2.6641 \times x_{\text{C}} + 7.9366 \times x_{\text{H}_2} + 0.9980 \times x_{\text{S}} - x_{\text{O}_2} \quad (16)$$

The components that leave the system of Figure 2.15 are all environmental components. That means that for the calculation of their exergy they only have to be expanded to their partial pressure in the environment. Then, the exergy of these components equals the work that is generated if the component is expanded isothermal from standard pressure to its partial pressure in the environment. The temperature of the reference environment is 25°C. The exergy values are calculated by using the tabulated data, which are primarily data taken from Baehr [2.2]. To get an idea of the differences between the environmental definition of Baehr and Szargut, the molar exergy values as calculated by Szargut [2.4] are mentioned too.

- The exergy of carbon dioxide at standard pressure can be calculated using the following equation (see Equation 2.17):

$$ex_{\text{CO}_2}^{\text{mol}}(T_0, p_0) = R^{\text{mol}} \cdot T_0 \cdot \ln \frac{P_0}{y_{\text{CO}_2} \cdot p_0}$$

$$ex_{\text{CO}_2}^{\text{mol}}(T_0, p_0) = 8.3143 \times 298.15 \times \ln \frac{1}{0.0003} = 20108 \text{ kJ/kmol (Szargut: 19 870$$

KJ/kmol)

$$ex_{\text{CO}_2}(T_0, p_0) = \frac{ex_{\text{CO}_2}^{\text{mol}}(T_0, p_0)}{M_{\text{CO}_2}} = \frac{20108}{44.010} = 456.90 \text{ kJ/kg}$$

- The exergy of water vapor at standard pressure:

$$ex_{\text{H}_2\text{O}_{(g)}}^{\text{mol}}(T_0, p_0) = R^{\text{mol}} \cdot T_0 \cdot \ln \frac{P_0}{y_{\text{H}_2\text{O}} \cdot p_0}$$

$$ex_{\text{H}_2\text{O}_{(g)}}^{\text{mol}}(T_0, p_0) = 8.3143 \times 298.15 \times \ln \frac{1}{0.0312} = 8595 \text{ kJ/kmol (Szargut: 9 500 KJ/kmol)}$$

## Appendix 2.3

$$ex_{\text{H}_2\text{O}_{(g)}}(T_0, p_0) = \frac{ex_{\text{H}_2\text{O}}^{\text{mol}}(T_0, p_0)}{M_{\text{H}_2\text{O}}} = \frac{8595}{18.0153} = 477.09 \text{ kJ/kg}$$

The exergy of liquid water at standard pressure and 298.15K is zero. Under these conditions liquid water is in equilibrium with saturated air.

$$ex_{\text{H}_2\text{O}_{(l)}}(T_0, p_0) = 0.0 \text{ kJ/kg}$$

- The exergy of nitrogen at standard pressure:

$$ex_{\text{N}_2}^{\text{mol}}(T_0, p_0) = R^{\text{mol}} \cdot T_0 \cdot \ln \frac{P_0}{y_{\text{N}_2} \cdot p_0}$$

$$ex_{\text{N}_2}^{\text{mol}}(T_0, p_0) = 8.3143 \times 298.15 \times \ln \frac{1}{0.7565} = 691.7 \text{ kJ/kmol (Szargut: 720 KJ/kmol)}$$

$$ex_{\text{N}_2}(T_0, p_0) = \frac{ex_{\text{N}_2}^{\text{mol}}(T_0, p_0)}{M_{\text{N}_2}} = \frac{691.7}{28.0134} = 24.69 \text{ kJ/kg}$$

- For the calculation of the exergy of sulfur dioxide at standard pressure an additional environmental model is necessary. Baehr [2.9] uses a model consisting: saturated humid air, liquid water, and the solids gypsum ( $\text{CaSO}_4 \cdot 2\text{H}_2\text{O}$ ) and calcium carbonate ( $\text{CaCO}_3$ ). Then, he finds:  $ex_{\text{SO}_2}(T_0, p_0) = 4783.4 \text{ kJ/kg}$

Szargut [2.4] has found a slightly different value:  $ex_{\text{SO}_2}(T_0, p_0) = 4892.1 \text{ kJ/kg}$

But it is not clear if this was based on the same assumptions regarding the environment.

For this study the value calculated by Baehr will be used.

- The exergy of oxygen at standard pressure:

$$ex_{\text{O}_2}^{\text{mol}}(T_0, p_0) = R^{\text{mol}} \cdot T_0 \cdot \ln \frac{P_0}{y_{\text{O}_2} \cdot p_0}$$

$$ex_{\text{O}_2}^{\text{mol}}(T_0, p_0) = 8.3143 \times 298.15 \times \ln \frac{1}{0.2030} = 3953 \text{ kJ/kmol (Szargut: 3 970 KJ/kmol)}$$

$$ex_{\text{O}_2}(T_0, p_0) = \frac{ex_{\text{O}_2}^{\text{mol}}(T_0, p_0)}{M_{\text{O}_2}} = \frac{3953}{31.9988} = 123.53 \text{ kJ/kg}$$

For the calculation of the reaction entropy Equation 2.46 can be used. The specific entropy for the considered components is:

$$s_{\text{CO}_2}(T_0, p_0) = \frac{s_{\text{CO}_2}^{\text{mol}}(T_0, p_0)}{M_{\text{CO}_2}} = \frac{213.67}{44.010} = 4.8550 \text{ kJ/(kg K)}$$

For liquid water:

$$s_{\text{H}_2\text{O}_{(l)}}(T_0, p_0) = \frac{s_{\text{H}_2\text{O}}^{\text{mol}}(T_0, p_0)}{M_{\text{H}_2\text{O}}} = \frac{69.95}{18.0153} = 3.8828 \text{ kJ/(kg K)}$$

and water vapour:

$$s_{\text{H}_2\text{O}_{(g)}}(T_0, p_0) = \frac{s_{\text{H}_2\text{O}}^{\text{mol}}(T_0, p_0)}{M_{\text{H}_2\text{O}}} = \frac{188.72}{18.0153} = 10.476 \text{ kJ/(kg K)}$$

For the other gaseous components:

$$s_{\text{SO}_2}(T_0, p_0) = \frac{s_{\text{SO}_2}^{\text{mol}}(T_0, p_0)}{M_{\text{SO}_2}} = \frac{248.1}{64.0628} = 3.8727 \text{ kJ/(kg K)}$$

$$s_{\text{N}_2}(T_0, p_0) = \frac{s_{\text{N}_2}^{\text{mol}}(T_0, p_0)}{M_{\text{N}_2}} = \frac{191.5}{28.0134} = 6.8360 \text{ kJ/(kg K)}$$

$$s_{\text{O}_2}(T_0, p_0) = \frac{s_{\text{O}_2}^{\text{mol}}(T_0, p_0)}{M_{\text{O}_2}} = \frac{205.03}{31.9988} = 6.4074 \text{ kJ/(kg K)}$$

With these data the following equations can be derived for the calculation of the exergy of the fuel with Equation 15:

$$\begin{aligned} \Delta Ex = & m_{\text{CO}_2} \cdot ex_{\text{CO}_2}(T_0, p_0) + m_{\text{H}_2\text{O}} \cdot ex_{\text{H}_2\text{O}}(T_0, p_0) + m_{\text{SO}_2} \cdot ex_{\text{SO}_2}(T_0, p_0) \\ & + m_{\text{N}_2} \cdot ex_{\text{N}_2}(T_0, p_0) - m_{\text{O}_2} \cdot ex_{\text{O}_2}(T_0, p_0) \end{aligned}$$

Then, if water leaves the system as liquid water:

$$\begin{aligned} \Delta Ex = & (3.6641 \times x_C \times 456.90) + (8.9366 \times x_{\text{H}_2} \times 0) + (1.9980 \times x_S \times 4783.4) \\ & + (x_{\text{N}_2} \times 24.70) - [(2.6641 \times x_C + 7.9366 \times x_{\text{H}_2} + 0.9980 \times x_S - x_{\text{O}_2}) \times 123.54] \end{aligned}$$

$$\begin{aligned} \Delta Ex = & 1674.1 \times x_C + 0 \times x_{\text{H}_2} + 9557.2 \times x_S + 24.70 \times x_{\text{N}_2} \\ & - [329.12 \times x_C + 980.49 \times x_{\text{H}_2} + 123.29 \times x_S - 123.54 \times x_{\text{O}_2}] \end{aligned}$$

Finally, the exergy difference becomes:

$$\Delta Ex = 1345.00 \times x_C - 980.49 \times x_{\text{H}_2} + 9433.84 \times x_S + 24.70 \times x_{\text{N}_2} + 123.54 \times x_{\text{O}_2} \quad (17)$$

If  $s_F(T_0, p_0)$  is the entropy of the fuel as received and  $s'_F(T_0, p_0)$  the entropy of the dry and ash free fuel (the part of the fuel with the reacting components) then, the relation between these entropy values is:  $s_F(T_0, p_0) = s'_F(T_0, p_0) \cdot (1 - x_{\text{water}} - x_{\text{ash}})$

then Equation 14 becomes:

$$\begin{aligned} \Delta_R S(T_0, p_0) = & m_{\text{CO}_2} \cdot s_{\text{CO}_2}(T_0, p_0) + m_{\text{H}_2\text{O}} \cdot s_{\text{H}_2\text{O}}(T_0, p_0) + m_{\text{SO}_2} \cdot s_{\text{SO}_2}(T_0, p_0) \\ & + m_{\text{N}_2} \cdot s_{\text{N}_2}(T_0, p_0) - s'_F(T_0, p_0) \cdot (1 - x_{\text{water}} - x_{\text{ash}}) - m_{\text{O}_2} \cdot s_{\text{O}_2}(T_0, p_0) \\ \Delta_R S(T_0, p_0) = & 3.6641 \times x_C \cdot s_{\text{CO}_2}(T_0, p_0) + 8.9366 \times x_{\text{H}_2} \cdot s_{\text{H}_2\text{O}}(T_0, p_0) + 1.9980 \times x_S \cdot s_{\text{SO}_2}(T_0, p_0) \\ & + x_{\text{N}_2} \cdot s_{\text{N}_2}(T_0, p_0) - s'_F(T_0, p_0) \cdot (1 - x_{\text{water}} - x_{\text{ash}}) - m_{\text{O}_2} \cdot s_{\text{O}_2}(T_0, p_0) \end{aligned}$$

And thus, if water leaves the system as liquid water:

$$\begin{aligned} \Delta_R S(T_0, p_0) = & 0.719 \times x_C - 16.154 \times x_{\text{H}_2} + 1.3431 \times x_S + x_{\text{N}_2} \times 6.8360 \\ & - s'_F(T_0, p_0) \cdot (1 - x_{\text{water}} - x_{\text{ash}}) + 6.4074 \times x_{\text{O}_2} \end{aligned} \quad (18)$$

With the ultimate analysis of the fuel and an estimated value for the entropy of the fuel, the fuel exergy can be calculated with Equation 13.

Baehr proposed the use of the following estimated values for entropy of coal and oil:

$$\text{solid fuels (coal)} \quad s'_F(T_0, p_0) = 1.7 \pm 1.0 \text{ kJ/kg K}$$

$$\text{liquid fuels (oil)} \quad s'_F(T_0, p_0) = 3.5 \pm 1.0 \text{ kJ/kg K}$$

## Appendix 2.3

2.2 The method of Baehr-II

The method of Baehr-II enables the calculation of the specific exergy of the fuel if only the heating value is known. Therefore the mass fractions of the fuel in the method of Baehr-I are eliminated by using the statistical relations between mass fractions and the heating value from F. Brandt [2.10]. Two sets of equations are taken from [2.10], one for coal and one for liquid fuels.

1) Coal (10 MJ/kg  $<LHV_F < 35$  MJ/kg)

The relations between mass fractions and heating value from [2.10]:

$$x_C = 0.054829 + 0.023736 \times LHV_F$$

$$x_{H_2} = 0.018054 + 0.0008215 \times LHV_F$$

$$x_S = 0.000555 + 0.000240 \times LHV_F$$

$$x_{O_2} = 0.158524 - 0.003385 \times LHV_F$$

$$x_{N_2} = 0.000909 + 0.0003935 \times LHV_F$$

$$x_{water} = 0.746737 - 0.023637 \times LHV_F$$

$$x_{ash} = 0.020392 + 0.001831 \times LHV_F$$

For the relation between the heating values:

$$HHV_F = 2.2180 + 0.9602 \times LHV_F$$

For the change of entropy of the combustion system used for the calculation of the specific exergy Equation 18 has been derived:

$$\begin{aligned} \Delta_R S(T_0, p_0) = & 0.719 \times x_C - 16.154 \times x_{H_2} + 1.3431 \times x_S + x_{N_2} \times 6.8360 \\ & - s'_F(T_0, p_0) \cdot (1 - x_{water} - x_{ash}) + 6.4074 \times x_{O_2} \end{aligned}$$

Replacing the mass fractions in this equation by the relations from Brandt gives:

$$\begin{aligned} \Delta_R S(T_0, p_0) = & 0.719 \times (0.054829 + 0.023736 \times LHV_F) \\ & - 16.154 \times (0.018054 + 0.0008215 \times LHV_F) \\ & + 1.3431 \times (0.000555 + 0.000240 \times LHV_F) \\ & + 6.8360 \times (0.000909 + 0.0003935 \times LHV_F) \\ & - s'_F(T_0, p_0) \cdot [1 - (0.746737 - 0.023637 \times LHV_F) \\ & \quad - (0.020392 + 0.001831 \times LHV_F)] \\ & + 6.4074 \times (0.158524 - 0.003385 \times LHV_F) \end{aligned}$$

For solid fuels (coal) Baehr proposed the following estimate:

$$s'_F(T_0, p_0) = 1.7 \pm 1.0 \text{ kJ/kg K}$$

Then, the change of entropy becomes:

$$\Delta_R S(T_0, p_0) = 0.37458 - 0.05159 \times LHV_F \pm (0.23287 + 0.021806 \times LHV_F) \quad (19)$$

This equation with only the  $LHV_F$  as the independent variable gives the entropy change in KJ/kg K.

For  $\Delta Ex$  Equation 17 was derived:

$$\Delta Ex = 1345.00 \times x_C - 980.49 \times x_{H_2} + 9433.84 \times x_S + 24.70 \times x_{N_2} + 123.54 \times x_{O_2}$$

Replacing the mass fractions in this equation gives:

$$\begin{aligned}\Delta Ex = & 1345.00 \times (0.054829 + 0.023736 \times LHV_F) - 980.49 \times (0.018054 + 0.0008215 \times LHV_F) \\ & + 9433.84 \times (0.000555 + 0.000240 \times LHV_F) + 24.70 \times (0.000909 + 0.0003935 \times LHV_F) \\ & + 123.54 \times (0.158524 - 0.003385 \times LHV_F)\end{aligned}$$

Which results into:

$$\Delta Ex = 80.8855 + 32.9751 \times LHV_F$$

With  $\Delta Ex$  in KJ/kg fuel. If  $\Delta Ex$  is presented in MJ/kg as needed for the final equation for the fuel exergy, this equation becomes:

$$\Delta Ex = 0.080886 + 0.032975 \times LHV_F \quad [\text{MJ/kg}] \quad (20)$$

Then the specific exergy of the fuel can be determined by using Equation 13:

$$ex_F = HHV_F(T_0, p_0) + T_0 \cdot \Delta_R S(T_0, p_0) + \Delta Ex$$

By using Eq. A3.3-19 and Eq. A3.3-20 and the following relation of Brandt:

$$HHV_F = 2.2180 + 0.9602 \times LHV_F$$

the exergy of coal becomes:

$$\begin{aligned}ex_F = & 2.2180 + 0.9602 \times LHV_F \\ & + 298.15 \times 10^{-3} \times [0.37458 - 0.05195 \times LHV_F \pm (0.23287 + 0.021806 \times LHV_F)] \\ & + 0.080886 + 0.032975 \times LHV_F\end{aligned}$$

Then:

$$ex_F = 2.4106 + 0.97949 \times LHV_F \pm (0.06943 + 0.0065015 \times LHV_F) \quad (\text{A3.3-21})$$

And with:  $HHV_F = 2.2180 + 0.9602 \times LHV_F$

$$ex_F = 0.14805 + 1.02004 \times HHV_F \pm (0.05441 + 0.00677 \times HHV_F) \quad (\text{A3.3-22})$$

## 2) Fuel oil ( $37 \text{ MJ/kg} < LHV_F < 43 \text{ MJ/kg}$ )

The relation between mass fractions and heating value from [2.10]:

$$\begin{aligned}x_C &= 0.68309 + 0.0040776 \times LHV_F \\ x_{H_2} &= -0.224265 + 0.0082625 \times LHV_F \\ x_S &= 0.276035 - 0.0062774 \times LHV_F \\ x_{O_2} &= 0.21356 - 0.0048612 \times LHV_F \\ x_{N_2} &= 0.05158 - 0.0012015 \times LHV_F\end{aligned}$$

For the relation between the heating values:

$$HHV_F = -4.8954 + 1.18036 \times LHV_F$$

For the change of entropy of the combustion system used for the calculation of the specific exergy Equation 18 has been derived:

$$\begin{aligned}\Delta_R S(T_0, p_0) = & 0.719 \times x_C - 16.154 \times x_{H_2} + 1.3431 \times x_S + x_{N_2} \times 6.8360 \\ & - s'_F(T_0, p_0) \cdot (1 - x_{\text{water}} - x_{\text{ash}}) + 6.4074 \times x_{O_2}\end{aligned}$$

Combining these equations and assuming that the fuel oil does not contain water or ash

( $x_{\text{water}} = x_{\text{ash}} = 0$  and  $s_F = s'_F$ ) gives:

## Appendix 2.3

$$\begin{aligned}\Delta_R S(T_0, p_0) = & 0.719 \times (0.68309 + 0.0040776 \times LHV_F) \\ & - 16.154 \times (-0.224265 + 0.0082625 \times LHV_F) \\ & + 1.3431 \times (0.276035 - 0.0062774 \times LHV_F) \\ & + 6.8360 \times (0.05158 - 0.0012015 \times LHV_F) - s_F(T_0, p_0) \\ & + 6.4074 \times (0.21356 - 0.0048612 \times LHV_F)\end{aligned}$$

Thus:

$$\Delta_R S(T_0, p_0) = 6.2056 - 0.17833 \times LHV_F - s_F(T_0, p_0)$$

For liquid fuels Baehr proposed the following estimate:  $s_F = 3.5 \pm 1.0$  kJ/kg

Then, the equation for the change of entropy becomes:

$$\Delta_R S(T_0, p_0) = 2.7056 - 0.17833 \times LHV_F [\text{MJ/kg}] \pm 1.0 \text{ kJ/kg} \quad (23)$$

This equation gives the entropy change in KJ/kg K.

Replacing the mass fractions in Equation 17: for the calculation of  $\Delta Ex$ :

$$\Delta Ex = 1345.00 \times x_C - 980.49 \times x_{H_2} + 9433.84 \times x_S + 24.70 \times x_{N_2} + 123.54 \times x_{O_2}$$

gives:

$$\begin{aligned}\Delta Ex = & 1345.00 \times (0.68309 + 0.0040776 \times LHV_F) \\ & - 980.49 \times (-0.224265 + 0.0082625 \times LHV_F) \\ & + 9433.84 \times (0.276035 - 0.0062774 \times LHV_F) \\ & + 24.70 \times (0.05158 - 0.0012015 \times LHV_F) \\ & + 123.54 \times (0.21356 - 0.0048612 \times LHV_F)\end{aligned}$$

Which finally results in:

$$\Delta Ex = 3770.4 - 62.467 \times LHV_F$$

This equation calculates the specific exergy in KJ/kg. As  $\Delta Ex$  has to be presented in MJ/kg the final equation becomes:

$$\Delta Ex = 3.7704 - 0.062467 \times LHV_F \quad (24)$$

Then the specific exergy of the fuel can be determined by using Equation 13:

$$ex_F = HHV_F(T_0, p_0) + T_0 \cdot \Delta_R S(T_0, p_0) + \Delta Ex$$

By using Equation 23 and Equation 24 and the following relation of Brandt:

$$HHV_F = -4.8954 + 1.18036 \times LHV_F$$

the exergy of fuel oil becomes:

$$ex_F = -4.0887 + 1.12719 \times LHV_F \pm 0.29815 + 3.7704 - 0.062467 \times LHV_F$$

and thus:

$$ex_F = -0.3183 + 1.0647 \times LHV_F \pm 0.29815 \quad \text{in MJ/kg} \quad (25)$$

Replacing the  $LHV_F$  by the  $HHV_F$  gives:

$$ex_F = -0.3183 + 1.0647 \times (4.1474 + 0.84720 \times HHV_F) \pm 0.29815$$

and thus:

$$ex_F = 4.0975 + 0.90203 \times HHV_F \pm 0.29815 \quad \text{in MJ/kg} \quad (26)$$



## **APPENDIX 3.1**

### **EVALUATION OF RENEWABLE ENERGY SOURCES**

#### **TABLE OF CONTENTS**

<b>1</b>	<b>INTRODUCTION</b>
<b>2</b>	<b>SYSTEM DESCRIPTION</b>
<b>2.1</b>	<b>The national energy system</b>
<b>2.2</b>	<b>Energy sources and demands</b>
<b>2.3</b>	<b>Energy storage</b>
<b>2.4</b>	<b>Energy conversion systems</b>
<b>3</b>	<b>SYSTEM EVALUATIONS</b>
<b>3.1</b>	<b>Introduction</b>
<b>3.2</b>	<b>Exploring system studies</b>
3.2.1	Introduction
3.2.2	Systems 1 and 2
3.2.3	System 3
3.2.4	System 4
3.2.5	Systems 5 to 7
3.2.6	Systems 8 and 9
3.2.7	System 10
3.2.8	Systems 11 and 12
3.2.9	Systems 13 and 14
<b>3.3</b>	<b>A systematic evaluation</b>
3.3.1	Introduction
3.3.2	Systems 1a and 1b
3.3.3	Systems 2a and 2b
3.3.4	Systems 3a and 3b
3.3.5	Systems 4a and 4b
3.3.6	Conclusions
<b>3.4</b>	<b>Selection of reference configurations</b>
3.4.1	Introduction
3.4.2	Evaluation and selection of production chains
3.4.3	Composition of reference configurations
3.4.4	Selected configurations
3.4.5	Conclusions
<b>3.5</b>	<b>The evaluation of wind turbines and energy storage</b>

3.5.1 Introduction

3.5.2 The systems with coal gas (SNG) as the secondary fuel

3.5.3 The systems with hydrogen as the secondary fuel

## 4 CONCLUSIONS

## REFERENCES

Note

Concepts used in this appendix:

- Demand control: the control of the demanded energy in such a way that the energy demand is reduced at moments of limited energy generation and is increased at moments of abundant energy generation. This can be realized e.g. by switching of or switching on energy consuming equipment, like cooling equipment or washing machines etc., which does not need instantaneous energy supply.
- Load factor: the load factor as used in this paper is defined as the actually generated power by the plant in a specific period divided by the power that should have been generated if the plant was operated continuously at design load. In this study the load factors are specified for one year.

## Appendix 3.1

### 1 INTRODUCTION

In this appendix a study executed by the Energy Systems group of the TU Delft during the years 1983-1988 is summarized. The most important results are presented; the method of evaluation is described as far as necessary to understand the meaning of the results. The study was started on request of the Dutch ministry of Economic Affairs in order to get a better insight in the possibilities and problems associated with the application of renewable sources like wind and solar energy. Attention should be paid in particular to the effect of the application of fuel cells in combination with hydrogen storage. The study should focus primarily on the following questions:

- What kind of energy sources have to be applied in the future if natural gas and oil are no longer available?
- Which systems and apparatuses have to be developed to enable the application of these sources?

At the start a limited number of energy systems have been defined to see what the consequences are of the application of selected technologies. Primarily attention was paid on the total yearly costs of the systems supposing that further evaluation of systems is useful only if systems have a chance to become economical feasible. It was assumed that the economical feasibility will depend on the ratio of total yearly costs of a new energy system and a reference system that primarily uses conventional technologies. The cost data are presented in the units as used in the study (Dutch guilders) because actually the cost ratios and not the absolute costs are used to come to conclusions regarding the application of new energy sources and conversion technologies. Furthermore, an update of the results is not feasible at this moment because of the time that will be required to update the computer program and to revise all the applied data. The various systems were considered for application in 2040; the applied cost data and conversion efficiencies are specified around 1985. The year 2040 was chosen because it was supposed that natural gas and oil should not longer be available for general use at that time.

The study has started with the evaluation of energy systems with one single energy source and one specific set of conversion technologies. This was done to recognize clearly the effects of the various energy sources. After that, the effect of combining energy sources and the application of alternative conversion technologies has been investigated. The results are presented in the reports [1] to [6]

### 2 SYSTEM DESCRIPTION

#### 2.1 The national energy system

The national energy system should comprise in principle all necessary systems for the conversion, transport and storage of energy in the Netherlands from the primary fuel or energy source to final use, the energy demand. The general outline of such a system (the reference

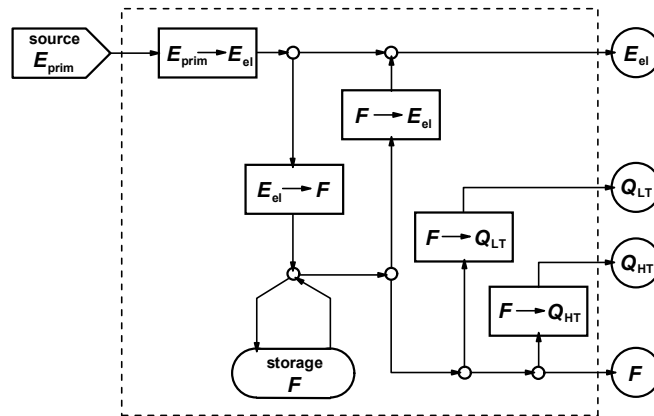


Figure 1a System diagram A

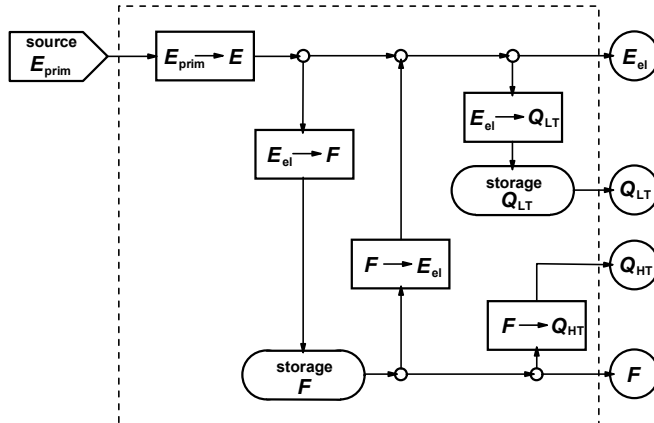


Figure 1b System diagram B

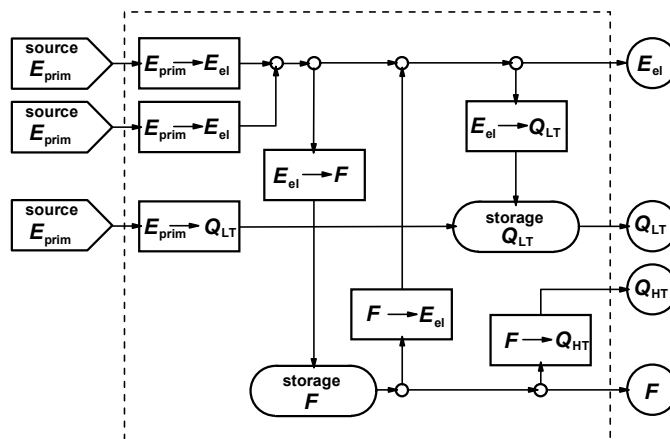


Figure 1c System diagram C

### Appendix 3.1

system) as used at the start of the study is presented in Figure 1a. The source of the primary energy is shown at the left side of the system and energy demands at the right side. The national energy demand is divided into four separate demands for electricity ( $E_{el}$ ), low temperature heat ( $Q_{LT}$ ), high temperature heat ( $Q_{HT}$ ) and fuel ( $F$ ). The specification of the demands is presented in a following section. At the start of the study the consequences of the application of various sources of primary energy have been investigated. Therefore one single energy source is depicted in the reference system. The primary source might be solar energy, wind energy or a fuel (fossil, nuclear or biomass). The system that connects the energy source and the energy demands should enable the delivery of the demanded energy by using the considered energy source. The primary energy is converted first into electricity (conversion  $E_{prim} \rightarrow E_{el}$ ). Storage of energy might be necessary because of the fluctuating energy demands and the autonomous behavior of the primary source in the case of solar and wind energy. For the reference system it is assumed that large scale storage of energy will take place by storing hydrogen (storage  $F$ ). Therefore, electricity must be converted into hydrogen fuel ( $E_{el} \rightarrow F$ ). This fuel will be used to meet the fuel demand ( $F$ ) for transport and will be used also for the generation of low and high temperature heat. If the electricity demand is at any time higher than the electricity generated by the primary source, the difference can be generated by converting fuel from the storage into electricity ( $F \rightarrow E_{el}$ ).

The computer program TASTE (Transport And Storage with Time dependent Energy flows) has been developed to calculate the power or capacity of the considered conversion and storage systems based on the specified energy demands, the characteristics of the energy source and the specified efficiencies of the conversion and storage systems. The calculated power or capacity is used to calculate also the capital costs and the total annual costs of the system.

Initially, the costs of energy transport (electricity, fuel and heat) have been ignored. The exploring calculations indicated that the costs of transport might be significant for drawing the right conclusions. Therefore, the program was extended with facilities that enable the estimation of the costs for transport and distribution of energy.

The estimated total yearly costs are an important characteristic to judge the attractiveness of system concepts for future application. But, other qualities of the systems have to be taken into account also. The environmental effects of a concept are supposed to be of primary importance. Therefore, the final version of TASTE is able to calculate also the total yearly emissions of the system ( $CO_2$ ,  $NO_x$ ,  $SO_2$  and particles) based on specified average emissions of the considered type of equipment.

## 2.2 Energy sources and demands

The availability of wind and sun as well as the characteristics of the energy demand are taken from available data for the year 1980. Because of the relation that exists between the climate and the energy demand, it was supposed to be important to use data recorded all for the

same year. It is assumed that fossil fuels as well as biomass can be made available on demand as usual. The systems needed for this kind of fuel storage are not included in the evaluations; the storage costs are supposed to be included in the applied market prices. Wind, solar radiation and the energy demands are continuously varying quantities. It was decided to apply averaged values per hour for each of these quantities to simplify the calculations. It was assumed that by doing so the accuracy will be sufficient for the purpose of this study.

The energy from the sources is specified in the program as a total installed power (peak electric power) for photovoltaic converters, solar collectors and/or wind turbines and the fraction generated per hour for all hours of the year. The energy demands (electricity, low temperature heat, high temperature heat and fuel) are specified as a total yearly demand and the fractions per hour for all hours of the year. How the applied data are derived is described below in more detail.

#### Solar energy

The data for solar energy are needed to calculate the electricity supplied by photovoltaic generators and the heat generated by solar collectors. For the influx of solar radiation data averaged values per hour were available from the KNMI for location De Bilt. The same data have been used for the photovoltaic generators and the solar collectors.

#### Wind energy

The calculated wind energy is based on averaged values per hour of the wind velocity at location Den Helder as available from the KNMI. The data are specified for a position 10 m above surface level. In general the height of the turbine rotor above the surface level will be more. Then, also the wind speed will be higher. The data from the KNMI are corrected to get the averaged wind velocity at the height of the rotor shaft by using the following equation:

$$V_h = V_{10m} \cdot \left(\frac{h}{10}\right)^\alpha$$

In this equation is  $V_{10m}$  the wind velocity as specified by the KNMI,  $V_h$  the wind velocity at the required height  $h$ . The exponent  $\alpha$  is set at 0.155, a value as specified for flat and open fields.

#### Electricity demand

The total electricity demand of the Netherlands in the year 1980 is derived from data of the CBS. A total demand of 206 PJ was calculated for the supply by the public grid and the electricity generated by independent generators. Because of the lack of detailed data from the independent generators, the hourly fractions are based on data of the averaged electricity supply per hour from the SEP. Since the electricity generated by the independent generators is roughly 10% of the total electricity demand, the inaccuracy caused by this assumption is limited. An impression of the development of the electricity demand is shown in Figures 2a to 2c.

#### High temperature heat demand

To distinguish between high temperature heat and low temperature heat it is assumed in principle that all heat generated at temperatures higher than 80°C is high temperature heat. However, the available CBS data didn't specify sufficient information to enable the use of this temperature limit. Therefore, it was assumed that the high temperature heat demand equals the

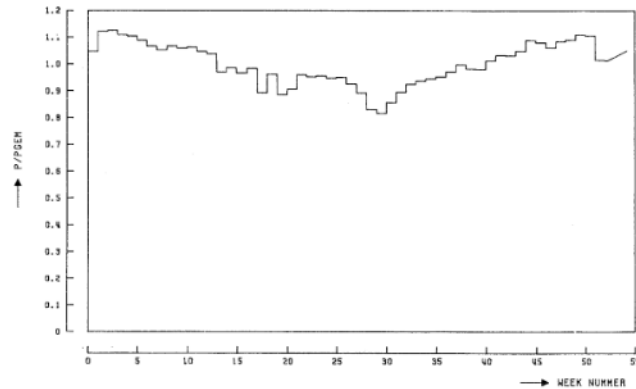


Figure 2a Electricity demand, average power per week over average power per year as function of the week number (1980,  $P_{\text{average of year}} = 6.51 \text{ GW}_e$ )

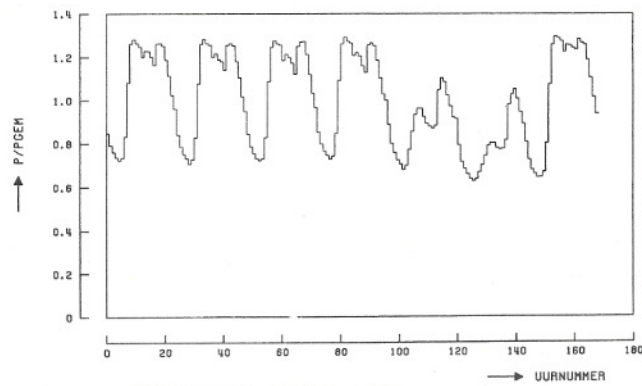


Figure 2b Electricity demand, average power per hour over average power per week as function of the hour number (week 3, 1980,  $P_{\text{average of week}} = 7.33 \text{ GW}_e$ )

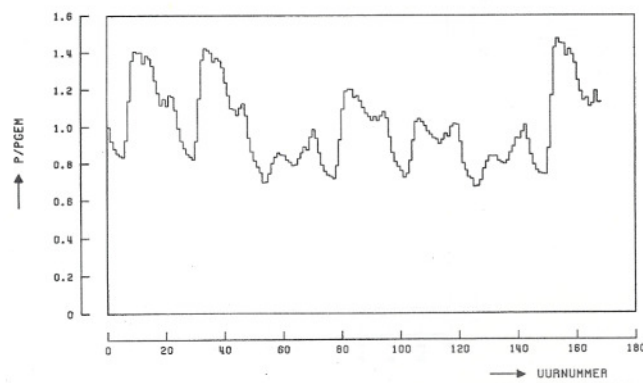


Figure 2c Electricity demand, average power per hour over average power per week as function of the hour number (week 20, 1980,  $P_{\text{average of week}} = 5.77 \text{ GW}_e$ )

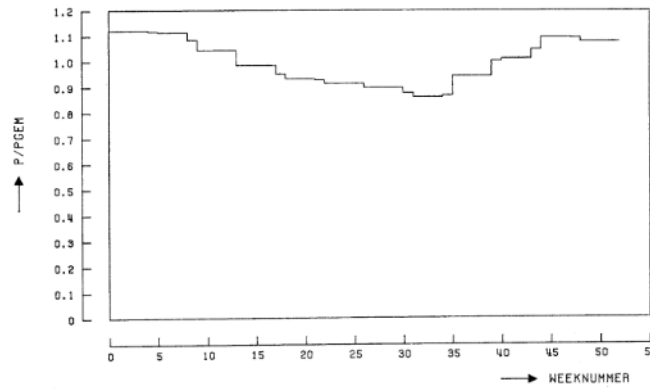


Figure 3a High temperature heat demand, average power per week over average power per year as function of the week number (1980,

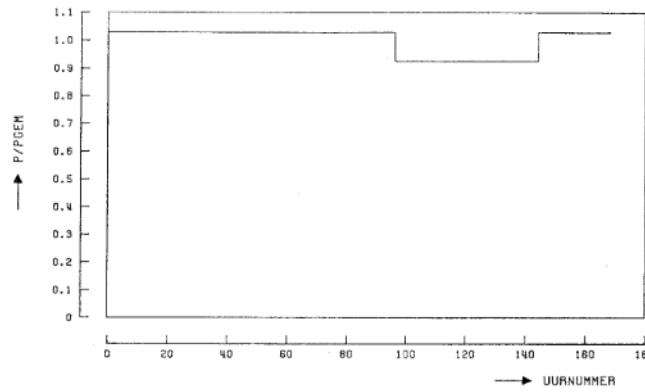


Figure 3b High temperature heat demand, average power per hour over average power per week as function of the hour number (week 3, 1980,  $P_{\text{average of week}} = 14.49 \text{ GW}_{\text{th}}$ )

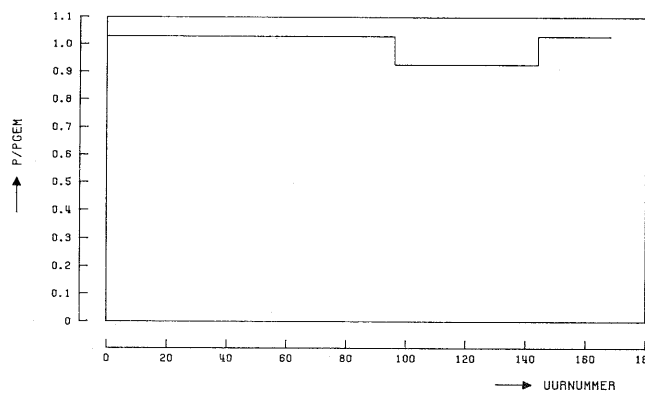


Figure 3c High temperature heat demand, average power per hour over average power per week as function of the hour number (week 20, 1980,  $P_{\text{average of week}} = 12.06 \text{ GW}_{\text{th}}$ )

## Appendix 3.1

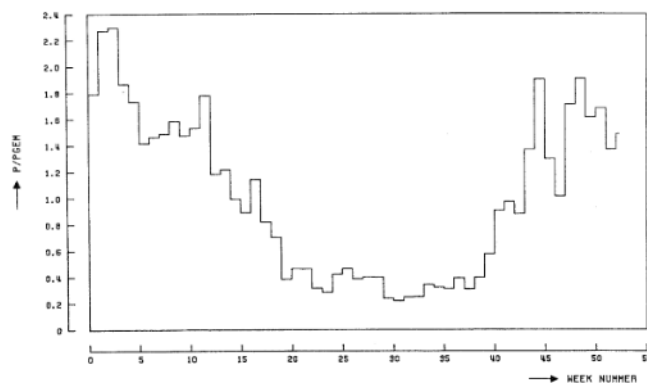


Figure 4a Low temperature heat demand, average power per week over average power per year as function of the week number (1980,  $P_{\text{average of year}} = 19.38 \text{ GW}_{\text{th}}$ )

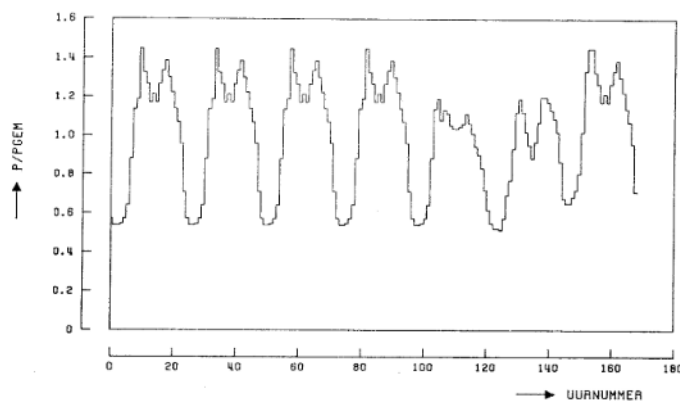


Figure 4b Low temperature heat demand, average power per hour over average power per week as function of the hour number (week 3, 1980,  $P_{\text{average of week}} = 44.43 \text{ GW}_{\text{th}}$ )

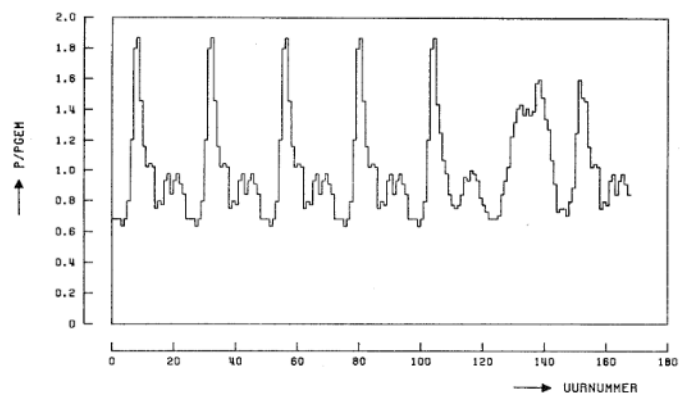


Figure 4c Low temperature heat demand, average power per hour over average power per week as function of the hour number (week 20, 1980,  $P_{\text{average of week}} = 7.46 \text{ GW}_{\text{th}}$ )

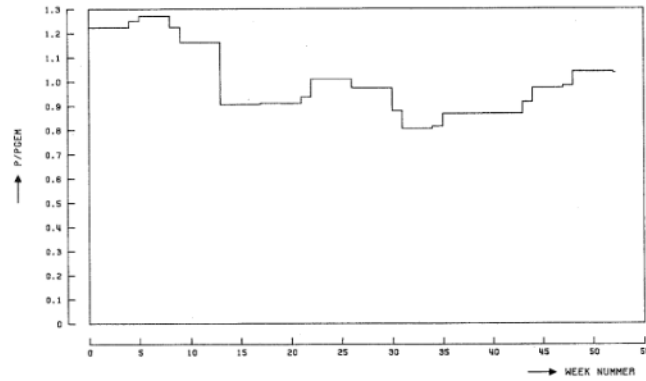


Figure 5a Fuel demand, average power per week over average power per year as function of the week number (1980,  $P_{\text{average of year}} = 9.99 \text{ GW}$ )

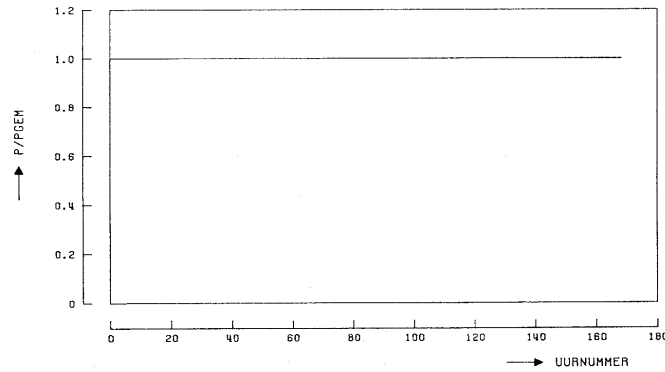


Figure 5b Fuel demand, average power per hour over average power per week as function of the hour number (week 3, 1980,  $P_{\text{average of week}} = 12.23 \text{ GW}$ )

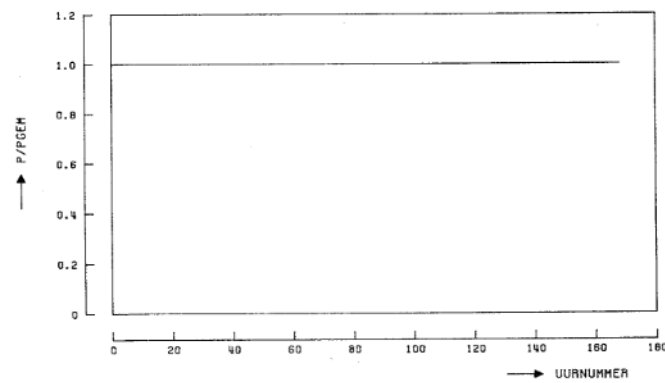


Figure 5c Fuel demand, average power per hour over average power per week as function of the hour number (week 20, 1980,  $P_{\text{average of week}} = 9.09 \text{ GW}_e$ )

### Appendix 3.1

total industrial energy consumption minus the industrial electricity consumption. Using the CBS data the high temperature heat demand was initially estimated to be 449 PJ. This value was used in reference [2]. In [3] a correction was made and the total demand was estimated to be 409 PJ. This value has been used for all the following evaluations. No proper information was available to find the hourly fractions of the high temperature heat demand. An estimate of the fractions was based on the total industrial gas consumption per month as published by the Gasunie. First, the total consumption per week was determined in proportion to the monthly consumption. Then, it was assumed that the consumption during the days of the weekend is 90% of the consumption during the normal working days. Finally, the hourly demand was determined by dividing the daily consumption in 24 equal parts. An impression of the development of the high temperature heat demand is shown in Figure 3a to 3c.

#### Low temperature heat demand

First the total heat demand was determined by using data of the CBS. The magnitude has been calculated by subtracting the fuel demanded for electricity generation and transport from the final demand of fuels for energy applications. It was assumed that from the remainder 80% of the available energy is used to meet the heat demand; that means that 20% is lost because of conversion and distribution losses. Then, the total (low temperature + high temperature) heat demand was calculated to be 1022 PJ. The low temperature heat demand was determined by subtracting the high temperature heat demand from the total heat demand. This resulted initially in a yearly low temperature heat demand of 573 PJ (see [2]). The correction of the high temperature heat demand in [3] resulted also in a correction of the low temperature heat demand. The value of 613 PJ has been used in [3] and all following calculations. After the hourly fractions are determined in two steps. First, the daily fractions were determined using the data of the gas distribution companies; they specified the total gas consumption per day without the power generating companies and large industries. Finally, the hourly fractions were determined by using the gas consumption data from the municipal energy company of The Hague. An impression of the development of the high temperature heat demand is shown in Figures 4a to 4c.

#### Fuel demand (for transport)

The total yearly fuel consumption for transport could be derived from data of the CBS. A value of 316.22 PJ was reported. The hourly fractions were determined in some steps. First, the monthly fractions are based on the variations in the total production of petrol, diesel oil and LPG. The weekly fractions are determined in proportion with the monthly fractions; the hourly fractions are just the weekly fractions divided by the number of hours in a week. This actually means that the fuel demand represents per week a continuous fuel flow to the fuel distribution system. An impression of the development of the high temperature heat demand is shown in Figures 5a to 5c.

The applied yearly energy demands are summarized in Table 1 together with some general data as used for the economic calculations. The economic life time of 20 years is applied if no more accurate information on the economic life time was available.

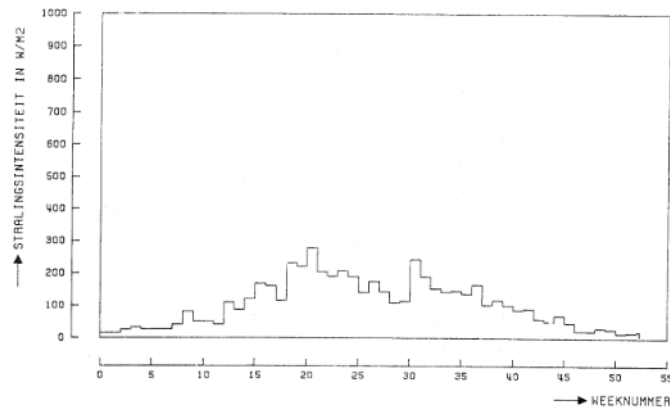


Figure 6a Averaged global solar radiation (average per week) as function of the week number (De Bilt, Netherlands 1980)

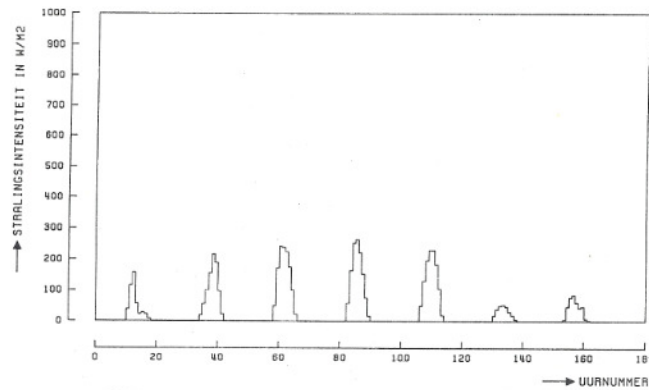


Figure 6b Averaged global solar radiation (average per hour) as function of the hour number (De Bilt, Netherlands; week 3, 1980)

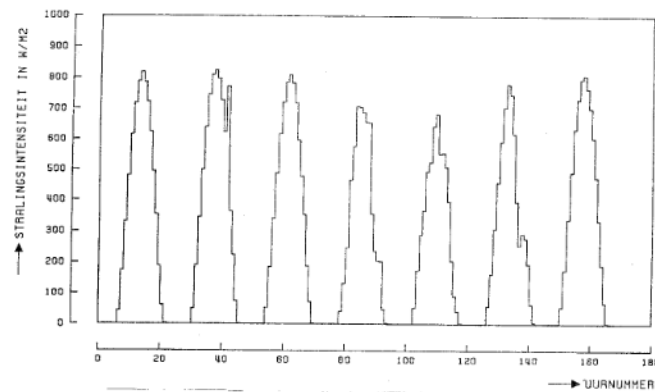


Figure 6c Averaged global solar radiation (average per hour) as function of the hour number (De Bilt, Netherlands; week 20, 1980)

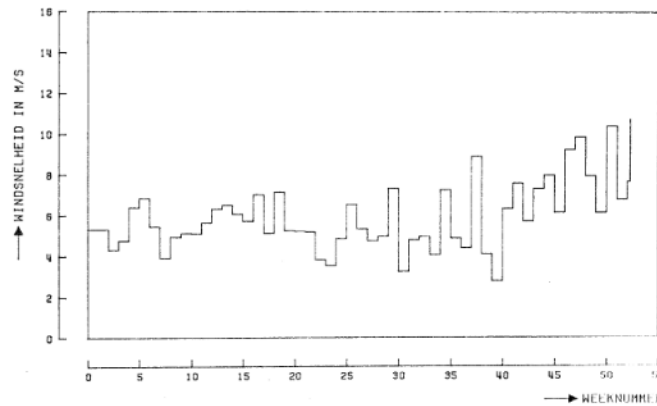


Figure 7a Averaged wind speed (average per week) as function of the week number (Den Helder, Netherlands; 1980)

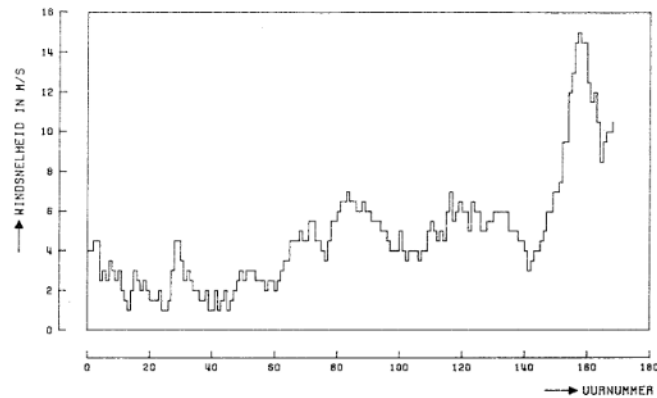


Figure 7b Averaged wind speed (average per hour) as function of the hour number (Den Helder, Netherlands; week 3, 1980)

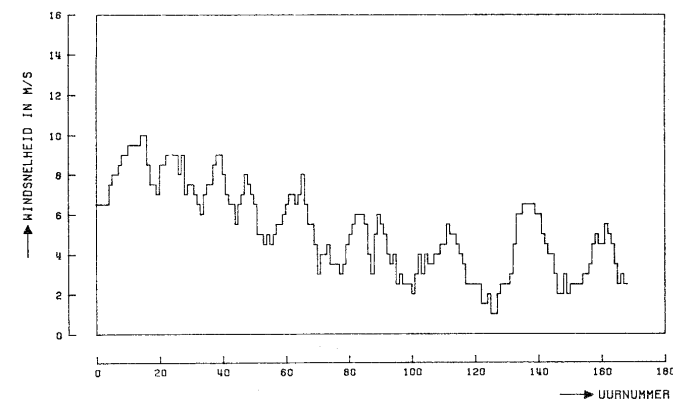


Figure 7c Averaged wind speed (average per hour) as function of the hour number (Den Helder, Netherlands; week 20, 1980)

### 2.3 Energy storage

It is assumed that energy can be stored in different ways. In Figure 1 energy is stored as a fuel (hydrogen), but also other options, like the storage of heat or storage of power by a pump accumulation system, are considered. It is assumed that the storage itself is free of losses. If necessary, additional losses can be combined with the conversion of the energy flow to or from the storage. In the calculation the storage has the task to assure the balance between generated energy and demanded energy if the energy source is not designed for load following operation. It is assumed that any surplus of energy will be transported to the energy storage and any shortage can be taken from the energy storage. During the system calculation for one year the content of the store is calculated. The capacity of the storage is calculated as the difference between maximum and the minimum level.

<i>Table 1 General data used for the systematic evaluation of alternative systems</i>	
Yearly energy demand	<i>value</i>
<ul style="list-style-type: none"> <li>• Electricity</li> <li>• Low temperature heat</li> <li>• High temperature heat</li> <li>• Fuel</li> </ul>	<p>206 PJ</p> <p>613 PJ (573 PJ)</p> <p>409 PJ (449 PJ)</p> <p>316 PJ</p>
Economic data	
<ul style="list-style-type: none"> <li>• Economic life time</li> <li>• Interest</li> <li>• Annuity factor</li> <li>• Fuel prices</li> </ul>	<p>20 years</p> <p>4%</p> <p>0.07358</p> <p>coal 8.0 Dfl/GJ</p> <p>uranium 2.6 Dfl/GJ</p>

### 2.4 Energy conversion systems

The energy from the primary source has to be converted into the demanded energy. Therefore, appropriate energy conversion systems are necessary. Also the storage of energy will require additional energy conversions. In the reference system (Figure 1) the primary energy is converted into electricity that can be used first to meet the electricity demand. The remainder will be converted into a secondary fuel, e.g. hydrogen. The secondary fuel is used to generate low and high temperature heat and to meet the demand of fuel for transportation. For each of the applied conversion systems a technology has to be specified including a conversion factor (e.g. efficiency or COP), the specific investment costs, the specific yearly operational costs and for the later versions of the program also the specific emissions. In Table 2 the data are shown as used for the

## Appendix 3.1

*Table 2 Data of conversion and storage systems*

system	Conversion factor	Specific investment costs	Specific yearly operating costs
Photovoltaic generators	-	1 000 Dfl/kW <sub>e</sub>	30 Dfl/(kW <sub>e</sub> .a)
Wind turbines	-	2 000 Dfl/kW <sub>e</sub>	60 Dfl/(kW <sub>e</sub> .a)
Nuclear power plants	0.32	3 600 Dfl/kW <sub>e</sub>	108 Dfl/(kW <sub>e</sub> .a)
Coal fired power plants	0.387	1 800 Dfl/kW <sub>e</sub>	54 Dfl/(kW <sub>e</sub> .a)
Solar collectors	-	2 000 Dfl/kW <sub>th</sub>	60 Dfl/(kW <sub>th</sub> .a)
Electrolysis plants	0.75	1 000 Dfl/kW <sub>e</sub>	30 Dfl/(kW <sub>e</sub> .a)
Fuel cell plants	0.50	1 000 Dfl/kW <sub>e</sub>	30 Dfl/(kW <sub>e</sub> .a)
Boilers	0.90	200 Dfl/kW <sub>th</sub>	6 Dfl/(kW <sub>th</sub> .a)
Heat pumps	2.0	700 Dfl/kW <sub>e</sub>	21 Dfl/(kW <sub>e</sub> .a)
Hydrogen storage	1.0	30 Dfl/GJ	0.3 Dfl/(GJ.a)
LT heat storage	1.0	500 Dfl/GJ	15 Dfl/(GJ.a)

exploring calculations. Costs are presented in Dutch guilders, the units as used in the original studies. The motivation of the selected data is discussed in the following for each of the considered technologies. In general, the specific yearly operational costs are supposed to be 3% of the specific investment cost. Only deviations of this assumption are discussed in the following.

#### Photovoltaic generators

Photovoltaic generators enable the direct conversion of solar energy into electricity. The actual specific investment costs in 1985 were estimated to be around 25,000 Dfl/kW<sub>e</sub> (peak power, output) for an operating power plant. It was expected that these costs could be reduced to roughly 1,000 Dfl/kW<sub>e</sub> for the year 2040. These specific investment costs were supposed to be the lower limit for this kind of equipment; this lower limit was used for the evaluations assuming that the large scale application of solar energy will become possible only if the conditions are favorable. The data of the averaged global radiation of location De Bilt (see Figure 4) have been used to determine the generated electricity of the photovoltaic generators during the year. The use of data for one specific location to determine the national power generation by photovoltaic generators is of course questionable. But it was decided that these data should be used, because:

- Only data of De Bilt were available at that time.
- The effects on the capacity of the energy storage facilities are supposed to be very limited if the storage capacity is primarily determined by the seasonal fluctuations which are highly the same for different locations within the Netherlands.
- The accuracy of the exploring evaluations is limited because of the uncertainty of many of the assumptions that have to be made.

It is supposed that the generated electricity is proportional with the global solar radiation. It will be clear from the data of Figure 6 that the average generated power is far less than the installed peak power. In order to determine the necessary area for the photovoltaic generators it was supposed that 1 kW<sub>e</sub> (peak power) will require 20 m<sup>2</sup> overall.

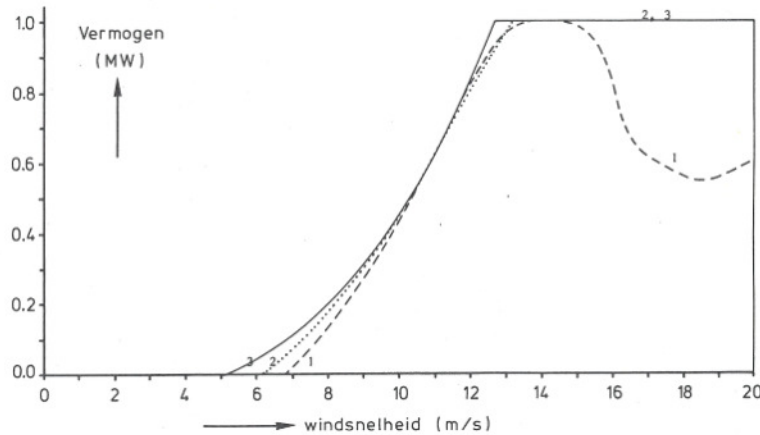


Figure 8 Power characteristics of a wind turbine, rotor diameter 50 m, nominal power  $P_r = 1.0$  MW, for three control strategies:

- 1) Constant speed, fixed blade angle
- 2) Constant speed, variable blade angle
- 3) Maximum  $C_p = 0.45$

### Wind turbines

Wind turbines are used to convert wind energy into electricity. At the time the study was executed a variety of wind turbines were under development, but the high speed turbine with horizontal axis was selected for the purpose of this evaluation. Wind speed data of the location Den Helder were used to determine the generated power. It was assumed that the rotor axis is positioned 40 m above surface level. The corresponding wind speeds are presented in Figure 7. The generated electrical power is determined using the power characteristic of the wind turbine as shown in Figure 8 (see [7]). The curve for the turbine at constant speed and variable blade angle (curve 2) was used for the evaluations. Then, the calculated power is based on the average values of the wind speed during an hour.

Large scale application of wind turbines will require that turbines are placed in wind parks. The vicinity of other turbines will cause a slight reduction of the power that can be generated in comparison with a solitary turbine. These effects, however, are ignored in the evaluations. The total investment costs of the wind turbines are fixed at 2,000 Dfl/kW<sub>e</sub>. This amount was based on a prognosis for large scale turbines (approx. 1 MW<sub>e</sub>) at that time if manufactured in high volumes. To estimate the necessary area for placing the wind turbines it was assumed that 10 MW<sub>e</sub>/km<sup>2</sup> can be placed.

### Nuclear power plants

The pressurized water reactor (PWR) was selected for this evaluation. The necessary data are taken from [2]. The unit size is 1,000 MW<sub>e</sub>. The net plant efficiency is 0.32 and the specific investment costs are 3,600 Dfl/kW<sub>e</sub> including the costs for interest during construction and dismantling. The fuel costs are 2.6 Dfl/GJ; in this price all costs of the fuel cycle are included.

### Appendix 3.1

The specific yearly operational costs are supposed to be 3% of the specific investment costs, resulting into 108 Dfl/(kW<sub>e</sub>.a) which is higher than the 61.2 Dfl/(kW<sub>e</sub>.a) mentioned in [8]. The need for backup power was ignored in the system calculations. This means that it is assumed that all plants are operating at 100% availability. As availability data were available only for the power generators that are used at large scale at that time, like coal fired power plants and nuclear plants, it was decided that the addition of the costs for backup power should not improve the accuracy of the results.

#### Coal fired power plants

The necessary data for the coal fired power plants are taken from [8]. The data are presented for a coal fired power plant of 600 MW<sub>e</sub>. The net efficiency of the power plant is supposed to be 38.7%; this efficiency is assumed to be the overall efficiency during one year of operation and includes the effects of starting up, shutting down and part load conditions. The investment costs, including the costs of interest during construction and dismantling, are supposed to be 1,800 Dfl/kW<sub>e</sub>. The specific yearly operational costs are assumed to be 3% of the specific investment costs: 54 Dfl/(kW<sub>e</sub>.a). This amount is somewhat lower than the 68.3 Dfl/(kW<sub>e</sub>.a) as specified in [8].

#### Solar collectors

The solar collectors are used in the system evaluations for the direct conversion of solar energy into low temperature heat for space heating. It is assumed that the solar collectors are placed on individual dwellings or buildings. But a connection with a common system is available to transport or exchange surplus heat and shortages. This might require the addition of heat storage equipment which can be a mix of individual and common storage facilities.

It is assumed that the generated heat is proportional with global the solar radiation, which means that the solar collectors operate at constant conversion efficiency. In practice the efficiency of a solar collector depends on the global solar radiation as well as the temperature difference between the solar collector and the surroundings. As the minimization of the heat losses is an important development goal, it is assumed that the effect of the these losses can be ignored for operation in the year 2040.

The specific investment costs are supposed to be 2,000 Dfl/kW<sub>th</sub> (peak power). The maximum of the global solar radiation in the Netherlands is approximately 1.0 kW/m<sup>2</sup>. Assuming a collector efficiency of 50%, the price of a solar collector is supposed to be 1,000 Dfl/m<sup>2</sup> collector surface. This price includes all equipment necessary inside the building to operate the system. The specific yearly operational costs are arbitrarily chosen as 3% of the specific investment costs, which amounts to 60 Dfl/(kW<sub>th</sub>.a).

#### Electrolysis plants

Electrolysis plants are used for the conversion of electricity into the secondary fuel hydrogen. Electrical energy from the public grid is used to generate hydrogen that is supplied to a hydrogen transport piping system. That means that the electrolysis plants must include the conversion of alternating current into direct current and also the compression of the hydrogen at a pressure that enables the supply to the hydrogen transport system. In 1985 large electrolysis plants at powers of 100 to 165 MW were under construction or in operation. The large scale

plants were all of the filter-press type, operating at temperatures of 60 to 90°C. It was assumed that these temperatures are too low to enable the use of waste heat.

The plant efficiency is actually the ratio of the higher heating value of the hydrogen entering the hydrogen transport system and the corresponding electrical energy taken from the public grid. The chosen efficiency of 75% is rather high in comparison with the actual efficiencies of existing plants. It was assumed that the actual efficiencies will increase because of higher development efforts if the total number of plants will increase substantially. The specific investment costs are based on the best available data from literature but are supposed not to be very accurate. No data were found for the specific yearly operational costs; therefore, these costs are arbitrarily fixed at 3% of the specific investment costs.

#### Fuel cell power plants

In the system evaluation fuel cells power plants are considered for the conversion of hydrogen into electricity. Hydrogen from the hydrogen transport system is used to fuel the plants and the generated electricity is delivered to the public grid; therefore, the direct current from the fuel cells must be converted into alternating current. The choices made with regard to the fuel cell power plants were based on the very limited knowledge as available in 1985. The largest plants build at that time were the phosphoric acid fuel cell plants in New York and Tokio with powers around 4.5 MW<sub>e</sub> to demonstrate the technology. The plant in Tokio started operation in 1984. The operating experiences were not available at that time. Also the future prospects of the molten carbonate fuel cells were highly estimated at that time. But, with hydrogen as the fuel, it was expected that the phosphoric acid fuel might be the most suitable candidate. The operation of the molten carbonate fuel cell requires the presence of CO<sub>2</sub> in the fuel entering the anode; in the case of a hydrogen fuelled system, CO<sub>2</sub> from an external source must be mixed with the fuel. This will complicate the plant design and requires a CO<sub>2</sub> handling system. The solid oxide fuel cell was not seen as a serious option at that time, thus, the phosphoric acid fuel cell (PAFC) was selected as the preferred technology. The conversion efficiency of the PAFC power stations was assumed to be 50% based on the higher heating value of the fuel and the generated net AC power. During the preliminary evaluations utilization of the waste heat from the PAFC power plants was neglected. But it was assumed that 35% of the heat from the fuel can be used in the case of combined heat and power operation.

Useful information about costs was not available at that time. It was assumed that fuel cell power stations will be build in the future only if the investment costs are acceptable. Therefore, specific investment costs of 1,000 Dfl/kW<sub>e</sub> are considered for this study and the specific yearly operational costs are assumed to be 3% of this amount.

#### Boilers

The generation of low temperature heat as well as high temperature heat is supposed to be done by the combustion of hydrogen. Hot water boilers are considered for the generation of low temperature heat and steam boilers for the generation of high temperature heat. This is obviously a serious simplification but acceptable for these evaluations. The thermal efficiency of hot water boilers and steam boilers was assumed to be 90% based on the higher heating value of the fuel and represents actually the average efficiency during the year.

### Appendix 3.1

The specific investment costs are assumed to be 200 Dfl/kW<sub>th</sub> and the specific yearly operational costs 3% of the investment costs. Actually these costs have to be representative for the average costs of a variety of boiler types.

#### Heat pumps

The generation of low temperature heat is also possible by the application of heat pumps. In 1985 the application of heat pumps for individual dwellings was not seen as a realistic option. Therefore, it was supposed that large heat pumps have to be used in combination with a heat distribution system. The higher temperatures that are required in such a system will result in a lower coefficient of performance. It was assumed that a yearly average COP of 2.0 might be achievable. Because of the high power the specific investment costs are assumed to be 700 Dfl/kW<sub>e</sub> and the specific yearly operational costs are 3% of this amount.

#### Hydrogen storage

Various options for the storage of hydrogen have been considered: compressed gaseous hydrogen, liquid hydrogen and chemical bounded as hydrides. Storage is conceivable in tanks over ground or underground in depleted oil or gas fields, aquifers or caverns in salt layers. In the case of large scale storage with primarily one loading cycle per year the capital costs of the storage capacity must be very low. That's why underground storage of pressurized hydrogen gas in depleted gas fields is chosen for this study. Large scale centralized storage will require probably additional decentralized small scale storage to ensure hydrogen delivery under all circumstances. However, this intermediate storage is ignored for the time being.

The transport of hydrogen to the large scale storage and back to the distribution system will require energy. This energy consumption can be considered as a consumption of hydrogen necessary for the generation of compression power. This consumption can be represented by an efficiency of the hydrogen storage system, which means that it is taken into account as a hydrogen loss by the storage system. The compression power, however, is very small in comparison with the energy content of the compressed fuel. At first it was assumed that this loss can be neglected and the efficiency of the storage is assumed to be 1.0.

The specific investment costs of hydrogen storage are derived from the costs of underground storage of natural gas and were supposed to be 30 Dfl/GJ. In this amount the costs of the over ground plants as well as the costs of the cushion gas are included; the costs of the cushion gas are approximately 75% of the total costs of the storage facility. The cushion gas is the gas that has to be injected to the storage but never can be recovered. The operational costs of storage facility are determined only by the over ground plants. Therefore, it was assumed that the specific yearly operational costs are only 0.3 Dfl/(GJ.a) which is 1% of the specific investment costs.

#### LT Heat storage

The storage of low temperature heat can be done in different ways. If heat storage should match heat generation and heat demand during the year minimum investment costs are of primary importance. The considered options for large scale heat storage are:

- Large cylindrical tanks
- Underground storage

- By heating coils in the soil
- In aquifers or caverns
- Isolated lakes

The preference for one of these options is also depending on the local situation. Since long distance transport of heat is not attractive, heat storage will be necessary on many locations distributed over the country. It is not very likely that in all cases one specific kind of heat storage will be preferred. Therefore the selected values for the performance and costs of heat storage have to be seen as average values of a variety of systems. The efficiency of the heat storage system was optimistically assumed to be 1.0 which means that losses are neglected. In practice the losses can be considerable but insufficient data appeared to be available to enable a reliable estimate of the heat losses in the far away future.

The specific investment costs were assumed to be 500 Dfl/GJ. This level of costs was found in literature for various storage systems. Only for isolated lakes significant lower costs were found. The specific yearly operational costs are supposed to be 15 Dfl/(GJ.a) which is 3% of the specific investment costs.

### **3 SYSTEM EVALUATIONS**

#### **3.1 Introduction**

This chapter gives an overview of the results of various system calculations made during the project. The results as taken from [2], [3], [4], [6] and [7] are reported in the original units. In the original reports the application of nuclear power plants was used as a reference; today the use of coal fired power plants is supposed more appropriate. Therefore, the numbering of the systems is slightly modified. Moreover, some of the results that are considered not to be useful for the purpose of this report are left out.

#### **3.2 Exploring system studies**

##### **3.2.1 Introduction**

The exploring system studies are reported in [2]; the results taken from this report are presented in Table 3a and 3b. The purpose of the study was to recognize the effects of the application of different energy sources on the costs of a hydrogen based energy system. First systems using only one single energy source are considered (systems 1 to 7). After that also modified systems using combinations of different sources are taken into account (systems 8 to 14). The results of the system calculations will be briefly discussed in this section.

##### **3.2.2 Systems 1 and 2 (initial system with coal fired power plants nuclear plants)**

The systems 1 and 2 are based on the system diagram A as presented in Figure 1a. In the case of system 1 the primary source is coal which is converted by conventional pulverized coal power plants into electricity. The power plants operate continuously at design power. The

### Appendix 3.1

generated electricity is used to meet the electricity demand and any surplus will be converted into hydrogen by electrolysis plants. If the electricity demand should be higher than the generated electricity the balance can be provided with fuel cell systems converting hydrogen into electricity. The hydrogen is primarily used to meet the fuel demand for transport and for the generation of low temperature and high temperature heat. The conversion into heat takes place in hydrogen fuelled boilers. Hydrogen generation and demand are balanced by using a large scale hydrogen storage facility. In the case of system 2 uranium is used as the primary source and nuclear plants (pressurized water reactors) will convert uranium into electricity. All other conversions are the same as in the case of system 1. The necessary powers of the various conversion systems are calculated from the supposed energy demands as described in Section 2.2 of this appendix and are presented in Table 3a. The total yearly energy demands, 206 PJ/a electricity, 1022 PJ/a heat and 316 PJ/a transport fuel, are presented in Table 3a. It appears that in such a system the total power of the power plants (coal fired or nuclear) must be 68  $\text{GW}_e$ . And the power of the electrolysis plants is 63  $\text{GW}_e$ . The difference is actually the minimum electricity demand. Since the power generated by the power plants is always higher than the electricity demand, the power of the fuel cell plants can be 0. For the systems 1 to 4 no distinction was made between the generation of low temperature and high temperature heat. The demand pattern of low temperature heat was used for the calculation of the total power. The total thermal power of the boilers is 107  $\text{GW}_{th}$ . The storage capacity of hydrogen must be 327 PJ. The calculated total yearly costs of system 1 are 67 GDfl/a and 52 GDfl/a for system 2. In the case of system 1 the specification of costs shows that the fuel costs (coal) are almost 2/3 of the total yearly costs. The lower costs of system 2 is only due to the lower costs (lower fuel costs) of the nuclear plants. All other contributions are the same.

The systems 1 and 2 are used to determine the effects of the application of wind and solar energy. But, the systems are far away from the conventional energy systems. In a later stage of the study an attempt was made to determine the costs of the energy system as used in 1980 in the same way as chosen for this study. For the 1980 system the total yearly costs were calculated to be 22 GDfl/a. Unfortunately, the assumptions made for this calculation were not exactly the same as for the systems discussed in this section. But it shows at least that hydrogen based systems as considered here will result in very high total costs. The total yearly costs of the nuclear system, system 2, are more than 2 times the costs of the conventional system and the expenses for the coal fired system are about 3 times the yearly costs of the conventional system.

#### 3.2.3 System 3 (initial system with wind turbines)

System 3 uses only wind energy as the primary energy source. All other conversions are the same as in the case of systems 1 and 2. It appears that in total 301  $\text{GW}_e$  of turbine power is necessary to generate the required energy. Because of the high fluctuations of the wind speed the generated power will also show large fluctuations. The electrolysis plants must convert a significant part of the generated electricity into hydrogen. The power of these plants should enable the conversion of all generated electricity minus the electricity demand. Since the

<i>Table 3a Exploring system calculations</i>										
			system number							
			Units	1	2	3	4	5	6	7
System diagram				A	A	A	A	A	A	A
conversion										
$F_C \rightarrow E$	Coal fired power stations	GW <sub>e</sub>	68	-	-	-	-	6.7	-	-
$F_U \rightarrow E$	Nuclear power stations	GW <sub>e</sub>	-	68	-	-	-	-	6.7	-
$E_{wind} \rightarrow E$	Wind turbines	GW <sub>e</sub>	-	-	301	-	-	-	-	61.4
$E_{solar} \rightarrow E$	Photovoltaic generators	GW <sub>e</sub>	-	-	-	547	-	-	-	-
$E \rightarrow F$	Electrolysis plants	GW <sub>e</sub>	63	63	298	539	3.1	3.1	3.1	58
$F \rightarrow E$	Fuel cell power plants	GW <sub>e</sub>	0	0	9.5	9.5	2.8	2.8	2.8	9.4
$F \rightarrow Q$	Boilers	GW <sub>th</sub>	107	107	107	107	-	-	-	-
storage	Hydrogen, underground	PJ	327	327	346	772	7.8	7.8	7.8	55.4
demand	Electricity	PJ/a	206	206	206	206	206	206	206	206
	Heat	PJ/a	1022	1022	1022	1022	-	-	-	-
	Fuel	PJ/a	316	316	316	316	-	-	-	-
Total costs										
	Coal fired power stations	GDfl/a	57.5	-	-	-	-	5.67	-	-
	Nuclear power stations	GDfl/a	-	42.5	-	-	-	-	4.27	-
	Wind turbines	GDfl/a	-	-	62.2	-	-	-	-	12.7
	Photovoltaic generators	GDfl/a	-	-	-	56.9	-	-	-	-
	Electrolysis plants	GDfl/a	6.5	6.5	30.7	56.0	0.32	0.32	0.32	6.0
	Fuel cell power plants	GDfl/a	-	-	1.0	1.0	0.29	0.29	0.29	1.0
	Boilers	GDfl/a	2.2	2.2	2.2	2.2	-	-	-	-
	Hydrogen, underground	GDfl/a	0.8	0.8	0.9	1.9	0.02	0.02	0.02	0.1
	Total	GDfl/a	67.0	52.0	97.0	118	6.3	4.9	4.9	19.8
Specification of total costs										
	Capital costs	GDfl/a	15.9	24.8	69.1	84.1	1.52	2.25	2.25	14.1
	Fuel costs	GDfl/a	44.8	17.3	-	-	4.42	1.74	1.74	-
	Operating costs	GDfl/a	6.3	9.9	27.9	33.9	0.36	0.91	0.91	5.7
<p>Systems 5 and 6 can be compared with the generation of electricity by nuclear and coal fired power plants without storage.</p> <p>For the generation of electricity without storage the following costs are calculated (assuming the same specific costs and 100% plant availability):</p> <ul style="list-style-type: none"> <li>• Generation with coal fired power plants 6.0 GDfl/a</li> <li>• Generation with nuclear plants 5.2 GDfl/a</li> </ul>										

## Appendix 3.1

		Units	system number							
			8	9	10	11	12	13	14	
System diagram			C	C	C	C	C	B	B	
conversion										
$F_C \rightarrow E$	Coal fired power stations	GW <sub>e</sub>	4.0	-	-	20.0	-	30.0	-	
$F_U \rightarrow E$	Nuclear power stations	GW <sub>e</sub>	-	4.0	-	-	20.0	-	30.0	
$E_{wind} \rightarrow E$	Wind turbines	GW <sub>e</sub>	3.0	3.0	-	15.0	15.0	25.0	25.0	
$E_{solar} \rightarrow E$	Photovoltaic generators	GW <sub>e</sub>	297	297	335	145	145	109	109	
$E_{solar} \rightarrow Q_{LT}$	Solar collectors	GW <sub>th</sub>	125	125	143	125	125	-	-	
$E \rightarrow F$	Electrolysis plants	GW <sub>e</sub>	285	285	327	160	160	80.4	80.4	
$F \rightarrow E$	Fuel cell power plants	GW <sub>e</sub>	5.5	5.5	9.5	-	-	-	-	
$F \rightarrow Q_{LT}$	Heat pumps	GW <sub>e</sub>	9.2	9.2	-	9.2	9.2	71.9	71.9	
$F \rightarrow Q_{HT}$	Boilers	GW <sub>th</sub>	16.4	16.4	16.4	16.4	16.4	16.4	16.4	
storage	Hydrogen, underground	PJ	281	281	318	143	143	58.5	58.5	
	LT heat	PJ	312	312	312	312	312	312	312	
demand	Electricity	PJ/a	206	206	206	206	206	206	206	
	LT heat	PJ/a	573	573	573	573	573	573	573	
	HT heat	PJ/a	449	449	449	449	449	449	449	
	Fuel	PJ/a	316	316	316	316	316	316	316	
Total costs										
Conversion	Coal fired power stations	GDfl/a	3.5	-	-	15.7	-	25.1	-	
	Nuclear power stations	GDfl/a	-	2.5	-	-	10.7	-	19.1	
	Wind turbines	GDfl/a	0.7	0.7	-	3.1	3.1	5.2	5.2	
	Photovoltaic generators	GDfl/a	30.9	30.9	34.6	15.0	15.0	11.5	11.5	
	Solar collectors	GDfl/a	25.9	25.9	29.5	26.0	26.0	-	-	
	Electrolysis plants	GDfl/a	29.7	29.7	33.7	16.6	16.6	8.4	8.4	
	Fuel cell power plants	GDfl/a	0.5	0.5	0.9	-	-	-	-	
	Heat pumps	GDfl/a	0.7	0.7	-	0.6	0.6	5.2	5.2	
	Boilers	GDfl/a	0.3	0.3	0.3	0.4	0.4	0.3	0.3	
storage	Hydrogen, underground	GDfl/a	0.6	0.6	0.8	0.4	0.4	0.1	0.1	
	LT heat	GDfl/a	16.2	16.2	16.2	16.2	16.2	16.2	16.2	
Total			GDfl/a	109	108	116	94.0	89.0	72.0	66.0
Specification of total costs										
	Capital costs	GDfl/a	75.7	76.1	82.5	58.6	61.0	37.3	41.4	
	Fuel costs	GDfl/a	2.6	1.0	-	13.2	5.1	19.5	7.7	
	Operating costs	GDfl/a	30.7	30.9	33.5	22.2	22.9	15.2	16.9	

electricity demand is much lower than the maximum power generated by the wind turbines, the power of the electrolysis plants (298 GW<sub>e</sub>) is only slightly lower than the power of the wind turbines. Wind turbines are not always able to generate the demanded electricity. Therefore fuel cell power plants are necessary for back-up. The calculated power of the fuel cell plants (9.5 GW<sub>e</sub>) equals almost the maximum electricity demand. The capacity of the hydrogen storage (346 PJ) is not much higher than in the case of the systems 1 and 2.

The total yearly costs of system 3 are calculated to be 97.0 GDfl/a. This is much higher than the calculated costs of the systems 1 and 2. Wind energy is available for free but the capital and operating costs for wind turbines and electrolysis plants are very high: roughly 96% of the total yearly costs of system 3.

#### 3.2.4 System 4 (initial system with photovoltaic generators)

System 4 uses only solar energy as the primary energy source. The solar energy is converted into electricity by photovoltaic generators. A total power of 547 GW<sub>e</sub> is required to meet all energy demands. And also the necessary power of the electrolysis plants (539 GW<sub>e</sub>) is much higher than for the other systems. The generation of electricity and consequently hydrogen will primarily take place during the summer period while the consumption of hydrogen for the generation of heat will be maximum during winter time. This mismatch between generation and consumption of hydrogen requires a high capacity of the hydrogen storage facility (772 PJ).

The total yearly costs (118 GDfl/a) are highly dominated by the capital and operating costs of the photovoltaic generators and the electrolysis plants. They determine roughly 96% of the total yearly costs. The specific investment costs of the photovoltaic generators are assumed to be 1 000 Dfl/kW<sub>e</sub>, which is extremely low. In spite of this optimistic assumption the total yearly costs of system 4 are significantly higher than the costs of the other systems.

#### 3.2.5 Systems 5 to 7 (systems with electricity supply only)

In the systems 1 to 4 each of the considered sources of primary energy is supposed to generate the electricity needed to meet all national energy demands. It appears that under the considered circumstances the application of renewable sources will result into a significant increase of the total yearly costs. For a better understanding of the effects of the application of renewable sources on the design of the national energy system, three additional system calculations are made for systems that have to meet only the national demand on electrical energy. The systems 5 and 6 use coal fired and nuclear power plants operating at constant power and using the storage of hydrogen to meet the fluctuations of the electricity demand. In system 7 the power plants are replaced by wind turbines and hydrogen storage is used to balance electricity generation and demand. Because of the lower costs of the nuclear plants the total yearly costs of system 6 are lower than for system 5. It is clear that the assumptions regarding investment costs and fuel prices are determining this difference. It should be realized also that the use of hydrogen storage has not a positive effect on the overall yearly costs. If the coal fired power plants and the nuclear power plants are considered in load following operation and when using the same calculation rules, the total yearly costs are 6.0 GDfl/a in the case of coal fired power plants and

### Appendix 3.1

5.2 GDfl/a in the case of nuclear plants (the bottom of Table 3a). The application of wind turbines (system 7) has a serious effect on the need for storing hydrogen. The capacity of the hydrogen storage plant increases from 7.8 PJ for the systems 5 and 6 to 55.4 PJ for system 7. Since all hydrogen is used for the generation of electricity, the need for hydrogen storage will reduce the overall conversion efficiency of the system significantly. At the same time they cause higher total yearly costs. The total yearly costs of system 7 (wind turbines) are roughly three times the total yearly costs of system 5 (coal fired power plants). Because of the additional conversion losses due to energy storage the electrical power generated by the wind turbines is roughly two times the electrical power generated by the power plants. High conversion efficiencies are necessary to make the application of renewable sources more attractive.

#### 3.2.6 Systems 8 and 9 (mixed primary sources: power plants 4 GW<sub>e</sub>, wind turbines 3 GW<sub>e</sub>, solar collectors 125 GW<sub>th</sub>)

So far only systems using one particular energy source are considered. The systems 8 to 12 are evaluated to get a first impression of the possibilities of the application of mixed energy sources and the use of alternative conversion techniques. All systems are based on system diagram C as presented in Figure 1c. The system diagram enables the application of more than one energy source for the generation of electricity. Only two sources are shown in the diagram, but actually also systems with three sources are considered. And in addition a separate energy source is shown for the generation of low temperature heat. This source is added for the evaluation of the application of solar collectors. The conversion of electricity into low temperature heat was added too in the system diagram to evaluate the application of electrical driven compression heat pumps. To balance the generated heat with the low temperature heat demand, a LT heat storage was included in the system.

The systems 8 and 9 are based on a mix of coal or nuclear, solar energy and wind energy. Solar energy is used for the generation of electricity as well as LT heat. The generation of electricity takes place by power stations with a total power of 4.0 GW<sub>e</sub>, wind turbines with an installed power of 3.0 GW<sub>e</sub> and photovoltaic generators for the remainder of the required electricity. From the system calculation it appears that 297 GW<sub>e</sub> of photovoltaic generators are needed. LT heat is generated by solar collectors and electrical driven heat pumps. It is assumed that the solar collectors will generate 500 PJ/a which requires an installed power of 125 GW<sub>th</sub>. The remainder is generated by the heat pumps. Because of the limited power of the power stations the total yearly costs of the systems 8 and 9 are almost similar. The costs are dominated by the costs of the photovoltaic generators, the solar collectors and the electrolysis plants. Also the costs of the LT heat storage are substantial. In comparison with system 4, with only photovoltaic generators for the conversion of primary energy, the reduction of the total yearly costs is limited. The necessary power of the photovoltaic generators is significantly reduced but this reduction is highly compensated by the additional costs of the solar collectors and the LT heat storage.

### 3.2.7 System 10 (solar energy only: with solar collectors generating all LT heat)

System 10 makes only use of solar energy, but with different conversion technologies: photovoltaic generators and solar collectors. The solar collectors are used to generate all necessary LT heat; the difference between generation and demand is balanced by the low temperature heat storage facilities. The other energy demands are met by the generation of electricity from photovoltaic generators. Thus, this system is highly similar to system 4. It appears from the system calculation that the application of solar collectors will cause a substantial reduction of the power from the photovoltaic generators (from 547 GW<sub>e</sub> to 335 GW<sub>e</sub>). The consequence of this reduction is that also the power of the electrolysis plants and the capacity of the hydrogen storage can be reduced. However, because of the relatively high specific costs of the solar collectors and the LT heat storage the calculated total yearly costs of system 10 are only slightly lower. If the optimistic assumption regarding the specific costs of the photovoltaic generators is taken into account, it may be concluded that the application of solar collectors for the generation of LT heat is more attractive than photovoltaic generators if this heat should be achieved from solar energy.

### 3.2.8 Systems 11 and 12 (mixed primary sources: power plants 20 GW<sub>e</sub>, wind turbines 15 GW<sub>e</sub>, solar collectors 125 GW<sub>th</sub>)

From the previous system calculations it appeared that a reduction of the power of the photovoltaic generators will result in a decrease of the total yearly costs of the system. In the systems 11 and 12 the total power of the coal fired and nuclear power plants are increased to 20 GW<sub>e</sub>, and the total power of the wind turbines is 15 GW<sub>e</sub>. The system calculation shows that this results in a decrease of the power of the photovoltaic generators to 145 GW<sub>e</sub>. And consequently the power of the electrolysis plants decreases to 145 GW<sub>e</sub> and the capacity of the hydrogen storage to 143 PJ. LT heat is generated by solar collectors and heat pumps, in the same way as for the systems 8 and 9. Because of the relatively high power of the power plants additional power generation by fuel cell systems is not necessary. The system calculations show that the reduced power of the photovoltaic generators results in a decrease of the total yearly costs of the system from 109 to 94 GDfl/a for the coal fired system and from 108 to 89 GDfl/a for the nuclear system.

### 3.2.9 Systems 13 and 14 (mixed primary sources: power plants 30 GW<sub>e</sub>, wind turbines 25 GW<sub>e</sub>, no solar collectors)

A further reduction of the power from the photovoltaic generators is evaluated with systems 13 and 14. In these systems the power from the power plants is increased to 30 GW<sub>e</sub>, and the installed power of the wind turbines to 25 GW<sub>e</sub>. At the same time the solar collectors are skipped; all LT heat is generated by electrical driven heat pumps that are operating proportional with the power from the photovoltaic generators. Then, the power of the heat pumps must be 71.9 GW<sub>e</sub>. And the capacity of the heat storage is the same as in the case of the systems 8 to 12. Under these conditions the installed power of the photovoltaic generators must be 109 GW<sub>e</sub>; the power of the electrolysis plants must be 80.4 GW<sub>e</sub> and a capacity of the hydrogen storage of 58.5 PJ is needed.

## Appendix 3.1

The calculated total yearly costs of system 13 (with coal fired power plants) are 72 GDfl/a and of system 14 (with nuclear power plants) 66 GDfl/a.

### 3.3 A systematic evaluation

#### 3.3.1 Introduction

The exploring system studies have shown that replacing the (more expensive) conventional power plants (coal fired or nuclear plants) by wind turbines or photovoltaic generators can increase the total costs of the national energy supply significantly. But high cost differences were achieved for the various systems. It appeared that the number of system options is high and it is not easy to predict the effect of the application of specific technologies. First of all a better understanding of the consequences of the use of the various options for energy conversion and storage will be necessary. Therefore, it was decided to make a systematic evaluation that starts with a system using only coal or uranium and then replacing part of the fossil or nuclear fuel by renewable sources. Only the most interesting results from this evaluation are presented in this appendix. For the systematic evaluation the data as presented in the Tables 1 and 2 and the system diagram C (Figure 1c) are used.

The results are shown in the Tables 4a and 4b. The results for nuclear plants are not presented. At this level of evaluation the behavior of the nuclear plants is the same as the coal fired plants and does not affect the power or capacity of the various conversions and storages. Further, only hydrogen was considered as the secondary fuel; other secondary fuels were not considered in this evaluation.

#### 3.3.2 Systems 1a and 1b (reference system with and without LT heat storage)

Coal is used as the primary source of these systems. LT heat is generated by electrical driven heat pumps operating continuously at full load. LT heat generation and demand are balanced by LT heat storage. It is assumed that the LT heat storage consists of a combination of and large scale and small scale heat stores. Small scale heat storage in warm water tanks will be available in the dwellings or buildings; large scale heat storage is done in underground reservoirs. Such a system requires also a hot water distribution system. HT heat is generated by hydrogen fuelled boilers. The installed power of these boilers must be  $14.9 \text{ GW}_{\text{th}}$ . The calculated total power of the power plants is  $48.7 \text{ GW}_{\text{e}}$ . The generated electricity is used directly to meet the electricity demand and to feed the electrical driven heat pumps. The surplus is converted into hydrogen by the electrolysis plants. A hydrogen storage system is applied to balance the hydrogen demand for transport and the generation of HT heat with the hydrogen generation.

In this system configuration the power of the electrolysis plants is relatively low ( $35.4 \text{ GW}_{\text{e}}$ ). Also the capacity of the hydrogen storage is limited to 39.1 PJ but the capacity of the LT heat storage system is quite high (167.5 PJ). The total yearly costs of system 1a are 54.4 GDfl/a; the expenses for fuel are almost 60% of these costs.

The systems discussed so far are almost all integrated systems that generate all the demanded energy. For system 1a it was checked what the savings are of such an integrated

		Units	system number			
			1a	1b	2a	2b
System diagram						
conversion						
$F_C \rightarrow E$	Coal fired power stations	$\text{GW}_e$	48.7	48.7	39.0	44.3
$E_{\text{wind}} \rightarrow E$	Wind turbines	$\text{GW}_e$	-	-	-	-
$E_{\text{solar}} \rightarrow E$	Photovoltaic generators	$\text{GW}_e$	-	-	-	-
$E_{\text{solar}} \rightarrow Q_{\text{LT}}$	Solar collectors	$\text{GW}_{\text{th}}$	-	-	158.5	158.5
$E \rightarrow F$	Electrolysis plants	$\text{GW}_e$	35.4	43.4	35.4	40.7
$F \rightarrow E$	Fuel cell power plants	$\text{GW}_e$	-	-	-	-
$F \rightarrow Q_{\text{LT}}$	Heat pumps	$\text{GW}_e$	9.7	34.3	-	33.5
$F \rightarrow Q_{\text{HT}}$	Boilers	$\text{GW}_{\text{th}}$	14.9	14.9	14.9	14.9
storage	Hydrogen, underground	PJ	39.1	100.9	39.1	107.5
	LT heat	PJ	167.5	-	338.1	3.5
demand	Electricity	PJ/a	206	206	206	206
	LT heat	PJ/a	613	613	613	613
	HT heat	PJ/a	409	409	409	409
	Fuel	PJ/a	316	316	316	316
Costs	Capital costs	GDfl/a	16.0	11.8	43.8	34.4
	Fuel costs	GDfl/a	31.9	31.8	25.4	29.0
	Operating costs	GDfl/a	6.5	4.8	17.9	13.8
	Total	GDfl/a	54.4	48.4	87.1	77.2

system in comparison with the use of independent conversion chains for the various energy demands using the same conversion and storage techniques. It appeared that the integration causes a reduction of the total yearly costs of approximately 2%.

In system 1b the same conversions are used for the generation of the various energy demands; but LT heat storage is not available in this case. Then, the power of the electrolysis plants must increase (to 43.4  $\text{GW}_e$ ) and also the power of the heat pumps (to 34.3  $\text{GW}_e$ ). The capacity of the hydrogen storage becomes 100.9 PJ. It appears that the total yearly costs of system 1b are 48.4 GDfl/a, which is seriously lower than the total yearly costs calculated for system 1a. The higher power of the heat pumps will require an extension of the electrical transport and distribution grid. The costs of the grid are not included in these calculations. That makes it difficult to draw firm conclusions at this stage.

## Appendix 3.1

<i>Table 4b Systematic evaluation (continued)</i>						
		Units	system number			
			3a	3b	4a	4b
System diagram						
conversion						
$F_C \rightarrow E$	Coal fired power stations	GW <sub>e</sub>	41.3	41.3	33.5	33.6
$E_{\text{wind}} \rightarrow E$	Wind turbines	GW <sub>e</sub>	-	-	60	60
$E_{\text{solar}} \rightarrow E$	Photovoltaic generators	GW <sub>e</sub>	60	60	-	-
$E_{\text{solar}} \rightarrow Q_{\text{LT}}$	Solar collectors	GW <sub>th</sub>	-	-	-	-
$E \rightarrow F$	Electrolysis plants	GW <sub>e</sub>	86.5	89.8	79.9	87.9
$F \rightarrow E$	Fuel cell power plants	GW <sub>e</sub>	-	1.5	-	9.3
$F \rightarrow Q_{\text{LT}}$	Heat pumps	GW <sub>e</sub>	9.7	34.3	9.7	34.3
$F \rightarrow Q_{\text{HT}}$	Boilers	GW <sub>th</sub>	14.9	14.9	14.9	14.9
storage	Hydrogen, underground	PJ	87.3	148	75.8	97.8
	LT heat	PJ	167.5	-	167.5	-
demand	Electricity	PJ/a	206	206	206	206
	LT heat	PJ/a	613	613	613	613
	HT heat	PJ/a	409	409	409	409
	Fuel	PJ/a	316	316	316	316
Costs	Capital costs	GDfl/a	23.3	19.0	26.2	22.6
	Fuel costs	GDfl/a	27.0	27.0	21.9	21.9
	Operating costs	GDfl/a	9.5	7.6	10.6	9.2
Total		GDfl/a	59.8	53.6	58.7	53.7

### 3.3.3 Systems 2a and 2b (reference system extended with solar collectors, with and without LT heat storage)

In system 2a LT heat is generated only by solar collectors. Then, a LT heat storage system is necessary to balance the heat generation and demand. It appears that the power of the solar collectors must be 158.5 GW<sub>th</sub> in total. The capacity of the heat storage system must be 338.1 PJ which is about two times the capacity needed in the case of system 1a. The total yearly costs are 87.1 GDfl/a, an increase of 60% in comparison with system 1a. It appears that the application of solar collectors with heat storage is quite expensive.

Usual solar collector systems include a small scale heat storage system that has a storage capacity for roughly one day. In the case of system 2b it has been assumed that no large scale heat storage system is available but only a storage that can meet the daily fluctuations. The power of the solar collectors is the same as for system 2a. In addition to the solar collectors heat pumps are used to generate the demanded heat. It appears that the power of the heat pumps must be 33.5

$\text{GW}_e$  to generate the demanded heat at any time. The high power of the heat pumps results in an increase of the power of the coal fired power stations and the electrolysis plants compared to system 2a. Also a higher capacity of the hydrogen storage system is necessary.

### 3.3.4 Systems 3a and 3b (systems with 60 $\text{GW}_e$ photovoltaic generators, with and without LT heat storage)

The difference between the systems 3a and 3b and the systems 1a and 1b is the application of 60  $\text{GW}_e$  photovoltaic generators. This results in a decrease of the required power of the coal fired power plants from 48.7  $\text{GW}_e$  to 41.3  $\text{GW}_e$ . However, the power of the electrolysis plants is more than doubled. The total yearly costs of the systems 3a and 3b are approximately 10% higher than the costs of the systems 1a and 1b. It should be mentioned that the moderate increase of total yearly costs of the systems 3 compared to the systems 1 is primarily caused by the low value of the specific investment costs of the photovoltaic generators used for this study.

### 3.3.5 Systems 4a and 4b (systems with 60 $\text{GW}_e$ wind turbines, with and without LT heat storage)

In the systems 4a and 4b it is assumed that 60  $\text{GW}_e$  wind turbines are used to replace part of the coal fired power plants of the systems 1a and 1b. The system calculations shows that the decrease of the necessary power of the coal fired power plants is stronger than in the case of the photovoltaic generators. But the increase of the power of the electrolysis plants is comparable. The application of the wind turbines requires a lower capacity of the hydrogen storage than the application of the photovoltaic generators. The total yearly costs of the systems 4a and 4b are almost the same as for the systems 3a and 3b. But again it has to be emphasized that this is primarily due to the low value of the specific investment costs of the photovoltaic generators.

<i>Table 5 Increase of total yearly costs due to the application of renewable energy</i>		
		increase of total yearly costs per $\text{GW}_e$ reduction of coal fired power plants [(GDF/a)/ $\text{GW}_e$ ]
Solar collectors	with LT heat storage (2a vs 1a)	3.4
	without LT heat storage (2b vs 1b)	6.5
Photovoltaic generators	with LT heat storage (3a vs 1a)	0.73
	without LT heat storage (3b vs 1b)	0.70
Wind turbines	with LT heat storage (4a vs 1a)	0.28
	without LT heat storage (4b vs 1b)	0.35

### 3.3.6 Conclusions

The results of the systematic evaluation show that replacement of a significant part of the fossil fired plants by generators using renewable sources is conceivable without an excessive increase of the total yearly costs. In the original evaluation the replacement of the power of the coal fired plants by generators using renewable sources was done in a number of steps. The effects on the necessary powers and total yearly costs appeared to be almost linear, therefore,

## Appendix 3.1

only the highest powers of the generators using renewable sources are presented in Table 4. The extra costs of the application of renewable energy can be calculated by dividing the difference of the total yearly costs between the systems using renewable energy and the reference systems by the reduction of the power of the coal fired power plants. The results are shown in Table 5.

Replacing fossil fired power plants can be done with the lowest increase of total yearly costs by using wind turbines; if due to the application of wind turbines the power of the coal fired power stations can be reduced with 1 GW<sub>e</sub> the increase of total yearly costs will be roughly 0.28 to 0.35 GDfl/a depending on the system design. To achieve the same reduction of fossil power by using photovoltaic generators the increase of the total yearly costs will be roughly 0.70 to 0.73 GDfl/a. Full replacement of the coal fired power station by wind turbines will increase the total yearly costs roughly with 15 GDfl/a, an increase of 30%. A similar increase will occur if the fuel prices will go up by 50%; thus this increase is supposed to be affordable. With the cost assumptions used for this evaluation the application of solar collectors appears to be not attractive at all. Also the application of large scale heat storage appears to be very expensive.

### 3.4 Selection of reference configurations

#### 3.4.1 Introduction

The third part of the study on energy systems for the future, reported in [4], was focusing on the design of system configurations that could be used as a reference for the evaluation of the various technologies. The need for and the attractiveness of certain technologies depends on the technologies cooperating in a system. The careful selection of an appropriate reference system is of main importance for useful conclusions with regard to the various technologies available or under development at the moment. For the purpose of this selection the following steps are done:

1. Evaluation of single production chains for the four energy demands.
2. Selection of suitable production chains for the composition of attractive reference configurations.
3. Composition and evaluation of a number of possible reference configurations.
4. Definition of some reference configurations that can be used for the further evaluation of the effects of alternative sources, conversion and storage technologies, alternative system configurations etc..

A comprehensive evaluation of various kinds of technologies was made. The details of these evaluations are not included in this section. Only the main results and insights are reported here.

#### 3.4.2 Evaluation and selection of production chains

The evaluation and selection of production chains was done to see what the most attractive technologies are for the generation of respectively electricity, LT heat, HT heat and transport fuel. For the selection of integrated reference systems, not only the most attractive system for each of the energy demands is important but also the deviation of the alternatives. Production chains for each of the energy demands are considered using uranium, coal, solar energy and wind as the

<i>Table 6 Data used for the selection of reference configurations</i>			
	system	Conversion factor	Specific investment costs
<b>Primary conversion systems</b>			
$F_U \rightarrow E$	Pressurized water reactor	0.32	3 600 Dfl/kW <sub>e</sub>
$F_U \rightarrow Q_{LT}$	Nuclear reactor for LT heat	1.0	650 Dfl/kW <sub>th</sub>
$F_C \rightarrow E$	Power station (pulverized coal)	0.39	2 000 Dfl/kW <sub>e</sub>
$F_C \rightarrow Q_{LT}$	Fluidized bed boilers (LT heat)	0.90	970 Dfl/kW <sub>th</sub>
$F_C \rightarrow Q_{HT}$	Fluidized bed boilers (HT heat)	0.90	760 Dfl/kW <sub>th</sub>
$F_C \rightarrow F''_C$	Coal gasification plant (intermediate calorific gas)	0.75	1 000 Dfl/kW <sub>th, out</sub>
	Coal gasification plant (high calorific gas / SNG)	0.60	1 200 Dfl/kW <sub>th, out</sub>
$F_C \rightarrow F'_C$	Coal liquefaction plant (direct conversion)	0.63	2 000 Dfl/kW <sub>th, out</sub>
$F_C \rightarrow E$	Fluidized bed boiler with back pressure turbine	0.11	8600 Dfl/kW <sub>e</sub>
$F_C \rightarrow Q_{LT}$		0.74	1260 Dfl/kW <sub>th</sub>
$F_C \rightarrow E$	Fluidized bed boiler with back pressure turbine	0.11	8600 Dfl/kW <sub>e</sub>
$F_C \rightarrow Q_{HT}$		0.74	1260 Dfl/kW <sub>th</sub>
$F_C \rightarrow F'_C$	SNG/liquefaction plant (SASOL-1)	0.19	6 800 Dfl/kW <sup>(1)</sup> <sub>th, out</sub>
$F_C \rightarrow F''_C$		0.37	
$F_C \rightarrow F'_C$	Ethylene/liquefaction plant (SASOL-2)	0.34	3 700 Dfl/kW <sup>(1)</sup> <sub>ft h out</sub>
$F_C \rightarrow F''_C$		0.04	
$F_C \rightarrow F'_C$	Coal gasification with PWR	0.90	1 500 Dfl/kW <sub>th, out</sub>
$F_U \rightarrow F'_C$		uranium 0.25	
$F_C \rightarrow F'_C$	Coal gasification with HTGR	1.0	2 500 Dfl/kW <sub>th, out</sub>
$F_U \rightarrow F'_C$		uranium 0.40	
$E_{wind} \rightarrow E$	Wind turbines	-	2 000 Dfl/kW <sub>e</sub>
$E_{solar} \rightarrow E$	Photovoltaic generators	-	1 000 Dfl/kW <sub>e</sub>
$E_{solar} \rightarrow Q_{LT}$	Solar collectors	-	2 000 Dfl/kW <sub>th</sub>
<b>Secondary conversion systems</b>			
$E \rightarrow Q_{LT}$	Electrical heat pumps	2.0	350 Dfl/kW <sub>th</sub>
$E \rightarrow Q_{LT}$	Electrical heaters	1.0	500 Dfl/kW <sub>th</sub>
$E \rightarrow F''_H$	Electrolysis plants	0.75	1 000 Dfl/kW <sub>e</sub>
$F''_C \rightarrow E$	MCFC Fuel cell plants	0.50	1 000 Dfl/kW <sub>e</sub>
	PAFC Fuel cell plants	0.45	1 000 Dfl/kW <sub>e</sub>
	Combined Cycle plants	0.50	1 100 Dfl/kW <sub>e</sub>
	Gas turbine plants	0.30	600 Dfl/kW <sub>e</sub>
	Gas fired power plants (steam turbine cycle)	0.40	1 200 Dfl/kW <sub>e</sub>
$F''_H \rightarrow E$	AFC Fuel cell plants	0.60	1 000 Dfl/kW <sub>e</sub>
	PAFC Fuel cell plants	0.55	800 Dfl/kW <sub>e</sub>

## Appendix 3.1

<i>Table 6 Data used for the selection of reference configurations (continued)</i>			
	system	Conversion factor	Specific investment costs
<b>Secondary conversion systems (continued)</b>			
$F''_C \rightarrow Q_{LT}$	Coal gas fired hot water boilers	0.90	200 Dfl/kW <sub>th</sub>
	Gas engine heat pumps	1.5	500 Dfl/kW <sub>th</sub>
	Absorption heat pumps	1.2	700 Dfl/kW <sub>th</sub>
$F''_H \rightarrow Q_{LT}$	Hydrogen gas fired hot water boilers	0.90	200 Dfl/kW <sub>th</sub>
$F''_C \rightarrow Q_{HT}$	Coal gas fired steam boilers	0.90	200 Dfl/kW <sub>th</sub>
$F''_H \rightarrow Q_{HT}$	Hydrogen gas fired steam boilers	0.90	200 Dfl/kW <sub>th</sub>
$F''_C \rightarrow E$ $\rightarrow Q_{LT}$	Combined cycle plants with back pressure turbine	0.35	1 100 Dfl/kW <sub>e</sub>
		0.43	830 Dfl/kW <sub>th</sub>
$F''_C \rightarrow E$ $\rightarrow Q_{LT}$	MCFC fuel cell plants	0.50	1 200 Dfl/kW <sub>e</sub>
		0.30	
$F''_C \rightarrow E$ $\rightarrow Q_{LT}$	PAFC fuel cell plants	0.45	1 200 Dfl/kW <sub>e</sub>
		0.25	
$F''_C \rightarrow E$ $\rightarrow Q_{HT}$	Gas turbine plants with waste heat boilers	0.26	1 250 Dfl/kW <sub>e</sub>
		0.45	730 Dfl/kW <sub>th</sub>
$F''_C \rightarrow E$ $\rightarrow Q_{HT}$	MCFC fuel cell plants	0.50	1 200 Dfl/kW <sub>e</sub>
		0.20	
$F_C$ $F_U \rightarrow F'_C$	Gas turbine with compressed air	1.08 air 0.49	300 Dfl/kW <sub>e</sub>
<b>Storage systems</b>			
$Q_{LT}$	Underground hot water reservoir	(1.0)	500 Dfl/GJ
	Large hot water tanks	(1.0)	700 Dfl/GJ
$F''_H$	Underground H <sub>2</sub> reservoir	0.94	30 Dfl/GJ
	Large pressurized H <sub>2</sub> tanks	0.94	10 000 Dfl/GJ
$F'_H$	Underground liquid H <sub>2</sub> reservoir		20-50 Dfl/GJ
	Large liquid H <sub>2</sub> tanks	0.98/day	500 Dfl/GJ
$F''_C$	Syngas/SNG in underground reservoir		30 Dfl/GJ
	Syngas/SNG in large tanks		10 000 Dfl/GJ
$E$	Pumped storage (capacity)	-	11 000 Dfl/GJ
	in (Kaplan turbine/pump)	0.85	1 200 Dfl/kW <sub>e</sub>
	out (Kaplan turbine/pump)	0.89	-----
	Underground pumped storage (capacity)	-	50 000 Dfl/GJ
	in (Francis turbine/pump)	0.85	350 Dfl/kW <sub>e</sub>
	out (Francis turbine/pump)	0.89	-----
	Compressed air underground (capacity)	1.0	20 000 Dfl/GJ
	in (compressor)	0.62	150 Dfl/kW <sub>e</sub>
	out (gas turbine)	0.74	300 Dfl/kW <sub>e</sub>

*Table 7 Additional data used for the selection of reference configurations*

Transport and distribution systems		
Transported medium	Characteristics	Specific costs
electricity	Transport grid	0.0069 MDfl/(km.GW <sub>e,a</sub> )
	Length transport grid 4 100 km	29 MDfl/(GW <sub>e,a</sub> )
	Distribution grid	142 MDfl/(GW <sub>e,a</sub> )
Low temperature heat	Transport network	2.7 MDfl/(km.GW <sub>th,a</sub> )
	Length transport network 5 km	13 MDfl/(GW <sub>th,a</sub> )
	Distribution network	33 MDfl/(GW <sub>th,a</sub> )
Gas (natural gas, SNG)	Transport network	0.0007 MDfl/(km.GW <sub>th,a</sub> )
	Length transport network 10 000 km	7 MDfl/(GW <sub>th,a</sub> )
	Distribution network	12 MDfl/(GW <sub>th,a</sub> )
Coal (decentralized units)	Train transport	0.0107 Dfl/(km.GJ)
	Average transport distance 100 km	1.07 Dfl/GJ
Fuel prices		
Uranium		2.6 Dfl/GJ
Coal		6.0 Dfl/GJ
Economic data		
Economic lifetime		20 a
Interest		4%
Annuity factor		0.07358
Operation and maintenance costs (percentage of investment costs)	Default	3%/a
	Underground gas storage	1%/a

primary source. The results of the production chains using renewable energy sources are only used indirectly during these evaluations, because the reference configurations have to be based on uranium and/or coal as the primary energy source. The use of renewable energy sources will require the storage of energy to meet the energy demands. Therefore the evaluation of various options for energy storage has been part of the evaluation of production chains.

### 3.4.3 Composition of reference configurations

The composition of reference configurations has been done more or less systematically by defining categories of systems based on the possibilities for energy distribution, the use of primary energy sources and the primary conversions. The used codes are presented Table 8. In the case of system configuration C(1a, 2acdfg) the system configuration is based on the distribution of electricity and LT heat and uranium and coal as the primary sources. Uranium is converted into electricity and coal is used to generate: electricity, HT heat in coal fired boilers, a gaseous fuel, electricity + LT heat in combined heat and power plants as well as electricity + HT heat in combined heat and power plants. Finally 13 system configurations were selected for further evaluation. Two of these configurations, called System 1980 and System 1984, are included to enable the comparison with respectively the actual situation in 1980 and with the previous calculations presented in [2] and summarized in the Section 3.1 of this appendix. In the evaluation of the reference configurations also the costs of transport and distribution of energy

## Appendix 3.1

Table 8 System codes for reference configurations		
Networks for energy distribution		
A	Electricity + gas (secondary fuel)	
B	Electricity	
C	Electricity + LT heat	
D	Electricity + gas (secondary fuel) + LT heat	
Primary energy sources		
1	Uranium	
2	Coal	
3	Uranium + coal	
Primary conversions		
a	$E_{\text{Prim}} \rightarrow E$	Primary energy into electricity
b	$E_{\text{Prim}} \rightarrow Q_{\text{LT}}$	Primary energy into LT heat
c	$F_{\text{C}} \rightarrow Q_{\text{HT}}$	Coal into HT heat
d	$F_{\text{C+U}} \rightarrow F'_{\text{C}}$	Coal or coal + uranium into a gaseous fuel
e	$F_{\text{C+U}} \rightarrow F''_{\text{C}}$	Coal or coal + uranium into a liquid fuel
f	$E_{\text{Prim}} \rightarrow E + Q_{\text{LT}}$	Primary energy into electricity and LT heat
g	$F_{\text{C}} \rightarrow E + Q_{\text{HT}}$	Coal into electricity and HT heat
h	$F_{\text{C}} \rightarrow E + F'_{\text{C}}$	Coal into electricity and gaseous fuel
i	$E_{\text{Prim}} \rightarrow F''_{\text{H}}$	Primary energy into hydrogen

carriers are considered. These costs were ignored in the previous studies. The results of System 1984 will show the additional (estimated) costs for energy transport and distribution. System 1980 represents the actual system configuration as available that year, based on the data from the CBS (Statistics Netherlands).

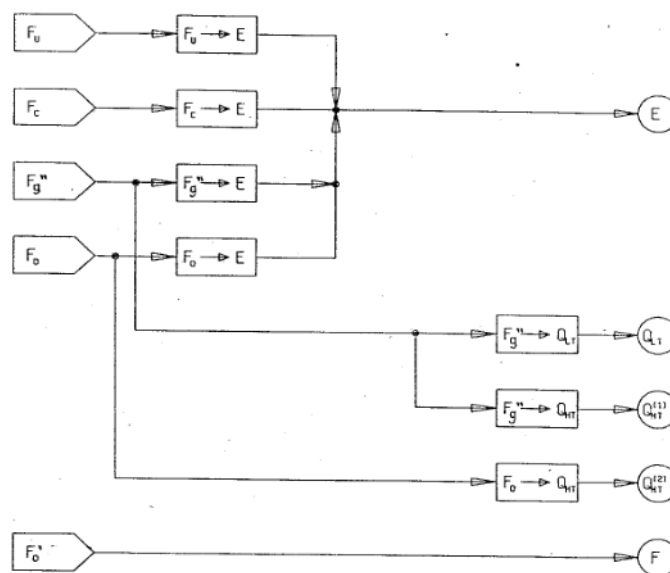


Figure 9 System diagram "System 1980"

		Units	system name				
			System 1980	System 1984	Ref. config.	Ref. coal gas	Ref. H <sub>2</sub> gas
System code					C(1a, 2acdfg)	A(1a, 2cde)	A(1a, 2ac)
Conversion							
$F_U \rightarrow E$	Nuclear power stations	GW <sub>e</sub>	0.5	-	2.7	3.6	22.2
$F_C \rightarrow E$	Coal fired power stations	GW <sub>e</sub>	0.8	48.7	17.3	-	108.5
$F_G \rightarrow E$	Nat. gas fired power stations	GW <sub>e</sub>	7.04	-	-	-	-
$F_O \rightarrow E$	Oil fired power stations	GW <sub>e</sub>	7.04	-	-	-	-
$F_C \rightarrow E$	Fluidized bed CHP plants	GW <sub>e</sub>	-	-	5.1	-	-
		GW <sub>th</sub>	-	-	7.2	-	-
$F_C \rightarrow E$	Fluidized bed CHP plants	GW <sub>e</sub>	-	-	1.5	-	-
		GW <sub>th</sub>	-	-	10.3	-	-
$F_G \rightarrow Q_{LT}$	Nat. gas fired boilers	GW <sub>th</sub>	68.7	-	-	-	-
$F_G \rightarrow Q_{HT}$	Nat. gas fired boilers	GW <sub>th</sub>	7.4	-	-	-	-
$F_O \rightarrow Q_{HT}$	Oil fired boilers	GW <sub>th</sub>	7.4	-	-	-	-
$F_C \rightarrow Q_{HT}$	Coal fired boilers	GW <sub>th</sub>	-	-	4.6	14.9	14.9
$F_O \rightarrow F'$	Oil refinery	GW <sub>th</sub>	24.0	-	-	-	-
$F_C \rightarrow F''$	Coal gasification plants	GW <sub>th</sub>	-	-	-	86.7	-
$F_C \rightarrow F'$	Coal liquefaction plants	GW <sub>th</sub>	-	-	12.7	12.7	-
$E \rightarrow F''_H$	Electrolysis plants	GW <sub>e</sub>	-	43.4	-	-	122.4
$E \rightarrow Q_{LT}$	Heat pumps	GW <sub>e</sub>	-	34.3	17.2	-	-
$F'' \rightarrow E$	Fuel cell power plants	GW <sub>e</sub>	-	-	-	6.1	-
$F'' \rightarrow Q_{LT}$	Gas fired boilers	GW <sub>th</sub>	-	-	-	68.7	68.7
$F'' \rightarrow Q_{HT}$	Gas fired boilers	GW <sub>th</sub>	-	14.9	-	-	-
$F'' \rightarrow F'$	Gas liquefaction plants	GW <sub>th</sub>	-	-	-	-	12.7
Transp/ distr	Electricity transport	GW <sub>e</sub>	9.7	48.7	26.5	9.7	130
	Electricity distribution	GW <sub>e</sub>	9.7	43.2	26.5	9.7	9.7
	Gas transport	GW <sub>th</sub>	92.3	32.6	-	86.7	91.8
	Gas distribution	GW <sub>th</sub>	76.3	32.6	-	76.3	76.3
	Coal transport	PJ/a	-	-	947	454	-
	Heat distribution	GW <sub>th</sub>	-	-	34.3	-	-
Storage	Hydrogen, underground	PJ	-	100.9	-	-	-
Emissions	CO <sub>2</sub>	Mtons/a	-	345	171	215	264
Demand	Electricity	PJ/a	206	206	206	206	206
	LT heat	PJ/a	613	613	613	613	613
	HT heat	PJ/a	409	409	409	409	409
	Fuel	PJ/a	316	316	316	316	316
Costs	Capital + operating costs	GDfl/a	9.2	25.4	21.8	21.6	53.4
	Fuel costs	GDfl/a	12.9	23.1	12.1	15.3	23.3
<b>Total</b>		<b>GDfl/a</b>	<b>22.1</b>	<b>48.5</b>	<b>33.9</b>	<b>36.9</b>	<b>76.7</b>

## Appendix 3.1

## 3.4.4 Selected configurations

System 1980 represents the actual situation at the time that the study was made. The system diagram as used for the calculations is shown in Figure 9. The oil refineries assumed for the conversion of crude oil into transport fuels and fuel oil are not visualized in the diagram, but are included in the system calculations. The powers of the various conversion technologies are shown in Table 9. The generation of electricity is primarily based on oil and natural gas; only limited powers of coal and uranium are used. It was assumed that LT heat is generated only with natural gas. HT heat is generated with natural gas and fuel oil. The calculated total yearly costs of this system are 22.1 GDF/a. The use of direct conversion processes of primary fuel into the demanded energy results in low capital costs and also relatively low fuel costs. The highest contributions to the total yearly costs are from the oil refineries (29%), the LT heat boilers (26%), electricity transport and distribution (12%) and the gas fired power stations (10%)

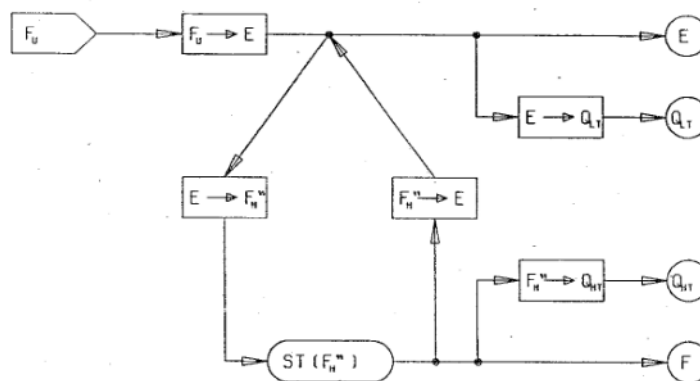
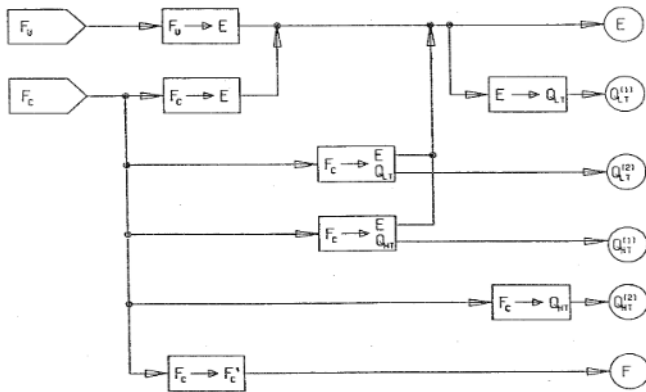


Figure 10 System diagram "System 1984"

System 1984 is actually the same as system 1b from the systematic evaluation (see Table 4a). The system diagram of System 1984 is shown in Figure 10; the powers and costs are presented in Table 9. Both systems use hydrogen as the secondary fuel and hydrogen storage to enable constant full load operation of the coal fired power plants. However, the total yearly costs differ only slightly from the costs of system 1b; the addition of the costs of transport and distribution of electricity and gas is almost counterbalanced by the lower coal price that is used for the evaluation of the selected configurations. It appears that the total yearly costs of System 1984 are more than twice the costs of System 1980. Apparently the straight forward application of hydrogen as a secondary fuel results in an excessive increase of the total yearly costs.

Reference configuration (C(1a,2acdfg))

The system diagram of the reference configuration is shown in Figure 11; the necessary powers and the resulting costs are presented in Table 9. Electricity is generated by nuclear as well as coal fired power stations and coal fired CHP plants. The LT heat demand as well as the HT heat demand are split to enable the use of different conversion technologies. LT heat is generated by electrical driven heat pumps and coal fired CHP plants; for the generation of HT heat CHP



C (1A, 2ACDFG)

Figure 11 System diagram "Reference configuration (C(1a, 2acdfg))"

plants and coal fired boilers are used. The production of liquid fuels for transport coal liquefaction plants are used. The selected reference configuration was one of the configurations with the lowest total yearly costs. Further cost reductions are achievable by increasing the power of the nuclear plants for the generation of electricity or heat. However, for the investigations on the effects of renewable sources and alternative technologies a further increase of the power of the nuclear plants was supposed not to be useful.

Transport and distribution of energy is done by an electrical grid and heat distribution grids. The high power of the transport and distribution grid is caused by the application of electrical driven heat pumps. The ample use of coal requires the transport of huge amounts of coal. The total yearly costs are 33.9 GDfl/a, which is relatively low but still 50% higher than the costs of System 1980. The higher costs are caused only by the higher capital costs of the system; the fuel costs are almost the same. It is obvious that the transition from the usual fossil fuels (oil and natural gas) to coal will result in a significant increase of the total yearly costs.

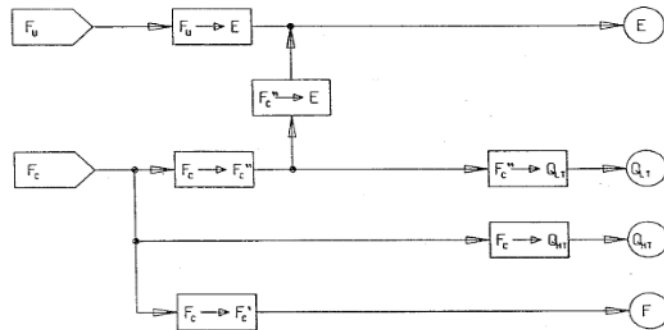
The preference for the reference configuration was primarily based on the relatively low costs and low CO<sub>2</sub> emissions and the prospects for further cost reductions and the addition of renewable sources and energy storage.

However, the reference configuration does not incorporate a gas distribution grid. To enable the evaluation of configurations in which the distribution of a

secondary gaseous fuel might be important two additional reference configurations have been chosen: one based on the distribution of coal gas, the other on the distribution of hydrogen.

Reference configuration with coal gas (A(1a, 2cde))

The system diagram of this configuration is shown in Figure 12; the necessary powers and calculated costs are presented in Table 9. Electricity is generated by nuclear power stations and fuel cell power plants. The nuclear power plants should generate the base load electricity and the



A (1A, 2CDE)

Figure 12 System diagram "Reference coal gas (A(1a, 2cde))"

## Appendix 3.1

fuel cell power plants generate the intermediate load and peak load power. The fuel cell power plants are fuelled with gas from the coal gasification plants. HT heat will be generated by coal fired boilers and LT heat by gas from coal gasification. It was assumed that because of the higher powers the industrial plants are able to use a solid fuel and the small powers of the boilers for the generation of LT heat require the use of gaseous fuels. Liquid fuels for transport are produced by coal liquefaction plants. Coal transport is necessary for the fuel supply of the industrial HT heat boilers. It is assumed that the costs of transport of coal to the power plants is included in the coal price; the transport of coal as mentioned in Table 9 represents only the transport of coal to dispersed locations. The total yearly costs of this configuration are almost 10% higher than the total yearly costs of the reference configuration. The capital costs are roughly the same, but the fuel costs are 26% higher than in the case of the reference configuration. This means that the overall conversion efficiency of the reference configuration is higher than the efficiency of reference configuration with coal gas. The lower efficiency causes also an increase of the yearly CO<sub>2</sub> emissions.

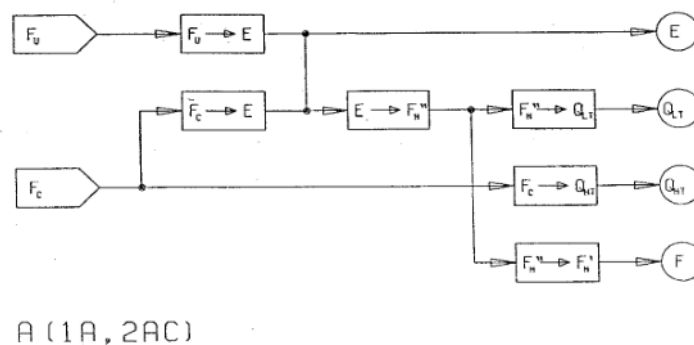


*Figure 13 System diagram "Reference hydrogen gas (A(1a, 2ac))"*

Reference configuration with hydrogen gas (A(1a, 2ac))

The system diagram of this configuration is shown in Figure 13; the necessary powers and calculated costs are presented in Table 9. Electricity is generated in this configuration by nuclear power stations and coal fired power stations. Because of the high electrical power that must be generated, the base load will be significantly higher and thus also the power of the nuclear power stations. HT heat for industrial purposes is generated in coal fired boilers. Hydrogen is used as secondary fuel necessary for transport fuel and for the generation of LT heat in hot water boilers. As no storage of hydrogen is supposed to be available, the powers of the electrolysis plants and the coal fired power stations are very high. But the load factors are quite low: the load factor of the coal fired power plants is 28.4% and of the electrolysis plants 38.0%. The low load factors of these plants are primarily responsible for the high total yearly costs of this configuration. It is assumed that the electrolysis plants are not located nearby the power stations and that transport of all generated electricity is necessary. Distribution of electricity is only needed for the electricity demand. The gas transport system is used also for the transport of transport fuel. The overall efficiency of the reference configuration with hydrogen gas appears to be much lower than for the

other selected reference systems as can be concluded from the yearly CO<sub>2</sub> emissions. In spite of the higher power of the nuclear power plants the CO<sub>2</sub> emissions are about 23% higher than in the case of coal gas distribution. The total yearly costs are 76.7 GDfl/a which is more than twice the costs of the reference configuration with coal gas.

#### 3.4.5 Conclusions

Various options for systems with hydrogen as the secondary fuel that should enable serious cost reductions have been evaluated. But only limited cost reductions were achieved. All alternatives were based on available or almost available technologies. Therefore, it was concluded that the application of hydrogen as a secondary fuel is very expensive. Only the development of very efficient and cheap technologies for the generation of hydrogen might cause a reconsideration of this conclusion.

### **3.5 The evaluation of wind turbines and energy storage**

#### 3.5.1 Introduction

In the last report [6] of the study on renewable energy systems the application of wind turbines and energy storage has been considered into more detail. The application of wind turbines was selected for this purpose because wind energy has better economic perspectives than solar energy. The generated power by the wind turbines is governed by the wind speed; the fluctuations do in general not follow the fluctuations of the energy demand. Additional facilities are necessary to balance energy generation and demand. In the case of the use of solar energy the same additional facilities can be used, but, as shown before, the powers and capacities must be higher. If large scale energy storage is not possible, sufficient backup power must be available to ensure the generation of the demanded energy at any time during the year. The use of energy storage can reduce the need for backup power. The application of energy storage will be beneficial only if the costs of energy storage are lower than the costs of backup power.

It was learned from the previous studies that only the large scale storage of a secondary fuel has a change to be attractive with regard to costs. To avoid the need for additional conversions, the stored fuel is supposed to be the same as the secondary fuel used for transport and distribution of energy. Two secondary fuels are considered in this evaluation: gaseous hydrogen and synthetic natural gas (SNG). The storage of secondary fuels is supposed to enable the storage of large quantities of fuel necessary to level off the seasonal fluctuations. In the case of a pumped-hydro energy storage facility, the costs of the storage capacity are relatively high (see Table 6) but the costs of the pumping system appears to be affordable. In order to check the feasibility of this type of energy storage a pumped-hydro energy storage plant was considered to level off the daily fluctuations of the wind turbines in addition to the large scale underground storage of a secondary fuel.

## Appendix 3.1

<i>Table 10 Data used for the evaluation of wind turbines and energy storage</i>			
	system	Conversion factor	Specific investment costs
<b>Primary conversion systems</b>			
$F_U \rightarrow E$	Nuclear power station (PWR)	0.32	3 600 Dfl/kW <sub>e</sub>
$F_C \rightarrow E$	Power station (pulverized coal)	0.39	1 800 Dfl/kW <sub>e</sub>
$F_C \rightarrow E$	Coal gasification CC	0.39	1 800 Dfl/kW <sub>e</sub>
$F_C \rightarrow F''_C$	Coal gasification plant (high calorific gas / SNG)	0.60	1 200 Dfl/kW <sub>th, out</sub>
$F_C \rightarrow F'_C$	Coal liquefaction plant (direct conversion)	0.63	2 000 Dfl/kW <sub>th, out</sub>
$F_C \rightarrow E$ $\rightarrow Q_{LT}$	Atmospheric fluidized bed CHP plant (back pressure turbine)	0.11	8600 Dfl/kW <sub>e</sub>
		0.74	1260 Dfl/kW <sub>th</sub>
$F_C \rightarrow E$ $\rightarrow Q_{HT}$	Atmospheric fluidized bed CHP plant (back pressure turbine)	0.11	8600 Dfl/kW <sub>e</sub>
		0.74	1260 Dfl/kW <sub>th</sub>
$E_{wind} \rightarrow E$	Wind turbines	-	2 000 Dfl/kW <sub>e</sub>
<b>Secondary conversion systems</b>			
$E \rightarrow F''_H$	Electrolysis plants	0.75	1 000 Dfl/kW <sub>e</sub>
$F''_C \rightarrow E$	Fuel cell power plants	0.55	1 000 Dfl/kW <sub>e</sub>
$F''_H \rightarrow E$	Fuel cell power plants	0.60	1 000 Dfl/kW <sub>e</sub>
$F''_C \rightarrow Q_{LT}$	Coal gas fired hot water boilers	0.90	200 Dfl/kW <sub>th</sub>
$F''_H \rightarrow Q_{LT}$	Hydrogen gas fired hot water boilers	0.90	200 Dfl/kW <sub>th</sub>
$F''_C \rightarrow Q_{HT}$	Coal gas fired steam boilers	0.90	200 Dfl/kW <sub>th</sub>
$F''_H \rightarrow Q_{HT}$	Gas fired hot water boilers	0.90	200 Dfl/kW <sub>th</sub>
<b>Storage systems</b>			
$F''_H$	Underground H <sub>2</sub> reservoir	-	30 Dfl/GJ
	H <sub>2</sub> compression	0.952	
	H <sub>2</sub> expansion	1.0	
$F''_C$	Underground coal gas reservoir	-	30 Dfl/GJ
	Coal gas compression	0.985	
	Coal gas expansion	1.0	
$E$	Pump storage (capacity)	-	11 000 Dfl/GJ
	in (Kaplan turbine/pump)	0.85	1 200 Dfl/kW <sub>e</sub>
	out (Kaplan turbine/pump)	0.89	-

The control strategies considered in this study are relatively simple. They enable the use of the program TASTE without further extensions. The use of more sophisticated strategies is not considered to be useful at this stage because of the lack of knowledge with regard to possibilities and effects.

<i>Table 11 Additional data used for the evaluation of wind turbines and energy storage</i>		
Transport and distribution systems		
Transported medium	Characteristics	Specific costs
electricity	Transport of electricity	29 MDfl/(GW <sub>e.a</sub> )
	Distribution of electricity	142 MDfl/(GW <sub>e.a</sub> )
Hydrogen	Transport of hydrogen	10.5 MDfl/(GW <sub>th.a</sub> )
	Distribution of hydrogen	18 MDfl/(GW <sub>th.a</sub> )
SNG	Transport of SNG	7 MDfl/(GW <sub>th.a</sub> )
	Distribution network	12 MDfl/(GW <sub>th.a</sub> )
Fuel prices		
Uranium		2.6 Dfl/GJ
Coal		6.0 Dfl/GJ
Economic data		
Economic lifetime		20 a
Interest		4%
Annuity factor		0.07358
Operation and maintenance costs (percentage of investment costs)		
	Default	3%/a
	Underground gas storage	1%/a

An important difference between the system evaluations presented in this section and the system evaluations reported in the previous sections is the energy demand. In the previous sections the energy demands have been determined using available data of the year 1980. In this section an attempt was made to determine demand data for the year 2040. The new values are mentioned in the Tables 12 and 13. It is assumed that the total electricity demand in 2040 will be 50% higher than in 1980; thus a yearly electricity demand of 309 PJ/a in 2040 against 206 PJ/a in 1980. Further it is assumed that the increase of electricity demand will be caused primarily by continuous processes. Therefore, the additional demand of 103 PJ/a is added completely to the base-load electricity demand. With regard to the low temperature heat demand it is assumed that the yearly demand will be decreased by 30% compared to the demand of 1980. This reduction can be achieved because of the lower heat demand of new dwellings and buildings and a better isolation of existing buildings and houses. Thus the yearly LT heat demand will be reduced from 613 PJ/a in 1980 to 439 PJ/a in 2040. The hourly fractions of the heat demand in 2040 are supposed to be the same as in 1980. For the HT heat demand only a small reduction of the total yearly demand was assumed. The expected reduction is 5% which means that the yearly HT heat demand of 409 PJ/a in 1980 was reduced to 389 PJ/a for the year 2040. Also here no serious reasons were found to change the hourly fractions. The fuel demand for transport in 2040 is supposed to be the same as in 1980 (316 PJ/a); also the hourly fractions are supposed to be the same. Because of the modification of the energy demands the calculated results for the system configurations are not exactly comparable with the results from the previous sections.

## Appendix 3.1

*Table 12 Some results of the evaluation of wind turbines and energy storage (SNG distribution)*

		Units	system				
			Ref. system	+ gas storage	1 GW <sub>e</sub> wind turb	5 GW <sub>e</sub> wind turb	10 GW <sub>e</sub> wind turb
Conversion							
$F_U \rightarrow E$	Nuclear power stations	GW <sub>e</sub>	6.8	6.8	6.1	2.1	0.0
$E_{wind} \rightarrow E$	Wind turbines	GW <sub>e</sub>	-	-	1.0	5.0	10.0
$F_C \rightarrow F''$	Coal gasification plants	GW <sub>th</sub>	67.3	24.2	24.9	30.3	32.4
$F_C \rightarrow E$	Atmospheric fluidized bed	GW <sub>e</sub>	1.3	1.3	1.3	1.3	1.3
	CHP plants	GW <sub>th</sub>	8.7	8.7	8.7	8.7	8.7
$F''_C \rightarrow E$	Fuel cell power plants	GW <sub>e</sub>	4.9	4.9	5.5	9.5	11.4
$F'' \rightarrow Q_{LT}$	Gas fired boilers	GW <sub>th</sub>	48.1	48.1	48.1	48.1	48.1
$F'' \rightarrow Q_{HT}$	Gas fired boilers	GW <sub>th</sub>	5.7	5.7	5.7	5.7	5.7
$F'' \rightarrow Q_{HT}$	Gas fired auxiliary boilers	GW <sub>th</sub>	6.1	6.1	6.8	6.8	8.5
$F_C \rightarrow F'$	Coal liquefaction plants	GW <sub>th</sub>	12.7	12.7	12.7	12.7	12.7
Transp/ distr	Electricity transport	GW <sub>e</sub>	13.0	13.0	13.0	13.0	13.0
	Electricity distribution	GW <sub>e</sub>	13.0	13.0	13.0	13.0	13.0
	Gas transport	GW <sub>th</sub>	67.3	24.2	24.9	30.3	32.4
	Gas distribution	GW <sub>th</sub>	53.4	53.4	53.4	53.4	53.4
	Coal transport	PJ/a	808	808	813	815	807
Storage	Undergr. coal gas storage	PJ	-	144	144	138	132
	Coal gas in	GW <sub>th</sub>	-	17.9	18.7	22.8	24.7
	Coal gas out	GW <sub>th</sub>	-	43.0	43.6	45.0	45.7
Emissions	CO <sub>2</sub>	Mtons/a	186	187	190	216	225
Demand (year 2040)	Electricity	PJ/a	309	309	309	309	309
	LT heat	PJ/a	429	429	429	429	429
	HT heat	PJ/a	389	389	389	389	389
	Fuel	PJ/a	316	316	316	316	316
Costs	Capital + operating costs	GDfl/a	19.6	14.3	14.4	14.9	17.2
	Fuel costs	GDfl/a	14.2	14.3	14.3	15.0	15.1
Total		GDfl/a	33.8	28.6	28.7	29.9	32.3

NB In the case of 10 GW<sub>e</sub> wind turbines a pumped-hydro energy storage plant with a capacity of 0.78 PJ is used to level off the daily fluctuations of the wind turbine power. The costs of the wind turbines + pumped storage plant are 3.69 GDfl/a.

The calculations for this evaluation are made with the final version of the computer program TASTE. An overview of the available system elements is shown in Figure 14. The following functions can be represented by these elements:

- Source: energy source (fossil, nuclear or renewable)
- Demand: energy demand (electricity, LT heat, HT heat or fuel)
- Nodsto: element that balances the actual energy flows to or from a storage element
- Forc: element that splits or combines energy flows

- Store: energy storage
- Traapp: energy transformation or conversion
- Sink: energy loss (unused energy)
- Cmprod: combined production (to kinds of energy from one)
- Transp/distr: transport and/or distribution (indicated by T respectively D)

The program will calculate the necessary power or capacity of the various elements and the total yearly costs. The final version of the program also calculates the yearly emissions to the environment based on defined specific emissions of the conversion systems. Only the calculated CO<sub>2</sub> emissions are presented in this section. The values of the other emissions are left out because they are probably not representative for the present gas cleaning technology.

*Table 13 Some results of the evaluation of wind turbines and energy storage (H<sub>2</sub> distribution)*

		Units	system					
			Ref. system	+ gas storage	1 GW <sub>e</sub> wind turb	5 GW <sub>e</sub> wind turb	10 GW <sub>e</sub> wind turb	
Conversion	$F_U \rightarrow E$	Nuclear power stations	GW <sub>e</sub>	35.4	61.7	61.5	60.5	59.1
	$F_C \rightarrow E$	Coal fired power stations	GW <sub>e</sub>	84.3	-	-	-	-
	$E_{wind} \rightarrow E$	Wind turbines	GW <sub>e</sub>	-	-	1.0	5.0	10.0
	$E \rightarrow F''_H$	Electrolysis plants	GW <sub>e</sub>	106.8	54.9	55.4	58.4	62.1
	$F''_H \rightarrow Q_{LT}$	Gas fired boilers	GW <sub>th</sub>	48.1	48.1	48.1	48.1	48.1
	$F''_H \rightarrow Q_{HT}$	Gas fired boilers	GW <sub>th</sub>	14.2	14.2	14.2	14.2	14.2
Transp/ distr	Electricity transport	GW <sub>e</sub>	13.0	13.0	13.0	13.0	13.0	
	Electricity distribution	GW <sub>e</sub>	13.0	13.0	13.0	13.0	13.0	
	Gas transport	GW <sub>th</sub>	80.1	80.1	80.1	80.1	80.1	
	Gas distribution	GW <sub>th</sub>	53.4	53.4	53.4	53.4	53.4	
Storage	Undergr. hydrogen storage	PJ	-	164	164	161	158	
	Hydrogen gas in	GW <sub>th</sub>	-	19.7	20.1	22.3	25.0	
Emissions	CO <sub>2</sub>	Mtons/a	189	0	0	0	0	
Demand (year 2040)	Electricity	PJ/a	309	309	309	309	309	
	LT heat	PJ/a	429	429	429	429	429	
	HT heat	PJ/a	389	389	389	389	389	
	Fuel	PJ/a	316	316	316	316	316	
Costs	Capital + operating costs	GDfl/a	45.2	34.3	34.5	35.2	36.1	
	Fuel costs	GDfl/a	21.7	15.8	15.8	15.5	15.2	
Total		GDfl/a	66.9	50.1	50.3	50.7	51.3	

### 3.5.2 The systems with coal gas (SNG) as the secondary fuel.

A reference system without energy storage and wind turbines was selected first. The system diagram is presented in Figure 15; in this diagram also elements representing the transport and distribution of energy are included. Uranium and coal were used as primary energy sources. It was assumed that nuclear power plants have to generate the base-load of the electricity demand;

Appendix 3.1

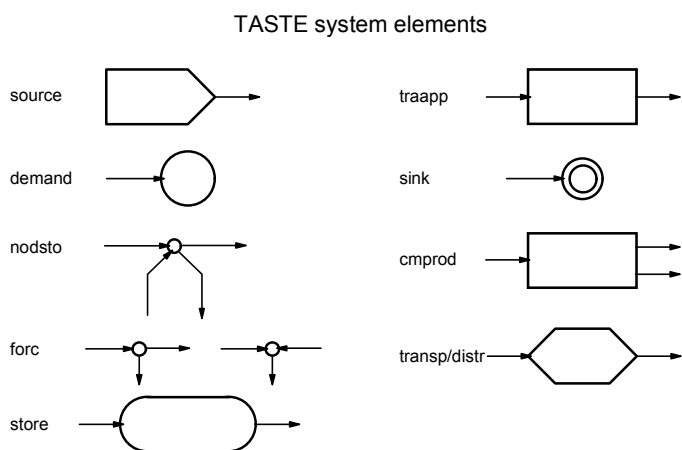


Figure 14 Overview of the TASTE system elements

it is assumed that they operate at constant power. Additional electric power is generated by coal fired industrial CHP plants and fuel cell plants operating on SNG. Coal is converted into a gaseous fuel (SNG) and liquid fuel for transport. The SNG is transported to the fuel cell power plants, the gas fired boilers and auxiliary boilers for industrial heat and the distribution network that supplies the boilers for low temperature heat. Because of the fluctuations in the demands of heat

and electricity, the generated power of coal gasification/SNG plants will not be constant. The storage capability of gas transport and distribution network is ignored in the calculations. That means that the coal gasification/SNG plants have to operate in load-following mode. The high temperature (industrial) heat demand is split; 40% of this demand is generated by gas fired industrial boilers the other 60% is generated by coal fired CHP plants based on atmospheric fluidized bed boilers. The heat from the fuel to the CHP plants is converted for 74% into heat and for 11% into electricity. The actual power of the CHP plants is controlled such that the generated electricity and heat will never exceed the actual demand. If the electrical demand does not enable the generation of sufficient heat, auxiliary gas fired boilers are available to generate the

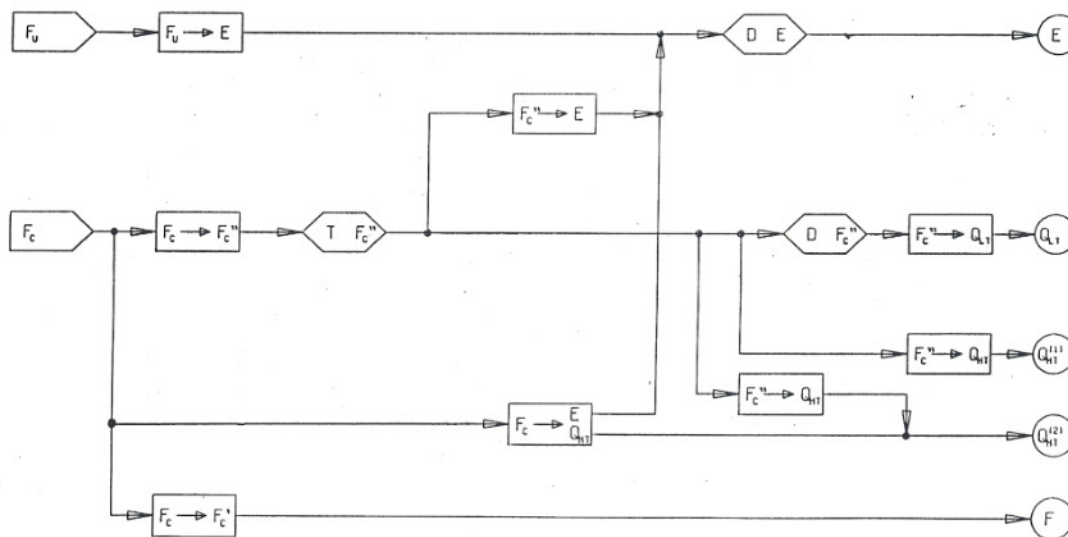


Figure 15 System diagram "Reference configuration with coal gas (SNG)"







## Appendix 3.1

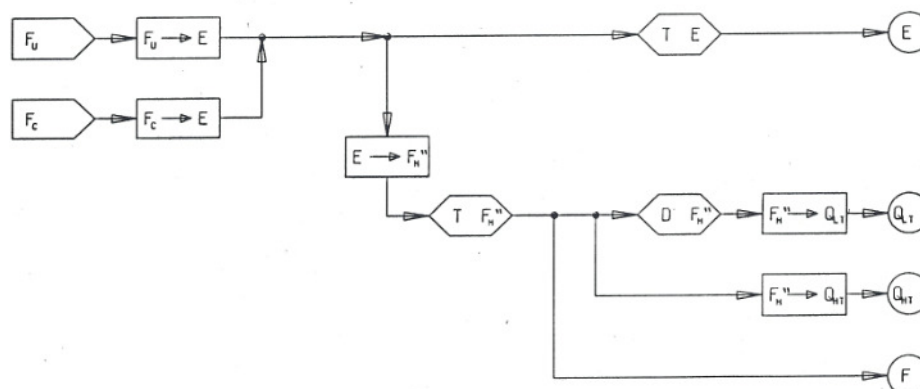


Figure 19 System diagram "Reference configuration with hydrogen gas"

### 3.5.3 The systems with hydrogen gas as the secondary fuel.

In Figure 19 a system configuration is presented that will be used as the reference system for the evaluation of the systems with hydrogen as the secondary fuel. In this case gaseous hydrogen is used for the energy demand of transport and to fuel boilers for the generation of LT heat and HT heat. In the reference system no storage of hydrogen gas is possible; the storage capacity of the transport and distribution system is ignored in the evaluations. Hydrogen is generated by electrolysis plants. Then, all primary energy must be converted first into electricity which results in very high powers of the power stations. It is assumed that the base load electricity is generated by nuclear power plants and that coal fired plants will generate the intermediate and peak loads. The results of the system calculation (see Table 13) show that the total power of the nuclear plants must be 35.4 GW<sub>e</sub> and the total power of the coal fired plants 84.3 GW<sub>e</sub>. For the generation of hydrogen the electrolysis plants must have a total power of 106.8 GW<sub>e</sub>. It appears that the total yearly costs of this system are 66.9 GDfl/a which is almost two times the costs of the reference system with SNG distribution. The conversion of primary fuels into hydrogen occurs in two steps: first the conversion into electricity and then the conversion of electricity into hydrogen. This appears to be expensive and inefficient, because in spite of the fact that compared to the reference system with SNG distribution the nuclear plants generate 5 times more power the coal consumption and also the CO<sub>2</sub> emissions of the two reference systems are almost the same.

The application of large scale hydrogen storage appears to be very useful to reduce the total yearly costs of the system. The system diagram of a system with hydrogen storage is presented in Figure 20. The results of the calculation of this system configuration are shown in the second column of Table 13. It was assumed that the storage system will be controlled such that the power stations will operate continuously at design load. As the generation of electricity occurs completely in base load, the generation can be done only by nuclear power plants. It appears that the total plant power must be 61.7 GW<sub>e</sub>. The electricity that is not needed to meet the electricity demand is converted into hydrogen by the electrolysis plants. Thus, the load factor of the

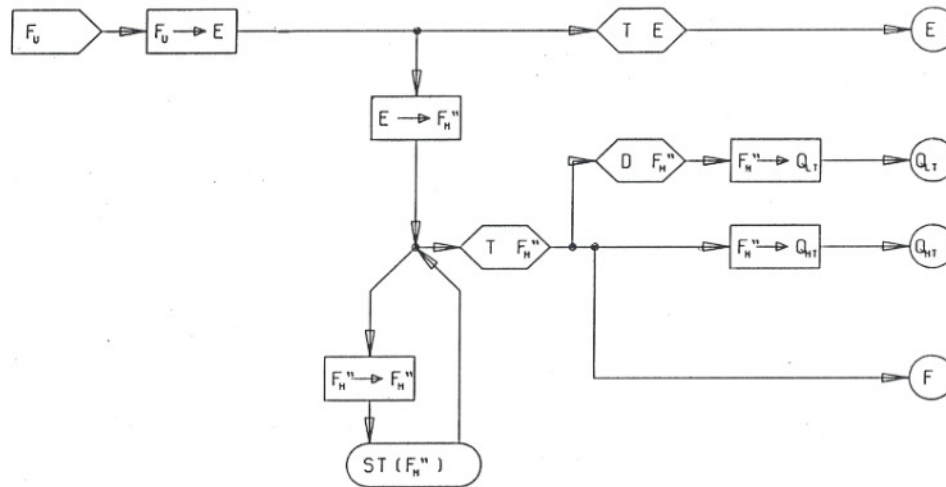


Figure 20 System diagram "Hydrogen gas with underground storage"

electrolysis plants is increased from 48% to 95%; therefore the power of the electrolysis plants can be decreased to 54.9 GW<sub>e</sub>. The generated hydrogen is used first to meet the demand of fuel, LT heat and HT heat. The difference will be extracted from or be supplied to the underground hydrogen storage. The capacity of the hydrogen storage must be 164 PJ. The total yearly costs of the system configuration with hydrogen distribution and underground hydrogen storage are 50.1 GDfl/a which is a reduction of 25% compared to the system without hydrogen storage. The system uses only uranium as the primary energy source.

The application of wind turbines is considered to reduce the consumption of other primary sources. Also in this case 3 alternative system configurations are considered with respectively 1, 5 and 10 GW<sub>e</sub> wind turbine power. All configurations are supposed to operate with large scale hydrogen storage. In the original study also configurations with additional pumped-hydro storage systems that level out the daily fluctuations of the wind turbines are considered. The results are not included in this summary because the differences in total yearly costs are 3% or less. The application of hydrogen as the secondary enables in principle the complete replacement of power stations by wind turbines. Thus the system configurations with hydrogen distribution and wind turbines are all based on the system diagram shown in Figure 21. As the nuclear power plants are operated at constant load the application of wind turbines results in higher fluctuations of the electric power that must be converted into hydrogen and thus in higher powers of the electrolysis plants as can be concluded from the data in Table 13. The load factor of the electrolysis plants decreases. The power decrease of the nuclear plants is limited of course because of the load factor of the wind turbines (approx. 25%). As the assumed load factor of the nuclear plants is 100% the application of 10 GW<sub>e</sub> will reduce the necessary power of the nuclear plants with about 2.5 GW<sub>e</sub>. Further it appears that the capacity of the hydrogen storage can be somewhat lower when using wind turbines. The application of wind turbines increases the total yearly costs of the system. The

## Appendix 3.1

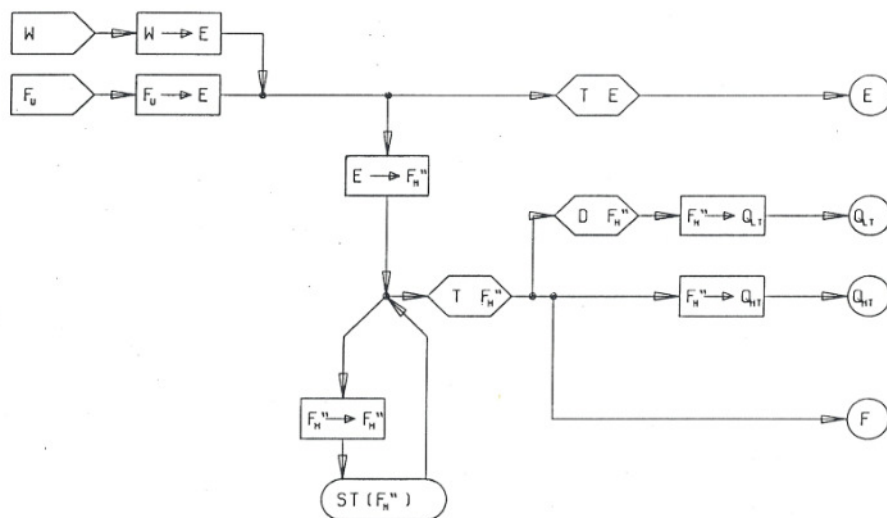


Figure 21 System diagram "Hydrogen gas with underground storage and wind turbines"

costs increase per GWe wind turbine power is distinctly lower than in the case of SNG distribution. But the level of the absolute costs of the systems with hydrogen distribution is about 60% higher.

#### 4 CONCLUSIONS

##### General

Various options for the energy supply in the future are evaluated in this study with the objective to understand what should be done to enable the application of high powers from renewable sources. The study represents a first evaluation of a variety of options; a simplified presentation of the systems appeared to be necessary to enable the possibility of quantitative results. It is obvious that apart from the considered technologies data and criteria used for this study can be questioned. And thus results cannot simply be taken for true but should be considered as an indication or warning. Nevertheless, it is believed that the study has delivered quite a number of useful results that will be helpful to find answers on various questions with regard to the development of new and coherent energy conversion technologies.

The study was based on the assumption that oil and natural gas are no longer available for large scale energy supply. From the conventional fuels coal and uranium are supposed to be abundantly available and the introduction of wind and solar energy was desired. Biomass was not considered for this study but the application is highly comparable with coal; in general plant costs will be somewhat higher and efficiencies lower. The future availability of biomass for energy conversion is still uncertain. Biomass should be used first for the generation of more valuable

products, but it is assumed that waste streams that can be used for the generation of electricity, heat and secondary fuels are always available.

The total yearly costs of the energy system are primarily used as indicator for the attractiveness of systems. Of course more criteria have to be used in the case of final decisions. But it is obvious that the total yearly costs will be highly determining.

The study confirms that the number of conversion steps necessary to convert energy from a primary source into demanded energy must be minimum. It appears that in general the use of more conversion steps results in higher costs and higher losses.

Conversion systems with high specific costs can be attractive only if they can be operated at high load factors. Therefore, energy storage systems can be useful not only for balancing the generated wind and solar energy with the energy demand but also for increasing the load factors of expensive conversion systems (e.g. gasification plants). The application of energy storage plants is beneficial only if the costs of these plants are sufficiently low.

#### Primary sources

The total yearly costs of the energy systems are primarily determined by the applied sources of primary energy. The study shows that the application of photovoltaic generators and wind turbines instead of power plants does result into significantly higher yearly costs. The higher costs are caused not only by the costs of the photovoltaic generators or the wind turbines but also by the additional costs for balancing the generated and demanded powers. Even the very optimistic assumptions regarding the capital costs of photovoltaic generators as used for this study are not able to make these generators more attractive than wind turbines. The calculated increase of the total yearly costs is roughly doubled if photovoltaic generators are used instead of wind turbines to replace conventional power plants. The difference is primarily caused by the higher yearly load factor of the wind turbines and the lower seasonal fluctuations of the wind energy. The applied data resulted in a load factor of the wind turbines of 25.3% and a load factor of the photovoltaic generators of 12.6%. During the winter time the energy demand is higher than during the summer period. But the power generation by the photovoltaic generators is highest in the summer period and lower during winter time. The power generation by the wind turbines is almost the same during the year. If the power of the photovoltaic generators or the wind turbines is higher than the electricity demand and the surplus electricity is used to generate a secondary fuel, the differences between wind and solar energy will also have consequences for systems that convert electricity into secondary fuel. This appears to be a serious disadvantage in the case of systems using hydrogen from electrolysis plants. The combination of photovoltaic generators and electrolysis plants is very expensive.

The application of solar collectors is evaluated using more realistic cost data than for the photovoltaic generators. But the used data result in a strong increase of the total yearly costs if solar collectors are used for the generation of LT heat. Also large scale heat storage appeared not to be attractive.

Balancing the generated and demanded powers requires back-up power plants or energy storage plants. The installed power of the back-up power plants is almost independent of the power of the photovoltaic generators or wind turbines. Increasing the power of the photovoltaic

### Appendix 3.1

generators or wind turbines will primarily decrease the load factor of the back-up power plants. If the powers are balanced using energy storage plants, an increase of the power of the photovoltaic generators or wind turbines will increase the power of the energy flows to and from the storage plant as well as its capacity.

The study uses fixed fluctuations of energy generation from renewable sources and the energy demands. The application of demand control can reduce the mismatch between power generation and demand. Thus demand control will reduce the needed power for back-up power plants or energy storage plants. Almost no information on the effects of demand control was available at the time the study was made. Therefore these effects are not further investigated.

#### System configurations and applied conversion technologies

Many system configurations and conversion technologies are considered in this study. The evaluated configurations and technologies are primarily determined by the chosen primary energy sources and the secondary fuel. Alternative technologies for one specific energy conversion process are in general direct competitors and it is not expected that they will cause significant differences in holistic system evaluations. The generation of LT heat, however, appears to be an exception in this respect. LT heat can be generated with very different technologies e.g. by the combustion of a secondary fuel, the application of electrical driven compression heat pumps, the use of CHP systems and the application of solar collectors. Unfortunately a comprehensive evaluation of the various technologies for the generation of LT heat was not made in this study and conclusions can be drawn only with reservation. The attractiveness of the combustion of secondary fuels depends primarily on the actual costs of the fuel. If the fuel is generated by an expensive system, as is the case with hydrogen, the actual costs of the fuel are high. Furthermore, the thermodynamic efficiency of the generation of LT heat by combustion is very poor (less than 15%). From the exploring system studies it appeared that the application of heat pumps is much more attractive than the combustion of hydrogen; but at that time the additional costs of the necessary extension of the grid for electricity transport and distribution were not included. It is not expected, however, that these additional costs will cancel out the advantages of the application of heat pumps. The application of solar collectors is primarily depending on the specific costs of the system including the required heat storage. With the used cost data, representing the costs at the time of evaluation, these collectors appeared not to be very attractive.

#### The secondary fuel and transport, distribution and storage of energy

The selection of an appropriate fuel for the transport, distribution and storage of energy will seriously affect the total yearly costs of the system. The application of hydrogen as the secondary fuel offers high flexibility with regard to the addition of power generated from renewable sources. Electricity from wind turbines and photovoltaic generators can be converted directly into hydrogen by using electrolysis plants. Serious disadvantages of hydrogen are the high costs. All hydrogen based systems appeared to be quite expensive; the high costs are primarily caused by the thermodynamic losses as well as the high capital costs of the conversion equipment of the conversion chain for the generation of hydrogen. Hydrogen will be attractive only for specific applications. Hydrogen will be used on large scale only if very cheap and efficient methods for the generation of hydrogen become available.

Systems with secondary fuels from coal have resulted in much lower total yearly costs than the hydrogen based systems. It was assumed that coal can be converted directly into gaseous or liquid hydrocarbon fuels. In comparison with hydrogen the generation of secondary fuels from coal is less expensive and more efficient. However, the introduction of wind turbine power or power from photovoltaic generators is limited by the electricity demand as electricity can not be used for the generation of the secondary fuel. If biomass has to be used instead of coal as the primary fuel the same system configuration can be used but the specific costs of the conversion processes will be higher and the conversion efficiencies will be lower. It is expected that systems with hydrocarbon fuels from biomass will be less expensive than hydrogen based systems.

The calculated total costs for transport and distribution of the considered energy carriers are in general not higher than 10 to 20% of the total yearly costs. These costs are dominated by the transport and distribution costs of electricity. It appears that the costs for transport and distribution of energy cannot be ignored, but they are also not really determining.

#### Miscellaneous

In the case of given energy demands the power of the primary conversion process (power plants or power generators using renewable energy) is determined by the efficiencies of the various processes necessary for the storage and the conversion of power into the demanded energy. The costs of the primary conversion processes are usually higher than 50% of the total yearly costs; thus they are highly determining the total yearly costs. Therefore, high efficiencies of the storage and conversion processes are very important to limit the costs of the primary conversion processes and to achieve affordable total yearly costs. The need for high efficiencies of the conversion processes is also true in the case of the application of renewable energy.

## REFERENCES

- [1] N. Woudstra, C. Heil, M. Hartman. De BB Cel. Methode van onderzoek en voorlopige resultaten. TU Delft, EV-1336, 1984.
- [2] N. Woudstra, C. Heil, M. Hartman. De BB Cel. Verkennende systeemstudies. TU Delft, EV-1346, 1985.
- [3] C. Heil, M. Hartman. De BB Cel, een systematisch onderzoek. TU Delft, EV-1418, 1986
- [4] C. Heil, M. Hartman. Selectie basisconfiguraties t.b.v. het onderzoek duurzame energie. TU Delft, EV-1419, 1986.
- [5] M. Hartman. Programmabeschrijving TASTE. TU Delft, EV-1479, 1988.
- [6] M. Hartman. Lange termijn energievoorziening, inzet van windturbines en energieopslag. TU Delft, EV-1492, 1988.
- [7] Perspectieven voor windenergie in Nederland, nationaal onderzoekprogramma windenergie 1976-1981, resultaten en aanbevelingen; BEOP-4; april 1981.
- [8] Kostenvergelijking van elektriciteit uit kolen- en kernenergiecentrales; KIVI/NIRIA; september 1982

## **APPENDIX 4.1**

### **EXERGY LOSSES OF A CONVENTIONAL POWER PLANT (A REFERENCE SYSTEM)**

#### **1 INTRODUCTION**

The conventional power plant with a fired boiler and steam cycle is often used as a basis for the comparison with newly proposed advanced energy systems. The Energy Systems group of the TU Delft has established a well defined reference system for that purpose. The system consists of a conventional coal fired boiler that transfers heat to a subcritical steam cycle. In this appendix first a description of the system design and the corresponding input data for a system calculation with Cycle-Tempo are presented. Also the results of the system calculation as well as a comprehensive presentation of the exergy losses are shown. Only the results of the design condition are discussed.

#### **2 SYSTEM DESCRIPTION AND INPUT DATA**

The system diagram as used for the evaluation of the exergy losses is presented in Figure 1. The system diagram includes all the apparatuses that are necessary for the process calculation by Cycle-Tempo. The left part of the diagram represents the boiler, the right part the steam cycle. Combustion air enters the boiler at source (101), is pressurized by the air fan (103) and heated to 250 °C by the air preheater (105). The input data are summarized in Table 1. An air recycle fan (131) is added to enable the control of the flue gas stack temperature. The preheated air is passed to the burners for the combustion of the fuel (pulverized coal). The applied fuel data are presented in Table 2. The hot flue gas is cooled first in the evaporator (221); evaporation occurs in the tubes that are cooling the furnace walls. For the purpose of the calculation it is assumed that complete combustion is achieved before the flue gas is cooled. In reality the heat transfer from the flue gas to the furnace walls will take place from the very beginning of the combustion process before complete combustion is achieved. The theoretical combustion temperature as calculated will never appear in the real boiler. However, the use of the theoretical combustion temperature simplifies the calculation and does not affect the total exergy losses of the boiler. After evaporation the steam is superheated in the first superheater (222). This superheater is placed in the top of the furnace and heated primarily by radiation. Further cooling of the flue gas occurs in so-called convection heat exchangers, respectively the final (third) superheater (225), the second reheater (205), the second superheater (224), the first reheater (203) and the economizer (219). In off-design condition cooled flue gas can be recycled to the boiler furnace by a flue gas recycle fan (151) to control the heat transfer process. After cooling in the air preheater the flue gas is passed to the stack by the forced draught fan (112). The forced draft fan keeps the furnace pressure somewhat below atmospheric pressure.

Life steam at a temperature of 530 °C and a pressure of 180 bar enters the HP steam turbine (201). The steam turbine has an extraction point to enable a high temperature of the

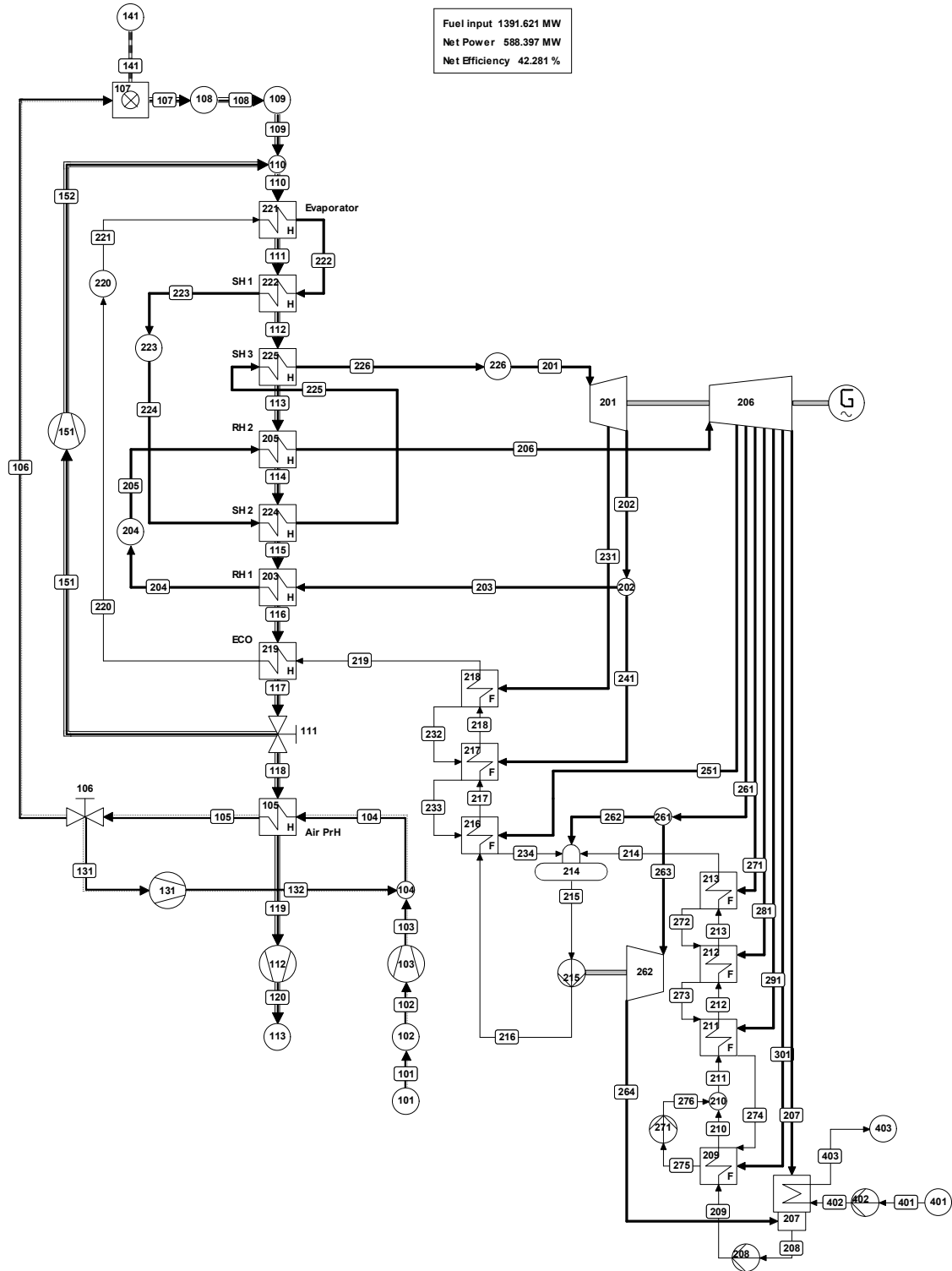


Figure 1 System diagram of the reference system

## Appendix 4.1

<i>Table 1a Input data system calculation</i>			
<b>SUBSYSTEM BOILER</b>			
Conditions at air inlet [101]	Press.	1.013	Bar
	Temp.	15	°C
Air fan [103]	Isentropic efficiency	0.87	-
	Mech. Efficiency	0.94	-
Air preheater [105]	Press. loss prim.	0.01	Bar
	Outlet temp. prim.	250	°C
	Press. loss sec.	0.01	Bar
Air recycle fan [131]	Isentropic efficiency	0.87	-
	Mech. Efficiency	0.94	-
Burner [107]	Air factor	1.16	-
	Press. loss	0.02	Bar
Evaporator [221]	Inlet press. prim.	230	Bar
	Inlet temp. prim.	310	°C
	Press. loss sec.	0.004	Bar
	Outlet temp. sec.	1100	°C
Superheater 1 [222]	Inlet press. prim.	200	Bar
	Outlet temp. prim.	435	°C
	Press. loss sec.	0.004	Bar
Superheater 3 [225]	Inlet press. prim.	192	Bar
	Press. loss sec.	0.004	Bar
Reheater 2 [205]	Inlet press. prim.	36	Bar
	Press. loss sec.	0.005	Bar
Superheater 2 [224]	Inlet press. prim.	196	Bar
	Outlet temp. prim.	480	°C
	Press. loss sec.	0.004	Bar
Reheater 1 [203]	Inlet press. prim.	37.42	Bar
	Outlet temp. prim.	415	°C
	Press. loss sec.	0.005	Bar
Economizer [219]	Outlet temp. sec.	318	°C
	Press. loss sec.	0.004	Bar
Flue gas recycle fan [151]	Isentropic efficiency	0.87	-
	Mech. Efficiency	0.94	-
Air preheater [105]	Press. loss prim.	0.01	Bar
	Outlet temp. prim.	250	°C
	Press. loss sec.	0.01	Bar
Flue gas fan [112]	Isentropic efficiency	0.90	-
	Mech. Efficiency	0.94	-
	Pressure increase	0.03	Bar
Flue gas stack [113]	Exhaust pressure	1.013	Bar

<i>Table 1b Input data system calculation (continued)</i>			
<b>SUBSYSTEM STEAM CYCLE</b>			
Turbine inlet [226]	Press.	180	Bar
	Temp.	530	°C
HP turbine [201]	TUCODE	10000	-
	GDCODE	1	-
IP and LP turbine [206]	Inlet press.	34.02	Bar
	Inlet temp.	530	°C
	TUCODE	52160	-
	GDCODE	1	-
	DIAOUT	2.3	-
	SLENG	0.85	-
Condensate pump [208]	Isentropic efficiency	0.78	-
	Mech. Efficiency	0.88	-
LP preheater 1 [209]	Press. loss prim.	0.5	Bar
	Inlet press. sec.	0.082	Bar
	Press. loss sec.	0	Bar
	$\Delta T_H$	3	K
	Outlet temp. sec.	Saturated	
Condensate pump [271]	Isentropic efficiency	0.78	-
	Mech. Efficiency	0.86	-
LP preheater 2 [211]	Inlet press. prim.	7.692	Bar
	Press. loss prim.	0.5	Bar
	Inlet press. sec.	0.236	Bar
	Press. loss sec.	0	Bar
	$\Delta T_H$	3	K
	$\Delta T_L$	5	K
LP preheater 3 [212]	Press. loss prim.	0.5	Bar
	Inlet press. sec.	0.676	Bar
	Press. loss sec.	0	Bar
	$\Delta T_L$	5	K
LP preheater 4 [213]	Press. loss prim.	0.5	Bar
	Inlet press. sec.	1.895	Bar
	Press. loss sec.	0	Bar
	$\Delta T_H$	3	K
	$\Delta T_L$	5	K
Deaerator [214]	Inlet press.	5.192	Bar
	Press. loss	0	Bar
Boiler feedwater pump [215]	Outlet press.	244.2	Bar
	Isentropic efficiency	0.83	-
BFWP turbine [262]	GDCODE	1	-
	Isentropic efficiency	0.80	-
	Mech. Efficiency	0.98	-

SUBSYSTEM STEAM CYCLE (continued)			
HP preheater 6 [216]	Press. loss prim.	1.0	Bar
	Inlet press. sec.	13.919	Bar
	Press. loss sec.	0	Bar
	$\Delta T_H$	0	K
	$\Delta T_L$	7	K
HP preheater 7 [217]	Press. loss prim.	1.0	Bar
	Press. loss sec.	0	Bar
	$\Delta T_H$	0	K
	$\Delta T_L$	7	K
HP preheater 8 [218]	Press. loss prim.	1.0	Bar
	Inlet press. sec.	71.472	Bar
	Press. loss sec.	0	Bar
	$\Delta T_H$	0	K
	$\Delta T_L$	7	K

boiler feedwater. The extraction steam is used to heat the last HP feedwater heater (218); the steam enters the feedwater heater at a pressure of 71.472 bar. The exhaust steam flow from the HP steam turbine is passed to the first reheater (203); a small flow is split off and goes to the second HP feedwater heater (217). The steam pressure is determined by the IP inlet pressure. In the two reheaters (203) and (205) the steam is reheated to 530 °C and enters the IP turbine at a pressure of 34.02 bar. The turbine efficiencies are calculated by Cycle-Tempo using the method described in [4.2]. The method combines the calculation of the IP turbine and the LP turbine; therefore these two turbine stages are presented in the system flow diagram as one turbine (206). The number of parallel turbine houses is defined by the input data of the turbine (TUCODE) together with some geometric data of the LP exhaust. The IP

Composition	
Species	Mass fraction
C	70.48
Cl	0.33
F	0.02
H <sub>2</sub>	4.98
H <sub>2</sub> O	11.77
N <sub>2</sub>	1.35
O <sub>2</sub>	9.48
S	1.59
<i>LHV</i>	28.953 MJ/kg

and LP steam turbine have a number of extraction points that deliver steam to respectively the first HP feedwater heater (216), the deaerator (214) and the boiler feedwater pump (BFWP) turbine (262), and the LP feedwater heaters (213), (212), (211) and (209). The turbine exhaust is connected with the main condenser (207) that operates at a design pressure of 0.027 bar. The cooling water has a temperature of 12 °C at the system inlet (source 401) and leaves the condenser at a temperature of 19.36 °C, assuming a temperature difference of 3 K between the condensing temperature and the cooling water outlet temperature. The condensate leaves the condenser at saturation temperature (22.36 °C). The condensate pump (208) pumps the condensate to the deaerator via the LP feedwater heaters. The first feedwater heater (209) gets saturated steam

*Table 3 System data (from Cycle-Tempo calculation)*

	No.	Apparatus	Type	Energy	Totals	Exergy	Totals
				[kW]	[kW]	[kW]	[kW]
<b>Absorbed power</b>	141	Fuel source	10	1391623		1474191	
					1391623		1474191
<b>Delivered gross power</b>	1	Generator	G	600000		600000	
	262	BFWP turbine	3	16245		16245	
	215	BFW pump	8	-16245		-16245	
					600000		600000
<b>Aux. power consumption</b>	208	Cond.pump	8	374		374	
	131	Air recirc.	29	0		0	
	112	Flue gas fan	29	2338		2338	
	151	Flue gas rec	29	0		0	
	103	Air fan	29	2211		2211	
	271	Add.cond. pu	8	65		65	
	402	CW-pump	8	1815		1815	
		Coal Mills		4800		4800	
					11603		11603
<b>Delivered net power</b>					588397		588397
<b>Efficiencies</b>	gross			43.12%		40.70%	
	net			42.28%		39.91%	

from the last extraction point of the LP turbine and cooled condensate from the second feedwater heater (211) to heat the feedwater. As the condensate from second feedwater heater enters the first feedwater heater it will flash because of the pressure difference between these heaters. A mixture of condensate with some steam will enter the first feedwater heater. The mixture is condensed and pumped into the main feedwater line by the condensate pump (271). The feedwater is heated to a temperature 3 K below the saturation temperature in the feedwater heater. The second feedwater heater (211) also receives saturated extraction steam from the LP turbine and cooled condensate from the third feedwater heater. The mixture is condensed and cooled in a feedwater heater with after-cooler. The condensate leaves the feedwater heater at a temperature 5 K higher than the feedwater inlet temperature. The feedwater leaves the feedwater heater at a temperature 3 K below the saturation temperature of the condensate. The third and fourth feedwater heaters receive slightly superheated steam from the steam turbine; the temperature differences at the hot and the cold side are the same as for the second feedwater heater. The condensate is passed to the previous feedwater heater. The deaerator is the fifth feedwater heater. In the deaerator (214) the feedwater is mixed with extraction steam and the condensate from the HP feedwater heaters. The mixture leaves the deaerator at saturation temperature and is pumped to the boiler via the HP feedwater heaters by the boiler feedwater pump (BFWP) (215). The outlet pressure of the feedwater pump is 244.2 bar. The feedwater is heated further in the three HP feedwater heaters (216, 217 and 218). All feedwater heaters are equipped with a desuperheater and a condensate cooler. Because of the desuperheater it is assumed that the temperature difference at the hot side of

## Appendix 4.1

the feedwater heater is 0 K. That means that the feedwater temperature at the outlet of de desuperheater equals the condensation temperature in the feedwater heater. The temperature difference at the cold side is 7 K; thus the temperature of the condensate that leaves the condensate cooler of the feedwater heater is 7 K higher than the temperature of the feedwater that enters the heater. The sixth feedwater heater (216) receives steam from the IP steam turbine and condensate from heater (217). The condensate from the heater goes to the deaerator. Feedwater heater (217) receives steam from the HP turbine outlet and the condensate from the last feedwater heater (218). Feedwater heater (218) is connected with the extraction point at the HP turbine; the pressure of the extraction steam (design pressure is 71.472 bar) determines the feedwater temperature at the boiler inlet.

### 3 RESULTS OF THE SYSTEM CALCULATION

The results of a system calculation with Cycle-Tempo are presented in a number of tables containing all useful data. For a quick overview of the results also some diagrams can be drawn by the program. Overall system data as presented by Cycle-Tempo are shown in Table 3. The table gives an overview of the powers transferred to and from the system; energy values as well as exergy values of the powers are given. The absorbed power is the power transferred to the system, in this case the power of the fuel (1391.62 MW). The fuel exergy calculated by Cycle-Tempo (1474.19 MW) is somewhat higher. Cycle-Tempo uses the method of Baehr-II (see Appendix 2.3). The gross electrical power generated by the system is 600 MW. The power of the BFWP turbine is absorbed directly by the BFW pump and does not contribute to the total generated power. The auxiliary powers for pumps and fans are listed as electrical powers. With exception of the power needed to drive the coal mills all auxiliary powers are calculated by the program. The power for the coal mills is estimated and added to the system calculation. The calculated auxiliary power (11.60 MW) includes the power of all the equipment necessary to operate the plant. In general the total auxiliary power of a power plant will be somewhat higher because of e.g. facilities for coal transport at the plant area and lighting of the buildings. The generated net electrical power then becomes 588.40 MW. The net thermal efficiency is 42.28% and the net exergy efficiency is 39.91%.

The overview of all pipe data, as presented in Table 4, is useful in the case of a more detailed analysis of the system results. The table gives an overview of all relevant parameters of the fluid flows between the various apparatuses. The pipe numbers refer to the numbers in the system diagram of Figure 1. The flows are presented as mass flows, molar flows as well as volume flows. The compositions of the fluids (medium) as calculated by Cycle-Tempo are presented in a separate table which is not included in this appendix. For each fluid flow the pressure, temperature, specific enthalpy, specific entropy and specific exergy are presented. For water/steam also the steam quality (= the steam fraction of the water/steam mixture) is given.

The table with an overview of the calculated exergy values facilitates the exergy analysis of the system. The calculated exergy values for the apparatuses shown in the system diagram (Figure 1) are presented in the Tables 5a, 5b and 5c for respectively the boiler, the steam cycle and the cooling water system. The numbers do correspond with the apparatus

*Table 4a Pipe data (from Cycle-Tempo calculation)*

Pipe no.	Medium (fluid)	Mass flow	Mole flow	Volume flow	Press.	Temp.	Enthalpy	Entropy	Exergy
		[kg/s]	[kmol/s]	[m <sup>3</sup> /s]	[bar]	[°C]	[kJ/kg]	[kJ/kg.K]	[kJ/kg]
101	GASMIX 1	531.585	18.423	435.71	1.013	15	-98.84	6.8653	0.14
				435.71	1.013	15	-98.84	6.8653	0.14
102	GASMIX 1	531.585	18.423	458.39	1.013	30	-83.69	6.9165	0.52
				458.39	1.013	30	-83.69	6.9165	0.52
103	GASMIX 1	531.585	18.423	446.61	1.053	33.87	-79.78	6.9182	3.96
				446.61	1.053	33.87	-79.78	6.9182	3.96
104	GASMIX 1	531.585	18.423	446.61	1.053	33.87	-79.78	6.9182	3.96
				446.61	1.053	33.87	-79.78	6.9182	3.96
105	GASMIX 1	531.585	18.423	768.31	1.043	250	141.23	7.4652	67.33
				768.31	1.043	250	141.23	7.4652	67.33
106	GASMIX 1	531.585	18.423	768.31	1.043	250	141.23	7.4652	67.33
				768.31	1.043	250	141.23	7.4652	67.33
107	GASMIX 2	579.65	19.501	3748.3	1.023	2091.94	-22.49	9.2662	1974.96
				3748.3	1.023	2091.94	-22.49	9.2662	1974.96
108	GASMIX 2	579.65	19.501	3726.3	1.023	2078.04	-41.9	9.2579	1957.92
				3726.3	1.023	2078.04	-41.9	9.2579	1957.92
109	GASMIX 2	579.65	19.501	3704.8	1.023	2064.49	-60.82	9.2499	1941.33
				3704.8	1.023	2064.49	-60.82	9.2499	1941.33
110	GASMIX 2	579.65	19.501	3704.8	1.023	2064.49	-60.82	9.2499	1941.33
				3704.8	1.023	2064.49	-60.82	9.2499	1941.33
111	GASMIX 2	579.65	19.501	2184.8	1.019	1100	-1368.57	8.5318	840.49
				2184.8	1.019	1100	-1368.57	8.5318	840.49
112	GASMIX 2	579.65	19.501	2011.5	1.015	986.11	-1515.59	8.4212	725.35
				2011.5	1.015	986.11	-1515.59	8.4212	725.35
113	GASMIX 2	579.65	19.501	1825.5	1.011	865.21	-1669.16	8.2941	608.4
				1825.5	1.011	865.21	-1669.16	8.2941	608.4
114	GASMIX 2	579.65	19.501	1589.4	1.006	713.06	-1858.25	8.1172	470.28
				1589.4	1.006	713.06	-1858.25	8.1172	470.28
115	GASMIX 2	579.65	19.501	1385.4	1.002	583.06	-2015.47	7.9474	361.98
				1385.4	1.002	583.06	-2015.47	7.9474	361.98
116	GASMIX 2	579.65	19.501	1115.5	0.997	412.84	-2214.11	7.6904	237.41
				1115.5	0.997	412.84	-2214.11	7.6904	237.41
117	GASMIX 2	579.65	19.501	965.17	0.993	318	-2320.95	7.5239	178.53
				965.17	0.993	318	-2320.95	7.5239	178.53
118	GASMIX 2	579.65	19.501	965.17	0.993	318	-2320.95	7.5239	178.53
				965.17	0.993	318	-2320.95	7.5239	178.53
119	GASMIX 2	579.65	19.501	666.63	0.983	131.06	-2523.63	7.1153	93.61
				666.63	0.983	131.06	-2523.63	7.1153	93.61

## Appendix 4.1

*Table 4b Pipe data (from Cycle-Tempo calculation)*

Pipe no.	Medium (fluid)	Mass flow	Mole flow	Volume flow	Press.	Temp.	Enthalpy	Entropy	Exergy
		[kg/s]	[kmol/s]	[m <sup>3</sup> /s]	[bar]	[°C]	[kJ/kg]	[kJ/kg.K]	[kJ/kg]
120	GASMIX 2	579.65	19.501	652.62	1.013	134.64	-2519.84	7.1162	97.13
				652.62	1.013	134.64	-2519.84	7.1162	97.13
131	GASMIX 1	0	0	0	1.043	250	141.23	7.4652	67.33
				0	1.043	250	141.23	7.4652	67.33
132	GASMIX 1	0	0	0	1.053	251.59	142.88	7.4656	68.87
				0	1.053	251.59	142.88	7.4656	68.87
141	FUEL 3	48.065	4.514	0.024516	1.043	30	-1833.2	2.0342	30670.84
				0.024516	1.043	30	-1833.2	2.0342	30670.84
151	GASMIX 2	0	0	0	0.993	318	-2320.95	7.5239	178.53
				0	0.993	318	-2320.95	7.5239	178.53
152	GASMIX 2	0	0	0	1.023	323.1	-2315.27	7.5252	183.85
				0	1.023	323.1	-2315.27	7.5252	183.85
201	WATERSTM	518.624	28.788	9.3035	180	530	3359	6.3366	1534.69
				9.5921	174.6	527.76	3359	6.3489	1531.15
202	WATERSTM	466.89	25.916	29.937	37.42	303.86	2981.56	6.4257	1131.59
				29.937	37.42	303.86	2981.56	6.4257	1131.59
203	WATERSTM	418.028	23.204	26.804	37.42	303.86	2981.56	6.4257	1131.59
				26.804	37.42	303.86	2981.56	6.4257	1131.59
204	WATERSTM	418.028	23.204	35.204	36	415	3257	6.8801	1276.09
				35.204	36	415	3257	6.8801	1276.09
205	WATERSTM	418.028	23.204	35.204	36	415	3257	6.8801	1276.09
				35.204	36	415	3257	6.8801	1276.09
206	WATERSTM	418.028	23.204	44.477	34.02	530	3519.19	7.2578	1429.46
				44.477	34.02	530	3519.19	7.2578	1429.46
207	WATERSTM	289.725	16.082	13282	0.027	22.36	2318.91	7.8598	55.71
				13282	0.027	22.36	2318.91	7.8598	55.71
208	WATERSTM	313.55	17.405	0.31425	0.027	22.36	93.71	0.3298	0.29
				0.31425	0.027	22.36	93.71	0.3298	0.29
209	WATERSTM	313.55	17.405	0.31414	8.192	22.42	94.76	0.3305	1.11
				0.31414	8.192	22.42	94.76	0.3305	1.11
210	WATERSTM	313.55	17.405	0.31577	7.692	39	163.96	0.5585	4.63
				0.31577	7.692	39	163.96	0.5585	4.63
211	WATERSTM	369.958	20.536	0.37265	7.692	39.47	165.92	0.5648	4.78
				0.37265	7.692	39.47	165.92	0.5648	4.78
212	WATERSTM	369.958	20.536	0.37632	7.192	60.71	254.64	0.8395	14.34
				0.37632	7.192	60.71	254.64	0.8395	14.34
213	WATERSTM	369.958	20.536	0.38218	6.692	86.04	360.78	1.1461	32.14
				0.38218	6.692	86.04	360.78	1.1461	32.14

*Table 4c Pipe data (from Cycle-Tempo calculation)*

Pipe no.	Medium (fluid)	Mass flow	Mole flow	Volume flow	Press.	Temp.	Enthalpy	Entropy	Exergy
		[kg/s]	[kmol/s]	[m <sup>3</sup> /s]					
214	WATERSTM	369.958	20.536	0.39082	6.192	115.53	485.08	1.4788	60.57
				0.39085	5.192	115.55	485.08	1.4791	60.49
215	WATERSTM	518.624	28.788	0.5676	5.192	153.27	646.28	1.8748	107.65
				0.5676	5.192	153.27	646.28	1.8748	107.65
216	WATERSTM	518.624	28.788	0.56146	244.2	157.13	677.6	1.8872	135.41
				0.56146	244.2	157.13	677.6	1.8872	135.41
217	WATERSTM	518.624	28.788	0.58486	243.2	194.77	839.6	2.2483	193.35
				0.58486	243.2	194.77	839.6	2.2483	193.35
218	WATERSTM	518.624	28.788	0.62653	242.2	244.64	1062.56	2.7011	285.84
				0.62653	242.2	244.64	1062.56	2.7011	285.84
219	WATERSTM	518.624	28.788	0.67841	241.2	287.2	1266.26	3.0792	380.59
				0.67841	241.2	287.2	1266.26	3.0792	380.59
220	WATERSTM	518.624	28.788	0.71978	230	310	1385.68	3.2907	439.07
				0.71978	230	310	1385.68	3.2907	439.07
221	WATERSTM	518.624	28.788	0.71978	230	310	1385.68	3.2907	439.07
				0.71978	230	310	1385.68	3.2907	439.07
222	WATERSTM	518.624	28.788	5.3112	200	404.29	2847.31	5.5983	1235.77
				5.3112	200	404.29	2847.31	5.5983	1235.77
223	WATERSTM	518.624	28.788	6.402	196	435	3011.63	5.8423	1329.76
				6.402	196	435	3011.63	5.8423	1329.76
224	WATERSTM	518.624	28.788	6.402	196	435	3011.63	5.8423	1329.76
				6.402	196	435	3011.63	5.8423	1329.76
225	WATERSTM	518.624	28.788	7.6409	192	480	3187.36	6.0906	1433.94
				7.6409	192	480	3187.36	6.0906	1433.94
226	WATERSTM	518.624	28.788	8.9307	187.5	533.07	3359	6.3203	1539.41
				9.3035	180	530	3359	6.3366	1534.69
231	WATERSTM	51.735	2.872	1.9196	73.68	393.28	3135.75	6.3943	1294.82
				1.9797	71.47	391.63	3135.75	6.4069	1291.21
232	WATERSTM	51.735	2.872	0.06464	71.47	251.64	1093.68	2.801	288.17
				0.11809	36.3	244.64	1093.68	2.8098	285.63
233	WATERSTM	100.596	5.584	0.1164	36.3	201.77	861.17	2.3442	187.3
				0.34847	13.92	194.77	861.17	2.3501	185.57
234	WATERSTM	126.517	7.023	0.14001	13.92	164.13	693.88	1.9828	124.13
				1.171	5.192	153.27	693.88	1.9864	123.09
241	WATERSTM	48.862	2.712	3.133	37.42	303.86	2981.56	6.4257	1131.59
				3.2308	36.3	302.52	2981.56	6.4384	1127.93

## Appendix 4.1

*Table 4d Pipe data (from Cycle-Tempo calculation)*

Pipe no.	Medium (fluid)	Mass flow	Mole flow	Volume flow	Press.	Temp.	Enthalpy	Entropy	Exergy
		[kg/s]	[kmol/s]	[m <sup>3</sup> /s]					
251	WATERSTM	25.921	1.439	5.6185	14.35	413.15	3285.88	7.3341	1174.16
				5.7928	13.92	412.86	3285.88	7.3479	1170.18
261	WATERSTM	45.974	2.552	21.13	5.694	301.82	3066.82	7.4057	934.45
				21.785	5.523	301.62	3066.82	7.4196	930.45
262	WATERSTM	22.149	1.229	10.495	5.523	301.62	3066.82	7.4196	930.45
				11.166	5.192	301.23	3066.82	7.4478	922.33
263	WATERSTM	23.826	1.323	11.29	5.523	301.62	3066.82	7.4196	930.45
				12.011	5.192	301.23	3066.82	7.4478	922.33
264	WATERSTM	23.826	1.323	1117.8	0.027	22.36	2371.09	8.0364	57.01
				1117.8	0.027	22.36	2371.09	8.0364	57.01
271	WATERSTM	18.622	1.034	20.158	1.954	190.26	2851.03	7.4763	698.33
				20.781	1.895	190.11	2851.03	7.4902	694.32
272	WATERSTM	18.622	1.034	0.019308	1.895	91.04	381.42	1.2045	35.94
				0.18848	0.676	89.04	381.42	1.2049	35.82
273	WATERSTM	34.134	1.895	0.034827	0.676	65.71	275.03	0.9021	16.69
				0.83488	0.236	63.71	275.03	0.9023	16.63
274	WATERSTM	46.846	2.6	0.047298	0.236	44.47	186.16	0.6314	5.82
				3.6112	0.082	42	186.16	0.6316	5.77
275	WATERSTM	56.408	3.131	0.056894	0.082	42	175.83	0.5988	4.89
				0.056894	0.082	42	175.83	0.5988	4.89
276	WATERSTM	56.408	3.131	0.056877	7.692	42.08	176.81	0.5995	5.67
				0.056877	7.692	42.08	176.81	0.5995	5.67
281	WATERSTM	15.512	0.861	37.843	0.6969	99.25	2678.57	7.5327	509.61
				39.012	0.676	99.11	2678.57	7.5466	505.61
291	WATERSTM	12.712	0.706	77.884	0.2433	64.39	2529.48	7.5815	346.47
				80.186	0.236	63.71	2529.48	7.595	342.59
301	WATERSTM	9.562	0.531	151.72	0.08454	42.58	2394.45	7.6257	198.71
				156.22	0.082	42	2394.45	7.6386	194.98
401	WATERSTM	22745.221	1262.557	22.754	1.013	12	50.47	0.1805	0.07
				22.754	1.013	12	50.47	0.1805	0.07
402	WATERSTM	22745.221	1262.557	22.754	1.613	12	50.55	0.1805	0.13
				22.754	1.613	12	50.55	0.1805	0.13
403	WATERSTM	22745.221	1262.557	22.78	1.013	19.36	81.28	0.2871	0.14
				22.78	1.013	19.36	81.28	0.2871	0.14

numbers in the system diagram. The type number is only for identification in Cycle-Tempo. The exergy transferred from the system is presented as the total exergy transfer, the exergy transfer into power and heat and the exergy loss in the considered apparatus. E.g. in the case

<b>BOILER</b>								
No.	Name	Type	Exergy transferred. from system [kW]			Relative Ex. Loss	Exergy eff.	Subsystem
			Total	Power/Heat	Losses	[%]	[%]	Total [kW]
107	Burner	13	365197	0	365197	24.75	74.56	<b>384690</b>
108	Radiation loss	10	9877	0	9877	0.67		
109	Unburned loss	10	9616	0	9616	0.65		
101	Air source	10	-75	0	-75	-0.01		<b>312241</b>
102	Heat recovery	10	-203	0	-203	-0.01		
103	Air fan	29	-1825	-2211	386	0.03	82.52	
104	Mixer	9	0	0	0	0.00		
105	Air preheater	6	15536	0	15536	1.05	68.44	
106	Valve	14	0	0	0	0.00		
141	Fuel source	10	-1474191	-1474191	0	0.00		
110	Mixer	9	0	0	0	0.00		
111	Valve	14	0	0	0	0.00		
112	Flue gas fan	29	-2042	-2338	296	0.02	87.35	
131	Air recirc.	29	0	0	0	0.00		
151	Flue gas recirc.	29	0	0	0	0.00		
219	ECO	6	3800	0	3800	0.26	88.87	
220	Dummy	10	0	0	0	0.00		
221	Evaporator	12	224920	0	224920	15.24	64.75	
222	Superheater 1	6	17992	0	17992	1.22	73.04	
223	Dummy	10	0	0	0	0.00		
224	Superheater 2	6	8748	0	8748	0.59	86.07	
225	Superheater 3	6	13090	0	13090	0.89	80.69	
203	Reheater 1	6	11800	0	11800	0.80	83.66	
204	Dummy	10	0	0	0	0.00		
205	Reheater 2	6	15951	0	15951	1.08	80.08	
141	Pipe		0		0	0.00		
113	Stack	10	56301	0	56301	3.82		
<b>TOTAL EXERGY LOSS BOILER</b>					<b>753232</b>	<b>51.05</b>		

of the air fan (103) the electrical power transferred to the fan is 2.221 MW and gets an minus sign because it not transferred from the system. The calculated exergy loss is 0.386 MW, thus the total exergy transferred from the system is -1.825 MW. The relative exergy loss is defined as the fraction of the fuel exergy lost in the considered apparatus. The exergy efficiencies of the apparatuses are defined in Appendix 2.2. The total exergy loss of the boiler is 753.31 MW, which is 51.06% of the fuel exergy. The exergy loss of the boiler consists primarily of the combustion loss, the heat transfer losses and the stack loss as discussed in Chapter 2; these losses are determined separately in Table 5a. The combustion losses include the exergy losses of the burner (107), the radiation loss (108) and the unburned loss (109); the last two contributions are based on estimated input data. Then, the combustion loss is 384.69 MW which is roughly 50% of the total exergy loss of the boiler. The exergy lost by the discharge

## Appendix 4.1

<i>Table 5b Calculated exergy values steam cycle</i>							
<b>STEAM CYCLE</b>							
No.	Name	Type	Exergy transferred from system [kW]			Relative Ex. Loss	Exergy eff.
			Total	Power/Heat	Losses	[%]	[%]
226	Turbine inlet	10	0	0	0	0.00	
201	HP Turbine	3	198781	187769	11012	0.75	94.46
202	Splitter	9	0	0	0	0.00	
206	MP+LP Turb.	3	480803	423414	57389	3.89	88.06
208	Cond.pump	8	-258	-374	115	0.01	69.12
209	LP-preheater	5	757	0	757	0.05	59.28
271	Add.cond. pu	8	-44	-65	20	0.00	68.70
210	Mixer	9	3	0	3	0.00	
211	LP preheater	5	1114	0	1114	0.08	76.05
212	LP-preheater	5	1355	0	1355	0.09	82.93
213	L.P.-preheat	5	1741	0	1741	0.12	85.80
214	Deaerator	7	2549	0	2549	0.17	87.26
215	BFW pump	8	-14392	-16245	1852	0.13	88.60
261	Splitter	9	0	0	0	0.00	
262	BFWP turbine	3	20617	16245	4372	0.30	78.79
216	HP preheater	5	3244	0	3244	0.22	90.26
217	HP preheater	5	3082	0	3082	0.21	93.96
218	HP preheater	5	2750	0	2750	0.19	94.70
201	Pipe		1833		1833	0.12	
214	Pipe		29		29	0.00	
216	Pipe		0		0	0.00	
217	Pipe		0		0	0.00	
226	Pipe		2448		2448	0.17	
231	Pipe		187		187	0.01	
232	Pipe		132		132	0.01	
233	Pipe		173		173	0.01	
234	Pipe		132		132	0.01	
241	Pipe		179		179	0.01	
251	Pipe		103		103	0.01	
261	Pipe		184		184	0.01	
262	Pipe		180		180	0.01	
263	Pipe		194		194	0.01	
271	Pipe		75		75	0.01	
272	Pipe		2		2	0.00	
273	Pipe		2		2	0.00	
274	Pipe		2		2	0.00	
281	Pipe		62		62	0.00	
291	Pipe		49		49	0.00	
301	Pipe		36		36	0.00	
<b>TOTAL EXERGY LOSS STEAM CYCLE</b>					<b>97356</b>	<b>6.60</b>	

<i>Table 5c Calculated exergy values cooling water system</i>							
<b>COOLING WATER SYSTEM</b>							
No.	Name	Type	Exergy transferred from system [kW]			Relative Ex. Loss	Exergy eff.
			Total	Power/Heat	Losses	[%]	[%]
207	Condenser	4	17160	0	17160	1.16	1.42
401	CW-source	10	-1498	0	-1498	-0.10	
402	CW-pump	8	-1362	-1815	454	0.03	75.00
403	CW-sink	10	3107	0	3107	0.21	
<b>TOTAL EXERGY LOSS COOLING WATER SYSTEM</b>					<b>19223</b>	<b>1.30</b>	

of hot flue gas to the stack (113) is 56.301 MW. The remaining losses (312.24 MW) are primarily exergy losses due to heat transfer from the flue gas to water/steam and combustion air. Cycle-Tempo facilitates the drawing of  $T, Q$ -diagrams and value diagrams of heat exchangers and combinations of heat exchangers that can be useful for a further evaluation of the processes in the boiler. Figure 2 presents the  $T, Q$ -diagram of the boiler. The flue gas temperature curve starts at the adiabatic combustion temperature (2064°C) and ends at the environmental temperature (15°C) and includes the cooling of the flue gas that occurs in the environment after leaving the stack. The curve is almost straight from the adiabatic combustion temperature till the point at which condensation of the available water vapor in the flue gas starts. Then, the heat transferred per degree temperature change increases significantly. Not all water vapor of the flue gas is condensed at environmental temperature; therefore the heat transferred from the flue gas is higher than the  $LHV$  of the fuel, but still somewhat lower than the  $HHV$ . The evaporator and the first superheater are located in the furnace of the boiler. The temperature difference between the primary and secondary fluid in the furnace is very high, even in the case of the actual process as heat transfer starts before combustion is completed. The evaporator is a once-through system with changing internal pressure; it is assumed that sub-cooled water enters the evaporator at supercritical pressure and that slightly superheated steam at subcritical pressure leaves the evaporator. Therefore, the temperature curve of the steam in the evaporator is not a straight line. The value diagram of the boiler is presented in Figure 3. The horizontal axis has the same dimensions as the  $T, Q$ -diagram in Figure 2, but at the vertical axis the term  $1 - (T_0 / T)$  is depicted instead of  $T$ . The shaded area in this diagram represents the exergy loss due to heat transfer in the respective heat exchanging sections of the boiler. Obviously the furnace and the superheaters 1 and 3 are primarily determining the exergy loss due to heat transfer. If the length of the horizontal axis should be the exergy of the fuel, then the area above the flue gas temperature curve should equal the exergy loss of combustion. However the length of the horizontal axis equals the heat transferred from the flue gas if cooled down from the adiabatic combustion temperature till environmental temperature and this amount of heat is not exactly the same as the fuel exergy.

The process of the steam cycle is depicted in the  $T, s$ -diagram of Figure 4. Feedwater enters the boiler at a pressure of 241.1 bar. The steam at the HP turbine inlet has a temperature of 530°C and a pressure of 180 bar. The large pressure difference is necessary to overcome the flow resistances of the boiler. In the HP turbine the steam is expanded to a pressure of 37.42 bar. During expansion steam is extracted at a pressure of 73.68 bar. The

Appendix 4.1

temperature curve of the extracted steam is also depicted in Figure 4. Some steam from the 7<sup>th</sup> feedwater heater, the main stream is returned to the

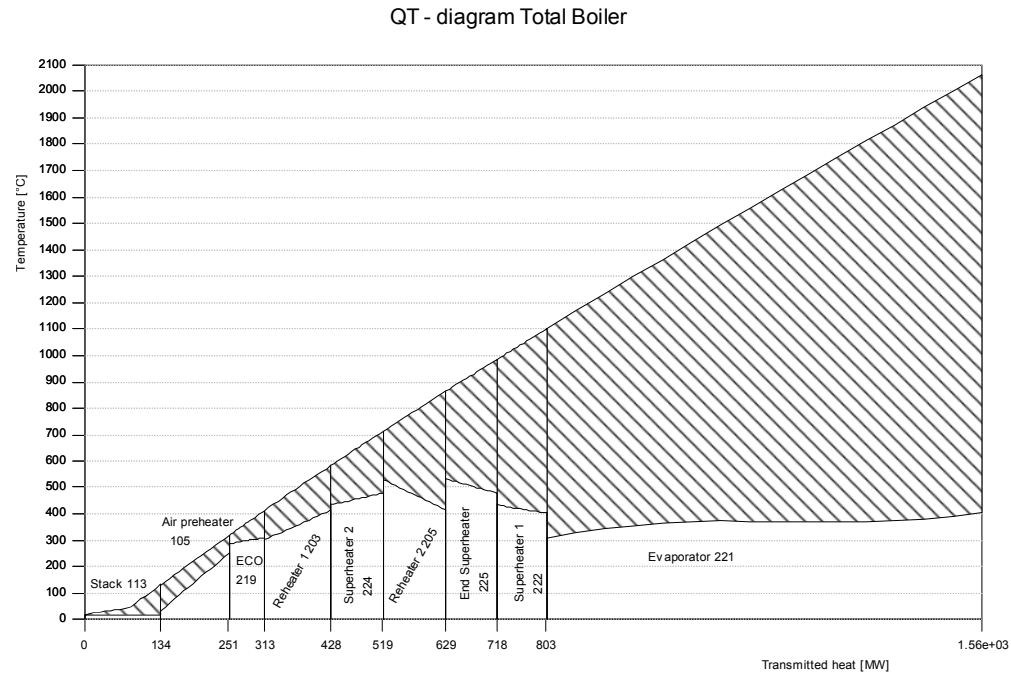


Figure 2 T,Q-diagram of the boiler

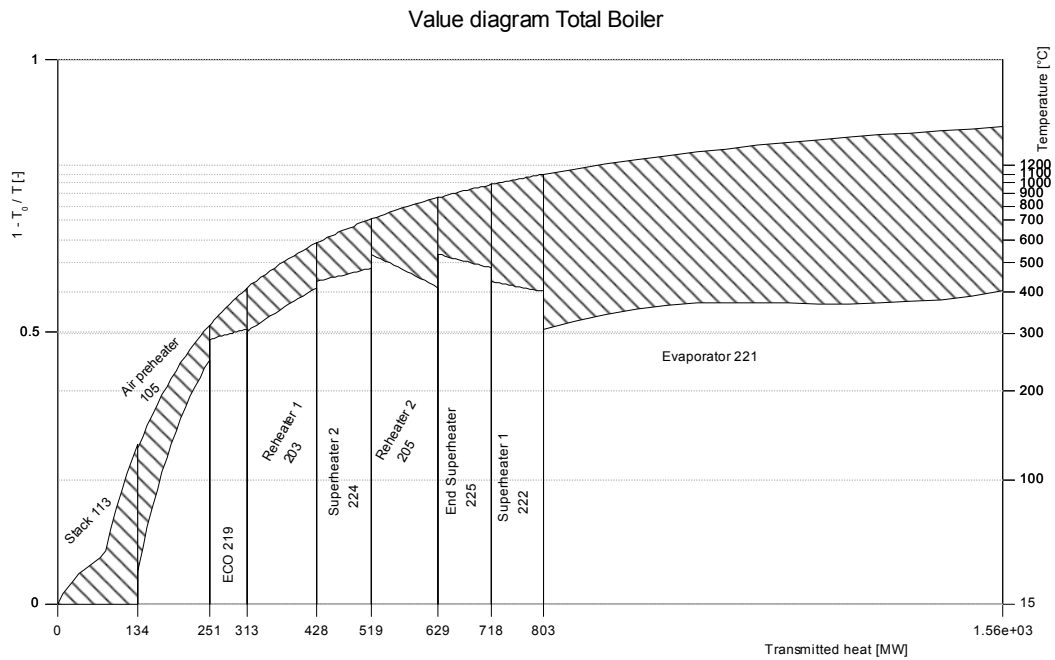


Figure 3 Value diagram of the boiler

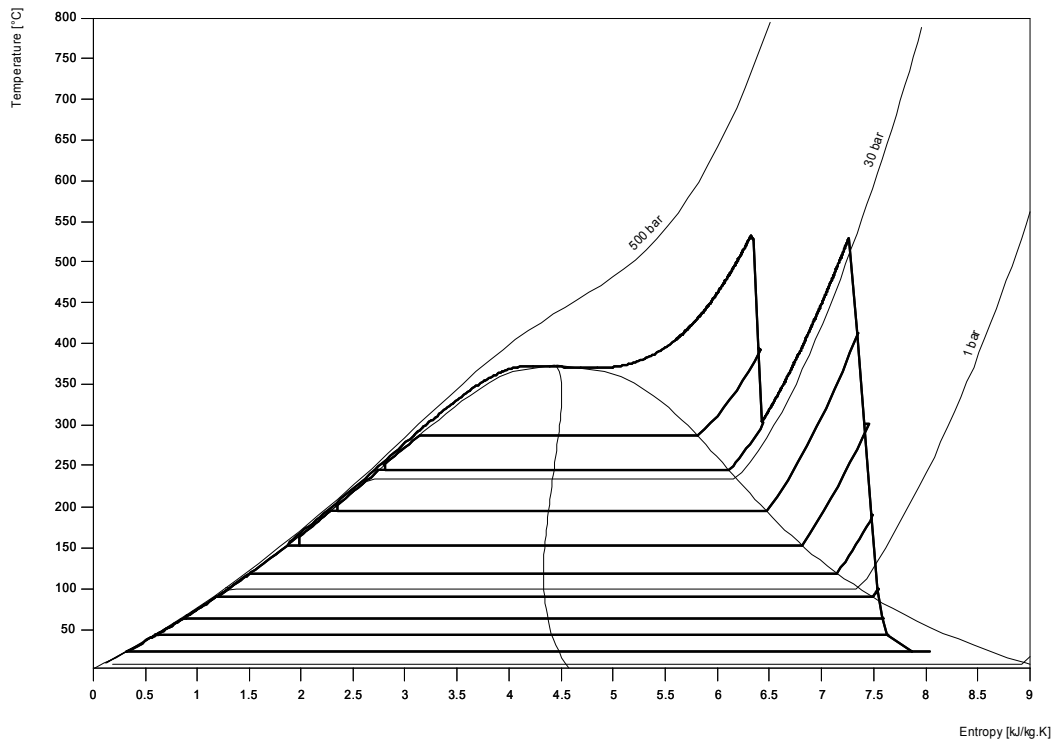


Figure 4  $T,s$ -diagram of the steam cycle

boiler and reheated. After reheat the steam enters the IP turbine at a pressure of 34.02 bar and a temperature of 530°C. The steam is expanded in the IP turbine and LP turbine till condenser pressure (0.027 bar). During expansion steam is extracted for feedwater heating at the respective steam pressures. The cooling curves of the extraction steam are depicted in the  $T,s$ -diagram of Figure 4. The turbine efficiencies are calculated by Cycle-Tempo based on the input data presented in Table 1b. The calculation method is taken from [1] and results in somewhat conservative efficiency values; however this is not a problem for this evaluation. The expansion curve in the  $T,s$ -diagram shows that the isentropic efficiency during expansion from extraction point of the first feedwater heater to the turbine outlet is significantly lower than the isentropic efficiency of the preceding expansion stages. The reason for this apparently lower expansion efficiency is that the expansion end point in the diagram is effected by the outlet loss of the LP turbine. After condensation the feedwater is preheated in the respective feedwater heaters to 287.2°C, the boiler inlet temperature. The temperature differences of the secondary and primary fluids in the feedwater heaters are shown in the  $T,Q$ -diagram of Figure 5. The value diagram of Figure 6 shows why the temperature differences in the LP feedwater heaters are smaller than in the HP feedwater heaters. The extraction pressures are determined by an optimization program that minimizes the exergy loss of the feedwater train. The total exergy loss of the steam cycle is 97.36 MW which is only 6.6% of the exergy of the fuel (see Table 5b). Roughly 2/3 of these losses are due to the expansion

## Appendix 4.1

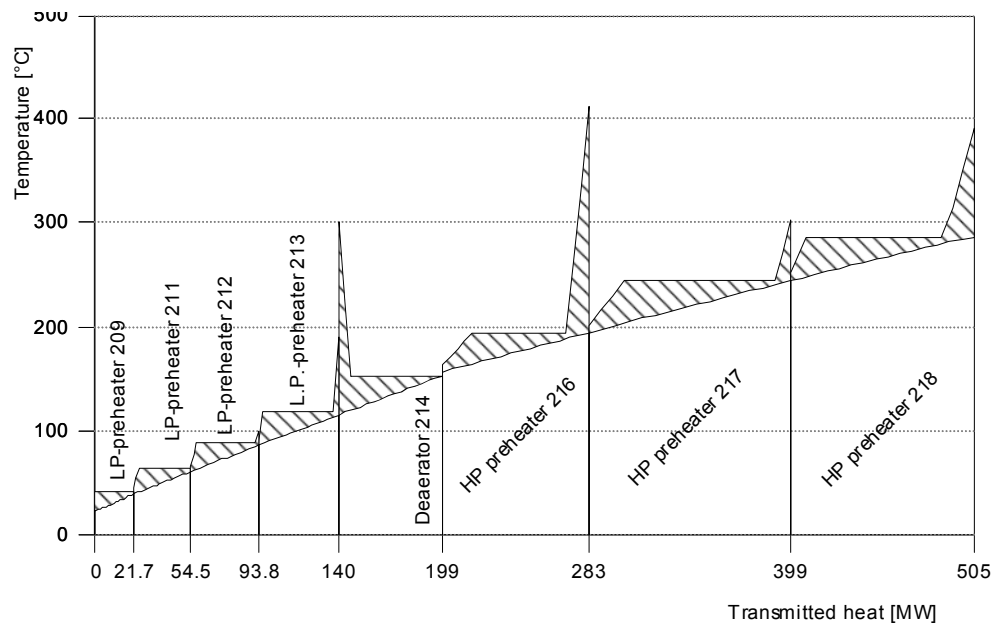


Figure 5 *T,Q*-diagram of the feedwater heaters

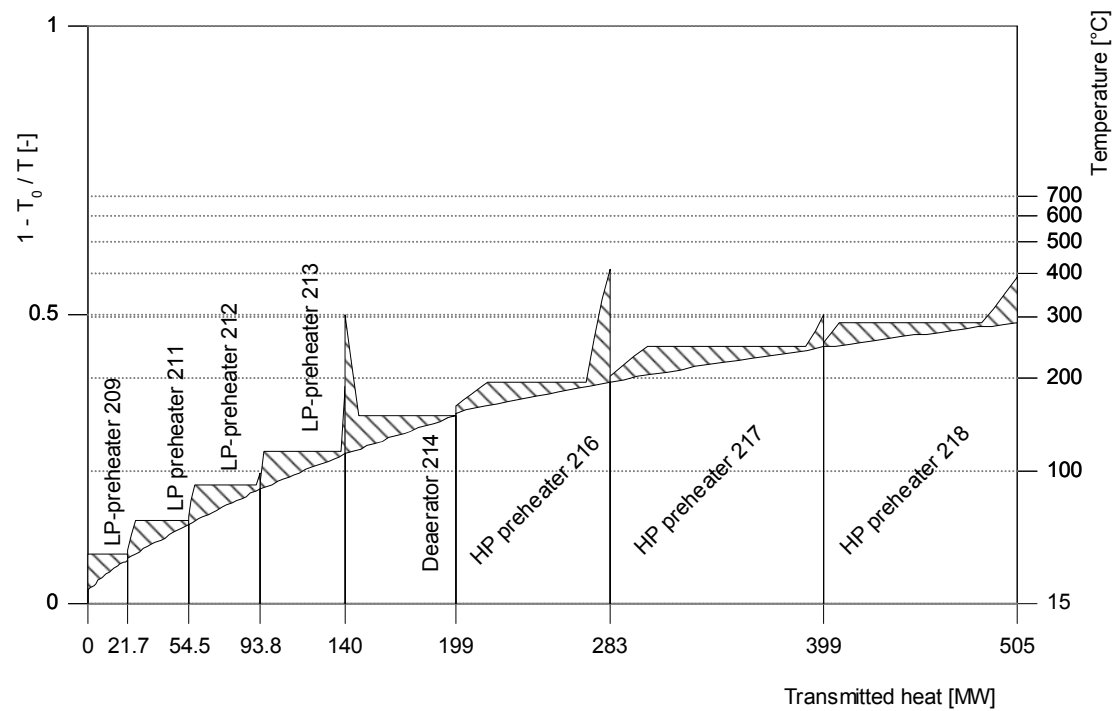


Figure 6 *Value* diagram of the feedwater heaters

process in the turbines. The remainders are the losses of the feedwater train. Table 6 gives an overview of the energy and exergy flows in the pipes of the system. The total exergy can easily be calculated using the data from Table 4. But in addition the total exergy flow is split into the thermo mechanical exergy and the chemical exergy. This is in particular useful for the

Pipe no.	Energy flows			Exergy flows		
	Total [kW]	Thermo Mech. [kW]	Chemical [kW]	Total [kW]	Thermo Mech. [kW]	Chemical [kW]
101	8266.86	8266.86	0	75.39	-10.89	86.28
	8266.86	8266.86		75.39	-10.89	
102	16319.17	16319.17	0	278	191.71	86.28
	16319.17	16319.17		278	191.71	
103	18397.64	18397.64	0	2102.67	2016.38	86.28
	18397.64	18397.64		2102.67	2016.38	
104	18397.64	18397.64	0	2102.67	2016.38	86.28
	18397.64	18397.64		2102.67	2016.38	
105	135881.22	135881.22	0	35794.04	35707.75	86.28
	135881.22	135881.22		35794.04	35707.75	
106	135881.22	135881.22	0	35794.04	35707.75	86.28
	135881.22	135881.22		35794.04	35707.75	
107	1594749.5	1594738	11.49	43159.19	2192.52	40966.67
	1594749.5	1594738		43159.19	2192.52	
108	1583497.5	1583486	11.49	43159.19	2192.52	40966.67
	1583497.5	1583486		43159.19	2192.52	
109	1572533.5	1572522	11.49	43159.19	2192.52	40966.67
	1572533.5	1572522		43159.19	2192.52	
110	1572533.5	1572522	11.49	43159.19	2192.52	40966.67
	1572533.5	1572522		43159.19	2192.52	
111	814495.25	814483.75	11.49	487189.38	446222.72	40966.67
	814495.25	814483.75		487189.38	446222.72	
112	729274.44	729262.94	11.49	420451.44	379484.78	40966.67
	729274.44	729262.94		420451.44	379484.78	
113	640257.88	640246.38	11.49	352661.69	311695.03	40966.67
	640257.88	640246.38		352661.69	311695.03	
114	530654.12	530642.62	11.49	272598.62	231631.95	40966.67
	530654.12	530642.62		272598.62	231631.95	
115	439518.66	439507.16	11.49	209821.73	168855.06	40966.67
	439518.66	439507.16		209821.73	168855.06	
116	324379.62	324368.12	11.49	137616.16	96649.48	40966.67
	324379.62	324368.12		137616.16	96649.48	
117	262449.34	262437.84	11.49	103486.22	62519.55	40966.67
	262449.34	262437.84		103486.22	62519.55	
118	262449.34	262437.84	11.49	103486.22	62519.55	40966.67
	262449.34	262437.84		103486.22	62519.55	
119	144965.75	144954.27	11.49	54259.02	13292.36	40966.67
	144965.75	144954.27		54259.02	13292.36	
120	147163.34	147151.86	11.49	56301.27	15334.6	40966.67
	147163.34	147151.86		56301.27	15334.6	
131	0	0	0	0	0	0
	0	0		0	0	

## Appendix 4.1

*Table 6b Energy and exergy flows in pipes (continued)*

Pipe no.	Energy flows			Exergy flows		
	Total	Thermo Mech.	Chemical	Total	Thermo Mech.	Chemical
	[kW]	[kW]	[kW]	[kW]	[kW]	[kW]
132	0	0	0	0	0	0
	0	0		0	0	
141	1458445.25	864	1457581.25	1471205.25	-4942.5	1476147.75
	1458445.25	864		1471205.5	-4942.25	
151	0	0	0	0	0	0
	0	0		0	0	
152	0	0	0	0	0	0
	0	0		0	0	
201	1709364.12	1709364.12	0	795926.25	795926.25	0
	1709364.12	1709364.12		794093.56	794093.56	
202	1362630	1362630	0	528325.88	528325.88	0
	1362630	1362630		528325.88	528325.88	
203	1220026	1220026	0	473034.75	473034.75	0
	1220026	1220026		473034.75	473034.75	
204	1335165.12	1335165.12	0	533439.94	533439.94	0
	1335165.12	1335165.12		533439.94	533439.94	
205	1335165.12	1335165.12	0	533439.94	533439.94	0
	1335165.12	1335165.12		533439.94	533439.94	
206	1444768.75	1444768.75	0	597552.38	597552.38	0
	1444768.75	1444768.75		597552.38	597552.38	
207	653581.75	653581.75	0	16139.55	16139.55	0
	653581.75	653581.75		16139.55	16139.55	
208	9618.36	9618.36	0	90.11	90.11	0
	9618.36	9618.36		90.11	90.11	
209	9947.26	9947.26	0	348.46	348.46	0
	9947.26	9947.26		348.46	348.46	
210	31645.93	31645.93	0	1450.51	1450.51	0
	31645.93	31645.93		1450.51	1450.51	
211	38063.7	38063.7	0	1767.68	1767.68	0
	38063.7	38063.7		1767.68	1767.68	
212	70886.5	70886.5	0	5303.93	5303.93	0
	70886.5	70886.5		5303.93	5303.93	
213	110152.29	110152.29	0	11889.17	11889.17	0
	110152.29	110152.29		11889.17	11889.17	
214	156140.23	156140.23	0	22408.46	22408.46	0
	156140.23	156140.23		22379.48	22379.48	
215	302482.66	302482.66	0	55832.38	55832.38	0
	302482.66	302482.66		55832.38	55832.38	
216	318727.19	318727.19	0	70224.84	70224.84	0
	318727.19	318727.19		70224.84	70224.84	
217	402743.19	402743.19	0	100276.16	100276.16	0
	402743.19	402743.19		100276.16	100276.16	

*Table 6c Energy and exergy flows in pipes (continued)*

Pipe no.	Energy flows			Exergy flows		
	Total	Thermo Mech.	Chemical	Total	Thermo Mech.	Chemical
	[kW]	[kW]	[kW]	[kW]	[kW]	[kW]
218	518377.75	518377.75	0	148242.25	148242.25	0
	518377.75	518377.75		148242.25	148242.25	
219	624023.12	624023.12	0	197384.02	197384.02	0
	624023.12	624023.12		197384.02	197384.02	
220	685953.38	685953.38	0	227713.75	227713.75	0
	685953.38	685953.38		227713.75	227713.75	
221	685953.38	685953.38	0	227713.75	227713.75	0
	685953.38	685953.38		227713.75	227713.75	
222	1443991.25	1443991.25	0	640899	640899	0
	1443991.25	1443991.25		640899	640899	
223	1529212.12	1529212.12	0	689644.75	689644.75	0
	1529212.12	1529212.12		689644.75	689644.75	
224	1529212.12	1529212.12	0	689644.75	689644.75	0
	1529212.12	1529212.12		689644.75	689644.75	
225	1620347.5	1620347.5	0	743673.88	743673.88	0
	1620347.5	1620347.5		743673.88	743673.88	
226	1709364.12	1709364.12	0	798374.12	798374.12	0
	1709364.12	1709364.12		795926.25	795926.25	
231	158965.41	158965.41	0	66986.7	66986.7	0
	158965.41	158965.41		66800.16	66800.16	
232	53320.04	53320.04	0	14908.48	14908.48	0
	53320.04	53320.04		14776.85	14776.85	
233	80289.45	80289.45	0	18841.52	18841.52	0
	80289.45	80289.45		18668.07	18668.07	
234	79812.55	79812.55	0	15705.16	15705.16	0
	79812.55	79812.55		15572.95	15572.95	
241	142603.95	142603.95	0	55291.14	55291.14	0
	142603.95	142603.95		55112.58	55112.58	
251	83539.11	83539.11	0	30435.32	30435.32	0
	83539.11	83539.11		30332.19	30332.19	
261	138096.52	138096.52	0	42960.59	42960.59	0
	138096.52	138096.52		42776.89	42776.89	
262	66529.89	66529.89	0	20608.35	20608.35	0
	66529.89	66529.89		20428.46	20428.46	
263	71566.63	71566.63	0	22168.54	22168.54	0
	71566.63	71566.63		21975.03	21975.03	
264	54990.61	54990.61	0	1358.2	1358.2	0
	54990.61	54990.61		1358.2	1358.2	
271	51916.76	51916.76	0	13003.89	13003.89	0
	51916.76	51916.76		12929.3	12929.3	
272	5928.81	5928.81	0	669.22	669.22	0
	5928.81	5928.81		667	667	

## Appendix 4.1

Pipe no.	Energy flows [kW]	Exergy flows Thermo Mech. [kW]	Chemical [kW]	Total [kW]	Thermo Mech. [kW]	Chemical [kW]
273	7236.14 7236.14	7236.14 7236.14	0	569.68 567.64	569.68 567.64	0
274	5767.79 5767.79	5767.79 5767.79	0	272.75 270.36	272.75 270.36	0
275	6362.27 6362.27	6362.27 6362.27	0	275.61 275.61	275.61 275.61	0
276	6417.77 6417.77	6417.77 6417.77	0	319.94 319.94	319.94 319.94	0
281	40573.12 40573.12	40573.12 40573.12	0	7905.3 7843.13	7905.3 7843.13	0
291	31354.45 31354.45	31354.45 31354.45	0	4404.48 4355.19	4404.48 4355.19	0
301	22293.15 22293.15	22293.15 22293.15	0	1900.11 1864.44	1900.11 1864.44	0
401	285743.06 285743.06	285743.06 285743.06	0	1497.51 1497.51	1497.51 1497.51	0
402	284036.5 284036.5	284036.5 284036.5	0	2859.16 2859.16	2859.16 2859.16	0
403	414917.47 414917.47	414917.47 414917.47	0	3106.74 3106.74	3106.74 3106.74	0

evaluation of plants with a variety of chemical conversions like e.g. plants with gasification and fuel cells.

The cooling water system is supposed to comprise the condenser and the cooling water cycle (see Table 5c). The exergy loss of the cooling water system is 19.22 MW which is 1.3% of the fuel exergy. The negative exergy value of the cooling water that enters the cooling

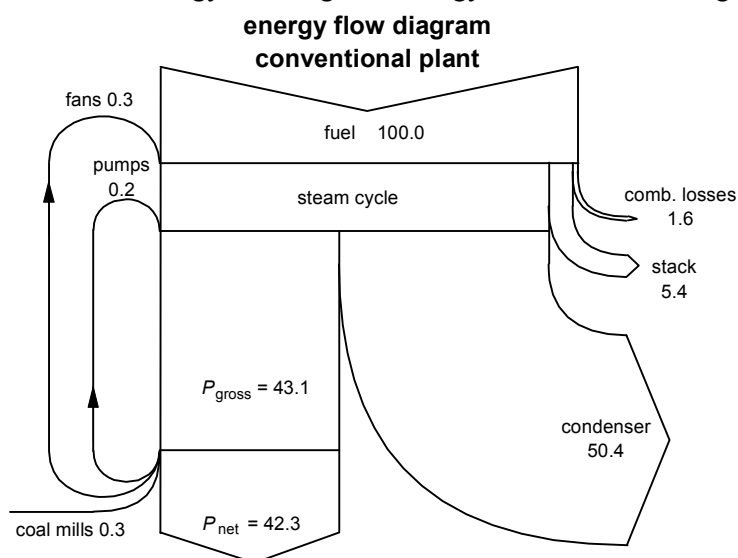


Figure 7 Energy flow diagram of the reference system

water cycle is caused by the fact that the exergy of the cooling water is transferred to the system. The temperature of the cooling water (12°C) is somewhat lower than the considered environmental temperature for the exergy calculation. It emphasizes the problem that the environment is not in equilibrium with itself. It was concluded in Section 2.3.2 that the thermo mechanical exergy of heat at a temperature below environmental temperature will be positive.

But in the case of an exergy balance the exergy difference between the water that enters the system and the water that leaves the system is the sum of the absolute exergy values of these water flows<sup>1</sup>. For this evaluation the effects are negligible.

For a quick overview of the system performance energy flow diagrams (Figure 7) or exergy flow diagrams (Figure 8) can be used. The energy flow diagram, however, can be

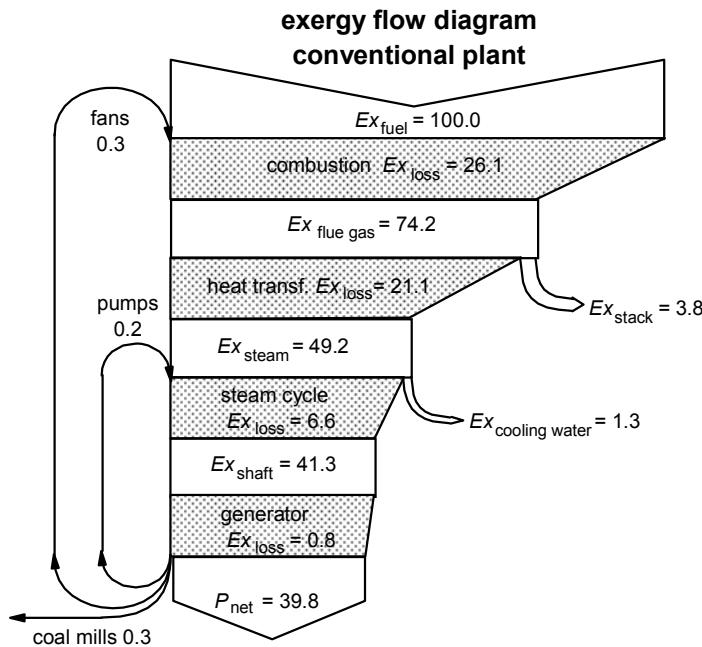


Figure 8 Exergy flow diagram of the reference system

misleading if an explanation is demanded for the causes of the system losses. The diagram just shows the quantity of energy flows but ignores the quality. The large energy flow that leaves the system through the condenser has stimulated in the past many people to search for solutions that enable useful applications of this heat. But, as the exergy flow diagram shows, the large thermodynamic losses of the system do not originate from the condenser, but are caused by the processes in the boiler. The exergy flow diagram obviously shows that the exergy losses due to combustion and heat transfer are primarily responsible for the limited overall exergy efficiency of the power plant. The losses in the steam cycle and (electrical) generator are reasonable and are the result of an economical balance between system efficiency and system capital costs. The exergy flow diagram gives a true indication of the origin of the various losses in the system and is therefore useful for further discussions on the possibilities for system improvements.

## REFERENCES

- [1] R.C. Spencer, K.C. Cotton, C.N. Cannon. A method for predicting the performance of steam turbine generators. *Journal of Engineering for Power*, Vol. 85, Oct. (1963), revised July 1974.

<sup>1</sup> In the Cycle-Tempo calculation these exergy values are added up which is not correct

**APPENDIX 4.2****THE THERMODYNAMIC EQUIVALENT TEMPERATURE OF HEAT TRANSFER TO THE GAS TURBINE CYCLE**

The exergy loss of combustion is in principle determined by the thermodynamic equivalent temperature of heat transfer to the gas turbine cycle. Two equations that can be used to calculate the thermodynamic equivalent temperature of heat transfer are derived in Chapter 2:

$$\bar{T} = \frac{H_{\text{out}} - H_{\text{in}}}{S_{\text{out}} - S_{\text{in}}} = \frac{m \cdot (h_{\text{out}} - h_{\text{in}})}{m \cdot (s_{\text{out}} - s_{\text{in}})} \quad (2.83)$$

$$\bar{T} = \frac{T_{\text{out}} - T_{\text{in}}}{\ln \frac{T_{\text{out}}}{T_{\text{in}}}} \quad (2.84)$$

These equations are derived for heat transfer to or from a fluid with constant composition. In the case of a temperature increase in a combustor these conditions are not obeyed; air and fuel are mixed and the composition changes because of the combustion reaction. That complicates the exact calculation of the thermodynamic equivalent temperature of heat transfer in the combustor. Equation 2.84 can be used for quick and dirty assessment; the accuracy is reasonable in the case of high air to fuel ratios. If the air to fuel ratio is smaller, e.g. in the case of low calorific fuels, very high combustion temperatures or low pressure ratios of the compressor, the deviation might become unacceptable high.

The accuracy of the estimated equivalent temperature of heat transfer  $\bar{T}_{\text{to}}$  based on Equation 2.84 can be checked by using this temperature for the calculation of the relative exergy loss of combustion of a gas turbine power cycle. The deviation of the exergy loss estimated by using  $\bar{T}_{\text{to}}$  (= the estimated exergy loss) with the actual exergy loss, as calculated using a Cycle-Tempo model, equals also the deviation of  $\bar{T}_{\text{to}}$ . The estimated exergy loss is determined by using a reversible thermal power cycle with  $T_{\text{H}} = \bar{T}_{\text{to}}$  and  $T_{\text{C}} = T_0$ . It is assumed further that the heat transferred to the cycle equals the total heat of combustion. Then, the power from this cycle is:

$$W = \left(1 - \frac{T_{\text{C}}}{T_{\text{H}}}\right) \cdot Q_{\text{H}} = \left(1 - \frac{T_0}{\bar{T}_{\text{to}}}\right) \cdot Q_{\text{comb}} \quad (1)$$

And the fuel exergy supplied to the system is:

$$Ex_{\text{fuel}} = f_{\text{ex, F}} \cdot Q_{\text{comb}} \quad (2)$$

The exergy loss of combustion can be written as:

$$Ex_{\text{loss, comb}} = Ex_{\text{fuel}} - W = f_{\text{ex, F}} \cdot Q_{\text{comb}} - \left(1 - \frac{T_0}{\bar{T}_{\text{to}}}\right) \cdot Q_{\text{comb}} \quad (3)$$

The relative exergy loss is found by dividing this exergy loss by the fuel exergy, thus

$$Ex_{\text{loss, rel}} = 1 - \frac{1}{f_{\text{ex, F}}} \cdot \left(1 - \frac{T_0}{\bar{T}_{\text{to}}}\right) \quad (4)$$

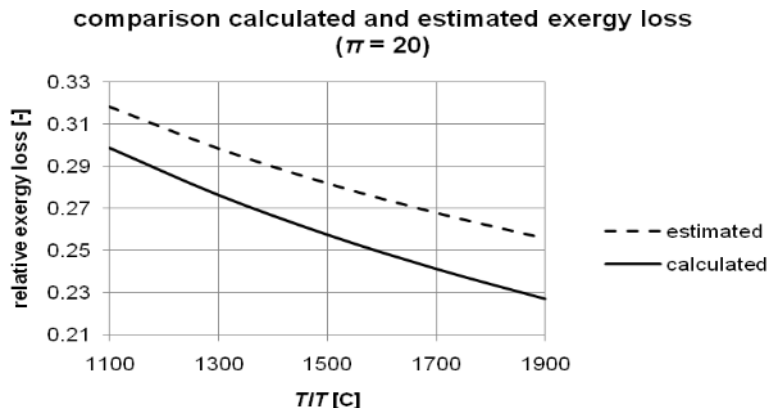


Figure 1 Comparison of the estimated and calculated exergy loss of combustion as function of the TIT ( $\pi = 20$ )

If  $\bar{T}_{to}$  is calculated with Equation 2.84, using the inlet and outlet temperature of the combustion chamber, an estimated value of the relative exergy loss of combustion can be achieved by using Equation 4.

The accuracy of the estimated exergy loss is determined by comparing this loss to

the actual exergy loss of combustion. The simple gas turbine model as described in Section 4.3 is used for this purpose. The results of this comparison are presented in the Figures 1 to 4.

In Figure 1 the relative exergy loss of combustion is shown for the case of a gas turbine with a pressure ratio ( $\pi$ ) of 20 and turbine inlet temperatures ( $TIT$ ) from 1100°C to 1900°C. The deviation of the estimated exergy loss from the calculated value is 6.6% at 1100°C and increases to 12.6% at a  $TIT$  of 1900°C. In the case of  $TIT = 1100^\circ\text{C}$  the air factor is 3.49 and decreases to 1.36 if the  $TIT = 1900^\circ\text{C}$  (see Figure 2). It appears that the deviation depends seriously on the composition of the flue gas which is primarily determined by the air factor. The deviation is smaller if the air factor is higher.

The Figures 3 and 4 present similar data for the case of a gas turbine system with  $\pi = 40$ . Then, the air factor is somewhat higher because of the higher air temperature after compression and the deviation of the estimated exergy loss from the calculated value is slightly lower (5.5% at  $TIT = 1100^\circ\text{C}$  and 11.0% at  $TIT = 1900^\circ\text{C}$ ) than for the case with  $\pi = 20$ . The air factor decreases from 4.49 to 1.50 by increasing the  $TIT$  from 1100 to 1900°C.

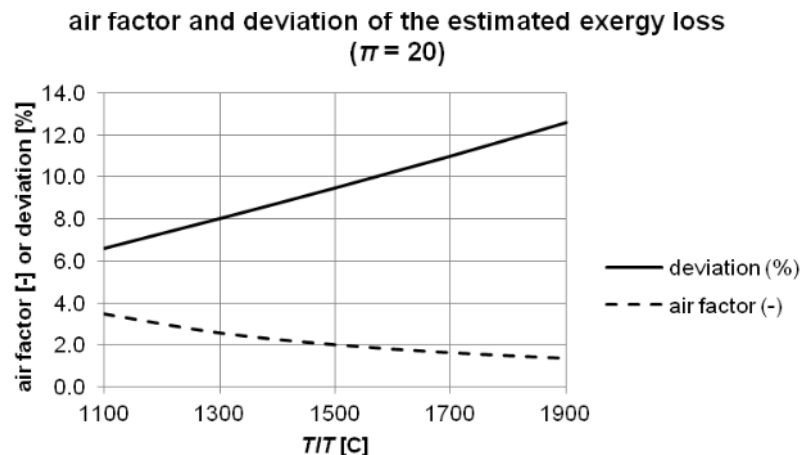


Figure 2 The air factor and the deviation of the estimated exergy loss as function of the TIT ( $\pi = 20$ )

It is concluded from this evaluation that the application of Equation 2.84 for a rough estimate of the thermodynamic equivalent temperature of heat transfer to the gas turbine cycle

## Appendix 4.2

( $\bar{T}_{to}$ ) is acceptable if no high accuracy is required. The evaluations are made for gas turbines using Slochteren quality natural gas as the fuel. At a turbine pressure ratio of 20 and turbine

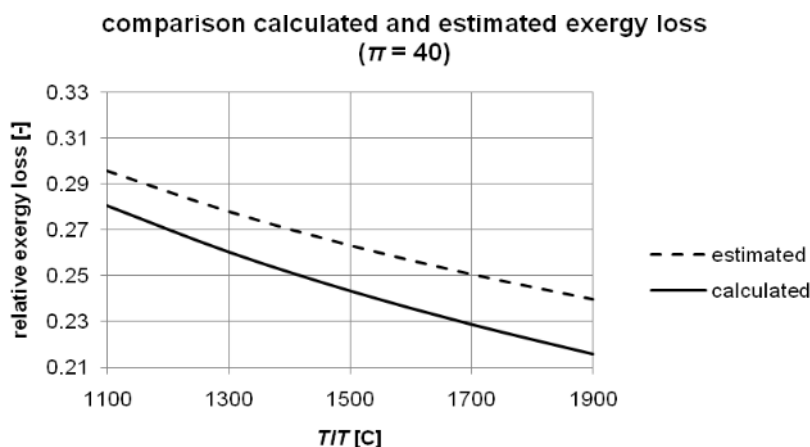


Figure 3 Comparison of the estimated and calculated exergy loss of combustion as function of the TIT ( $\pi = 40$ )

inlet temperatures up to 1500°C the deviation of  $\bar{T}_{to}$  is such that the inaccuracy of the resulting exergy loss is less than 10%. In the case of a pressure ratio of 50 an inaccuracy of 10% is reached at a turbine inlet temperature of approximately 1800°C. The slope of the curves in Figures

1 and 2 are almost the same. This means that Equation 2.84 is appropriate for the assessment of tendencies.

The highest turbine inlet temperatures today are in the area of 1300 to 1500°C, which means that the application of the discussed estimation method for  $\bar{T}_{to}$  can be used with reasonable accuracy for systems with Slochteren natural gas. The heating value of pure methane is somewhat higher than the heating value of Slochteren gas. The effect on the deviation of the

estimated exergy loss is shown in Figure 5. The higher heating value requires a higher air factor and results into a slightly lower deviation. The use of a gas from biomass gasification with a LHV of 4.88

MJ/kg will raise the inaccuracy

from 6.6 to 9.1% for a gas turbine system with  $\pi = 20$  and  $TIT = 1100^\circ\text{C}$ . At higher values of the  $TIT$  the inaccuracy of the resulting exergy loss of combustion is higher than 10%. Thus, the application of Equation 2.84 for gas turbine systems using low calorific gas might become very rough.

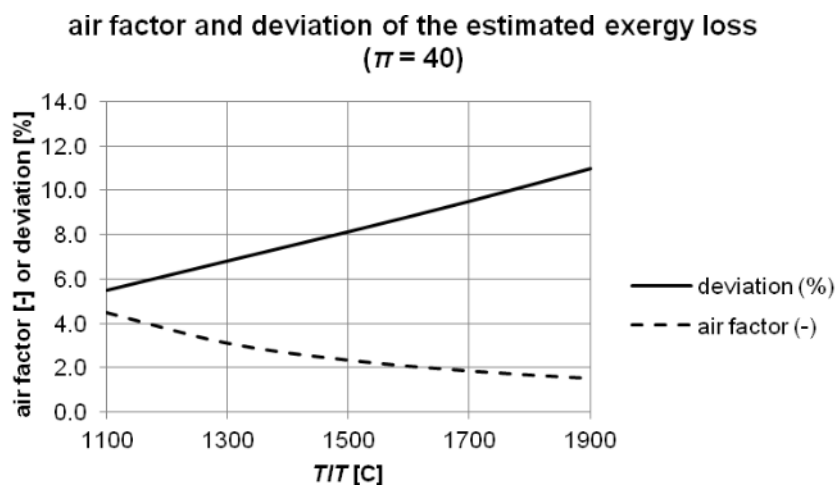


Figure 4 The air factor and the deviation of the estimated exergy loss as function of the TIT ( $\pi = 40$ )

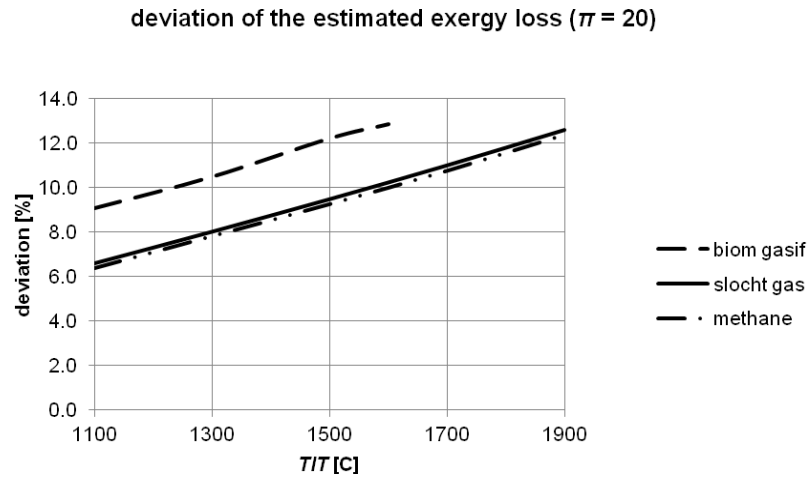


Figure 5 The deviation of the estimated exergy loss for gas from biomass gasification, Slochteren natural gas and methane as function of the TIT ( $\pi = 20$ )

### APPENDIX 4.3 FUEL DATA

In this appendix an overview is given of collected fuel data that might be useful for system evaluations with Cycle-Tempo. Data are presented for some frequently used fuels: solid fuels (coal in Table 1, lignite in Table 2, biomass in Table 3), liquid fuels in Table 4 (petrol, diesel oil, fuel oil) and gaseous fuels in Table 5 (natural gas, coal gas, coke oven gas and refinery gas). For the solid fuels data can be specified for three conditions: the actual condition (as received), the dry condition and the dry and ash free condition. These conditions are all specified in the Tables 1 to 3. For the classification of coal the ASTM standard as presented below is used.

Classification of coal (ASTM):		fixed carbon	
		dry %	moist %
anthracite	1. meta-anthracite	> 98	> 92
	2. anthracite	92 - 98	89 - 95
	3. semianthracite	86 - 92	81 - 89
bituminous	1. low-volatile	78 - 86	73 - 81
	2. medium-volatile	69 - 78	65 - 73
	3. high-volatile A	< 69	58 - 65
	4. high-volatile B	57	53
	5. high-volatile C	54	45
subbituminous	1 subbituminous A	55	45
	2 subbituminous B	56	43
	3 subbituminous C	53	37
lignite	1 lignite A	52	32
	2 lignite B	52	26

### REFERENCES

- [1] Heikki Oravainen. Flue gas condensing and heat recovery at biomass fired district heating plants. Euroheat & Power International, June 1998, p 26 -
- [2] H.D. Baehr. Thermodynamik, Vierte berichtigte Auflage. Springer-Verlag Berlin 1978 (Tabelle 10.12, p.431)
- [3] N. Woudstra, a.o.. Systeemstudie hoge temperatuur gasreiniging bij KV-STEG-systemen. Novem, Ref.nr. 90-310, november 1990
- [4] W. Traupel. Thermische Turbomaschinen, Erster Band. Springer-Verlag, Berlin, 1958
- [5] A.J. Munday, R.A. Farrar. An Engineering Data Book. The Macmillan Press LTD, London, 1979
- [6] K. Schröder. Grosse Dampfkraftwerke, Dritter Band, Teil A, p.5. Springer-Verlag, Berlin, 1966
- [7] W. Bartok, A.F. Sarofim. Fossil Fuel Combustion. John Wiley & Sons, Inc., New York, 1991
- [8] Fluor Daniel B.V.. Integrated coal gasification combined cycle power plant study. Ministry of economic affairs, The Netherlands

## Appendix 4.3

[9a] W. Leibrock. Kennzahlen und Verbrennungskontrolle von Heizöl S und EL. Wärme Band 89, Heft 2

[9b] W. Leibrock. Benzin: Kennzahlen, Verbrennungskontrolle. Wärme Band 91, Heft 5

[10] Gasunie. Physical properties of natural gases

[11] Hoppesteijn. Personal communication (Bart Buhre) 1998

<b>Table 1 Solid fuels (coal)</b>								
FUEL		coke	coal [antracite, C>0.81]		coal [bituminous, 0.81>C>0.45]			
name			Ruhr Anthrazit	Ruhr Magerkohle	Ruhr Esskohle	Ruhr Fettkohle	Saar Fettkohle	Ruhr, Gas flammkohle
source		[2]	[2]	[2]	[2]	[2]	[2]	[2]
<b>a) actual condition</b>								
water	[-]	0.0900	0.0250	0.0250	0.0250	0.0250	0.0250	0.0250
as	[-]	0.0900	0.0600	0.0600	0.0600	0.0600	0.0600	0.0600
C	[-]	0.7995	0.8400	0.8345	0.8317	0.8116	0.7896	0.7604
H	[-]	0.0024	0.0329	0.0375	0.0403	0.0448	0.0503	0.0494
O	[-]	0.0025	0.0238	0.0220	0.0229	0.0375	0.0531	0.0824
N	[-]	0.0082	0.0119	0.0137	0.0146	0.0147	0.0128	0.0146
S	[-]	0.0074	0.0064	0.0073	0.0055	0.0064	0.0092	0.0082
Cl	[-]	0	0	0	0	0	0	0
F	[-]	0	0	0	0	0	0	0
total	[-]	1.0000	1.0000	1.0000	1.0000	1.0000	1.0000	1.0000
HHV	[MJ/kg]	27.39	32.85	33.12	33.31	33.03	32.57	31.48
LHV	[MJ/kg]	27.11	32.07	32.24	32.37	31.99	31.41	30.34
<b>b) dry condition</b>								
as	[-]	0.0989	0.0615	0.0615	0.0615	0.0615	0.0615	0.0615
C	[-]	0.8786	0.8615	0.8559	0.8531	0.8324	0.8099	0.7799
H	[-]	0.0027	0.0338	0.0385	0.0413	0.0460	0.0516	0.0507
O	[-]	0.0027	0.0244	0.0225	0.0235	0.0385	0.0544	0.0845
N	[-]	0.0090	0.0122	0.0141	0.0150	0.0150	0.0132	0.0150
S	[-]	0.0081	0.0066	0.0075	0.0056	0.0066	0.0094	0.0084
Cl	[-]	0	0	0	0	0	0	0
F	[-]	0	0	0	0	0	0	0
total	[-]	1.0000	1.0000	1.0000	1.0000	1.0000	1.0000	1.0000
HHV	[MJ/kg]	30.10	33.69	33.97	34.16	33.88	33.41	32.28
LHV	[MJ/kg]	30.04	32.95	33.13	33.26	32.88	32.28	31.18
<b>c) dry, ash free condition</b>								
C	[-]	0.9750	0.9180	0.9120	0.9090	0.8870	0.8630	0.8310
H	[-]	0.0030	0.0360	0.0410	0.0440	0.0490	0.0550	0.0540
O	[-]	0.0030	0.0260	0.0240	0.0250	0.0410	0.0580	0.0900
N	[-]	0.0100	0.0130	0.0150	0.0160	0.0160	0.0140	0.0160
S	[-]	0.0090	0.0070	0.0080	0.0060	0.0070	0.0100	0.0090
Cl	[-]	0	0	0	0	0	0	0
F	[-]	0	0	0	0	0	0	0
total	[-]	1.0000	1.0000	1.0000	1.0000	1.0000	1.0000	1.0000
HHV	[MJ/kg]	33.40	35.90	36.20	36.40	36.10	35.60	34.40
LHV	[MJ/kg]	33.34	35.11	35.30	35.44	35.03	34.40	33.22

## Appendix 4.3

<b>Table 1 Solid fuels (coal) (continued)</b>								
FUEL		coal [bituminous, 0.81>C>0.45]						
name		Drayton coal	Saar Flammkohle	Ohoi #6	El Cerrejon	Illinois #6	Indiana #3	Wambo
source		[8]	[2]	[7]		[7]	[7]	[3]
<b>a) actual condition (mass fractions)</b>								
water	[-]	0.0950	0.0250	0.0215	0.1670	0.1610	0.1370	0.0910
as	[-]	0.1220	0.0600	0.0636	0.0741	0.1007	0.1278	0.1022
C	[-]	0.6499	0.7539	0.7505	0.6114	0.5890	0.5886	0.6599
H	[-]	0.0423	0.0485	0.0499	0.0499	0.0386	0.0412	0.0434
O	[-]	0.0697	0.0897	0.0607	0.0841	0.0747	0.0535	0.0820
N	[-]	0.0117	0.0101	0.0137	0.0149	0.0117	0.0113	0.0167
S	[-]	0.0094	0.0128	0.0401	0.0083	0.0243	0.0406	0.0043
Cl	[-]	0	0	0	0.0003	0	0	0.0004
F	[-]	0	0	0	0	0	0	0.0001
total	[-]	1.0000	1.0000	1.0000	1.0000	1.0000	1.0000	1.0000
HHV	[MJ/kg]	26.89	30.65	31.91	25.31	24.47	24.97	27.25
LHV	[MJ/kg]	25.73	29.53	30.77	24.03	23.23	23.74	26.08
<b>b) dry condition (mass fractions)</b>								
as	[-]	0.1348	0.0616	0.0650	0.0890	0.1200	0.1481	0.1124
C	[-]	0.7181	0.7733	0.7670	0.7337	0.7020	0.6822	0.7260
H	[-]	0.0467	0.0497	0.0510	0.0480	0.0460	0.0477	0.0477
O	[-]	0.0770	0.0920	0.0620	0.1009	0.0890	0.0620	0.0902
N	[-]	0.0130	0.0103	0.0140	0.0180	0.0140	0.0130	0.0184
S	[-]	0.0104	0.0131	0.0410	0.0100	0.0290	0.0470	0.0047
Cl	[-]	0	0	0	0.0004	0	0	0.0005
F	[-]	0	0	0	0	0	0	0.0001
total	[-]	1.0000	1.0000	1.0000	1.0000	1.0000	1.0000	1.0000
HHV	[MJ/kg]	29.71	31.44	32.62	30.38	29.16	28.94	29.98
LHV	[MJ/kg]	28.69	30.35	31.50	29.33	28.16	27.90	28.94
<b>c) dry, ash free condition (mass fractions)</b>								
C	[-]	0.8300	0.8240	0.8203	0.8056	0.7977	0.8006	0.8180
H	[-]	0.0540	0.0530	0.0545	0.0526	0.0523	0.0561	0.0537
O	[-]	0.0890	0.0980	0.0663	0.1108	0.1011	0.0728	0.1016
N	[-]	0.0150	0.0110	0.0150	0.0197	0.0159	0.0153	0.0207
S	[-]	0.0120	0.0140	0.0439	0.0109	0.0330	0.0552	0.0053
Cl	[-]	0	0	0	0.0004	0	0	0.0006
F	[-]	0	0	0	0	0	0	0.0001
total	[-]	1.0000	1.0000	1.0000	1.0000	1.0000	1.0000	1.0000
HHV	[MJ/kg]	34.34	33.50	34.88	33.35	33.14	33.97	33.77
LHV	[MJ/kg]	33.16	32.34	33.69	32.20	32.00	32.74	32.60

<b>Table 2 Solid fuels (lignite)</b>			
FUEL		lignite C < 0.32	
name		Rheinland	briquet
source		[2]	[2]
<b>a) actual condition (mass fractions)</b>			
water	[-]	0.5700	0.1500
as	[-]	0.1200	0.0700
C	[-]	0.2133	0.5366
H	[-]	0.0155	0.0390
O	[-]	0.0766	0.1927
N	[-]	0.0031	0.0078
S	[-]	0.0015	0.0039
Cl	[-]	0	0
F	[-]	0	0
total	[-]	1.0000	1.0000
<i>HHV</i>	[MJ/kg]	8.308	20.90
<i>LHV</i>	[MJ/kg]	6.577	19.69
<b>b) dry condition (mass fractions)</b>			
as	[-]	0.2791	0.0823
C	[-]	0.4960	0.6313
H	[-]	0.0360	0.0459
O	[-]	0.1781	0.2267
N	[-]	0.0072	0.0092
S	[-]	0.0036	0.0046
Cl	[-]	0	0
F	[-]	0	0
total	[-]	1.0000	1.0000
<i>HHV</i>	[MJ/kg]	19.32	24.59
<i>LHV</i>	[MJ/kg]	18.53	23.59
<b>c) dry, ash free condition (mass fractions)</b>			
C	[-]	0.6880	0.6880
H	[-]	0.0500	0.0500
O	[-]	0.2470	0.2470
N	[-]	0.0100	0.0100
S	[-]	0.0050	0.0050
Cl	[-]	0	0
F	[-]	0	0
total	[-]	1.0000	1.0000
<i>HHV</i>	[MJ/kg]	26.80	26.80
<i>LHV</i>	[MJ/kg]	25.71	25.71

<b>Table 3 Solid fuels, biomass</b>					
FUEL		wood		wood chips	peat
source		[1]	[2]	[1]	[1]
<b>a) actual condition (mass fractions)</b>					
water	[-]	0.4940	0.2000	0.3030	0.4820
as	[-]	0.0322	0.0050	0.0059	0.0231
C	[-]	0.2844	0.3975	0.3562	0.2849
H	[-]	0.0300	0.0477	0.0427	0.0285
O	[-]	0.1493	0.3498	0.2890	0.1717
N	[-]	0.0094	0	0.0031	0.0088
S	[-]	0.0007	0	0.0001	0.0010
Cl	[-]	0	0	0	0
F	[-]	0	0	0	0
total	[-]	1.000	1.000	1.000	1.000
<i>HHV</i>	[MJ/kg]	11.09	16.06	13.36	10.89
<i>LHV</i>	[MJ/kg]	9.229	14.53	11.69	9.094
<b>b) dry condition (mass fractions)</b>					
as	[-]	0.0636	0.0063	0.0084	0.0446
C	[-]	0.5620	0.4969	0.5110	0.5500
H	[-]	0.0594	0.0596	0.0612	0.0550
O	[-]	0.2951	0.4372	0.4148	0.3314
N	[-]	0.0185	0	0.0044	0.0170
S	[-]	0.0014	0	0.0002	0.0020
Cl	[-]	0	0	0	0
F	[-]	0	0	0	0
total	[-]	1.000	1.000	1.000	1.000
<i>HHV</i>	[MJ/kg]	21.92	20.07	19.17	21.03
<i>LHV</i>	[MJ/kg]	20.62	18.77	17.83	19.83
<b>c) dry, ash free condition (mass fractions)</b>					
C	[-]	0.6002	0.5000	0.5153	0.5757
H	[-]	0.0634	0.0600	0.0617	0.0575
O	[-]	0.3151	0.4400	0.4183	0.3469
N	[-]	0.0198	0	0.0045	0.0178
S	[-]	0.0015	0	0.0002	0.0021
Cl	[-]	0	0	0	0
F	[-]	0	0	0	0
total	[-]	1.000	1.000	1.000	1.000
<i>HHV</i>	[MJ/kg]	23.41	20.20	19.33	22.01
<i>LHV</i>	[MJ/kg]	22.02	18.89	17.99	20.76

## Appendix 4.3

FUEL		petrol		kerosene	diesel oil	
source		[2]	[9b]	[5]	[2]	[5]
density	kg/dm <sup>3</sup>	0.726	0.735	0.780	0.840	0.840
mass fractions						
C	[-]	0.8550	0.8540	0.8590	0.8600	0.8570
H	[-]	0.1445	0.1455	0.1400	0.1320	0.1340
O	[-]	0	0	0	0.0010	0
N	[-]	0	0	0	0.0010	0
S	[-]	0.0005	0.0005	0.0010	0.0060	0.0090
total	[-]	1.0000	1.0000	1.0000	1.0000	1.0000
HHV	[MJ/kg]	46.50	47.00	46.50	45.40	45.40
LHV	[MJ/kg]	43.35	43.85	43.44	42.52	42.48

FUEL		fuel oil						
		light			intermediate	heavy		
source		[4]	[2]	[6]	[2]	[2]	[6]	[9a]
density	kg/dm <sup>3</sup>		0.850	0.880	0.920	0.980	0.970	0.970
mass fractions								
C	[-]	0.8440	0.8570	0.8550	0.8530	0.8490	0.8400	0.8700
H	[-]	0.1380	0.1310	0.1250	0.1160	0.1060	0.1100	0.1080
O	[-]	0.0130	0.0010	0.0080	0.0030	0.0050	0.0111	0.0010
N	[-]	0	0.0010	0	0.0030	0.0050	0.0039	0.0010
S	[-]	0.0050	0.010	0.0120	0.0250	0.0350	0.0350	0.0200
total	[-]	1.0000	1.0000	1.0000	1.0000	1.0000	1.0000	1.0000
HHV	[MJ/kg]	42.00	45.40	44.80	43.30	42.30	42.71	41.90
LHV	[MJ/kg]	38.99	42.54	42.07	40.77	39.99	40.31	39.54





## Appendix 5.1

**APPENDIX 5.1****STEAM CYCLES WITH ADVANCED STEAM CONDITIONS.****ASSUMPTIONS WITH REGARD TO SYSTEM DESIGN AND DESIGN PARAMETERS.****1 INTRODUCTION**

The results of the system calculation of a steam turbine cycle are depending on various assumptions concerning system design and design parameters. The evaluation of the effects of a variation of main design parameters requires a systematic selection of further design parameters that are affected by the variation of the main design parameters. This appendix summarizes the assumptions and the main design parameters chosen for the system calculations made with the computer program Cycle-Tempo together with the results as presented more comprehensively in [5.2]. The system calculations demonstrate in a systematic way the effect of advanced steam conditions on the performance of the steam cycle.

Two system configurations are considered for this evaluation: a steam cycle with single reheat (see Figure 5.1) and one with double reheat (see Figure 5.2). The assumptions for each of these system configurations are described separately in this appendix.

**2 STEAM CYCLES WITH SINGLE REHEAT**

The single reheat steam cycle is supposed to be a conventional cycle for large fossil fired power plants. The following assumptions have been used for the system calculations:

- The steam turbine generator is supposed to be a single shaft unit consisting of a single flow high pressure (HP) section, a double flow intermediate pressure (IP) section and three double flow low pressure (LP) sections in parallel<sup>1</sup>. The design power of the generator is 600 MWe. The exhaust area of the last LP turbine stage is 6 x 6.14 m<sup>2</sup>.
- The boiler is a once through unit with a pressure loss that equals 30% of the HP turbine inlet pressure. The pressure loss of the reheater is 10% of the inlet pressure of the IP turbine inlet pressure.

*Table 1 The inlet pressure ( $p_{IP, in}$ ) of the IP turbine with  $T_{HP, in}$  and  $p_{HP, in}$  as independent parameters (single reheat)*

$T_{HP, in}$ [°C]	$p_{HP, in}$ [bar]			
	180	250	300	350
530	34.02	45.25	52.50	57.75
560	33.30	45.30	52.98	60.48
580	32.94	45.40	53.34	61.04
600	32.58	45.50	53.70	61.60
620	32.29	45.70	54.54	63.28
650	32.04	45.75	55.80	65.80

<sup>1</sup> The procedure that determines the performance of the steam turbine [2] considers the IP turbine and the LP turbine as a single unit. Therefore, the efficiency of these sections is reported as the efficiency of the combined IP and LP section.

- The steam temperatures at the inlet of the IP section (after reheat) are the same as the temperatures at the inlet of the HP section. The steam pressures at the inlet of the IP section are depending on the inlet pressure of the HP section and are chosen by using data from [1]. In this book the influence of the main process parameters on a large number of process conditions is investigated. The selected pressures are presented in Table 1.
- The performance of the steam turbines are determined with the procedures published in [2]. These procedures are implemented in Cycle-Tempo. For the HP section, however, it was decided to choose a turbine with sliding pressure control. In [2] only procedures for HP turbines with a control stage are available. Therefore, the procedure for IP sections is applied with some corrections that reduce the isentropic efficiency with 1.5%.
- The condenser pressure is fixed on 0.027 bar. This is based on the assumption that cooling water with 12°C is available for condenser cooling.
- Feedwater heating occurs in 5 LP feedwater heaters and 3 HP feedwater heaters. The last LP feedwater heater is the deaerator which is heated with extraction steam from the IP exhaust. The other LP feedwater heaters are heated with steam extracted from the LP turbine. The condensate from the surface heat exchangers is throttled and passed to the previous feedwater heater. Condensate from the first feedwater heater is pumped into the main condensate line. The first HP feedwater heater is heated with steam extracted from the IP section. The other HP feedwater heaters receive steam from the HP turbine. Then the HP turbine needs to have an extraction point which was not common practice at the time that the calculations were made.

- Because of the application of an extraction point at the HP turbine the final feedwater temperature is not fixed by the pressure of the reheater. Therefore the final feedwater temperatures (boiler inlet temperatures) were selected using [1]. The selected final feedwater temperatures are presented in Table 2.

*Table 2 Final feedwater temperatures (in °C) of the steam cycles with single reheat with  $T_{HP, in}$  and  $p_{HP, in}$  as independent parameters (single reheat)*

$T_{HP, in}$ [°C]	$p_{HP, in}$ [bar]			
	180	250	300	350
530	287.2	307.9	317.9	321.8
560	286.8	307.9	319.1	329.0
580	286.8	307.9	319.1	329.0
600	286.8	307.9	319.1	330.3
620	286.8	308.6	320.5	330.3
650	286.8	308.6	321.8	331.5

- The boiler feedpump is driven by an auxiliary turbine during normal operation. The turbine feed is extracted from the exhaust of the IP turbine. The turbine exhaust is connected with an auxiliary condenser operating at the same pressure (0.027 bar) as the main condenser. The other pumps are driven by electric motors.
- The thermal efficiency of the cycle is defined as the electrical power of the generator minus the auxiliary power necessary for the electrical driven pumps divided by the heat transferred to the cycle in de boiler (including reheater).

The results of the cycle calculations with Cycle-Tempo are presented in Table 3. The independent variables, the pressure and temperature at the inlet of the HP turbine, are shown in the first columns. In the other columns are respectively presented the calculated isentropic

## Appendix 5.1

*Table 3 Results of the system calculations (with single reheat): isentropic efficiencies of the HP section ( $\eta_{s,HP}$ ) and the combined IP and LP section ( $\eta_{s,IP+LP}$ ), the exhaust loss ( $E_{loss,exhaust}$ ), the steam quality at the LP section exhaust ( $x_{exhaust}$ ) and the net thermal efficiency of the cycle ( $\eta_{th,cycle}$ ).*

$p_{HP,in}$ [bar]	$T_{HP,in}$ [°C]	$\eta_{s,HP}$ [-]	$\eta_{s,IP+LP}$ [-]	$E_{loss,exhaust}$ [kJ/kg]	$x_{exhaust}$ [-]	$\eta_{th,cycle}$ [°C]
180	530	0.8962	0.8709	56.38	0.886	0.4581
	560	0.8967	0.8776	54.40	0.896	0.4660
	580	0.8969	0.8819	53.11	0.903	0.4711
	600	0.8971	0.8858	51.84	0.909	0.4760
	620	0.8973	0.8896	50.57	0.915	0.4808
	650	0.8974	0.8949	48.73	0.924	0.4876
250	530	0.8934	0.8733	48.04	0.872	0.4658
	560	0.8936	0.8800	45.85	0.881	0.4745
	580	0.8936	0.8839	44.55	0.887	0.4799
	600	0.8936	0.8878	43.29	0.893	0.4851
	620	0.8935	0.8913	42.15	0.899	0.4900
	650	0.8935	0.8962	40.65	0.908	0.4970
300	530	0.8915	0.8742	43.67	0.865	0.4681
	560	0.8916	0.8806	41.40	0.874	0.4775
	580	0.8915	0.8847	40.15	0.880	0.4833
	600	0.8915	0.8884	39.02	0.886	0.4887
	620	0.8912	0.8917	37.93	0.891	0.4938
	650	0.8908	0.8962	36.43	0.899	0.5010
350	530	0.8897	0.8747	40.52	0.861	0.4683
	560	0.8895	0.8810	37.85	0.868	0.4788
	580	0.8895	0.8849	36.61	0.874	0.4850
	600	0.8895	0.8885	35.48	0.879	0.4907
	620	0.8889	0.8916	34.44	0.884	0.4961
	650	0.8882	0.8959	33.00	0.891	0.5035

efficiencies of the HP turbine ( $\eta_{s,HP}$ ) and the combined IP and LP turbine ( $\eta_{s,IP+LP}$ ), the exhaust loss of the LP turbine ( $E_{loss,exhaust}$ ), the steam quality at the LP exhaust ( $x_{exhaust}$ ) and the thermal efficiency of the cycle ( $\eta_{th,cycle}$ ). The effect of the exhaust loss of the LP turbine is included in the isentropic efficiency of the combined IP and LP turbine section.

### 3 STEAM CYCLES WITH DOUBLE REHEAT

The system configuration of the double reheat steam cycle is almost the same as the configuration of the single reheat cycle. But the addition of a second reheater requires some modifications. This resulted into the following assumptions for the double reheat system calculations:

- The expansion of the steam starts in a single flow super pressure (SP) turbine and is continued, after the first reheat, in the single flow high pressure (HP) turbine section.

Further expansion occurs in the double flow IP pressure turbine and three double flow LP turbines. The exhaust area of the last LP turbine stage is also  $6 \times 6.14 \text{ m}^2$ .

*Table 4 The inlet pressure of HP turbine ( $p_{\text{HP, in}}$ ) and the IP turbine ( $p_{\text{IP, in}}$ ) with  $T_{\text{HP, in}}$  and  $p_{\text{HP, in}}$  as independent parameters (double reheat)*

$T_{\text{HP, in}}$ [°C]	$p_{\text{HP, in}}$ [bar]							
	180		250		300		350	
	$p_{\text{HP, in}}$	$p_{\text{IP, in}}$	$p_{\text{HP, in}}$	$p_{\text{IP, in}}$	$p_{\text{HP, in}}$	$p_{\text{IP, in}}$	$p_{\text{HP, in}}$	$p_{\text{IP, in}}$
530	66.32	15.94	88.13	22.28	102.4	25.34	117.8	28.11
560	65.08	15.46	87.06	20.60	102.3	24.56	117.4	27.66
580	63.84	14.98	86.35	19.49	102.3	24.03	117.1	27.37
600	62.60	14.50	85.64	18.37	102.2	23.51	116.9	27.07
620	61.36	14.02	84.93	17.25	102.1	22.99	116.6	26.77
650	59.50	13.30	83.86	15.68	102.0	22.20	116.2	26.33

- The pressure loss of the once through boiler is 30% of the HP turbine inlet pressure. The pressure loss of the reheaters is 10% of respectively the inlet pressure of the HP section and the inlet pressure of the IP inlet section.
- The steam temperatures at the inlet of the HP section and the IP section are the same as the steam temperature at the inlet of the SP section. The steam pressures at the inlet of the HP section and the IP section are chosen by using data from [1]. The selected pressures are presented in Table 4.
- The SP turbine is also a sliding pressure turbine. The procedure for the performance calculation is the same as for the HP section of the single reheat steam cycle. The performance of the HP section of the double reheat steam cycle is determined using the procedure from [2] for a IP turbine section.
- The number of feedwater heaters for the double reheat cycle is the same as for the single reheat cycle. But in the case of the double reheat cycle the deaerator and also the feedpump turbine are fed by extraction steam from the IP turbine. This results generally in slightly higher inlet pressures for these apparatuses.
- The last feedwater heater is heated with steam from the exhaust of the SP turbine section. Then, the final feedwater temperature is determined by the inlet pressure of the first reheater.

The results of the cycle calculations with Cycle-Tempo are presented in Table 5. Values for the isentropic efficiency of the SP turbine section ( $\eta_{s, \text{SP}}$ ) are given in the third column; the other columns show the same parameters as for the single reheat cycle.

*Table 5 Results of the system calculations (with double reheat): isentropic efficiencies of the SP section ( $\eta_{s, SP}$ ), the HP section ( $\eta_{s, HP}$ ) and the combined IP and LP section ( $\eta_{s, IP+LP}$ ), the exhaust loss ( $E_{loss, exhaust}$ ), the steam quality at the LP section exhaust ( $x_{exhaust}$ ) and the net thermal efficiency of the cycle ( $\eta_{th, cycle}$ ).*

$p_{SP, in}$ [bar]	$T_{SP, in}$ [°C]	$\eta_{s, SP}$ [-]	$\eta_{s, HP}$ [-]	$\eta_{s, IP+LP}$ [-]	$E_{loss, exhaust}$ [kJ/kg]	$x_{exhaust}$ [-]	$\eta_{th, cycle}$ [°C]
180	530	0.8737	0.8967	0.8751	58.27	0.922	0.4655
	560	0.8746	0.8970	0.8820	56.08	0.933	0.4736
	580	0.8755	0.8973	0.8864	54.65	0.940	0.4789
	600	0.8763	0.8977	0.8905	53.24	0.948	0.4840
	620	0.8772	0.8980	0.8945	51.86	0.955	0.4890
	650	0.8783	0.8985	0.9001	49.87	0.966	0.4963
250	530	0.8703	0.8941	0.8794	49.65	0.906	0.4743
	560	0.8710	0.8957	0.8863	47.54	0.919	0.4831
	580	0.8714	0.8968	0.8907	46.22	0.928	0.4886
	600	0.8718	0.8979	0.8948	45.01	0.937	0.4940
	620	0.8721	0.8991	0.8987	43.93	0.945	0.4992
	650	0.8726	0.9007	0.9042	42.37	0.959	0.5067
300	530	0.8676	0.8938	0.8815	45.26	0.900	0.4778
	560	0.8681	0.8945	0.8882	43.07	0.911	0.4869
	580	0.8683	0.8949	0.8921	41.85	0.918	0.4925
	600	0.8685	0.8954	0.8959	40.68	0.925	0.4979
	620	0.8686	0.8958	0.8995	39.58	0.932	0.5013
	650	0.8687	0.8965	0.9046	37.98	0.942	0.5105
350	530	0.8639	0.8937	0.8932	41.68	0.895	0.4796
	560	0.8649	0.8940	0.8895	39.63	0.905	0.4892
	580	0.8653	0.8942	0.8933	38.41	0.912	0.4951
	600	0.8657	0.8943	0.8970	37.25	0.918	0.5007
	620	0.8659	0.8945	0.9005	36.15	0.925	0.5060
	650	0.8662	0.8948	0.9053	34.78	0.934	0.5136

## REFERENCES

- [1] K. Knizia. Die Thermodynamik des Dampfprozesses, Band I. Springer Verlag, Berlin (1966).
- [2] R.C. Spencer, K.C. Cotton, C.N. Cannon. A method for predicting the performance of steam turbine generators. Journal of Engineering for Power, Vol. 85, Oct. (1963), revised July 1974.



**APPENDIX 5.2****THERMODYNAMIC PERFORMANCE OF CLOSED CYCLE GAS TURBINE SYSTEMS****1 INTRODUCTION**

The flow diagram of a simple closed cycle gas turbine is depicted in Figure 1. The system consists of a compressor (1), gas heater (2), expansion turbine (3) and gas cooler (4)<sup>1</sup>. The cycle process in the  $T,s$ -diagram is presented in the left diagram of Figure 2. In this figure the pressure losses in heat exchangers

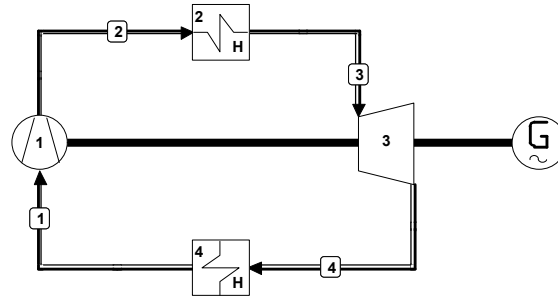


Figure 1 Closed cycle gas turbine system

and the entropy production in compressor and expander are ignored. After compression from condition 1 to 2, heat is transferred to the cycle from condition 2 to 3 at a thermodynamic equivalent temperature  $\bar{T}_H$ . After expansion from condition 3 to 4, heat transfer from the system occurs from condition 4 to 1 at a thermodynamic equivalent temperature  $\bar{T}_C$ . The highest fluid temperature ( $T_{\max}$ ) is achieved at the outlet of the gas heater (condition 3) and the lowest fluid temperature ( $T_{\min}$ ) at the outlet of the gas cooler (condition 1). Since the temperature at condition 4 is not really higher than the temperature at condition 2 heat transfer from the cooled fluid to the heated fluid is not possible. It is obvious that:

$$1 - \frac{\bar{T}_C}{\bar{T}_H} \ll 1 - \frac{T_{\min}}{T_{\max}}$$

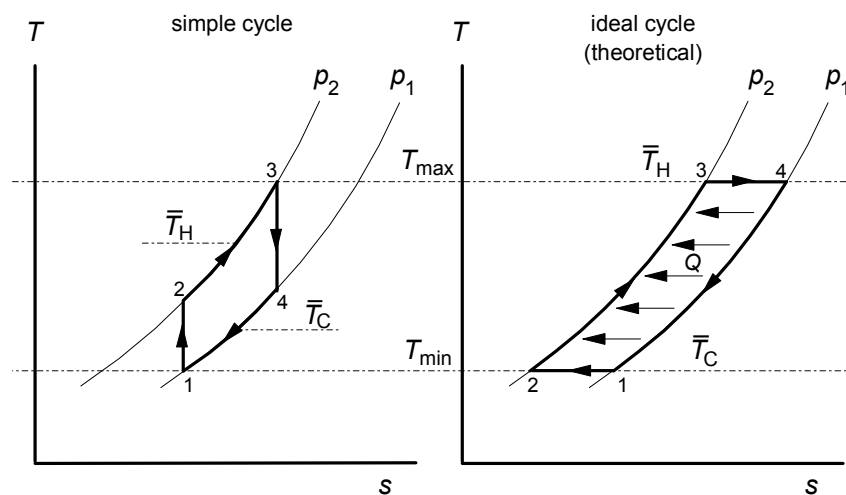


Figure 2 Theoretical gas turbine cycles

<sup>1</sup> The numbers refer to the apparatus numbers in the system diagram

The highest efficiency of a thermal cycle is achieved if all heat transfer to the cycle occurs at the maximum temperature of the cycle and all heat transfer from the cycle at the minimum temperature. This is conceivable in the ideal cycle as presented in the diagram at the right of Figure 2. Compression from condition 1 to 2 occurs isothermal. That means that compression and cooling of the gas should occur simultaneously. After compression the gas is heated from condition 2 to 3 by transferring heat from the expanded gas. In the ideal cycle it is assumed that heat transfer is possible without temperature difference. Isothermal expansion from condition 3 to 4 requires simultaneous expansion and heat transfer to the cycle. Cooling of the expanded gas from condition 4 to 1 is done by internal heat transfer. Since heat is transferred to the cycle at  $T_{\max}$  and from the cycle at  $T_{\min}$  this imaginary cycle will enable the highest cycle efficiency. However, the simultaneous heat transfer and compression or expansion is technically not feasible. Thus, the ideal cycle is used only as an idea that has to be approached as good as possible taking into account the technical and economic limitations.

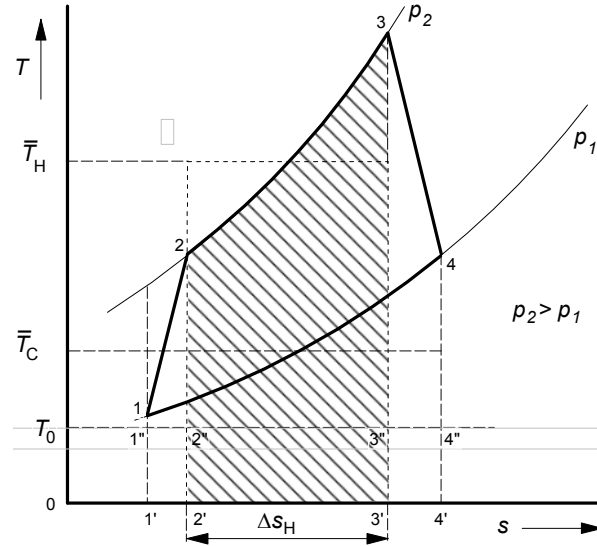


Figure 3 The gas turbine cycle in the  $T,s$ -diagram. The shaded area equals  $Q_H$

## 2 THERMODYNAMIC EVALUATION OF THE GAS TURBINE CYCLE

### 2.1 Exergy losses

The presentation of the simple gas turbine cycle in the  $T,s$ -diagram is useful to discuss the thermodynamic characteristics of the cycle (see Figure 3). The numbering of the various conditions is in agreement with the previous figures. Considering 1 kg of the cycle fluid, the thermodynamic equivalent temperature of heat transfer to the cycle can be written as:

$$\bar{T}_H = \frac{h_3 - h_2}{s_3 - s_2} = \frac{Q_H}{s_3 - s_2} \quad (1)$$

In general for a reversible process it is known that  $dQ = T \cdot ds$ . If the pressure loss during the heat transfer to and from the cycle is ignored, the heat transfer to the cycle becomes:

$$Q_H = \int_2^3 T \cdot ds = \bar{T}_H \cdot (s_3 - s_2) \quad (2)$$

And the heat transfer from the cycle:

$$Q_C = \int_4^1 T \cdot ds = \bar{T}_C \cdot (s_1 - s_4) \quad (3)$$



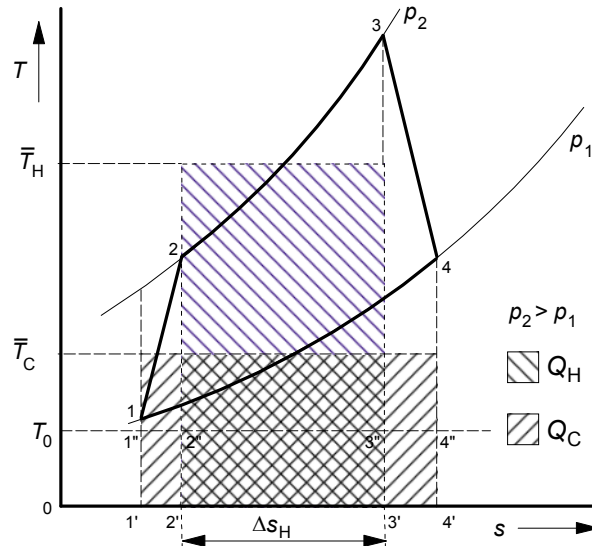


Figure 5 The gas turbine cycle in the  $T,s$ -diagram. The shaded areas equal  $Q_H$  and  $Q_C$

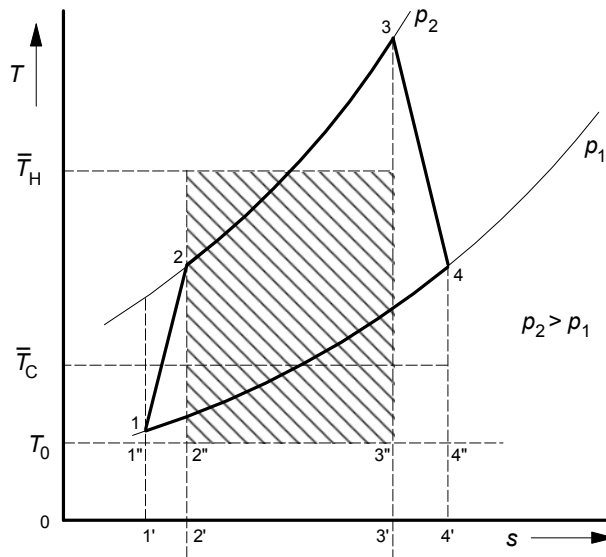


Figure 6 The gas turbine cycle in the  $T,s$ -diagram. The shaded area equals  $Ex_H$

equivalent temperature of heat transfer to and from the cycle are discussed. The cycle parameters that primarily determine the cycle performance are the turbine inlet temperature and the pressure ratio. In general the cooling conditions and thus the temperatures of heat transfer from the cycle are in the case of closed gas turbine cycles usually determined by external circumstances.

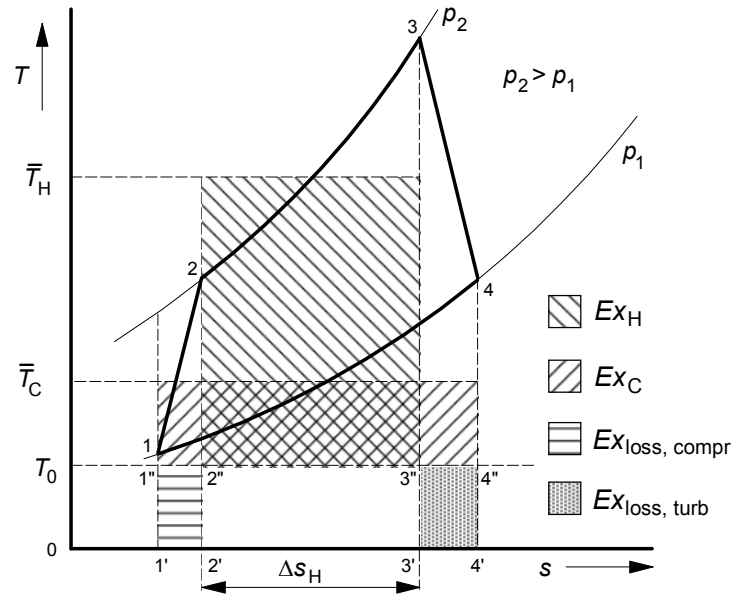


Figure 7 The gas turbine cycle in the  $T,s$ -diagram. With shaded areas for  $Ex_H$ ,  $Ex_C$ ,  $Ex_{\text{loss, compr}}$  and  $Ex_{\text{loss, turb}}$

#### Increase of turbine inlet temperature

Apparently the thermodynamic equivalent temperature of heat transfer to the cycle can be raised by increasing the turbine inlet temperature. In Figure 8 it is supposed for a reversible cycle that the turbine inlet temperature is increased from  $T_3$  to  $T_5$  without changing the pressure ratio. In this diagram 3 cycles can be distinguished: cycle 1-2-3-4-1, cycle 1-2-5-6-1 and cycle 4-3-5-6-4. If the cycle fluid is supposed to be an ideal gas with constant  $c_p$  it can be proven that all cycles have the same thermal efficiency. Thus, an increase of the turbine inlet temperature has no effect on the cycle efficiency in the case of a reversible cycle with an ideal gas with constant  $c_p$  as the cycle fluid. Air can be considered to be an ideal gas if the pressure is not too high ( $< 30$  bar), but the  $c_p$  will slightly increase with temperature. Then, the efficiency of the reversible air cycle will even be lower at higher temperatures. In Table 1 the thermal efficiencies of a number of reversible air turbine cycles are presented with turbine inlet temperatures from 500 to 900°C

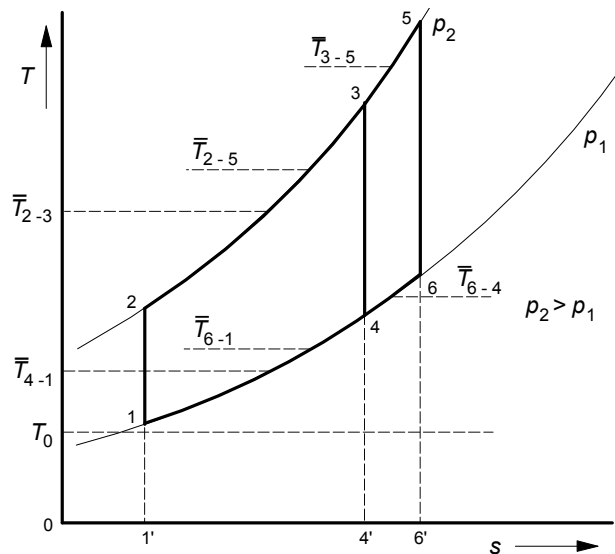


Figure 8 The effect of an increased turbine inlet temperature in the case of a reversible cycle

and pressure ratios of 3, 5 and 7. The calculated values do confirm the expected behavior. But, e.g. in the case of a reversible helium cycle the efficiency of the cycle will be constant. In

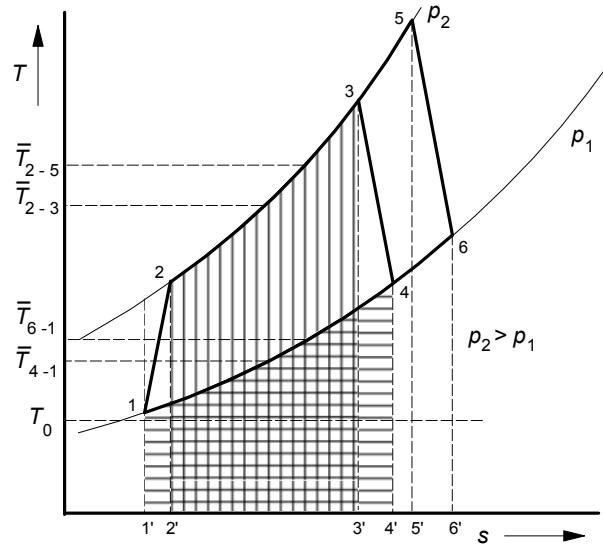


Figure 9 The effect of an increased turbine inlet temperature in the case of an irreversible cycle

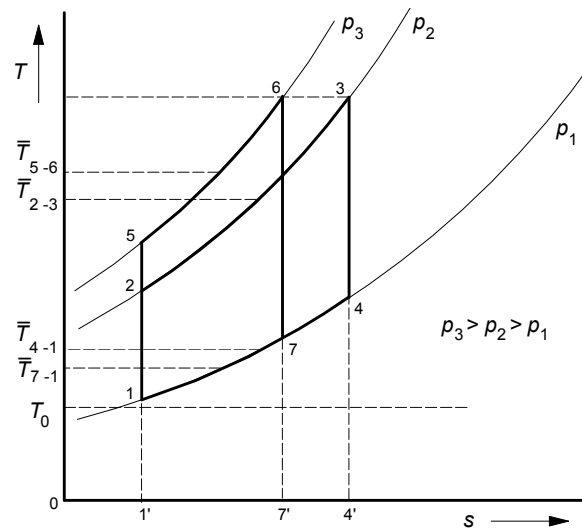


Figure 10 The effect of an increased turbine inlet pressure in the case of a reversible cycle

a real cycle, however, the irreversibility's in the compressor and the turbine cannot be ignored. In Figure 9 it is supposed that the turbine inlet temperature  $T_3$  of the irreversible cycle 1-2-3-4-1 is increased to  $T_5$ . With Eq. 2 and 3 the thermal efficiency of the original cycle can be written as:

## Appendix 5.2

$$\eta_{th(T_3)} = 1 - \frac{|Q_C|}{|Q_H|} = 1 - \frac{\bar{T}_{4-1} \cdot |\Delta s_{4-1}|}{\bar{T}_{2-3} \cdot |\Delta s_{2-3}|} \quad (9)$$

And the thermal efficiency of the cycle with increased turbine inlet temperature is:

$$\eta_{th(T_5)} = 1 - \frac{\bar{T}_{6-1} \cdot |\Delta s_{6-1}|}{\bar{T}_{2-5} \cdot |\Delta s_{2-5}|} \quad (10)$$

Since  $\frac{\bar{T}_{4-1}}{\bar{T}_{2-3}} \approx \frac{\bar{T}_{6-1}}{\bar{T}_{2-5}}$  but  $\frac{|\Delta s_{4-1}|}{|\Delta s_{2-3}|} > \frac{|\Delta s_{6-1}|}{|\Delta s_{2-5}|}$  the thermal efficiency of the cycle with the increased turbine inlet temperature will be higher than the thermal efficiency of the original cycle. Thus:  $\eta_{th(T_5)} > \eta_{th(T_3)}$

It is concluded that the effect of an increase of the turbine inlet temperature will be higher if:

- the irreversible losses of compressor and turbine are higher
- the pressure ratio of the cycle is higher
- the turbine inlet temperature is lower.

#### Increase of pressure ratio

In cycle diagram of Figure 10 the pressure ratio of the cycle is increased by increasing the turbine inlet pressure from  $p_2$  to  $p_3$ . The turbine inlet temperature remains unchanged. It is obvious from this diagram that the pressure increase results in a higher thermodynamic temperature of heat transfer to the cycle (from  $\bar{T}_{2-3}$  to  $\bar{T}_{5-6}$ ) and a lower thermodynamic equivalent temperature of heat transfer from the cycle (from  $\bar{T}_{4-1}$  to  $\bar{T}_{7-1}$ ). This will result in a higher thermal efficiency of the cycle. This is also confirmed by the calculated thermal efficiencies in Table 1. In an irreversible cycle a higher pressure ratio will result in higher irreversibility's in the compressor and the turbine. The effects are depicted in Figure 11. Due to the higher pressure ratio the entropy production of the compressor grows from  $\Delta s_{1-2}$  to  $\Delta s_{1-5}$  and the entropy production of the turbine from  $\Delta s_{3-4}$  to  $\Delta s_{6-7}$ . And consequently also the exergy losses will increase. It is concluded that the effect of an increase of the pressure ratio will be higher if:

- the irreversible losses of compressor and turbine are lower
- the turbine inlet temperature is higher

It is obvious that the cycle efficiency can be increased by increasing the turbine inlet temperature and the pressure ratio of the cycle. But the two

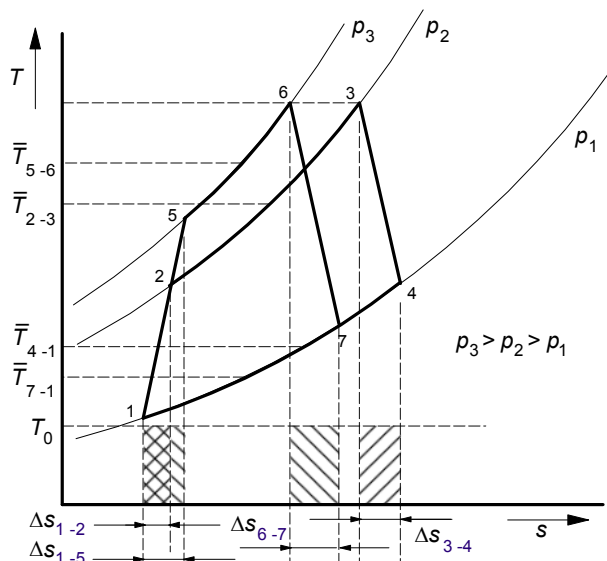


Figure 11 The effect of an increased turbine inlet pressure in the case of an irreversible cycle

parameters appear to be mutual dependent. And the optimum value of both will also depend on the isentropic efficiencies of compressor and turbine.

### 2.3 Cycle configurations

The temperatures of heat transfer to and from the cycle are basically determining the thermal efficiency of a power cycle. These temperatures can also be affected also by alterations of the cycle configuration. The characteristics of some frequently proposed cycle modifications are discussed in this section.

#### Gas turbine cycle with recuperator

If the turbine outlet temperature is significantly higher than the outlet temperature of the compressor, heat from the turbine exhaust gas can be used to heat the compressed fluid. The cycle process is depicted in the  $T,s$ -diagram of Figure 12. In the considered configuration the

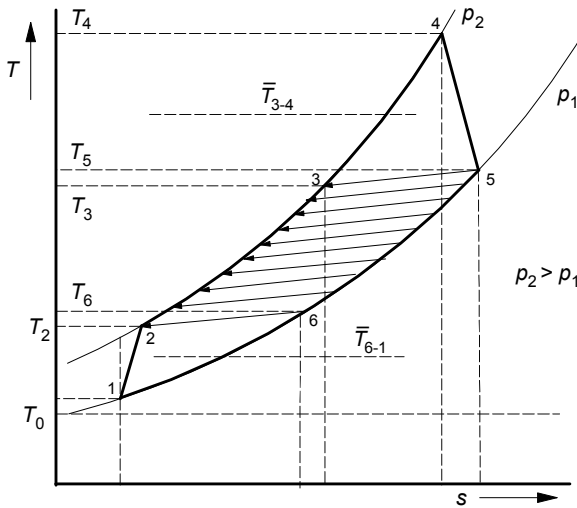


Figure 12 Closed gas turbine cycle with recuperator

compressed fluid is heated from the conditions 2 to 3 in the recuperator with heat from the expanded gas as indicated by the arrows<sup>2</sup>. Further heating from the conditions 3 to 4 occurs in the gas heater by external heat. Thus the thermodynamic temperature of heat transfer to the cycle is  $\bar{T}_{3-4}$ . After expansion the gas is cooled in the recuperator from the conditions 5 to 6. Heat transfer in the gas cooler to the surroundings cools the gas from the conditions 6 to 1. Then, the thermodynamic equivalent temperature of heat transfer from the cycle is  $\bar{T}_{5-6}$ .

From the diagram it will be obvious that the ratio of the temperatures of heat transfer to and from the cycle is much higher than in the case of the same cycle without recuperator. It will be clear also that the effect of the recuperator depends on the temperature difference  $T_5 - T_2$ . This temperature difference is determined primarily by the turbine inlet temperature and the cycle pressure ratio.

Table 1 Thermal efficiencies of reversible closed air turbine cycles

$T_{in, turb}$	$T_{in, compr}$	$\eta_{th}$		
		$\pi = 3$	$\pi = 5$	$\pi = 7$
[°C]	[°C]			
500	50	0.2619	0.3595	0.4166
600	50	0.2598	0.3571	0.4141
700	50	0.2577	0.3545	0.4114
800	50	0.2556	0.3520	0.4087
900	50	0.2536	0.3495	0.4050

<sup>2</sup> A temperature difference between the hot and the cold fluid in the recuperator is considered for heat transfer.

## Appendix 5.2

The limited density of the fluids in the recuperator, in particular the density of the hot fluid, requires large heating areas. The large heating areas together with the high fluid temperatures will result in high capital costs of the recuperator. The size of the heating areas depends primarily on the temperature difference between the hot and the cold fluid and the allowable pressure drop of each of the fluids in the recuperator. Higher pressure drops will increase the internal exergy losses of the cycle. In general a system optimization must balance the recuperator capital costs against the cycle performance.

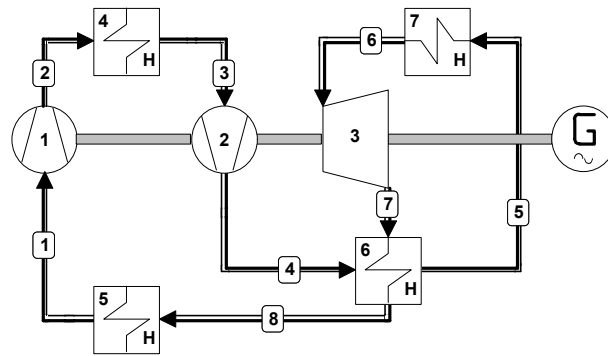


Figure 13 Closed gas turbine cycle with recuperator and intercooler

#### Gas turbine cycle with intercooled compressor and recuperator

Intercooling during compression will reduce the volume of the compressed fluid and consequently the work that is required per unit mass. Thus it increases the net power that is generated by the cycle. The flow diagram of a closed cycle gas turbine system with recuperator and compression in two stages with intercooling in between is presented in Figure 13. The representation of the cycle process in the  $T,s$ -diagram is depicted in Figure 14. After the first stage of compression from condition 1 to 2 the gas is cooled from condition 2 to 3 and compressed further from 3 to 4. The temperature after compression is significantly lower than in the case of compression without intercooling. In a cycle without recuperator intercooling increases the heat that must be transferred by the gas heater and reduces the thermodynamic equivalent temperature of heat transfer to the cycle. In general the effect on

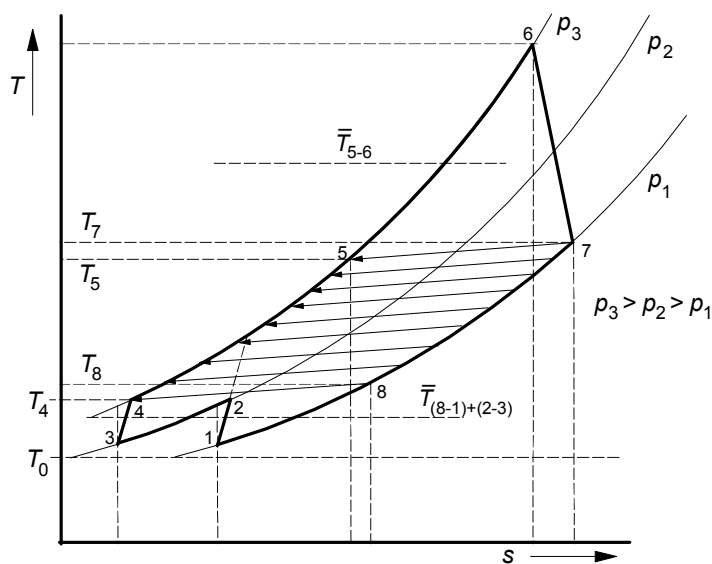


Figure 14 Closed gas turbine cycle with recuperator and intercooling

system efficiency is practically negligible. The reduction of the compression power is almost eliminated by the extra heat necessary for heating the gas to  $T_6$ . In the case of a gas turbine cycle with recuperator no extra heat is required from the gas heater. The lower temperature of the gas after compression increases the total heat that must be transferred in the recuperator and results in a lower thermodynamic equivalent temperature of heat transfer from the cycle ( $\bar{T}_{(8-1)+(2-3)}$ ). The value can be calculated as follows:

$$\bar{T}_{(5-6)+(7-8)} = \frac{\Phi_m \cdot [(h_8 - h_1) + (h_2 - h_3)]}{\Phi_m \cdot [(s_8 - s_1) + (s_2 - s_3)]} \quad (11)$$

The extra heat transfer by the recuperator and the intercooler will cause additional internal losses due to friction in heat exchangers and piping. Nevertheless, intercooling in combination with recuperation can be beneficial in a well designed system.

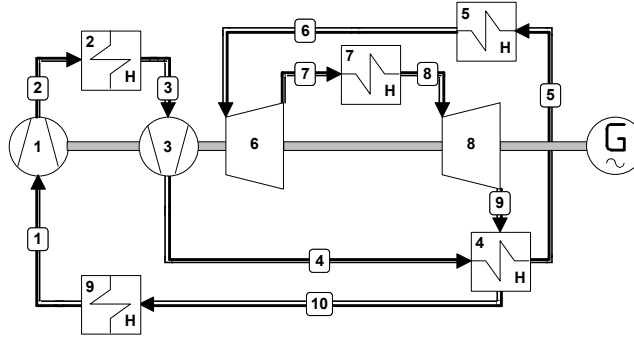


Figure 15 Closed gas turbine cycle with recuperator, intercooler and reheat

Gas turbine cycle with intercooled compressor, reheat turbine and recuperator

A further increase of the ratio between the thermodynamic equivalent temperature of heat transfer to and from the cycle can be achieved by the application of a turbine with reheat. The flow diagram of a system with recuperator, two stage compression with intercooler and

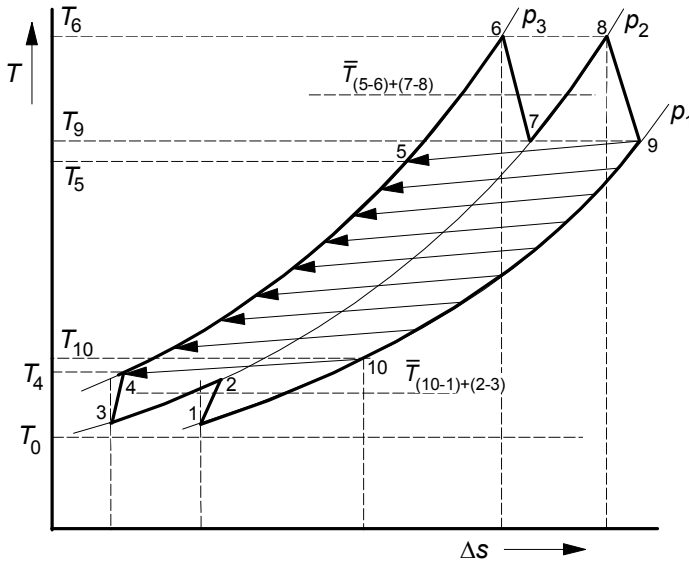


Figure 16 Closed gas turbine cycle with recuperator, intercooling and reheat

two stage expansion with reheat is presented in Figure 15. The representation of the cycle in the  $T,s$ -diagram is depicted in Figure 16. After expansion from condition 6 to 7 the cycle fluid is reheated to condition 8 at the intermediate pressure  $p_2$  and expanded further to condition 9 at pressure  $p_1$ , the compressor inlet pressure. In the diagram of Figure 16 the intermediate pressures for reheat and intercooling were arbitrarily chosen to be the same, but these pressures can be selected independently. The thermodynamic equivalent

temperature of heat transfer to the cycle is the average of the heat transfer from the conditions 5 to 6 and 7 to 8. Thus:

$$\bar{T}_{(5-6)+(7-8)} = \frac{\Phi_{m, 5-6} \cdot (h_6 - h_5) + \Phi_{m, 7-8} \cdot (h_8 - h_7)}{\Phi_{m, 5-6} \cdot (s_6 - s_5) + \Phi_{m, 7-8} \cdot (s_8 - s_7)} \quad (12)$$

## Appendix 5.2

In the closed cycle system as discussed here the mass flows through the gas heater and the reheater are the same, but in open gas turbine cycles they will differ. For that reason in Equation 12 the mass flows are presented separately. From the presentation in the  $T,s$ -diagram it is obvious that intercooling and reheat in combination with recuperation will increase the thermal efficiency of the theoretical (reversible) cycle. With multiple intercooling and reheat as shown in Figure 17 a system is conceivable with thermodynamic equivalent temperatures of heat transfer to and from the cycle very close to respectively the maximum and minimum temperature of the cycle. Such a cycle approaches the ideal cycle as depicted in Figure 2.

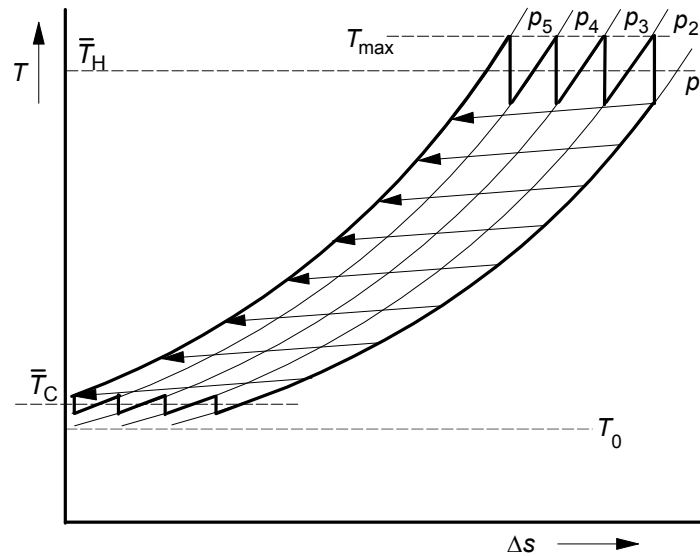


Figure 17 Closed gas turbine cycle with recuperator, multiple intercooling and multiple reheat

A serious drawback of the closed gas turbine cycle with recuperation, intercooling and reheat is the high number of heat exchangers. In particular the large dimensions of the recuperator, gas heater and reheater together expensive materials necessary because of the high fluid temperatures will result in very high equipment costs. The pressure loss due to friction in these heat exchangers will have a negative effect on the internal cycle efficiency.

A very limited number of closed gas turbine cycles have been build in the past. Simple cycles with helium as cycle fluid are applied in gas cooled nuclear reactor plants. Closed air cycles with recuperator and intercooling are applied as CHP plants for district heating with maximum pressures up to 40 bar and turbine inlet temperatures of 750 – 850°C. An attractive quality of closed cycle gas turbines is the off-design performance. The power of the cycle can be controlled by the supply or relief of cycle fluid. This will change the pressures in the cycle but it does not change the pressure ratio and the gas temperatures. Then the cycle efficiency during part load is almost the same as the full load efficiency.

### 3 INTERNAL EFFICIENCY OF A SIMPLE CYCLE CLOSED GAS TURBINE

The internal efficiency of the simple closed cycle gas turbine is primarily determined by the isentropic efficiencies of the compressor and the turbine and the flow resistance of the gas heater and gas cooler and their connecting pipes. To demonstrate the effect of the various parameters on the internal efficiency cycle calculations have been made with Cycle-Tempo for a number of cases as shown in Table 2. The system diagram of Figure 1 has been used for this purpose. The input parameters are shown in the shaded part of the table; the lower part presents the calculated results. For all cases the turbine inlet temperature is fixed at 850°C and

*Table 2 Sensitivity of the internal cycle efficiency*

case		1	2	3	4	5	6	7	8
$p_{\text{compr, in}}$	[bar]	10	10	10	10	10	10	10	10
$T_{\text{compr, in}}$	[°C]	50	50	50	50	50	50	50	50
$\eta_{\text{s, compr}}$	[-]	1	0.87	0.87	0.87	0.87	0.87	0.87	0.87
$\pi$	[-]	3	3	3	3	3	3	5	7
$\Delta p_{\text{gas heater, rel}}$	[-]	0	0	0	0.01	0.01	0.03	0.03	0.03
$T_{\text{turb, in}}$	[°C]	850	850	850	850	850	850	850	850
$\eta_{\text{s, turb}}$	[-]	1	1	0.89	0.89	0.89	0.89	0.89	0.89
$\Delta p_{\text{gas cooler, rel}}$	[-]	0	0	0	0	0.01	0.03	0.03	0.03
$\bar{T}_{\text{to}}$	[K]	737.60	749.37	749.37	747.15	747.15	742.75	791.05	824.28
$\bar{T}_{\text{from}}$	[K]	549.80	549.80	561.67	562.43	564.72	570.97	534.14	511.74
$\eta_{\text{th, ideal}}$	[-]	0.2546	0.2663	0.2505	0.2472	0.2442	0.2313	0.3248	0.3792
$\eta_{\text{th}}$	[-]	0.2546	0.2363	0.1894	0.1866	0.1836	0.1713	0.2321	0.2607
$\eta_{\text{ex, intern}}$	[-]	1.0000	0.8874	0.7562	0.7547	0.7518	0.7405	0.7147	0.6875

compressor inlet temperature at 50°C. A pressure ratio of 3 is used for the first six cases; for the cases 7 and 8 the pressure ratio is increased to respectively 5 and 7.

Case 1 is the ideal cycle with isentropic compression and expansion and no pressure losses in the gas heater and gas cooler. The ideal efficiency, calculated by using the thermodynamic equivalent temperatures  $\bar{T}_{\text{to}}$  and  $\bar{T}_{\text{from}}$ , and the thermal efficiency calculated by Cycle-Tempo are the same and thus the internal efficiency is 1. In case 2 it is assumed that the compressor has an isentropic efficiency of 0.87 which results in a higher exhaust temperature. This increases the ideal efficiency but because of the irreversible entropy increase of the compressor the thermal efficiency of the cycle decreases. The resulting internal exergy efficiency is 0.8874. In case 4 also the irreversibility's of the turbine are included applying an isentropic efficiency of 0.89. The higher exhaust temperature of the turbine results into a higher thermal equivalent temperature of heat transfer from the cycle and consequently a decrease of the ideal efficiency. The irreversibility's of the turbine causes a serious decrease of the thermal efficiency of the cycle. They decrease the internal exergy efficiency to 0.7562. The next steps are the introduction of the flow resistances of the gas heater and the gas cooler. These resistances are supposed to cause a relative pressure loss of 1% for the cases 4 and 5. In case 4 only the resistance of the gas heater is considered, in case 5 also the resistance of the gas cooler is taken into account. The effects on the thermal efficiency as well as the internal exergy efficiency are limited. If the pressure losses of the gas heater and gas cooler are supposed to be 3% of the prevailing pressure, as assumed for case 6, the thermal efficiency is reduced to 0.1713 and the internal exergy efficiency to 0.7405. Thus the friction in the heaters causes a decrease of the thermal efficiency of 1.81% (points) and a

## Appendix 5.2

decrease of the internal exergy efficiency of 1.57% (points) in that case. In the cases 1 to 6 for the compressor a pressure ratio of 3 was assumed. For the cases 7 and 8 this pressure ratio is increased to respectively 5 and 7. The higher pressure ratio causes a serious increase of the ideal efficiencies. But the effect on the thermal efficiencies is mitigated because of the lower internal exergy efficiency of the cycle.

In the cases that all losses are considered the internal exergy efficiency of the closed gas turbine cycle is significantly lower than the internal efficiencies of the steam cycles presented in Section 5.2.2. With the assumptions used for this evaluation a higher pressure ratio of the cycle results in a considerable decrease of the internal exergy efficiency. During the theoretical evaluation it was emphasized that a higher pressure ratio causes a higher irreversible entropy increase in the compressor and turbine. These effects are primarily responsible for the decrease of the internal efficiency.

In Section 2.6.4 a simplified method was mentioned for the calculation of the thermodynamic equivalent temperature. In the case of an ideal gas with constant  $c_p$  the equation:

$$\bar{T} = \frac{h_{\text{out}} - h_{\text{in}}}{s_{\text{out}} - s_{\text{in}}} \quad (13)$$

can be converted into:

$$\bar{T} = \frac{T_{\text{out}} - T_{\text{in}}}{\ln \frac{T_{\text{out}}}{T_{\text{in}}}} \quad (14)$$

case		1	2	3	4	5	6	7	8
Calculated values									
$\bar{T}_{\text{to}}$	[K]	737.60	749.37	749.37	747.15	747.15	742.75	791.05	824.28
$\bar{T}_{\text{from}}$	[K]	549.8	549.80	561.67	562.43	564.72	570.97	534.14	511.74
$\eta_{\text{th, ideal}}$	[-]	0.2546	0.2663	0.2505	0.2472	0.2442	0.2313	0.3248	0.3792
Estimated values									
$\bar{T}_{\text{to}}$	[K]	729.80	741.94	741.94	741.94	741.94	741.94	793.79	829.92
$\bar{T}_{\text{from}}$	[K]	545.35	545.35	556.62	557.33	558.05	560.99	525.62	503.87
$\eta_{\text{th, ideal}}$	[-]	0.2527	0.2650	0.2498	0.2488	0.2478	0.2439	0.3378	0.3929
deviation	[%]	-0.73	-0.51	-0.28	0.64	1.51	5.45	4.02	3.61

The use of temperatures instead of enthalpies and entropies can be convenient for quick calculations where no high accuracy is required. In the case of ideal gas without a constant  $c_p$  Equation 14 can be used for a quick estimate. For a better insight of the accuracy of the estimated values Table 3 presents a comparison of the actual values (calculated with Equation 13) with the estimated values (with Equation 14). In the case of thermal power cycles the temperatures are often used to determine the ideal (reversible) cycle efficiency. Therefore the ideal cycle efficiencies are used for the actual comparison. In the last row of Table 3 the

deviation of the estimated ideal efficiency from the calculated efficiency is shown. It appears that the estimated value can deviate more than 5% from the actual value and the deviation is higher at lower pressure ratios.

## APPENDIX 5.3 EVALUATION OF METHODS TO DETERMINE THE INTERNAL EXERGY EFFICIENCY

### 1 INTRODUCTION

The concept of the internal exergy efficiency of a thermal power cycle ( $\eta_{ex, intern}$ ) is defined in Chapter 3 by the Equations 3.77 and 3.78:

$$\eta_{ex, intern} = \frac{W}{W_{rev}} \quad (3.77)$$

$$\eta_{th} = \eta_{ex, intern} \cdot \left(1 - \frac{\bar{T}_C}{\bar{T}_H}\right) \quad (3.78)$$

The internal exergy efficiency actually represents the ratio between the thermal efficiency of the actual cycle and efficiency of a reversible cycle operating at the same temperatures of heat transfer to and from the cycle. The problem with the open gas turbine cycle is that a true calculation of  $\eta_{ex, intern}$  is not possible. With a system calculation the true work or power generated by the cycle can be calculated but the work generated by the corresponding reversible cycle is not well defined if the thermodynamic equivalent temperatures of heat transfer to and from the cycle are not available. Application of the equation

$$\bar{T} = \frac{h_{out} - h_{in}}{s_{out} - s_{in}}$$

to determine the temperature  $\bar{T}_H$  is not possible as heat transfer to the cycle occurs by the combustion of fuel. The determination of  $\bar{T}_C$  is complicated because of the condensation of water vapor from the flue gas when it is cooled to environmental temperature. Furthermore, the composition and the mass of the flue gas that is transferred to the environment differs from the incoming air. To find an appropriate method to determine useful estimated values of the internal exergy efficiency various options will be discussed first. To check the quality of these options the resulting equations are applied on two cycles: the reference cycle and a reversible cycle. The reversible cycle has the same cycle parameters as the reference cycle, but without the irreversibilities. That means that the isentropic efficiencies of compressor and turbine are 100% and the pressure losses and heat loss are zero. The differences between the two cycles are shown in Table 1. The

Reference cycle		Reference cycle	Reversible cycle
$P_{fuel}$	[MW]	611.60	642.36
$P_{shaft}$	[MWe]	238.42	334.35
$\pi$	[-]	17	17
$T_{compr, out}$	[°C]	410.27	364.38
$TIT$	[°C]	1200	1200
$T_{turb, out}$	[°C]	562.26	473.3
$\eta_{th}$	[-]	0.3889	0.5205

cycle calculations are based on the assumption that the air flow through the compressor is the same (600 kg/s).

## 2 Evaluation of various methods

### OPTION 1

If it is assumed that the cycle fluid is an ideal gas with constant  $c_p$  the thermodynamic equivalent temperature of heat transfer can be calculated as follows:

$$\bar{T}_H = \frac{T_7 - T_4}{\ln \frac{T_7}{T_4}}$$

And the thermodynamic equivalent temperature from the cycle:

$$\bar{T}_C = \frac{T_8 - T_0}{\ln \frac{T_8}{T_0}}$$

The results of the calculations for the two cycles are presented in Table 2. The results show that the thermodynamic equivalent temperatures of heat transfer to and from the system are lower in the case of the reversible cycle. With the thermodynamic equivalent temperatures of the reference cycle a reversible efficiency (Carnot efficiency) of 0.5000 was calculated

reference cycle		option 1	option 2	option 3	option 4	option 5	option 6	option 7
$\bar{T}_H$	[°C]	755.08	837.93	595.81	749.91	749.91		
$\bar{T}_C$	[°C]	240.98	209.04	209.04	201.45	236.14		
$\eta_{rev}$	[-]	0.5000	0.5660	0.4451	0.5361	0.5022		
$\eta_{ex, intern}$	[-]	0.7797	0.6887	0.8758	0.7272	0.7763	0.8608	0.8790
reversible cycle		option 1	option 2	option 3	option 4	option 5	option 6	option 7
$\bar{T}_H$	[°C]	724.54	808.69	579.55	723.96	723.96		
$\bar{T}_C$	[°C]	208.33	178.51	178.51	169.11	213.44		
$\eta_{rev}$	[-]	0.5174	0.5825	0.4703	0.5565	0.5120		
$\eta_{ex, intern}$	[-]	1.0060	0.8936	1.1067	0.9354	1.0166	1.0000	1.0188

resulting in an internal exergy efficiency of the reference cycle of 0.7797. In the case of the reversible cycle the internal exergy efficiency must be 1.0. The calculated value is 1.0060 a deviation of less than 1%. The accuracy of the calculated value for the reference cycle can be questioned since the fluids do not fulfill the conditions for which the applied equations are derived. But the calculated value for  $\eta_{ex, intern}$  seems to be reasonable. Further options are

## Appendix 5.3

considered to check if more appropriate methods are conceivable. In the last rows of Table 2 the ratios of  $\eta_{\text{rev}}$  and  $\eta_{\text{ex, intern}}$  are shown for comparison with the other options.

OPTION 2

An alternative way to determine a value for  $\bar{T}_H$  starts with the equation for determining the exergy that is transferred to a thermal power cycle:

$$Ex_H = \left(1 - \frac{T_0}{\bar{T}_H}\right) \cdot Q_H$$

Then, the following equation for the thermodynamic equivalent temperature is found:

$$\bar{T}_H = \frac{T_0}{1 - \frac{Ex_H}{Q_H}}$$

With this equation  $\bar{T}_H$  can be calculated if  $Ex_H$  and  $Q_H$  are determined first. Using the results from the Cycle-Tempo calculations the exergy and the heat transferred to the cycle are calculated as follows:

$$Ex_H = Ex_F - Ex_{\text{loss, app 5}} - Ex_{\text{loss, pipe 5}} \quad \text{and} \quad Q_H = Q_{F(LHV)}$$

The exergy transferred to the cycle equals the fuel exergy minus the exergy lost due to throttling the fuel (in pipe 5) and to the combustion process (in apparatus 5). The heat transferred to the cycle is supposed to equal the heat based on the lower value of the fuel.

The temperature  $\bar{T}_C$  can be calculated using the following equation:

$$\bar{T}_C = \frac{h_8 - h_9}{s_8 - s_9}$$

This temperature represents the thermodynamic equivalent temperature of the heat that is transferred from the flue gas when this gas is cooled down from the exhaust temperature of the turbine to the temperature of the environment. However the application of this equation results in a rather low value of  $\bar{T}_C$ . Alternatively a similar equation as for  $\bar{T}_H$  can be used:

$$\bar{T}_C = \frac{T_0}{1 - \frac{Ex_C}{Q_C}}$$

With  $Ex_C = Ex_{\text{pipe 8}} - Ex_{\text{pipe 1}}$  and  $Q_C = Q_{\text{pipe 8}} - Q_{\text{pipe 1}}$

the results as presented in Table 2 are determined. Thus the exergy transferred from the cycle equals the exergy flow leaving the turbine exhaust minus the exergy flow of the air that enters the cycle. The heat transferred from the cycle is determined in a similar way using the heat that is obtained from the considered flows if they are brought into equilibrium with the environment.

For option 2 the results are not really credible. The calculated thermodynamic equivalent temperature of heat transfer to the cycle is quite high and the temperature of heat transfer from the cycle is rather low. For the reference cycle this results into an reversible efficiency of 0.5660 and 0.5824 for the reversible cycle. These values are much higher than in the case of option 1 but the ratio between these efficiencies is almost the same as in the case of option 1. The higher values of reversible efficiencies result into lower values for the

internal exergy efficiencies. For the reversible cycle an internal exergy efficiency of 0.8938 was calculated. This very low value is the reason to reject option 2.

#### OPTION 3

For option 3 the same equations are applied as for option 2. The only difference is that in option 3 the higher heating value is used instead of the lower heating value for the

calculation of  $\bar{T}_H$ , thus:  $Q_H = Q_{F(HHV)}$

The result is a significant decrease of the thermodynamic equivalent temperature of heat transfer to the cycle (from 837.93 to 595.81°C for the reference cycle and from 808.69 to 579.55°C for the reversible cycle). Then, the reversible efficiencies are significantly lower and the internal exergy efficiencies higher. The deviation of the internal exergy efficiency from the actual value 1.0 is almost the same as in the case of option 2. Option 3 is then rejected for the same reason.

#### OPTION 4

So far only total exergy values are used to determine the internal exergy efficiency. However, a thermal power cycle converts heat into power, a conversion in which only thermo-mechanical exergy plays a role. By replacing the total exergies in option 2 by the thermo-mechanical exergies, the following equations are obtained:

$$\bar{T}_H = \frac{T_0}{1 - \frac{Ex_H^{tm}}{Q_H}} \quad \text{with} \quad Ex_H^{tm} = Ex_{\text{pipe 6}}^{tm} - Ex_{\text{pipe 4}}^{tm} - Ex_{\text{pipe 5}}^{tm} \quad \text{and}$$

$$Q_H = Q_{F(LHV)}$$

$$\bar{T}_C = \frac{T_0}{1 - \frac{Ex_C^{tm}}{Q_C}} \quad \text{with} \quad Ex_C^{tm} = Ex_{\text{pipe 8}}^{tm} - Ex_{\text{pipe 1}}^{tm} \quad \text{and}$$

$$Q_C = Q_{\text{pipe 8}} - Q_{\text{pipe 1}}$$

The thermo-mechanical exergy of the air flow in pipe 1 is actually zero since air at ambient pressure and temperature enters the system. The exergy is included in the equation however for completeness.

The value of  $\bar{T}_H$  is 749.91°C rather close to the value of option 1. However, a very low value (201.45°C) is calculated for  $\bar{T}_C$ . Then, the internal exergy efficiencies are low in comparison with the values calculated in the case of option 1. The internal exergy efficiency of the reversible cycle is 0.9354 which is far from 1.0. Therefore, also option 4 is rejected.

#### OPTION 5

The values of  $Ex_C^{tm}$  and  $Q_C$  in option 4 are determined by calculating respectively the exergy and the heat that are generated when the flue gas flow leaving the turbine is cooled down to ambient temperature. The high fraction of water vapor in the flue gas causes condensation at lower temperatures. The heat of condensation is more than 10% of the total heat of the flue gas. As this heat does not play a role in the generation of power it should be excluded for the determination of the internal exergy efficiency. The same might be the case for the exergy of condensation. The problem is however that this exergy is not easily to determine. Therefore, in option 5 only the effect of the heat of condensation is included in the

### Appendix 5.3

calculations. For the reference cycle the heat of condensation ( $Q_{\text{cond}}$ ) appears to be 50 079 kW and for the reversible cycle 63 018 kW. Then  $Q_C$  is calculated in this case as:

$$Q_C = Q_{\text{pipe 8}} - Q_{\text{pipe 1}} - Q_{\text{cond}}$$

The results in Table 2 show that the temperatures  $\bar{T}_C$  calculated in this case are very close to the calculated values for option 1. Since also the temperatures of heat transfer to the cycle are almost similar, the internal exergy efficiencies do agree quite well. However, the deviation of the internal exergy efficiency of the reversible cycle from 1.0 is about 1% higher than in the case of option 1. Thus, the accuracy of option 5 does not seem to be higher than the accuracy of option 1.

#### OPTION 6

In principle the internal exergy efficiency can be determined too by comparing the actual generated power by the cycle with the power generated by a reversible cycle operating with the same temperatures of heat transfer to and from the cycle (see Equation 2.87). If it is assumed that the power generated the reversible cycle equals the exergy that is available for power generation, which is actually the difference between the exergy transferred to the cycle and the exergy transferred from the cycle. Then:

$$\eta_{\text{ex, intern}} = \frac{P_{\text{shaft}}}{Ex_H - Ex_C}$$

with:  $Ex_H = Ex_F - Ex_{\text{loss, app 5}} - Ex_{\text{loss, pipe 5}}$  and  $Ex_C = Ex_{\text{pipe 8}} - Ex_{\text{pipe 1}}$

Actually this is the exergy efficiency of the cycle by applying the usual definition of the exergy efficiency (see Equation 2.66). In this case the internal exergy efficiencies are directly calculated by using the exergy values from the cycle calculations. It is not necessary to determine the temperatures of heat transfer or the reversible efficiency. Therefore, in Table 2 only the internal exergy efficiencies are presented. As may be expected in this case the internal exergy efficiency of the reversible cycle is exactly 1.0. For the reference cycle a value of 0.8608 is calculated.

#### OPTION 7

One more option is included in this evaluation to check the use of the thermo-mechanical exergy values when applying the equation of option 6. Then:

$$\eta_{\text{ex, intern}} = \frac{P_{\text{shaft}}}{Ex_H^{\text{tm}} - Ex_C^{\text{tm}}}$$

with:  $Ex_H^{\text{tm}} = Ex_{\text{pipe 6}}^{\text{tm}} - Ex_{\text{pipe 4}}^{\text{tm}} - Ex_{\text{pipe 5}}^{\text{tm}}$  and  $Ex_C^{\text{tm}} = Ex_{\text{pipe 8}}^{\text{tm}} - Ex_{\text{pipe 1}}^{\text{tm}}$

The results in Table 2 show that the use of the thermo-mechanical exergy values only reduces the accuracy of the calculated values for the internal exergy efficiency.

### 3 CONCLUSIONS

From the evaluation of the various options it is concluded that the options 1 and 6 are the most appropriate methods for the evaluation of gas turbine cycles. Option 6 gives actually the exergy efficiency of the cycle instead of the internal exergy efficiency. Since  $Ex_C$  depends on the irreversibility's of the power cycle, the efficiency calculated by the method of option 6

will not present the true power ratio of the actual cycle and the reversible cycle. Also option 6 does not provide temperatures of heat transfer to and from the cycle. For that reason option 1 is more general applicable. It has the advantage that only temperatures are needed to calculate the thermodynamic equivalent temperatures of heat transfer to and from the cycle as well as the internal exergy efficiency. Also in the case of option 1 the calculated thermodynamic equivalent temperatures of heat transfer to and from the cycle are affected by the irreversibilities of the cycle. The temperatures calculated for the reference cycle are higher than for the reversible cycle and consequently the estimated efficiency of the reversible cycle (0.5000) is somewhat lower than the true reversible efficiency (0.5174). Thus, option 1 only gives a reasonable approximation of  $\eta_{\text{ex, intern}}$ .

## APPENDIX 6.1 THERMODYNAMICS OF FUEL CELLS.

### 1 INTRODUCTION

The thermodynamics of the processes in fuel cells are usually described as part of a more comprehensive description of fuel technology. Then, the thermodynamics are in general somewhat underexposed. Therefore, an accurate description of the thermodynamics of fuel cells might be helpful for a better understanding of the processes related to the generation of power and heat. The processes in the fuel cell are depending on the type of fuel cell. At the moment the Proton Exchange Membrane Fuel Cell (PEMFC), the Molten Carbonate Fuel Cell (MCFC) and the Solid Oxide Fuel Cell (SOFC) are supposed to be the most promising candidates for future power application. Therefore, the description of the thermodynamics is limited to these three types.

Today, the generation of power is primarily based on the conversion of a fuel into heat and the subsequent conversion of heat into power by a thermal power cycle. The conversion of the chemical energy of a fuel into heat by thermal combustion processes appears to be a highly irreversible and the following conversion of heat into power causes a further reduction of the achievable conversion efficiency. The fuel cell enables the direct conversion of a fuel into power and with the fuel cell a reversible process is conceivable. Therefore, the relations for reversible fuel cell processes are described first and the Nernst equation is derived for the considered fuel cell types.

Real fuel cells are of course not free of irreversibility's. A short overview of the various irreversibility's might be helpful for a better understanding of the losses. In addition some equations are presented that are often used to include these losses in fuel cell calculations. Fuel cells can be easily operated at different loads. For economic application the selection of the optimum design point is important. Therefore the process parameters that are determining the optimum design load are discussed. During part load the effect of various irreversibility's on the performance of the fuel cell will diminish. A short description of the part load behavior of fuel cells is presented.

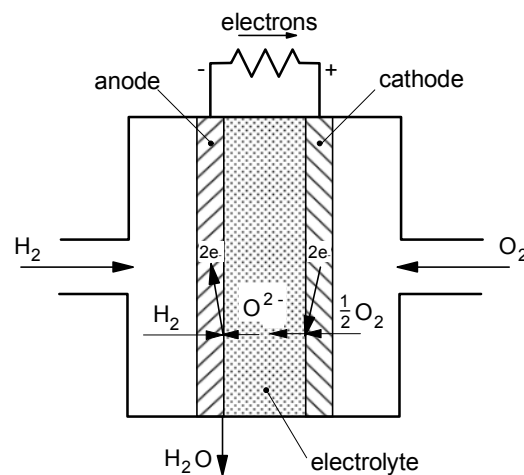
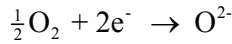


Figure 1 Fuel cell principle

### 2 REVERSIBLE CONVERSION OF FUEL INTO POWER

The thermal combustion of a fuel is inherently irreversible because of the chaotic process in which reactants and products are mixed and heat transfer occurs with high temperature gradients. The electrochemical reaction of oxygen and fuel offers actually a well

controlled combustion process. Reversible combustion is conceivable as a electrochemical cell or fuel cell. Figure 1 can be used to explain the principle of the hydrogen fuel cell<sup>1</sup>. The cell consists of an electrolyte enclosed by two electrodes: the anode and the cathode. The anode is in contact with a gas atmosphere that contains hydrogen; the cathode with a gas atmosphere containing oxygen. The electrodes are porous so that gas molecules are able to reach the interface between electrode and electrolyte. The electrolyte is gas tight. Only ions can be transferred across the electrolyte. Oxygen molecules that enter the cathode are converted into oxygen ions by accepting 2 electrons from the electrode:



This reaction occurs in principle at the cathode-electrolyte interface. If the oxygen ions are transferred through the electrolyte to the anode-electrolyte interface, they will react with hydrogen molecules from the anode:



The reaction delivers 2 electrons per hydrogen molecule and produces one molecule of water. The overall reaction is the sum of the two electrode reactions:

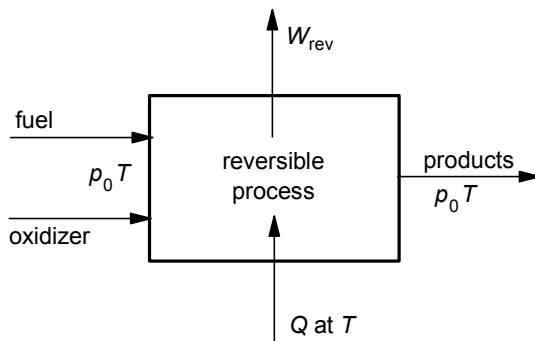
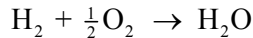


Figure 2 System with a reversible fuel cell process

The reverse reaction is the well known electrolysis reaction. The reaction as described before is able to generate power because of the potential difference that exists between the two electrodes. This potential difference is determined by the chemical potential of the reactants. If the two electrodes are brought into contact via an external resistance the potential difference will result into a flow of electrons from the anode to the cathode generating power (work).

To determine the work that can be achieved from an quantity of fuel converted in a reversible operating fuel cell a system as presented in Figure 2 is considered. Fuel and oxidizer are entering the system at environmental pressure and an arbitrarily chosen temperature. Only reversible processes are taking place in the system. The reaction products are leaving the system at environmental pressure and the same temperature as at the inlet. All processes within the system are isothermal. Heat transfer to or from the system occurs also at the same temperature. The work that is generated by the system must be the reversible work. The energy balance of the system is in general written as:

$$Q + \sum H_{\text{in}} = \sum H_{\text{out}} + W_{\text{rev}}$$

If the flows to and from the system consist of various components this equation can be rewritten as:

$$Q = \sum n_{\text{out}} \cdot h_{\text{out}}^{\text{mol}} - \sum n_{\text{in}} \cdot h_{\text{in}}^{\text{mol}} + W_{\text{rev}} \quad (1)$$

<sup>1</sup> Almost all fuel cells under development at the moment are in principle hydrogen-oxygen fuel cells.

## Appendix 6.1

Since the processes in the system are reversible and isothermal:

$$Q = T \cdot \left( \sum n_{\text{out}} \cdot s_{\text{out}}^{\text{mol}} - \sum n_{\text{in}} \cdot s_{\text{in}}^{\text{mol}} \right) \quad (2)$$

Combining equations (1) and (2) and taking into account that the entropy values are at standard pressure the following equation for the reversible work from a quantity of fuel is derived:

$$W_{\text{rev}} = - \left[ \left( \sum n_{\text{out}} \cdot h_{\text{out}}^{\text{mol}} - \sum n_{\text{in}} \cdot h_{\text{in}}^{\text{mol}} \right) - T \cdot \left( \sum n_{\text{out}} \cdot s_{\text{out}}^{0, \text{mol}} - \sum n_{\text{in}} \cdot s_{\text{in}}^{0, \text{mol}} \right) \right] \quad (3)$$

For this derivation it is assumed that the fluids may be considered as ideal gas<sup>2</sup>. Equation 3 can be written in a somewhat different way:

$$W_{\text{rev}} = - \left[ \left( \sum_{\text{out}} n \cdot \left( h^{\text{mol}} - T \cdot s^{0, \text{mol}} \right) - \sum_{\text{in}} n \cdot \left( h^{\text{mol}} - T \cdot s^{0, \text{mol}} \right) \right) \right] \quad (4)$$

The molar Gibbs free energy is defined as:  $g^{\text{mol}} = h^{\text{mol}} - T \cdot s^{\text{mol}}$

Then, the reversible work from the system can be written as:

$$W_{\text{rev}} = - \left[ \left( \sum_{\text{out}} n \cdot g^{0, \text{mol}} - \sum_{\text{in}} n \cdot g^{0, \text{mol}} \right) \right] = -\Delta G^0 \quad (5)$$

In Figure 1 a fuel cell was shown with gas connections that are only able to transport gas into the cell. The reaction product (water) is supposed to be drained off. With pure hydrogen and oxygen no other components have to leave the fuel cell. In actual fuel cells the fuel will be a mixture with hydrogen and usually air will be the oxidizer. That means that hydrogen and oxygen are in general not available at standard pressure but at their partial pressures in the gas

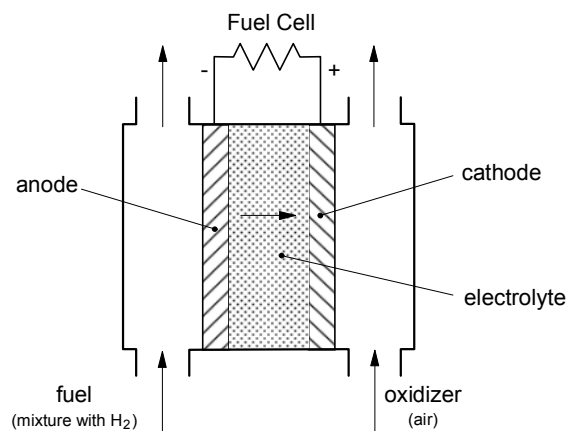


Figure 3 The basic components of a fuel cell

flows. Non converted components in the fuel and oxidizer flows have to be removed and thus a configuration as depicted in Figure 3 will be necessary. Fuel gas and air will enter the anode respectively the cathode chamber at one side and will leave the chamber on the other side. When flowing along the electrode, oxygen and hydrogen will be removed from the gas and diluted flows are leaving the cell. Depending on the fuel cell type the reaction product (water) is removed by the anode flow and/or the cathode flow. In the following it is assumed that the reaction product water will become available as water vapor.

To include the effects of the partial pressure of hydrogen and oxygen in the respective flows a system will be used that first brings the reactants isothermally at standard pressure, then converts the reactants isothermally into the products at standard pressure and finally brings the products isothermally at their partial pressure in the fuel flow respectively the air flow. For the calculation of the reversible work from this system, the system is split into 4

<sup>2</sup> With the pressures and temperatures in the fuel cells under development today the assumption that the fluids are considered as ideal gas is appropriate.

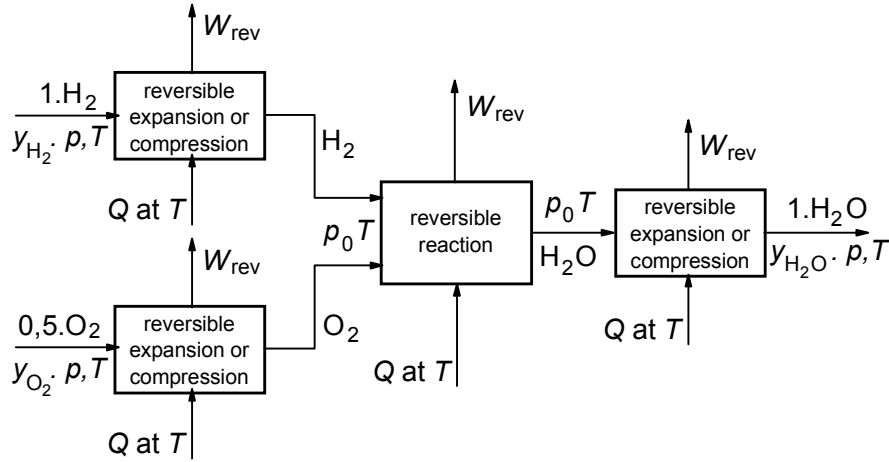


Figure 4 The subsystems used for the calculation of the work from a reversible isothermal fuel cell

subsystems as depicted in Figure 4. All subsystems are assumed to operate reversible and isothermal. The figure is considering a hydrogen-oxygen fuel cell. In the case of a fuel cell based on another conversion reaction, e.g. the solid carbon fuel cell, the system must be adapted to that reaction. The work generated by a reversible fuel cell equals the sum of the work from the subsystems:

$$W_{\text{FC, rev}} = \sum_i W_{\text{rev}} \quad (6)$$

It was assumed that the fluids are considered as ideal gas. Then, the following equations are used to calculate the work from the subsystems necessary to compress or expand the fluids, assuming the formation of 1 kmol of H<sub>2</sub>O or the conversion of 1 kmol of hydrogen.

For the compression or expansion of hydrogen:

$$W_{\text{rev}} = -v_{\text{H}_2} \cdot R^{\text{mol}} \cdot T \cdot \ln \frac{p_0}{y_{\text{H}_2} \cdot p} = R^{\text{mol}} \cdot T \cdot \ln \left( \frac{y_{\text{H}_2} \cdot p}{p_0} \right) \quad (7)$$

For the compression or expansion of oxygen:

$$W_{\text{rev}} = -v_{\text{O}_2} \cdot R^{\text{mol}} \cdot T \cdot \ln \frac{p_0}{y_{\text{O}_2} \cdot p} = R^{\text{mol}} \cdot T \cdot \ln \left( \frac{y_{\text{O}_2} \cdot p}{p_0} \right)^{0.5} \quad (8)$$

For the compression or expansion of water vapor:

$$W_{\text{rev}} = -v_{\text{H}_2\text{O}} \cdot R^{\text{mol}} \cdot T \cdot \ln \frac{y_{\text{H}_2\text{O}} \cdot p}{p_0} = R^{\text{mol}} \cdot T \cdot \ln \left( \frac{p_0}{y_{\text{H}_2\text{O}} \cdot p} \right) \quad (9)$$

And Equation 5 was derived for the reversible reaction at standard pressure in the cell.

Considering the formation of 1 mole (or 1 kmol) of water:

$$W_{\text{rev}} = -\Delta_f g^{0, \text{mol}}$$

The total reversible work from the chemical reaction in the fuel results from combining the equations 5 to 9:

$$W_{\text{FC, rev}} = -\Delta_f g^{0, \text{mol}} + R^{\text{mol}} \cdot T \cdot \ln \left( \frac{y_{\text{H}_2} \cdot y_{\text{O}_2}^{0.5}}{y_{\text{H}_2\text{O}}} \cdot \left( \frac{p}{p_0} \right)^{0.5} \right) = -\Delta g^{\text{mol}} \quad (10)$$

## Appendix 6.1

So far, the fuel cell was considered as a chemical reactor. But the fuel cell must be considered also as an electrical generator. The work from this electrical generator must be:

$$W_{\text{electr, rev}} = n \cdot F \cdot V_{\text{rev}} \quad (11)$$

In this equation is  $n$  the number of electrons per fuel molecule and  $F$  the Faraday constant and  $V_{\text{rev}}$  the voltage of the reversible fuel cell<sup>3</sup>. The product  $n \cdot F$  is the electrical charge of one mole (or kmol) of fuel. In the case of a reversible fuel cell, the electrical work must equal the work from the chemical reaction, thus:

$$W_{\text{electr, rev}} = W_{\text{FC, rev}} \quad (12)$$

Combining the Equations 10 to 12 results into the following equation for the reversible cell voltage:

$$V_{\text{rev}} = \frac{-\Delta g^{\text{mol}}}{n \cdot F} = \frac{-\Delta_f g^{0, \text{mol}}}{n \cdot F} + \frac{R^{\text{mol}} \cdot T}{n \cdot F} \cdot \ln \left( \frac{y_{\text{H}_2} \cdot y_{\text{O}_2}^{0.5}}{y_{\text{H}_2\text{O}}} \cdot \left( \frac{p}{p_0} \right)^{0.5} \right)$$

or with: 
$$V^0 = \frac{-\Delta_f g^{0, \text{mol}}}{n \cdot F}$$

$$V_{\text{rev}} = V^0 + \frac{R^{\text{mol}} \cdot T}{n \cdot F} \cdot \ln \left( \frac{y_{\text{H}_2} \cdot y_{\text{O}_2}^{0.5}}{y_{\text{H}_2\text{O}}} \cdot \left( \frac{p}{p_0} \right)^{0.5} \right) \quad (13)$$

In the case of the hydrogen-oxygen reaction the number of electrons per fuel molecule is 2. This equation and the resulting equations derived in the next chapter for specific fuel cells are called “Nernst equations”.

### 3 NERNST EQUATIONS FOR SPECIFIC FUEL CELLS

The Nernst equations of various fuel cells are not exactly the same. They might differ because of differences of the ions transported through the electrolyte and the cell reactions. In this chapter it shown how the actual Nernst equations for the PEMFC, the MCFC and the SOFC are derived.

#### The proton exchange membrane fuel cell (PEMFC)

The electrolyte of the PEMFC is an ion conducting polymer. Today

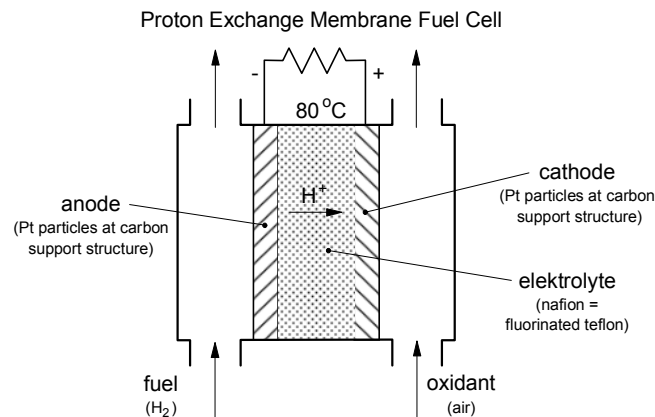


Figure 5 The principle of the PEMFC

<sup>3</sup> With regard to values and dimensions of these parameters:

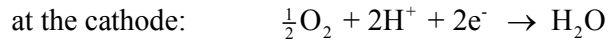
A mole of substance always has the same number of entities (e.g. molecules), the Avogadro number:

$N_A = 6.022137 \times 10^{26} \text{ kmol}^{-1}$ . The charge of 1 electron is:  $e = 1.602177 \times 10^{-19} \text{ C}$  (Coulomb is the unit of

charge) and a kmol of electrons equals  $6.022137 \times 10^{26}$  electrons. The Faraday constant represents the charge of 1 mole or kmol electrons, thus:  $F = N_A \cdot e = 6.022137 \times 10^{26} \times 1.602177 \times 10^{-19} = 96485 \times 10^3 \text{ C/kmol}$ .

(1 Coulomb = 1 A · s ; 1 V · A · s = 1 J)

Nafion, a registered trademark of Dupont, is usually applied. The principle of the PEMFC is shown in Figure 5. In this figure also the usual applied materials for the electrodes are mentioned. Operating temperature are usually not higher than 80°C. For appropriate operation of the fuel cell nafion should contain a certain amount of water. It might be necessary to humidify the fuel and air flow to control the water balance within the fuel cell. This will reduce the reactant concentrations. Hydrogen protons are generated at the anode and transferred through the electrolyte to the cathode. At the cathode hydrogen protons react with oxygen forming water. The reactions are:



Water is generated at the cathode. However, the water is not simply discharged to the cathode flow. Water transport in the cell might occur because of the drag of water from the anode to the cathode by protons moving through the electrolyte. But water may also diffuse back from the cathode to the anode if the humidity at the cathode is higher than at the anode. The net water transport is not easily to predict.

With the reactions at anode and cathode as presented the Nernst equation of the PEMFC can be derived from Equation 13:

$$V_{\text{rev}} = V^0 + \frac{R^{\text{mol}} \cdot T}{2 \cdot F} \cdot \ln \left( \frac{y_{\text{H}_2, (\text{a})} \cdot y_{\text{O}_2, (\text{c})}^{0.5}}{y_{\text{H}_2\text{O}, (\text{c})}} \cdot \left( \frac{p}{p_0} \right)^{0.5} \right) \quad (14)$$

In the case of the PEMFC the equation is the same as Equation 13, only is indicated whether the concentrations at the anode or the cathode side have to be used.

#### The molten carbonate fuel cell (MCFC)

The electrolyte of the MCFC is a molten mixture of alkali metal carbonates e.g. a binary mixture of lithium and potassium. This is retained in a ceramic matrix of  $\text{LiAlO}_2$ . The MCFC operates at temperatures of 600-700°C. At these high temperatures the alkali carbonates form a highly conductive molten salt. As shown in Figure 6 the charge transfer through the electrolyte occurs by  $\text{CO}_3^{2-}$  ions from cathode to anode. To generate these ions at the cathode oxygen as well as carbon dioxide should be available in the cathode gas. At the anode the  $\text{CO}_3^{2-}$  ions react

with hydrogen into water and carbon dioxide. The reactions are:

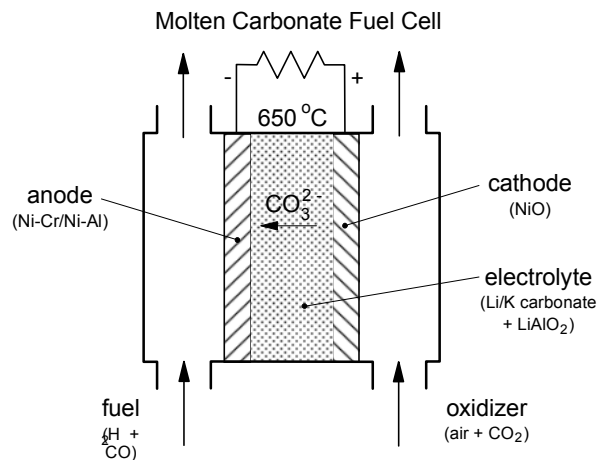
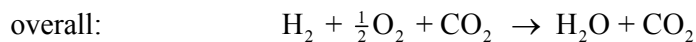


Figure 6 The principle of the MCFC

## Appendix 6.1



The reaction products  $\text{H}_2\text{O}$  and  $\text{CO}_2$  come free at the anode and are discharged by the anode flow.

With the reactions at anode and cathode as presented the following Nernst equation of the MCFC can be derived:

$$V_{\text{rev}} = V^0 + \frac{R^{\text{mol}} \cdot T}{2 \cdot F} \cdot \ln \left( \frac{y_{\text{H}_2, (a)} \cdot y_{\text{O}_2, (c)}^{0.5} \cdot y_{\text{CO}_2, (c)}}{y_{\text{H}_2\text{O}, (c)} \cdot y_{\text{CO}_2, (a)}} \cdot \left( \frac{p}{p_0} \right)^{0.5} \right) \quad (15)$$

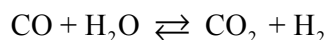
In the case of the MCFC also the concentrations of carbon dioxide have to be considered in the Nernst equation. Carbon dioxide acts as a reactant at the cathode and as a product at the anode. The concentrations at anode and cathode will be different in general.  $\text{CO}_2$  is absorbed at the cathode, thus the concentration of  $\text{CO}_2$  along the cathode will decrease. At the anode  $\text{CO}_2$  is formed. In the case of a carbon containing fuel more  $\text{CO}_2$  will be formed at the anode than is absorbed at the cathode.

#### The solid oxide fuel cell (SOFC)

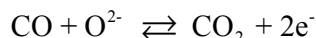
The SOFC uses an ion-conducting ceramic material as the electrolyte. SOFC's are primarily based on an electrolyte of zirconia ( $\text{ZrO}_2$ ) stabilized with a small percentage of yttria ( $\text{Y}_2\text{O}_3$ ). At high temperatures ( $> 800^\circ\text{C}$ ) zirconia is a good oxygen-ion ( $\text{O}^{2-}$ ) conductor. Zirconia based SOFC's operate at temperatures between  $800\text{-}1000^\circ\text{C}$ . Air can be used as oxidizer at the cathode. Oxygen molecules are converted into oxygen-ions at the cathode-electrolyte interface. The oxygen-ions move through the electrolyte to the anode as can be seen in Figure 7. At the electrolyte-anode interface the oxygen-ions react with hydrogen from the fuel gas into water (vapor). The reactions are:



If the fuel gas contains also carbon monoxide, the CO might be converted into hydrogen due to the following equilibrium reaction:



Thus, one mole of carbon monoxide will deliver one mole hydrogen that can be converted in the cell. But CO is also directly converted at the anode due to the reaction:



Which processes actually happen in the cell is not easy to observe. The two options are thermodynamically similar. In the case of system calculations it is usually assumed that carbon monoxide is converted first into hydrogen.

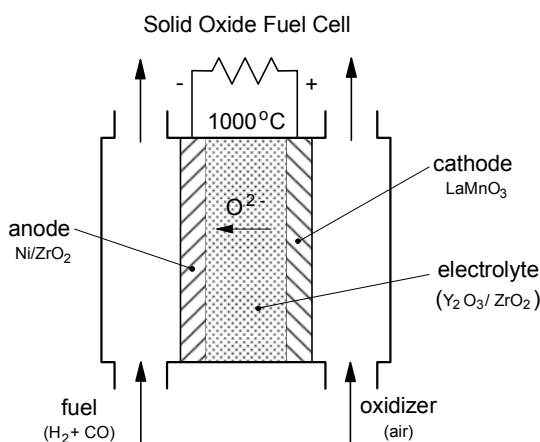


Figure 7 The principle of the SOFC

With the reactions at the cathode and anode as presented the Nernst equation of the SOFC can be written as follows:

$$V_{\text{rev}} = V^0 + \frac{R^{\text{mol}} \cdot T}{2 \cdot F} \cdot \ln \left( \frac{y_{\text{H}_2, (\text{a})} \cdot y_{\text{O}_2, (\text{c})}^{0.5}}{y_{\text{H}_2\text{O}, (\text{a})}} \cdot \left( \frac{p}{p_0} \right)^{0.5} \right) \quad (16)$$

In this case water is generated at the anode, thus, the water concentration at the anode has to be used in the denominator.

The cell voltage at standard pressure ( $V^0$ ) can easily be calculated. With the following values at 25°C:

$$\Delta_f h_{298, \text{H}_2\text{O} (\text{g})}^{0, \text{mol}} = -241.83 \text{ kJ/mol}$$

$$s_{298, \text{H}_2\text{O} (\text{g})}^{0, \text{mol}} = 0.18872 \text{ kJ}/(\text{mol K})$$

$$s_{298, \text{H}_2}^{0, \text{mol}} = 0.13057 \text{ kJ}/(\text{mol K})$$

$$s_{298, \text{O}_2}^{0, \text{mol}} = 0.20503 \text{ kJ}/(\text{mol K})$$

the change of Gibbs free energy of the water formation reaction is:

$$\Delta_f g_{298, \text{H}_2\text{O} (\text{g})}^{0, \text{mol}} = 228.60 \text{ kJ/mol}$$

Then, the reversible voltage at standard pressure and 25°C becomes:

$$V^0 = \frac{-\Delta_f g_{298, \text{H}_2\text{O}}^{0, \text{mol}}}{n \cdot F} = \frac{228.60}{2 \times 96486.7} = 1.18 \text{ V}$$

If the reaction occurs at higher temperatures the change of Gibbs free energy will decrease and also the reversible voltage. The effect of the reaction temperature (cell temperature) on the reversible voltage is shown in Figure 8. As the work from the cell is proportional with the voltage, also the work will decrease. However, the heat from the fuel is almost independent from the reaction temperature. Thus, at higher temperatures the reversible work from the fuel decreases and the heat from the reversible reaction increases. If it should be possible to convert the total enthalpy into work, the “equivalent cell voltage” should be 1.25 V. The ratio of the reversible voltage and this “equivalent cell voltage” equals the work to heat ratio of the reversible cell. Figure 8 shows that in the case of high temperature fuel cells the reversible cell voltage is lower than in the case of low temperature fuel cells. However, the irreversible losses are in general higher at lower temperatures.

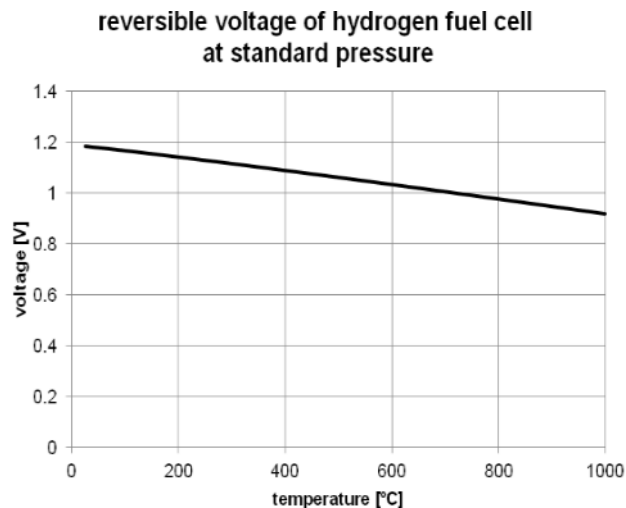


Figure 8 The reversible cell voltage at standard pressure as function of the reaction temperature

## Appendix 6.1

## 4 IRRIVERSIBLE FUEL CELLS

## 4.1 Introduction

The cell voltage of real fuel cells is in general significantly lower than the reversible cell voltage. In Figure 9 an example of the actual  $i, V$ -curve of a fuel cell is shown. The reversible cell voltage ( $V_{rev}$ ) is represented by the dotted line at the top of the diagram. For the

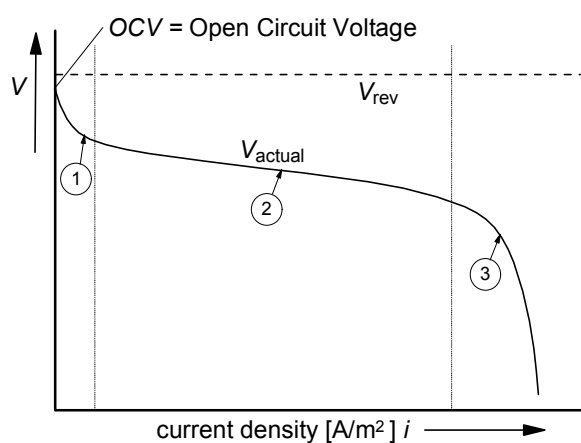


Figure 9 The  $i, V$ -curve of a real fuel cell

difference between the actual voltage and the reversible voltage different names are used like polarization, overvoltage or overpotential, irreversibility, losses and voltage drop. The different names originate from the various disciplines involved in fuel cell development. For a discussion of the thermodynamic performance just thermodynamic losses or irreversibility's are considered to be most appropriate. The deviation of the actual voltage from the reversible voltage originates from various phenomena. With increasing current density different phenomena are dominating the irreversibility's. In Figure 9 three regions are distinguished. In region 1 the irreversibility's are primarily caused by activation losses. Even at zero current density the measured cell voltage, the open circuit voltage (OCV), is usually lower than the reversible voltage. The initial increase of the current density causes a rapid fall of the cell voltage. This rapid fall results from the slowness of the reactions taking place on the surface of the electrodes. In region 2 the voltage falls more slowly and the  $i, V$ -curve is fairly linear. The irreversibility's in this region are dominated by the resistance of the flow of ions in the electrolyte and the flow of electrons through the electrodes. The voltage drop is essentially proportional to current density and is therefore called an ohmic loss. At higher current densities, in region 3, the irreversibility's are dominated by losses due to mass transport, the transport of reactants to the surface of the electrodes and of reaction products from the electrodes. Mass transport loss is considered to be an appropriate name for these losses. Since this results in deviations from the composition of the bulk fluid these losses are also called concentration losses. As the effect of such losses is modeled by the Nernst equation, the mass transport losses are sometimes indicated as Nernst losses. Another cause of losses, not indicated

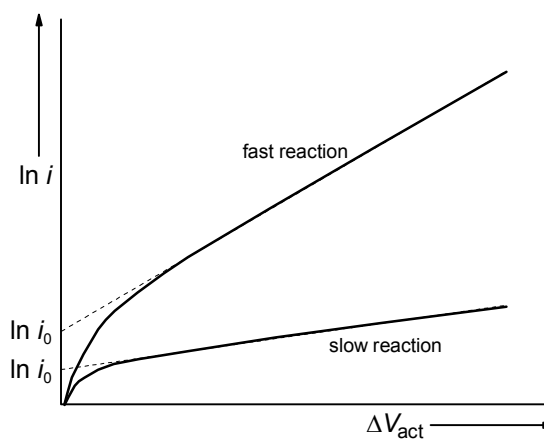


Figure 10 Tafel plots for slow and fast electrochemical reactions

in Figure 9, are the fuel crossover and internal currents. The electrolyte has to be made such that it will not conduct electrons and it must be gas tight. In actual fuel cells, however, the diffusion of fuel and the flow of electrons cannot always be avoided completely. A more comprehensive description of the various losses is presented in the following sections.

## 4.2 Activation losses

Similar as in chemical reactions the reaction species in an electrochemical reaction have to overcome an activation energy. In the case of an electrochemical reaction as in a fuel cell this results into a voltage drop<sup>4</sup>. From experiments with a great variety of electrochemical reactions, Tafel observed a similar pattern, as shown in a slightly modified way in Figure 10. The  $\ln i / \Delta V_{\text{act}}$ -plots are called Tafel plots and are used to determine  $i_0$ , the exchange current density. The value for  $i_0$  is found by the intercept of the extrapolated best fit line and the  $\ln i$  axis at  $\Delta V_{\text{act}} = 0$ . The current density  $i_0$  is actually the current density at which the voltage drop begins to move from zero. The so-called Tafel plot can be described by the following equation:

$$\Delta V_{\text{act}} = C_1 \cdot \ln\left(\frac{i}{i_0}\right) \quad (17)$$

This equation is true only if  $i > i_0$ . For a slow reaction the constant  $C_1$  is higher and for a fast reaction the constant  $i_0$  is higher. Further theoretical considerations have shown that the constant  $C_1$  can be replaced as follows:

$$\Delta V_{\text{act}} = \frac{R^{\text{mol}} \cdot T}{2 \cdot \alpha \cdot F} \cdot \ln\left(\frac{i}{i_0}\right) \quad (18)$$

The constant  $\alpha$  is called the charge transfer coefficient. Its value must be in the range of 0 to 1.0 and depends on the reaction involved and the material the electrode is made from. If a fuel cell has no other losses than the activation loss, the voltage can be given by the equation:

$$V = V_{\text{rev}} - \frac{R^{\text{mol}} \cdot T}{2 \cdot \alpha \cdot F} \cdot \ln\left(\frac{i}{i_0}\right) \quad (19)$$

In general the activation losses have to be determined for both the anode and the cathode. The values for each of the electrodes can be highly different. The overall activation loss of the fuel can be calculated with the equation:

$$\Delta V_{\text{act, cell}} = \frac{R^{\text{mol}} \cdot T}{2 \cdot \alpha_{\text{an}} \cdot F} \cdot \ln \frac{i}{i_{0, \text{an}}} + \frac{R^{\text{mol}} \cdot T}{2 \cdot \alpha_{\text{cat}} \cdot F} \cdot \ln \frac{i}{i_{0, \text{cat}}} \quad (20)$$

This equation can be expressed as:

$$\Delta V_{\text{act, cell}} = C_1 \cdot \ln \frac{i}{b} \quad (21)$$

<sup>4</sup> The voltage drop is described by electro-chemist as an overvoltage. In the case of a fuel cell an overvoltage reduces the actual cell voltage. The overvoltage is usually indicated as a voltage ( $V$ ). Here it is presented as a voltage difference ( $\Delta V$ ).

## Appendix 6.1

Where:

$$C_1 = \frac{R^{\text{mol}} \cdot T}{2 \cdot \alpha_{\text{an}} \cdot F} + \frac{R^{\text{mol}} \cdot T}{2 \cdot \alpha_{\text{cat}} \cdot F} = C_{1, \text{an}} + C_{1, \text{cat}} \quad (22)$$

and:

$$b = i_{0, \text{an}} \left( \frac{1}{\frac{\alpha_{\text{an}}}{1 + \alpha_{\text{cat}}}} \right) + i_{0, \text{cat}} \left( \frac{1}{\frac{\alpha_{\text{cat}}}{1 + \alpha_{\text{an}}}} \right) = i_{0, \text{an}} \left( \frac{C_{1, \text{an}}}{C_1} \right) + i_{0, \text{cat}} \left( \frac{C_{1, \text{cat}}}{C_1} \right) \quad (23)$$

In low and intermediate temperature fuel cells the activation loss is the most important irreversibility. The value of the exchange current density  $i_0$  is primarily determining the height of the activation losses. In the case of hydrogen fuel cells it occurs mainly at the cathode. The activation losses become less important at higher temperatures and pressures.

### 4.3 Ohmic losses

The ohmic losses is a fuel cell do include losses due the voltage drop in the electrodes and electrical connections but also due to the resistance of the transfer of ions in the electrolyte. It is actually a loss due to various phenomena which results into a quasi ohmic loss, a loss that can be characterized as an ohmic loss. Therefore, the quasi electrical resistance is called here the equivalent cell resistance ( $R_{\text{equiv}}$ ). The quasi ohmic losses are proportional to the current, thus, the voltage drop due to the quasi ohmic resistance can be written as:

$$\Delta V_{\text{ohm}} = i \cdot R_{\text{equiv}} \quad (24)$$

The equivalent cell resistance includes electronic, ionic and contact resistances, thus, in principle:

$$R_{\text{equiv}} = R_{\text{electronic}} + R_{\text{ionic}} + R_{\text{contact}}$$

The current density  $i$  (in  $\text{A}/\text{m}^2$ ) is used instead of the total current through the cell in order to be consistent with the other equations for voltage losses. Then, the resistance must be represented by the area specific resistance  $R_{\text{equiv}}$  (in  $\Omega \cdot \text{m}^2$ ). In proper fuel cells the cell equivalent resistance is dominated by the ionic resistance of the electrolyte. The actual resistance depends on various parameters like operating pressure and temperature, the fluid compositions, cell design and dimensions, materials and manufacturing. Impedance spectroscopy can be used to determine the equivalent cell resistance<sup>5</sup>.

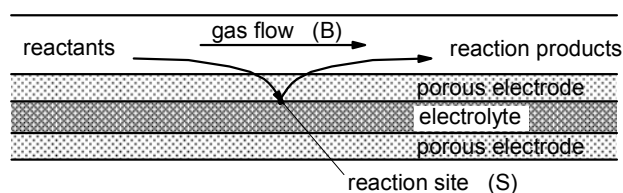


Figure 11 Cross-section of a fuel cell

<sup>5</sup> Sometimes researchers define area specific resistances that include the ohmic losses as well as the activation and concentration losses.

#### 4.4 Mass transport losses

In the cross-section of a fuel cell as shown in Figure 11 the electrolyte with the two electrodes and one gas channel are depicted. The electrodes have to be porous to allow the gas to flow to the actual reaction sites. The reaction occurs at sites where electrolyte and electrode are in contact with each other. These sites are inside the porous electrode. Therefore, reactants from the bulk gas flow (B) in the gas channel have to move through the electrode to the reaction sites (S) and eventually reaction products have to move from the reaction sites in the electrode back to the bulk gas flow in the channel. If the reactants are supplied in a gas mixture the conversion of reactants at the reaction sites might reduce the partial pressure at the location of the reaction sites in comparison with the bulk flow in the gas channel. The lower partial pressure, or lower concentration, of the reactants will result into a lower cell voltage. Since air is normally used at the cathode concentration losses will also occur at the cathode. The mass transport from the bulk flow to the reaction sites is in general controlled by diffusion. In the case of low temperature fuel cells liquid water can be available in the pores of the electrode which might affect the transport of reactants and reaction products. Diffusion of the reactants from the bulk flow to a reaction site can be described by Fick's first law:

$$i = \frac{n \cdot F \cdot D \cdot (p_{i,B} - p_{i,S})}{\delta} \quad (25)$$

In this equation is  $D$  the diffusion coefficient of the reacting specie,  $p_{i,B}$  its partial pressure in the bulk flow and  $p_{i,S}$  its partial pressure at the reaction site. The thickness of the diffusion layer  $\delta$  is the actual transport distance of the specie. From Equation 25 it is obvious that a higher current density will require a higher difference in partial pressure between the bulk flow and the reaction site. The maximum current density is achieved if the partial pressure at the reaction site ( $p_{i,S}$ ) is zero. This maximum current density is called the limiting current:

$$i_1 = \frac{n \cdot F \cdot D \cdot p_{i,B}}{\delta} \quad (26)$$

Combining Equations 25 and 26 results into:

$$\frac{p_{i,S}}{p_{i,B}} = 1 - \frac{i}{i_1} \quad (27)$$

The voltage loss caused by the difference in partial pressure  $p_{i,B} - p_{i,S}$  between the bulk gas and the reaction site can be determined by applying the Nernst equation:

$$\Delta V_{\text{mass transp}} = V_{\text{rev}, p_i=p_{i,B}} - V_{\text{rev}, p_i=p_{i,S}} = \frac{R^{\text{mol}} \cdot T}{n \cdot F} \cdot \ln \left( \frac{p_{i,S}}{p_{i,B}} \right)^{-1} \quad (28)$$

Replacing the pressure ratio of Equation 27 in this equation gives:

$$\Delta V_{\text{mass transp}} = \frac{R^{\text{mol}} \cdot T}{n \cdot F} \cdot \ln \left( 1 - \frac{i}{i_1} \right)^{-1} \quad (29)$$

When using this equation it must be realized that  $n = 2$  in the case of hydrogen and  $n = 4$  in the case of oxygen. This equation can be written too as:

## Appendix 6.1

$$\Delta V_{\text{mass transp}} = -C_2 \cdot \ln \left( 1 - \frac{i}{i_1} \right) \quad (30)$$

in which  $C_2$  is constant at the considered temperature. From practical experiences it appears that in general the voltage loss calculated with Equation 29 deviates seriously from measured values. Therefore, it is necessary to use values for the constant  $C_2$  that deviate from the theoretical value. Obviously the value of  $C_2$  must include the mass transport effects at the anode as well as at the cathode.

#### 4.5 Losses due to fuel crossover and internal currents

As mentioned before the electrolyte should be gas tight and not able to conduct electrons. In actual fuel cells this cannot always be realized completely. Conduction of small amounts of electrons might occur and some hydrogen might diffuse through the electrolyte from the anode to the cathode. In practical fuel cells hydrogen diffusion is probably the most important. This diffusion is called fuel crossover. The hydrogen that diffuses through the electrolyte will react directly with oxygen at the cathode without contributing to the external current of the cell. The two phenomena, internal current and fuel crossover, are essentially equivalent. Therefore, the fuel crossover is usually assigned to as an internal current. The equivalence of the internal currents and the fuel crossover is just an approximation. For practical calculations, however, it appears to be useful.

Because of the internal current the actual cell current is not zero, even if the external current is zero. That means that also in the case of an open circuit the internal current density has a positive value. This explains the deviation of the OCV from the theoretical cell voltage. Thus, the actual current density in the cell is higher than the current density calculated from the external current. If  $i_n$  is the current density because of the internal currents and fuel crossover,  $i$  the current density based on the external current and  $i_{\text{act}}$  the actual current density, then:

$$i_{\text{act}} = i + i_n \quad (31)$$

The higher current density might affect the various losses discussed in the previous sections.

#### 4.6 Actual cell performance

The actual cell voltage equals the reversible cell voltage minus the various voltage losses which can be written as:

$$V_{\text{cell}} = V_{\text{rev}} - \Delta V_{\text{act, cell}} - \Delta V_{\text{ohm}} - \Delta V_{\text{mass transp}} \quad (32)$$

Combining this equation with the Equations 21, 24 and 30 the following equation for the actual cell voltage is achieved:

$$V_{\text{cell}} = V_{\text{rev}} - C_1 \cdot \ln \frac{i}{b} - i \cdot R_{\text{equiv}} + C_2 \cdot \ln \left( 1 - \frac{i}{i_1} \right) \quad (33)$$

The constant  $b$  is the exchange current density of the cell as discussed in Section 4.2. The effect of internal currents and fuel crossover can be taken into account by replacing the

external current  $i$  through the actual current as presented by Equation 31. Then, Equation 33 can be written as:

$$V_{\text{cell}} = V_{\text{rev}} - C_1 \cdot \ln \frac{i+i_n}{b} - (i+i_n) \cdot R_{\text{equiv}} + C_2 \cdot \ln \left( 1 - \frac{i+i_n}{i_1} \right) \quad (34)$$

constant	units	Low temperature (PEMFC)	High temperature (SOFC)
$V_{\text{rev}}$	V	1.18	1.0
$i_n$	A/m <sup>2</sup>	20	20
$R_{\text{equiv}}$	Ω.m <sup>2</sup>	3*10 <sup>-6</sup>	30*10 <sup>-6</sup>
$b$	A/m <sup>2</sup>	0.67	3000
$C_1$	V	0.06	0.03
$C_2$	V	0.05	0.08
$i_1$	A/m <sup>2</sup>	9000	9000

This equation can be used to depict the  $i, V$ -curve of a fuel cell if the necessary constants are known. In Table 1 constants are presented for reference cases of a low temperature fuel cell, e.g. a PEMFC, and a high temperature fuel, e.g. an SOFC. The data are taken from [7.1]; only for the

reversible voltage of the low temperature fuel cell a value of 1.18 was used instead of 1.20. These data are used here to discuss some characteristics of  $i, V$ -curves.

The  $i, V$ -curve of a PEMFC based on the data of Table 1 is presented in Figure 12. The curve clearly shows the high initial voltage drop due to the activation losses which are primarily determined by the constant  $C_1$  and the exchange current density  $b$ . Since the internal current density  $i_n = 20$  is higher than the exchange current density  $b = 0.67$  the term  $i+i_n$  is always higher than the exchange current density. Thus, the second term of Equation 34 is valid for all considered external current densities. At high current densities the curve shows a fast decrease of the cell voltage. A limiting current of  $i_1 = 9000$  was used. Since the last term of Equation 34 is only valid if  $i+i_n < i_1$ , then

$i < 8980 \text{ A/m}^2$ . Higher current densities cannot be achieved in this case. For current densities in between 2000 and 7000 A/m<sup>2</sup> the curve is almost linear. Within this range the voltage drop with increasing current density is dominated by the equivalent cell resistance ( $R_{\text{equiv}}$ ).

The  $i, V$ -curve of a SOFC based on the data of Table 1 is shown in Figure 13 as the reference curve. The problem with this curve is, however,

**$i, V$ -curve PEMFC**  
(reference conditions)

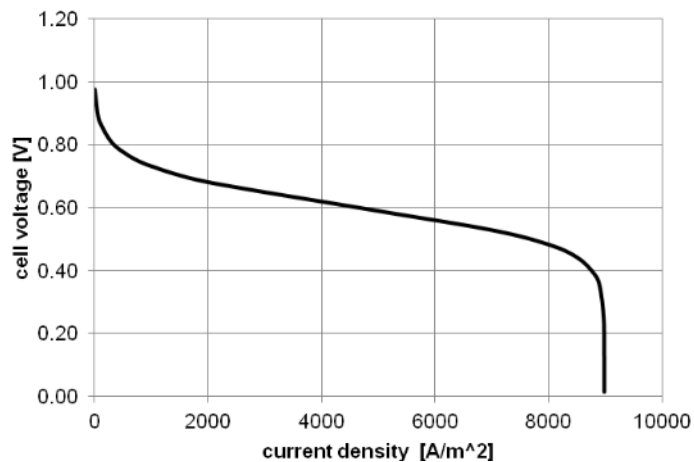


Figure 12 The  $i, V$ -curve of a PEMFC based on the data for a reference case

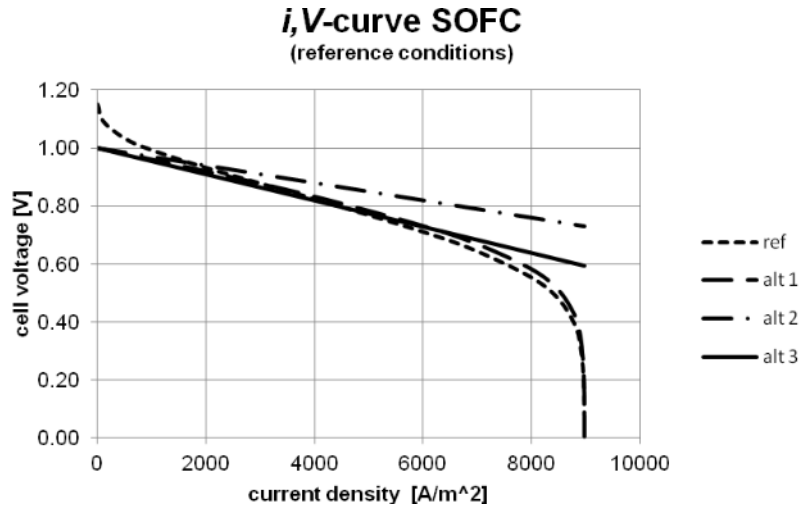


Figure 13 The  $i, V$ -curves of a SOFC based on the data for a reference case and 3 alternatives

that the second term of Equation 34 is valid only if  $i + i_n > b$  which means that the curve is only true for current densities higher than  $2980 \text{ A/m}^2$ . The second term represents the activation loss. In general the activation losses are very small at high temperatures and are often ignored for practical evaluations. The resulting curve (for  $C_1 = 0$ ) is presented in Figure 13 as alternative 1. It appears that the deviation from the reference curve is very small for higher current densities (the valid area of the reference curve). For practical fuel cell operation high cell voltages are preferred because of the efficiency targets. Operation near to the limiting current has to be avoided for that reason. To simplify the modeling of high temperature fuel cells the last term of Equation 34 is often ignored too. Then, the following equation can be used:

$$V_{\text{cell}} = V_{\text{rev}} - (i + i_n) \cdot R_{\text{equiv}} \quad (35)$$

If  $R_{\text{equiv}} = 30 \times 10^{-6} \Omega \cdot \text{m}^2$ , then the curve of alternative 1 in Figure 13 is obtained. The calculated cell voltages are significantly higher than for the reference curve and alternative 1. An increase of the equivalent cell resistance with 50% ( $R_{\text{equiv}} = 45 \times 10^{-6} \Omega \cdot \text{m}^2$ ) gives the curve of alternative 3. It appears that the curve of alternative 3 fits quite well with the curve of alternative 1 within the range of current densities from  $1000$  to  $7000 \text{ A/m}^2$ . Thus, Equation 35 can be applied for high temperature fuel cells provided that the equivalent cell resistant is determined in an appropriate way.

#### 4.7 The effect of fuel utilization

All fuel cells as mentioned so far are hydrogen fuel cells or they behave like hydrogen fuel cells. High temperature fuel cells are usually fueled by gas mixture containing hydrogen. As the fuel flows along the anode area the hydrogen is converted while the other components in the gas remain unaffected. Depending on the type of fuel cell the gas might become diluted by reaction products from the reaction zone at the anode. The concentration of the hydrogen

in the fuel gas will change when flowing from anode inlet to anode outlet. And thus the reversible cell voltage will change according to the Nernst equation, e.g. for the SOFC (Equation 16):

$$V_{\text{rev}} = V^0 + \frac{R^{\text{mol}} \cdot T}{2 \cdot F} \cdot \ln \left( \frac{y_{\text{H}_2, (\text{a})} \cdot y_{\text{O}_2, (\text{c})}^{0.5}}{y_{\text{H}_2\text{O}, (\text{a})}} \cdot \left( \frac{p}{p_0} \right)^{0.5} \right) \quad (16)$$

In Figure 14 the reversible cell voltage is shown as a function of the fuel utilization in the case of a high temperature fuel cell. The curve is depicted for a fuel utilization from  $u_F = 0$  to  $u_F = 1$ , the case of total utilization of the hydrogen in the fuel. As the reversible cell voltage ( $V_{\text{rev}}$ ) must be higher than the actual cell voltage ( $V_{\text{cell}}$ ) total utilization is not possible, thus in real fuel cells the utilization at the anode outlet must be lower than 1. Values between 0.8 and 0.9 are achievable. This means that not all fuel can be converted in the fuel cell.

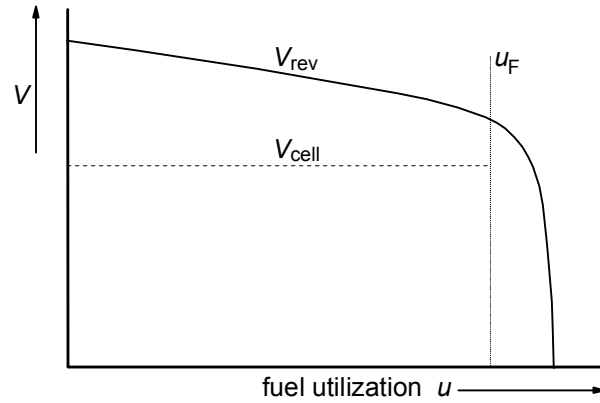


Figure 14 Cell voltage as function of the fuel utilization (for a high temperature fuel cell)

Unconverted fuel can be combusted in an after burner. Appropriate system design should enable efficient use of this heat.

The fuel utilization ( $u_F$ ) is defined as the fraction of the fuel, that enters the anode area, that is converted at the anode. If it is assumed that hydrogen and carbon monoxide can react at the anode and hydrogen, carbon monoxide and methane are the components in the fuel that can be converted in the fuel cell, the utilization can be defined as:

$$u_F = \frac{\sum (n_{\text{H}_2} + n_{\text{CO}})_{\text{converted}}}{\sum (n_{\text{H}_2} + n_{\text{CO}} + n_{\text{CH}_4})_{\text{in}}} \quad (36)$$

Equation 35 can be used to determine the cell current density:

$$i + i_n = \frac{V_{\text{rev}}(u_F) - V_{\text{cell}}}{R_{\text{equiv}}}$$

Obviously, as the reversible cell voltage changes with the fuel utilization while the actual cell voltage is constant, also the current density will decrease along the anode area. The current density must be integrated over the anode area to determine the total current through the cell.

In the case of low temperature fuel cells, e.g. the PEMFC, pure hydrogen is often used as the fuel. The hydrogen might contain some water vapor because of the water balance of the electrolyte. In principle 100% hydrogen conversion can be achieved in the PEMFC. In practice the periodic blow-off of anode gas appears to be necessary to avoid the storage of inert gases in the anode chamber.

## 5 FUEL CELL OPERATION

Fuel cells are developed for operation at very different temperatures from around 70°C for the alkaline and proton exchange membrane (solid polymer) fuel cells up to 1000°C for the solid electrolyte fuel cell. The low temperature fuel cells have the advantage of a higher reversible cell voltage but it appears that the irreversible losses are in general higher at low temperatures as roughly indicate in Figure 15. Therefore, the actual cell voltages are not strongly depending on the operation temperature. The performance of low temperature fuel cells is negatively affected by the presence of even small concentrations of carbon monoxide and sulfur in the fuel. Serious cleaning of the fuel gas is necessary for trouble-free operation. At higher temperatures fuel cells are less sensitive for these components but even a few ppm of sulfur might affect the performance of high temperature fuel cells, the MCFC as well as the SOFC.

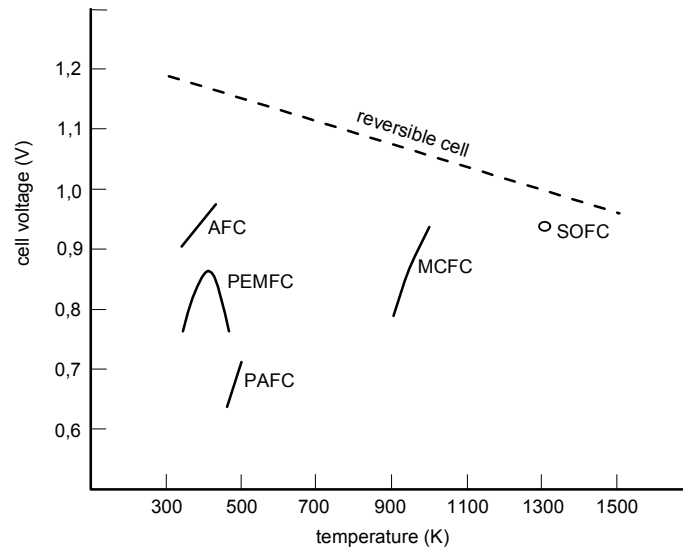


Figure 15 Indication of the performance of various fuel cells

The thermodynamic losses of a fuel cell are determined by the difference between the actual voltage and the reversible voltage of the cell. Thus, the fuel cell efficiency<sup>6</sup> can be defined by the ratio of the actual cell voltage and the reversible cell voltage:

$$\eta_{FC} = \frac{V_{\text{cell}}}{V_{\text{rev}}} \quad (37)$$

In the case of fuel cells with a fuel utilization lower than 1.0 the unconverted fuel might result into additional losses. Whether it is a loss or not depends on the processes that are used for the conversion of the residual fuel. Thus, it should not be considered as a loss of the fuel cell. The reversible work from a fuel cell is defined by the Equations 11 and 12. Since  $n \cdot F$  is the charge of one mole or kmol of fuel, the work is presented here as a molar value:

$$W_{FC, \text{rev}}^{\text{mol}} = n \cdot F \cdot V_{\text{rev}} \quad (38)$$

Then, the actual work from the fuel cell becomes:

$$W_{FC}^{\text{mol}} = \eta_{FC} \cdot n \cdot F \cdot V_{\text{rev}} = n \cdot F \cdot V_{\text{cell}} \quad (39)$$

<sup>6</sup> This ratio can be considered to be the ratio of the actual work and the reversible work from the fuel cell. Thus, it might be considered to be the exergy efficiency but it is certainly not the thermal efficiency of the fuel cell.

The thermal efficiency of the fuel cell is defined as the generated work divided by the heating value of the fuel:

$$\eta_{th,FC} = \frac{W_{FC}^{mol}}{LHV_F^{mol}} = \frac{n \cdot F \cdot V_{cell}}{LHV_F^{mol}} \quad (40)$$

In the case of a hydrogen fuel cell the conversion of one mole (or kmol) of hydrogen must be considered. Combining Equations 10, 11 and 12 gives:

$$n \cdot F \cdot V_{rev} = -\Delta g^{mol} \quad (41)$$

Then, Equation 40 can be written as:

$$\eta_{th,FC} = -\frac{\Delta g^{mol}}{LHV_F^{mol}} \cdot \frac{V_{cell}}{V_{rev}} \quad (42)$$

Apparently, the efficiency as defined by Equation 37 must be multiplied with (the absolute value) the ratio of  $\Delta g$  and  $LHV$  to find the thermal efficiency. In the case of a hydrogen fuel cell operating at standard conditions and a temperature of 25°C this ratio becomes (see also Chapter 3):

$$-\frac{\Delta g^{mol}}{LHV_F^{mol}} = \frac{\Delta g^{mol}}{\Delta_f h_{298, H_2O(g)}^{0, mol}} = \frac{228.60}{241.83} = 0.9453$$

That means that even in the case of ideal operation the thermal efficiency cannot reach 100%.

For the design of a fuel cell system the design parameters of the fuel cell have to be chosen such that a high efficiency will be achieved at reasonable fuel cell costs. A useful optimization of the fuel cell parameters requires the availability of all relevant data. Only for specific design studies this will be the case. A general discussion of some important aspects might be helpful to understand the evaluations that have to be done. Therefore, a fuel cell with idealized cell behavior as shown in Figure 16 is considered first. According to Equation 35 the cell voltage decreases linearly with the current density. In this equation the limiting current is already ignored. If also the fuel cross-over and the internal current are assumed to be zero, the cell voltage is a straight line described by the following equation:

$$V_{cell} = V_{rev} - i \cdot R_{equiv}$$

At  $i = 0$  the voltage curve intersects the vertical axis at  $V_{cell} = V_{rev}$ . The cell voltage decreases with increasing current density and will be zero as the product  $i \cdot R_{equiv}$  equals the reversible cell voltage. The electrical power generated by the fuel cell is the product of the cell voltage and the total current through the cell and can be written as:

$$P_{cell} = I \cdot V_{cell} = i \cdot A_{cell} \cdot V_{cell} \quad (43)$$

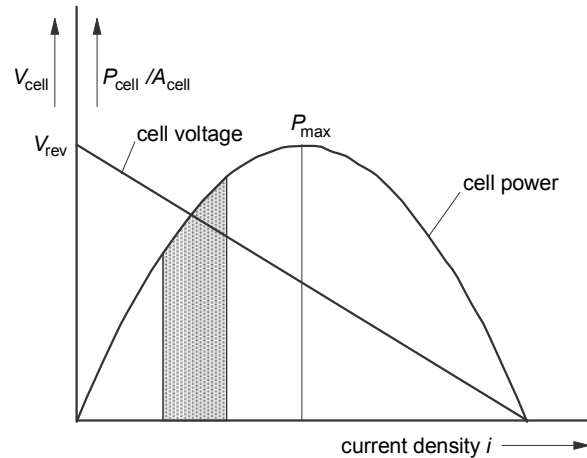


Figure 16 Cell voltage and power as function of the current density (for assumed linear  $i, V$ -curve)

## Appendix 6.1

In this equation  $A_{\text{cell}}$  is the active cell area which is used here as a constant. In Figure 16 the specific cell power ( $P_{\text{cell}} / A_{\text{cell}}$ ) is depicted as a function of the current density. Then, at zero current density the specific cell power will be zero. If the current density increases from zero also the specific power will increase. With increasing current density, however, the cell voltage will decrease. The lower cell voltage will moderate the specific power at higher current densities causing a maximum at the current density at which the cell voltage is 50% of the reversible cell voltage. A further increase of the current density will result in a decrease of the generated power by the fuel cell. In the extreme case that the cell voltage is zero the specific cell power will also be zero. From Equation 42 it is obvious that high cell efficiencies require high cell voltages and thus low current densities. At low current densities also the specific power is low. The price of fuel cells is in principle proportional with the cell area. Thus, low area specific power will result into high power specific costs. Minimum power specific costs are achieved at  $P_{\text{cell}} = P_{\text{max}}$  but at that point the cell efficiency is rather low. The optimum design current density should be not too low but anyhow lower than the current density at which  $P_{\text{cell}} = P_{\text{max}}$ . Usually the optimum value of the current density will be within the shaded area in Figure 16.

The behavior of high temperature fuel cells corresponds reasonably with the idealized behavior as discussed before. The behavior of low temperature fuel cells in general differs seriously. In Figure 17 the cell power is added to the diagram of the cell voltage as presented in Figure 12 for a reference case. From this diagram it will be obvious that optimum current densities have to be lower than around  $7000 \text{ A/m}^2$  and higher than  $3000 \text{ A/m}^2$ .

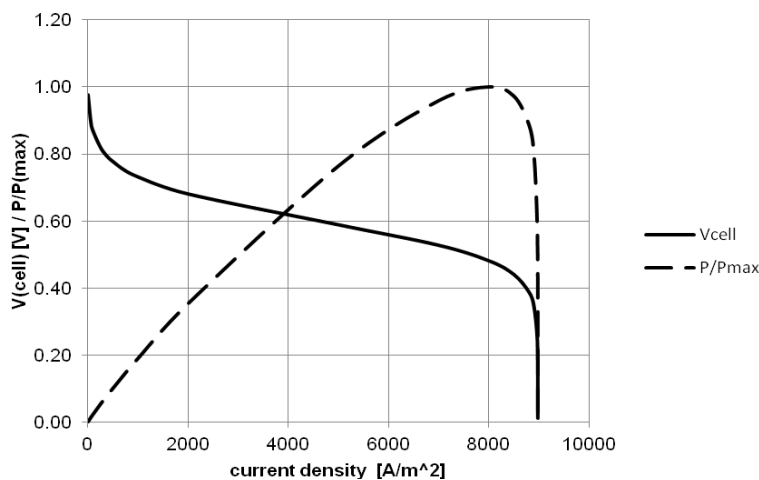


Figure 17 Cell voltage and power as function of the current density for the  $i, V$ -curve of the PEMFC reference case



**APPENDIX 6.2****CONVERSION OF MOLAR RATIOS INTO MASS RATIOS FOR DIFFERENT FUELS**

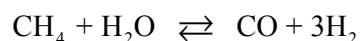
For the design of fuel conversion processes the steam to carbon ratio (S/C) and oxygen to carbon ratio (O/C) are important design parameters. These ratios are usually specified as molar ratios. The development of Cycle-Tempo has been started by mechanical engineers who are using mass flows and also mass ratios for the specification of flow rates. Furthermore, in the process calculations fuel, steam and air are used as the reactants. Thus, the molar ratios S/C and O/C have to be converted into mass ratios  $m_{\text{steam}}/m_{\text{fuel}}$  and  $m_{\text{air}}/m_{\text{fuel}}$  respectively. The respective conversion factors are calculated for two different fuels: pure methane (CH<sub>4</sub>) and Slochteren natural gas. The necessary data for Slochteren natural gas are shown in Table 1. The data for standard air with a temperature of 15°C and a relative humidity of 60% are presented in Table 2.

component	molar mass [kg/kmol]	mole fraction	mass fraction
CH <sub>4</sub>	16.043	0.8129	0.6997
C <sub>2</sub> H <sub>6</sub>	30.069	0.0287	0.0463
C <sub>3</sub> H <sub>8</sub>	44.096	0.0038	0.0090
C <sub>4</sub> H <sub>10</sub>	58.123	0.0015	0.0047
C <sub>5</sub> H <sub>12</sub>	72.150	0.0004	0.0016
C <sub>6</sub> H <sub>14</sub>	86.177	0.0005	0.0023
N <sub>2</sub>	28.0134	0.1432	0.2152
O <sub>2</sub>	31.9988	0.0001	0.0002
CO <sub>2</sub>	44.010	0.0089	0.0210
total	18.637	1.0000	1.0000

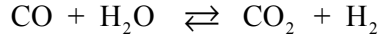
component	molar mass [kg/kmol]	mole fraction	mass fraction
N <sub>2</sub>	28.0134	0.7729	0.7504
O <sub>2</sub>	31.9988	0.2075	0.2301
H <sub>2</sub> O	18.0153	0.0101	0.0063
Ar	39.948	0.0092	0.0127
CO <sub>2</sub>	44.010	0.0003	0.0005
total	28.8541	1.0000	1.0000

Conversion of pure methane

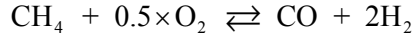
In the case of steam reforming of methane 1 mole of methane reacts with 1 mole of steam into 1 mole of carbon monoxide and 3 moles of hydrogen, due to the following reaction equation:



If sufficient steam has to be available to convert also the carbon monoxide into carbon dioxide in the subsequent shift reaction another mole of steam is required per mole of carbon:



In the case of autothermal reforming the conversion of methane is a mixture of the steam reforming reaction and the partial oxidation reaction:



Since a part of the methane is converted by the partial oxidation reaction, less steam is necessary in the case of the autothermal reforming process.

The mass ratio steam to fuel can be written as:

$$\frac{m_{\text{H}_2\text{O}}}{m_{\text{fuel}}} = \frac{M_{\text{H}_2\text{O}}}{M_{\text{fuel}}} \cdot \frac{n_{\text{H}_2\text{O}}}{n_{\text{fuel}}} = \frac{M_{\text{H}_2\text{O}}}{M_{\text{CH}_4}} \cdot \frac{n_{\text{H}_2\text{O}}}{n_{\text{C}}} = \frac{18.0153}{16.043} \times \frac{n_{\text{H}_2\text{O}}}{n_{\text{C}}} \quad (1)$$

thus: 
$$\frac{m_{\text{H}_2\text{O}}}{m_{\text{fuel}}} = 1.123 \times \frac{n_{\text{H}_2\text{O}}}{n_{\text{C}}}$$

Since:  $n_{\text{fuel}} = n_{\text{CH}_4} = n_{\text{C}}$

And the mass ratio air to fuel can be written as:

$$\frac{m_{\text{air}}}{m_{\text{fuel}}} = \frac{M_{\text{air}}}{M_{\text{fuel}}} \cdot \frac{n_{\text{air}}}{n_{\text{fuel}}} = \frac{M_{\text{air}}}{M_{\text{CH}_4}} \cdot \frac{n_{\text{air}}}{n_{\text{O}_2}} \cdot \frac{n_{\text{O}_2}}{n_{\text{C}}} = \frac{28.8541}{16.043} \times \frac{1}{0.2075} \times \frac{n_{\text{O}_2}}{n_{\text{C}}} \quad (2)$$

thus: 
$$\frac{m_{\text{air}}}{m_{\text{fuel}}} = 8.668 \times \frac{n_{\text{O}_2}}{n_{\text{C}}}$$

In the case of complete conversion of methane the stoichiometric steam to carbon ratio is 2. Practical steam to carbon ratios are in general higher to assure that the formation of solid carbon is avoided. Usual values for the S/C ratio are between 2.0 and 3.5. Thus, in the case of methane, the mass ratio steam to fuel should be within the range of 2.246 and 3.930 (roughly 2.5 and 4.0).

In the case of autothermal reforming a wide range of S/C ratios are proposed in the literature from 1.1 up to 3.5. But usual values seem to be between 1.1 and 2.0. These values correspond with steam to fuel mass ratios of 1.235 to 2.246 (roughly 1.3 to 2.5). The air to fuel ratios in the case of ATR depend on the reaction temperature; they can be converted into oxygen to carbon ratios with Equation (2).

#### Conversion of Slochteren natural gas

In the case of Slochteren natural gas  $n_{\text{fuel}} \neq n_{\text{C}}$  since:

$$\frac{n_{\text{C}}}{n_{\text{fuel}}} = \sum x \cdot n_{\text{C}_x\text{H}_y} + n_{\text{CO}_2} = 0.8927 + 0.0089 = 0.9016 \quad (3)$$

For the mass ratio steam to fuel can be written:

$$\frac{m_{\text{H}_2\text{O}}}{m_{\text{fuel}}} = \frac{M_{\text{H}_2\text{O}}}{M_{\text{fuel}}} \cdot \frac{n_{\text{H}_2\text{O}}}{n_{\text{fuel}}} = \frac{M_{\text{H}_2\text{O}}}{M_{\text{fuel}}} \cdot \frac{n_{\text{C}}}{n_{\text{fuel}}} \cdot \frac{n_{\text{H}_2\text{O}}}{n_{\text{C}}} = \frac{18.0153}{18.637} \times 0.9016 \times \frac{n_{\text{H}_2\text{O}}}{n_{\text{C}}} \quad (4)$$

thus: 
$$\frac{m_{\text{H}_2\text{O}}}{m_{\text{fuel}}} = 0.8715 \times \frac{n_{\text{H}_2\text{O}}}{n_{\text{C}}}$$

And the air to fuel ratio can be written as:

## Appendix 6.2

$$\frac{m_{\text{air}}}{m_{\text{fuel}}} = \frac{M_{\text{air}}}{M_{\text{fuel}}} \cdot \frac{n_{\text{air}}}{n_{\text{fuel}}} = \frac{M_{\text{air}}}{M_{\text{fuel}}} \cdot \frac{n_{\text{air}}}{n_{\text{O}_2}} \cdot \frac{n_{\text{C}}}{n_{\text{fuel}}} \cdot \frac{n_{\text{O}_2}}{n_{\text{C}}} = \frac{28.8541}{18.637} \times \frac{1}{0.2075} \times 0.9016 \times \frac{n_{\text{O}_2}}{n_{\text{C}}} \quad (5)$$

thus: 
$$\frac{m_{\text{air}}}{m_{\text{fuel}}} = 6.727 \times \frac{n_{\text{O}_2}}{n_{\text{C}}}$$

In the case of SR usual values for the S/C ratio are between 2.0 and 3.5. The usual values for the steam to fuel ratios then are between 1.743 and 3.050 (roughly between 1.8 and 3.0).

In the case of ATR usual values of the S/C ratio are between 1.1 and 2.0. Usual value for the steam to fuel ratios then are between 0.957 and 1.743 (roughly between 1.0 and 1.8). The air to fuel ratios in the case of ATR depend on the reaction temperature; they can be converted into oxygen to carbon ratios with Equation (2).



**APPENDIX 6.3****CALCULATION OF THE SOFC TARGET SYSTEM WITH CYCLE-TEMPO**

Input data and results of the Cycle-Tempo calculation of the SOFC target system are shown in this Appendix. The system diagram with pipe numbers and apparatus numbers is presented in Figure 1. In this diagram also the three considered subsystems, the fuel cell subsystem, the gas turbine subsystem, and the heat recovery subsystem, are outlined. The input data of the Cycle-Tempo calculation are shown in Table 1. The results from the Cycle-Tempo calculation are presented in the Tables 2-12. The exergy balances of the subsystems needed to draw the exergy flow diagram are presented in Table 13.

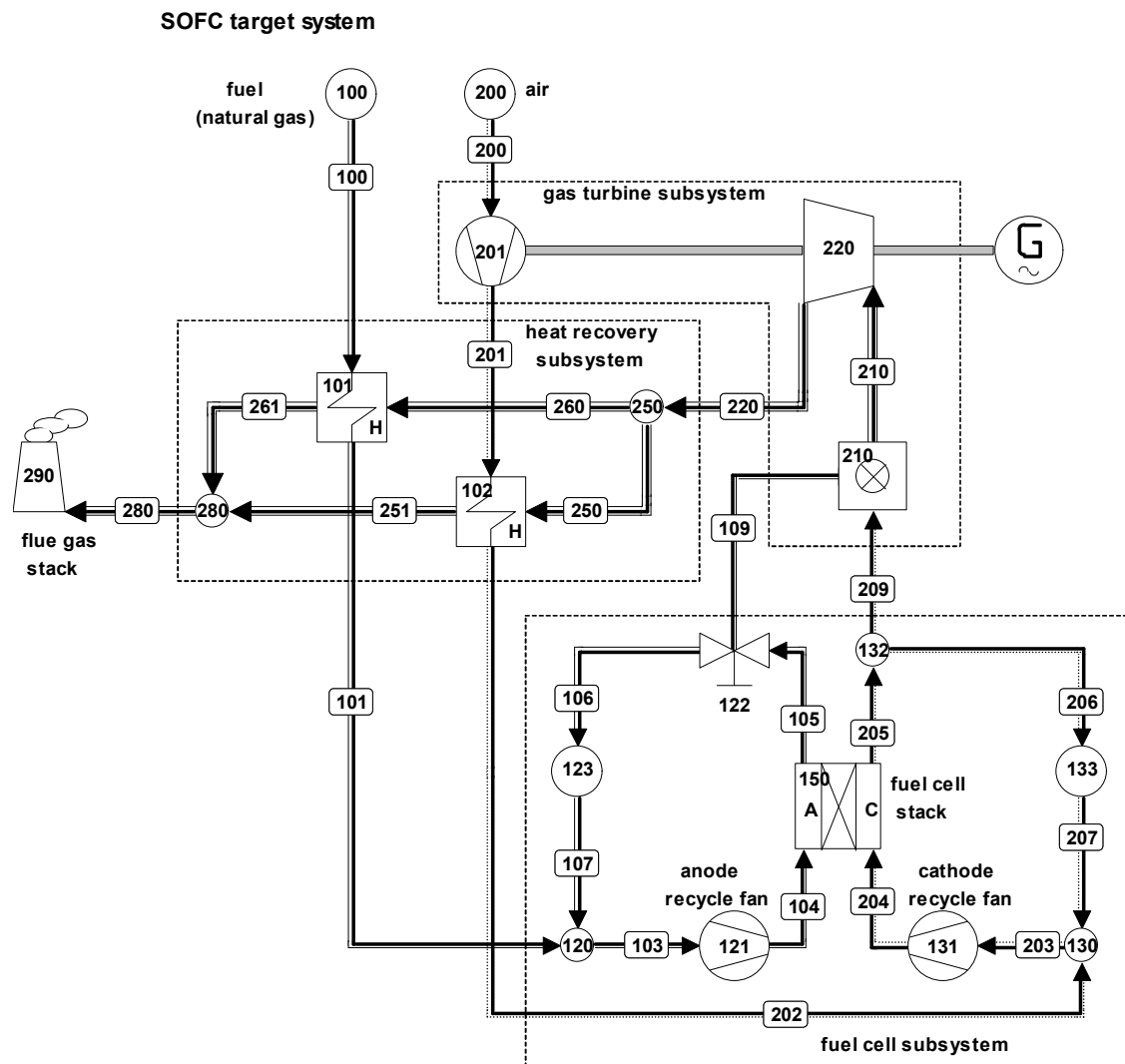


Figure 1 System diagram SOFC target system

Table 1 Input data

Description	
System data:	NAPP=19, NLIN=24, NCYCLE=1, NPRODF=1, MAXITM=50, NPRINT=4
Apparatus:	NO=100, TYPE=10, APNAME='Sink/Source', TOUT= 15, DELM= 1
Apparatus:	NO=101, TYPE=12, APNAME='Heat Exchgr.', DELP1=0.16, DELP2=0.02, TOUT2= 110
Apparatus:	NO=102, TYPE=6, APNAME='Heat Exchgr.', DELP1=0.16, DELP2=0.02
Apparatus:	NO=120, TYPE=9, APNAME='Node', DELP=0
Apparatus:	NO=121, TYPE=29, APNAME='Compressor', ETHAI=0.8
Apparatus:	NO=122, TYPE=14, APNAME='Valve', DELP=0, PIPE= 106, FLOW= 6.178 kg/s
Apparatus:	NO=123, TYPE=10, APNAME='Sink/Source', DELP=0, DELH=0
Apparatus:	NO=130, TYPE=9, APNAME='Node', DELP=0
Apparatus:	NO=131, TYPE=29, APNAME='Compressor', ETHAI=0.8
Apparatus:	NO=132, TYPE=14, APNAME='Valve', DELP=0, PIPE= 206, FLOW=0.64 of mass flow in pipe 205
Apparatus:	NO=133, TYPE=10, APNAME='Sink/Source', DELP=0, DELH=0
Apparatus:	NO=150, TYPE=21, APNAME='Fuel Cell', FCTYPE='SOFC-DIR', DELPAN=0.16, TINAN= 650, TOUTPS= 750, DELPCA=0.16, TINCA= 650, DCAC=0.97, PFCCELL= 8, TFCCELL= 700, UFL=0.8, ESTMFL= 1, ESTMOX= 20
Apparatus:	NO=200, TYPE=10, APNAME='Sink/Source', POUT= 1.01325, TOUT= 15
Apparatus:	NO=201, TYPE=29, APNAME='Compressor', PRATI= 8, ETHAI=0.8415, ETHAM=0.99
Apparatus:	NO=210, TYPE=13, APNAME='Combustor', DELP=0.16, ESTOFR= 4, TREAT= 1000, PREAT= 8
Apparatus:	NO=220, TYPE=3, APNAME='Turbine', TUCODE=0, GDCODE= 1, ETHAI=0.9133, ETHAM=0.99
Apparatus:	NO=250, TYPE=9, APNAME='Node'
Apparatus:	NO=280, TYPE=9, APNAME='Node'
Apparatus:	NO=290, TYPE=10, APNAME='Stack', PIN= 1.01325
Generator:	NO=1, IGAPP=220, ETAGEN=0.98
Medium:	Pipe No = 100, Type = 'GASMIX' Standard Natural Gas
Medium:	Pipe No = 107, Type = 'GASMIX', Estimation Specie = H2O Mole % = 100
Medium:	Pipe No = 200, Type = 'GASMIX' Standard Air
Medium:	Pipe No = 207, Type = 'GASMIX', Estimation Standard Air
Shaft:	IPUMP=201, ITURBP=220
Production Func.:	Apparatus 101, Power = 0
User subroutines:	Apparatus numbers: 201,220
Name of user executable:	C:\Documents and Settings\Administrator\Mijn documenten\prom\CT files\CT-SOFC-target\circ02\UserSub\Debug\
Geometry data:	Apparatus NO=150, FCTYPE='SOFC-DIR', FLOW=0, RCELL=5e-05, ACELL= 10000
Environment:	User defined environment
	Environment composition:
	Specie = AR CL2 CO2 H2O N2 O2 S(S)
	Mole % = 0.91 0.01 0.03 1.68 76.76 20.6 0.01
	Environment pressure: 1.01325 bar
	Environment temperature: 15 °C
	Heating values calculated at 1 atm, 25 °C
State functions for water/steam calculation: IAPWS Industrial Formulation 1997 (IAPWS-IF97)	

## Appendix 6.3

No.	Apparatus	Type	Energy [kW]	Totals [kW]	Exergy [kW]	Totals [kW]
Absorbed power	100	Sink/Source	37999.18		39653.27	
				37999.18		39653.27
Delivered gross power	1	Generator	4256.1		4256.1	
	150	Fuel Cell	27140.38		27140.38	
				31396.49		31396.49
Aux. power consumption	121	Compressor	64.23		64.23	
	131	Compressor	269.72		269.72	
				333.95		333.95
Delivered net power						
				31062.54		31062.54
Efficiencies	gross		82.62%		79.18%	
	net		81.75%		78.34%	

No.	Name	Type	Energy loss (enthalpy) [kW]	Energy loss (HHV) [kW]	Energy loss (LHV) [kW]
220	Turbine	3	8757.61	8757.61	8757.61
102	Heat Exchgr.	6	0	0	0
120	Node	9	0	-0.71	-0.49
130	Node	9	0	-0.02	-0.01
250	Node	9	0	0	0
280	Node	9	0	0	0
123	Sink/Source	10	0	0	0
133	Sink/Source	10	0	0	0
200	Sink/Source	10	1514.39	-238.17	0
100	Sink/Source	10	3642.08	-42107.15	-37999.18
290	Stack	10	-37301.08	10245.66	5859.46
101	Heat Exchgr.	12	-0.26	-0.26	-0.26
210	Combustor	13	0	-3.87	1.34
122	Valve	14	0	0	0
132	Valve	14	0	0	0
150	Fuel Cell	21	27979.77	27939.43	27974.04
121	Compressor	29	-56.97	-56.97	-56.97
131	Compressor	29	-251.75	-251.75	-251.75
201	Compressor	29	-4283.79	-4283.79	-4283.79
	Total:		0	0	0

Composition number	1	2	3	4	5	6	7
CH <sub>4</sub>	0.8129	0.1461	0.0002				
C <sub>2</sub> H <sub>6</sub>	0.0287	0.0052					
C <sub>3</sub> H <sub>8</sub>	0.0038	0.0007					
C <sub>4</sub> H <sub>10</sub>	0.0015	0.0003					
C <sub>5</sub> H <sub>12</sub>	0.0004	0.0001					
C <sub>6</sub> H <sub>14</sub>	0.0005	0.0001					
N <sub>2</sub>	0.1432	0.0679	0.0514	0.7729	0.8628	0.9231	0.7136
O <sub>2</sub>	0.0001	0		0.2075	0.1154	0.0534	0.0266
CO <sub>2</sub>	0.0089	0.2446	0.2962	0.0003	0.0003	0.0004	0.0828
H <sub>2</sub> O		0.4458	0.5433	0.0101	0.0113	0.0121	0.1686
AR				0.0092	0.0103	0.011	0.0083
H <sub>2</sub>		0.0668	0.0815				
H <sub>2</sub> S							
CO		0.0225	0.0274				
HCl							
C(S)		0	0				0
SO <sub>2</sub>							
Avg. molemass [kg/kmol]	18.64	24.02	25.2	28.85	28.49	28.24	27.86
LHV [kJ/mol]	708.3	149.78	27.58	0	0	0	0
HHV [kJ/mol]	784.88	166.48	31.18	0	0	0	0

Composition number	LHV [kJ/kg]	HHV [kJ/kg]	LHV (without water) [kJ/kg]	HHV (without water) [kJ/kg]
1	37999.18	42107.15	37999.18	42107.15
2	6235.84	6931.02	9367.55	10411.86
3	1094.48	1237.25	1789.58	2023.02
4	0	0	0	0
5	0	0	0	0
6	0	0	0	0
7	0.01	0.01	0.02	0.02

## Appendix 6.3

*Table 6 Data for all pipes*

Pipe no.	Medium	Flow			Press. [bar]	Temp. [°C]	Enthalpy [kJ/kg]	Entropy [kJ/kg.K]	Exergy [kJ/kg]
		Mass [kg/s]	Mole [kmol/s]	Volume [m <sup>3</sup> /s]					
100	GASMIX 1	1	0.054	0.15858	8.106	15	-3642.08	9.4321	39653.27
				0.15858	8.106	15	-3642.08	9.4321	39653.27
101	GASMIX 1	1	0.054	0.3146	7.946	287.2	-3035.59	10.8963	39837.86
				0.3146	7.946	287.2	-3035.59	10.8963	39837.86
103	GASMIX 2	7.178	0.299	2.8719	7.946	645.92	-8025.66	9.6109	7376.26
				2.8719	7.946	645.92	-8025.66	9.6109	7376.26
104	GASMIX 2	7.178	0.299	2.8278	8.106	650	-8017.72	9.6126	7383.7
				2.8278	8.106	650	-8017.72	9.6126	7383.7
105	GASMIX 3	9.943	0.395	4.2218	7.946	750	-8833.38	9.1765	2186.99
				4.2218	7.946	750	-8833.38	9.1765	2186.99
106	GASMIX 3	6.178	0.245	2.6232	7.946	750	-8833.38	9.1765	2186.99
				2.6232	7.946	750	-8833.38	9.1765	2186.99
107	GASMIX 3	6.178	0.245	2.6232	7.946	750	-8833.38	9.1765	2186.99
				2.6232	7.946	750	-8833.38	9.1765	2186.99
109	GASMIX 3	3.765	0.149	1.5986	7.946	750	-8833.38	9.1765	2186.99
				1.5986	7.946	750	-8833.38	9.1765	2186.99
200	GASMIX 4	15.32	0.531	12.554	1.013	15	-98.85	6.8652	0.15
				12.554	1.013	15	-98.85	6.8652	0.15
201	GASMIX 4	15.32	0.531	3.0553	8.106	287.89	180.77	6.9474	256.09
				3.0553	8.106	287.89	180.77	6.9474	256.09
202	GASMIX 4	15.32	0.531	4.2073	7.946	484.16	390.98	7.274	372.17
				4.2073	7.946	484.16	390.98	7.274	372.17
203	GASMIX 5	37.64	1.321	12.681	7.946	644.13	562.52	7.4916	495.7
				12.681	7.946	644.13	562.52	7.4916	495.7
204	GASMIX 5	37.64	1.321	12.51	8.106	650	569.21	7.4931	501.97
				12.51	8.106	650	569.21	7.4931	501.97
205	GASMIX 6	34.875	1.235	13.22	7.946	750	680.26	7.6071	590.24
				13.22	7.946	750	680.26	7.6071	590.24
206	GASMIX 6	22.32	0.79	8.4606	7.946	750	680.26	7.6071	590.24
				8.4606	7.946	750	680.26	7.6071	590.24
207	GASMIX 6	22.32	0.79	8.4606	7.946	750	680.26	7.6071	590.24
				8.4606	7.946	750	680.26	7.6071	590.24
209	GASMIX 6	12.555	0.445	4.7591	7.946	750	680.26	7.6071	590.24
				4.7591	7.946	750	680.26	7.6071	590.24
210	GASMIX 7	16.32	0.586	7.6203	7.786	945.05	-1514.52	8.2506	877.52
				7.6203	7.786	945.05	-1514.52	8.2506	877.52

*Table 6 Data for all pipes (continued)*

Pipe no.	Medium	Flow			Press. [bar]	Temp. [°C]	Enthalpy [kJ/kg]	Entropy [kJ/kg.K]	Exergy [kJ/kg]
		Mass [kg/s]	Mole [kmol/s]	Volume [m <sup>3</sup> /s]					
220	GASMIX 7	16.32	0.586	37.792	1.033	528.59	-2051.14	8.3158	322.1
				37.792	1.033	528.59	-2051.14	8.3158	322.1
250	GASMIX 7	15.08	0.541	34.922	1.033	528.59	-2051.14	8.3158	322.1
				34.922	1.033	528.59	-2051.14	8.3158	322.1
251	GASMIX 7	15.08	0.541	27.729	1.013	351.17	-2264.69	8.0209	193.54
				27.729	1.013	351.17	-2264.69	8.0209	193.54
260	GASMIX 7	1.24	0.044	2.8708	1.033	528.59	-2051.14	8.3158	322.1
				2.8708	1.033	528.59	-2051.14	8.3158	322.1
261	GASMIX 7	1.24	0.044	1.3985	1.013	110	-2540.16	7.4645	78.4
				1.3985	1.013	110	-2540.16	7.4645	78.4
280	GASMIX 7	16.32	0.586	29.152	1.013	333.33	-2285.61	7.9869	182.41
				29.152	1.013	333.33	-2285.61	7.9869	182.41

*Table 7 Energy and exergy flows in the pipes*

Pipe no.	ENERGY			EXERGY		
	Total [kW]	Thermo Mechanical [kW]	Chemical [kW]	Total [kW]	Thermo Mechanical [kW]	Chemical [kW]
100	42107.15	0	42107.15	39653.27	267.31	39385.96
	42107.15	0		39653.27	267.31	
101	42713.64	606.49	42107.15	39837.86	451.89	39385.96
	42713.64	606.49		39837.86	451.89	
103	63321.38	13570.51	49750.87	52946.78	6012.75	46934.04
	63321.38	13570.51		52946.78	6012.75	
104	63378.35	13627.48	49750.87	53000.19	6066.16	46934.04
	63378.35	13627.48		53000.19	6066.16	
105	33165.27	20863.35	12301.93	21745.18	9255.69	12489.49
	33165.27	20863.35		21745.18	9255.69	
106	20607.03	12963.31	7643.72	13511.22	5750.96	7760.26
	20607.03	12963.31		13511.22	5750.96	
107	20607.03	12963.31	7643.72	13511.22	5750.96	7760.26
	20607.03	12963.31		13511.22	5750.96	
109	12558.25	7900.04	4658.2	8233.95	3504.73	4729.23
	12558.25	7900.04		8233.95	3504.73	
200	238.17	238.17	0	2.23	0	2.23
	238.17	238.17		2.23	0	

## Appendix 6.3

*Table 7 Energy and exergy flows in the pipes*

Pipe no.	ENERGY			EXERGY		
	Total [kW]	Thermo Mechanical [kW]	Chemical [kW]	Total [kW]	Thermo Mechanical [kW]	Chemical [kW]
201	4521.97	4521.97	0	3923.35	3921.13	2.23
	4521.97	4521.97		3923.35	3921.13	
202	7742.42	7742.42	0	5701.67	5699.44	2.23
	7742.42	7742.42		5701.67	5699.44	
203	25996.34	25996.34	0	18657.94	18560.79	97.15
	25996.34	25996.34		18657.94	18560.79	
204	26248.09	26248.09	0	18893.96	18796.81	97.15
	26248.09	26248.09		18893.96	18796.81	
205	28521.74	28521.74	0	20584.53	20299.57	284.96
	28521.74	28521.74		20584.53	20299.57	
206	18253.91	18253.91	0	13174.1	12991.72	182.37
	18253.91	18253.91		13174.1	12991.72	
207	18253.91	18253.91	0	13174.1	12991.72	182.37
	18253.91	18253.91		13174.1	12991.72	
209	10267.83	10267.83	0	7410.43	7307.84	102.58
	10267.83	10267.83		7410.43	7307.84	
210	22829.94	22829.71	0.24	14321.11	13622.13	698.98
	22829.94	22829.71		14321.11	13622.13	
220	14072.34	14072.1	0.24	5256.69	4557.71	698.98
	14072.34	14072.1		5256.69	4557.71	
250	13003.38	13003.16	0.22	4857.39	4211.5	645.88
	13003.38	13003.16		4857.39	4211.5	
251	9782.94	9782.72	0.22	2918.57	2272.69	645.88
	9782.94	9782.72		2918.57	2272.69	
260	1068.95	1068.94	0.02	399.31	346.21	53.1
	1068.95	1068.94		399.31	346.21	
261	462.72	462.7	0.02	97.19	44.09	53.1
	462.72	462.7		97.19	44.09	
280	10245.66	10245.42	0.24	2976.91	2277.93	698.98
	10245.66	10245.42		2976.91	2277.93	

No.	Name	Type	Exergy transferred from system [kW]			Relative Exergy Loss [%]	Exergy efficiency [%]	Univ. Exergy efficiency [%]
			Total	Power or Heat	Losses			
220	Turbine	3	9064.42	8670.03	394.39	0.99	95.65	97.25
102	Heat Exchgr.	6	160.5	0	160.5	0.4	91.72	98.17
120	Node	9	402.3	0	402.3	1.01		99.25
130	Node	9	217.83	0	217.83	0.55		98.85
250	Node	9	0	0	0	0		100
280	Node	9	38.85	0	38.85	0.1		98.71
123	Sink/Source	10	0	0	0	0		100
133	Sink/Source	10	0	0	0	0		100
101	Heat Exchgr.	12	117.53	0	117.53	0.3	61.1	99.71
210	Combustor	13	1323.27	0	1323.27	3.34	67.98	91.54
122	Valve	14	0	0	0	0		100
132	Valve	14	0	0	0	0		100
150	Fuel Cell	21	29564.45	27140.38	2424.07	6.11	91.8	96.63
121	Compressor	29	-53.41	-64.23	10.82	0.03	83.16	99.98
131	Compressor	29	-236.02	-269.72	33.7	0.08	87.51	99.82
201	Compressor	29	-3921.13	-4327.07	405.94	1.02	90.62	90.62
	Medium to/from env.							
200	Sink/Source	10	-2.23	0	-2.23	-0.01		
100	Sink/Source	10	-39653.27	-39653.27	0	0		
290	Stack	10	2976.91	0	2976.91	7.51		
	Total:		0	-8503.87	8503.87	21.44		

## Appendix 6.3

App.	Name	Type	Isentropic efficiency	Mechanical efficiency
no.			[%]	[%]
220	Turbine	3	91.33	99.0
121	Compressor	29	80.0	100.0
131	Compressor	29	80.0	100.0
201	Compressor	29	84.15	99.0

No.	Name	Type	Mechanical efficiency [%]	Electrical efficiency [%]	Mechanical*Electrical efficiency [%]
1	Generator	G			98.0
121	Compressor	29			88.70
131	Compressor	29			93.34

App. no.	Name	Type	Low end temperature diff. [K]	High end temperature diff. [K]	Transmitted heat flow [kW]
102	Heat Exchgr.	6	63.28	44.43	3220.45
101	Heat Exchgr.	12	95	241.39	606.49

Apparatus nr. 150		units	
cell voltage		[V]	0.8390
current density		[A/m <sup>2</sup> ]	3334.83
cell area		[m <sup>2</sup> ]	10000
cell resistance		[Ω m <sup>2</sup> ]	0.00005
		[Ω cm <sup>2</sup> ]	0.5
power density		[kW/m <sup>2</sup> ]	2.7980
stack	DC-power	[kW]	27979.7738
	AC-power	[kW]	27140.3806
fuel utilization/pass		[-]	0.8000
O <sub>2</sub> utilization/pass		[-]	0.5670

<i>Table 13 Exergy balances subsystems SOFC target system</i>			
	[kW]	[kW]	[%]
<b>FUEL CELL SUBSYSTEM</b>			
Exergy in			
pipe 101	39837.86		100.47
pipe 202	5701.67		14.38
electrical power	333.95		0.84
total in		<b>45873</b>	<b>115.69</b>
Exergy out			
pipe 109	8233.95		20.76
pipe 209	7410.43		18.69
electrical power	27140.38		68.44
total out		<b>42785</b>	<b>107.90</b>
Exergy loss		<b>3089</b>	<b>7.79</b>
<b>GAS TURBINE SUBSYSTEM</b>			
Exergy in			
pipe 109	8233.95		20.76
pipe 209	7410.43		18.69
pipe 200	2.23		0.01
total in		<b>15647</b>	<b>39.46</b>
Exergy out			
pipe 201	3923.35		9.89
pipe 220	5256.69		13.26
electrical power	4256.10		10.73
total out		<b>13436</b>	<b>33.88</b>
Exergy loss		<b>2210</b>	<b>5.57</b>
<b>HEAT RECOVERY SUBSYSTEM</b>			
Exergy in			
pipe 100	39653.27		100.00
pipe 201	3923.35		9.89
pipe 220	5256.69		13.26
total in		<b>48833</b>	<b>123.15</b>
Exergy out			
pipe 101	39837.86		100.47
pipe 202	5701.67		14.38
pipe 280	2976.91		7.51
total out		<b>48516</b>	<b>122.35</b>
Exergy loss		<b>317</b>	<b>0.80</b>

## **APPENDIX 7.1**

### **OFF-DESIGN EVALUATION OF CHP SYSTEMS**

#### **1 INTRODUCTION**

CHP plants are designed to generate two products: electricity as well as heat. The electricity demand as well as the heat demand are in general independent and are varying continuously. Depending on the application and the operational conditions the actual plant operating point is determined by the heat demand or the power demand. The optimum operation point depends on the availability of alternative generation capacity in the case of larger systems or in the case of single plants on the connections with a heat distribution system and the electricity grid together with the tariffs for import and export of heat and electricity.

In the case of large industrial plants, power and heat are usually generated in a central power station consisting of one or more CHP units, power generating units and boilers. The connection with the grid enables in many cases only the import of electricity. The export or import of heat is getting more interest but the number of applications is limited. In the nineties several CHP plants have been built by industry in cooperation with power companies. Industrial Combined Cycle plants with steam extraction (see Section 4.2.2) appeared to be favorable for this purpose. These plants deliver power to the public grid while the heat is delivered to the industrial plant. Since the subsidy regulations have been changed it is no longer attractive to build this kind of plants. Saturated steam is often used to distribute heat to the various heat consumers at industrial plants. Optimum operation of an industrial CHP plant depends on a variety of, in general very specific, conditions for the considered plant. It is not usual in industrial plants today to increase the freedom of generation by the application of heat storage.

Large district heating systems are supplied in general by a number of large CHP plants, usually steam turbine plants and combined cycle plants. These plants offer high flexibility with regard to the heat to power ratio. Their low maximum heat to power ratio is in general not a problem because they primarily generate power for the public grid. Auxiliary boilers are used sometimes to generate additional heat. Optimum operating conditions require custom-made solutions.

Small scale systems consisting of a single CHP unit require careful optimization first of all in the design phase but also during operation. It is obvious that the accurate assessment of the electricity and heat demand is very important for these optimizations. Usually the electricity and heat demand of the considered consumer are available for this purpose in a load duration curve. However, this curve does not provide all information necessary for an appropriate optimization of the plant in the design phase. In this appendix the application of the heat to power matrix will be proposed<sup>1</sup>. Further it will be explained how the heat to power

---

<sup>1</sup> The heat to power matrix was originally proposed by employees of Heineken Zoeterwoude. Together with TU Delft possibilities for more general application have been investigated.

matrix can be combined with the realization diagram of a specific plant in order to check if this diagram matches decently with the demand matrix. The information about energy demand as well as the performance of CHP plants needed for such an evaluation is in general not easily to obtain. This appears to be an obstacle for the universal application of the method. Further extension of the method will be necessary to enable the accurate prediction of the fuel consumption of a plant.

## 2 THE HEAT TO POWER MATRIX

In general the heat and power demand of an individual CHP plant will fluctuate during the day as well as during the seasons. The imaginary heat and power demand for a CHP plant during a short period is presented in Figure 1. The curves show both the heat and power demand at a specific moment. However, companies are not very willing to provide the demand information in this way because it might include information about their production processes. Therefore, this

information is usually summarized into load duration curves as shown in Figure 2. The curves show actually the time during which the demanded power is higher than the indicated power. The load duration curve presents the energy demand in a very compact way. Unfortunately, it does not consider the coherence between the heat demand and the electricity demand. And this coherence is important for the design and operation of CHP plants. The heat to power (or electricity) matrix enables the presentation of the heat and power demands in a way that the coherence is assured but information about the time at which a specific combination of heat and power demand is not shown. An example of an heat to power matrix is presented in Figure 3. To establish this matrix small intervals of heat and power demand are considered. During a short time interval, e.g. an hour but preferably a quarter of an

hour, the actual heat and power demand is measured and assigned to the appropriate heat and power intervals. The heat and power intervals are depicted in the diagram of Figure 3 resulting into boxes for all combinations of heat and power demands that will occur. In each

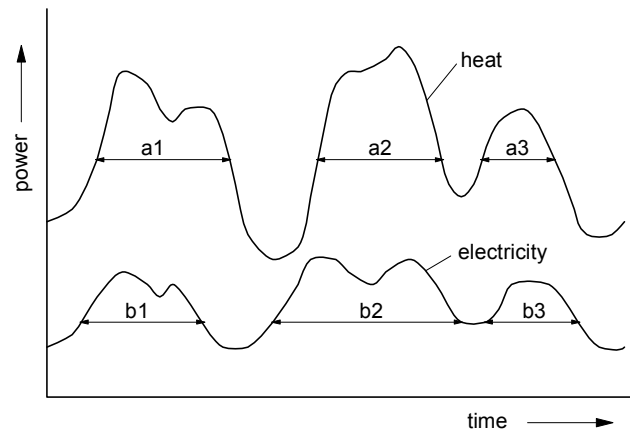


Figure 1 Actual electricity and heat demand of a CHP plant

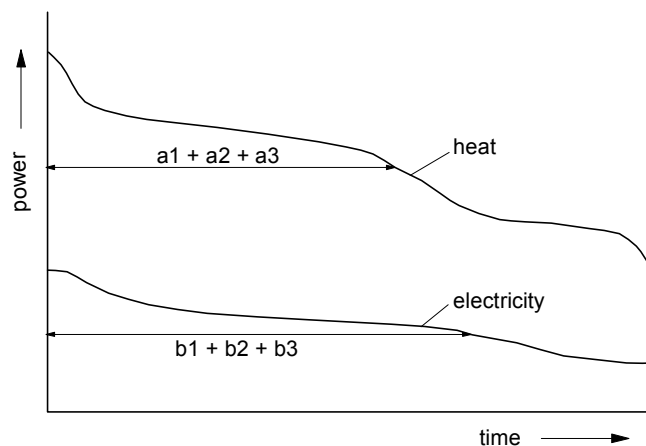


Figure 2 Load duration curve of a CHP plant

## Appendix 7.1

of the boxes the number of time intervals, or frequency, is presented in which the specific

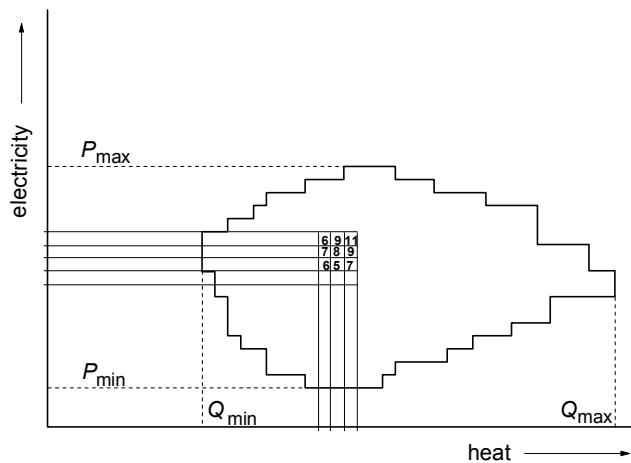


Figure 3 Energy demand presented in a heat to power matrix

combination of heat and power demand is measured<sup>2</sup>. In Figure 3 the frequency is depicted only for some of the boxes and the outline of the area with all the boxes is shown. This area is further called the “heat to power matrix (H/P matrix)”. In general the highest frequencies will be found in the center of the H/P matrix. Near the borders of the matrix the frequencies are usually low. Depending on the characteristics of the energy consumers the H/P matrix might show one or more areas with a local maximum of the frequency values.

### 3 THE CHP PLANT OPERATION AREA

The CHP plant operation area presents the combinations of heat and power generation that can be covered by the considered CHP plant. The plant operation area might be helpful to find the optimum CHP plant for a specific energy demand as shown by the H/P matrix. Each type of CHP plant will have a characteristic operation area. A CHP plant consisting e.g. of a gas turbine (GT) and a waste heat boiler (WHB) can be used to generate power by the gas turbine while the waste heat boiler is used for the generation of heat (steam or hot water). The heat and power generation are primarily determined by the power control of the gas turbine. The gas turbine cannot be operated below a certain minimum power ( $P_{\min}$ ). At this operation point also the heat production is minimum ( $Q_{\min}$ ). If the generated power is increased to  $P_{\max}$ , the produced heat increases to  $Q_{\max}$ . In Figure 4 a roughly linear relation between the generated power

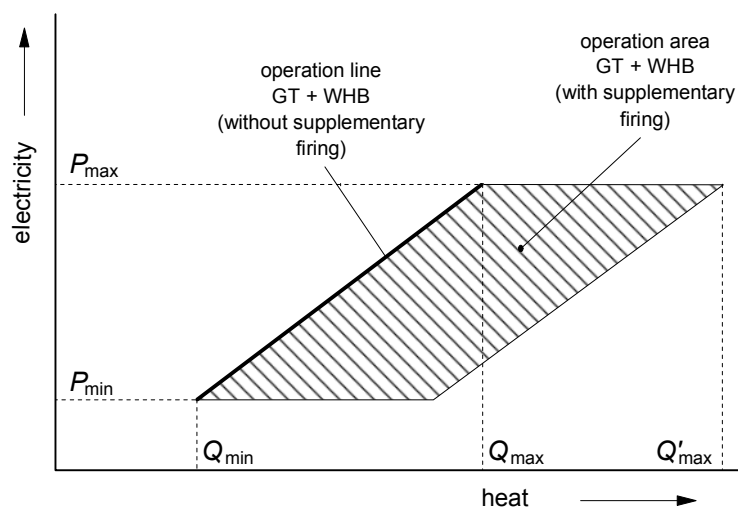


Figure 4 Operation area of a gas turbine plant with and without supplementary firing

<sup>2</sup> In a 3D-diagram the frequency can also be presented as the length of a bar.

and heat is assumed. In many applications the heat demanded by a consumer is significantly higher than the power demand. In the case of a gas turbine plant with waste heat boiler the generation of heat can be increased by the application of supplementary firing in the waste heat boiler. Then the maximum generated heat can be increased from  $Q_{\max}$  to  $Q'_{\max}$ . The generation of additional heat at part load operation of the gas turbine is also possible by supplementary firing in the waste heat boiler. In Figure 4 it is assumed that at minimum load of the gas turbine the additional heat generated by supplementary firing is roughly the same as at maximum load of the gas turbine. It might be clear that in principle the maximum heat power of supplementary firing is determined by the available oxygen in the gas turbine exhaust flow. The shaded area represents all possible operation points of the gas turbine with supplementary firing and is called the operation area of the gas turbine plant with supplementary firing.

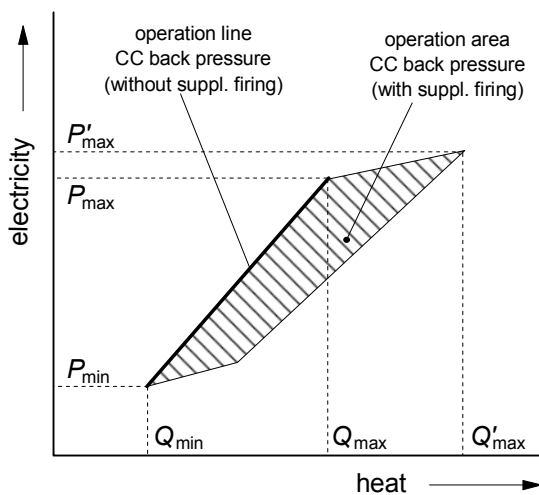


Figure 5 Operation area of a CC back pressure plant with and without supplementary firing

CC plants are also often used as CHP plants. In Figure 5 the operation area of a CC plant with back pressure steam turbine is shown. Such a plant can be built with or without supplementary firing in the HRSG. If no supplementary firing is applied, the generated heat is determined by the gas turbine load. Increasing the power of the gas turbine will also result into an increase of the generated heat. The operation area of this plant is just a single curve. With supplementary firing more steam will be generated in the HRSG. The higher steam flow will increase the power of the steam turbine as well as the heat transferred in the (high pressure) condenser. Thus, the generated

power as well as the generated heat are increased by supplementary firing. The shaded area represents the operation area of the CC plant with back pressure steam turbine and supplementary firing.

A very popular CHP plant for large scale heat generation is the CC plant with steam extraction. These plants are often used as heat supply for district heating because of the high efficiencies that can be achieved and the high flexibility with regard to the heat to power ratio. The operation area of such a plant is shown in Figure 6. The maximum power ( $P_{\max}$ ) of this plant is achieved if no steam extraction is used for the generation of heat. If steam is extracted for heat generation at constant gas turbine load, the power of the steam turbine

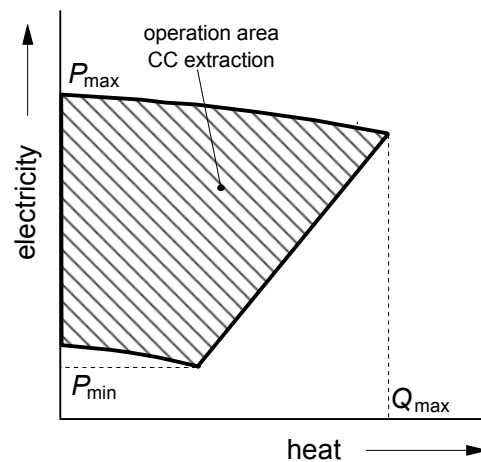


Figure 6 Operation area of a CC plant with steam extraction

## Appendix 7.1

decreases. Thus at maximum heat production the generated electricity is somewhat lower than at maximum power. The generated heat can easily be controlled from zero to  $Q_{\max}$  if no limitations of the electrical power have to be considered.

To get an impression of the fuel consumption of the CHP plant in the various operation points lines of constant fuel consumption or constant efficiency can be depicted in the operation area. Accurate values can be got by system calculations if sufficient information of the plant design and control is available.

### 4 MATCHING PLANT OPERATION AND H/P MATRIX

In order to check if a CHP plant is suitable for a specific application, the H/P matrix and the operation area of the considered plant are combined in the heat to power diagram as shown in Figure 7 for a gas turbine plant with waste heat boiler and supplementary firing. It appears that the operation area of the CHP plant covers a serious part of the H/P matrix. For a reasonable match it is not necessary that the H/P matrix is completely covered by the operation area. The CHP operation point is not necessarily the same as the demand point. E.g. if the export of electricity is beneficial at the time of operation it is possible that the generation of heat fits to the heat demand while the electricity generation is higher than the demand. If export of electricity is not possible or beneficial, then the power level has to be adjusted and additional heat might be generated by auxiliary boilers. In the case of low heat and high electricity demands the plant can be operation might be matched with the heat demand and the remaining electricity can be obtained from the public grid. It seems to be likely that the highest frequencies have to be covered by the operation area.

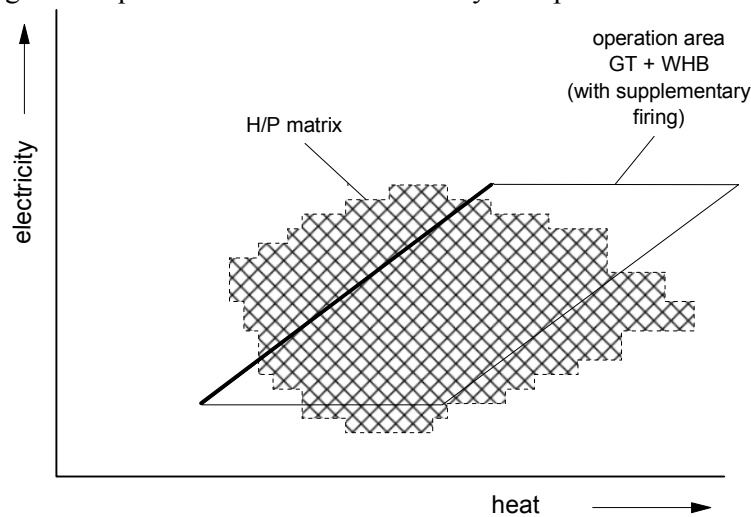


*Figure 7 Match of H/P matrix with operation area of a gas turbine plant with supplementary firing*

In Figure 8 also the operation areas are shown of a CC plant with back pressure steam turbine and supplementary firing and a CC plant with steam extraction. The power range of the CC plants do fit well with the electricity demand but the ranges of heat generation have little overlap with the H/P matrix. In this case the operation area of the gas turbine plant with

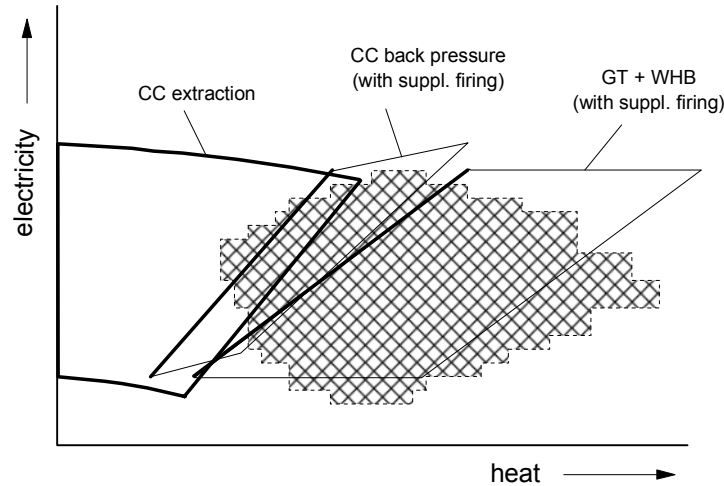


Figure 8 H/P matrix with operation areas of various plants

waste heat boiler and supplementary firing provides the highest overlap with the H/P matrix. However, further system calculations and economic evaluations are necessary to find out which option results into lowest fuel consumption and the best economic performance. The H/P matrix and the depicted operation area can be used also to discuss and evaluate the optimum design power of CHP plants. In Figure 9 the H/P matrix is depicted together with a gas turbine plant with design power A and gas turbine plant with higher design power B. The plant with design power A has a waste heat boiler with supplementary firing. The plant with design power B has a waste heat boiler without supplementary firing. Region 1 (see Figure 9) of the H/P matrix is completely covered by the operation area of plant A. No import or export of electricity is necessary and no heat from auxiliary boilers is required. If the demand is in region 2 it is likely that the CHP will be operated along the left border of the operation area.

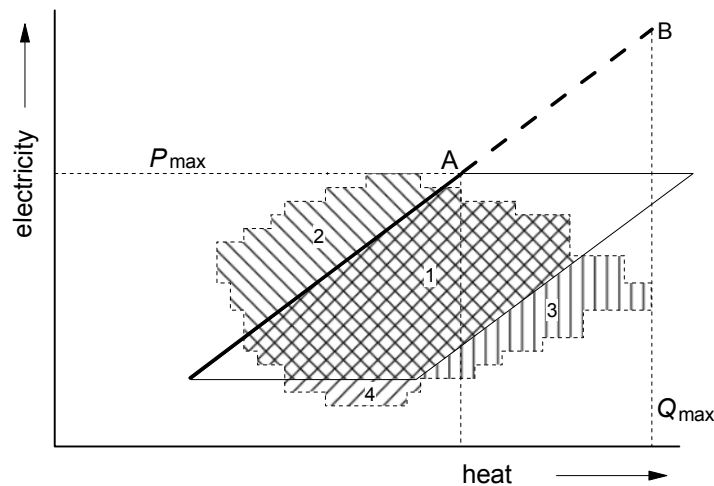


Figure 9 H/P matrix with operation area of a GT plant with WHB and supplementary firing (design power A) and a GT plant with WHB (design power B)

## Appendix 7.1

It has to be decided, however, whether the operation point of the CHP plant should equal the electricity or the heat demand. If it equals the heat demand, additional electricity must be imported. If it equals the electricity demand, heat must be discharged. The most beneficial operation depends on fuel consumption and fuel costs and the electricity prices. Demands in region 3 will require the export of electricity if it is beneficial to generate all heat by the CHP plant. If export of electricity is unfavorable, additional heat has to be generated with auxiliary boilers. In region 4 the electricity demand is lower than the minimum power that can be generated by the CHP plant. Electricity must be exported or, if this is not favorable, the CHP plant must be shut down and electricity must be imported while heat has to be generated by auxiliary boilers.

Plant B is able to generate more electricity than plant A. If the plant is controlled in a way that it first of all generates the demanded heat, in many circumstances export of electricity is needed. The design point B is chosen such that the plant is able to generate the maximum demanded heat. Plant B is primarily of interest in cases with high export prices of electricity. Obviously various plant designs, design powers and operation modes of CHP plants have to be considered to find the optimum configuration for a specific case. In general highly flexible operation might be advantageous because it is in general not assured that all parameters will remain constant during the plant lifetime.

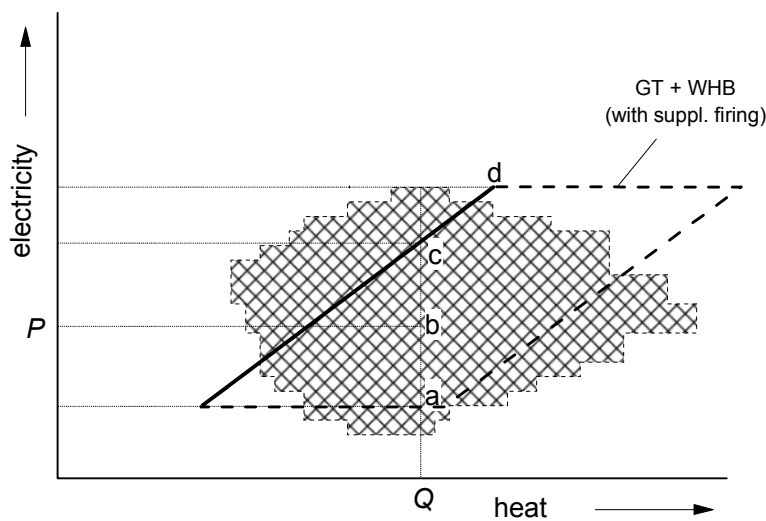


Figure 10 H/P matrix with operation area of a GT plant with WHB and supplementary firing

## 5 EVALUATION OF CHP PLANT OPERATION

The H/P matrix and the plant operation area can also be used to optimize the operation of existing CHP plants. As an example the H/P matrix and the operation area from previous figures are used (see Figure 10). It is supposed that point b in this figure represents the energy demand at a certain moment. The CHP plant can be operated in a way that generation equals both the electricity demand and the heat demand. But, if the price of electricity export is high at that moment, it might be beneficial to operate the CHP plant at point c and export the extra

generated electricity. Are electricity export prices very high even operation at point d has to be considered. In that case the discharge of a certain heat power is necessary which means that equipment for heat rejection should be available. At moments that the electricity import is very cheap, even cheaper than if generated with the CHP plant, it might be decided to operate the CHP plant at point a. In extreme cases the plant can be switched off and the heat must be generated by an auxiliary boiler.

It is obvious that the diagrams as shown in this appendix are primarily useful to discuss the various options for design and operation of CHP plants. For the actual optimization comprehensive system calculations and economic evaluations are required.

**REFERENCES****CHAPTER 1 INTRODUCTION**

- [1.1] Jakob de Swaan Arons, Hedzer van der Kooi, Krishnan Sankaranarayanan. Efficiency and sustainability in the energy and chemical industries. Marcel Dekker, Inc. New York
- [1.2] Naim H. Afgan, Maria G. Carvalho and Nikolai V. Hovanov. Energy system assessment with sustainability indicators. *Energy Policy* 28 (2000) 603-612.
- [1.3] Christos A. Frangopoulos and Despoina E. Keramioti. Multi-Criteria Evaluation of Energy Systems with Sustainability Considerations. *Entropy* 2010, 12, 1006-1020;
- [1.4] G. Assefa, B. Frostell. Social sustainability and social acceptance in technology assessment: A case study of energy technologies. *Technology in Society* 29 (2007) 63-78
- [1.5] Naim H. Afgan, Maria G. Carvalho. Multi-criteria assessment of new and renewable energy power plants. *Energy* 27 (2002) 739-755
- [1.6] Fajik Begić, Naim H. Afgan. Sustainability assessment tool for the decision making in selection of energy system - Bosnian case. *Energy* 32 (2007) 1979-1985
- [1.7] K. Kaygusuz and S. Bilgen. Thermodynamic Aspects of Renewable and Sustainable Development. *Energy Sources, Part A*, 31:287-298, 2009
- [1.8] Our Common Future. Report of the World Commission on Environment and Development. United Nations August 1987.
- [1.9] Algemene Rekenkamer. Energiebesparing: ambities en resultaten. ISSN 0921 - 7371, 's-Gravenhage 2011
- [1.10] Ecofys. The energy report. ISBN 978-2-940443-26-0, 2010.

**CHAPTER 2 EXERGY ANALYSIS**

- [2.1] H.D. Baehr, E. Bergmann, F. Bošnjaković, P. Grassmann, J.J.C. van Lier, Z. Rant, H Rögner, K.R. Schmidt. *Energie und Exergie. Die Anwendung des Exergiebegriffs in der Energietechnik.* VDI-Verlag Dusseldorf; 1965.
- [2.2] H.D. Baehr. *Thermodynamik.* ISBN 0-387-10777-0
- [2.3] J.J.C. van Lier. *Thermodynamische processen in de centrale en mogelijkheden tot het verbeteren van deze processen.* Argus, Amsterdam; 1963.
- [2.4] Jan Szargut, David R. Morris, Frank R. Steward. *Exergy analysis of thermal, chemical, and metallurgical processes.* Springer Verlag, Berlin. ISBN 3-540-18864-9
- [2.5] T.J. Kotas. *The exergy method of thermal plant analysis.* Krieger publishing company, Malabar, Florida. ISBN 0-89464-941-8
- [2.6] Michael J. Moran, Howard N. Shapiro. *Fundamentals of Engineering Thermodynamics,* 5<sup>th</sup> edition. ISBN-10 0-470-03037-2
- [2.7] Sabine Jansen, Nico Woudstra. Understanding the exergy of cold: theory and practical examples. *International Journal of Exergy* 7 (6) 693-713
- [2.8] H.D. Baehr. *Exergie der Brennstoffe.* *Brennst.-Wärme-Kraft* 31 (1979)
- [2.9] H.D. Baehr. *Die Exergie von Kohle und Heizöl.* *BWK* 39 (1987)
- [2.10] F. Brandt. *Brennstoffe und Verbrennungsrechnung.* Vulkan-Verlag Essen 1981.
- [2.11] S. Kelly, G. Tsatsaronis, T. Morosuk. Advanced exergetic analysis: Approaches for splitting the exergy destruction into endogenous and exogenous parts. *Energy* 34 (2009) 384-391.

- [2.12] T. Morosuk, G. Tsatsaronis. Advanced exergetic evaluation of refrigeration machines using different working fluids. *Energy* 34 (2009) 2248-2258.
- [2.13] N. Razmara, R. Khoshbakhti Saray. A simple gas turbine system and co-generation power plant improvement based on endogenous and exogenous exergy destruction.
- [2.14] Valero A, Correas L, Zaleta A, Lazzaretto A, Verda V, Reini M, Rangel V. On the thermoeconomic approach to the diagnosis of energy system malfunctions: Part 1-the TADEUS problem. *Energy* 29 (2004) 1875-1887.
- [2.15] Valero A, Correas L, Zaleta A, Lazzaretto A, Verda V, Reini M, Rangel V. On the thermoeconomic approach to the diagnosis of energy system malfunctions. Part 2- Malfunction definitions and assessment. *Energy Int. J* 2004;29: 1889–907.
- [2.16] Kotas, T.J. Exergy Criteria of Performance for Thermal Plant. *Int. J. Heat & Fluid Flow*, Vol.2, No.4
- [2.17] Tsatsaronis, G. Thermoeconomic analysis and optimization of energy systems. *Prog. Energy Combust. Sci.* 1993, Vol 19
- [2.18] George Tsatsaronis, Moungh-Ho Park. On avoidable and unavoidable exergy destructions and investment costs in thermal systems. *Energy Conversion and Management* 43 (2002) 1259-1270
- [2.19] Frank Cziesla, George Tsatsaronis, Zengliang Gao. Avoidable thermodynamic inefficiencies and costs in an externally fired combined cycle power plant. *Energy* 31 (2006) 1472–1489
- [2.20] Tatiana Morosuk, George Tsatsaronis. A new approach to the exergy analysis of absorption refrigeration machines. *Energy* 33 (2008) 890–907
- [2.21] Andrea Lazzaretto, George Tsatsaronis. SPECO: A systematic and general methodology for calculating efficiencies and costs in thermal systems. *Energy* 31 (2006) 1257–1289
- [2.22] A. Valero, M. A. Lozano and J. L. Bartolomé. On-line monitoring of power-plant performance, using exergetic cost techniques. *Applied Thermal Engineering*, Vol. 16, No. 12, pp. 933-948, 1996.
- [2.23] M. Dentice d'Accadia, M. Sasso. Exergetic cost and exergoeconomic evaluation of vapour-compression heat pumps. *Energy* Vol. 23, No. 11, pp. 937–942, 1998
- [2.24] J.J.C. van Lier. Bewertung der Energieumwandlung mit dem Exergiebegriff bei der Strom- und/oder Wärmeerzeugung. *Brennst.-Wärme-Kraft* 30 (1978) Nr. 12 Dezember.

### **CHAPTER 3 OPTIONS FOR FUTURE ENERGY SYSTEMS**

- [3.1] Nico Woudstra. Towards sustainable energy systems. ECOS2000, Enschede, The Netherlands (5-7 July, 2000), p. 965-978
- [3.2] Jaap Koppejan, Wolter Elbersen, Prem Bindraban. Beschikbaarheid van Nederlandse biomassa voor elektriciteit en warmte in 2020. Rapportage in opdracht van SenterNovem. November 2009; projnr. 200809
- [3.3] Richard Toonssen. Sustainable power from biomass. Thesis TU Delft, July 2010. ISBN 978-90-5335-297-7

### **CHAPTER 4 FUEL COMVERSION**

- [4.1] N. Woudstra, T. van der Stelt. Exergy analysis of combustion systems. ECOS 2003, Copenhagen, Denmark, June 30 - July 2, 2003, Vol.II: 835 - 842

## References

- [4.2] W.R. Dunbar, N. Lior. Sources of combustion irreversibility. *Combust. Sci. and Tech.* 1994, Vol. 103, pp 41-61.
- [4.3] Lier, J.J.C. van. Bewertung der Energieumwandlung mit dem Exergiebegriff bei der Strom- und/oder Wärmeerzeugung. *Brennstoff Wärme Kraft* 30 (1978), Nr. 12, Dezember, 475-484
- [4.4] Baehr, H.D. Die exergie von Kohle und Heizöl. *Brennstoff Wärme Kraft* 39 (1987)
- [4.5] S.K. Som, A. Datta. Thermodynamic irreversibilities and exergy balance in combustion processes. *Progress in Energy Combustion Science* 34 (2008) 251-376.
- [4.6] M.J. Prins, K.J. Ptasinski. Energy and exergy analysis of the oxidation and gasification of carbon. *Energy* 30 (2005) 982-1002.
- [4.7] Krzysztof J. Ptasinski. Thermodynamic efficiency of biomass gasification and biofuels conversion. *Biofuels, Bioprod. Bioref.* 2 (2008) 239-253.
- [4.8] A. Franco, N. Giannini. Perspectives for the use of biomass as fuel in combined cycle power plants. *International Journal of Thermal Sciences* 44 (2005) 163-177.
- [4.9] Carmen Martin, Miguel A. Villamañán, Cesar R. Chamorro, Juan Otero, Andrés Cabanillas, José J. Segovia. Low-grade coal and biomass co-combustion on fluidized bed: exergy analysis. *Energy* 31 (2006) 330–344.
- [4.10] M. Sorin, J.-C. Bonhivers, J. Paris. Exergy efficiency and conversion of chemical reactions. *Energy Convers. Mgmt* vol. 39, no. 16-18, pp. 1863-1868 (1998)
- [4.11] M. Sorin, J. Lambert, J. Paris. Exergy flows analysis in chemical reactors. *Trans IChemE*, vol 76, Part A, March 1998, 389-395.
- [4.12] M. J. Prins, K. J. Ptasinski, F. J. J. G. Janssen. Thermodynamics of gas-char reactions: first and second law analysis. *Chemical Engineering Science* 58 (2003) 1003–1011.
- [4.13] M. Sorin, A. Hammache, O. Diallo. Exergy load distribution approach for multi-step process design. *Applied Thermal Engineering* 20 (2000) 1365-1380.
- [4.14] S.S. Mondal. Modelling of transport processes and associated thermodynamic irreversibilities in ignition and combustion of a pulverized coal particle. *International Journal of Thermal Sciences* 47 (2008) 1442-1453
- [4.15] Hiroshi Taniguchi, Kunihiko Mouri, Takefumi Nakahara, Norio Arai. Exergy analysis on combustion and energy conversion processes. *Energy* 30 (2005) 111–117
- [4.16] Jerald A. Caton. On the destruction of availability (exergy) due to combustion processes - with specific application to internal-combustion engines. *Energy* 25 (2000) 1097–1117
- [4.17] M. Imroz Sohel, Michael W. Jack. Thermodynamic analysis of lignocellulosic biofuel production via a biochemical process: Guiding technology selection and research focus. *Bioresource Technology* 102 (2011) 2617–2622
- [4.18] A. Boyano, A.M. Blanco-Marigorta, T. Morosuk, G. Tsatsaronis. Exergoenvironmental analysis of a steam methane reforming process for hydrogen production. *Energy* 36 (2011) 2202-2214
- [4.19] Th. Woudstra, N. Woudstra. Exergy analysis of hot-gas clean-up in IGCC systems. *Journal of the Institute of Energy*, September 1995, 68, pp 157-166.
- [4.20] Richard Toonssen. Sustainable power from biomass. Thesis TU Delft, July 2010. ISBN 978-90-5335-297-7

**CHAPTER 5 THERMAL POWER CYCLES**

- [5.1] Th. Woudstra, W. Wester. Stoomsystemen met geavanceerde condities. TU Delft, EV 1365, December 1985.
- [5.2] Zen Fan, Archie Roberson, Steve Goidich. 800 MWe Circulating Fluidized Bed Boiler with 1300°F Supercritical Steam. 33<sup>rd</sup> International Technical Conference on Coal Utilization and Fuel Systems; Clearwater, Florida. June 1-8, 2008.
- [5.3] Miro R. Susta. Ultra-Supercritical Pulverized Coal Fired Power Plants. Coalgen 2006, Cincinnati-USA. August 16-18, 2006.
- [5.4] Frank Czesla, Herman Kremer, Ulrich Much, Jan-Erik Riemschneider, Rainer Quinkertz. Advanced 800+ MW Steam Power Plants and Future CCS Options. COAL-GEN Europe 2009; Katowice, Poland. September 1-4, 2009.
- [5.5] János M. Beér. High efficiency electric power generation: The environmental role. *Progress in Energy and Combustion Science* 33 (2007) 107-134.
- [5.6] Stephen J. Goidich, Kenneth P. Melzer, Robert V. Roche. Innovation in Supercritical Boiler Technology – The 750 MWe Longview Power Project. PowerGen Europe; Cologne, Germany. May 26-28, 2006.
- [5.7] H.G. Neft, G. Franconville. Neue Dampfturbinenkonzepte für höhere Eintrittsparameter und längere Endschaufeln. *VGB Kraftwerkstechnik* 73 (1993), Heft 5, 409-415.
- [5.8] H. Noppenau, S. Hansen. Designstudie eines kohle- und gasbefeueten Kraftwerkes mit fortgeschrittenen Dampfdaten. *VGB Kraftwerkstechnik* 74 (1994), Heft 2, 119-123.
- [5.9] P. Havenaar, H. Kotschenreuther. Das Kraftwerk Hemweg 8. *VGB Kraftwerkstechnik* 75 (1995), Heft 5, 407-411.
- [5.10] S. Kjær, F. Thomsen. Stand der fortgeschrittenen überkritischen fossilbefeueten Dampfkraftwerke im ELSAM-Bereich. *VGB Kraftwerkstechnik* 6/99, 31-35.
- [5.11] H.-J. Meier, M. Alf, M. Fishedick, B. Hillebrand, H. Lichte, J. Meier, M. Neubronner, D. Schmitt, W. Victor, M. Wagner. Reference Power Plant North Rhine-Westphalia (RPP NRW). *VGB Power Tech* 5/2004, 76-89.
- [5.12] A.P. Fraas. A potassium-steam-gas vapor cycle. ORNL-NSF-EP-6, August 1971
- [5.13] G.E. Rajakovics. Exrem hohe Kraftwerkswirkungsgrade durch Dreifach-Dampfprozess. *ÖZE*, Hef 4, 1974.
- [5.14] R.J. Rossbach. Potassium topping cycles for stationary power. NASA CR-2518, March 1975
- [5.15] Evaluation of phase 2 conceptual designs and implementation assessment resulting from the energy conversions alternative study (ECAS). NASA TMX-73515, April 1977.
- [5.16] G. Samuels et al. Design study of a 200 MWe alkali metal/steam binary power plant using a coal fired fluidized bed furnace. ORNL/TM-6041, April 1978.
- [5.17] N. Woudstra. Potassium topping cycles; System studies (in Dutch). TU Delft, EV-1325, August 1983.
- [5.18] Gianfranco Angelino, Constante Invernizzi. Binary conversion cycles for concentrating solar power technology. *Solar Energy* 82 (2008) 637-647.
- [5.19] Nico Woudstra, Theo Woudstra, Armando Pirone, Teus van der Stelt. Thermodynamic evaluation of combined cycle plants. *Energy Conversion and Management* 51 (2010) 1099-1110

## References

- [5.20] Ivar S. Ertesvåg, Hanne M. Kvamsdal, Olav Bolland. Exergy analysis of a gas-turbine combined-cycle power plant with precombustion CO<sub>2</sub> capture. *Energy* 30 (2005) 5-39.
- [5.21] Alessandro Franco, Claudio Casarosa. Thermoeconomic evaluation of the feasibility of highly efficient combined cycle power plants. *Energy* 29 (2004) 1963-1982
- [5.22] Frank Czesla, George Tsatsaronis, Zengliang Gao. Avoidable thermodynamic inefficiencies and costs in an externally fired combined cycle power plant. *Energy* 31 (2006) 1472-1489.
- [5.23] Mehmet Kanoglu, Ibrahim Dincer, Marc A. Rosen. Understanding energy and exergy efficiencies for improved energy management in power plants. *Energy Policy* 35 (2007) 3967-3978
- [5.24] T.W. Song, J.L. Sohn, J.H. Kim, T.S. Kim, S.T. Ro. Exergy-based performance analysis of the heavy-duty gas turbine in part-load operating conditions. *Exergy, an International Journal* 2 (2000) 105-112.
- [5.25] B.V. Reddy, K. Mohamed. Exergy analysis of a natural gas fired combined cycle power generation unit. *Int. J. Exergy*, Vol. 4, No. 2, 2007.
- [5.26] M. Mohagheghi, J. Shayegan. Thermodynamic optimization of design variables and heat exchangers layout in HRSGs for CCGT, using generic algorithm. *Appl. Therm. Eng.* (2008) doi:10.1016/j.applthermaleng.2008.02.035.
- [5.27] Y. Sanjay, Onkar Singh, B.N. Prasad. Energy and exergy analysis of steam cooled reheat gas-steam combined cycle. *Applied Thermal Engineering* 27 (2007) 2779-2790.
- [5.28] Samuel José Sarraf Borelli, Silvio de Oliveira Junior. Exergy-based method for analyzing the composition of the electricity cost generated in gas-fired combined cycle plants. *Energy* 33 (2008) 153-162.
- [5.29] Daniele Fiaschi, Giampaolo Manfrida. Exergy analysis of the semi-closed gas turbine combined cycle (SCGT/CC). *Energy Convers. Mgmt Vol.* 39, No. 16-18, pp. 1643-1652, 1998.
- [5.30] E. Kakaras, A. Doukelis, R. Leithner, N. Aronis. Combined cycle power plant with integrated low temperature heat (LOTHECO). *Applied Thermal Engineering* 24 (2004) 1677-1686.
- [5.31] Deng-Chern Sue, Chia-Chin Chuang. Engineering design and exergy analysis for combustion gas turbine based power generation system. *Energy* 29 (2004) 1183-1205.
- [5.32] [www.cycle-tempo.nl](http://www.cycle-tempo.nl) (version June 2008)
- [5.33] J.J.C. van Lier. Bewertung der Energieumwandlung mit dem Exergiebegriff bei der Strom- und/oder Wärmeerzeugung (Evaluation of energy conversion processes for the generation of power and heat by applying the exergy concept). *Brennst.-Wärme-Kraft* 30 (1978)
- [5.34] Gas Turbine World, 2004 Performance Specs, 22<sup>nd</sup> Edition
- [5.35] Gas Turbine World, 2008 Performance Specs, 25<sup>th</sup> Edition
- [5.36] R.C. Spencer, K.C. Cotton, C.N. Cannon. A method for predicting the performance of steam turbine generators, 16,500 kW and larger. Revised 1974 and reprinted by The General Electric Company.
- [5.37] P.J. Mago, L.M. Chamra, C. Somayaji Performance analysis of different working fluids for use in organic Rankine cycles. *Proc. ImechE Vol.* 221 part A: J. Power and Energy 255-263

**CHAPTER 6 FUEL CELL SYSTEMS**

- [6.1] James Larminie, Andrew Dicks. Fuel Cell Systems Explained. John Wiley & Sons, LTD. ISBN 0 471 49026 1
- [6.2] N. Woudstra, T.P. van der Stelt, K. Hemmes. Thermodynamic Evaluation and optimization of Fuel Cell Systems. Journal of Fuel Cell Science and Technology, Volume 3, Number 2, May 2006 (p.155-164)
- [6.3] Fuel Cell Handbook. EG&G Technical Services, Inc.. Under Contract No. DE-AM26-99FT40575 U.S. Department of Energy, November 2004.
- [6.4] Frank de Bruijn. The current status of fuel cell technology for mobile and stationary applications. Green Chem., 2005, 7, 132-150.
- [6.5] Mark A.J. Cropper, Stefan Geiger, David M. Jollie. Fuel Cells: a survey of current developments. Journal of Power Sources 131 (2004) 57-61.
- [6.6] C. Barnay, M. Marchand, M. Cassir. Prospects of different fuel cell technologies for vehicle applications. Journal of Power Sources 108 (2002) 139-152.
- [6.7] L. Carrette, K.A. Friedrich, U. Stimming. Fuel Cells – Fundamentals and Applications. Fuel Cells 2001, No. 1, 5-39.
- [6.8] E. Turpeinen, R. Raudaskoski, E. Pongrácz, R.L. Keiski. Thermodynamic analysis of conversion of alternative hydrocarbon-based feedstocks to hydrogen. International Journal of hydrogen energy 33 (2008) 6635-6643
- [6.9] Omer Faruk Dilmac, Semra K. Özkan. Energy and exergy analyses of a steam reforming process for hydrogen production. Int. J. Exergy, Vol. 5, No. 2, 2008
- [6.10] Atilla Ersoz, Hayati Olgun, Sibel Ozdogan. Reforming options for hydrogen production from fossil fuels for PEM fuel cells. Journal of Power Sources 154 (2006) 67-73
- [6.11] J. Pasel, J. Meißner, Z. Porš, C. Palm, P. Cremer, R. Peters, D. Stolten. Hydrogen Production via Autothermal Reforming of Diesel Fuel. Fuel Cells 2004, 4, No. 3
- [6.12] H.P. Schmid, J.A. Wüning. Steam Reforming for PEM Fuel Cell Systems. Fuel Cells, 4(4) (2004), p. 256–263
- [6.13] J. Mathiak, A. Heinzl, J. Roes, T. Kalk, H. Kraus, H. Brandt. Coupling of a 2.5 kW Steam Reformer With a 1 kWel PEM Fuel Cell. Journal of Power Sources, 131 (2004), p. 112–119
- [6.14] J. Lampert. Selective catalytic oxidation: a new approach to the desulfurization of natural gas and liquid petroleum gas for fuel cell reformer applications. Journal of Power Sources 131 (2004) 27-34.
- [6.15] D.P.J. Barz, U.K. Trägner, V.M. Schmidt, M. Koschowitz. Thermodynamics of Hydrogen Generation from Methane for Domestic Polymer Electrolyte Fuel Cell Systems. Fuel Cells, 3(4) (2003), p. 199–207
- [6.16] R. Peters, H.G. Düsterwald, B. Höhle. Investigation of a methanol reformer concept considering the particular impact of dynamics and long-term stability for use in a fuel-cell-powered passenger car. Journal of Power Sources 86 (2000) 507–514
- [6.17] Doohwan Lee, Hyun Chul Lee, Kang Hee Lee, Soonho Kim. A compact and highly efficient natural gas fuel processor for 1-kW residential polymer electrolyte membrane fuel cells. Journal of Power Sources 165 (2007) 337–341

## References

- [6.18] Yu Taek Seo, Dong Joo Seo, Jin Hyeok Jeong, Wang Lai Yoon. Development of compact fuel processor for 2 kW class residential PEMFCs. *Journal of Power Sources* 163 (2006) 119–124
- [6.19] Richard Toonssen. Sustainable power from biomass. Thesis TU Delft, July 2010.
- [6.20] R. v. Helmolt. Fuel Cell Vehicles at General Motors. *Fuel Cells* 2004, 4, No. 4; 264-268
- [6.21] U. Winter, M. Hermann. Hydrogen Automobile Heads Toward Series Production. Hydrogen 3 puts Fuel Cells on the Road. *Fuel Cells* 2003, 3, No. 3; 141-145
- [6.22] U. Winter, H. Weidner. Hydrogen for Mobility of the Future. Results of GM/Opel's Well-to-Wheel Studies in North America and Europe. *Fuel Cells* 2003, 3, No. 3; 76-83
- [6.23] [www.fuelcells.org/info/charts/carchart.pdf](http://www.fuelcells.org/info/charts/carchart.pdf)
- [6.24] R. Cozzolino, S.P. Cicconardi, E. Galloni, M. Minutillo, A. Perna. Theoretical and experimental investigations on thermal management of a PEMFC stack. *International journal of hydrogen energy* 36 (2011) 8030-8037
- [6.25] A. Arsalis, Mads P. Nielsen, Søren K. Kær. Modeling and parametric study of a 1 kW<sub>e</sub> HT-PEMFC-based residential micro-CHP system. *International journal of hydrogen energy* 36 (2011) 5010-5020
- [6.26] Alexandros Arsalis, Mads P. Nielsen, Søren K. Kær. Modeling and off-design performance of a 1 kW<sub>e</sub> HT-PEMFC (high temperature-proton exchange membrane fuel cell)-based residential micro-CHP (combined-heat-and-power) system for Danish single-family households. *Energy* 36 (2011) 993-1002
- [6.27] José Geraldo de Melo Furtado, George Cassani Gatti, Eduardo Torres Serra, Silvio Carlos Anibal de Almeida. Performance analysis of a 5 kW PEMFC with a natural gas reformer. *International Journal of Hydrogen Energy* 35 (2010) 9990–9995
- [6.28] I. Staffell, R.J. Green. Estimating future prices for stationary fuel cells with empirically derived experience curves. *International journal of hydrogen energy* 34 (2009) 5617-5628
- [6.29] Ph. Moçotéguy, B. Ludwig, J. Scholta, R. Barrera, S. Ginocchio. Long Term Testing in Continuous Mode of HT-PEMFC Based H<sub>3</sub>PO<sub>4</sub>/PBI Celtec-P MEAs for  $\mu$ -CHP Applications. *Fuel Cells* 09, 2009, No. 4, 325–348
- [6.30] M. Ferraro, F. Sergi, G. Brunaccini, G. Dispenza, L. Andaloro, V. Antonucci. Demonstration and development of a polymer electrolyte fuel cell system for residential use. *Journal of Power Sources* 193 (2009) 342–348
- [6.31] M. Radulescu, V. Ayel, O. Lottin, M. Feidt, B. Antoine, C. Moyne, D. Le Noc, S. Le Doze. Natural gas electric generator powered by polymer exchange membrane fuel cell: Numerical model and experimental results. *Energy Conversion and Management* 49 (2008) 326–335
- [6.32] Mihai Radulescu, Olivier Lottin, Michel Feidt, Christophe Lombard, David Le Noc, Stéphane Le Doze. Experimental results with a natural gas cogeneration system using a polymer exchange membrane fuel cell. *Journal of Power Sources* 159 (2006) 1142–1146
- [6.33] Charles-Emile Hubert, Patrick Achard, Rudolf Metkemeijer. Study of a small heat and power PEM fuel cell system generator. *Journal of Power Sources* 156 (2006) 64-70
- [6.34] Mihai Radulescu, Olivier Lottin, Michel Feidt, Christophe Lombard, David Le Noc, Stéphane Le Doze. Experimental and theoretical analysis of the operation of a natural gas

- cogeneration system using a polymer exchange membrane fuel cell. *Chemical Engineering Science* 61 (2006) 743 – 752
- [6.35] P. Britz, N. Zartnar. PEM-Fuel Cell System for Residential Applications. *Fuel Cells*, 4(4) (2004), p. 269–275
- [6.36] [http://www.microchap.info/pem\\_fuel\\_cells.htm](http://www.microchap.info/pem_fuel_cells.htm)
- [6.37] Michaela Wilhelm, Michael Jeske, Roland Marschall, Welch Leite Cavalcanti, Pia Tölle, Christof Köhler, Dietmar Koch, Thomas Frauenheim, Georg Grathwohl, Jürgen Caro, Michael Wark. New proton conducting hybrid membranes for HT-PEMFC systems based on polysiloxanes and SO<sub>3</sub>H-functionalized mesoporous Si-MCM-41 particles. *Journal of Membrane Science* 316 (2008) 164–175
- [6.38] Jens Oluf Jensen, Qingfeng Li, Chao Pan, Andreas P. Vestbø, Kasper Mortensen, Henrik Nybo Petersen, Christian Lau Sørensen, Thomas Nedergaard Clausen, Jesper Schramm, Niels J. Bjerrum. High temperature PEMFC and the possible utilization of the excess heat for fuel processing. *International Journal of Hydrogen Energy* 32 (2007) 1567 – 1571
- [6.39] Jianlu Zhang, Zhong Xie, Jiujun Zhang, Yanghua Tang, Chaojie Song, Titichai Navessin, Zhiqing Shi, Datong Song, Haijiang Wang, David Wilkinson, Zhong-Shen Liu, Steven Holdcroft. High temperature PEM fuel cells. *Journal of Power Sources* 160 (2006) 872–891
- [6.40] M. Farooque, A. Kush, A. Leo, H. Maru, A. Skok. Direct Fuel Cell Development and Demonstration Activities At Energy Research Corporation. Abstracts from the 1998 Fuel Cell Seminar, Palm Springs, CA, November 16–19, p. 13–16
- [6.41] G. Huppmann. The MTU Fuel Cell HotModule for Decentralised Combined Power and Heat Generation. *European Fuel Cell News*, 1(1) (2002), p. 12–15
- [6.42] N. Woudstra, A.G. Melman, G. Peppink. The Application of Molten Carbonate Fuel Cell for Power Generation—A System Study. *Fuel Cell Technology and Applications*, International Seminar (1987), The Netherlands, 26–29 October, p. 112–119
- [6.43] G. Angelino, P. Collonna di Paliano. Organic Rankine Cycles (ORCs) for Energy Recovery from Molten Carbonate Fuel Cells. 35th Intersociety Energy Conversion Engineering, 24–28 July 2000, Las Vegas, NV
- [6.44] F.R.A.M. Standaert. Analytical Fuel Cell Modelling and Exergy Analysis of Fuel Cells, Ph.D. thesis, Delft University of Technology, December 1998
- [6.45] S.F. Au. Innovative High Temperature Fuel Cell Systems. Ph.D thesis, Delft University of Technology, January 2003
- [6.46] K. Hemmes, W.H.A. Peelen, J.H.W. de Wit. Molten Carbonate Fuel Cell with Separate CO<sub>2</sub> Gas Supply. *Electrochem. Solid-State Lett.*, 2(3) (1999), p. 103–106
- [6.47] Beomjoo Kim, Do Hyung Kim, Junghyun Lee, Seung Won Kang, Hee Chun Lim. The Ejector Performance of a 75 kW Molten Carbonate Fuel Cell System. *Journal of Fuel Cell Science and Technology*, February 2011, Vol. 8 / 014503-1
- [6.48] Jung-Ho Wee. Molten carbonate fuel cell and gas turbine hybrid systems as distributed energy resources. *Applied Energy* 88 (2011) 4252–4263
- [6.49] <http://www.energyagency.at/fileadmin/aea/pdf/energietechnologien/molten-carbonate.pdf>

## References

- [6.50] A.L. Dicks, R.G. Fellows, C.M. Mescal, C. Seymour. A Study of SOFC-PEM Hybrid Systems. *Journal of Power Sources*, 86 (2000), p. 501–506
- [6.51] H.E. Vollmar, C.U. Maier, C. Nölscher, T. Merklein, M. Poppinger. Innovative Concepts for the Coproduction of Electricity and Syngas with Solid Oxide Fuel Cells. *Journal of Power Sources*, 86 (2000) 90–97
- [6.52] Kas Hemmes, Anish Patil, Nico Woudstra. Flexible Coproduction of Hydrogen and Power Using Internal Reforming Solid Oxide Fuel Cells System. *Journal of Fuel Cell Science and Technology* November 2008, Vol. 5
- [6.53] Wolfgang Winkler, Hagen Lorenz. Design studies of mobile applications with SOFC-heat engine modules. *Journal of Power Sources* 106 (2002) 338-343
- [6.54] P. Lamp, J. Tachtler, O. Finkenwirth, S. Mukerjee, S. Shaffer. Development of an Auxiliary Power Unit with Solid Oxide Fuel Cells for Automotive Applications. *Fuel Cells*, 3(3) (2003), p. 146–152
- [6.55] A.D. Hawkes, P. Aguiar, B. Croxford, M.A. Leach, C.S. Adjiman, N.P. Brandon. Solid oxide fuel cell micro combined heat and power system operating strategy: Options for provision of residential space and water heating. *Journal of Power Sources* 164 (2007) 260–271
- [6.56] E. Fontell, T Kivisaari, N. Christiansen, J.-B. Hansen, J. Pålsson. Conceptual study of a 250 kW planar SOFC system for CHP application.
- [6.57] A.L. Dicks, R.J. Carpenter, E. Erdle, D.F. Lander, P.D. Lilley, A.G. Melman, N. Woudstra. Solid Oxide Fuel Cell Systems Study. TNO report, Ref. No. 88-315, March 1990, prepared for the Commission of the European Community (EN 3E-0165-NL)
- [6.58] Simon P. Harvey, Horst J. Richter. Improved Gas Turbine Power Plant Efficiency by use of recycled Exhaust Gases and Fuel Cell Technology. AES-Vol. 266, Thermodynamics and the Design, Analysis, and Improvement of Energy Systems. ASME 1993
- [6.59] S. Campanari, E. Macchi. Thermodynamic Analysis of Advanced Power Cycles Based Upon Solid Oxide Fuel Cells, Gas Turbines and Rankine Bottoming Cycles. ASME 98-GT-585, International Gas Turbine & Aeroengine Congress & Exhibition, 1998 June 2–5, Stockholm, Sweden
- [6.60] Azra Selimovic, Jens Pålsson. Networked solid oxide fuel cell stacks combined with a gas turbine cycle. *Journal of Power Sources* 106 (2002) 76–82
- [6.61] Mario L. Ferrari, Alberto Traverso, Loredana Magistri, Aristide F. Massardo. Influence of the anodic recirculation transient behavior on the SOFC hybrid system performance. *Journal of Power Sources* 149 (2005) 22–32
- [6.62] K. Hassmann. SOFC Power Plants, the Siemens-Westinghouse Approach. *Fuel Cells*, 1(1) (2001) 78–84
- [6.63] F. Calise, M. Dentice d'Accadia, A. Palombo, L. Vanoli. Simulation and exergy analysis of a hybrid Solid Oxide Fuel Cell (SOFC)–Gas Turbine System. *Energy* 31 (2006) 3278–3299
- [6.64] Jin Sik Yang, Jeong L. Sohn, Sung Tack Ro. Performance characteristics of part-load operations of a solid oxide fuel cell/gas turbine hybrid system using air-bypass valves. *Journal of Power Sources* 175 (2008) 296–302
- [6.65] Winston Burbank Jr., Dennis Witmer, Frank Holcomb. Model of a novel pressurized solid oxide fuel cell gas turbine hybrid engine *Journal of Power Sources* 193 (2009) 656–664

- [6.66] Brian Tarroja, Fabian Mueller, Jim Maclay, Jacob Brouwer. Parametric Thermodynamic Analysis of a Solid Oxide Fuel Cell Gas Turbine System Design Space. *Journal of Engineering for Gas Turbines and Power*, July 2010, Vol. 132
- [6.67] Yingru Zhao, Nilay Shah, Nigel Brandon. Comparison between two optimization strategies for solid oxide fuel cell-gas turbine hybrid cycles. *International Journal of Hydrogen Energy* 36 (2011) 10235-10246
- [6.68] Yingru Zhao, Jhuma Sadhukhan, Andrea Lanzini, Nigel Brandon, Nilay Shah. Optimal integration strategies for a syngas fuelled SOFC and gas turbine hybrid. *Journal of Power Sources* 196 (2011) 9516– 9527
- [6.69] T. Suther, A. S. Fung, M. Koksall, F. Zabihian. Effects of operating and design parameters on the performance of a solid oxide fuel cell–gas turbine system. *Int. J. Energy Res.* 2011; 35:616–632
- [6.70] Kaushik Rajashekara, James Grieve, David Daggett. Hybrid Fuel Cell Power in Aircraft. *IEEE Industry Applications Magazine*, July/Aug 2008
- [6.71] K.J. Bosch. Designing Solid Oxide Fuel Cell – Gas Turbine hybrid systems. Master thesis TU Delft, ET 2198, March 2006.
- [6.72] K.J. Bosch, N. Woudstra, K.V. van der Nat. Designing solid oxide fuel cell gas turbine hybrid systems using exergy analysis. Fourth International Conference on Fuel Cell Science, Engineering and Technology; June 19-21, Irvine, California (FuelCell2006-97084).
- [6.73] P.V. Aravind. Studies on High Temperature Energy Systems Based on Biomass Gasifiers and Solid Oxide Fuel Cells with Ni/GDC Anodes. Thesis TU Delft, November 2007. ISBN-13: 978-90-9022534-0
- [6.74] Richard Toonssen. Sustainable power from biomass. Thesis TU Delft, July 2010. ISBN 978-90-5335-297-7
- [6.75] Zuopeng Qu. Simulation and Analysis of an Anode-Supported Solid Oxide Fuel Cell and Stack. Thesis TU Delft, April 2011. ISBN 978-90-8570-747-9
- [6.76] Eduardo Hernández-Pacheco, Devinder Singh, Phillip N. Hutton, Nikhil Patel, Michael D. Mann. A macro-level model for determining the performance characteristics of solid oxide fuel cells. *Journal of Power Sources* 138 (2004) 174-186
- [6.77] P. Aguiar, C.S. Adjiman, N.P. Brandon. Anode-supported intermediate temperature direct internal reforming solid oxide fuel cell. I: model-based steady-state performance. *Journal of Power Sources* 138 (2004) 120-136
- [6.78] C. Xia, Y. Lang, G. Meng. Recent Advances to the Development of Low-Temperature Solid Oxide Fuel Cells. *Fuel Cells* 2004, 4, No. 1-2, 41-47
- [6.79] Paola Costamagna, Azra Selimovic, Marco Del Borghi, Gerry Agnew. Electrochemical model for the integrated planar solid oxide fuel cell (IP-SOFC). *Chemical Engineering Journal* 102 (2004) 61-69
- [6.80] F.J. Gardner, M.J. Day, N.P. Brandon, M.N. Pashley, M. Cassidy. SOFC technology development at Rolls-Royce. *Journal of Power Sources* 86 (2000) 122-129

## **CHAPTER 7 COMBINED HEAT AND POWER SYSTEMS**

- [7.1] Nico Woudstra, Theo Woudstra, Armando Pirone, Teus van der Stelt. Thermodynamic evaluation of combined cycle plants. *Energy Conversion and Management* 51 (2010) 1099-1110

## References

- [7.2] Aviel Verbruggen. The merit of cogeneration: Measuring and rewarding performance. *Energy Policy* 36 (2008) 3069–3076
- [7.3] Monteiro E et al. Planning of micro-combined heat and power systems in the Portuguese scenario. *Applied Energy* 86 (2009) 290–298
- [7.4] Hawkes, A.D., Leach, M.A. On policy instruments for support of micro combined heat and power. *Energy Policy* 36 (2008) 2973–2982
- [7.5] Torchio MF, et al. Merging of energy and environmental analyses for district heating systems. *Energy* 34 (2009) 220–227
- [7.6] Michel De Paepe, David Mertens. Combined heat and power in a liberalised energy market. *Energy Conversion and Management* 48 (2007) 2542–2555
- [7.7] Marko P. Hekkert, Robert Harmsen, Arjen de Jong. Explaining the rapid diffusion of Dutch cogeneration by innovation system functioning. *Energy Policy* 35 (2007) 4677–4687
- [7.8] M.A. Mujeebu, S. Jayaraj, S. Ashok, M.Z. Abdullah, M. Khalil. Feasibility study of cogeneration in a plywood industry with power export to grid. *Applied Energy* 86 (2009) 657–662
- [7.9] Magnus Karlsson, Alemayehu Gebremedhin, Sofia Klugman, Dag Henning, Bahram Moshfegh. Regional energy system optimization – Potential for a regional heat market. *Applied Energy* 86 (2009) 441–451
- [7.10] S.R. Allen, G.P. Hammond, M.C. McManus. Prospects for and barriers to domestic micro-generation: A United Kingdom perspective. *Applied Energy* 85 (2008) 528–544
- [7.11] Jeremy Cockroft, Nick Kelly. A comparative assessment of future heat and power sources for the UK domestic sector. *Energy conversion and management* 47(2006) 2349-2360
- [7.12] A.D. Hawkes, P. Aguiar, C.A. Hernandez-Aramburo, M.A. Leach, N.P. Brandon, T.C. Green, C.S. Adjiman. Techno-economic modelling of a solid oxide fuel cell stack for micro combined heat and power. *Journal of Power Sources* 156 (2006) 321–333
- [7.13] Michel De Paepe, Peter D’Herdt, David Mertens. Micro-CHP systems for residential applications. *Energy Conversion and Management* 47 (2006) 3435–3446
- [7.14] Petar Varbanov, Jiří Klemeš. Analysis and integration of fuel cell combined cycles for development of low-carbon energy technologies. *Energy* 33 (2008) 1508–1517
- [7.15] Deng J. et al. Exergy cost analysis of a micro-trigeneration system based on the structural theory of thermoeconomics. *Energy* 33 (2008) 1417–1426
- [7.16] Ivar S. Ertesvåg. Exergetic comparison of efficiency indicators for combined heat and power (CHP). *Energy* 32 (2007) 2038–2050
- [7.17] Svein J. Nesheim, Ivar S. Ertesvåg. Efficiencies and indicators defined to promote combined heat and power. *Energy Conversion and Management* 48 (2007) 1004-1015
- [7.18] Ozgur Balli, Haydar Aras, Arif Hepbasli. Exergetic performance evaluation of a combined heat and power system (CHP) in Turkey. *Int. J. Energy Res.* 2007; 31:849–866
- [7.19] S. Bonnet, M. Alaphilippe, P. Stouffs. Energy, exergy and cost analysis of a micro-cogeneration system based on an Ericsson engine. *International Journal of Thermal Sciences* 44 (2005) 1161–1168
- [7.20] M.A. Smith, P.C. Few. Second law analysis of an experimental domestic scale cogeneration plant incorporating a heat pump. *Applied Thermal Engineering* 21 (2001) 93-110

- [7.21] N. Woudstra, T. van der Stelt. Exergy analysis of combustion systems. ECOS 2003, Copenhagen, Denmark, June 30 - July 2, 2003, Vol.II: 835 - 842
- [7.22] K.J. Bosch, N. Woudstra, K.V. van der Nat. Designing Solid Oxide Fuel Cell Gas Turbine Hybrid Systems using Exergy Analysis. Fourth International ASME Conference on Fuel Cell Science, Engineering and Technology, June 19-21, 2006, Irvine, California.
- [7.23] N. Woudstra, T.P. van der Stelt, K. Hemmes. Thermodynamic Evaluation and optimization of Fuel Cell Systems. *Journal of Fuel Cell Science and Technology*, Volume 3, Number 2, May 2006 (p.155-164)
- [7.24] Anders R. Korsgaard, Mads P. Nielsen, Søren K. Kær. Part two: Control of a novel HTPeM-based micro combined heat and power fuel cell system. *International Journal of Hydrogen Energy* 33 ( 2008 ) 1921 – 1931
- [7.25] Ignacio Zabalza, Alfonso Aranda, María Dolores de Gracia. Feasibility analysis of fuel cells for combined heat and power systems in the tertiary sector. *International Journal of Hydrogen Energy* 32 (2007) 1396 – 1403
- [7.26] A.D. Peacock, M. Newborough. Impact of micro-CHP systems on domestic sector CO<sub>2</sub> emissions. *Applied Thermal Engineering* 25 (2005) 2653-2676
- [7.27] Kari Alanne, Arto Saari, V. Ismet Ugursal, Joel Good. The financial viability of an SOFC cogeneration system in single-family dwellings. *Journal of Power Sources* 158 (2006) 403-416
- [7.28] G. Gigliucci, L. Petrucci, E. Cerelli, A. Garzisi, A. La Mendola. Demonstration of a residential CHP system based on PEM fuel cells. *Journal of Power Sources* 131 (2004) 62–68
- [7.29] N. Woudstra. Towards sustainable energy systems. ECOS2000, Enschede, The Netherlands (5-7 July, 2000), p. 965-978
- [7.30] J. Matics, G. Krost. Micro combined heat and power home supply: Prospective and adaptive management achieved by computational intelligence techniques. *Applied Thermal Engineering* 28 (2008) 2055–2061
- [7.31] M.A. Smith, P.C. Few. Domestic-scale combined heat-and-power system incorporating a heat pump: analysis of a prototype plant. *Applied Energy* 70 (2001) 215–232

## ACKNOWLEDGEMENTS

Many people have influenced and contributed to the work described in this thesis. It is impossible to mention them all at this place. I will restrict myself primarily to the persons that have affected my activities or have contributed seriously to the results. Of course, many more have been of importance to me. I hope they will forgive me that I didn't mention them too.

The man who gave me the chance to start the research on advanced energy systems was Fred Braun, at that time director of the TNO-PgK (Project group for Nuclear Energy). He also started the cooperation with the TU Delft with regard the Potassium Topping Cycle and I am still grateful that he offered me the opportunity to join this work. Through him I came into contact with Jan van Lier (initially prof.ir. J.J.C. van Lier, the Dutch expert on exergy analysis) who taught me the fundamentals and the application of thermodynamics for energy systems as well as the exergy analysis. This thesis is actually my extension of his work. I am very grateful for the lessons, the support and the friendship I received from him. Without his contributions this thesis never would have been realized.

Another man who taught me in particular the properties of steam and specific problems of steam cycles is Kees van Paassen. I like to thank him for all the discussions, the disagreements as well as the friendship we had during the years we worked together.

Several studies presented in this thesis result from two STW projects. During the first project Michiel Hartman and Kees Heil did research on long term energy supply systems. At the same time Wiebe Wester and Theo Woudstra (Ir. Th. Woudstra) were involved in the evaluation of thermal power cycles and the development of Cycle-Tempo. I have appreciated very much their contributions and their dedication to the activities of the group. I also like to thank the group of the second project: Arend de Groot, Marianne Meijer, Bart de Melker and again Theo Woudstra. Their inspiring contributions to the development of exergy analysis, fuel cell systems and Cycle-Tempo have been of great help. During these projects also Teus van der Stelt was appointed and supported the development of Cycle-Tempo. I am extremely grateful for all the work Teus and Theo did around the development and application of Cycle-Tempo. Without their calm, dutiful, and always helpful support the software never should have reached the present high level for the analysis of energy systems.

The interest for exergy analysis within the TU Delft has resulted into the TU Delft Exergy Group. Information exchange and dissemination of knowledge have been the main activities of the group. I like to thank in particular Lydia Stougie, Hedzer van der Kooi, and Gerard Bart for all the discussions on principles and applications and for their contributions to the activities of the group. I have highly appreciated their support and friendship.

I further like to express my gratitude to Kas Hemmes for all his help to focus the research of the energy systems group more on fuel cell systems. Our cooperation in the PhD projects of Frans Standaert and Siu Fai Au has been very instructive to me. Our contacts are characterized by different backgrounds, different opinions but always friendly and stimulating discussions. I will thank Frans and Siu Fai too for their constructive contributions to these discussions.

A further intensification of the fuel cell research has been realized by Aravind Purushothaman Vellayani, short Aravind PV. He extended the studies on high temperature fuel cell systems with the experimental activities we had in mind. I have appreciated very

much his integrity, sincerity and frankness. Together with Aravind I like to thank Zuopeng Qu and Richard Toonssen. The PhD work of Zuopeng, executed in cooperation with ECN, has seriously improved my understanding the processes within the fuel cell stack. The PhD study of Richard has offered a valuable overview of possibilities to combine biomass gasification with SOFC systems. His knowledge of chemical engineering appeared to be very useful to me.

Of course I have to express my gratitude to Ad Verkooijen, my promoter. He offered me the freedom to write this thesis in my way. I have admired the way he gave his critical comments. I also like to thank him for the support he has given to the activities of the energy systems group.

Finally I have to thank my wife Marjan and my children, Martijn, Mark, Marcela and Elizabeth. They didn't contribute directly to this thesis, hindered by their lack of interest for thermodynamics. But at least they kept the "fool on his cloud" down to earth so that I could always feel their warmth. The capacity of this source has been increased during the years and includes also Sasja with Sverre, Serein and Laure, Annemarie with Yannick, Laurens and Ruben, and Joao. The exergy I have got from this source seems to be significant higher than the temperature suggests. I am grateful for all the exergy I received.

## CURRICULUM VITAE

Nico Woudstra was born on April 12<sup>th</sup> 1945 in Sneek (The Netherlands). He graduated at the Johannes Bogerman Lyceum (HBS-B) in 1963 and started his study Mechanical Engineering at the TU Eindhoven. He completed his study in 1973 with a Master thesis on ship propulsion systems.

After his study he was appointed at Verolme Machinefabriek IJsselmonde as engineer engine room systems. From 1975 to 1991 he was employed at TNO (Netherlands Organization for Applied Research) at various positions. He started as systems engineer in the Project group for Nuclear Energy (PgK) (1975 – 1979). During this period he was posted at Neratoom in the Hague. From 1979 – 1983 he was project manager of the Potassium topping cycle project, a cooperation of TNO-PgK and Neratoom, supported by the Dutch government partly as an IEA project with German and Austrian partners. After this period he continued as research engineer within TNO, first in the Institute for Mechanical Engineering and from 1985 – 1991 in the Institute of Environmental and Energy Technology. From 1983 to 1991 he was posted at the TU Delft in the section Thermal Power Engineering of the faculty Mechanical Engineering. During this period he was supervisor of two STW projects on advanced energy systems for the future. The further improvement and extension of the computer program Cycle-Tempo and the participation in system studies on IGCC and fuel cell systems has been part of these projects.

In 1991 he was appointed at the TU Delft as UD (assistant professor) in the section of Thermal Power Engineering (faculty of Mechanical Engineering). Besides the continuation the activities of the previous period, his research did focus more and more on the exergy analysis of energy systems. His involvement in education started with the supervision of MSc students during their final assignments. In the beginning various studies on CHP (Combined Heat and Power) have been executed. Around the year 2000 his focus moved to fuel cell systems, in particular high temperature fuel cell systems. In that time he became involved too in the supervision of PhD projects on fuel cell systems. Further he coordinated the first year energy project during several years and started teaching activities. His teaching included primarily the lecturing Thermodynamics of Energy Systems (wb 4302), a course in the master program of ET, and the bachelor course Thermodynamics 2 (wb 1224). He contributed also to the bachelor course Energy Conversion (wb 4304) and a course on Sustainable Energy (ie 3320). Finally he started a course on Fuel Cell Systems (wb 4425) in the master program.

In 2010 he retired and decided to write this thesis.

